

UNIVERSITY OF THE BASQUE COUNTRY
UNIVERSITY OF BORDEAUX

OPTIMIZED MONITORING TECHNIQUES AND DATA ANALYSIS DEVELOPMENT FOR IN-SITU CHARACTERIZATION OF THE BUILDING ENVELOPE'S REAL ENERGETIC BEHAVIOUR



PhD Candidate:
Catalina Giraldo Soto

Supervisors:
Aitor Erkoreka (UPV/EHU)
Laurent Mora (UBX)

(cc) 2021 Catalina Giraldo Soto (cc by-nc-nd 4.0)

January 2021

ACKNOWLEDGEMENTS

First of all, I would like to thank my thesis directors Aitor Erkoreka and Laurent Mora, whose help has been decisive throughout the scientific direction of this thesis. My gratitude is infinite for their valuable advice and all the time dedicated in these years.

I am also grateful for the sponsorship received from the University of the Basque Country (UPV/EHU) and the University of Bordeaux (UBX), which has positively enriched the research work I have developed. I extend this gratitude to the ENEDI and I2M institute research groups, the Department of Energy Engineering (UPV/EHU), the Department of Mechanics (UBX) and all my colleagues who have accompanied me during the development stages of my doctorate. I would also like to thank doctors Iván Flores, Koldo Martín and Luis del Portillo for their support within the PhD program during these years, Ander Barragan Elorza for his help in the experimental test carried out and Joaki Rodríguez for the help in the administrative process in the acquisition of material and equipment for the experimental phase of my thesis.

I am grateful for the support received by Dr Iván Flores, Carlos García Gafaro, Daniel Pérez (Laboratory for the Quality Control in Buildings), Amaia Uriarte (Tecnalia) and Isabel Pineda (Ensanche 21). Their collaboration has been essential in order to carry out the ambitious project of monitoring the residential building and to make it possible to integrate this project into all the phases of refurbishment. I would like to thank Wahbi Jomaa, Thomas Recht and Philippe Lagiere from the University of Bordeaux for their generosity and support during my doctoral stay in the cottage, and now during the final phase of my doctorate.

My family has been a fundamental part of these years of work. I thank my mother, my father and my brother for the unconditional support and encouragement that you have given me during these years in my doctoral work. I would also like to thank my partner for his encouragement and his optimism he has shown during this period in which he has always been by my side.

Finally, I would like to emphasise in particular my thanks to Aitor Erkoreka. His constant support and great involvement have been decisive in the whole process. Only he knows how much I owe him. Furthermore, thanks to with Jose María Sala, I was offered the opportunity to start my professional and personal journey in the Basque Country four years ago. This journey is now materialised in this research work.

RESUMEN

Aunque la eficiencia energética de los edificios ha mejorado durante los últimos años, todavía se encuentra una importante "brecha de rendimiento" entre su diseño y el consumo real de energía. Esta brecha de rendimiento tiene tres fuentes principales: el comportamiento del usuario del edificio, el rendimiento real de los sistemas del edificio y el rendimiento energético real de la envoltura del edificio. Los resultados de la tesis tienen como objetivo avanzar en la fiabilidad de la comprensión y la cuantificación de la brecha de rendimiento debido al rendimiento energético en uso de la envoltura del edificio. El valor del Coeficiente de Pérdida de Calor de Diseño (HLC) de la envolvente del edificio suele estar disponible en los Certificados de Rendimiento Energético para los edificios nuevos o reformados, pero todavía existen problemas de fiabilidad en los métodos que permiten estimar el HLC de los edificios en uso. La HLC es la pérdida total de calor de un edificio que resulta de la transferencia de calor a través de la envoltura (UA) y de la infiltración y/o ventilación (C_v) por grado de diferencia de temperatura entre el interior y el exterior en $W/^\circ C$.

La tesis comienza analizando y presentando en detalle dos métodos para la estimación de la HLC. El conocido Método de Co-calentamiento, que está cerca de ser un estándar para medir la HLC de las envolventes de edificios desocupados. Mientras que el Método de Promedio permite la estimación de la HLC de las envolventes de edificios en uso. El Método de Promedio se basa principalmente en los ya extendidos sistemas de monitorización de edificios donde se miden los parámetros asociados al confort interior y calidad del aire, consumos de energía de los sistemas de edificios y datos meteorológicos. Además, utilizando CO_2 antropogénico, como gas trazador, y los datos de monitorización del sistema de ventilación, se expone el método para la estimación de C_v . De esta forma, el la estimación del HLC de la envolvente del edificio en uso HLC, podría ser desacoplada por una simple sustracción $HLC = UA + C_v$.

El objetivo general de este proyecto de tesis doctoral es avanzar en la fiabilidad y optimización de los Sistemas de Monitorización y Control para la estimación y el desacoplamiento del HLC, para en el futuro, poder definir un mínimo Kit de Monitorización energético para edificios residenciales o terciarios. Estos Kits de Monitorización deben ser lo más discretos posible y deben permitir monitorizar de forma fiable la mínima cantidad de datos que, junto con un análisis correcto, deben permitir caracterizar el comportamiento real de la envoltura del edificio.

Así pues, después de presentar los métodos existentes para estimar y desacoplar de HLC en uso, se realiza el análisis del estado del arte sobre el uso los Sistemas de Monitorización y Control para la caracterización energética de la envoltura de los edificios en uso. Gracias a este análisis sobre los Sistemas de Monitorización y Control, se ha comprobado que, en la bibliografía existente, la incertidumbre general de la temperatura interior y exterior (cuando se presenta) se considera siempre como la precisión del fabricante. Utilizar sólo la precisión del fabricante como la incertidumbre global para estas dos importantes mediciones, que son necesarias para la estimación de las HLC de edificios en uso, podría conducir a una fuerte subestimación de su incertidumbre real y esta subestimación se propagaría en el valor estimado del HLC. Para analizar en profundidad

este tema, que podría generar serios problemas de fiabilidad en los valores HLC, se ha diseñado e implementado unos sistemas de monitorización tridimensional en las oficinas de un edificio terciario. Para analizar la incertidumbre general de la medición de la temperatura del aire interior, se han monitorizado cuatro zonas térmicas del edificio terciario con un enfoque tridimensional. Para analizar la incertidumbre general de la medición de la temperatura del aire exterior, también se ha aplicado un enfoque de monitorización tridimensional alrededor de la envolvente del edificio.

Los resultados de este análisis han permitido identificar la mejor ubicación de los sensores de temperatura interior y exterior en el edificio monitorizado. Igualmente, se han analizado las discrepancias entre el valor de la precisión del sensor dado por el fabricante y el valor experimental de la precisión del sensor más el sistema de Monitorización y Control. En este análisis se encuentra la principal contribución de esta tesis: donde se ha desarrollado una metodología para cuantificar de la incertidumbre global de medida de variables intensivas en los edificios en uso, como lo son la temperatura del aire interior y la temperatura del aire exterior. Esta metodología no sólo permite obtener el valor global de la incertidumbre de las medidas (denominada Incertidumbre de Medida), la cual contiene todas las fuentes de incertidumbre, sino que también permite desacoplar dicha incertidumbre en de la incertidumbre asociada a los errores aleatorios y los errores sistemáticos. Este desacoplamiento separa el valor de la varianza asociada a la incertidumbre global (Incertidumbre de Medida) en la suma de dos varianzas, una asociada a los errores sistemáticos (denominada en el estudio, Incertidumbre Medición del Sensor) y otra asociada a los errores aleatorios (denominada en el estudio, Incertidumbre Espacial de Medida).

Por otro lado, a partir del análisis del Método de Co-heating y del Método Promedio para estimar el HLC, se ha diseñado e implementado un sistema de Sistema de Monitorización y Control extremadamente detallado en un edificio residencial. El objetivo de este sistema de monitorización es poder analizar cuál es el conjunto mínimo de sensores necesarios para estimar y desacoplar los valores del HLC de un edificio en uso con una fiabilidad suficiente. Los sensores seleccionados tienen la mayor precisión posible que se podría encontrar para la aplicación en el sector de la construcción. También se incluye un análisis económico detallado para este Sistema de Monitorización y Control. Debido al COVID-19, no ha sido posible obtener suficientes datos de este sistema implementado para realizar el análisis previsto. Aun así, se presentan las directrices sobre cómo analizar los datos de este Sistema de Monitorización y Control para obtener el número mínimo de sensores para la estimación y desacople del HLC en edificios en uso.

La cuantificación de la diferencia entre el diseño y los HLC, UA y C_v en uso no sólo es el primer paso para reducir el consumo de energía real de los edificios, sino que podría ser el comienzo de una nueva era para la certificación de edificios en uso, basada en los datos obtenidos del Sistema de Monitorización y Control.

Palabras clave: Sistemas de monitorización y Control energética, Incertidumbre de Medida, Pérdida de Calor (HLC), Rendimiento energético del edificio (EPB).

ABSTRACT

Although the energy efficiency of buildings has improved over the last few years, there is still an important 'performance gap' between their design and actual energy consumption. This performance gap has three main sources: the building user's behaviour, the building systems' real performance and the building envelope's actual energy performance. The thesis results aim to advance in the reliability of the understanding and quantification of the performance gap due to the building envelope in-use energy performance. The design Heat Loss Coefficient (HLC) value of building envelopes are usually available in the Energy Performance Certificates of new or retrofitted buildings, but there are still reliability problems in the methods that permits to estimate the HLC of in-use buildings. HLC is the total heat loss from a building resulting from heat transfer through the envelope (UA) and from infiltration and/or ventilation (C_v) per °C of indoor to outdoor temperature difference in $W/°C$.

The thesis starts by analysing and presenting in detail two methods for HLC estimation. The well-known Co-heating Method is already close to being a standard to measure the HLC of unoccupied building envelopes. While the Average Method permits the estimation of the HLC of in-use building envelopes. The Average Method relies mainly on already widespread building monitoring systems comprising just indoor comfort and air quality parameters, building systems energy consumptions and weather data. In addition, using anthropogenic CO_2 as the tracer gas and ventilation system monitored data, the method for C_v estimation will also be presented. Then, the in-use building envelope HLC could be decoupled by simple subtraction $HLC = UA + C_v$.

The general objective of this doctoral thesis project is to advance in the reliability and optimisation of Monitoring and Control Systems for HLC estimation and decoupling, so as to be able to define a minimum energy Monitoring Kit for residential or tertiary buildings in the future. These monitoring kits should be as unobtrusive as possible and should allow the minimum amount of data to be reliably monitored which, together with a correct analysis, should allow the real behaviour of the building envelope to be characterised.

Thus after presenting the existing in-use HLC estimation and decoupling methods, the analysis of the State of the Art on monitoring and control systems for in-use building envelope energy characterisation is performed. Thanks to this review on monitoring and control systems analysis, it has been found that the overall uncertainty of indoor and outdoor temperature (when presented) is always considered to be the manufacturer's accuracy in the existing literature. Using only the manufacturer's accuracy as the overall uncertainty for these two important measurements required for the in-use HLC estimation, might lead to strongly underestimating their real uncertainty and this underestimation would be propagated to the estimated HLC values. To deeply analyse this topic, which could generate serious reliability issues for the estimated HLC values, a three-dimensional monitoring system has been designed and deployed in an office building. To analyse the overall uncertainty of the indoor air temperature measurement, four thermal zones within the office building have been monitored with a three-dimensional approach. To analyse the overall uncertainty of the outdoor air temperature measurement, a three-dimensional monitoring approach has also been

implemented around the building envelope.

Furthermore, the results of this analysis have allowed the identification of the best location for the indoor and outdoor temperature sensors on the monitored building. Besides, the quantification of the discrepancies between the value of the sensor accuracy given by the manufacturer and the experimental value of the sensor accuracy plus the monitoring and control system has also been analysed. Here, the main contribution of this thesis can be found: the methodology developed to allow the quantification of the overall uncertainty of intensive variable measurements such as indoor air temperature and outdoor air temperature on in-use buildings. This methodology not only allows us to obtain the overall value of these measurements' uncertainty containing all sources of uncertainty (called Measurement Uncertainty), but also allows us to decouple the Measurement Uncertainty into the uncertainty associated to the random and systematic errors. This decoupling separates the value of the variance associated with the overall uncertainty into the sum of two variances, one variance associated with the uncertainty related to the systematic errors (called in the study, Sensor Measurement Uncertainty) and another associated with the uncertainty related to the random errors (called in the study, Measurement's Spatial Uncertainty).

On the other hand, from the analysis of the Co-heating and the Average method to estimate the HLC, an extremely detailed monitoring system has been designed and implemented in a residential building. The aim of this extremely detailed monitoring system is to be able to analyse what the minimum required set of sensors to estimate and decouple the in-use HLC values with sufficient reliability. The selected sensors have the highest possible accuracy that could be found for building sector applications. A detailed economic analysis is also included for this extremely detailed monitoring. Due to the COVID-19, it has not been possible to obtain sufficient data of this implemented monitoring and control system to perform the planned analysis. However, the guidelines of how to analyse the data of this monitoring and control system to obtain the minimum sensor number for in-use HLC estimation and decoupling are presented.

Quantifying the difference between the design and in-use HLC, UA and C_v is not only the first step to reduce the buildings' actual energy consumption, but could be the beginning of a new building certification era based on in-use building monitored data.

Keywords: Energy monitoring and control system, Measurement Uncertainty, Heat Loss Coefficient (HLC), Energy Performance Buildings (EPB).

Contents

Contents	x
List of Figures	xv
List of Tables	xxi
1 INTRODUCTION	39
2 LITERATURE REVIEW	49
2.1 Introduction	50
2.1.1 Energy consumption of buildings in Europe	50
2.1.2 The the role of MCS in Energy Performance Certificates and the HLC to characterize the Thermal Envelope Performance (TEP) of buildings	52
2.1.3 The Monitoring Systems (MSs) used to estimate the Heat Loss Coefficient (HLC) to determine the Thermal Envelope Performance (TEP) of Buildings	54
2.1.4 Fault Diagnostic, Detection (FDD) and Calibration in Building Monitoring Systems	55
2.2 Monitoring and Control Systems (MCSs) used to estimate the Heat Loss Coefficient (HLC) using the Average Method and the Co-Heating Method	55
2.2.1 Different methods to characterize the building envelope energy behaviour	56
2.2.2 General mathematical development to estimate the Heat Loss Coefficient (HLC) through the Average Method	57
2.2.3 Co-Heating Method	68
2.2.4 Decoupling the building's HLC by estimating the Infiltration/Ventilation Heat Loss Coefficient (C_v) by means of the metabolic CO_2 decay method	71
2.2.5 Importance of the in-use HLC estimation and relation of the measurement uncertainty with the HLC estimation uncertainty	73
2.2.6 Error propagation	75
2.2.7 Sensor accuracy of Monitoring Systems (MSs) used in an experimental test to estimate the building envelope HLC for an in-use building	75
2.3 Analysis of the state of the art of Monitoring and Control Systems (MCSs) implemented to estimate the Heat Loss Coefficient (HLC)	78

2.3.1	Literature review’s study of Monitoring and Control Systems’ (MCSs) equipment used in research projects to estimate the Heat Loss Coefficient (HLC) and characterize the Thermal Envelope Performance(TEP) of Buildings	87
2.3.2	Quantitative and qualitative analysis of monitoring and control systems of the reviewed literature	92
2.3.3	Conclusions	101
3	METHODOLOGY	105
3.1	Introduction	106
3.2	Uncertainty analysis for intensive variables measurement of in-use buildings	106
3.2.1	Statistical basis of the uncertainty estimation	109
3.2.2	Methodology to decouple systematic and random uncertainties of Type A samples	118
3.2.3	Vertical analysis of Measurement Uncertainty (U_M): vertical stratification’s behaviour	126
3.2.4	Impact of spatial localisation over U_M	127
3.2.5	Impact of number of sensors installed at the same height, but in different horizontal locations to decrease the Measurement Uncertainty (U_M) in an MZ	127
3.3	Design of Monitoring and Control Systems (MCS) for HLC estimation for buildings . . .	127
3.4	Conclusions	131
4	RESULTS AND DISCUSSION	133
4.1	Introduction	134
4.2	Design of a Mobile Monitoring System (MMS) to analyse the overall uncertainties of T_{in} and T_{out} measurements in the administrative building of the UPV/EHU	134
4.3	Measurement uncertainty analysis of indoor and outdoor air temperature in the administrative building of the UPV/EHU	148
4.3.1	Indoor air temperature global uncertainty results for the UPV/EHU administrative building	150
4.3.2	Outdoor air temperature global uncertainty results for the UPV/EHU administrative building	181
4.4	Design and deployment of an Experimental Monitoring and Control System (MCS) for an in-use residential building of Vitoria-Gasteiz to analyse the sensor requirements so as to be able to estimate and decouple the HLC	204
4.5	Conclusions	218
5	Final Conclusions, contributions and New Research Lines	223
5.1	Final conclusions	224
5.2	Contributions	228
5.2.1	Research papers of this thesis	228
5.2.2	Research papers related to this thesis work	229
5.2.3	Data repositories related to this thesis work	229

5.2.4	International conferences	229
5.3	New research lines:	230
	Bibliography	233
	Appendix	247
A	MMS' sensor installed in the in-use tertiary building	247
B	Histograms of T_{in} uncertainty for tertiary building	271
C	Histograms of T_{out} uncertainty for tertiary building	279
D	MCS' sensor installed in the residential building	293
E	Budgets and invoices for the investment of tertiary building's MMS	311
F	Budgets and invoices for the investment of residential building's MCS	329

List of Figures

1.1	Measured (through the co-heating test) versus predicted whole house's Heat Loss Coefficient (HLC) (W/K) for 18 new build dwellings in the UK [16].	41
1.2	Schematic of main energy and mass exchanges through the building envelope.	43
1.3	Scheme of optimized MCS scope.	47
2.1	Scheme of tools to determinate the gap between performances at design and operation phases of buildings: the HLC and TEP estimation role to know the envelope energy behaviour in order to generate EPCs related to the building envelope.	51
2.2	Traditional estimation of Thermal Envelope Performance (TEP) versus the new estimation trend through the Heat Loss Coefficient (HLC) estimation.	56
2.3	Scheme of all energy and mass exchanges through the control volume defined by the building envelope.	58
2.4	Scheme of all heat and mass exchanges through the multi-volume building.	69
2.5	Scheme of MCSs used in reviewed literature to estimate the HLC and characterize the TEP.	78
2.6	Classification scheme for AFDD methods based on previous research [113, 114]	88
3.1	Scheme of differential volumes of Monitored Zones (MZ) and Monitored Spaces (MS) in a building composed by several floors.	111
3.2	Scheme of $[(\overline{M}_{vw})_{MZ}]_{range}$ and $[(\overline{M}_a)_{MZ}]_{range}$ estimation based on the U_M estimation.	124
3.3	Scheme of $[(\overline{M}_{vw})_{MZ}]_{band}$ and $[(\overline{M}_a)_{MZ}]_{band}$ estimation when one or some MSs are monitored to measure a intensive variable in an MZ.	124
3.4	Scheme of MCS requirement of Co-Heating test to estimate the HLC.	129
3.5	Scheme of MCS requirement of Average method to estimate the HLC.	131
4.1	Location of tertiary building. City/Town/Region: Leioa/Bizkaia/Basque Country. Country: Spain. Latitude and longitude: 43.3316308, -2.9716170.	136
4.2	The UPV/EHU administrative building in Leioa post-retrofitting: a) northern façade, b) West Façade, c) southern façade, d) Roof.	137
4.3	Scheme of the uncertainty of T_{in} measurement for different Thermal Zones (TZs) and Thermal Spaces (TSs) identified in the in-use tertiary building.	151

4.4 Scheme of the uncertainty of T_{in} measurement for different Thermal Zones (TZs) and Thermal Spaces (TSs) identified in an in-use tertiary building. 154

4.5 T_{dvi} evolution in 24 hours of data collected from the TT test between 30th June 2019 at 0:00 to 24:00. (TT test ([149])). 156

4.6 T_{dvi} evolution during 24 hours of data collected from the OT test ([149]): a. OT1 data 11th June 2019 from 0:00 to 24:00. b. OT2 data of 11th June 2019 from 0:00 to 24:00. c. OT3 data of 29th May 2019 from 0:00 to 24:00. d. OT4 data of 24th April 2019 from 0:00 to 24:00. 158

4.7 Temperature Histogram of T_{dvi} from MMS in OT1 for a sample size equal to 28,733 t_N with measurement frequency equal to ten seconds. 159

4.8 Standard deviation tendency by vertical height for each tripod with one sensor. 166

4.9 Standard deviation tendency by tripod with two sensors for each vertical height. 166

4.10 Standard deviation tendency by vertical height for each tripod with one sensors. 167

4.11 Standard deviation tendency by tripod with one sensor for each vertical height. 167

4.12 Mean standard deviation tendency by sensor based on vertical location for RAD ON and RAD OFF samples. 170

4.13 Mean standard deviation tendency by sensor based on vertical location for Ph ON and Ph OFF samples. 170

4.14 Mean standard deviation tendency by sensor based on vertical location for Pw ON and Pw OFF samples. 170

4.15 Mean standard deviation tendency by sensor based on vertical location for RAD ON and RAD OFF samples. 172

4.16 Mean standard deviation tendency by sensor based on vertical location for Ph ON and Ph OFF samples. 173

4.17 Mean standard deviation tendency by sensor based on vertical location for Pw ON and Pw OFF samples. 173

4.18 Uncertainty evolution for each $(\theta_{dvi})_{vw}$ by Instant of Time (t_N), in function of the number of sensors (T_{dvi} values) installed at high level in OT4. 180

4.19 Scheme of the uncertainty of the T_{out} measurement for different Thermal Zones (TZs) and Thermal Spaces (TSs) identified in an in-use tertiary building. 182

4.20 Scheme of the uncertainty of the T_{out} measurement for different Thermal Zones (TZs) and Thermal Spaces (TSs) identified in an in-use tertiary building. 182

4.21 T_{dvi} evolution for October 19th, 2020 from 0:00 to 23:59 of data collected from the E.R3.s.25 and E.R3.s.26 sensors of the MMS. 185

4.22 T_{dvi} evolution on October 19th, 2020 from 0:00 to 23:59 of data collected from E.F1.n.20, E.F1.n.21, E.F1.w.22, E.F1.s.23, E.F2.s.24, E.R3.s.25, E.R3.s.26 and E.R3.n.27 sensors of the MMS. 187

4.23 T_{dvi} and solar radiation evolution on October 19th, 2020 from 0:00 to 23:59 of data collected from MMS' BEAs (north Façade, southern façade and roof). 194

4.24 (T_{dv_i}) evolution during 10 hours from 4 th May 2019 at 0:15:00 to 10:10:00 of data collected from the E.R3.s.25 and E.R3.s.26 sensors, there is no solar radiation.	197
4.25 Location of residential building. City/Town/Region: Vitoria-Gasteiz/Álava/Basque Country. Country: Spain. Latitude and longitude: 42.8500434, -2.6738711.	205
4.26 The residential building in Vitoria-Gasteiz: a) Pre-retrofitting, b) Post-retrofitting.	206
A.5 Interior 3D MMS tripods and sensors all together during the TT test [139].	250
A.6 OT1 sensor layout, located in F2. Based on A2PBEER project’s architecture plans [76] [139].	251
A.7 OT2 sensor layout, located in F2. Based on A2PBEER project’s architecture plans [76] [139].	252
A.8 OT3 sensor layout, located in F2. Based on A2PBEER project’s architecture plans [76] [139].	253
A.9 OT4 sensor layout, located in F3. Based on A2PBEER project’s architecture plans [139].	254
A.10 Sensors and Hardware installed in UPV/EHU administrator building [139].	255
A.11 Installed interior MMS’ pictures [139].	255
A.12 Exterior Together (ET) test pictures [139].	257
A.13 Exterior MMS’ layout [139].	258
A.14 Southern sensors layout of Exterior MMS [139].	259
A.15 Western sensor layout of Exterior MMS [139].	260
A.16 Northern sensors layout of Exterior MMS [139].	261
A.17 Installed exterior MMS sensors’ pictures [139].	262
A.1 F0 of the UPV/EHU admin building in Leioa. Based on A2PBEER project’s architecture plans [76].	264
A.2 F1 of the UPV/EHU admin building in Leioa. Based on A2PBEER project’s architecture plans [76].	265
A.3 F2 of the UPV/EHU admin building in Leioa. Includes the position of the three selected measurement points of the existing BAS referred to in Table A.6. Based on A2PBEER project’s architecture plans [76].	266
A.4 F3 of the UPV/EHU admin building in Leioa, including the position of the three selected measurement points of the existing BAS referred to in Table A.6. Note that T9.md.142143 is the signal created by adding the measurements T9.md.142 and T9.md.143. Based on A2PBEER project’s architecture plans [76].	267
B.1 Temperature Histogram of T_{dv_i} from nineteen sensors measuring together (eighteen EE800-M1213 sensors and one EE071-HTPC sensor), for a sample size equal to 868 t_N with measurement frequency equal to five minutes.	272
B.2 Temperature Histogram of $(\theta_{dv_i})_{wsm}$ from nineteen sensors measuring together (eighteen EE800-M1213 sensors and one EE071-HTPC sensor), for a sample size equal to 868 t_N with measurement frequency equal to five minutes.	272

B.3 Temperature Histogram of $(\theta_{dv_i})_{vw}$ from MMS in OT1 for a sample size equal to 28,733 t_N with measurement frequency equal to ten seconds. 272

B.4 Temperature Histogram of Tdv_i from MMS in OT2 for a sample size equal to 28,705 t_N with measurement frequency equal to ten seconds. 273

B.5 Temperature Histogram of $(\theta_{dv_i})_{vw}$ from MMS in OT2 for a sample size equal to 28,705 t_N with measurement frequency equal to ten seconds. 273

B.6 Temperature Histogram of Tdv_i from MMS in OT3 for a sample size equal to 18,861 t_N with measurement frequency equal to fifty seconds. 273

B.7 Temperature Histogram of $(\theta_{dv_i})_{vw}$ from MMS in OT3 for a sample size equal to 18,861 t_N with measurement frequency equal to fifty seconds. 274

B.8 Temperature Histogram of Tdv_i from MMS in OT4 for a sample size equal to 35,381 t_N with measurement frequency equal to forty seconds. 274

B.9 Temperature Histogram of $(\theta_{dv_i})_{vw}$ from MMS in OT4 for a sample size equal to 35,381 t_N with measurement frequency equal to forty seconds. 274

B.10 Temperature Histogram of Tdv_i from MMS in OT3.2C3.2 for a sample size equal to 18,861 t_N with measurement frequency equal to fifty seconds. 275

B.11 Temperature Histogram of $(\theta_{dv_i})_{wsm}$ from MMS in OT3.2C3.2 for a sample size equal to 18861 t_N with measurement frequency equal to fifty seconds. 275

B.12 Temperature Histogram of Tdv_i from MMS in OT3.2C3.3 for a sample size equal to 18,861 t_N with measurement frequency equal to fifty seconds. 275

B.13 Temperature Histogram of $(\theta_{dv_i})_{wsm}$ from MMS in OT3.2C3.3 for a sample size equal to 18,861 t_N with measurement frequency equal to fifty seconds. 276

B.14 Temperature Histogram of Tdv_i from MMS in OT3.2C3.5 for a sample size equal to 18,861 t_N with measurement frequency equal to fifty seconds. 276

B.15 Temperature Histogram of $(\theta_{dv_i})_{wsm}$ from MMS in OT3.2C3.5 for a sample size equal to 18,861 t_N with measurement frequency equal to fifty seconds. 276

B.16 Temperature Histogram of Tdv_i from MMS in OT3.2C3.9 for a sample size equal to 18,861 t_N with measurement frequency equal to fifty seconds. 277

B.17 Temperature Histogram of $(\theta_{dv_i})_{wsm}$ from MMS in OT3.2C3.9 for a sample size equal to 18,861 t_N with measurement frequency equal to fifty seconds. 277

C.1 Temperature Histogram of Tdv_i from E.R3.s.25 and E.R3.s.26 sensors of the MMS for a sample size equal to 50,958 t_N with and without solar radiation. 280

C.2 Temperature Histogram of $(\theta_{dv_i})_{la}$ with data centred on the Local Average Temperature $(T_a)_{la}$ for E.R3.s.25 and E.R3.s.26 sensors of the MMS for a sample size equal to 50,958 t_N with and without solar radiation. 280

C.3 Temperature Histogram of $(\theta_{dv_i})_{la}$ with data centred on the Local Average Temperature $(T_a)_{la}$ for E.R3.s.25 and E.R3.s.26 sensors of the MMS for a sample size equal to 17,527 t_N with solar radiation. 280

C.4 Temperature Histogram of $(\theta_{dv_i})_{la}$ with data centred on the Local Average Temperature $(T_a)_{la}$ for E.R3.s.25 and E.R3.s.26 sensors of the MMS for a sample size equal to 29,05 t_N without solar radiation. 281

C.5 Temperature Histogram of (T_{dv_i}) from E.F1.n.20, E.F1.n.21, E.F1.w.22, E.F1.s.23, E.F2.s.24, E.R3.s.25, E.R3.s.26 and E.R3.n.27 sensors of MMS for a sample size equal to 50,958 t_N with and without solar radiation. 281

C.6 Temperature Histogram of (T_{dv_i}) from E.F1.n.20, E.F1.n.21, E.F1.w.22, E.F1.s.23, E.F2.s.24, E.R3.s.25, E.R3.s.26 and E.R3.n.27 sensors of the MMS for a sample size equal to 17,527 t_N with solar radiation. 281

C.7 Temperature Histogram of (T_{dv_i}) from E.F1.n.20, E.F1.n.21, E.F1.w.22, E.F1.s.23, E.F2.s.24, E.R3.s.25, E.R3.s.26 and E.R3.n.27 sensors of the MMS for a sample size equal to 29,05 t_N without solar radiation. 282

C.8 Temperature Histogram of $(\theta_{dv_i})_{ta}$ with data centred on the Total Average Temperature $((T_a)_{ta})$ for E.F1.n.20, E.F1.n.21, E.F1.w.22, E.F1.s.23, E.F2.s.24, E.R3.s.25, E.R3.s.26 and E.R3.n.27 sensors of MMS for a sample size equal to 50,958 t_N with and without solar radiation. 282

C.9 Temperature Histogram of $(\theta_{dv_i})_{ta}$ with data centred on the Total Average Temperature $((T_a)_{ta})$ for E.F1.n.20, E.F1.n.21, E.F1.w.22, E.F1.s.23, E.F2.s.24, E.R3.s.25, E.R3.s.26 and E.R3.n.27 sensors of MMS for a sample size equal to 17,527 t_N with solar radiation. . . 282

C.10 Temperature Histogram of $((\theta_{dv_i})_{ta})$ with data centred on the Total Average Temperature $((T_a)_{ta})$ for E.F1.n.20, E.F1.n.21, E.F1.w.22, E.F1.s.23, E.F2.s.24, E.R3.s.25, E.R3.s.26 and E.R3.n.27 sensors of MMS for a sample size equal to 29,05 t_N without solar radiation. 283

C.11 Temperature Histogram of $(\theta_{dv_i})_{ta}$ with data centred on the Total Average Temperature $((T_a)_{ta})$ for E.F1.n.20 and E.F1.n.21 sensors of MMS for a sample size equal to 50,958 t_N with and without solar radiation. 283

C.12 Temperature Histogram of $(\theta_{dv_i})_{ta}$ with data centred on the Total Average Temperature $((T_a)_{ta})$ for E.F1.n.20 and E.F1.n.21 sensors of MMS for a sample size equal to 17,527 t_N with solar radiation. 283

C.13 Temperature Histogram of $((\theta_{dv_i})_{ta})$ with data centred on the Total Average Temperature $((T_a)_{ta})$ for E.F1.n.20 and E.F1.n.21 sensors of MMS for a sample size equal to 29,05 t_N without solar radiation. 284

C.14 Temperature Histogram of $((\theta_{dv_i})_{ta})$ with data centred on the Total Average Temperature $((T_a)_{ta})$ for E.F1.s.23 and E.F2.s.24 sensors of MMS for a sample size equal to 50,958 t_N with and without solar radiation. 284

C.15 Temperature Histogram of $((\theta_{dv_i})_{ta})$ with data centred on the Total Average Temperature $((T_a)_{ta})$ for E.F1.s.23 and E.F2.s.24 sensors of MMS for a sample size equal to 17,527 t_N with solar radiation. 284

C.16 Temperature Histogram of $((\theta_{dv_i})_{ta})$ with data centred on the Total Average Temperature $((T_a)_{ta})$ for E.F1.s.23 and E.F2.s.24 sensors of MMS for a sample size equal to 29,05 t_N without solar radiation. 285

C.17 Temperature Histogram of $(\theta_{dv_i})_{ta}$ with data centred on the Total Average Temperature $((T_a)_{ta})$ for E.R3.s.25, E.R3.s.26 and E.R3.n.27 sensors of MMS for a sample size equal to 50,958 t_N with and without solar radiation. 285

C.18 Temperature Histogram of $(\theta_{dv_i})_{ta}$ with data centred on the Total Average Temperature $((T_a)_{ta})$ for E.R3.s.25, E.R3.s.26 and E.R3.n.27 sensors of MMS for a sample size equal to 17,527 t_N with solar radiation. 285

C.19 Temperature Histogram of $(\theta_{dv_i})_{ta}$ with data centred on the Total Average Temperature $((T_a)_{ta})$ for E.R3.s.25, E.R3.s.26 and E.R3.n.27 sensors of MMS for a sample size equal to 29,05 t_N without solar radiation. 286

C.20 Temperature Histogram of T_{dv_i} from E.F1.n.20 and E.F1.n.21 sensors of the MMS for a sample size equal to 50,958 t_N with and without solar radiation. 286

C.21 Temperature Histogram of T_{dv_i} from E.F1.n.20 and E.F1.n.21 sensors of the MMS for a sample size equal to 17,527 t_N with solar radiation. 286

C.22 Temperature Histogram of T_{dv_i} from E.F1.n.20 and E.F1.n.21 sensors of MMS for a sample size equal to 29,05 t_N without solar radiation. 287

C.23 Temperature Histogram of T_{dv_i} from E.F1.s.23 and E.F2.s.24 sensors of the MMS for a sample size equal to 50,958 t_N with and without solar radiation. 287

C.24 Temperature Histogram of T_{dv_i} from E.F1.s.23 and E.F2.s.24 sensors of the MMS for a sample size equal to 17,527 t_N with solar radiation. 287

C.25 Temperature Histogram of T_{dv_i} from E.F1.s.23 and E.F2.s.24 sensors of the MMS for a sample size equal to 29,05 t_N without solar radiation. 288

C.26 Temperature Histogram of T_{dv_i} from E.R3.s.25, E.R3.s.26 and E.R3.n.27 sensors of the MMS for a sample size equal to 50,958 t_N with and without solar radiation. 288

C.27 Temperature Histogram of T_{dv_i} from E.R3.s.25, E.R3.s.26 and E.R3.n.27 sensors of the MMS for a sample size equal to 17,527 t_N with solar radiation. 288

C.28 Temperature Histogram of T_{dv_i} from E.R3.s.25, E.R3.s.26 and E.R3.n.27 sensors of MMS for a sample size equal to 29,05 t_N without solar radiation. 289

C.29 Temperature Histogram of $(\theta_{dv_i})_{la}$ with data centred on the Local Average Temperature $((T_a)_{la})$ for E.F1.n.20 and E.F1.n.21 sensors of MMS for a sample size equal to 50,958 t_N with and without solar radiation. 289

C.30 Temperature Histogram of $(\theta_{dv_i})_{la}$ with data centred on Local Average Temperature $((T_a)_{la})$ for E.F1.n.20 and E.F1.n.21 sensors of MMS for a sample size equal to 17,527 t_N with solar radiation. 289

C.31 Temperature Histogram of $(\theta_{dv_i})_{la}$ with data centred on Local Average Temperature $((T_a)_{la})$ for E.F1.n.20 and E.F1.n.21 sensors of the MMS for a sample size equal to 29,05 t_N without solar radiation. 290

C.32 Temperature Histogram of $(\theta_{dv_i})_{la}$ with data centred on Local Average Temperature $((T_a)_{la})$ for E.F1.s.23 and E.F2.s.24 sensors of the MMS for a sample size equal to 50,958 t_N with and without solar radiation. 290

C.33 Temperature Histogram of $(\theta_{dv_i})_{la}$ with data centred on Local Average Temperature $((T_a)_{la})$ for E.F1.s.23 and E.F2.s.24 sensors of MMS for a sample size equal to 17,527 t_N with solar radiation. 290

C.34 Temperature Histogram of $(\theta_{dv_i})_{la}$ with data centred on Local Average Temperature $((T_a)_{la})$ for E.F1.s.23 and E.F2.s.24 sensors of the MMS for a sample size equal to 29,05 t_N without and without solar radiation. 291

C.35 Temperature Histogram of $(\theta_{dv_i})_{la}$ with data centred on Local Average Temperature $((T_a)_{la})$ for E.R3.s.25, E.R3.s.26 and E.R3.n.27 sensors of MMS for a sample size equal to 50,958 t_N with and without solar radiation. 291

C.36 Temperature Histogram of $(\theta_{dv_i})_{la}$ with data centred on Local Average Temperature $((T_a)_{la})$ for E.R3.s.25, E.R3.s.26 and E.R3.n.27 sensors of the MMS for a sample size equal to 17,527 t_N with solar radiation. 291

C.37 Temperature Histogram of $(\theta_{dv_i})_{la}$ with data centred on Local Average Temperature $((T_a)_{la})$ for E.R3.s.25, E.R3.s.26 and E.R3.n.27 sensors of the MMS for a sample size equal to 29,05 t_N without solar radiation. 292

C.38 Temperature Histogram of T_{dv_i} from E.R3.s.25 and E.R3.s.26 sensors of MMS for a sample size equal to 233 t_N with measurement frequency equal to five minutes and without solar radiation. 292

C.39 Temperature Histogram of $(\theta_{dv_i})_{la}$ with data centred on Local Average Temperature $(T_a)_{la}$ for E.R3.s.25 and E.R3.s.26 sensors of MMS for a sample size equal to 233 t_N with measurement frequency equal to five minutes and without solar radiation. 292

D.8 Sensors and Hardware installed in residential building at Vitoria-Gasteiz. 298

D.9 Layout of 3D monitoring in Z2 and Z4 of F1. 299

D.10 Installed indoor sensors of Fixed MCS pictures in F0. 300

D.11 Installed indoor sensors of Fixed MCS pictures in F1. 301

D.12 Installed indoor sensors of Fixed MCS pictures in F2. 302

D.13 Installed outdoor sensors of Fixed MCS pictures in roof. 302

D.14 Hardware and electricity meters of Mobile MCS (Co-Heating Co-Heating). 303

D.15 Hardware and electricity meters of Mobile MCS (mobile Co-Heating). 303

D.1 Sensor Layout of Fixed MCS in F0. 304

D.2 Sensor Layout of Fixed MCS in F1. 305

D.3 Sensor Layout of Fixed MCS in first level of F2. 306

D.4 Sensor Layout of Fixed MCS in second level of F2. 307

D.5 Sensor Layout of Mobile MCS in F0 for Co-Heating test. 308

D.6 Sensor Layout of Mobile MCS in F1 for Co-Heating test. 309

D.7 Sensor Layout of Mobile MCS in F2 for Co-Heating test. 310

List of Tables

- 2.1 Physical variables measured in the Average Method. 67
- 2.2 Physical variables measured in the Co-Heating test. 71
- 2.3 Monitoring system of a public building of the University of the Basque Country. 76
- 2.4 Control system (CS) of a public building of the University of the Basque Country. 77
- 2.5 Differences between the Wired and Wireless communication protocols [78]. 80
- 2.6 The main sensors and meters used for control in building automation based on previous research [24, 82]. 84
- 2.7 Examples of impacts produced by sensor errors in some study cases. 85
- 2.8 List of publications used in the MCS to characterize the TEP of in-situ buildings through HLC estimation and other estimates used to determinate energy behaviour of the buildings. 90
- 2.9 MCSs in the reviewed literature from 1979–2018, specified by the authors to characterize the TEP of buildings. 91
- 2.10 Description of the level quantification used to analyse the MCSs presented in the reviewed literature. 92
- 2.11 Criteria to evaluate the specification level of MCS. 93
- 2.12 Qualitative analysis of the specification level’s degree of the analysed criteria for the devices, hardware, and software of MCSs used in buildings or prototypes in each publication studied. Criteria based on Table 2.11. 96
- 2.13 Quantitative analysis of specification level’s degree of the analysed criteria of MCSs used in buildings or prototypes in all reviewed literature. 97
- 2.14 Quantitative analysis of specification level’s degree of the analysed criteria of MCSs used in buildings or prototypes in all reviewed literature with Co-Heating Method (HLC estimation). 97
- 2.15 Quantitative analysis of specification level’s degree of the analysed criteria of MCSs used in buildings or prototypes in all reviewed literature with Regression Method (HLC estimation). 97
- 2.16 Quantitative analysis of specification level’s degree of the analysed criteria of MCSs used in buildings or prototypes in all reviewed literature with Average Method (HLC estimation). 98

2.17 Quantitative analysis of specification level’s degree of the analysed criteria of MCSs used in buildings or prototypes in all reviewed literature with Corrected Average Method (HLC estimation). 98

2.18 Quantitative analysis of specification level’s degree of the analysed criteria of MCSs used in buildings or prototypes in all reviewed literature implementing other methods. 98

2.19 Quantitative analysis of the references studied by methodology: Global analysis of the method used, the fault detection and sensor type used for measuring physical variables in the MCSs in each methodology. 99

2.20 Quantitative analysis of references studied by methodology: Global analysis of the method, actuators, controls systems, and devices used in each methodology. 100

3.1 Matrix of measured raw data for a sample composed of several t_j 115

3.2 Matrix of zero centred data with respect to $(M_{vw})_{MZ}$ with a Normal Distribution $N(\mu, \sigma)$ for each t_j 115

3.3 Matrix of data centred on M_a with a Normal Distribution $N(\mu, \sigma)$ for each t_j , also being applicable to data centred on $(M_a)_{MZ}$ (Equation3.9) or $(M_a)_{MS}$ (Equation3.10) 116

3.4 Matrix of statistical parameters of the Normal Distributions $N(\mu, \sigma)$ for each t_j 116

3.5 Matrix of global statistical parameters of the Normal Distributions $N(\bar{\mu}, \bar{\sigma})$ for the t_N sample. 116

3.6 Expanded uncertainties of measurements. 116

4.1 Areas, heights and volumes of OT and WS based on the architectural drawings shown in Figure A.6, Figure A.7, Figure A.8 and Figure A.9. 141

4.3 Investment of MMS and its integration in the BAS of UPV/EHU building [139]. 145

4.2 Technical characteristics of sensors, gateway and protocol communications of interior MMS. 147

4.4 OWS typologies based on the OWSR. 152

4.5 CWS Typologies based on DF. 153

4.6 Results of the office characterization based on the studied thermal zones. 153

4.7 Names of particularized variables for the uncertainty study of the T_{in} measurement. . 155

4.8 Statistical results of Temperature Sensor Uncertainty ($U_{T(S)}$) analysis for the Mobile Monitoring System (MMS). 157

4.9 Sample statistical results and Temperature Uncertainty (U_T) estimation of OT $(\theta_{dv_i})_{vw}$ values (Equation 3.7), with temperature measurement (T_{dv_i}) centred on $(T_{vw})_{OT}$ (Equation 3.6). 159

4.10 Sample statistical results and Temperature Uncertainty (U_T) estimation of OT $(\theta_{dv_i})_{wsm}$ values (Equation 3.10), with temperature measurement (T_{dv_i}) centred on $(T_a)_{WS}$ (Equation 3.6). 160

4.11 Decoupling of global standard deviation values of temperature measurement for four OT volumes. 162

4.12 Decoupling of global standard deviation values of temperature measurement for each WS.	162
4.13 Example of the range in which, the representative value of the Average Temperature of a WS for the whole monitored period $((\bar{T}_a)_{WS})$ can be with a confidence interval of 95%.	163
4.14 Example of the range in which the representative value of the Volume Weight Average Temperature of a OT for the whole monitored period $((\bar{T}_{vw})_{OT})$ can be with a confidence interval of 95%.	163
4.15 Statistical results of vertical uncertainty analysis by sensor in OT3.	166
4.16 Statistical results of vertical uncertainty analysis by group of two sensors in OT3.	167
4.17 Statistical results of vertical uncertainty analysis by group of three sensors in OT3.	168
4.18 Relation of On-Off Sample Groups (OSGs) to analyse U_{VT} estimation based on radiation, heating cycle and electricity consumption effects.	169
4.19 Statistical parameters by one sensor of the OSGs to study the solar radiation effect on the vertical uncertainty.	171
4.20 Statistical parameters by one sensor of the OSGs to study the heating system effect on the vertical uncertainty.	171
4.21 Statistical parameters by one sensor of the OSGsto study the electricity consumption effect on the vertical uncertainty.	172
4.22 Statistical parameters by two sensors of the OSGs to study the solar radiation effect on the vertical uncertainty.	173
4.23 Statistical parameters by two sensors of the OSGs to study the heating system effect on the vertical uncertainty.	174
4.24 Statistical parameters by two sensors of the OSGs to study the electricity consumption effect on the vertical uncertainty.	174
4.25 Statistics results by sensor analysing values of $(\theta_{dv_i})_{vw}$ for high-level sensors in OT4 in order to determine the best spatial location.	175
4.26 Statistics results by two-sensor group analysing values of $(\theta_{dv_i})_{vw}$ for high-level sensors in OT4 in order to determine the best spatial location.	176
4.27 Statistics results by three-sensor group analysing values of $(\theta_{dv_i})_{vw}$ for high-level sensors in OT4.	177
4.28 Statistics results by four-sensor group analysing values of $(\theta_{dv_i})_{vw}$ for high-level sensors in OT4 in order to determine the best spatial location.	178
4.29 Statistics results by five-sensor group analysing values of $(\theta_{dv_i})_{vw}$ for high-level sensors in OT4 in order to determine the best spatial location.	179
4.30 Statistics results for six-sensor group analysing values of $(\theta_{dv_i})_{vw}$ for high-level sensors in OT4 in order to determine the best spatial location.	179
4.31 Names of particularized variables for the uncertainty study of the T_{out} measurement.	184

4.32 Temperature Uncertainty (U_T) estimation of $(\theta_{dv_i})_{la}$ with data centred on the Local Average Temperature $((T_a)_{la})$ of the E.R3.s.25 and E.R3.s.26 sensors for each t_j with and without solar radiation, with solar radiation and without solar radiation cases. . . . 186

4.33 Temperature Uncertainty (U_T) estimation of $((\theta_{dv_i})_{ta})$ for each BEA with data centred on the Total Average Temperature $((T_a)_{ta})$ for each t_j with and without solar radiation. Including data with and without solar radiation measurement data. 188

4.34 Temperature Uncertainty (U_T) estimation of $((\theta_{dv_i})_{ta})$ for each BEA with data centred on the Total Average Temperature $((T_a)_{ta})$ for each t_j with solar radiation. 189

4.35 Temperature Uncertainty (U_T) estimation of $((\theta_{dv_i})_{ta})$ for each BEA with data centred on the Total Average Temperature $((T_a)_{ta})$ for each t_j without solar radiation. 190

4.36 Temperature Uncertainty (U_T) estimation of $((\theta_{dv_i})_{ta})$ for the eight installed sensors with data centred on the Total Average Temperature $((T_a)_{ta})$ for each t_j with and without solar radiation. 190

4.37 Example of the Total Average Temperature Band $([(\bar{T}_a)_{ta}]_{band})$ analysis, in which the average temperature of air surrounding the tertiary building or BAV for the whole monitored period $(\bar{T}_a)_{ta}$ can lie, if only one Building Envelope Area (BEA) is monitored. 193

4.38 Temperature Uncertainty (U_T) estimation of $(\theta_{dv_i})_{la}$ for each BEA with data centred on the Local Average Temperature $((T_a)_{la})$ for each t_j with and without solar radiation. 195

4.39 Temperature Uncertainty (U_T) estimation of $(\theta_{dv_i})_{la}$ for each BEA with data centred on the Local Average Temperature $((T_a)_{la})$ for each t_j with solar radiation. 195

4.40 Temperature Uncertainty (U_T) estimation of $(\theta_{dv_i})_{la}$ for each BEA with data centred on the Local Average Temperature $((T_a)_{la})$ for each t_j without solar radiation. 196

4.41 Statistical results from manufacturer’s accuracy of the EE071-HTPC sensor. 197

4.42 Statistical results from experimental accuracy of the EE071-HTPC sensor. 198

4.43 Decoupling of T_{out} measurement with data centred on the Total Average Temperature $((T_a)_{ta})$ for the eight installed sensors around the building for the RAD ON-OFF, RAD ON and RAD OFF cases. 199

4.44 Example of estimation the Average Temperature Range $([(\bar{T}_a)_{ta}]_{range})$, within which the representative temperature of the air surrounding the building or BAV for the whole monitored period $(\bar{T}_a)_{ta}$, can lie with a 95% confidence for the studied tertiary building. 200

4.45 Decoupling of the T_{out} measurement from the BEA with data centred on the Local Average Temperature $((T_a)_{la})$ for each t_j with and without solar radiation. 201

4.46 Decoupling of the T_{out} measurement from the BEA with data centred on the Local Average Temperature $((T_a)_{la})$ for each t_j with solar radiation. 201

4.47 Decoupling of the T_{out} measurement from the BEA with data centred on the Local Average Temperature $((T_a)_{la})$ for each t_j without solar radiation. 202

4.48 Example of the estimation of the limits of the range within which the average temperature of the air surrounding the Building Envelope Area (BEA) $(\bar{T}_a)_{la}$ can lie for the whole monitored period. $([\bar{T}_a)_{la}]_{range}$ (Equation 3.44) 203

4.49 Number of sensors installed in the Fixed MCS and Mobile MCS of the residential building. 212

4.50 Number of sensors installed in the Fixed MCS of the residential building. 212

4.51 Number of hardware and software elements used in the Fixed MCS and Mobile MCS of the residential building. 212

4.52 Number of hardware and software elements used in the Fixed MCS of the residential building. 213

4.53 Accuracy and references of digital sensors installed in Fixed MCS and Mobile MCS of the residential building. 214

4.54 Accuracy and references of analogue sensors installed in Fixed MCS and Mobile MCS of the residential building. 215

4.55 Monitoring kit's investment of Vitoria-Gasteiz' MCS. 216

4.56 Control kit's investment of Vitoria-Gasteiz' MCS. 216

4.57 Equipment investment of Vitoria-Gasteiz' MCS. 217

4.58 Installing investment of Vitoria-Gasteiz' MCS. 217

4.59 Setup investment of Vitoria-Gasteiz' MCS. 217

4.60 Total investment of Vitoria-Gasteiz' MCS. 217

A.2 Sensor references installed on the eight tripods and level location. 248

A.3 Sensor layout by OT in each OT volume [139]. 249

A.4 Exterior (E) Layout of EE071-HTPC sensors installed around the building envelope [139]. 256

A.1 BAS sensors installed at the UPV/EHU administrative building in Leioa: Reference, measurements, accuracies and protocol communication. 263

A.5 Interior MMS codes: file name codes, file column code and sensor reference [139]. . . . 268

A.6 Exterior MMS codes: file name codes, file column code and sensor reference [139]. . . . 269

A.7 Existing BAS codes: file name codes, file column code and sensor reference [139]. . . . 270

D.1 Spatial Location in F0 of Fixed MMS' Sensor based on Figure D.1. 294

D.2 Spatial Location in F1 of Fixed MMS' Sensor based on Figure D.2. 295

D.3 Spatial Location in F2 of Fixed MMS' Sensor based on Figures D.3 and D.4. 296

D.4 Spatial Location of Mobile MMS' Sensor of Co-Heating test based on Figure D.5, Figure D.6 and Figure D.7. 297

Acronyms

°C Degree Celsius.

A2PBEER Affordable and Adaptable Public Buildings through Energy Efficient Retrofitting.

ACH_{avg} Air Change per hour [h^{-1}].

AFDD Automated Fault Detection and Diagnosis.

AHU Air Handling Unit.

ANSI American National Standards Institute.

ARMAX Autoregressive Moving Average Model.

ARX Autoregressive Model.

ASHRAE American Society of Heating, Refrigeration and Air Conditioning Engineers.

ASTM American Society for Testing and Materials.

B0 Basement of building.

BACnet Building Automation and Control Networks.

BACS Building Automation and Control System.

BAV Building Air's Volume or Air Surrounding Building.

BEA Building Envelope Area.

BIM Building Information Modelling.

BMS Building Management System.

c_i Specific Heat of Incompressible Material [$\text{kJ}/\text{kg}^\circ\text{C}$].

c_{p,air} Specific Heat at Constant Pressure of the Air [$\text{kJ}/\text{kg}^\circ\text{C}$ or kJ/kgK].

C_T Thermal Capacitancy.

C_v Ventilation and/or Infiltration Heat Loss Coefficient [kW/°C or kW/K].

c_{water} Specific Heat of Water [kJ/kg°C or kJ/kgK].

χ Measurements of HLC Variables.

cm Centimetre.

CO Cardinal Orientation.

CO₂ Carbon Dioxide.

CPU Central Processing Unit.

CS Control System.

CSIC Superior Council of Scientific Investigations.

cv Control Volume.

DF_{OT} Division Factor of a OT [%].

DHW Domestic Hot Water.

dv_i Differential Volume.

E Exterior.

E_{cv} Control Volume's Accumulated Energy [kJ].

E_k Kinetic Energy [kJ].

E_m Energy Exchanged by the System due to Mass Flows [kW].

E_p Potential Energy.

EBC Energy Buildings and Communities.

EED Energy Efficiency Directive.

ENERPAT Co-creation of Energetically efficient territorial solutions of Patrimonial Residential habitat Ecorenovation in SUDOE historical centres.

EPB Energy Performance of Buildings.

EPBD Energy Performance of Buildings Directive.

ε Number of Materials Within a Control Volume or Building.

et East.

ET Exterior Together.

η Heat Recovery Efficiency.

EU European Union.

F Façades.

F0 Ground Floor.

F1 Floor One.

F2 Floor Two.

F3 Floor Three.

F_i Floor of a Building.

F_{i,j} Sub-Spaces of a Building's Floor.

FDD Fault Detection and Diagnosis.

FP7 7th Framework Program for Research.

FR Facility Room.

g Number of Differential Volume in an MZ Volume / Acceleration of Gravity [m/s^2].

g – Value Solar Factor Coefficient.

GUM Guide to the Expression of Uncertainty in Measurement.

H Height Level.

h_{air_{exh}} Specific Enthalpy of Air's Exhaust [kJ/kg].

h_{air_{sup}} Specific Enthalpy of Air's Supply [kJ/kg].

h_{exh} Specific Enthalpy of Fluid's Exhaust [kJ/kg].

H_{sol} Horizontal Global Solar Radiation [W/m^2].

h_{sup} Specific Enthalpy of Fluid's Supply [kJ/kg].

h_{water_{exh}} Specific Enthalpy of Water's Exhaust [kJ/kg].

h_{water_{sup}} Specific Enthalpy of Water's Supply [kJ/kg].

hg High.

HLC Heat Loss Coefficient [$\text{W/}^\circ\text{C}$].

HLC_{range} Maximum and Minimum Limits within which is the Representative Value of the Heat Loss Coefficient of an in-use Building can be [W/°C].

HS Hardware and Systems Software.

HSW Hot Sanitary Water.

HTC Heat Transfer Coefficient.

HVAC Heating, Ventilation and Air Conditioning.

ID Identification.

IEA International Energy Agency.

IEC International Electrotechnical Commission.

IEEE Institute of Electrical and Electronic Engineers.

IoT Internet of Things.

ISO International Organization for Standardization.

K Kelvin Degrees.

K_e Heat Gains due to Electrical Consumption of Control Volume Devices, Excluding the Heating System) [kW].

K_o Heat Gains due to Occupants' Metabolic Generation [kW].

K_T Interior Heat Gains (Sum of Occupants and Electricity gains), Excluding the Heating Gains [kW].

κ Index Observation for a Period Consisting.

kg Kilogram.

kg/s Kilogram per Second.

kJ/kg Kilojoule per Kilogramme.

KPI Key Performance Indicator.

kW Kilowatt.

kW/m² Kilowatt per Square Meter.

kWh Kilowatt Hour.

l Litre.

l/s Litre per Second.

lw Low.

m Meter.

$(\overline{\mathbf{M}}_{vw})$ Volume Weight of the Measurement for a Whole Monitored Period.

$(\overline{\mathbf{M}}_a)$ Average Measurement for a Whole Monitored Period.

$(\overline{\mathbf{M}}_a)_{MZ}$ Average Measurement of an MZ for a whole Monitored Period.

m/s Meter per Second.

m/s² Meter per Square Second.

m² Same Equivalence as m².

m³ Cubic Meter.

m³/s Cubic Meter per Second.

M_a Average Measurement of a Volume for each t_j .

$(\mathbf{M}_a)_{MS}$ Average Measurement of an MS volume for each t_j .

$(\mathbf{M}_a)_{MZ}$ Average Measurement of an MZ Volume for each t_j .

$[\mathbf{M}_a]_{range}$ Maximum and Minimum limits in which M_a fluctuates.

m_{air} Air Mass Flow Rate [kg/s].

M_{dvi} Sensor Measurement for each t_j .

m_{exh} Exhaust Air Mass Flow Rate [kg/s].

m_i Mass of Materials within a Control Volume or Building [Kg].

m_{sup} Supply Air Mass Flow Rate [kg/s].

$(\mathbf{M}_{vw})_{MZ}$ Volume-Weighted Measurement of an MZ for each t_j .

$[\mathbf{M}_{vw}]_{range}$ Maximum and Minimum limits in which M_{vw} fluctuates.

m_{water} Water Mass Flow Rate [kg].

$[(\overline{\mathbf{M}}_a)_{MZ}]_{band}$ Total Average Measurement Bandwidth in which the Estimated Average Measurement of an MZ can be.

MCS Monitoring and Control System.

md Medium.

MMS Mobile Monitoring System.

MS Monitored Space.

$\bar{\mu}$ Mean of t_N samples.

μ_{t_N} Mean of Measurement Differentials θ_{dvi} for each t_j .

MWh Megawatt per hour.

MZ Monitored Zone.

n Number of MS volumes contained in an MZ.

N Number of Instants of Time in a Period.

N_{cws} Number of Compact Workspaces in Office Typology (OT).

N_{ows} Number of Open Workspaces in Office Typology (OT).

Nm³ Cubic Meter in Normal Conditions.

nt North.

nZEB nearly Zero Energy Building.

OSG On-Off Sample Group.

OSGI Open Services Gateway Initiative.

OT Office Typology.

OT1 Office Typology 1.

OT2 Office Typology 2.

OT3 Office Typology 3.

OT4 Office Typology 4.

O_{WSR}_{OT} Open Workspace Ratio of Office Typology (OT) [%].

p Number of M_{dvi} in an MZ for each t_j .

Pa Pascal.

PC Protocol Communication.

ph Power of Heating System [W].

Ph OFF or ph.off Heating Power Off [W].

Ph ON or ph.on Heating Power On [W].

PLC Programmable Logic Controller.

ppm Parts Per Million.

pw Electricity Power.

PW Active Power [kW].

Pw OFF or pw.off Active Power Off [kW].

Pw ON or pw.on Active Power On [kW].

q Number of M_{dvi} in an MS for each t_j .

Q_{cv} Heat Exchanged Rate through the Control Volume.

Q_{inf} Infiltration Heat Loss of Control Volume [kW].

Q_{trans} Heat Transmission Effects that depend on the UA-Value [kW].

Q_{vent} Ventilation Heat Loss Rate of Control Volume [kW].

Q_h or Q All Heating System's Inputs Inside the Control Volume [kW].

R Roof.

R_(S) Ratio of Mean Variance of t_N samples due to $U_{M(S)}$ with respect to Mean Variance of a t_N Samples due to U_M [%].

R_(SP) Ratio of Mean Variance of t_N samples due to $U_{M(SP)}$ with respect to Mean Variance of a t_N Samples due to U_M [%].

rad Solar Radiation [W/m^2].

RAD OFF or rad.off Without Solar Radiation [W/m^2].

RAD ON or rad.on With Solar Radiation [W/m^2].

RAD ON-OFF Without Solar Radiation [W/m^2].

RD&D Research, Development and Design.

RH Relative Humidity [%].

ρ_{air} Air Density [Kg/m^3].

rms Root Mean Square.

R-Value Thermal Resistance [m^2K/W].

s Second.

S_a Solar Aperture [m²].

SAP Standard Assessment Procedure.

SCADA Supervisory Control And Data Acquisition.

SI International System of Units.

$\bar{\sigma}^2$ Mean Variance of t_N samples.

$\bar{\sigma}_{\mathbf{t}_N(\text{SP})}^2$ Variance of Z Measurement Differential (θ_{dv_i}) of a t_N sample due to $U_{M(\text{SP})}$.

$\bar{\sigma}_{\mathbf{VM}}^2$ Mean Variance of t_N samples associated to U_{VM} .

$\bar{\sigma}_{\mathbf{t}_N(\text{S})}^2$ Variance of Z Measurement Differential (θ_{dv_i}) of a t_N sample due to $U_{M(\text{S})}$.

$\bar{\sigma}_{\mathbf{M}}^2$ Mean Variance of t_N samples associated to U_M .

$\bar{\sigma}_{\mathbf{M}}$ Mean Standard Deviation of t_N samples associated to U_M .

$\bar{\sigma}_{(\text{S})}^2$ Mean Variance of t_N samples associated to $U_{M(\text{S})}$.

$\bar{\sigma}_{(\text{SP})}^2$ Mean Variance of t_N samples associated to $U_{M(\text{SP})}$.

$\bar{\sigma}_{\mathbf{t}_N}^2$ Variance of Z Measurement Differential (θ_{dv_i}) of a t_N sample.

$\sigma_{\mathbf{t}_N}^2$ Variance of Measurement Differentials θ_{dv_i} for each t_j .

$\bar{\sigma}_{(\text{S})}$ Mean Standard Deviation of t_N samples associated to $U_{M(\text{S})}$.

$\bar{\sigma}_{(\text{SP})}$ Mean Standard Deviation of t_N samples associated to $U_{M(\text{SP})}$.

$\sigma_{\mathbf{t}_N}$ Experimental Standard Deviation of Measurement Differentials θ_{dv_i} for each t_j .

$\bar{\sigma}_{\mathbf{VM}}$ Mean Standard Deviation of t_N samples associated to U_{VM} .

Q_{recovery} Heat Exchanged inside the Heat Exchanger [kW].

st South.

SUDOE Southwest European Space Territorial Cooperation Programme.

T Temperature [K or °C].

T_{air_{exh}} Exhaust Air Temperature [K or °C].

T_{air_{sup}} Supply Air Temperature [K or °C].

T_i Temperature of Material Within in a Control Volume or Building [K or °C].

T_{in} Indoor Air Temperature [K or °C].

t_N Instants of Time Sample of a Period.

T_{out} Outdoor Air Temperature [K or °C].

T_{sup} Surface Temperature [K or °C].

T_{water_{exh}} Exhaust Water Temperature [K or °C].

T_{water_{sup}} Supply Water Temperature [K or °C].

TCP/IP Transmission Control Protocol / Internet Protocol.

$(\theta_{dvi})_a$ Measurement Differential of M_{dvi} centred on an Average Measurement for each t_j .

$(\theta_{dvi})_{MS}$ Measurement Differential of M_{dvi} centred on an Average Measurement of an MS for each t_j .

$(\theta_{dvi})_{MZ}$ Measurement Differential of M_{dvi} centred on an Average Measurement of an MZ for each t_j .

$(\theta_{dvi})_{vw}$ Measurement Differential with respect to the Volume-Weighted Temperature of an MZ for each t_j .

T Tripod.

TT Tripod Together.

U Internal Energy [kJ].

\bar{U} Expanded uncertainty of Measurements.

U_{HLC} Maximum and Minimum Limits within which is the Representative Value of the Heat Loss Coefficient of an in-use Building can be [W/°C].

U_M Measurement Uncertainty.

U_{M(S)} Measurement Sensor Uncertainty.

U_{M(SP)} Measurement's Spatial Uncertainty.

U_{VM} Vertical Measurement Uncertainty.

UA Heat Transfer Coefficient or Transmission Heat Loss Coefficient [kW/°C or KW/K].

UPnP Universal Plug and Play.

UPV/EHU University of the Basque Country.

U-Value Thermal Transmittance [W/(m²K)].

$\dot{V}_{air(inf)}$ Infiltration Volumetric Air Flow Rate [m³/s].

- $\dot{V}_{\text{air(vent)}}$ Ventilation Volumetric Air Flow Rate [m^3/s].
- v_{exh} Exhaust Fluid Velocity [m/s].
- V_{Fi} Volume of a Building's Floor [m^3].
- $V_{\text{i,j}}$ Sub-Volumes of a Building's Floor [m^3].
- V_{MS} MS Volume [m^3].
- V_{MZ} MZ Volume [m^3].
- V_{OT} Volume of Office Typology (OT) [m^3].
- V_{OWS} Open Workspace Volume within an Office Typology (OT) [m^3].
- V_{sol} Vertical Global Solar Radiation [W/m^2].
- v_{sup} Supply Fluid Velocity [m/s].
- VAV** Variable Air Volume.
- V_{Fi} Volume of a Building's Floor (F) [m^3].
- w** Week of Year.
- W** Watt.
- W-m2 or W/m2** Same Equivalence as W/m^2 .
- W_{cv} Work Exchanged through the Control Volume.
- Wh** Watt per hour.
- W/m^2 Watt per Square Meter.
- WPAN** Wireless Personal Area Networks.
- WS** workspaces.
- wt** North.
- XY** A Unit of Sensor Measurement of International System Unit.
- y** Number of Differential Volume in an MS Volume.
- z_{sup} Supply Fluid Elevation [m].
- z_{exh} Exhaust Fluid Elevation [m].

Chapter 1

INTRODUCTION

We all live in buildings, and most of us work inside buildings where we spend most of our lives, but we care little about the most important part of the buildings regarding our comfort and the building's in-use energy performance. This is the building envelope. Everything related to the building's indoor comfort conditions and its real energy consumption starts in the building envelope. If a high performance building envelope is designed according to the local environmental conditions (correctly considering building use, weather and orientation of the building), and the building is constructed as designed, only then, is it possible to have a highly efficient building. For in-use building systems (e.g., boilers, heat pumps etc.), seasonal Key Performance Indicators (KPI) are currently well defined for different building system typologies and are usually obtained as the measured heat or cold provided by the system divided by the measured gas or electricity consumed. Then a control over the evolution of the system's performance can be done during the buildings life. Making a performance evolution control similar to the KPIs related to the in-use building envelope energy performance is a crucial issue. It can be achieved through the continuous evaluation of the in-use Heat Loss Coefficient (HLC), transmission heat loss coefficient (UA) and Infiltration and/or ventilation heat loss coefficient (C_v) during the buildings life. Obtaining a highly efficient envelope in a building will allow, for two main reasons, energy consumption, building systems and user behaviour to be properly handled.

On the one hand, the building's systems (boilers, heat pumps, air conditioning systems, solar panels for heating etc.) will require a considerably smaller size (or design power) due to low power requirements compared to those corresponding to poorly behaving building envelopes. Thus, systems and their maintenance will be cheaper and their energy consumption will be lower. Furthermore, the inclusion of renewable energies can become economically and technically feasible even when they have to cover 100% of the annual energy demand of the building (Nearly Zero Energy Buildings [1]). Even more important are the optimal operating conditions required by the heating and cooling system's heat transfer fluids to supply the temperatures required by buildings with high performing envelopes. In winter, the heating system working fluid supply temperature can be low (30 - 40 °C) and could be used in such heating distribution systems as underfloor heating. This type of systems not only

provide better comfort conditions to users, but also permit the use of high performing devices such as heat pumps or hybrid systems with solar collectors to be optimised. Even natural gas boilers will work under their most efficient mode, as condensing boilers, if this type of underground distribution systems is possible thanks to the high performing building envelope. Note that usual radiators require hot water at 60 °C to 70 °C and do not permit the uses of boilers and heat pumps in their most efficient modes. Regarding cooling systems, their heat transfer fluids supply temperatures (15-20 °C) that may be closer to the indoor comfort temperature (23-25 °C) [2]. This will again permit the use of the underfloor systems in the refreshing mode without producing condensation problems and the cooling systems chillers will work with higher efficiencies as compared to current ones where colder heat transfer fluid production is required (5-10°C). It is even possible to use the ventilation system alone to provide heating and cooling requirements if the building envelope performance is similar to the demanding 'Passivhaus' [3] requirements. There, heating and cooling distribution systems are avoided and comfort conditions can only be achieved with the mandatory ventilation system.

Together with the building system's real energy performance and the building envelope's actual energy performance, the user behaviour is the third main reason for energy consumption in buildings. If any of these three real-life performances is not as expected during the design phase, the actual energy consumption of the building will be different from the predicted one. Note though, that, in building with a high performing envelope and high performing systems, it is much easier to maintain comfort conditions within the building, and the effect of the building user in the energy consumption discrepancy, will usually be smaller in comparison to the same user in a low performing building. The automatic control of comfort conditions in highly efficient buildings is simpler and the indoor comfort air temperature is lower in winter and higher in summer. For example, in a poorly insulated building, in winter, the inner surface of the building envelope walls might be as cold as 15 °C so the user will try to increase the indoor air temperature to 24-25 °C to try to obtain comfort conditions to compensate for the radiant energy losses against cold walls. However, the heating process of the indoor air will reduce the indoor air relative humidity and generate uncomfortable hygrothermal conditions. Furthermore, the energy consumption will be higher compared to the same building, under the same outdoor conditions, but with a high performing envelope where the indoor surface envelope temperatures will be close, for example, at 20 °C an air temperature of 21-23 °C will be sufficient to obtain indoor thermal comfort conditions [2]. The relative humidity will decrease less due to the lower heating of the indoor air and the dryness feeling may not appear. There, the heating energy demand is much lower due to the two factors, since the walls are better insulated less heat is being lost and, since the required indoor comfort air temperature is lower with the high performing envelope, the indoor to outdoor temperature difference is smaller, which will also reduce the heating energy demand. In summer, similar effects occur, but with the cooling system, where high performance building envelopes will provide better comfort and lower energy consumptions.

Thus, although there are three main reasons for real buildings to consume up to 2.5 times more than designed [4, 5], namely building envelope [6-8], systems [9-11] and users [12-14], the building envelope's real energy performance is the key to drastically reducing the energy consumption of

buildings. Excluding by experts in the building physics field, the building envelope is taken as just a simple static component of the building that should not require complex methods to test if it is working as expected or if it has been built as designed. Making a parallelism with the transport sector, we could say that the building envelope's in-use energy characterization is 30 years beyond the car's in-use energy behaviour characterization. It is common to hear in non-technical conversations about the in-use fuel consumption (usually in litres/100 km) of car owners and most car owners, even remember the design fuel consumption of their cars. Thus, a real awareness has been generated among the population related to the transport in-use energy efficiencies. Much thought should be given to how it is possible for the transport sector, representing 33% of the 2016 energy consumption in Europe, has produced general awareness about the real energy efficiencies of our cars, while the building sector, representing 40% of the energy consumption in 2016, has not generated this awareness among the population [15].

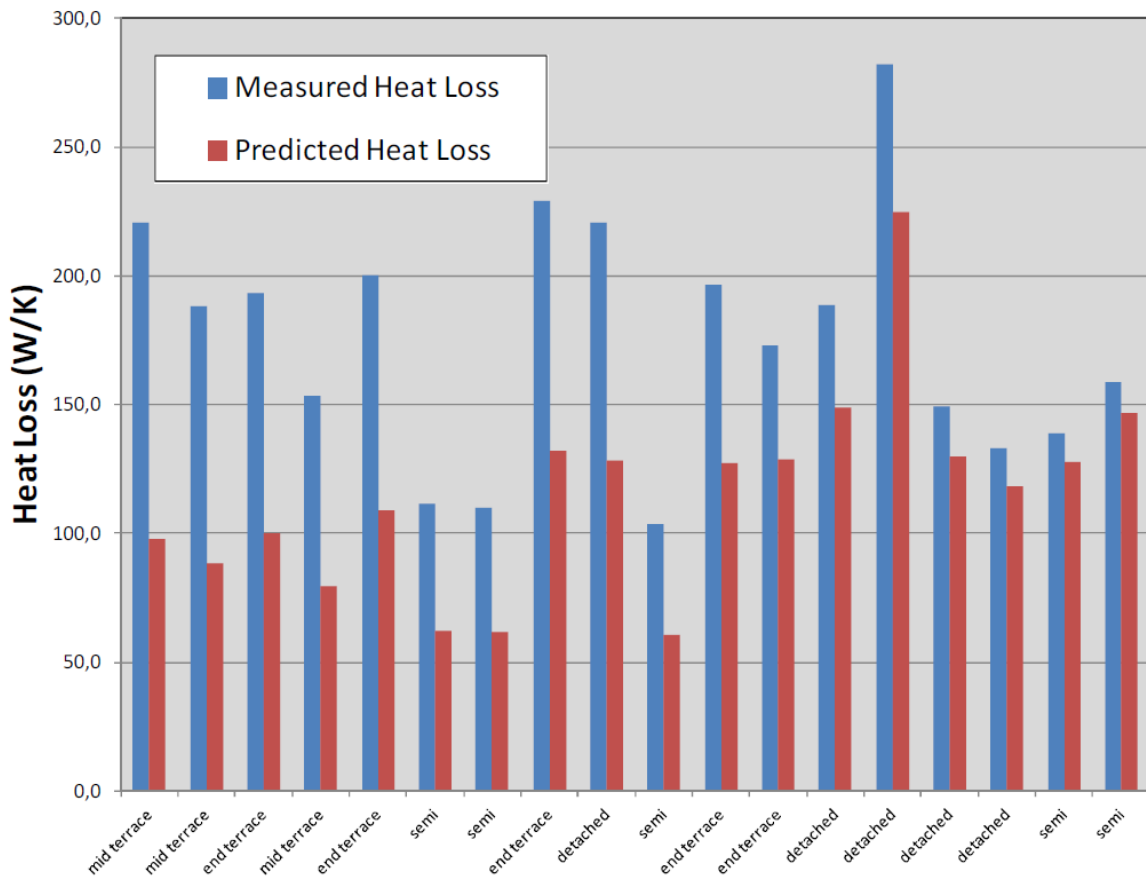


Figure 1.1: Measured (through the co-heating test) versus predicted whole house's Heat Loss Coefficient (HLC) (W/K) for 18 new build dwellings in the UK [16].

Europeans are now starting to become aware of the importance of a building's energy performance thanks to the building energy certification schemes implemented in the last few years. However, these certificates are not based on the real monitored data results of the building's actual energy performance, but rather on the design phase parameters, essential annual estimation of energy consumption. These estimations are based on a building model where the different areas of the building envelope with their corresponding design transmittance (U-value) for opaque elements, plus

the design solar factor coefficient (g-Value) in the case of semi-transparent elements, are considered. Then, based on the building's systems design seasonal performance, different software tools apply the corresponding EU member state regulation calculations, as defined by article 3 of [17]. Finally, the building is energetically classified and a design annual energy consumption and design CO₂ emissions are given. Then, how is it possible that such a complex device as a car has had design and in-use energy characterization parameters since the nineties? However, considering the huge importance of the building envelope's real energy behaviour in population comfort and European energy consumption, how is it possible that a seemingly simple static device such a building envelope cannot be characterized under its in-use conditions? As highlighted by [16] in Figure 1.1, the building envelope measured Heat Loss Coefficient (HLC) can deviate up by to 100% from its design value.

There are still some gaps in the knowledge in the building physics area that do not allow us to reliably develop an in-use energy characterization method for occupied buildings' envelopes. Since the development of the Co-heating method for estimating an unoccupied building's HLC and its equivalent solar aperture (S_a) regarding the south global vertical solar radiation in 1985 [18] (new edition in 2013 [19]), only one standard regarding the in-situ envelope characterization has been developed. The ISO 9869 standard from 1994 (updated in 2014 [20]) was developed only for in-situ U-value estimation of opaque walls. Remember, that the HLC considers both, the heat transmission through the envelope (walls, windows, roof and floor; UA value) and the Infiltration and/or Ventilation losses (C_v) in W/ °C. The ISO 9869 method only provides the in-situ U-value [W/m² °C] of opaque walls, where one-dimensional heat flow can be assumed. Although it might be valid to test some specific areas of an in-use building envelope, it is not useful for obtaining the global UA value of a whole building envelope. The ISO 9869 cannot be applied to ventilated façades, green roofs or walls, windows, frames, corners, joints, thermal bridges etc., where mass transfer effects occur and where multidimensional heat transfer mechanism effects also occur.

The Co-heating method can estimate the HLC of unoccupied buildings, but requires about a 3 week testing period with dedicated monitoring of the whole building in the winter season. Its indoor temperature must be controlled by specific electric radiators that will generate a high indoor to outdoor artificial temperature difference. As detailed in [19], by regressing the measured $(Q+K)/\Delta T$ of Equation 1.1 against the measured $V_{sol}/\Delta T$, the whole building HLC (remember $HLC = UA + C_v$ [W/°C] [21]) and the equivalent whole building solar aperture regarding south vertical global radiation (S_a [m²]) can be estimated under the co-heating testing conditions.

$$(Q + K)/\Delta T = HLC - (S_a V_{sol})/\Delta T [W/°C] \quad (1.1)$$

All measured parameters Equation 1.1 are daily averaged; Q : all energy inputs inside the building due to heating and ventilating systems [W]; K : internal heat gains inside the building due to all electricity consumed and dissipated within the building and metabolic heat gains due to occupants (not present

in co-heating tests) [W]; $\Delta T = T_{in} - T_{out}$: indoor to outdoor daily average temperature difference; V_{sol} : south vertical global solar radiation [m^2].

Note that the Co-heating Method requires all the ventilation ducts and to close all the blinds to be closed to minimize the effect of the solar gains on the entire regression of Equation 1.1 regression. Thus, the co-heating HLC will not consider the in-use Infiltration/Ventilation behaviour and the estimated solar aperture will not represent the reality of the use of the building where it is common to have open blinds during winter periods. Moreover, the HLC is only obtained once in the co-heating, usually after the building is constructed or refurbished. Applying the Co-heating test could also considerably the building's delivery to the owners if it is finished in spring or summer. It is not practical to vacate buildings for three weeks and fill them with sensors and actuators once it is in operation. Therefore, the need to evaluate the HLC under in-use conditions is of vital importance. It could thus be evaluated continuously during the building's life under its real in-use conditions by using the building's own monitoring system. So, why is it so difficult to obtain the in-use HLC for a building envelope?

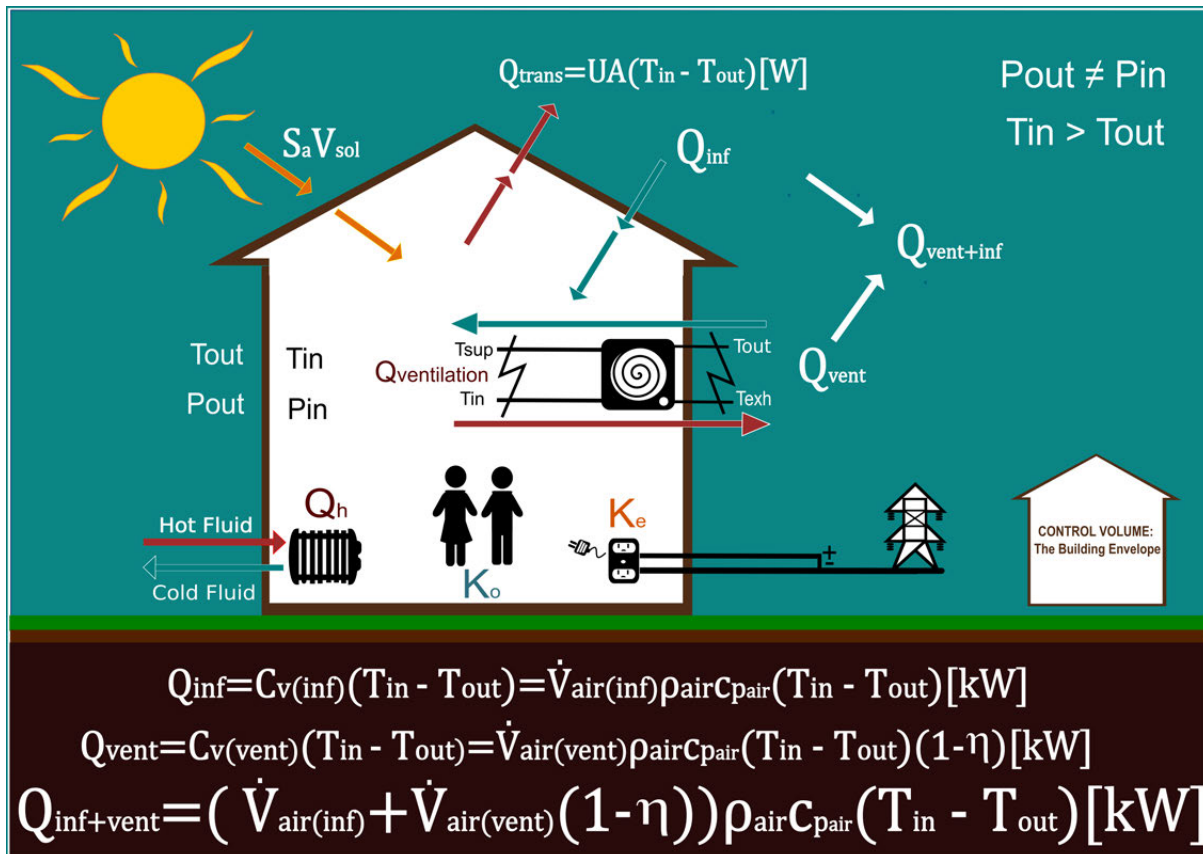


Figure 1.2: Schematic of main energy and mass exchanges through the building envelope.

Let us review the principal energy and mass exchanges occurring through a typical in-use building envelope in the heating season, see Figure 1.2. There are different energy gains within the building: the heating heat input typically provided by water or glycol-water as heat transfer fluid ($Q_{heating}$), metabolic heat gain produced by building users ($K_{occupants}$), electricity heat gains produced by all the

electric devices consuming and dissipating electricity within the building envelope ($K_{electricity}$) and possible solar gains ($S_a V_{sol}$).

We also have heat losses through the envelope due to:

- Transmission effects (Q_{trans}) dependant on the building envelope's UA value and the T_{in} to T_{out} temperature difference (equation in Figure 1.2).
- Infiltration effects (Q_{inf}), dependant on the infiltration heat loss coefficient ($C_{v(inf)}$), which depends on the building envelope's total permeability to the air infiltration that will produce different infiltration volumetric air flow rates $V_{air(inf)}$ (also dependant on wind velocity, direction, and T_{in} to T_{out} temperature difference), and proportional to the air density (ρ_{air}), the air constant pressure specific heat (c_{pair}) and the T_{in} to T_{out} temperature difference (see equation in Figure 1.2).
- Ventilation effects (Q_{vent}), dependant on the ventilation heat loss coefficient ($C_{v(vent)}$) which depends on the ventilation volumetric air flow rates $V_{air(vent)}$ (ventilation rates could be constant and scheduled or controlled by some indoor parameter such as indoor CO₂ concentration or relative humidity), and inversely proportional to the (if existing) Heat Recovery Efficiency (η), to ρ_{air} , to c_{pair} and the T_{in} to T_{out} temperature difference (see equation in Figure 1.2).

If we sum, as in the equation of Figure 1.2 equation, $Q_{inf+vent} = Q_{inf} + Q_{vent}$, taking $(T_{in} - T_{out})$ as the common factor, and reordering, we get Equation 1.2 for the most general case for the whole building's Infiltration/Ventilation heat loss coefficient. Note that buildings without heat recovery in their ventilation system are represented by $\eta = 0$.

$$C_v = \dot{V}_{air(vent)} \rho_{air} c_{pair} (1 - \eta) + \dot{V}_{air(inf)} \rho_{air} c_{pair} [KW/^\circ C] \quad (1.2)$$

HLC and the equivalent solar aperture (S_a) are the KPIs for the unoccupied building envelope energy performance characterization by the Co-heating method [19]. Few research works to estimate these KPI in monitored in-use buildings exist [22]. Furthermore, none of them has carried out the decoupling of the HLC into its UA and C_v coefficients, just using data sets from monitored in-use buildings.

One of the objectives of this thesis is to help to understand and reliably quantify the 'performance gap' between the design HLC and the actual HLC of building envelopes. Therefore, the first aim is to analyse the existing HLC estimation methods for in-use building envelopes. Among the few methods to estimate the HLC of in-use buildings, we can find the average method [23]. This method requires data sets obtained by a building monitoring system, comprising at least indoor and outdoor temperatures, heating systems energy inputs to the building, electricity consumptions and weather data. For reliable and robust in-use HLC estimation, the quantification of the overall uncertainty of

each of these measured parameters is of crucial importance.

The average method applies the energy conservation principle to the building schematic of Figure 1.2. This energy conservation equation analysis (developed in detail within the literature review) allows to relate the HLC and the solar gains $((S_a V_{sol})_{\kappa})$ to measurable variable parameters. These parameters are the heating system energy supply $(Q_{h_{\kappa}})$, all internal gains due to occupant metabolic heat generation and the consumption of electric devices within the building envelope $(K_{T_{\kappa}})$, as well as the $T_{in,\kappa}$ to $T_{out,\kappa}$ temperature difference present in Equation 1.3, where κ stands for an arbitrary measurement point. Building monitoring systems usually measure the Equation 1.3 measurable parameters $(T, Q, K$ and $V_{sol})$ in frequencies where ΔT could range from 1 min to 1 hour.

In [24], Equation 1.3 has been applied to different cold and cloudy short winter periods of 3 to 5 days, where Q and $(T_{in} - T_{out})$ were high. Thus, their measurement uncertainty was minimum. On the other hand, in these cloudy periods, the uncertain solar gains $(S_a V_{sol})$ were low compared to $(Q + K)$ and thus although solar gains were only roughly estimated, Equation 1.3 was applied.

$$HLC = \frac{\sum_{\kappa=1}^N (Q_{h_{\kappa}} + K_{T_{\kappa}} + (S_a V_{sol})_{\kappa})}{\sum_{\kappa=1}^N (T_{in_{\kappa}} - T_{out_{\kappa}})} [kW/{}^{\circ}C] \quad (1.3)$$

Although promising results have been obtained by Equation 1.3 in [24], among others, it will be impossible to obtain a generic reliable HLC estimation method until the following issue is solved:

- The non-uniformity of the indoor air temperature, even within a thermal zone of a building, is very common. The same happens for the outdoor air temperature measurements, where significant differences can be found depending on the orientation and height. Thus, quantifying the overall uncertainty of the indoor and outdoor temperature (T_{in} and T_{out}) measurements in in-use buildings and its propagation to the HLC estimations is crucial. This quantification is the main contribution of this thesis, since, following a detailed literature review on monitoring systems, it has been found that this issue is still unresolved, so a method to quantify these two measurements' overall uncertainty has been developed and implemented.

Finally, the anthropogenic CO₂ as tracer gas, in combination with direct measurements on the ventilation system, could be used to estimate the Infiltration/Ventilation heat loss coefficient (C_v) (this is fully developed in the literature review section). Usually, the UA value can be assumed to be constant in a building. However, the C_v value will be dependent on both: the user selected set points and regulation of the ventilation system as well as the behaviour of the infiltrations, which are mainly dependent on the window opening pattern, wind velocity and indoor to outdoor temperature variations.

OBJECTIVES

The research carried out in this thesis has, as its main objective, to help in the optimisation and reliability of the energy Monitoring and Control System (MCS) of buildings to be integrated in Building Automation Systems (BAS) in the future, so as to characterize the Thermal Envelope Performance (TEP) of Buildings through the reliable in-use HLC estimation and decoupling. The increase in reliability of the in-use HLC estimations and decoupling, could enable the emission of Energy Performance Certifications (EPCs) after the construction or retrofitting of a building and during the building's life cycle. Because of the important role of the MCS, they must be reliable in order to ensure that accurate and precise measurement values are obtained, along with the correct capture of data and storage of measurements. Figure 1.3 shows a diagram of the optimization process from the MCS scope.

To achieve this main objective, the following specific objectives have been identified in this thesis:

- Identification and analysis of the MCS used by different methods to estimate the TEP of Buildings in order to compare the different systems used in the literature.
- Develop a methodology to estimate the overall uncertainty of intensive variables of in-use buildings, such as the indoor air temperature of different thermal zones within a building or the outdoor air temperature surrounding the building envelope. The method should also permit this uncertainty to be decoupled in order to know which part of the uncertainty is due to random errors and which part is due to systematic errors.
- Design, testing and installation a three dimensional MCS to collect data in an in-use office building to analyse the developed methodology for the overall measurement uncertainty of the indoor and outdoor air temperatures.
- Based on the detailed analysis of the HLC estimation and decoupling methods, the analysed MCS in the literature review and the developed methodology for overall uncertainty analysis of the intensive variables required for HLC estimation and decoupling: the design and deployment of an extremely detailed MCS for a residential building integrated into the design and rehabilitation phase of the building. The aim of this extremely detailed monitoring system is to be able to analyse what is the minimum set of sensors required to estimate and decouple the in-use HLC values with sufficient reliability. The selected sensors should have the greatest possible accuracy that can be found for building sector applications. A detailed economic analysis should also be included for this extremely detailed monitoring. The guidelines on how to analyse the data of this monitoring and control system to obtain the minimum sensor number for in-use HLC estimation and decoupling will be developed.

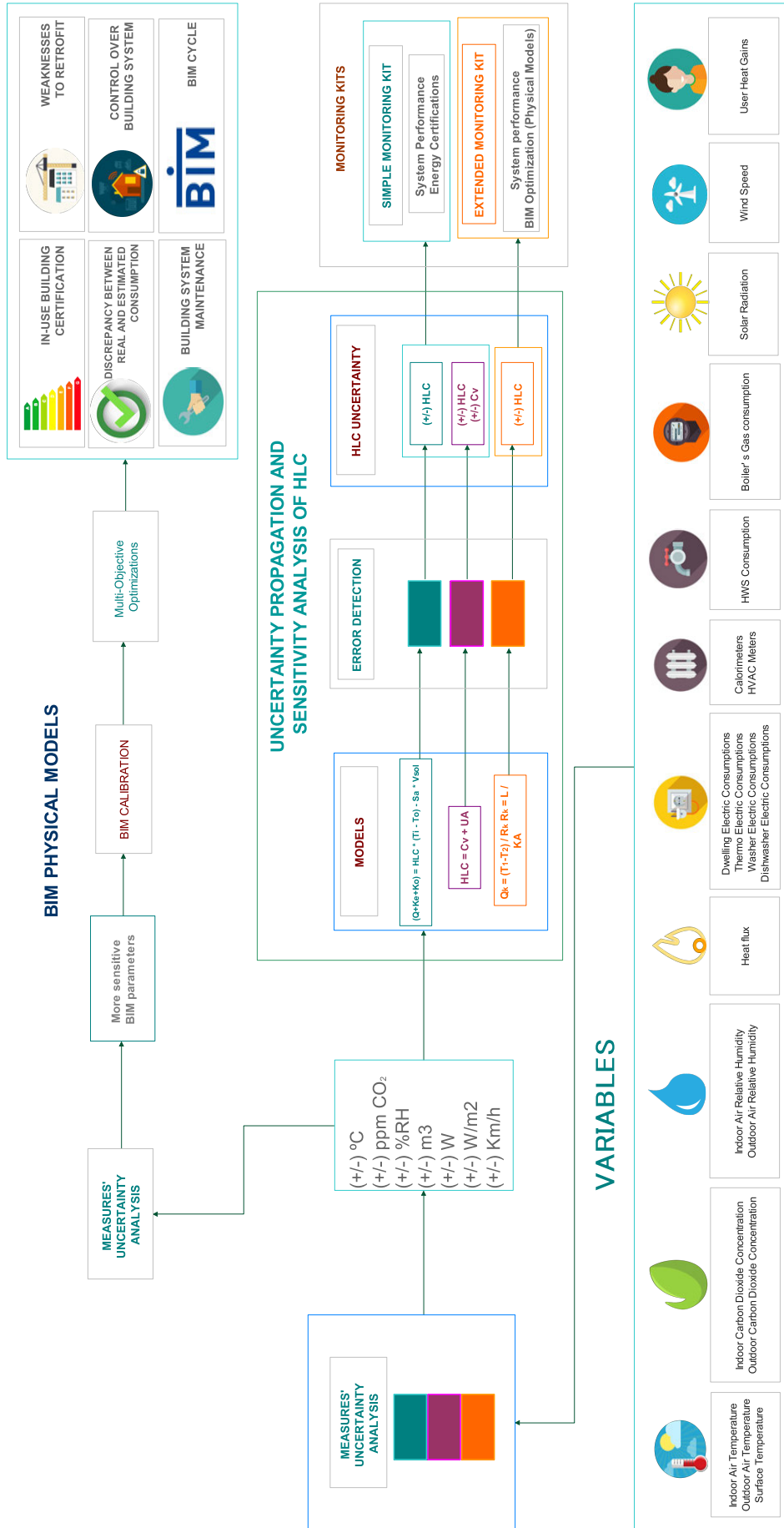


Figure 1.3: Scheme of optimized MCS scope.

Chapter 2

LITERATURE REVIEW

This chapter investigates the question of building energy monitoring systems used for data collection to estimate the Heat Loss Coefficient (HLC) with existing methods, in order to determine the Thermal Envelope Performance (TEP) of a building. The data requirements of HLC estimation methods are related to commonly used methods for fault detection, calibration, and supervision of energy monitoring systems in buildings. Based on an extended review of experimental tests to estimate the HLC undertaken since 1978, qualitative and quantitative analyses of the Monitoring and Controlling System (MCS)¹ specifications have been carried out. The results show that no Fault Detection and Diagnosis (FDD) methods have been implemented in the reviewed literature. Furthermore, it was not possible to identify a trend of technology type used in sensors, hardware, software, and communication protocols, because a high percentage of the reviewed experimental tests do not specify the model, technical characteristics, or selection criteria of the implemented MCSs. Although most actual Building Automation Systems (BAS) or Building Management System (BMS)² may measure the required parameters, further research is still needed to ensure that these data are accurate enough to rigorously apply HLC estimation methods.

¹The general definition of an MCS is a 'system designed to control large or complex facilities such as factories, power plants, network operations centres, airports, and spacecraft, with some degree of automation' [25], which can be implemented also in buildings.

²A building Automation System (BAS) or Building Management Systems (BMS) is a computer-based control system installed in buildings that controls and monitors the building's mechanical and electrical equipment, such as ventilation, lighting, power systems, fire systems, and security systems [26].

2.1 Introduction

In order to provide some background to the role of the Monitoring and controlling system (MCS) to evaluate a Building's Envelope Energy Performance by estimating its Heat Loss Coefficient (HLC), an introduction to the energy consumption in Europe is shown along with the role of the Heat Loss Coefficient (HLC) estimation in understanding the envelope's effect on the Energy Performance of Buildings (EPB). The monitoring systems used for this estimation are also set out together with the role of fault detection in building energy monitoring systems.

Butler and Dengel [19] define the Heat Loss Coefficient (HLC) as the total heat loss from a building resulting from heat transfer through the envelope (walls, roof and floor) and from background ventilation per °C of temperature difference between inside and outside (expressed as W/K). This review defines the Thermal Envelope Performance (TEP) as a characteristic that can be used to evaluate the energy performance of a building envelope. The TEP can be characterized by the estimation of the Heat Loss Coefficient (HLC), the energy consumption due to the envelope performance or the envelope elements' characterization (Thermal Resistance (R-value) or Thermal Transmittance (U-value), dynamic thermal models of the envelope...).

Estimating the Heat Loss Coefficient (HLC) and the Thermal Envelope Performance (TEP) characterization of buildings is important to better understand their energy efficiency, so as to generate Energy Performance Certificates (EPCs) (Figure 2.1 shows a scheme of the MCS, the HLC and TEP estimation so as to know the Energy Performance of Buildings (EPB) in order to generate EPCs). These can be used as a tool to determine the discrepancies between performances at the design and operation phases of buildings. Actual TEP, actual energy equipment performance, and user behaviour are the three main reasons for a building to consume energy differently from what its design conditions suggest. European regulations emphasise the quality of the EPC and its reliability and remark the importance of the use of reliable methodologies to characterize the Energy Performance of Buildings (EPB) [27]. The use of HLC estimation, as a methodology to generate EPCs, needs to be fed with physical variables collected and processed by a Monitoring and Controlling System (MCS), which is composed of elements with the necessary precision to generate reliable EPCs. Likewise, MCS require faults to be detected and minimized to guarantee a higher level of accuracy in the results by minimizing the error in calculations. Currently, existing smart buildings are monitored and controlled with various building systems (e.g., Heating, Ventilation and Air Conditioning (HVAC), heating, light systems), but do not have an integrated MCS of the type currently used in experimental tests to estimate the HLC.

2.1.1 Energy consumption of buildings in Europe

The potential for energy demand growth from connected devices in buildings, whether they are smart or not, has already been noted in many European Union (EU) markets, according to a study carried out by the Statistics in the Control and Connectivity segment, where 'the number of active households is expected to amount to 43.7 m by 2022' [28]. In the International Energy Agency (IEA) Central Scenario, 50% of household electricity demand for appliances by 2040 is expected to come from

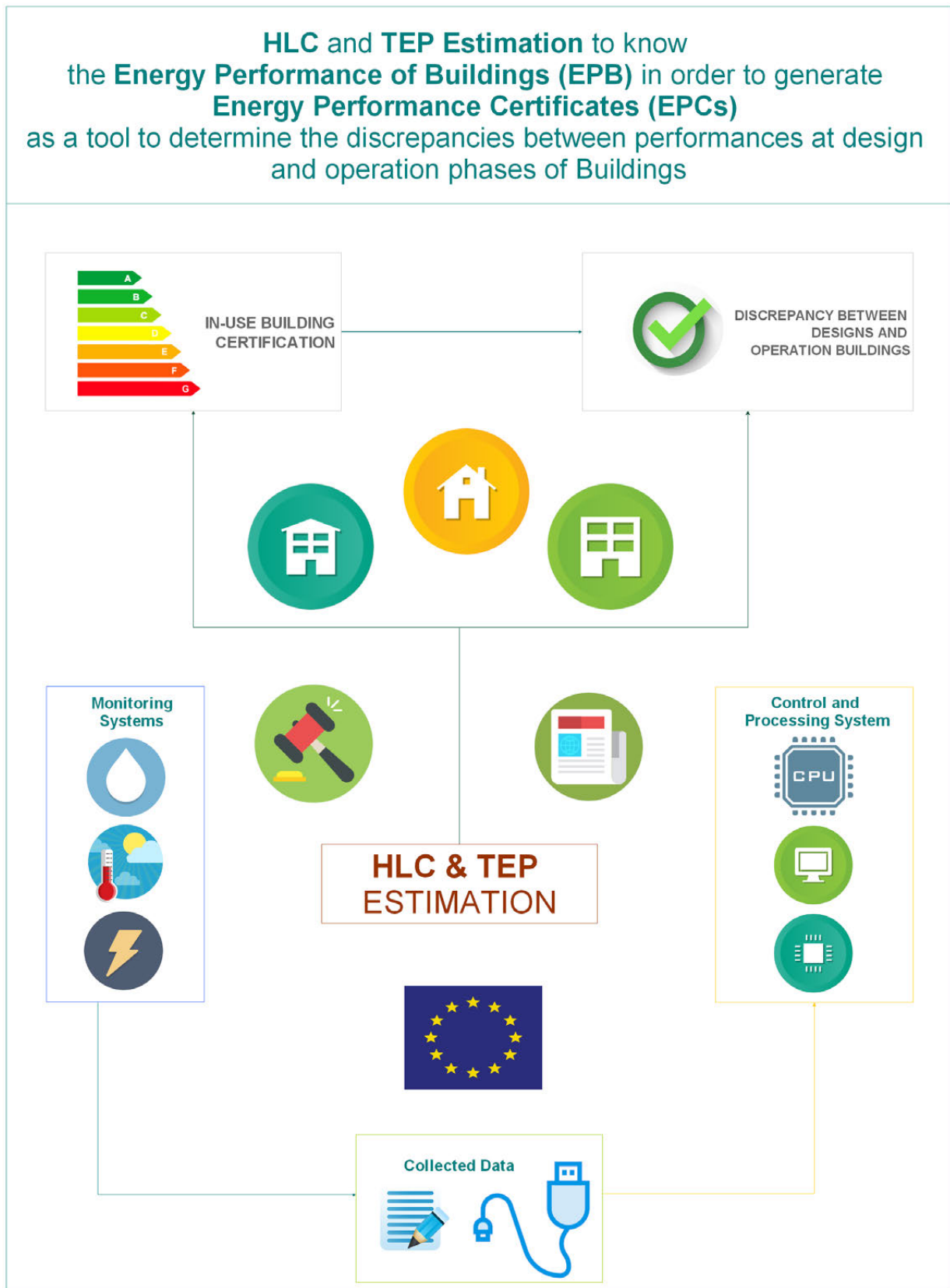


Figure 2.1: Scheme of tools to determinate the gap between performances at design and operation phases of buildings: the HLC and TEP estimation role to know the envelope energy behaviour in order to generate EPCs related to the building envelope.

connected devices, presenting opportunities for a smart demand response, but also increasing the need for standby power. 'Improving the operational efficiency of buildings by using real-time data could lower total energy consumption between 2017 and 2040 by as much as 10% compared with the Central Scenario, assuming limited rebound effects in consumer energy demand' [29].

Increasing the energy efficiency of buildings can generate economic, social, and environmental benefits and improve the building performance, providing better levels of comfort and well-being to users as health can be benefited by indoor climate improvements. It is necessary to reduce the energy consumption of buildings, which represents approximately 40% of energy consumption in Europe, in order to reduce Carbon Dioxide (CO₂) emissions [17].

Approximately 35% of buildings in the EU are over 50 years old. Of this percentage, only around 0.4–1.2% (depending on the country) are renewed annually. This implies that a greater renovation of existing buildings could generate significant energy savings through the reduction of 5–6% of the EU's total energy consumption, and 5% of the total (CO₂) emissions [30]. The 'Action Plan for Energy Efficiency: Realizing the Potential' calls on all regional and local authorities to develop energy efficiency plans and to transpose the directives on the energy performance of buildings into national legislation [31].

On 30 November 2016, the European Commission presented a proposal for a modest review of Directive 2010/31/EU on the Energy Efficiency of Buildings [32]. Some of the measures in the Clean Energy Package aim to meet the objectives of energy and climate of the EU 2030, together with the the Energy Efficiency of Buildings Directive (EPBD) [33], which is aimed at achieving the EU's energy efficiency objectives that are also addressed in the Energy Efficiency Directive (EED) [34]. The proposed revision of the EED (part of the Clean Energy Package) establishes a greater number of energy efficiency measures by 2030, so that for Member States can achieve at least 20% improvements in energy efficiency by 2020 [34, 35]. This reduction of 20% is a matter of urgency in the action plan and is equivalent to around 390 Mtoe. This energy reduction is supported by the Green Paper on energy efficiency [36, 37].

Energy efficiency and renewable energy technologies were the leading areas of Research, Development and Design (RD&D) investment of the European Commission in 2015, reaching significant shares (24% and 26%, respectively) of the total energy RD&D budget. RD&D for fossil fuels had the smallest share, accounting for 6% of the total budget in 2015 [38], and everything indicates that this investment trend will be maintained in order to carry out the measures in the Clean Energy Package and meet the 2030 goals.

2.1.2 The the role of MCS in Energy Performance Certificates and the HLC to characterize the Thermal Envelope Performance (TEP) of buildings

The Energy Performance of Buildings Directive 2010/31/EU [32] proposes granting powers to the European Union for rating the smart readiness of buildings in order to guarantee uniform conditions for its application. These powers must be exercised in accordance with Regulation (EU) No. 182/2011

of the European Parliament and of the Council [39]. This regulation specifies the need to have a smartness indicator that is used to measure the capacity of buildings to use Information and Communication Technologies and electronic systems, so as to optimize the operation of the building and to be able to interact with the network. The smartness indicator will create awareness among the owners of buildings and their occupants about the value that lies behind the automation of buildings and the electronic monitoring of technical building systems, increasing the confidence of the occupants in the ability to obtain a real savings when introducing new improved features in their dwellings.

In the same way, this directive states the importance of comparing EPCs issued before and after renewal. To do so, a transparent method provided by the installer of the certification or qualification level must be used to measure the performance of the equipment or material used for the renovation, thus guaranteeing their best use in the renovation of buildings in terms of the renovation quality, and to measure the associated financial impact and energy efficiency of buildings. To meet the objectives of the energy efficiency policy for buildings, the transparency of EPCs should be improved by ensuring that all the necessary variables for calculations, for both certification and minimum energy performance requirements, are set out and applied consistently.

A report by the EPBD [40, 41] stresses on the importance of implementing Monitoring and Control Systems (MCSs) to achieve quality assurance. These are an essential part of assessing compliance rates, which require confidence validation in source data and legitimacy in order to issue compliance reports and they can then be used for certification, such as the EPCs.

According to Article 3 of the EPBD [17], the EU Member must estimate a building's energy performance using a specific methodology, at the very least using standardized conditions specified by national regulations. There, the HLC could play an important role, since it is one of the Key Performance Indicators (KPIs) [24] of the energy performance of building envelopes.

To estimate the Heat Loss Coefficient (HLC), it is necessary to collect physical variable data of an in-use building or an unoccupied building, depending on the calculus methodology employed, to estimate the HLC. The sensors should measure, among other parameters, the temperature, heating inputs, ventilation rates, solar radiation, and different energy consumptions [24, 42] to demonstrate the energy performance of the building's envelope. In-use building monitoring will be developed in the next few years to collect physical variables, and could be used to obtain the building's envelope's thermal characteristics.

The Thermal Envelope Performance (TEP) of a whole building is often quantified by the Heat Transfer Coefficient (HTC). 'HTC' is interchangeable with a second term, the heat loss coefficient (HLC), which has often been used when reporting Co-Heating results and will be used in this thesis to refer to the Heat Transfer Coefficient. 'HTC' has been adopted as a standard term in line with the naming convention used in ISO³ 52016-1:2017 [44], the international standard method for calculating the

³ISO: 'International Organization for Standardization' [43].

energy performance of a building, which cancels the previous standard ISO 13790:2008 [45]. The HLC is a useful metric that describes the total, time-averaged rate of heat transfer (in Watts (W)) from a building in a per-degree-Kelvin difference between indoor and outdoor air temperatures. Each building can be assumed to have a constant HLC—a value that is estimated as a metric in building energy models such as the Standard Assessment Procedure (SAP), which ‘is the United Kingdom (UK) government standard to calculate a building’s energy efficiency and carbon emissions’ [46]. By estimating the HLC, the thermal performance of the complete building envelope, as built, can be directly compared with the designed thermal performance, independent of occupant behaviour and weather conditions.

2.1.3 The Monitoring Systems (MSs) used to estimate the Heat Loss Coefficient (HLC) to determine the Thermal Envelope Performance (TEP) of Buildings

Given the importance of measuring buildings’ energy performance, this thesis reviews the monitoring systems used to show the energy efficiency level of buildings through physical data collected by sensors. These data are used to estimate the energy performance using specific methodologies, which in future will guarantee transparent EPCs for minimum energy consumption. This thesis focuses on the energy monitoring used in projects to estimate the HLC with two methods: the Average Method [24] and the Regression Method, which is known as the Co-Heating method [19, 47]. These, along with other methods, can be used to calculate the Thermal Envelope Performance (TEP) of buildings.

The latest report of Digitalization & Energy [29] of the International Energy Agency (IEA) in 2017 stated that there is a greater potential for energy saving in heating, cooling and lighting, since these together in 2015 accounted for more than 60% of the total demand for final energy in buildings. The report also highlights the fact that sensors, intelligent controls, and connected devices consume energy to maintain connectivity, even when they are in standby mode. To improve the energy performance of the building, this necessitates, for example, the use of intelligent thermostats to improve the management of heating and cooling loads, allowing an improved and even remote control of the temperatures throughout the building.

Without automated monitoring and fault detection of the sensors and controls, the performance can degrade. The number and range of types of sensors installed in commercial buildings is inadequate to provide sufficient automated (or even visual) monitoring [48]. The characterization of the TEP of in-use buildings and systems requires a monitoring system that provides real data, which in turn requires a minimum sensor set to obtain a correct characterization. The data collected from the sensor set then needs to be analysed with different and robust methodologies due to the large amount of data obtained from the building monitoring systems.

Currently, some energy monitoring systems are integrated in domotic systems in order to information about the energy consumption and perform the control of user comfort parameters. However, in order to characterize the TEP of in-use buildings, there is no evidence of the integration of an energy MCS with a minimum sensor set in domotic systems. This sensor set integer in Building Automation

Systems (BAS) or domotic systems would allow us to know the real energy performance of building envelopes through the TEP characterization after the construction or retrofit of buildings.

2.1.4 Fault Diagnostic, Detection (FDD) and Calibration in Building Monitoring Systems

Buildings may have operational problems due to degraded equipment, failed sensors, incorrect installation, poor maintenance, and improperly implemented controls. Currently, most problems related to building systems are detected through complaints from occupants or alarms provided by a Building Automation System (BAS). Detection and diagnosis can be performed automatically by integrating the experience required to detect and diagnose operational problems into software tools that take advantage of existing sensors and control systems. These tools are not designed to replace the people who operate the building systems, but to help them improve the functioning of those systems. The automatic start-up and diagnosis technologies for systems and building equipment are expected to reduce and act on problems, as well as improve the functioning of the building, through the automatic and continuous detection of performance problems and maintenance requirements that are communicated to the building operators, who can then perform the necessary corrective actions [48].

Due to the large amount of data collected from sensor sets, it is necessary to address which calibration system and methodologies are applied in the building energy monitoring systems, and to know the sensor set necessary to characterize the energy performance of in-use buildings' envelopes. The literature related to fault detection and calibration in building monitoring is focused on the building systems, including fan coils, Heating, Ventilation and Air Conditioning systems (HVACs), heat pumps, air conditioners, commercial refrigerators, lighting, water heaters, chillers and cooling towers, Air Handling Units (AHUs), and Variable Air Volume (VAV) boxes. From all the works reviewed, a specific methodology that could be applied to the entire sensor set of the BAS and domotic systems was not found.

2.2 Monitoring and Control Systems (MCSs) used to estimate the Heat Loss Coefficient (HLC) using the Average Method and the Co-Heating Method

In order to introduce the study carried out concerning the review of MCS used in different projects published to estimate the HLC, the monitoring requirements of the Average Method and Co-Heating Method are analysed showing the main physical variables required. To introduce both methods, different mathematical modelling techniques, used to identify the real energy behaviour of buildings or building components based on measurements, are first set out.

2.2.1 Different methods to characterize the building envelope energy behaviour

The traditional methods to characterize the TEP are based on the estimation of the energy behaviour of the building through the estimation of the R-value and/or U-Value to characterize the building's envelop elements, estimating overall heating energy consumption and measuring the infiltrations rates of the building. The new trend to characterize TEP is through the estimation of the Heat Loss Coefficient (HLC), which allows us to know how much heat the building loses, per each indoor to outdoor centigrade degree, due to Heat Transmission (UA) plus air infiltration/ventilation (C_V), Equation 2.10.

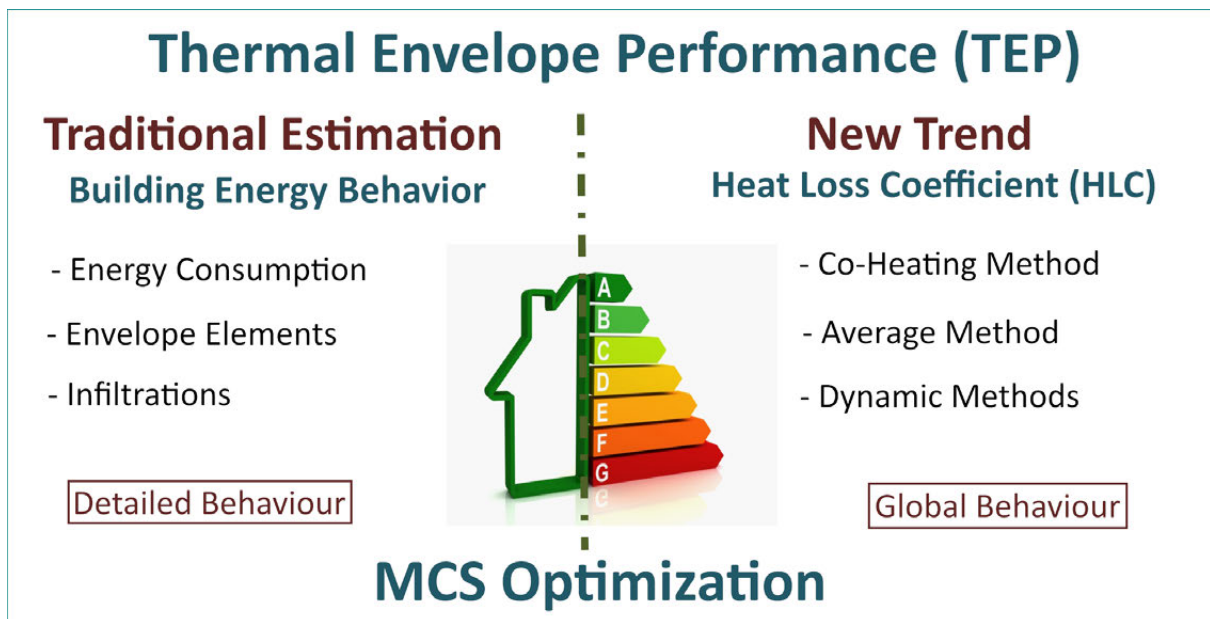


Figure 2.2: Traditional estimation of Thermal Envelope Performance (TEP) versus the new estimation trend through the Heat Loss Coefficient (HLC) estimation.

To estimate the HLC value of a building, there is a method which has been used since 1978 [49], named the Co-Heating method. This method is implemented in unoccupied buildings and requires a specific indoor condition to be maintained during the test. In the present, the scientific community is working to improve the HLC estimations in occupied buildings; one of these methods is the Average Method⁴ [23], which is implemented in different experimental studies and currently is a candidate of The Executive Committee of the International Energy Agency (IEA) in Energy in Buildings and Communities (EBC) programme named the 'IEA-EBC Annex 71: Building energy performance assessment based on in-situ measurements' [50].

Summerfield [51] established that energy saving methods should be based on empirical methods instead of model estimations, where the simulations assume standard operation conditions without considering the occupation and real heat requirements, overestimating the energy demand of old buildings and underestimating it in new buildings, unless the models are fed with monitored occupation and HVAC system data. Since MCSs are not usually implemented in in-use buildings, the use of advanced mathematical modelling techniques, is common. Such physical statistical approaches

⁴The first development of the Average Method was developed by A. Erkoreka in 2016 [24].

are used [52] to identify the real energy behaviour of buildings or building components based on measurements [53]. For this reason, the multiple linear regression, Autoregressive Model (ARX), Autoregressive Moving Average Model (ARMAX) [54, 55] and Grey Box modelling (state space models) [56–58] have been used by different authors to identify such building characteristics as U-values, R-value, Thermal Capacitances (C_T) and Solar Apertures (S_a), among others.

When the designed or simulated energy consumption are compared to real ones, a 'performance gap' [4] is usually observed. This gap can be affected by user behaviour and the building systems' real energy performance [59], but the building envelope also has a considerable influence on it. Some parameters have an influence in increasing the 'performance gap', making it difficult to accurately model such aspects as the simulation error related to the occupancy [12, 14], weather data [60], material uncertainty [8], etc.

Different Energy Performance of Building (EPB) estimation methods, which use building simulation software based on thermal models, have been developed by many countries in the European Union [61, 62]. The most commonly used Key Performance Indicators (KPI), which are used to characterize the energy performance of a building's envelope, are the Heat Loss Coefficient (HLC), which considers Transmission Heat Losses through the envelope, or Heat Transfer Coefficient (UA), plus Ventilation and/or Infiltration Heat Losses (C_v) [21], as well as the solar gains [19]. Although there are some research works that estimate these KPI in monitored in-use buildings [22], it is still far from being a general method. Of the existing methods to estimate the building envelope Heat Loss Coefficient, the Co-heating method is the most developed, and it also includes specific testing procedures [18, 19, 63]. This method is not prepared for working with in-use buildings, due to the difficulties when estimating such parameters as solar gains or occupancy [64, 65]. However, an Average Method has been developed to estimate the HLC of an in-use building in [24].

2.2.2 General mathematical development to estimate the Heat Loss Coefficient (HLC) through the Average Method

The origin of the method has been studied in detail to understand its limits when used in dynamic problems such as an in-use building. Figure 2.3 shows the system to be analysed from the Thermodynamics Open System (and not stationary) viewpoint. As can be seen in Figure 2.3, the building's envelope is the Control Volume (cv), or the boundary of the system through which heat and mass can be exchanged with the surroundings and the ground. Equation 2.1 states the energy conservation principle of a generic Thermodynamic Open System [66].

Applying the energy conservation principal to the control volume shown in Figure 2.3, the variation of the Control Volume's Accumulated Energy⁵ (E_{cv}) over time (Equation 2.1) is obtained, whose value in turn is equal to the variation of Internal Energy (U), the Kinetic Energy (E_k) and the Potential Energy (E_p) over time. E_k and E_p are usually constant and their derivatives over time are equal to zero.

Applying the First Law of thermodynamics to these open systems, the Control Volume's Accumulated

⁵This term represents the energy accumulation in the system.

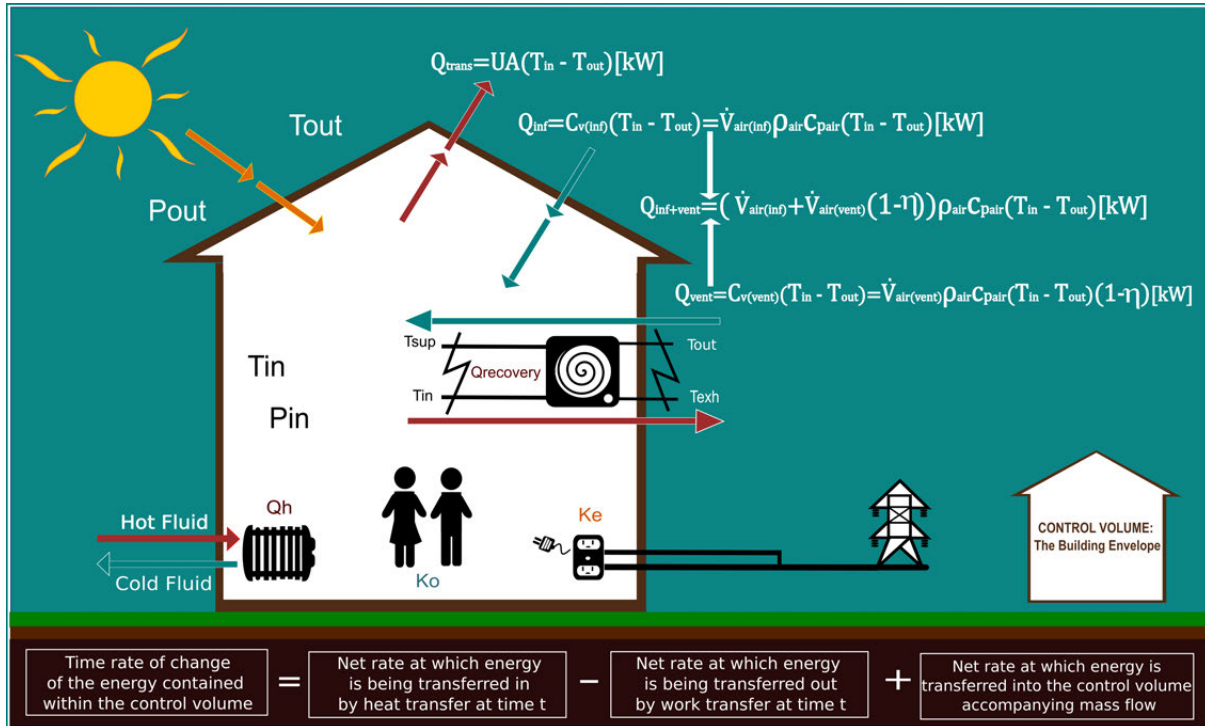


Figure 2.3: Scheme of all energy and mass exchanges through the control volume defined by the building envelope. .

Energy (E_{cv}) over time is equal to the Heat Exchange occurring through the building envelope (Control Volume (cv)) (Q_{cv}) over time minus the Work Exchanged through the Control Volume (W_{cv}) over time, plus the Energy Exchanged through the envelope due to Mass Flows over time (E_m), shown in Equation 2.3. Likewise, Equation 2.2 defines the Internal Energy (U) variation over time.

$$\frac{dE_{cv}}{dt} = \frac{dU}{dt} + \frac{dE_k}{dt} + \frac{dE_p}{dt} = \frac{dU}{dt} \quad (2.1)$$

Where Equation 2.2 shows $\frac{dU}{dt}$ in function of the different Mass Types (m_i) within the building (the analysed system), such as concrete, bricks, furniture, wood (the sum goes up to ϵ different types of mass present within the building), together with its Specific Heats (c_i), and the variation of the Temperature of the Building's Mass (T_i) over time. The m_i might change their temperatures (and thus their internal energy) when going from time instant t_1 to t_N . The c_i represents the different specific heats of the different masses within the system. For the air within the building, the specific heat at constant volume should be used.

$$\frac{dU}{dt} = \sum_i^{\epsilon} m_i \frac{du_i(t)}{dt} = \sum_i^{\epsilon} m_i c_i \frac{dT_i(t)}{dt} [kW] \quad (2.2)$$

Likewise, the $\frac{dE_{cv}}{dt}$ term can be defined by:

$$\frac{dE_{cv}}{dt} = \dot{Q}_{cv} - \dot{W}_{cv} + \sum_{sup} \dot{m}_{sup} \left(h + \frac{v^2}{2} + gz \right)_{sup} - \sum_{exh} \dot{m}_{exh} \left(h + \frac{v^2}{2} + gz \right)_{exh} \quad (2.3)$$

Being \dot{Q}_{cv} , $-\dot{W}_{cv}$ and $E_m = \sum_{sup} \dot{m}_{sup} \left(h + \frac{v^2}{2} + gz \right)_{sup} - \sum_{exh} \dot{m}_{exh} \left(h + \frac{v^2}{2} + gz \right)_{exh}$ terms equal to:

$$\dot{Q}_{cv} = S_a V_{sol} + K_{occupancy} - UA(T_{in} - T_{out}) \quad (2.4)$$

$$-\dot{W}_{cv} = K_{electricity} \quad (2.5)$$

$$\begin{aligned} \sum_{sup} \dot{m}_{sup} \left(h + \frac{v^2}{2} + gz \right)_{sup} - \sum_{exh} \dot{m}_{exh} \left(h + \frac{v^2}{2} + gz \right)_{exh} = \\ \dot{m}_{air} (h_{air_{sup}} - h_{air_{exh}}) + \dot{m}_{water} (h_{water_{sup}} - h_{water_{exh}}) = \\ - [\dot{V}_{air(vent)} \rho_{air} c_{p_{air}} (T_{in} - T_{out}) (1 - \eta) + \dot{V}_{air(inf)} \rho_{air} c_{p_{air}} (T_{in} - T_{out})] + \\ \dot{m}_{water} c_{water} (T_{water_{sup}} - T_{water_{exh}}) = \dot{m}_{water} c_w (T_{water_{sup}} - T_{water_{exh}}) - \\ C_v (T_{in} - T_{out}) = Q_h - Q_{vent+inf} [kW] \quad (2.6) \end{aligned}$$

The \dot{Q}_{cv} term takes into account all the pure heat exchanges occurring through the Control Volume boundary (the building envelope). In this case, the heat gained through the solar radiation entering the building and the metabolic heat generated by the occupants of the building are considered to be inputs (Equation 2.4). Nevertheless, the added negative inputs are transmission heat losses through the envelope of the building. The next term, \dot{W}_{cv} , considers the pure work exchanged through the Control Volume. In this case, the consumed electricity is considered as work. However, as the electricity is converted into heat within the system, the considered negative work is presented as positive heat gain (Equation 2.5). Finally, the terms, $E_m = \sum_{sup} \dot{m}_{sup} \left(h + \frac{v^2}{2} + gz \right)_{sup} - \sum_{exh} \dot{m}_{exh} \left(h + \frac{v^2}{2} + gz \right)_{exh}$, consider the net energy exchanged by the system due to the mass flow rates of the water (it could be an other Heat Transfer Fluid) in the heating system and the air mass flow rates of the ventilation and/or infiltration air exchanges. Here, the heat provided by the heating system is considered in the energy balance equation as the flow and return hot water of the heating system circuit (Equation 2.6). The hot water for the heating system could be produced by different technologies. If electrical heating is present, this would be considered in the \dot{W}_{cv} term (Equation 2.5).

Likewise, the heat exchanges associated to the Mass Flow, if the heat recovery system is added to the building is equal to:

$$\dot{Q}_h = Q = \dot{m}_{water} c_{water} (T_{water_{sup}} - T_{water_{exh}}) [kW] \quad (2.7)$$

$$\dot{Q}_{vent+inf} = Q_{vent} + Q_{inf} = C_v (T_{in} - T_{out}) = \dot{V}_{air(vent)} \rho_{air} c_{p_{air}} (T_{in} - T_{out}) (1 - \eta) + \dot{V}_{air(inf)} \rho_{air} c_{p_{air}} (T_{in} - T_{out}) [kW] \quad (2.8)$$

For buildings without a ventilation system or a ventilation system without heat recovery, then the term $[\dot{V}_{air(vent)} \rho_{air} c_{p_{air}} (T_{in} - T_{out}) + \dot{V}_{air(inf)} \rho_{air} c_{p_{air}} (T_{in} - T_{out})]$ represents the heat exchanged by the building with the outdoor ambient due to both phenomena, being the term, $(1 - \eta)$, of Equation 2.6 and Equation 2.8, being equal to one ($\eta = 0$). If no ventilation system is present in the building, the ventilation term disappears. Then, the ventilation and/or infiltration heat losses can be calculated using the specific heat at constant pressure of the air, $c_{p_{air}}$, and the indoor to outdoor temperatures. The kinetic and potential energy variations of both flows can be neglected.

However, if the building is working on a ventilation system with heat recovery, Q_{vent} should be calculated considering the heat recovery system efficiency ($1 - \eta \neq 1$ or $\eta \neq 0$), then $Q_{vent} = \dot{V}_{air(vent)} \rho_{air} c_{p_{air}} (T_{in} - T_{out}) (1 - \eta)$, as shown in Equations 2.6 and 2.8. The whole mathematical development of these terms is carried out in [23]. The schematic of the different temperatures involved in a generic heat recovery system for a ventilation system, are shown in Figure 2.3.

The heat recovery system works with four main temperatures: The outdoor or ambient air temperature (T_{out}), the renewed or supply air temperature (T_{sup}), the indoor air temperature (T_{in}) and the exhaust air temperature (T_{exh}). The supplied and exhaust air temperatures are those obtained after crossing the recovery system by both the flow and return of the air flows. The supply temperature is that obtained after the external temperature crosses the recovery system. In winter, this temperature will increase. Considering an adiabatic heat exchanger and the same volumetric flow rates for supply and exhaust flows, the heat from the exhaust stream will be used to heat up the cold inlet stream. Thus, the temperature drop of the exhaust stream should be equal to the inlet stream temperature increase across the heat exchanger. Therefore, the percentage of heat recovered would be defined as: $\eta = \frac{T_{air_{sup}} - T_{out}}{T_{in} - T_{out}}$. Where $Q_{recovery} = \dot{V}_{air(vent)} \rho_{air} c_{p_{air}} (T_{in} - T_{air_{exh}}) = \dot{V}_{air(vent)} \rho_{air} c_{p_{air}} (T_{air_{sup}} - T_{out})$. Then, taking into account the percentage of heat recovered (η) in $Q_{vent} = \dot{V}_{air(vent)} \rho_{air} c_{p_{air}} (T_{in} - T_{air_{sup}})$, it is possible to have the $T_{air_{sup}}$ value in function of η , T_{in} and T_{out} , thus, $Q_{vent} = \dot{V}_{air(vent)} \rho_{air} c_{p_{air}} (T_{in} - T_{out}) (1 - \eta)$ (Equation 2.8).

Then, replacing the Equations 2.4, 2.5 and 2.6 in Equation 2.1, the Internal Energy (U) rate is obtained with respect to the solar radiation gains, heating system gains, electricity and occupancy gains, infiltration/ventilation losses and heat transmission losses (Equation 2.9) [23].

$$\frac{dU}{dt} = S_a V_{sol,k}(t) + K_o(t) - UA(T_{in} - T_{out})(t) + K_e(t) + Q_h(t) - C_v(T_{in} - T_{out})(t) = S_a V_{sol}(t) + K_o(t) + K_e(t) - (UA + C_v)(T_{in} - T_{out})(t) [kW] \quad (2.9)$$

Both the heat losses to the ground and the long wave radiative heat exchange occurring in the building envelope have been considered within the HLC value, as if they were working against $(T_{in} - T_{out})$. This assumption is also made in the original Co-Heating Method [19], where the UA and C_v values are also considered to be constant, so it is possible to obtain a relation between the Internal Energy variation rate $(\frac{dU}{dt})$ and the HLC value through Equations 2.11 and 2.12, if Equation 2.10 is replaced in Equation 2.9. Moreover, the HLC value can be decoupled through Equation 2.10 as the sum of the transmission heat loss coefficient and the infiltration and/or ventilation heat loss coefficient [21].

Analysing Equation 2.11, it could be said that if the building's HLC is to be estimated by means of measurements, it would be necessary to make an instantaneous measurement of the energy rate being stored in the building $(\frac{dU}{dt})$, the exact solar gains at the same instant $(S_a V_{sol}(t))$, the exact instantaneous heating gains $(Q_h(t))$, the exact instantaneous internal gains due to occupants and electricity consumption $(K_o(t) + K_e(t))$ and the exact indoor to outdoor temperature difference $(T_{in} - T_{out})$. Obviously, the instantaneous accumulation term is nearly impossible to measure accurately and the exact instantaneous solar gains are also difficult to measure in an in-use building. The rest of the terms could be measured accurately and instantaneously.

$$HLC = (UA + C_v) [kW/^\circ C] \quad (2.10)$$

$$\frac{dU}{dt} = S_a V_{sol}(t) + K_o(t) - UA(T_{in} - T_{out})(t) + K_e(t) + Q_h(t) - C_v(T_{in} - T_{out})(t) = Q_h(t) + S_a V_{sol}(t) + K_o(t) + K_e(t) - HLC(T_{in} - T_{out})(t) [kW] \quad (2.11)$$

$$-\frac{dU}{dt} + Q_h(t) + K_o(t) + K_e(t) = HLC(T_{in} - T_{out})(t) - S_a V_{sol}(t) [kW] \quad (2.12)$$

Integrating Equation 2.12 from an initial time equal to t_1 to a final time t_N , Equation 2.13 is obtained. Since the data from monitoring systems are discrete, with measurements every Δt , the integers from Equations 2.13 would become sums from $k = 1$ (in t_1) to $k = N$ (in t_N), obtaining the Equation 2.14:

$$-\int_{t_1}^{t_N} U(t)dt + \int_{t_1}^{t_N} Q_h(t)dt + \int_{t_1}^{t_N} K_o(t)dt + \int_{t_1}^{t_N} K_e(t)dt = HLC \int_{t_1}^{t_N} (T_{in} - T_{out})(t)dt + \int_{t_1}^{t_N} S_a V_{sol}(t)dt [kJ] \quad (2.13)$$

$$\begin{aligned}
 - \sum_{i=1}^{\epsilon} m_i c_i (T_i(t_N) - T_i(t_1)) + \sum_{\kappa=1}^N Q_{h\kappa}(\Delta t) + \sum_{\kappa=1}^N K_{o\kappa}(\Delta t) + \sum_{\kappa=1}^N K_{e\kappa}(\Delta t) = \\
 HLC \sum_{\kappa=1}^N (T_{in\kappa} - T_{out\kappa})(\Delta t) + \sum_{k=1}^N (S_a V_{sol})_{\kappa}(\Delta t) [kJ] \quad (2.14)
 \end{aligned}$$

Solving the HLC from the Equation 2.14, the HLC's general Equation for the control volume (or whole building) is obtained in function of its internal energy (U), the indoor (T_{in}) and outdoor (T_{out}) air temperatures, solar radiation gains $S_a V_{sol}$, heating system gains (Q_h), electricity (K_e) gains and occupancy gains (K_o), (Equation 2.15). This general equation can be simplified if the occupancy and electricity gains are included in the K_T term (Equation 2.16), obtaining the HLC's simplified general equation shown in Equation 2.17, where Δt cannot be cancelled because the thermal storage is a property that depends solely on the initial and final thermal level of the building and not on the time dependant path, as are the rest of the variables of this equation.

$$HLC = \frac{\sum_{i=1}^{\epsilon} m_i c_i (T_i(t_1) - T_N(t_N)) + \sum_{\kappa=1}^N (Q_{h\kappa} + K_{o\kappa} + K_{e\kappa} + (S_a V_{sol})_{\kappa})(\Delta t)}{\sum_{\kappa=1}^N (T_{in\kappa} - T_{out\kappa})(\Delta t)} [kW/^{\circ}C] \quad (2.15)$$

$$K_{T\kappa} = K_{o\kappa} + K_{e\kappa} \quad (2.16)$$

$$HLC = \frac{\sum_{i=1}^{\epsilon} m_i c_i (T_i(t_1) - T_i(t_N)) + \sum_{\kappa=1}^N (Q_{h\kappa} + K_{T\kappa} + (S_a V_{sol})_{\kappa})}{\sum_{\kappa=1}^N (T_{in\kappa} - T_{out\kappa})} [kW/^{\circ}C] \quad (2.17)$$

The following is a description of each term that make up the analytical development to obtain the HLC General Equation:

- $\frac{dE_{cv}}{dt}$ is the Accumulated Energy Rate of the Control Volume [kW].
- $\frac{dU}{dt}$ is the Internal Energy Variation Rate of the Control Volume [kW].
- $\frac{dE_k}{dt}$ is the Kinetic Energy Variation Rate of the Control Volume [kW].
- $\frac{dE_p}{dt}$ is the Potential Energy Variation Rate of the Control Volume [kW].
- $\frac{dQ_{cv}}{dt} = \dot{Q}_{cv}$ is the heat exchange rate through the control volume [kW].
- $\frac{dW_{cv}}{dt} = \dot{W}_{cv}$ is the work exchange rate through the control volume [kW].

- \dot{m}_{sup} is the supply air mass flow rate [kg/s].
- \dot{m}_{exh} is the exhaust air mass flow rate [kg/s].
- h_{sup} is the fluid's supply enthalpy [kJ/kg].
- h_{exh} is the fluid's exhaust enthalpy [kJ/kg].
- v_{sup} is the fluid's supply Velocity [m/s].
- v_{exh} is the fluid's exhaust Velocity [m/s].
- z_{sup} is the fluid's supply elevation [m].
- z_{exh} is the fluid's exhaust elevation [m].
- g – value is the acceleration due to gravity [m/s²].
- UA is the heat transfer coefficient or transmission heat loss coefficient of the Control Volume [kW/°C].
- S_a is the solar aperture [m²].
- V_{sol} is the vertical global south solar radiation [W/m²].
- K_o are the heat gains due to occupants' metabolic generation [kW].
- K_e are the heat gains due to electricity consumed in the control volume [kW].
- K_T are the interior heat gains (sum of occupants and electricity gains) excluding the heating gains and solar radiation gains.
- T_{in} is the indoor air temperature [K or °C].
- T_{out} is the outdoor air temperature [K or °C].
- \dot{m}_{water} is the water mass flow rate [kg].
- \dot{m}_{air} is the air mass flow rate [kg].
- c_{water} is the water specific heat [kJ/kg°C or kJ/kgK].
- $\dot{V}_{air(vent)}$ is the ventilation volumetric air flow rate [m³/s].
- $\dot{V}_{air(inf)}$ is the infiltration volumetric air flow rate [m³/s].
- ρ_{air} is the air density [Kg/m³].
- $c_{p_{air}}$ is the constant pressure specific heat of the air [kJ/kg°C or kJ/kgK].
- C_v is the infiltration and/or ventilation heat loss coefficient [kW/°C or kW/K].

- $h_{water_{sup}}$ is the water's supply enthalpy [kJ/kg].
- $h_{water_{exh}}$ is the water's exhaust enthalpy [kJ/kg].
- $h_{air_{sup}}$ is the air's supply enthalpy [kJ/kg].
- $h_{air_{exh}}$ is the air's exhaust enthalpy [kJ/kg].
- $T_{water_{sup}}$ is the water's supply temperature [K or °C].
- $T_{water_{exh}}$ is the water's exhaust temperature [K or °C].
- $Q_h = Q$ is the heating system's inputs inside the control volume [kW].
- Q_{vent} is the ventilation heat loss rate of control volume [kW].
- Q_{inf} is the infiltration heat loss rate of control volume [kW].
- U is the internal energy of the control volume [kJ].
- m_i are the different mass types within the building or control volume [Kg].
- c_i are the specific heats of incompressible materials [kJ/kg°C].
- T_i are the temperature of different mass types within a the control volume [K or °C].
- HLC is the heat loss coefficient of the building envelope [kW]
- κ is the index observation for the period consisting of N measurements of all variables (having as many measures as instants of time (t_N)).
- ϵ is the number of different materials within the control volume or building.
- t_N is N is the time at instant N .

Average Method

A. Erkoreka in 2016 [24] proposed the Average Method [23], with similarities to the ISO 9869 standard [20], to estimate the Heat Loss Coefficient (HLC) of whole in-use buildings. This method takes into account the κ observation of all heat gains inside the building, represented by $(Q + K)$, and the Solar Gains ($S_a V_{sol}$) (Equation 2.18) in specific periods where:

- There is very low solar radiation and it is possible to roughly estimate the building's solar heat gains. To minimize the uncertainty effect of roughly estimating the solar gains, these should be less than 10% compared to the sum of all the rest of the accurately measurable heat gains inside the building $(Q + K)$.
- The interior to exterior average temperature difference during the selected testing period should be higher than 15°C and never less than 10°C. Furthermore, the building's average

temperature must be the same at the start and end times of the method to make the effect of the change in internal energy of the building negligible.

In Equation 2.17, it can be seen that the longer the considered period is, the smaller the impact of the difference in the thermal level of the building on the HLC estimate. Since the internal energy of the building is a property, it only depends on the initial and final states of the building, while the denominator increases, the longer the period is. The accumulation term is very hard to estimate accurately. The proposed average method is formed by selected periods, where the initial indoor and outdoor temperatures (at t_1) and final indoor and outdoor temperatures (at t_N) are equal. In other words, both indoor and outdoor temperatures must be equal at the start and end of the periods. Thus, the average temperature between the indoor and outdoor temperatures will also be equal at t_1 and t_N . If this is fulfilled, it can be assumed that there will be no accumulated heat in the building, since the start and end points of the analysed period will have the same thermal level. Then, the energy accumulation inside the building will be negligible between these two time instants and it will be possible to ensure similar conditions, as in the stationary stage for the selected period. Since the longer the period is, the smaller the impact of the accumulation term, as proved in Equation 2.17; if the period fulfils the same initial and final thermal level conditions, applying the method to periods of at least 72 hours (three days), the accumulation term effect on the HLC will be negligible. Then, for the selected period, where $T_i(t_1) = T_i(t_N)$, the Internal Energy Variation ($U(t_N) - U(t_1)$) term can be considered equal to zero such that $U(t_N) - U(t_1) = \sum_{i=1}^{\epsilon} m_i c_i (0) = 0$. If, in Equation 2.17, the Internal Energy Variation ($U(t_N) - U(t_1)$) value is equal to zero, and taking Δt as common factor and cancelling it, Equation 2.18 is obtained. Then, through this equation the air to air HLC estimation is carried out using the Average Method.

$$HLC_{N,air-to-air} = \frac{\sum_{\kappa=1}^N (Q_{\kappa} + K_{T_{\kappa}} + S_a V_{sol,\kappa})}{\sum_{\kappa=1}^N (T_{in\kappa} - T_{out\kappa})} [kW/^{\circ}C] \quad (2.18)$$

- $HLC_{N,air-to-air}$ [kW/ $^{\circ}C$ or kW/K] is the air to air Heat Loss Coefficient of the building envelope.
- Q are all the heating and ventilating systems' energy inputs inside the building [kW].
- K_T are all the other heat gains inside the building (illumination, all other electrical device consumption, and heat gains due to people, except solar radiation and heating system gains, which are not included) [kW].
- T_{in} is the indoor air temperature [K or $^{\circ}C$].
- T_{out} is the outdoor air temperature [K or $^{\circ}C$].
- S_a is the solar aperture [m²].
- V_{sol} is the vertical south global solar radiation [W/m²].
- κ is the observation index for the period consisting of N measurements of all variables.

The second term introducing uncertainties in the method application are the solar gains of Equation 2.18. The method proposes using periods, not only with the same initial and final temperatures of the building, but also with cold and cloudy periods where solar radiation is very low and could thus be considered purely diffuse [67]. For cloudy periods, where the radiation can be considered purely diffuse, any orientation of global radiation measurement can be used, since any of these measurements will be similar to a diffuse solar radiation measurement. These periods can easily be found in countries or areas where cloudy and cold days are common in winter. It must be possible to ensure that the solar heat gains for these periods compared to the rest of the heat gains (heating (Q) plus all internal gains excluding solar radiation (K_T)) of the building are less than 10%. Then, if these roughly estimated solar gains have an uncertainty as large as 100%, their effect on the HLC estimation would only be 10%. Accurately measuring heating and internal gains is possible, while measuring solar gains accurately is a hard task. However, if only cloudy days are present in the studied period and it can be considered that only diffuse solar radiation is affecting the whole building envelope, then it is possible to make a rough estimate of the solar gains.

To do so, it can be considered that by multiplying the total window area of the building envelope by a g-value of 0.5 [68], a rough estimation of the solar aperture regarding the diffuse radiation can be obtained. Since diffuse radiation can be considered to be similar in all orientations, if this value is multiplied by the solar aperture, the internal gains created by the solar radiation can be estimated. Therefore, it is reasonably easy to make rough estimates of the ($S_a V_{sol}$) term in cloudy periods. Hence, due to the similarity between the results of $S_a V_{sol}$ and $S_a H_{sol}$ ⁶ in cloudy periods, the method could be applied using any of them indistinctly.

The Average Method has some similar characteristics regarding the mathematical estimation method used by the ISO 9869-1 method [20] for obtaining in-situ U-values of walls. The method described by the ISO 9869-1 requires the accumulated average U-value to be plotted during the periods considered valid for the estimation. On these plots, a stabilization band of $\pm 2\%$ of the final estimate during the last 24 hours of the testing period is required. Based on the mathematical development carried out in this paper for the whole building in-use HLC estimation method, due to the complexity of a whole building when compared to a single wall analysis and considering the uncertainty limits imposed, this band will be expanded to $\pm 10\%$. In other words, the proposed average method will also perform the HLC accumulated average plots for the selected periods and should be able to provide stable HLC values within a $\pm 10\%$ during the previous 24 hours in order to ensure a reliable HLC estimation.

To solve the HLC estimation through the Average Method, the required variables are obtained from five different types of sensors, shown in Table 2.1.

The measurement of the variables in an in-use building to estimate the HLC through the Average Method have associated uncertainties; all these variables have systematic errors, while some of them have both systematic and random errors, where:

⁶ H_{sol} is the Horizontal Global Solar Radiation

Typology	Sensor Measure	International System Unit
Energy Consumption	Electricity consumed within the building envelope	Wh, kWh, MWh
	Energy supplied by the Heating System	Wh, kWh, MWh
Weather	Outdoor temperature	°C
	Horizontal global solar radiation	W/m ²
Indoor Conditions	Indoor Temperature	°C

Table 2.1: Physical variables measured in the Average Method.

- The systematic errors of Q , K_e , K_o , V_{sol} , T_{in} and T_{out} can be obtained through the manufacturer's accuracy.
- On the contrary, the random errors depend on not controlled causes and should be estimated through methods to evaluate the uncertainty due to this type of errors. In the case of K_o , there are studies that allow the number of persons in a space to be predicted with high precision⁷. Since the selected periods to estimate the HLC through the Average Method are cloudy and cold, it ensures that Q , K_o and K_e have big enough value with respect to Solar Gains ($S_a V_{sol}$), so it is possible to assume associated uncertainty of less than 10% for the solar gains. For the T_{in} and T_{out} of the thermal zones within buildings, there is currently no specific method to estimate their associated random uncertainties, so it is necessary to estimate them in order to study their propagation to the HLC through the Average Method. The latter is one of the main research gaps solved in this Thesis through the proposition and testing of an innovative method to estimate these random errors for the T_{in} and T_{out} . Furthermore, the proposed method is valid to estimate the random error values for any intensive, variable such as the CO₂ ppm concentration or Relative Humidity within a building thermal zone or for the ambient surrounding a building.

HLC general expression applied to a multi-volume building

Buildings can be considered Control Volumes composed by multi-volumes or thermal zones, as is shown in the schema of Figure 2.4, where each Floor Volume (V_{F_i}) is affected by several mass and heat exchanges between other volumes, the ground or the exterior. At the same time, each Floor (F_i) can be composed by Sub-Spaces ($F_{i,j}$) or Sub-Volumes ($V_{F_{i,j}}$) with an Indoor Temperature ($T_{F_{i,j}}$), where each volume is affected by different heat and mass exchanges, coming either from other volumes, the ground or the exterior. Several heat gains and losses have been considered when estimating the Heat Loss Coefficient for a whole building enclosed in a control volume. However, the demonstration only considers the HLC estimation for a whole building with homogeneous indoor temperature.

Taking into account the building's multi-volumes, which have L floors and M sub-volumes per floor, the total HLC of the building can be estimated by applying Equation 2.19, where the HLC value of the whole building is defined as the sum of the HLCs of the individual sub-volumes ($HLC_{(F_{i,j})}$). The HLCs

⁷As an example, based on the measurement of metabolic carbon dioxide and through the use of mathematical models, it is possible to predict, with an accuracy of 94.68%, the count of human occupation indoors in a small room [25].

of these sub-volumes are estimated through Equation 2.20, which is based on the HLC estimation by applying Equation 2.18 directly to each volume as if they were only affected by $(T_{F_{i,j}} - T_{out})$. Thus, replacing Equation 2.20 in Equation 2.19 for each $HLC_{(F_{i,j})}$ term, it is possible to develop a precise estimation of the HLC of the whole building, estimating the Heat Loss Coefficients (HLC) for each volume and summing them through Equation 2.21. This estimation considers:

- The effects of the transmissions and infiltration through the walls between the volumes ($V_{F_{i,j}}$) are cancelled out in the sum.
- The effects of energy transfers through internal walls due to transmission and infiltration between the considered sub-volumes are cancelled out in the sum, and only heat and mass transfers between indoor and outdoor air are considered by the aggregation of all individual HLC values.

The analytical development to obtain this general equation has been developed in depth in the publication named 'Mathematical development of an average method for estimating the reduction of the Heat Loss Coefficient of an energetically retrofitted occupied office building' [23].

$$HLC = \sum_{i=1}^L \sum_{j=1}^M HLC_{(F_{i,j})} = HLC_{F_{0,1}} + HLC_{F_{0,2}} + \dots + HLC_{F_{0,j}} + \dots + HLC_{F_{1,j}} + \dots + HLC_{F_{i,j}} [kW/^{\circ}C] \quad (2.19)$$

$$HLC_{(F_{i,j})} = \frac{\sum_{\kappa=1}^N (Q_{h_{(F_{i,j})\kappa}} + K_{T_{(F_{i,j})\kappa}} + (S_a V_{sol})_{(F_{i,j})\kappa})}{\sum_{\kappa=1}^N (T_{in_{(F_{i,j})\kappa}} - T_{out\kappa})} [kW/^{\circ}C] \quad (2.20)$$

$$HLC = \sum_{i=1}^L \sum_{j=1}^M HLC_{(F_{i,j})} = \sum_{i=1}^L \sum_{j=1}^M \sum_{k=1}^N \frac{(Q_{h_{(F_{i,j})\kappa}} + K_{T_{(F_{i,j})\kappa}} + (S_a V_{sol})_{(F_{i,j})\kappa})}{(T_{in_{(F_{i,j})\kappa}} - T_{out\kappa})} [kW/^{\circ}C] \quad (2.21)$$

2.2.3 Co-Heating Method

The Co-Heating test [19] has existed for more than three decades and has been used for many purposes. The performance parameters of the building of interest, in the form of the Heat Loss Coefficient (HLC) and the equivalent solar aperture, are determined by applying a linear regression analysis, assuming a simplified thermal equilibrium and aggregate performance data. Therefore, we observe the aggregate performance of its components. A common method to evaluate this is the Co-Heating test. This test essentially represents an almost stationary test based on the linear regression analysis of the aggregate building performance data acquired during the appropriate

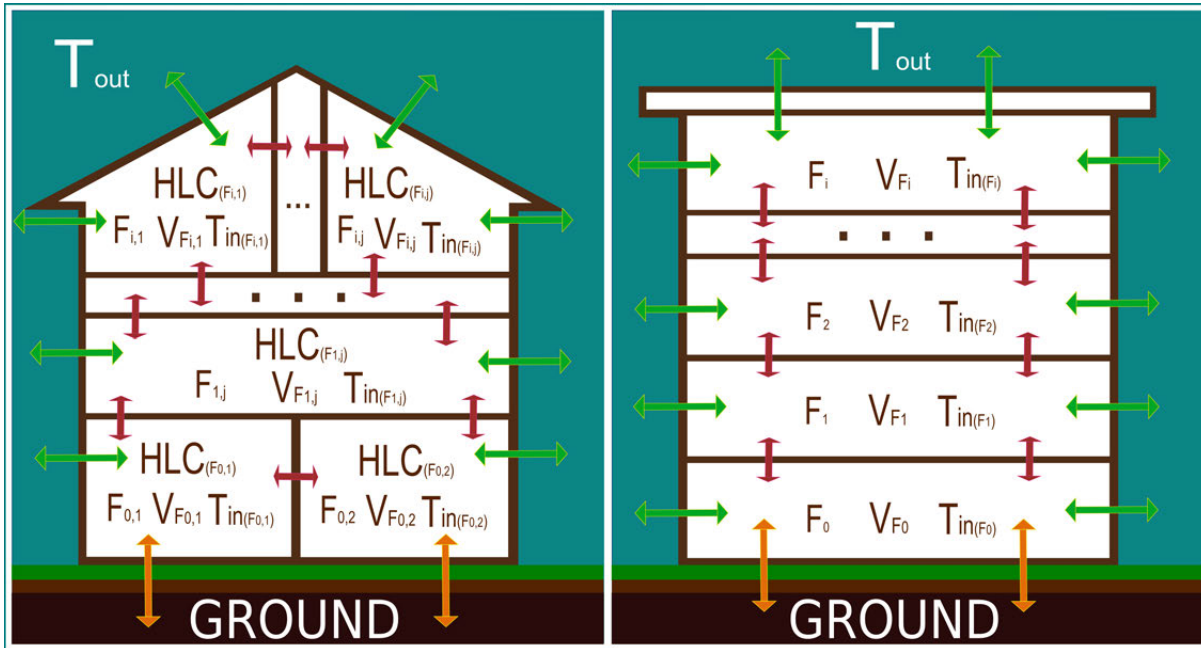


Figure 2.4: Scheme of all heat and mass exchanges through the multi-volume building.

heating experiments. During a Co-Heating test, the investigated dwelling is heated homogeneously to an indoor temperature of a steady state of 25 °C, using electric heaters and fans scattered throughout the building. The use of electrical energy, indoor and outdoor air temperatures and relative humidity, wind speed and direction, and solar radiation are controlled throughout the test. The influence of the transient effects induced by the loading and unloading of the thermal mass of the building can be reduced by carefully selecting the period of the experiment and averaging the collected data usually daily over a sufficient period.

Using the regression analysis to the daily averaged data points, the indoor and outdoor supervised conditions are related to the electric heating energy necessary to maintain a constant indoor air temperature. The coefficient that describes this relationship, representing the thermal performance characteristics of interest, is the Heat Loss Coefficient (HLC) in W/K. The total HLC constitutes a combined loss due to heat transmission and infiltration/ventilation. To decouple both, a Co-Heating test is usually combined with a blower door test or tracer gas test [19, 42, 47, 63, 69].

According to the specifications of the standard ISO 13790 [45], it is possible to obtain measurements to estimate the HLC of a dwelling through a Co-Heating test, determining the heat loss coefficient of the building envelope. The heat loss coefficient of the building achieved by the Co-Heating test has some advantages over other possible estimates of individual mechanisms of heat loss; for example, infiltration measurements [70] or point measurements (e.g., measurements of the building envelope's independent component U-values [20]).

D. Butler (2013) [19] used the regression methodology to estimate the HLC (Equation 2.22) and the solar aperture (Sa) of the whole building with reference to the south vertical global solar radiation. The Co-Heating test is carried out in winter to reduce the uncertainty effect of solar radiation on the

estimated HLC value and requires some conditions for the indoor air temperature to be kept at 25°C in order to carry out the HLC estimation. The requirements to perform the test are:

- Unoccupied Building.
- All conducts closed.
- Interior doors open.
- Exterior doors and windows closed.
- Sensors without direct solar radiation incidence.
- Indoor and outdoor air temperature difference must be superior to 10 °C ($T_{in}-T_{out}\geq 10^{\circ}C$).
- Keep indoor air temperature constant at 25°C.
- Five minute logging intervals.
- Once uniform mean temperature is achieved monitor for 1-3 weeks.

$$(Q + K_T) = HLC(\Delta T) - S_a V_{sol} \quad (2.22)$$

- Q is all heating and ventilating systems' energy inputs inside the building [kW].
- K_T is all the other heat gains inside the building (metabolic, solar and heating gains are not included) [kW].
- ΔT is the difference between T_{in} (the Indoor Air Temperature) and T_{out} (the Outdoor Air Temperature) [K or °C].
- S_a [m²] is the equivalent solar aperture of the whole building with reference to the south vertical global solar radiation.
- V_{sol} is the vertical south global solar radiation [kW/m²].

To perform this regression and obtain the HLC and $S_a V_{sol}$ of Equation 2.22, the variables are obtained from five different types of sensors, shown in Table 2.2.

All the measurements of variables in an unoccupied building to estimate the HLC through the Co-Heating Method have associated uncertainties due to systematic errors, T_{out} being, the only intensive variable that, besides having associated systemic errors, also has random errors. In the case of the T_{in} variable, its measurement does not have random errors because, during the test, the value of this variable remains constant and homogeneous in all points of the volume⁸. Since Solar Gains ($S_a V_{sol}$)

⁸The radiators heat the air mass to keep the temperature constant and the fans avoid the stratification of the air temperature to guarantee a homogeneous air temperature in the all volumes.

Typology	Sensor Measure	International System Unit
Energy Consumption	Electricity consumed within the building's envelope	Wh, kWh, MWh
	Energy consumption by the heaters and fans	Wh, kWh, MWh
Weather	Outdoor temperature	°C
	Vertical global south solar radiation	W/m ²
Indoor Conditions	Indoor Temperature	°C

Table 2.2: Physical variables measured in the Co-Heating test.

are estimated together with the HLC through the regression method, the random errors associated to the solar gains (V_{sol}) are eliminated.

2.2.4 Decoupling the building's HLC by estimating the Infiltration/Ventilation Heat Loss Coefficient (C_v) by means of the metabolic CO_2 decay method

Using the occupants' metabolic CO_2 concentration decay analysis to estimate in-use C_v , is a step forward in the attempt to decouple the estimated in-use HLC values into its Transmission Heat Loss Coefficient (UA) and Infiltration Heat Loss Coefficient (C_v), where: $HLC = UA + C_v$ (Equation 2.10) [21].

The metabolic CO_2 of the building occupants can be used as tracer gas to estimate the total air infiltration plus the ventilation volumetric flow rates by means of CO_2 concentration decay analysis, as detailed in [71]. The use of CO_2 generated from occupants as a tracer gas to determine air change rates in buildings, is described in the ASTM D6245-12 'Standard Guide for Using Indoor Carbon Dioxide Concentrations to Evaluate Indoor Air Quality and Ventilation' [72]. According to this guide, and together with the ASTM E741-11 Method [73], air change rates (or Air Changes per Hour of the analysed whole volume, ACH in [h^{-1}]) can be estimated using the tracer gas decay technique in which occupant-generated CO_2 is used as a tracer gas.

In small buildings where the indoor whole volume CO_2 concentration fulfils the ASTM method's homogeneity criteria, it would provide the total infiltration/ventilation volumetric flow rate as in Equation 2.23, where V is the total indoor volume of the building in [m^3] and ACH should be converted to [s^{-1}] to obtain Equation 2.23 units.

From Equation 2.6, the most general form of the infiltration and/or ventilation heat loss coefficient (C_v) is extracted (Equation 2.24), where, for buildings without a ventilation system, $\dot{V}_{air_{tot}} = \dot{V}_{air_{inf}}$ and $\dot{V}_{air_{vent}} = 0$. In the case of buildings with mechanical ventilation without heat recovery ($\eta = 0$), the C_v general form can be reordered as Equation 2.25, and theoretically, even without making any direct measurement in the ventilation system, it would be possible to obtain the C_v just from the ACH value estimation with the ASTM method.

$$\dot{V}_{air_{tot}} = V \cdot ACH = \dot{V}_{air_{vent}} + \dot{V}_{air_{inf}} [m^3/s] \quad (2.23)$$

$$C_v = \dot{V}_{air_{vent}} \rho_{air} c_{p_{air}} (1 - \eta) + \dot{V}_{air_{inf}} \rho_{air} c_{p_{air}} [W/^\circ C] \quad (2.24)$$

$$C_v = (\dot{V}_{air_{vent}} + \dot{V}_{air_{inf}}) \rho_{air} c_{p_{air}} [W/^\circ C] \quad (2.25)$$

However, for buildings with mechanical ventilation with heat recovery, we will again need the $\dot{V}_{air_{tot}}$ estimation by means of the ASTM method, but we will also need dedicated measurements in the ventilation system ducts to measure $\dot{V}_{air_{vent}}$ and η of Equation 2.24. For correctly compensated ventilation systems where supply and exhaust volumetric flows are equal ($\dot{V}_{air_{sup}} = \dot{V}_{air_{exh}} = \dot{V}_{air_{vent}}$), the heat recovery efficiency η for each instant can be estimated by measuring the four temperatures of $\eta = \frac{T_{air_{sup}} - T_{out}}{T_{in} - T_{out}}$. However if the ventilation system is not compensated, and the supply volumetric flow rate $\dot{V}_{air_{sup}}$ is different from the exhaust volumetric flow rate $\dot{V}_{air_{exh}}$, then it can be proven, that $Q_{vent} = \dot{V}_{air(vent)} \rho_{air} c_{p_{air}} (T_{in} - T_{out})(1 - \eta)$ will have the form of Equation 2.26. Then it will be at least necessary to measure, in the ventilation system, the supply and return volumetric flow rates and the supply (T_{sup}) and indoor (T_{in}) temperatures (See Figure 2.3). For such cases, the C_v value would be estimated as in Equation 2.27. Based on this development, it is possible to estimate the C_v for buildings with homogeneous CO₂ distribution within the whole volume. There, fulfilling the ASTM method requirements will give us the total infiltration/ventilation volumetric flow rates. However, two requirements established by the ASTM D6245-12 guide will need important research for the C_v estimation.

$$C_v = \left(\frac{\dot{V}_{air_{exh}} \rho_{air} c_{p_{air}} T_{in} - \dot{V}_{air_{sup}} \rho_{air} c_{p_{air}} T_{sup}}{T_{in} - T_{out}} \right) (T_{in} - T_{out}) [W] \quad (2.26)$$

$$C_v = \left(\frac{\dot{V}_{air_{exh}} \rho_{air} c_{p_{air}} T_{in} - \dot{V}_{air_{sup}} \rho_{air} c_{p_{air}} T_{sup}}{T_{in} - T_{out}} \right) (\dot{V}_{air_{inf}} \rho_{air} c_{p_{air}}) [W/^\circ C] \quad (2.27)$$

The ASTM D6245-12 section 9.3.1 states that the decay technique is based on the assumption that there is no source of tracer gas in the building, which in the case of CO₂ means that the building is no longer occupied. In in-use buildings there is usually one daily period where this method can be

applied. For example, when the occupants leave their house in the mornings or once office buildings are unoccupied after a working day. Thus, theoretically, every time a building is unoccupied an ACH value can be obtained that is valid for the 1 to 4 hours decay period (decay study length depends on total ventilation rate) after the building is unoccupied. During this period, there is an important knowledge gap in the ACH estimation, this value being valid for the HLC decoupling. Note that the HLC will be estimated using building monitoring data of several days in a row, since the estimated $HLC = UA + C_v$, the embedded C_v part will consider the average C_v of that whole period. However, the C_v value is not constant even during a single day, since window openings, ventilation system controls or set points variations, wind velocity and direction variations generate changes in it during the day. Thus, a rigorous research has to be done to understand the reliability of these estimated C_v values. For mechanically ventilated buildings, the ventilation part, $\dot{V}_{air_{vent}}$, can be measured continuously over 24 hours, and its corresponding $C_{v_{vent}}$ averaged for the HLC estimation period. However, the $\dot{V}_{air_{tot}}$ will only be available daily for the 1 to 4 hours discharging periods where the ASTM method can be applied. Thus, severe assumptions, such as considering the infiltration part constant or dependant on some measured variables, will have to be proved for a reliable C_v estimation and further HLC decoupling. Other aspects related to the automatic detection of the suitable periods for the decay analysis, depending on the building use, will also require a deep analysis.

The ASTM D6245-12 section 9.3.5 refers to ASTM E741-11, where the indoor tracer gas concentration at multiple points (at least two points) within the analysed volume is required to differ by less than 10% of the average concentration in the studied volume (at least at the beginning and end of the sampling period). When using CO₂, this concentration uniformity requirement should be applied to the difference between the indoor to outdoor concentration. Then, in theory, for the case of Figure 2.4, if $ACH_{(F_{0,1})}$, $ACH_{(F_{0,2})}$, ..., $ACH_{(F_{i,j})}$ are estimated by the ASTM method, those ACH values could be used to obtain the total Infiltration/Ventilation rates ($\dot{V}_{air_{tot}(F_{0,1})}$, $\dot{V}_{air_{tot}(F_{0,2})}$, ..., $\dot{V}_{air_{tot}(F_{i,j})}$). Here, there is a great challenge to the C_v estimation; since those individual ACH are affected by the CO₂ exchange between indoor volumes with different concentrations, the correlation between the CO₂ decay analysis ACHs and the real volumetric flow rates against the exterior must be obtained. In any case, through the mass conservation principle, the total sum of all the ASTM method individual $\dot{V}_{air_{tot}(F_{i,j})}$ should give us the $\dot{V}_{air_{tot}} = \dot{V}_{air_{vent}} + \dot{V}_{air_{inf}}$ of the whole building, where the inner volumes mass exchanges have been cancelled out.

2.2.5 Importance of the in-use HLC estimation and relation of the measurement uncertainty with the HLC estimation uncertainty

The HLC estimation depends on heat gains, electricity gains, occupancy gains, solar radiation gains, outdoor temperature and indoor air temperature of a building, which are shown in Equations 2.18 and 2.22. Through an optimized Monitoring and Control System (MCS) installed in a building, it is possible to obtain the measurements necessary to estimate the HLC value by reducing the measurement uncertainties due to systematic errors. However, it is also necessary to analyse the Monitoring System

(MS)⁹ based on the estimation of the measurement uncertainty due to random error. Thus, knowledge of the overall uncertainties of the measurements is necessary to obtain as reliable a value for the HLC as possible, where the overall uncertainty includes the uncertainties due to systematic and random errors. For this, it is necessary to install enough sensors with a good accuracy to obtain the measurements to estimate the HLC value: interior and exterior air temperature, energy consumptions and solar radiation; and also, to estimate the measurement uncertainty due to systematic and random errors.

The identification of all measurement uncertainties collected by the sensors to obtain the HLC value, allows us to know, with a certain confidence level, what the HLC estimation error is. To do so, it is necessary to estimate the overall uncertainties of the HLC function's variables based on Equation 2.28¹⁰ ($HLC = f(Q, K_e, K_o, S_a H_{sol}, T_{in}, T_{out})$), where it is possible to obtain this Equation if averaged variable values are used for the period, t_N . Once the uncertainties of these variables have been estimated, it is necessary to propagate these uncertainties in the HLC function, taking into account that its variables are not independent of each other. In this way the propagation of the HLC Uncertainty (U_{HLC}) would be estimated based on the propagation error exposed by Taylor [74]. Thus, it is possible to calculate the HLC_{range} (Equation 2.29 and Equation 2.30) taking into account all the uncertainty sources of the different variable measurements in the HLC error. This allows us to obtain the representative reliable value of the HLC, which will be in a range of values.

Estimating reliable in-use HLC values of buildings is important to better understand their energy efficiency, and to permit the generation of reliable Energy Performance Certificates (EPCs), which can be employed as a tool to determine the discrepancies between performances at the design and operation phases of buildings. This is an important reason to estimate the HLC values with the greatest precision and accuracy as possible, which is why it is necessary to know all the uncertainties associated to HLC estimation.

$$HLC = \frac{\sum_{\kappa=1}^N (Q_{\kappa} + K_{T_{\kappa}} + S_a V_{sol,\kappa})}{\sum_{\kappa=1}^N (T_{in\kappa} - T_{out\kappa})} = \frac{\sum_{\kappa=1}^N \frac{(Q_{\kappa} + K_{T_{\kappa}} + S_a V_{sol,\kappa})}{N}}{\sum_{\kappa=1}^N \frac{(T_{in\kappa} - T_{out\kappa})}{N}} = \frac{\overline{Q} + \overline{K_T} + \overline{S_a V_{sol}}}{\overline{T_{in}} - \overline{T_{out}}} [kW/^{\circ}C] \quad (2.28)$$

$$HLC_{range} = HLC \pm U_{HLC} [KW] \quad (2.29)$$

$$HLC - U_{HLC} \leq HLC_{range} \leq HLC + U_{HLC} [KW/^{\circ}C] \quad (2.30)$$

Where,

- HLC_{range} : Maximum and Minimum limits within which is the representative value of the Heat

⁹The Monitoring System (MS) is composed of the equipment used to measure variables and collect data, through the Control System (CS), which is made up of hardware, so that actuators and software, the data from the sensors can be collected and processed to control a process [25].

¹⁰In Equation 2.28, the \overline{Q} , $\overline{K_T}$, $\overline{S_a V_{sol}}$, $\overline{T_{in}}$ and $\overline{T_{out}}$ are the average values for the studied period (t_N)

Loss Coefficient of an in-use Building can be.

- U_{HLC} : HLC uncertainty, obtained by the error propagation of the different uncertainty sources of each of the variables [kW/K].

2.2.6 Error propagation

The propagation error for the addition and subtraction [74] for the Equation 2.28, first is estimated through Equation 2.31, where all terms' uncertainties are considered, including that of the roughly estimated solar gain. Finally, the propagation error for division in Equation 2.32 must be calculated to estimate the propagation error when estimating the HLC of the building or of a volume within the building. This equation should be also evaluated based on the general equation of the statistical error through the Taylor theorem [74].

$$HLC = \frac{(\overline{Q} \pm \delta\overline{Q}) + (\overline{K_T} \pm \delta\overline{K_T}) + (\overline{S_a V_{sol}} \pm \delta\overline{S_a V_{sol}})}{(\overline{T_{in}} \pm \delta\overline{T_{in}}) - (\overline{T_{out}} \pm \delta\overline{T_{out}})} = \frac{(\overline{Q} + \overline{K_T} + \overline{S_a V_{sol}}) \pm (\delta\overline{Q} + \delta\overline{K_T} + \delta\overline{S_a V_{sol}})}{(\overline{T_{in}} - \overline{T_{out}}) \pm (\delta\overline{T_{in}} + \delta\overline{T_{out}})} [kW/^\circ C] \quad (2.31)$$

$$HLC_{range} = \frac{(\overline{Q} + \overline{K_T} + \overline{S_a V_{sol}}) \pm (\delta\overline{Q} + \delta\overline{K_T} + \delta\overline{S_a V_{sol}})}{(\overline{T_{in}} - \overline{T_{out}}) \pm (\delta\overline{T_{in}} + \delta\overline{T_{out}})} [kW/^\circ C] = \frac{\overline{Q} + \overline{K_T} + \overline{S_a V_{sol}}}{(\overline{T_{in}} - \overline{T_{out}})} \pm \left| \frac{\overline{Q} + \overline{K_T} + \overline{S_a V_{sol}}}{\overline{T_{in}} - \overline{T_{out}}} \right| \left(\frac{\delta\overline{Q} + \delta\overline{K_T} + \delta\overline{S_a V_{sol}}}{|\overline{Q} + \overline{K_T} + \overline{S_a V_{sol}}|} + \frac{\delta\overline{T_{in}} - \delta\overline{T_{out}}}{|\overline{T_{in}} - \overline{T_{out}}|} \right) [kW/^\circ C] \quad (2.32)$$

2.2.7 Sensor accuracy of Monitoring Systems (MSs) used in an experimental test to estimate the building envelope HLC for an in-use building

In order to have a reference from and know the current accuracy of the experimental test to estimate the HLC, this section presents the sensors used in a large, occupied office building (Table 2.3), together with the communication protocol, hardware, and software (Table 2.4) that was implemented. The MCS was implemented in a public building of the University of the Basque Country under the 7th Framework Program for Research (FP7) [75] project A2PBEER [76, 77], in which an energy characterization [24] was carried out. This building has been retrofitted and is currently being energetically monitored. Their MCS had not implemented any Fault Detection and Diagnostic (FDD) methods.

This project is a sample of how the automation of buildings is being implemented in research. This example, and the literature studied in the next section, demonstrate the need to implement MCSs in experimental tests to obtain the energy characterization of the building envelope and a correct estimate of the HCL.

Typology	Measurement	Device Identification	Accuracy
Energy Consumption	Heating system	7 Calorimeter: Kamstrup Multical 602 for heating; F0 1 calorimeter; F1, F2 and F3 2 calorimeters per floor, for the set sensors	$E_T \pm (0.4 + 4/\Delta T)\%$
	Lighting system	4 Electricity Power Meter: 1 ABB EM/S 3.16.1 meter, 3 ABB A43 meters (1 per floor)	$\pm 2\%$ for all
Indoor Conditions	Illuminance (lux)	13 Illuminance sensors: Siemens 5WG1 255-4AB12	- - -
	Air Quality (ppm CO ₂)	13 Air quality, temperature and humidity sensors: ARCUS	$\pm 1\%$ Measurement Error
	Temperature (°C)	SK04-S8-CO ₂ -TF	$\pm 0.5\text{ }^\circ\text{C}$
Weather	Relative Humidity (%)		$\pm 3\%$ RH
	Illuminance (lux)	1 Weather Station on roof: ELSNER 3595 Sun tracer KNX basic	$\pm 35\%$ at 0...150,000 lux
	Temperature (°C)		$\pm 0.5\text{ }^\circ\text{C}$
	Wind Speed (m/s)		$\pm 25\%$ at 0...1.5 m/s
	Rain (yes/no)		- - -
	Temperature (°C)	1 Outdoors temperature and humidity sensor on roof: ARCUS	$\pm 0.5\text{ }^\circ\text{C}$
	Relative Humidity (%)	SK01-TFK-AF	$\pm 3\%$ RH
Global Solar Radiation (W/m ²)	1 Pyranometer on roof (horizontal radiation): ARCUS SK08-GLBS	$\pm 5\%$	

Table 2.3: Monitoring system of a public building of the University of the Basque Country.

Typology	Technology	Device Specifications	Descriptions
Communications	KNX Protocol	Bus KNX	The installation is based on device communication via a communication bus KNX that will allow communication between all the devices present in the installation.
	Cable	Twisted pair (TP1) of the type Y (St) Y 2×2×0.8 mm ²	Red (+) and black (-) for the bus line. The two remaining wires are yellow and white, which will be used for additional applications, additional power supply of certain components, or as an additional bus line or reserve for breakdowns.
Hardware	KNX/IP Interface	Weinzierl 730	Four lines of the Measuring System and of the lines set out are done through IP connections. Each line has a KNX/IP Interface located on the KNX board of each floor.
	Web Server	For the control and monitoring of the installation, the Cambridge Studio Evolution Server (CBSE) of IPAS is used	This device must be connected to a LAN network of each building and provided with Internet access. It communicates with the KNX network using KNX/IP gateways.
	Switch and router	Used by university	The university has several routers and switches that were used.
Software	Specific KNX software tool	Unique Standard Application for Programming KNX Systems Software	The programming occurs in two different phases. The first phase is the creation of the topological structure of the installation, parametrization of the devices, and assigning of the physical addresses and groups. The second phase consists of the physical programming of the installation directly into the building.

Table 2.4: Control system (CS) of a public building of the University of the Basque Country.

2.3 Analysis of the state of the art of Monitoring and Control Systems (MCSs) implemented to estimate the Heat Loss Coefficient (HLC)

To guarantee transparent EPCs for minimum Energy Performances of Buildings (EPB), it is necessary to estimate the energy performance using specific methodologies in order to determine the energy efficiency level of buildings. Physical data collected from the sensors of a monitoring system are necessary for this purpose. This section will focus on the study of energy monitoring systems used in projects to estimate the Heat Loss Coefficient (HLC) with two methods: the Averaging Method [24] and the Co-Heating Method, or similar [19, 47].

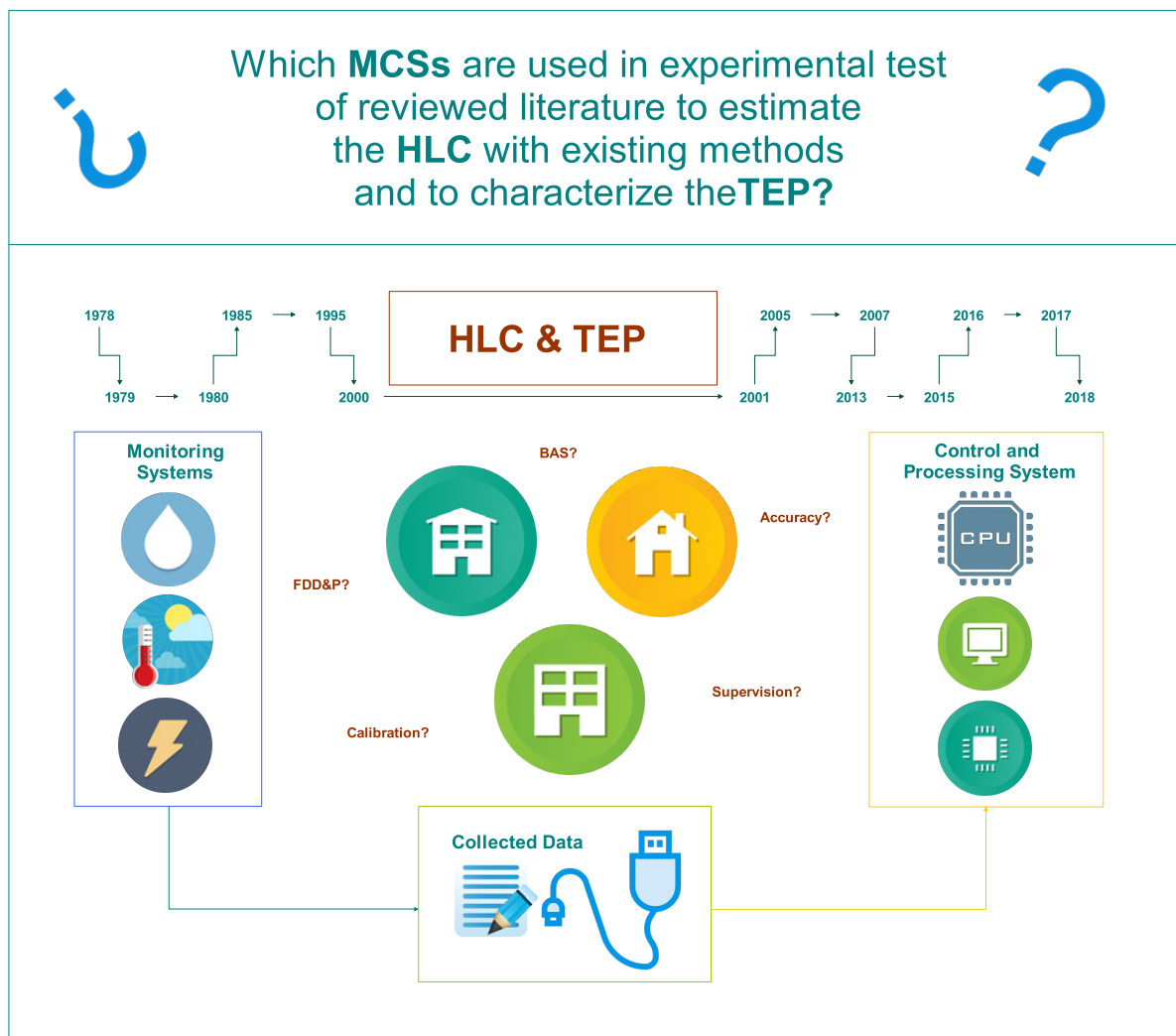


Figure 2.5: Scheme of MCSs used in reviewed literature to estimate the HLC and characterize the TEP.

The analysis of the state of the art carried out begins with a review of building automation, communication protocols, sensors and the fault detection methods most used in building control systems. This gives a perspective on the monitoring and Control of the system that is necessary in building automation. In order to identify and analyse the MCSs implemented in current research projects, a review of the literature was undertaken that, through experimental tests, estimated the

HLC using the Average Method, the Co-Heating Method, and other methods to characterize the TEP. This reviewed literature allowed the equipment that makes up the MCSs, and that is used to collect and process the physical variables in these experimental tests, to be identified. Figure 2.5 shows an abbreviated outline of the development of this section.

Building Automation

The Building Control System, also termed the Building Automation System (BAS) or Building Management System (BMS), is the control system composed of integrated hardware and software networks that monitors and controls the indoor climatic conditions in building facilities [26].

The Building Automation System (BAS) is installed to monitor and control the heating, cooling, ventilation, air conditioning, lighting, shading, life safety, alarm security, and other building systems [78]. The system can be divided into four areas: applications, hardware, communications, and oversights [48]. The BAS is a part of the Intelligent Building, where this 'intelligence' implies capturing the current state of the building and its devices through the collection of physical variables and signal processing to make the appropriate adjustments, so that the building inhabitants experience increased marginal utility in terms of comfort and energy cost. Intelligent buildings increase this marginal utility through sensor system integration, computer automation, information and communication systems, smart home appliance devices, and new materials [79].

'Domotic' is another term frequently used in reference to building automation; it is defined by S. Millán-Anglés [80] as 'a scalable set of services integrated into the home that are provided by systems that can configure one or several internal networks of the habitat and that, in turn, can communicate with networks outside the home'. These services have functions related to energy saving, the technical management of facilities, information, communication, leisure, accessibility, assistance, comfort, and more.

Georgios Lilis [81] defined three hierarchical level of functionality in a BAS. The management level is where all information is collected, aggregated, and represented for further management by the operator. The automation level includes the entire infrastructure for controlling and applying the management of the data or system supervision, in which interacting devices range from environmental sensors for luminosity, humidity, temperature, presence, and so forth, to actuators controlling passive devices and environmental parameters such as heating, lighting, and access to premises. Finally, the field level is where all the end-devices and field buses, which interface the physical world and are used in the automation of industrial processes and buildings, and which are limited solely to point-to-point communication within the BAS, belong.

The functions of a Building Automation System (BAS) generally include the Heating, Ventilation and Air Conditioning systems (HVACs); domestic hot water; lighting system control; shading systems control; energy conversion and storage (heating and cooling); onsite power generation; monitoring and data acquisition; and communications and security management [82]. Building automation integrates technology in a closed space with intelligent designs, which in turn can be integrated by

indoor and outdoor communication networks—wired or wireless—so that energy management is efficient and includes the air conditioning and boiler controls, awning controls, and electric shutter and electricity management.

Economic and legal restrictions regarding energy consumption and environmentalism define building energy borders [79]. House system optimization is possible through the Control System of the BAS, which helps to improve the comfort of the occupants while reducing the energy consumption and expediting the operation, monitoring, and maintenance of the building [78]. The reduction of electricity consumption and improvement in the occupant comfort level make the building an energetically efficient system, which is largely achieved by the interaction of a wide range of sensors that such collect physical variables, as the temperature, CO₂ concentration, zone airflow, daylight levels, occupancy levels, and so forth [48]. Even so, energy management is conditioned by user behaviour and comfort conditions have to take into account the lighting control and heating and cooling system control in the building automation.

Protocol communication used in a Building Automation

Communications play a major role in enabling building-wide controls. The communication protocols let communication between devices occur, and are central to data transmission in order to share essential information that allows effective control functioning. This transmission uses physical media through which control information and commands pass between devices via twisted-pair wiring or wireless devices, and has a substantial impact on the installed cost of building controls in building automation systems [48]. Table 2.5 shows various analogies between the wired and wireless communication protocols.

Wired	Wireless
High bandwidth	Low-medium bandwidth
High performance	Higher latency
Robust	Interference
Reliable	Unreliable by nature
Installation expensive	Installation cheap
“Unlimited” resources	Low power, memory
Static network	Mobile network
Less security problems	More security problems

Table 2.5: Differences between the Wired and Wireless communication protocols [78].

Today, building automation systems can be created using a multitude of different standards. In the 2010 International Symposium on Industrial Electronics organised by the Institute of Electrical and Electronic Engineers (IEEE), the main building automation protocols were identified as [83]:

1. KNX is an international standard (ISO/IEC 14543-3), European (CENELEC EN 50090 and CEN EN 13321-1) and Chinese (GB/T 20965), open for control in both commercial and residential buildings [84];

2. LonWorks standard is based on the scheme proposed by LON (Local Operating Network). The standard has been ratified by the American National Standards Institute (ANSI)(ANSI) organization as official in 1999 (ANSI/EIA 709.1-A-1999 [85]);
3. The Data communication protocol for Building Automation and Control Networks (BACnet) was developed under the auspices of the American Society of Heating, Refrigerating and Air-Conditioning Engineers (ASHRAE) 13 5-1995-7 and was published in 1995. The BACnet standard has the objective of providing a solution to the systems of automation and control of buildings of different sizes and types [86];
4. EnOcean is the standard based on the Institute of Electrical and Electronics Engineers (IEEE) 802.15.4. Here the modules based on EnOcean technology combine micro power converters with very low power electronics. This technology allows wireless communication between wireless sensors without batteries, switches, controllers and gateways. EnOcean is a wireless energy capture technology used in building automation systems and other industrial applications, transportation, logistics and smart homes [87];
5. Zigbee specifies a set of high-level wireless communication protocols with low-power digital transmission, based on the IEEE 802.15.4 standard for Wireless Personal Area Networks (WPAN) [88].

Currently, the BACnet, LonWorks, KNX and ZigBee technologies (based on IEEE 802.15.4) have attained considerable weight in the global market, as KNX has a strong presence in the European market [28]. Other technologies frequently used in BAS are:

1. INSTEON is a domotic network technology designed by SmartLabs, Inc. (Irvine, CA, USA). It is designed to allow devices such as switches, thermostats, sensors (movement, heat, smoke etc.) to be connected in a network through the power line and the radio frequency [89];
2. Modbus is a communications protocol located at level 7 of the Open System Interconnection (OSI) Model, based on the master/slave architecture (Remote Terminal Unit), or client/server (Transmission Control Protocol/Internet Protocol (TCP/IP)), designed in 1979 by Modicon for its range of Programmable Logic Controllers (PLCs). Developed into a de facto standard communications protocol in the industry, it has the greatest availability for the connection of industrial electronic devices [90];
3. Z-Wave is a wireless communications protocol used mainly for home automation. It is a mesh network that uses low-energy radio waves to communicate from one device to another, allowing wireless control of appliances and other devices [91].

The low-power wireless communication protocols such as EnOcean and Z-Wave are generally used in home automation and industry. Similarly, INSTEON is not restricted and gives support for wireless communication, and, while it is generally used for home automation, it is not limited to this [78]. According to a report from the Superior Council of Scientific Investigations (CSIC) of Spain (CSIC

report (2014)) [80], the most used communication protocols are Wifi, Ethernet, and Bluetooth. As for the control protocols, these are the European Installation Bus and KNX.

On the other hand, the most used framework platforms are Lonworks, Universal Plug and Play (UPnP) architecture, which is an open architecture and allows the interconnection between devices such as personal computers, home appliances, consumer electronics devices and wireless devices [92].

Moreover, Open Services Gateway Initiative (OSGi), which began in 1999 as a set of standards for a Java-based service framework that could be managed remotely, was originally conceived as a gateway to manage smart devices and other Internet-enabled devices in the home [93].

Gateways are used to translate the protocol information used in an initial network, to the protocol used in the destination network. The approach based on gateway has several disadvantages, storage of large mapping tables is required, and this is a factor that limits the scalability of the BAS, since the effort required for configuration and maintenance increases with the translation of all the relevant data points that are incorporated from the appropriate segments. This is a significantly large mapping table to be stored and can be a limiting factor with respect to BAS scalability. In addition, having a front door can introduce a single point of failure and a security risk [94]. The literature demonstrates designs for multi-protocol devices, since this is a gateway-free solution that eliminates the need for specialised gateways for inter-protocol communication, increasing the potential product range available for each manufacturer and decreasing the installation cost and number of devices needed for building automation [94].

Unfortunately, protocols used in building automation are often not compatible with each other; therefore, inter-operation across system boundaries requires special gateway solutions. To counteract these limitations, several middleware solutions have been developed that allow the communication of adjacent sides so there is abstraction of the specific details of the provider of the BAS components [95]. This solution (Middleware) is a software that allows interaction and communication between various applications or packages of programs, networks, hardware, and/or operating systems. The communication hid the heterogeneities of the software resources, operating system, protocols, etc., determining the interoperability between them [96].

Currently, there is no intrusion detection and prevention available for the BAS networks, which are increasingly extending their functionalities and their connection to internet. This significantly increases the exposure of BAS networks to cyber-attacks due to the significant increase in the attack surface. This also increases the interconnection between communication protocols due to the increase in information services and advanced network technologies. The need for Cloud Computing and Fog Computing also increases in order to provide solutions for the automation of final physical devices [97]. This allows integration on the Internet through a virtual representation, namely the vision of the Internet of Things (IoT) [98]. The building automation devices are considered for an integration in the IoT in order to have a smart and sustainable building operation [99]. In addition, the main difference between Cloud and Fog computing is that the former the Cloud computing 'refers to

both the applications delivered as services over the Internet and the Hardware and Systems Software (HS) in the data centres that provide those services' [99], while Fog computing is a 'paradigm that extends Cloud computing and services to the edge of the network. Similar to Cloud, Fog provides data, computing, storage, and application services to end-users' [100].

Sensors used in Building Automation

The sensor systems are required in advanced intelligent buildings to provide comfort, high performance and automation, energy and resource savings, and security [79]. In 2010, many modern automated buildings contained a limited number of wired sensors in such control systems as BACnet or LonWorks. This is mainly because the wired sensors need additional wiring for each sensor, which is a significant barrier in wired sensor deployment due to the increased installation cost. The entrance into the market of low-cost wireless sensors without a need for wire has opened up opportunities in the market to increase the number of connected sensors in buildings, thus allowing for improved sensing of the different necessary variables to achieve efficient and effective automation and consequently improve user comfort [101].

For the correct control of the interior conditions, a considerable number of sensors is necessary to control unwanted levels by the users and to achieve optimum levels in the use of energy. It is also necessary to use optimal control techniques in the system and throughout the building to achieve the levels of performance necessary to ensure that the conditions inside the building are of high quality with a minimum consumption of net energy [48, 78, 79, 102].

Previous research has specified the use of sensors and meters for controlling building performance, where the most installed environmental sensors are those measuring temperature, Relative Humidity (RH), and Carbon Dioxide (CO₂), which are used to control the HVAC operation. This control through environmental variables looks to maximize user comfort with an optimal performance of the HVAC systems [82]. The sensor used to meter electrical power/current is one of the most important types of sensor employed for monitoring energy efficiency. Table 2.6 shows a list of the main sensors and meters used for control in building automation.

In the literature, there is no specification of the monitoring system necessary to estimate the energy performance of a building's envelope using a specific methodology, according to Article 3 of the EPBD [17]. However, there are many studies that have been carried out to estimate the HLC in order to characterize the building's thermal envelope performance, together with other estimations to characterize the energetic behaviour of the building envelope. The monitoring systems needed to measure the user's behaviour and comfort are studied in depth in many papers through the control of heating, cooling, and lighting systems, measuring the electrical consumption of homes and buildings in order to know the energy performance of the users. In the next section, we will present the monitoring system necessary to estimate the HLC using the Average Method [24] and the Co-Heating Method or similar method [46, 47] and will present a review of different monitoring systems used in different studies developed to estimate the HLC.

Typology	Sensor Measure	International System Unit
Total Consumption:	Electricity Consumption	Wh, kWh, MWh
	Energy Consumption for Heating	Wh, kWh, MWh
	Water Consumption	L, m ³
	Fuel Consumption	Wh, kWh, MWh, L, Nm ³ , m ³
Weather:	Temperature	°C
	Relative humidity	%
	Global Solar Radiation	W/m ²
	Wind Velocity	km/h
	Wind Direction	(0°–360°)
Indoor Conditions:	Temperature	°C
	Relative Humidity	%
	CO ₂ Concentration	ppm
	Illuminance Level (Lux)	lux
Building Systems:	Fluid Temperature of Circuit: AHU/HVAC and Hot Water	°C
	AHU/HVAC Relative Humidity	%
	Flows	L/s, m ₃ /s
	Pressures	kPa, Pa
	Presence Sensors	0–100%, 0–1, ON/OFF, 0/1
	CO ₂ Sensors	0–100%, 0–1, ON/OFF, 0/1
Frequency to Collect Data	High, Medium and Low Frequency	s, min, h, day, month, year

Table 2.6: The main sensors and meters used for control in building automation based on previous research [24, 82].

Fault Detection and Diagnostics (FDD), prognostics and calibration in Building Monitoring Systems

Evaluating uncertainties in a test can lead to comprehension errors due to the absence of knowledge about the “true” value of a measured variable, especially systematic errors due to the absence of a reference between the true value and the measured value. The true value of a measurement can never be known, but when the HLC of a building is estimated, it varies in an unknown way and is difficult to predict, and this makes it difficult to assess the uncertainty of the estimate [103]. Some authors have studied the uncertainty in the calculation of the HLC, such as Stamp S. [104], who investigated the uncertainties related to solar gains through field tests and simulated Co-Heating tests.

Sensor errors greatly affect the performance of control, diagnosis, and optimization systems within building energy systems, negatively affecting energy efficiency. Calibrated measurements improve the accuracy of energy performance analysis for a building energy system by up to 18% [105]. It

has been reported that the exponential increase of the number of maintenance requests for building energy systems in the past decades is due to an increase in building operational faults [106]. Typical operational faults may arise from improper installation, equipment degradation, sensor offset or failures, or control logic problems. The latter can be split into several categories: control faults, sensor offset, equipment performance degradation, fouling faults, stuck faults, and others [107].

Table 2.7 shows the impact of sensor errors in a monitoring system, which reflect the need to implement and integrate a tool to detect, predict, diagnose and calibrate the sensor and monitoring systems in all building automation systems in an integral way.

Reference	Error and Fault Analysed	Impact
R. Zhang, T. Hong [108]	Outdoor air temperature sensor errors and thermostat errors on energy consumption.	Increase in cooling energy consumption by 0.8–13.6%, combined cooling and heating energy consumption increases 19.07–34.24%.
J. Verhelst, G. V. Ham [109]	HVAC performance under the fault sensors and actuators in a concrete core activated office building.	Economic impact from +7% to +1000% due to simultaneous sensor and actuator faults (realistic, randomly distributed and non-correlative).
K. Roth, D. Westphalen [110]	Identify thirteen key faults based on literature review, developing bottom-up energy impact range.	Increase of 4–18% in the annual energy consumption of the sum of commercial building HVAC, lighting, and refrigeration energy consumption. It is consistent with the typical range of energy waste reported in building commissioning studies.
J.Y. Kao, E.T. Pierce [111]	Simulation of error effects in the sensors of automatic controls for HVAC systems, in an office building of lightweight construction.	In annual building-energy requirements, an increase of 30–50% attributable to an air handling system.
W. Kim [112]	Fault detection and diagnosis for air conditioners and heat pumps based on virtual sensors.	Reduction of approximately 20% of the cooling capacity and 15% of the energy efficiency if the refrigerant undercharging is in the range of 25%.

Table 2.7: Examples of impacts produced by sensor errors in some study cases.

Automated Fault Detection and Diagnosis (AFDD) is an area of investigation concerned with automating the processes of detecting faults [113], whereby faulty operations, degraded performance, and broken components in a physical system are detected and understood. AFDD tools are based on algorithms that process data to determine if the source of the data is experiencing an error. The tool can be passive if the operation of the equipment/system is analysed without modifying any reference

points or control outputs, or active if the changes are made automatically to produce or simulate the operating conditions of a wider range of conditions that could not be modified for some time in a normal operation [48]. The impact of the failures allows the determination of the priority of repairs, directly affecting the reduction of energy use and costs and achieving greater comfort and useful life of the equipment, as well as a reduction in service costs. The severity of the failure and its impact on energy consumption must be considered in order to prioritize repairs. Assessing the failure or evaluating the impact (energy and cost) is one of the main steps in the AFDD process. However, determining the severity of the failure is difficult because, in many cases, the information necessary to perform the evaluation is not readily available [113].

The sensor and control performance can degrade without automated monitoring and fault detection. The number and range of the types of sensors installed in buildings today is inadequate to provide sufficient automated (or even visual) monitoring. Performance monitoring, automated fault detection and diagnosis, commissioning, optimal control, and the use of developed environments, design tools, and trainers are complementary technologies, with a notable potential to realize significant energy savings and other performance improvements in commercial buildings, including existing buildings [48]. All sensor systems are facing a noticeable upward trend in performance requirements for maintenance, downtime, reliability, fault tolerance, fault recovery, and adaptability [79].

The main fault detection and calibration methodologies in building systems include fan coils, HVACs, heat pumps, air conditioners, commercial refrigerators, lighting, water heaters, chillers and cooling towers, AHUs, and VAV boxes [113].

The AFDD methods can be classified into quantitative model-based, qualitative model-based, and process history-based methods [113–115] (Figure 2.6). The history-based process is the most used when the theoretical model of system behaviour is inappropriate to explain its behaviour, or it is not easy to create the model. In this AFDD method, the Black Box is the most used because of its simplicity. The qualitative model-based (rule-based) method is the second most used AFDD method. The quantitative model-based method needs a precise mathematical model of system behaviour and reliable sensors for the acquisition of data—as it is the most complex model and the least popular, it is more often used for industrial purposes than building landscapes. There are also AFDD methods that combine these three methods, which are used to improve the efficiency of individual methods and detect failures simultaneously (e.g., rule-based combined with statistical methods to reduce the noise, disturbances, and uncertainty of monitoring) [113].

AFDD can be integrated into an automatic start-up process. Start-up (new buildings) and commissioning (existing buildings) involve functional tests carried out to determine if a device or system is working correctly. In the commissioning process, the proper functioning of the equipment is verified by observing a series of functional tests; however, it is not guaranteed that the equipment can continue to function properly. Only continuous monitoring of the state of the equipment and its performance can guarantee continuous operation. The AFDD system constantly monitors the equipment and identifies failures and loss of performance, and is a fundamental system in the commissioning of

buildings. While the intervention of a human operator or repair technician is essential to complete the start-up cycle, without the automated monitoring system operating continuously many problems may not be detected for days, weeks, months, or even years [48].

All studies on the reviewed fault detection and calibration of monitoring systems did not apply AFDD methodologies in the energy monitoring system to characterize the TEP or to understand the energy efficiency of in-use buildings' envelopes through HLC estimation. The methods currently lack a holistic approach to predict the global impacts of faults at the building level [113].

2.3.1 Literature review's study of Monitoring and Control Systems' (MCSs) equipment used in research projects to estimate the Heat Loss Coefficient (HLC) and characterize the Thermal Envelope Performance (TEP) of Buildings

In order to know the MCSs used to measure the physical variables necessary to estimate the HLC and TEP, a range of literature has been selected. The purpose of this selection is to identify the sensors, controls, hardware and software employed in research studies to determine, for example, what kind of accuracy and technical sheet the used sensors have. In addition, the technology used is analysed in the discussion section to understand the possibility of implementing the MCSs used in BAS and domotic systems to characterize TEP.

The choice of literature took into account several requirements to ensure the literature was based not only on an analytical study of HLC estimation and TEP characterization, but also had an experimental basis. The experimental basis should be specific to buildings, housing or prototypes. Within the selection, studies based on simulations or that are purely theoretical or analytical were not taken into account. The requirements for the research to be considered were:

- 1) Studies based on experimental tests of buildings, houses, or prototypes on a small scale.
- 2) Studies that were developed with the objective of characterizing TEP in experimental buildings, houses or prototypes on a small scale, and that also used one or more of following methods:
 - a) Co-Heating Method.
 - b) Energy Balance.
 - c) Average Method.
 - d) Other methods (e.g., statistical methods) for estimating the building envelope energy behaviour, but that also include at least one of the following studies:
 - Energy Consumption.
 - Energy Balance.
 - Infiltration.
 - Local U-Value.

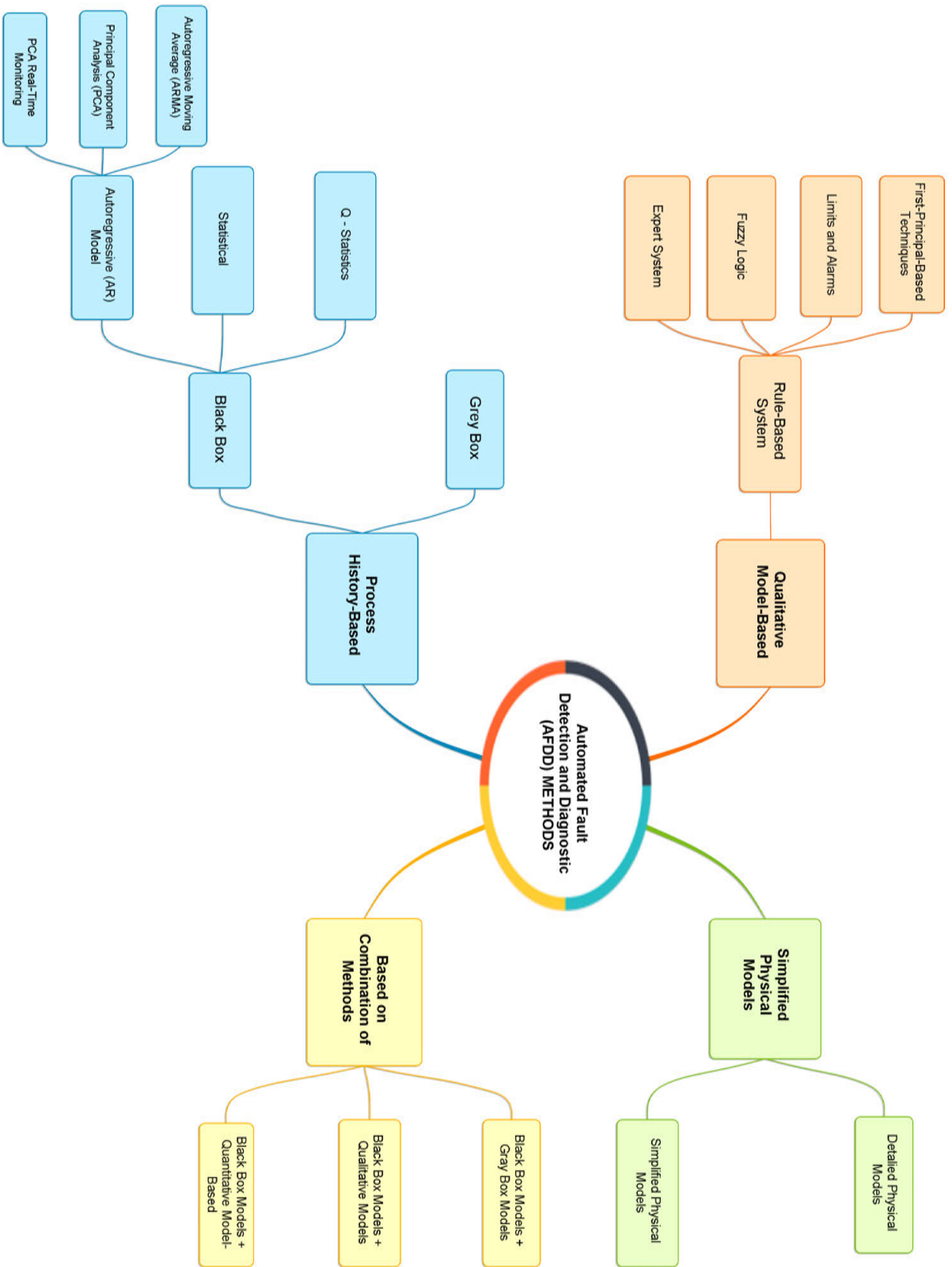


Figure 2.6: Classification scheme for AFDD methods based on previous research [113, 114]

- Other energy analysis (e.g., estimation of the heat dynamic of buildings).

Table 2.8 shows the relationship of the references selected for this study with the corresponding methods and studies carried out from 1978–2018. The references include reports, journal articles, and conference publications. The literature that was studied includes reports of the first studies of the Co-Heating Method in the 1970s [49], developed by the U.S. Energy Department [116], which analysed the sensors, controls, instrumentation, hardware and software necessary for MCSs to achieve HLC estimation and other buildings' envelope energy behaviour parameter estimation to characterize the TEP of buildings. Moreover, in the second decade of the 21st century, an increase in experimental tests was observed, with a greater concentration of publications occurring in 2015, 2016, and 2017. A study from 2018 [117] exists in which a sensitive analysis was carried out to determine the level of uncertainty in the HLC estimation due to the measurements obtained by the sensors. This type of analysis is necessary in order to identify which type of sensors should be implemented in the MCSs of buildings in order to characterize their TEP.

Table 2.9 shows the sensors, controls, hardware, software, and devices used in the experimental tests of each selected reference, together with the verification of the FDD method that was used, which was not implemented in any of the experimental tests studied. In the next section, the results and analysis of MCSs are developed through qualitative and quantitative analyses. Additionally, the methodology and criteria used to obtain the results are described.

		TEP CHARACTERIZATION THROUGH									
Reference	Publication Year	HLC Estimation				Estimation of Building Envelope Energy Behaviour Through					
		Co-Heating Method	Regression Method	Average Method	Corrected Average Method	Energy Consumption	Energy Balance Estimation	Infiltration Estimation	U-Value Estimation	R-Value Estimation	Other Estimations and Methods^{1,1}
[49]	1978	X				X		X			
[118]	1979	X									
[119]	1979	X									X
[120]	1980	X						X			
[121]	1985		X				X	X			X
[18]	1985		X				X				X
[122]	1995										X
[7]	2000	X				X					
[123]	2001					X					
[124]	2005	X									
[6]	2007	X									
[125]	2013	X						X	X		
[126]	2015	X									
[127]	2015										X
[128]	2015	X						X			
[129]	2015					X	X				X
[130]	2016	X						X	X		
[24]	2016		X		X						
[131]	2016	X							X		
[132]	2017	X									
[133]	2017	X						X	X		
[134]	2017		X	X							X
[135]	2018	X									
[117]	2018	X									

Table 2.8: List of publications used in the MCS to characterize the TEP of in-situ buildings through HLC estimation and other estimates used to determinate energy behaviour of the buildings.

Reference	Publication Year	Type of publication	FDD	Sensors														Actuators		Control System				Other Devices																							
				Indoor Air Temperature	Surface Temperature(out and indoor)	Indoor CO ₂	Indoor Relative Humidity	Heat Fluxes	Infiltration	Infrared Thermography	Illuminance Level (Lux)	Total Electricity Meter	Gas Meter	Heat Meter	HVAC Air Flow	Light Electricity Meter	Outdoor Air Temperature	Exterior Relative Humidity	Global Vertical Solar Radiation Intensity	Global Horizontal Solar Radiation Intensity	Diffuse Solar Radiation Intensity	Outdoor Illuminance Level (Lux)	Wind Speed Anemometer	Wind Direction	Atmospheric Pressure	Rainfall	Thermostat	Other Building Devices to Control	Protocol Communication	Gateway or Transmitters	Data logger	SCADA	Computer	Building Heating Systems	HVAC	Fans	Electric Radiator										
[49]	1978	Report	No	X													X	X	X	X	X						X																				
[118]	1979	Paper	No	X													X	X	X	X	X						X																				
[119]	1979	Report	No	X													X	X	X	X	X						X																				
[120]	1980	Report	No	X													X	X	X	X	X						X																				
[121]	1985	Report	No	X													X	X	X	X	X						X																				
[18]	1985	Report	No	X													X	X	X	X	X						X																				
[122]	1995	Paper	No	X													X	X	X	X	X						X																				
[7]	2000	Paper	No	X													X	X	X	X	X						X																				
[123]	2001	Paper	No	X													X	X	X	X	X						X																				
[124]	2005	Paper	No	X													X	X	X	X	X						X																				
[6]	2007	Paper	No	X													X	X	X	X	X						X																				
[125]	2013	Paper	No	X													X	X	X	X	X						X																				
[126]	2015	Conference Paper	No	X													X	X	X	X	X						X																				
[127]	2015	Conference Paper	No	X													X	X	X	X	X						X																				
[128]	2015	Conference Paper	No	X													X	X	X	X	X						X																				
[129]	2015	Paper	No	X													X	X	X	X	X						X																				
[130]	2016	Paper	No	X													X	X	X	X	X						X																				
[24]	2016	Paper	No	X													X	X	X	X	X						X																				
[131]	2016	Paper	No	X													X	X	X	X	X						X																				
[132]	2017	Paper	No	X													X	X	X	X	X						X																				
[133]	2017	Paper	No	X													X	X	X	X	X						X																				
[134]	2017	Paper	No	X													X	X	X	X	X						X																				
[135]	2018	Paper	No	X													X	X	X	X	X						X																				
[117]	2018	Paper	No	X													X	X	X	X	X						X																				

Table 2.9. MCSs in the reviewed literature from 1979–2018, specified by the authors to characterize the TEP of buildings.

2.3.2 Quantitative and qualitative analysis of monitoring and control systems of the reviewed literature

The qualitative and quantitative analysis of the equipment and the technical specification level of the MCSs used in the 24 reviewed bibliographies that were reviewed, has been carried out. The objective of the qualitative and quantitative analyses is to identify the MCSs currently used to estimate the HLC and TEP in order to:

- Identify the technology used in experimental tests.
- Analyse the integration of MCSs into BAS.
- Identify the current state of FDD methods implemented in MCSs.

Based on the data recompilation of Table 2.9, a qualitative and quantitative analysis was undertaken in terms of the function of the equipment and technical specification level of the MCSs' described and presented in the methodology reviewed from the literature.

To analyse the MCS technologies used in the experimental tests of the selected bibliography, different levels have been defined according to technical specifications that selected publications describe in their experimental methodology. For this, the MCS equipment implemented to collect and process the physical variables to develop the methods for the TEP characterization, which these publications propose, is characterized. The three levels are defined as Levels A, B, and C and they are quantified as 1, 0.5 and 0, respectively, and the degree of detail that defines each level is shown in Table 2.10.

Levels	Detail Degree of Technical Specifications	Quantitative Value
Level-A	High degree specification	1
Level-B	Partial specification	0.5
Level-C	There is not specification	0

Table 2.10: Description of the level quantification used to analyse the MCSs presented in the reviewed literature.

The evaluated criteria has been divided into two groups: one to analyse the Monitoring System that includes the sensors, and another to analyse the Control System that includes controls, communication protocols, software and hardware. Table 2.11 shows the criteria considered to analyze the MCSs' specification of the degree of technologies used in research projects in the reviewed literature. The MCSs' specification degree helps to identify the degree of importance of MCSs in HLC estimation and in other estimates used to determine the energy behaviour of the buildings, so as to characterize the TEP. This allows us know the reason why there is a difficulty in identifying MCS technologies used in experimental tests.

Table 2.12 shows the review bibliography with the analysed criteria and the corresponding level for each of them. In analysing the Monitoring System's device criteria, more than 50% of the literature studied falls into level C—where it has not been possible to identify the type or model of the sensors

Device Type	Criteria Type	Analysed criteria
Monitoring System	MS-1	Specify the Model or Type
	MS-2	Specify the Data Sheet
	MS-3	Details the Accuracy
	MS-4	Specify the criterion used for select the Type of Monitoring System
Control System	DS-1	Specify the Model or Type of control devices
	DS-2	Specify the Data Sheet
	DS-3	Specify the Protocol Communications
	DS-4	Specify the Operating Characteristics of Hardware and Software
	DS-5	Specify the Hardware and Software type
	DS-6	Specify the criterion used for select the type of Control System used

Table 2.11: Criteria to evaluate the specification level of MCS.

used in those experimental tests. Of 24 bibliographies reviewed, 83.3% did not specify the data sheet, and 58.3% did not specify the sensor's accuracy either. A total of 79.2% did not describe the decision criteria used to select the sensors (economic, technical, or other criteria). Furthermore, a 67% used the Co-Heating Method and 17% used other regression methods. One publication estimated the HLC with the Corrected Average Method and another with the Average Method, with each one representing 4% of total publications reviewed. To estimate local U-Values, two of four publications used ISO9869:1994, one publication does not specify the methodology implemented, and another was based on ISO 6946:2007 [127]. Seven publications, or 29%, implemented other methodologies to characterize the TEP—for example, statistical methods. These values are specified in Tables 2.13, 2.14, 2.15, 2.16, 2.17, 2.18, 2.19 and 2.20.

Regarding the Control System devices, they showed a similar tendency as the Monitoring System devices, with only around 12.5% giving a complete description specifying the model or type of control devices, the data sheet, and the criteria used to determinate the Control System in terms of the function of its technical requirements. On the other hand, 20.8% specified the protocol communication, software, and hardware used. In addition, just 25% specified the operating characteristics of the hardware and software used to control and process the collected data. Around 21% and 13%, respectively, specify the hardware and software type and the criterion used to determine the control system implemented.

By studying the publications, it was often possible to determine the sensors and devices used when these were not included explicitly in the methodologies because they were specified in the analysis, tables, and/or data graphics. In this way, it was possible to know, in some cases, the sensors used in the experimental test. Even so, there are publications that did not specify the devices used and just gave the results, making it impossible to identify the devices used in the experimental test. Tables 2.13, 2.14, 2.15, 2.16, 2.17, 2.18, 2.19 and 2.20 show the sensors, devices, software and hardware identified in the selected literature. It was possible to identify, in 100% of literature the use of sensors to measure the interior temperature, in 83% those used to measure the exterior temperature, and in around 13% those used to measure surface temperatures. The difference between the exterior and interior temperatures may be because these data were collected using weather stations, but neither

literature specify if this measure was collected by a station. In the tests, just 13% and 17% had used sensors to measure the indoor CO₂ level and indoor relative humidity, respectively.

In 21% of experimental tests, infrared thermographics were used, and 50% used different devices to estimate the infiltration. Only 33% used local heat flow sensors. The meteorological conditions were measured in several tests, of which 50% specified the horizontal global radiation, 63% the vertical global radiation, and 33% the diffuse radiation and relative humidity sensors.

In 83% of the reviewed literature, an electricity meter was used to measure the total energy consumption. Likewise, in determining the use of other meter sensors, 17% used gas meters, 25% used heat meters, and 8% used HVAC air flow and specific sensors to measure the light electricity consumption.

A total of 67% used the Co-Heating Method for their experimental tests, whereas 94% specify the use of a meter to measure the total electricity consumption and 81% the use of a sensor to measure the exterior temperature; of these, 25% measured the exterior RH and only 13% measured the interior RH. Respectively, 50% and 38% measured the global vertical and global horizontal solar radiation, while 19% measured wind speed and 25% measured diffuse solar radiation and wind direction, only 56% and 50%, respectively, described the use of electrical radiators and fans. A total of 56% measured air infiltration, 31% used infrared thermographics, 38% used heat flow, and only 6% measured surface temperatures. 25% and 19% used heating and HVAC systems. The use of these building systems in some cases was to maintain the internal conditions when a building prototype was being tested, or to avoid stratification during different tests. The physical variables shown in Table 2.2 are those measured in the Co-Heating Methods developed in selected publications.

Experimental tests in 75% of the reviewed cases that used other regression methods used sensors to measure the total electricity consumption, outdoor temperature, exterior relative humidity, vertical solar radiation, and wind direction, while 50% measured the surface temperature, indoor CO₂ concentration, heat flow, gas consumption, and diffuse solar radiation. All of the reviewed research experiments used sensors to measure global horizontal radiation, wind speed, and heating meters. Another 25% with sensors measured the interior relative humidity, infiltration, interior illumination level, light electricity consumption, and exterior illuminance.

The Average Method used in experimental tests, specified devices, besides the use of heating meters, to measure the interior, exterior and surface temperature, heat flow, electricity consumption, exterior relative humidity, horizontal, vertical and diffuse solar radiation, direction and wind speed. The Corrected Average Method specified measures of the interior and exterior temperature, indoor CO₂ concentration, interior and exterior RH and light power consumption, indoor and outdoor illumination levels and horizontal solar radiation, wind speed, and also uses heating meters. Each of these methods were used by only one of the experimental tests.

Seven papers (29%) used methods different to Co-Heating, regressions, the Average Method, and the Corrected Average Method for TEP characterization. Two publications used devices to measure the

surface temperature, heat flow, indoor CO₂ concentration, and gas consumption. Six experimental tests did not measure the interior RH, interior illuminance level, and HVAC airflow. A total of 71% used a sensor meter to measure the total electricity consumption and measure the global horizontal solar radiation, 86% measured the outdoor temperature, and 100% measured the global vertical solar radiation. A total of 57% measured the diffuse radiation, and 43% the exterior RH. Only one publication used an electrical radiator or a heating system, while in two publications an HVAC system was used. 43% used heat meters and measure infiltrations, while 57% measure the direction and speed of the wind.

Analysing the devices of Control Systems of all literatures, around 42% used a thermostat and 25% used any other device for another purpose, for example to open or close windows. Around 56% of publications that analysed the Co-Heating test used thermostats, versus 14% that implemented other methods to estimate the energy performance of buildings' envelopes. Furthermore, the 50% used fans and 56% electric radiators, versus 33% and 42%, respectively, of all literatures.

No project mentions the use of a Supervisory Control and Data Acquisition (SCADA) for collecting and processing data, although around 54% used a data logger and approximately 33% a data processor.

The communication protocols that were used were not identified; only around 21% of publications specified some characteristic of data transmission, and only one publication specified the use of a gateway or transmitter. A total of 29% of all publications specified the use of a computer. The experimental tests that implemented the Co-Heating and other methods to estimate the energy behaviour of buildings' envelopes to characterize TEP have the same tendency.

The results show that no publication has implemented an FDD method to detect, identify, and correct the error in MCSs used during experimental tests.

Specification level's degree of analysed criteria in the reviewed literature													
Reference	Publication Year	Type of publication	MS' Devices			CS' Devices							
			MS-1	MS-2	MS-3	MS-4	DS-1	DS-2	DS-3	DS-4	DS-5	DS-6	
[49]	1978	Report	Level-C	Level-C	Level-C	Level-C	Level-C	Level-B	Level-A	Level-A	Level-A	Level-B	Level-C
[118]	1979	Paper	Level-C	Level-C	Level-C	Level-C	Level-C	Level-C	Level-C	Level-C	Level-C	Level-C	Level-C
[119]	1979	Report	Level-A	Level-A	Level-A	Level-A	Level-A	Level-A	Level-A	Level-A	Level-A	Level-A	Level-A
[120]	1980	Report	Level-C	Level-C	Level-C	Level-C	Level-C	Level-C	Level-C	Level-C	Level-C	Level-C	Level-C
[121]	1985	Report	Level-B	Level-B	Level-B	Level-B	Level-B	Level-B	Level-B	Level-B	Level-B	Level-B	Level-B
[18]	1985	Report	Level-B	Level-B	Level-B	Level-B	Level-B	Level-B	Level-B	Level-B	Level-B	Level-B	Level-B
[122]	1995	Paper	Level-C	Level-C	Level-C	Level-C	Level-C	Level-C	Level-C	Level-C	Level-C	Level-C	Level-C
[7]	2000	Paper	Level-C	Level-C	Level-C	Level-C	Level-C	Level-C	Level-C	Level-C	Level-C	Level-C	Level-C
[123]	2001	Paper	Level-C	Level-C	Level-C	Level-C	Level-C	Level-C	Level-C	Level-C	Level-C	Level-C	Level-C
[124]	2005	Paper	Level-B	Level-C	Level-C	Level-C	Level-C	Level-A	Level-C	Level-C	Level-C	Level-C	Level-B
[6]	2007	Paper	Level-A	Level-C	Level-C	Level-C	Level-C	Level-A	Level-A	Level-A	Level-A	Level-A	Level-C
[125]	2013	Paper	Level-C	Level-C	Level-C	Level-C	Level-C	Level-C	Level-C	Level-C	Level-C	Level-C	Level-C
[126]	2015	Conference Paper	Level-C	Level-C	Level-C	Level-C	Level-C	Level-C	Level-C	Level-C	Level-C	Level-B	Level-B
[127]	2015	Conference Paper	Level-C	Level-C	Level-C	Level-C	Level-C	Level-C	Level-C	Level-C	Level-C	Level-B	Level-B
[128]	2015	Conference Paper	Level-C	Level-C	Level-C	Level-C	Level-C	Level-C	Level-C	Level-C	Level-C	Level-C	Level-C
[129]	2015	Paper	Level-C	Level-C	Level-C	Level-C	Level-C	Level-C	Level-C	Level-C	Level-C	Level-A	Level-C
[130]	2016	Paper	Level-B	Level-C	Level-B	Level-C	Level-C	Level-C	Level-C	Level-C	Level-C	Level-C	Level-C
[24]	2016	Paper	Level-A	Level-C	Level-A	Level-B	Level-C	Level-C	Level-C	Level-C	Level-C	Level-C	Level-C
[131]	2016	Paper	Level-A	Level-C	Level-A	Level-C	Level-C	Level-C	Level-C	Level-C	Level-C	Level-B	Level-C
[132]	2017	Paper	Level-A	Level-C	Level-B	Level-C	Level-C	Level-C	Level-A	Level-B	Level-B	Level-B	Level-C
[133]	2017	Paper	Level-A	Level-C	Level-A	Level-B	Level-C	Level-C	Level-C	Level-B	Level-B	Level-B	Level-C
[134]	2017	Paper	Level-A	Level-C	Level-C	Level-C	Level-C	Level-C	Level-C	Level-C	Level-C	Level-C	Level-C
[135]	2018	Paper	Level-C	Level-B	Level-B	Level-C	Level-C	Level-C	Level-C	Level-C	Level-C	Level-C	Level-C
[117]	2018	Paper	Level-A	Level-C	Level-B	Level-C	Level-C	Level-C	Level-C	Level-C	Level-C	Level-C	Level-C

Table 2.12: Qualitative analysis of the specification level's degree of the analysed criteria for the devices, hardware, and software of MCSs used in buildings or prototypes in each publication studied. Criteria based on Table 2.11.

All Reviewed Literature										
Number of references considering the analysed criteria of MCS										
All Methods	MS' Devices				CS' Devices					
24 references (100%)	MS-1	MS-2	MS-3	MS-4	DS-1	DS-2	DS-3	DS-4	DS-5	DS-6
Level-A	8 33.34%	1 4.17%	4 16.67%	1 4.17%	3 12.50%	3 12.50%	5 20.83%	6 25.00%	5 20.83%	3 12.50%
Level-B	4 16.67%	3 12.50%	6 25.00%	4 16.67%	1 4.17%	7 29.17%	1 4.17%	5 20.83%	8 33.33%	4 16.67%
Level-C	12 50.00%	20 83.33%	14 58.33%	19 79.17%	20 83.33%	14 58.33%	18 75.00%	13 54.17%	11 45.83%	17 70.83%

Table 2.13: Quantitative analysis of specification level's degree of the analysed criteria of MCSs used in buildings or prototypes in all reviewed literature.

Reviewed Literature with Co-Heating Method (HLC estimation)										
Number of references considering the analysed criteria of MCS										
Co-Heating Method	MS' Devices				CS' Devices					
16 references (67%)	MS-1	MS-2	MS-3	MS-4	DS-1	DS-2	DS-3	DS-4	DS-5	DS-6
Level-A	6 37.50%	1 6.25%	3 18.75%	1 6.25%	3 18.75%	3 18.75%	5 31.25%	4 25.00%	2 12.50%	1 6.25%
Level-B	2 12.50%	1 6.25%	4 25.00%	1 6.25%	0 0.00%	5 31.25%	0 0.00%	4 25.00%	6 37.50%	2 12.50%
Level-C	8 50.00%	14 87.50%	9 56.25%	14 87.50%	13 81.25%	8 50.00%	11 68.75%	8 50.00%	8 50.00%	13 81.25%

Table 2.14: Quantitative analysis of specification level's degree of the analysed criteria of MCSs used in buildings or prototypes in all reviewed literature with Co-Heating Method (HLC estimation).

Reviewed Literature with Regression Method (HLC estimation)										
Number of references considering the analysed criteria of MCS										
Regression Methods	MS' Devices				CS' Devices					
4 references (17%)	MS-1	MS-2	MS-3	MS-4	DS-1	DS-2	DS-3	DS-4	DS-5	DS-6
Level-A	2 50.00%	0 0.00%	1 25.00%	0 0.00%	1 25.00%	0 0.00%	0 0.00%	0 0.00%	2 50.00%	1 6.25%
Level-B	2 50.00%	2 50.00%	2 50.00%	3 75.00%	0 0.00%	1 25.00%	1 25.00%	0 0.00%	0 0.00%	2 12.50%
Level-C	0 0.00%	2 50.00%	1 25.00%	1 25.00%	0 0.00%	3 75.00%	3 75.00%	4 100%	2 50.00%	2 50.00%

Table 2.15: Quantitative analysis of specification level's degree of the analysed criteria of MCSs used in buildings or prototypes in all reviewed literature with Regression Method (HLC estimation).

Reviewed Literature with Average Method (HLC estimation)										
Number of references considering the analysed criteria of MCS										
Average Method	MS' Devices				CS' Devices					
1 reference (4%)	MS-1	MS-2	MS-3	MS-4	DS-1	DS-2	DS-3	DS-4	DS-5	DS-6
Level-A	1 100%	0 0.00%	0 0.00%	0 0.00%	0 0.00%	0 0.00%	0 0.00%	0 0.00%	0 0.00%	0 0.00%
Level-B	0 0.00%	0 0.00%	0 0.00%	0 0.00%	0 0.00%	0 0.00%	0 0.00%	0 0.00%	0 0.00%	0 0.00%
Level-C	0 0.00%	1 100%	1 100%	1 100%	1 100%	1 100%	1 100%	1 100%	1 100%	1 100%

Table 2.16: Quantitative analysis of specification level's degree of the analysed criteria of MCSs used in buildings or prototypes in all reviewed literature with Average Method (HLC estimation).

Reviewed Literature with Corrected Average Method (HLC estimation)										
Number of references considering the analysed criteria of MCS										
Corrected Average Method	MS' Devices				CS' Devices					
1 reference (4%)	MS-1	MS-2	MS-3	MS-4	DS-1	DS-2	DS-3	DS-4	DS-5	DS-6
Level-A	1 100%	0 0.00%	1 100%	0 0.00%	0 0.00%	0 0.00%	0 0.00%	0 0.00%	0 0.00%	0 0.00%
Level-B	0 0.00%	0 0.00%	0 0.00%	1 100%	0 0.00%	0 0.00%	0 0.00%	0 0.00%	0 0.00%	0 0.00%
Level-C	0 0.00%	1 100%	0 0.00%	0 0.00%	1 100%	1 100%	1 100%	1 100%	1 100%	1 100%

Table 2.17: Quantitative analysis of specification level's degree of the analysed criteria of MCSs used in buildings or prototypes in all reviewed literature with Corrected Average Method (HLC estimation).

Reviewed Literature implementing other methods										
Number of references considering the analysed criteria of MCS										
Other methods applied ¹²	MS' Devices				CS' Devices					
7 references (29%)	MS-1	MS-2	MS-3	MS-4	DS-1	DS-2	DS-3	DS-4	DS-5	DS-6
Level-A	1 14.29%	0 0.00%	0 0.00%	0 0.00%	0 0.00%	0 0.00%	0 0.00%	2 28.57%	3 42.86%	2 28.57%
Level-B	2 28.57%	2 28.57%	2 28.57%	2 28.57%	1 14.29%	2 28.57%	1 14.29%	1 14.29%	2 28.57%	2 28.57%
Level-C	4 57.14%	5 71.43%	5 71.43%	5 71.43%	6 85.71%	5 71.43%	6 85.71%	4 57.14%	2 28.57%	3 42.86%

Table 2.18: Quantitative analysis of specification level's degree of the analysed criteria of MCSs used in buildings or prototypes in all reviewed literature implementing other methods.

Literatures by methods		Total/Rate	Sensors																						
Global Analysis		Total references 24	Indoor Air Temperature	Indoor CO ₂	Interior Relative Humidity	Heat Fluxes	Infiltration	Infrared Thermography	Illuminance Level (Lux)	Total Electricity Meter	Gas Meter	Heat Meter	HVAC Air Flow	Light Electricity Meter	Outdoor Air Temperature	Exterior Relative Humidity	Global Vertical Solar Radiation Intensity	Global Horizontal Solar Radiation Intensity	Diffuse Solar Radiation Intensity	Outdoor Illuminance Level (Lux)	Wind Speed Anemometer	Wind Direction	Atmospheric Pressure	Precipitation	
All Literatures Studied		Percentage rate 100%	24 100%	3 12.50%	4 16.67%	8 33.33%	12 50.00%	5 20.83%	2 8.33%	20 83.33%	4 16.67%	6 25.00%	2 8.33%	2 8.33%	20 83.33%	8 33.33%	15 62.50%	12 50.00%	8 33.33%	1 4.17%	8 33.33%	8 33.33%	0 0.00%	1 4.17%	
Co-Heating Method		Percentage rate 66.67%	16 100%	0 0.00%	2 12.50%	6 37.50%	9 56.25%	5 31.25%	0 0.00%	15 93.75%	2 12.50%	2 12.50%	1 6.25%	1 6.25%	13 81.25%	4 25.00%	8 50.00%	6 37.50%	4 25.00%	0 0.00%	0 0.00%	3 18.75%	4 25.00%	0 0.00%	1 6.25%
Regression Method		Percentage rate 16.67%	4 100%	2 50.00%	1 25.00%	2 50.00%	1 25.00%	0 0.00%	1 25.00%	3 75.00%	2 50%	4 100%	0 0.00%	1 25.00%	3 75.00%	3 75.00%	3 75.00%	4 100%	2 25.00%	1 12.50%	1 12.50%	4 100%	3 75.00%	0 0.00%	0 0.00%
Average Method		Percentage rate 4.17%	1 100%	0 0.00%	0 0.00%	1 100%	0 0.00%	0 0.00%	0 0.00%	1 100%	0 0.00%	1 100%	0 0.00%	0 0.00%	1 100%	1 100%	1 100%	1 100%	1 100%	0 0.00%	0 0.00%	1 100%	1 100%	0 0.00%	0 0.00%
Corrected Average Method		Percentage rate 4.17%	1 100%	1 100%	1 100%	0 0.00%	0 0.00%	0 0.00%	1 100%	0 0.00%	0 0.00%	1 100%	0 0.00%	1 100%	1 100%	1 100%	0 0.00%	1 100%	1 100%	0 0.00%	1 100%	1 100%	0 0.00%	0 0.00%	0 0.00%
Other Methods Applied		Percentage rate 29.17%	7 100%	2 28.57%	1 14.29%	2 28.57%	3 42.86%	0 0.00%	1 14.29%	5 71.43%	2 28.57%	3 42.86%	1 14.29%	1 14.29%	6 85.71%	3 42.86%	7 100%	5 71.43%	4 57.14%	0 0.00%	0 0.00%	4 57.14%	4 57.14%	0 0.00%	1 14.29%

Table 2.19: Quantitative analysis of the references studied by methodology: Global analysis of the method used, the fault detection and sensor type used for measuring physical variables in the MCSs in each methodology.

Literatures grouping by methods	Type of publication	Global Analysis											
		Actuators			Control System				Other Devices				
		Thermostat	Other Building Devices to Control	Protocol Communication	Getaway or Transmitters	Data logger	Data Processor	SCADA	Computer	Building Heating Systems	HVAC	Fans	Dedicated Electric Radiator
All Literatures Studied	Total references Percentage rate	10 41.67%	6 25.00%	5 20.83%	1 4.17%	13 54.17%	8 33.33%	0 0.00%	7 29.17%	5 20.83%	5 20.83%	8 33.33%	10 41.67%
Co-Heating Method	Total references Percentage rate	9 56.25%	3 18.75%	4 25.00%	1 6.25%	9 56.25%	5 31.25%	0 0.00%	4 25.00%	4 25.00%	3 18.75%	8 50.00%	9 56.25%
Regression Method	Total references Percentage rate	1 25.00%	1 25.00%	0 0.00%	0 0.00%	2 50.00%	1 25.00%	0 0.00%	2 50.00%	0 0.00%	0 0.00%	0 0.00%	0 0.00%
Average Method	Total references Percentage rate	0 0.00%	0 0.00%	0 0.00%	0 0.00%	0 0.00%	0 0.00%	0 0.00%	0 0.00%	0 0.00%	0 0.00%	0 0.00%	0 0.00%
Corrected Average Method	Total references Percentage rate	0 0.00%	0 0.00%	0 0.00%	0 0.00%	0 0.00%	0 0.00%	0 0.00%	0 0.00%	0 0.00%	0 0.00%	0 0.00%	0 0.00%
Other Methods Applied	Total references Percentage rate	1 14.29%	3 42.86%	1 14.29%	0 0.00%	4 57.14%	3 42.86%	0 0.00%	3 42.86%	1 14.29%	2 28.57%	0 0.00%	1 14.29%

Table 2.20: Quantitative analysis of references studied by methodology: Global analysis of the method, actuators, controls systems, and devices used in each methodology.

2.3.3 Conclusions

There is evidence that energy efficiency research is primarily focused on the use of automated projects to collect physical data, transfer the information using standard communication protocols, and through the use of software, to process all information to control and monitor physical variables and undertake data treatment. Researchers could use centralised automation in their projects to facilitate the collection of a large amount of data. This could help them to not only understand the building envelope behaviour, but also to develop new services to be integrated into the market of Thermal Envelope Performance.

Currently in Building Automation Systems, there is no evidence of the integration of in-use building energy monitoring systems to characterize the Thermal Envelope Performance. However, it would be useful to know how efficient the envelope is after the construction or retrofit so as to determine the discrepancy between the building's design and the building in-use, and to identify future retrofits of the building envelope.

The equipment necessary to carry out the Thermal Envelope Performance characterization includes sensors, controllers, software, hardware, communication protocols, and other devices and components of Monitoring and Control Systems. At the end of the 1970s and the beginning of the 1980s, studies were undertaken regarding the different monitoring technologies and cost/precision criteria for equipment selection used in the energy monitoring of buildings to characterize the Thermal Envelope Performance of buildings with the estimation of the Heat Loss Coefficient, together with other estimations. There is currently no evidence from recent studies comparing the different sensors and equipment used in energy monitoring with existing technologies. There is also no evidence for which monitoring systems should be used to characterize the Thermal Envelope Performance in Building Automation Systems or domotic systems.

The reviewed publications do not specify the selection criteria of the monitoring systems used in research projects, which shows that there is no standardization in the type of Monitoring and Controlling System that should be used to perform experimental tests in these estimations. It is also evident that experimental tests tend to focus more on developing methods to estimate the Heat Loss Coefficient and other estimations to determine the envelope energy behaviour of buildings to characterize the Thermal Envelope Performance, rather than carrying out an analysis to determine the criteria to choose the Monitoring and Control Systems. This trend is apparent even though the sensors used to measure physical variables are critical to the reliability of the data collected to perform the Thermal Envelope Performance characterization. It has been also observed that the Monitoring and Control Systems used to estimate Heat Loss Coefficient allow the analysis and estimation of other parameters used to characterize the buildings' the Thermal Envelope Performance. The physical variables necessary for these estimations are collected in current Building Automation Systems and domotic systems in order to determine user comfort, electricity consumption, and for the control of the building systems. This makes it possible for the experimental tests used to characterize Thermal Envelope Performance to be designed from the perspective of Building Automation Systems and

domotic systems, in order to introduce this characterization into these automation systems. For this to be effective, the experimental tests should develop selection criteria for the Monitoring and Control Systems in the research projects to standardize them.

The standardization of the Monitoring and Control Systems used in the Thermal Envelope Performance characterization in experimental tests needs further research in order to ensure that the physical data are accurate enough to rigorously apply the Heat Loss Coefficient estimation methods. In this way, the Heat Loss Coefficient estimates for the emission of reliable Energy Performance Certificates, according to the requirements of the legislation, may be used if they are able to be integrated into Building Automation Systems and domotic systems. It is also necessary to emphasise the importance of defining the criteria in Monitoring and Control System selection in order to guarantee that the technologies are accurate, reliable, profitable, and safe from cyber-attacks.

No publication has been found that develops Automated Fault Detection and Diagnosis methods for the whole monitoring system of a Building Automation System or domotic system. Studies that characterize the Thermal Envelope Performance by testing different sensor technologies to understand any discrepancies in the Heat Loss Coefficient estimation, and what the sensor response is in building energy monitoring systems, are also lacking. The methods analysed to estimate the Heat Loss Coefficient and other estimates to determine the envelope energy behaviour of buildings only take into account the errors and the manufacturing precision of the devices used. As an example, to understand the measured discrepancies of temperature, RH, CO₂ levels, energy consumption, solar radiation, and other physical variables, it is necessary to know the sensor characteristics used in a building's automation in the research projects that characterize the Thermal Envelope Performance. For this, it is essential to know in real-time the faults that occur during the experimental tests, in order to analyse their impact and determine the error discrepancies with the manufacturing data sheet. All of this information is necessary for the implementation of Automated Fault Detection and Diagnosis methods in the Monitoring and Control Systems of experimental tests.

The literature studied in this thesis evidences the use of Automated Fault Detection and Diagnosis methods in such building systems as fan coils, Heating, Ventilation and Air Conditioning systems, heat pumps, air conditioners, commercial refrigerators, lighting, water heaters, chillers, cooling towers, Air Handling Units and Variable Air Volume boxes. However, a specific method for all Monitoring and Control Systems used in Building Automation Systems and domotic systems has not been found, while this is essential in order to integrate Fault Detection and Diagnosis methods for all parties that make up these Monitoring and Control Systems. It is necessary to develop Fault Detection and Diagnosis methods to calibrate, predict and detect the error of all devices in a Monitoring and Controlling System. This would facilitate the maintenance of the system, allowing its self-regulation and calibration so as to increase the accuracy and reliability of the studies.

When the measurement uncertainty or measurement error is taken into account in the literature reviewed, only the manufacturer's accuracy (systematic errors) of sensors is taken into account, without considering the measurement uncertainties associated to random errors or other uncertainty

sources.

The Co-Heating Method for HLC estimation has the advantage of being a method in which random errors are minimised. The random errors due to solar radiation disappears since they are estimated through the regression method together with the HLC value. The rest of the variables (indoor air temperature, electricity consumption and heating) have associated only systematic errors, so the outdoor air temperature is the only variable that has associated systematic and random errors. In this method, thanks to the air fans being used to continuously mix the indoor air, the indoor air temperature measurement does not have associated random errors. On the other hand, this method to estimate the HLC does not consider the user behaviour and its impact on the Energy Efficiency of a Building, and although the method requires less investment in Monitoring and Control Systems, as they are usually mobile systems, it has the disadvantage that the dwelling or building must be unoccupied for a considerable period of time, which makes it difficult to carry out the test on dwellings or buildings that are already inhabited.

The Average Method has the advantage that it is possible to know the impact of user behaviour in the Energy Efficiency Building, as it is not necessary to have a dwelling or building unoccupied, but this method requires more investment in the Monitoring and Control Systems. Furthermore, the effect of the random errors are considerably increased with respect to the Co-Heating Method because the variables such as solar radiation gains are measured from sensors and not estimated by regression methods. The estimation of users' metabolic gains must also be taken into account, and the indoor air temperature is a measure that is not fixed homogeneously within the thermal zones that make up the building. These variable uncertainties, together with the outdoor air temperature uncertainty, give the HLC value a higher uncertainty, where systematic and random errors are associated to more variables with respect to the HLC estimation of the Co-Heating method. Here, one of the main aims of this Thesis is to develop and test a method that can provide the overall uncertainty of the indoor and outdoor air temperatures, considering both, the systematic and random errors. Note that, in the literature review, it has been highlighted, that all the research works dealing with the HLC estimation only consider the systematic error associated to the manufacturer's accuracy, forgetting the random error sources.

This study shows the need to focus on the effect of the estimation of the Heat Loss Coefficient and other estimations to determine the envelope energy behaviour of buildings using different sensor technologies, with laboratory accuracy and market sensor accuracy. This type of research could allow the development of a monitoring kit and control specifications to define the Building Automation Systems, together with their layout in buildings, so as issue reliable Energy Performance Certificates in the future. In addition, it is necessary to know the discrepancy in the estimations of the Heat Loss Coefficient and other estimations to determinate the envelope energy behaviours of buildings. This discrepancy can be determined using the technology of current Building Automation Systems and domotic systems to know if, with the market technology, it is possible to determine the Thermal Envelope Performance of buildings after the new building construction or retrofit of

existing buildings. Therefore, knowing how to integrate the standardised Monitoring and Control Systems used to estimate the Heat Loss Coefficient and other estimations to determinate the envelope energy behaviours of buildings, which characterize the Thermal Envelope Performance in Building Automation Systems and domotic systems for new and existing buildings, is essential. Here, we found the second aim of this thesis. After presenting in detail the average method to estimate the in-use HLC and the possible decoupling method for those in-use HLC; a detailed monitoring system for a residential building will be designed and implemented to be able so as to analyse in detail the MCS requirements and its associated costs.

Chapter 3

METHODOLOGY

This chapter shows the methodology and criteria used to design MCSs in order to be optimized and thus characterize the TEP and estimate the HLC in monitored buildings. The theoretical basis of the GUM method is also presented to estimate the overall uncertainties in random samples, independent from each other and with a normal distribution. The proposed method permits the overall uncertainties of intensive variables such as temperature, relative humidity or CO₂ concentration values within monitored volumes to be estimated. These volumes could be thermal zones within a building or the volume surrounding the building envelope. In addition, a methodology to decouple these overall Measurement Uncertainties in two types of uncertainty is also developed; one of these uncertainties is associated to the random errors (Measurement's Spatial Uncertainty ($U_{M(SP)}$)) and the other is associated to the systematic errors (Sensor Measurement Uncertainty ($U_{M(S)}$)).

3.1 Introduction

Based on the literature review of section 2.3.3, the design of MCS with the necessary measurements to estimate the HLC through the Average Method and the Co-Heating Method (section 3.3) should be optimized. These measurements have associated uncertainties due to systematic and random errors, where the heating and ventilating systems' energy (Q) and electricity gains (K_e) only have associated measurement uncertainty due to systematic errors. Meanwhile, the solar gains ($S_a V_{sol}$), occupants' metabolic gains (K_o), indoor and outdoor temperature (T_{in} and T_{out}), all have associated measurement uncertainties due to systematic errors and random errors. In the case of HLC estimation through the Average Method (section 2.2.2), the effect of $S_a V_{sol}$ and K_o have a low uncertainty effect over the HLC estimation with respect to the Q and K_e being measurements, since the method is applied in cold and cloudy periods, Q and K_e the highest heat gains in the building. Thus, the overall measurement uncertainty of T_{in} and T_{out} is crucial and must be estimated in order to improve the HLC estimation. Understanding the overall uncertainty of T_{in} and T_{out} will permit us to design the MCS in order to quantify and reduce these uncertainties due to systematic and random errors.

On the other hand, when the HLC is estimated through the Co-Heating Method, only the T_{out} has associated both system and random errors, since the rest of the variables (Q , K_e , $S_a V_{sol}$ and T_{in}) only have associated measurement uncertainty due to systematic errors, as explained in section 2.2.3.

The methodology carried out to estimate the overall measurement uncertainty has been developed within this research to apply the GUM method to the intensive variables measurements used to characterize the TEP and the HLC. In addition, a decoupling uncertainty method (section 3.2.2) has been developed (section 3.2.1) with the objective of separating the uncertainties due to systematic and random error of the estimated overall uncertainty. Finally, the developed methodology has been used to analyse the vertical stratification of the measurements (section 3.2.3). Together with the uncertainty analysis, the estimation of the representative value of a measurement is explained using the estimation of the measurement uncertainty.

Finally, the MCS' general criteria to measure the variables involved in the HLC estimation and its decoupling through the Co-Heating Method and Average Method are presented. Likewise, other optional measurements of variables are included to estimate the infiltration and/or ventilation heat loss coefficients, the one dimensional transmission heat transfer coefficient (U-Value) of the envelope elements and the gas consumption to characterize the boiler's seasonal efficiencies.

3.2 Uncertainty analysis for intensive variables measurement of in-use buildings

Measurements of physical quantities have a degree of uncertainty. The variability of the results of repeated measurements is due to the fact that it is impossible to keep constant the variables that can affect the result of such a measurement. One of the reasons associated with this, is that the

manufacture of measurement equipment has a certain degree of quality that cannot be measured accurately even if actions are taken to limit the degree of uncertainty.

Estimating the uncertainty and indicating it properly allows data to be correctly interpreted and valid conclusions to be drawn, which implies that the measurement is not just the average value of the measurements. It is equally important to know how accurate and precise the measurement result is. Therefore, every measurement must have both the numerical value with its corresponding physical units and the degree of uncertainty associated with the measured value. In this way, the uncertainty, at a specified confidence level, will characterize a range of values within which the measured quantity can lie.

The methodology for estimating the uncertainty value is a process detailed in the ISO Guide to the Expression of Uncertainty in Measurement (GUM) [103], where there are terminologies associated to measurement, some of which are:

Error: is the difference between a measurement and the true value of the measuring does not include mistakes and it is not possible to completely eliminate error in a measurement, it can be only controlled and characterized. Error is what causes values to differ when a measurement is repeated and none of the results can be preferred over the others. The total error is a combination of systematic error and random error.

Systematic error: tends to displace all measurements systematically, so that after a series of measurements, the average value is constantly shifted or varies in a predictable way. The causes may be known or unknown, but must always be corrected when they are present. Systematic error can only be corrected when the 'true value' (such as the value assigned to a calibration or reference specimen) is known.

Random error: is a component of the total error which, after a series of measurements, varies in an unpredictable way. It is not possible to correct the random error.

Accuracy: is the closeness between a measured value and the true value. Accuracy is an expression of the lack of error, no two measurements are exactly the same, thus some deviations can be controlled and some cannot. Some deviations can be controlled by careful adjustment of the experimental procedure. These types of deviations are *systematic errors* which are sometimes referred to as determinate errors.

Precision: is the closeness of agreement between independent measurements of a quantity under the same conditions. It is a measure of how well a measurement can be made without reference to a theoretical or true value. Since precision is not based on a true value, there is no bias or systematic error in the value, but instead it depends only on the distribution of *random errors*.

Repeatability: is simply the precision determined under conditions where the same methods and equipment are used by the same operator to make measurements on identical specimens. Reproducibility is simply the precision determined under conditions where the same methods but

different equipment are used by different operators to make measurements on identical specimens.

Uncertainty (of measurement): this is a parameter, associated with the result of a measurement, that characterizes the dispersion of the values that could reasonably be attributed to the measuring. Uncertainty of measurement comprises, in general, many components. Some of these components may be evaluated from the statistical distribution of the results of measurements' series and can be characterized by experimental standard deviations. The uncertainty is a value that characterizes the range of values within which the true value is asserted to lie. These value estimates should address error from all possible effects (both systematic and random) and, therefore, is usually the most appropriate means of expressing the accuracy of results. Uncertainty characterizes the range of values within which the true value is asserted to lie with some level of confidence.

Expanded uncertainty: quantity defining an interval about the result of a measurement that may be expected to encompass a large fraction of the distribution of values that could reasonably be attributed to the measuring.

On the basis of all that is involved in the measurements, there is a discrepancy between the real measured value of an intensive variable of a volume within a building (or Monitored Zone) and the individual measurements from sensors of an MCS. It will never be possible to know with certainty the real value of a measure, because its uncertainty is due to both systematic errors (can be controlled and eliminated) and different errors from random causes (cannot be controlled and eliminated). The measurement uncertainty associated to systematic error is given by the sensor accuracy (which is given by the manufacturer) and by the monitoring system where the sensor is installed. However, random errors are due to different causes, such as user behaviour, incidence of solar radiation, or effects produced by the ventilation and heating system, among others. The overall uncertainty of the measurement could be estimated by combining uncertainties of the systematic and random errors. The different influences or causes that have an impact on the temperature measurement or any measurement are the following [103]:

- Repeatability.
- Resolution.
- Reproducibility.
- Reference.
- Standard Uncertainty.
- Reference Standard Stability.
- Environmental Factors.
- Measurement specific contributors: Alignment, scale, evaporation, mismatch, etc.

- Contributions required by method: ASTM¹, ISO/IEC², Military Procedure, etc.
- Accreditation requirements.

This section starts with the state of the art of uncertainty analysis methods and the developed methodology is then described for the following analysis:

- Measurement Sensor Uncertainty ($U_{M(S)}$) analysis: the uncertainty associated to systematic errors of the sensors and monitoring system is estimated.
- Measurement Uncertainty (U_M) analysis: the overall uncertainty analysis of the measurement for each Monitored Zone is performed. In this estimation, all uncertainty sources on the measurement are considered (systematic and random errors).
- Measurement Spatial Uncertainty ($U_{M(SP)}$) analysis: the uncertainty associated to random errors is estimated. For this, the Measurement Uncertainty (U_M) of the measurement is decoupled into sensor uncertainty and spatial uncertainty.

The statistical method for estimating the Measurement Uncertainty (U_M) and the Measurement Sensor Uncertainty ($U_{M(S)}$) is the same, so it is first introduced as a general uncertainty analysis method at the start, then the specific application of the method to each of these two cases is detailed.

3.2.1 Statistical basis of the uncertainty estimation

The theoretical framework of the statistical analysis carried out to estimate the uncertainty is explained in this subsection. Data must be formed by experimental observations whose bell-shaped distribution is best represented by the normal distribution, also called the Gaussian distribution ([136], [103]), where, for a sample size N with Z measures per sample, it is possible to obtain the Mean (μ), the Variance (σ^2) and the Standard Deviation (σ) for each sample (Z values), as well as the Mean ($\bar{\mu}$), Mean Variance ($\bar{\sigma}^2$) and the Mean Standard Deviation ($\bar{\sigma}$) of the sample (N values).

In addition, for the sample with a normal distribution centred on the μ and σ values, it is known a priori that the Mean (μ) of any sample has a 68% probability of falling within the interval $\bar{\mu} \pm \bar{\sigma}$. Measurements involve uncertainties, where repeated measurements give an indication of the measurement uncertainty through the dispersion in its measured values. In the case of independent observation series of 30 or more, the evaluation of uncertainty by statistical analysis is called Type A evaluations based on the GUM³ method [103].

In the statistical analysis of the Type A assessment, the sample's Mean Standard Deviation ($\bar{\sigma}$) of a probability distribution reflects the uncertainty value, where the Standard Uncertainty (U) is the measurement uncertainty expressed in terms of a sample's Mean Standard Deviation ($U = \bar{\sigma}$). If the U value is multiplied by a Coverage Factor (k) in a Type A distribution with sample size greater than

¹ASTM: "American Society for Testing and Materials"

²IEC: "International Electrotechnical Commission".

³GUM: "Guide to the Expression of Uncertainty in Measurement".

30, an “Expanded Uncertainty” is obtained, which is expected to be within the 95% confidence level interval if the k-value is equal to 2 ($\bar{U} = 2\bar{\sigma}$), or 99% if it is equal to 3 ($\bar{U} = 3\bar{\sigma}$) [103]. When there are fewer than 30 repeated measurements, the appropriate k-value is based on the Student t-distributions [103].

In this document, the overall Expanded Uncertainty \bar{U} value of the Measurement (M) from sensors is called “Measurement Uncertainty (U_M)”, with a U value multiplied by a k-value equal to 2. In addition, there are two different contributions of uncertainties, one due to systematic error (identified in this manuscript as Measurement Sensor Uncertainty ($U_{M(S)}$), and another due to random fluctuations (identified in this manuscript as Measurement Spatial Uncertainty ($U_{M(SP)}$), both estimated as Expanded Uncertainties (\bar{U}), but they are independent of each other.

The other type of uncertainty assessment set out in the GUM method [103] is the Type B distributions, which are not systematic errors and are not based on repeated measurements; therefore, Type B uncertainties have infinity degrees of freedom. Such distributions include manufacturer’s specifications, ASTM standards, experience, etc. This type of uncertainty is not applied in the methodology described here.

General method of uncertainty analysis applied to the measurement of intensive variables associated with the HLC estimation

The method set out in this section is developed in this research for measurements with a Type A sample. The analysis carried out can be applied to Indoor and Outdoor Air Temperature (T_{in} and T_{out}), indoor and outdoor Carbon Dioxide (CO_2) concentration, Relative Humidity (RH) and any measurement that has the characteristics of a Type A sample.

To carry out the statistical study to estimate the measurement uncertainty of intensive variables, the samples should be the Instant of Times (t_j) with $j = 1, \dots, N$. In each (t_j), different Sensor Measurements (M_{dv_i}) values have been acquired in a Differential Volume (dv_i) of a Monitored Zone (MZ), in which, in turn, the (dv_i) represents the volume where a sensor is located. M_{dv_i} represents one measurement point of the whole volume to be monitored, so that it is possible to know the estimated measurement value of the whole monitored volume. A diagram of these measurements is shown in Figure 3.1, which represents a building with several floors with Monitored Zones (MZ). Each MZ can be composed of a number of volumes called Monitored Spaces (MS). A building has x MZ volumes composed of g Differential Volumes (dv_i) and n MS volumes composed of Differential Volumes (dv_i); in turn, each MZ has p M_{dv_i} measurements and each MS has q M_{dv_i} measurements.

Equation 3.1 defines the MZ volume (V_{MZ}) as the sum of n volumes of the MS (V_{MS}) that makes up the MZ. Equation 3.2 defines the MS volume (V_{MS}) as the sum of y dv_i contained in each MS. Equation 3.3 shows the general equation to calculate the Average Measurement (M_a), while Equation 3.4 shows the Average Measurements of an MZ ($(M_a)_{MZ}$) defined by the sum of p units of M_{dv_i} measurement in an MZ divided by p . Also, Equation 3.5 shows the Average Measurement of an MS ($(M_a)_{MS}$) defined by the sum of q units of M_{dv_i} measurements in an MS divided by q . Equation 3.6 defines the Volume-Weighted

Measurement of an MZ $(M_{vw})_{MZ}$, which is calculated as the sum of the Average Measurement of an MS $((M_a)_{MS})$ multiplied by its volume weight in the MZ. The volume weight is equal to the MS Volume (V_{MS}) divided by the MZ Volume (V_{MZ}) . The units of each equation set out in this document are expressed generically as [SI], which corresponding to the International System of Units (SI) based on the unit of measure studied.

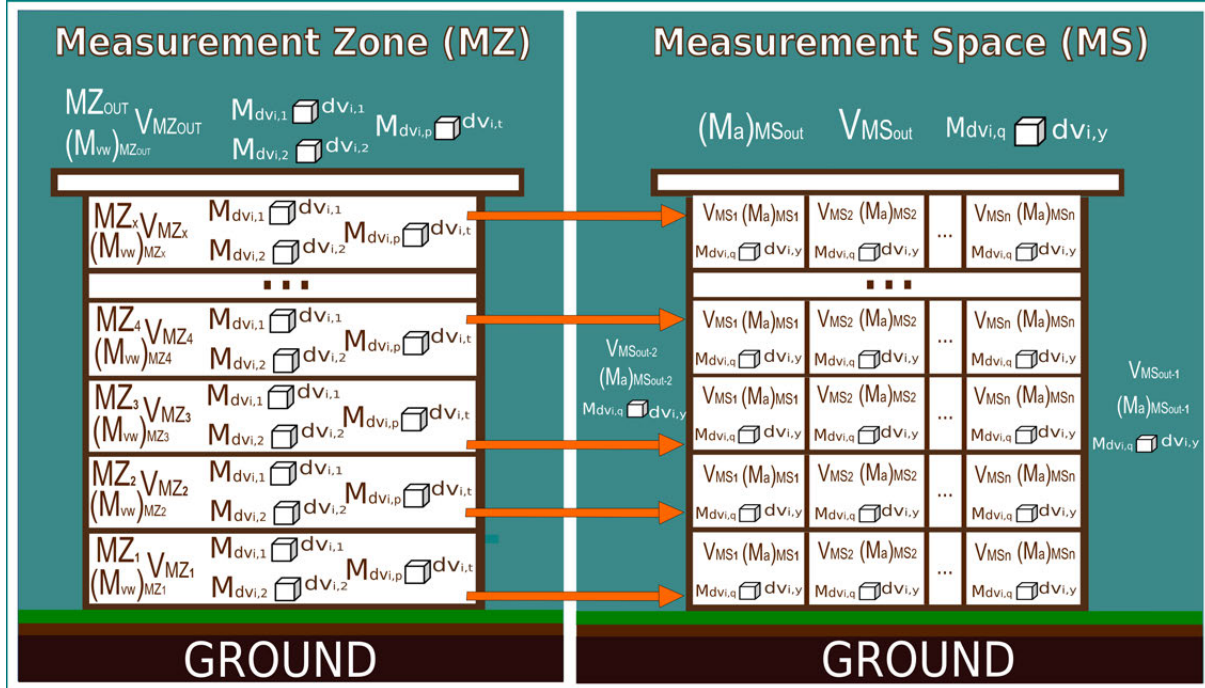


Figure 3.1: Scheme of differential volumes of Monitored Zones (MZ) and Monitored Spaces (MS) in a building composed by several floors.

As stated previously, the samples of the experimental study carried out are composed of N Instants of Time (t_j), for which independent Z measurements of M_{dvi} were collected from sensors located at different heights and positions; henceforth, each t_j has Z M_{dvi} measurements. The proposed statistical analysis carried out to estimate the uncertainties associated with measurements must be performed at M_{dvi} values centred with respect to an Average Measurement (M_a) (of MZ $(M_a)_{MZ}$ or MS $(M_a)_{MS}$) or Volume-Weighted Measurement (M_{vw}) (of MZ $(M_{vw})_{MZ}$); for which Equations 3.7, 3.8, 3.9 or 3.10 are used in order to have a new measurement value in each sensor measurement point, in this document, called Measurement Differential (θ_{dvi}). From this point on, each Instant of Time (t_j) has Z new measurement values (the Measurement Differentials (θ_{dvi})), which are centred on zero. For these new measurement values, the statistical uncertainty study is carried out to estimate the measurement uncertainties. Note that, for other analysis purposes, different reference measurements could be used to centre the M_{dvi} values.

Once the measurements have been centred with respect to an Average Measurement or a Volume-Weighted Average Measurement, the hypothesis that the centred instants of time are independent from each other can be considered. Now that we are working with the centred measurement differentials, for each time instant, the variations of θ_{dvi} are due to systematic and random variations

of the measurements from sensors within the Monitored Zone. Furthermore, the data collected over a long time span, and which have a large sample size, ensures that the data collected follows a type A distribution [103].

In the case where there is only one sensor measurement in a volume (or thermal zone), the M_{dv_i} value cannot be centred with respect to a reference measurement, so the proposed statistical analysis cannot be applied to these volumes.

$$V_{MZ} = \sum_{j=1}^n V_{MS_j} = \sum_{i=1}^g dv_i [m^3] \quad (3.1)$$

$$V_{MS} = \sum_{j=1}^y dv_j [m^3] \quad (3.2)$$

Where,

- V_{MZ} : MZ Volume [m^3].
- V_{MS} : MS Volume [m^3].
- dv_i : Differential Volume contained in an MZ or an MS [m^3].
- g : Number of Differential Volume in an MZ volume.
- y : Number of Differential Volume in an MS volume.
- n : Number of MS volumes contained in an MZ.

$$M_a = \sum_{i=1}^Z \frac{M_{dv_i}}{Z} [SI] \quad (3.3)$$

where for an MZ and MS volumes, M_a is defined by Equations 3.4 and 3.5:

$$(M_a)_{MZ} = \sum_{i=1}^p \frac{M_{dv_i}}{p} [SI] \quad (3.4)$$

$$(M_a)_{MS} = \sum_{i=1}^q \frac{M_{dv_i}}{q} [SI] \quad (3.5)$$

where,

- M_a : Average Measurement of a Volume for each t_j .
- $(M_a)_{MZ}$: Average Measurement of an MZ Volume for each t_j .
- $(M_a)_{MS}$: Average Measurement of an MS volume for each t_j .
- M_{dv_i} : Sensor Measurement for each t_j .
- p : Number of M_{dv_i} in an MZ for each t_j .
- q : Number of M_{dv_i} in an MS for each t_j .

$$(M_{vw})_{MZ} = \frac{1}{V_{MZ}} \sum_{j=1}^n V_{MS_j} \left(\frac{\sum_{i=1}^q (M_{dv_i})_{MS_i}}{q} \right) = \frac{1}{V_{MZ}} \sum_{j=1}^n V_{MS_j} (M_a)_{MS_j} [SI] \quad (3.6)$$

where,

- $(M_{vw})_{MZ}$: Volume-Weighted Measurement of an MZ for each t_j .
- $(M_{dv_i})_{MS}$: Sensor Measurement (M_{dv_i}) of an MS for each t_j .
- V_{MS} : Volume of an MS [m^3].
- V_{MZ} : Volume of an MZ [m^3].
- q : Number of M_{dv_i} in an MS for each t_j .
- n : Number of MS volumes contained in an MZ.

$$(\theta_{dv_i})_{vw} = (M_{dv_i} \text{ or } M_a) - (M_{vw})_{MZ} [SI] \quad (3.7)$$

where,

- $(\theta_{dv_i})_{vw}$: Measurement Differential with respect to the Volume-Weighted Measurement of an MZ for each t_j .
- M_{dv_i} : Sensor Measurement for each t_j .
- M_a : Average Measurement for each t_j .
- $(M_{vw})_{MZ}$: Volume Weighted Measurement of an MZ for each t_j .

$$(\theta_{dv_i})_a = M_{dv_i} - M_a[SI] \quad (3.8)$$

where for an MZ and MS volumes, θ_a is defined by Equations 3.9 and 3.10:

$$(\theta_{dv_i})_{MZ} = M_{dv_i} - (M_a)_{MZ}[SI] \quad (3.9)$$

$$(\theta_{dv_i})_{MS} = M_{dv_i} - (M_a)_{MS}[SI] \quad (3.10)$$

Where,

- $(\theta_{dv_i})_a$: Measurement Differential of M_{dv_i} centred on an Average Measurement for each t_j .
- $(\theta_{dv_i})_{MZ}$: Measurement Differential of M_{dv_i} centred on an Average Measurement of an MZ for each t_j .
- $(\theta_{dv_i})_{MS}$: Measurement Differential of M_{dv_i} centred on an Average Measurement of an MS for each t_j .
- M_{dv_i} Sensor Measurement for each t_j .
- M_a : Average Measurement for each t_j .
- $(M_a)_{MZ}$: Average Measurement of an MZ Volume for each t_j .
- $(M_a)_{MS}$: Average Measurement of an MS Volume for each t_j .

The zero centred data collected from sensor measurements follows a Type A distribution, M_{dv_i} , where the large sample size is composed of different time instants (t_j) and there are several measurements on each t_j . Table 3.1 shows the matrix of the raw data collected from the sensors.

The steps carried out for the statistical analysis to estimate the uncertainty of measurement are:

1. For more than one M_{dv_i} for each t_j :
 - (a) Transform the raw data of each time instant (t_j) (Table 3.1) into a centred Measurement Differential $(\theta_{dv_i})((\theta_{dv_i})_{vw}$ (Equation 3.7), $(\theta_{dv_i})_a$ (Equation 3.8), $(\theta_{dv_i})_{MZ}$ (Equation 3.9) or $(\theta_{dv_i})_{MS}$ (Equation 3.10)) for each instant of time (t_j), according to the volume type to be studied, V_{MZ} or V_{MS} analysis to be carried out. Now, for each time instant (t_j), a new normal distribution $N(\mu, \sigma)$ with mean, μ , and standard deviation, σ , (Table 3.2 or Table 3.3) is obtained.

- (b) Calculate the statistical parameters for θ_{dv_i} values of each t_j : the mean (μ), standard deviation (σ) and variance (σ^2) values, as well as the maximum (Max) and minimum (Min) values are obtained for each time instant (Table 3.4).
- (c) Calculate the Mean ($\bar{\mu}$), Mean Variance ($\bar{\sigma}^2$) and the Mean Standard Deviation ($\bar{\sigma}$) of the sample composed of N Instants of Time (t_N) (Table 3.5), based on the GUM method [103]. These statistical parameters are associated with the Measurement Uncertainty (U_M) estimation.
- (d) Estimate the Measurement Uncertainty (U_M), with a confidence interval of 95%, multiplying $\bar{\sigma}$ by $k=2$ (Table 3.6), based on the GUM method [103].

2. For volumes with a single M_{dv_i} measurement for each t_j , the method is not applicable.

In the case of the statistical analysis carried out in this research, Tables 3.4 and 3.5, the μ values are equal or close to zero. On the other hand, the σ and $\bar{\sigma}$ values determine the precision of the measurement, referring to how close the measured value is to the real one.

$M_{dv(i,t_j)} t_N$	t_1	t_2	t_3	...	t_N
$M_{dv(1,t_j)}$	$M_{dv(1,1)}$	$M_{dv(1,2)}$	$M_{dv(1,3)}$...	$M_{dv(1,N)}$
$M_{dv(2,t_j)}$	$M_{dv(2,1)}$	$M_{dv(2,2)}$	$M_{dv(2,3)}$...	$M_{dv(2,N)}$
$M_{dv(3,t_j)}$	$M_{dv(3,1)}$	$M_{dv(3,2)}$	$M_{dv(3,3)}$...	$M_{dv(3,N)}$
...
$M_{dv(Z,t_j)}$	$M_{dv(Z,1)}$	$M_{dv(Z,2)}$	$M_{dv(Z,3)}$...	$M_{dv(Z,N)}$

Table 3.1: Matrix of measured raw data for a sample composed of several t_j .

$(\theta_{dv(i,t_j)})_{vw}$ (Equation 3.7) t_N	t_1	t_2	t_3	...	t_N
$(\theta_{dv(1,t_j)})_{vw}$	$(\theta_{dv(1,1)})_{vw}$	$(\theta_{dv(1,2)})_{vw}$	$(\theta_{dv(1,3)})_{vw}$...	$(\theta_{dv(1,N)})_{vw}$
$(\theta_{dv(2,t_j)})_{vw}$	$(\theta_{dv(2,1)})_{vw}$	$(\theta_{dv(2,2)})_{vw}$	$(\theta_{dv(2,3)})_{vw}$...	$(\theta_{dv(2,N)})_{vw}$
$(\theta_{dv(3,t_j)})_{vw}$	$(\theta_{dv(3,1)})_{vw}$	$(\theta_{dv(3,2)})_{vw}$	$(\theta_{dv(3,3)})_{vw}$...	$(\theta_{dv(3,N)})_{vw}$
...
$(\theta_{dv(Z,t_j)})_{vw}$	$(\theta_{dv(Z,1)})_{vw}$	$(\theta_{dv(Z,2)})_{vw}$	$(\theta_{dv(Z,3)})_{vw}$...	$(\theta_{dv(Z,N)})_{vw}$

Table 3.2: Matrix of zero centred data with respect to $(M_{vw})_{MZ}$ with a Normal Distribution $N(\mu, \sigma)$ for each t_j .

$(\theta_{dv(i,t_j)})_a$ (Equation3.8) t_N	t_1	t_2	t_3	...	t_N
$(\theta_{dv(1,t_j)})_a$	$(\theta_{dv(1,1)})_a$	$(\theta_{dv(1,2)})_a$	$(\theta_{dv(1,3)})_a$...	$(\theta_{dv(1,N)})_a$
$(\theta_{dv(2,t_j)})_a$	$(\theta_{dv(2,1)})_a$	$(\theta_{dv(2,2)})_a$	$(\theta_{dv(2,3)})_a$...	$(\theta_{dv(2,N)})_a$
$(\theta_{dv(3,t_j)})_a$	$(\theta_{dv(3,1)})_a$	$(\theta_{dv(3,2)})_a$	$(\theta_{dv(3,3)})_a$...	$(\theta_{dv(3,N)})_a$
...
$(\theta_{dv(Z,t_j)})_a$	$(\theta_{dv(Z,1)})_a$	$(\theta_{dv(Z,2)})_a$	$(\theta_{dv(Z,3)})_a$...	$(\theta_{dv(Z,N)})_a$

Table 3.3: Matrix of data centred on M_a with a Normal Distribution $N(\mu, \sigma)$ for each t_j , also being applicable to data centred on $(M_a)_{MZ}$ (Equation3.9) or $(M_a)_{MS}$ (Equation3.10)

Statistical Parameters t_N	t_1	t_2	t_3	...	t_N
μ_{t_j} (Equation3.11)	μ_{t_1}	μ_{t_2}	μ_{t_3}	...	μ_{t_j}
$\sigma_{t_j}^2$ (Equation3.12)	$\sigma_{t_1}^2$	$\sigma_{t_2}^2$	$\sigma_{t_3}^2$...	$\sigma_{t_j}^2$
σ_{t_j} (Equation3.13)	σ_{t_1}	σ_{t_2}	σ_{t_3}	...	σ_{t_j}
Max_{t_j}	Max_{t_1}	Max_{t_2}	Max_{t_3}	...	Max_{t_j}
Min_{t_j}	Min_{t_1}	Min_{t_2}	Min_{t_3}	...	Min_{t_j}

Table 3.4: Matrix of statistical parameters of the Normal Distributions $N(\mu, \sigma)$ for each t_j .

Statistical Parameters	MZ	MS
$\bar{\mu}_{t_N}$ (Equation3.14)	$\bar{\mu}_{MZ}$	$\bar{\mu}_{MS}$
$\bar{\sigma}_{t_N}^2$ (Equation3.15)	$\bar{\sigma}_{MZ}^2$	$\bar{\sigma}_{MS}^2$
$\bar{\sigma}_{t_N}$ (Equation3.16)	$\bar{\sigma}_{MZ}$	$\bar{\sigma}_{MS}$

Table 3.5: Matrix of global statistical parameters of the Normal Distributions $N(\bar{\mu}, \bar{\sigma})$ for the t_N sample.

Measurement Uncertainty	Measurement Sensor Uncertainty	Measurement's Spatial Uncertainty
U_M (Equation3.17)	$U_{M(S)}$ (Equation3.17)	$U_M(SP)$ (Equation3.17)

Table 3.6: Expanded uncertainties of measurements.

$$\mu_{t_j} = \frac{1}{Z} \sum_{i=1}^Z \theta_{dv(i,t_j)} |_{j=1,2,\dots,N} [SI] \quad (3.11)$$

$$\sigma_{t_j}^2 = \frac{1}{Z-1} \sum_{i=1}^Z \left(\theta_{dv(i,t_j)} - \mu_{t_j} \right)^2 |_{j=1,2,\dots,N} [SI] \quad (3.12)$$

$$\sigma_{t_j} = \sqrt{\sigma_{t_j}^2 |_{j=1,2,\dots,N}[SI]} \quad (3.13)$$

$$\bar{\mu} = \frac{1}{N} \sum_{t_j=1}^N \mu_{t_j}[SI] \quad (3.14)$$

$$\bar{\sigma}^2 = \frac{1}{N} \sum_{t_j=1}^N \sigma_{t_j}^2[SI] \quad (3.15)$$

$$\bar{\sigma} = \sqrt{\bar{\sigma}^2}[SI] \quad (3.16)$$

$$\bar{U} = 2\bar{\sigma}[SI] \quad (3.17)$$

where,

- $\theta_{dv(i,t_j)}$: Measurement Differential, defined by the difference of M_{dv_i} with respect to M_a , $(M_a)_{MZ}$ or $(M_a)_{MS}$ for each t_j .
- μ_{t_j} : Mean of Measurement Differentials θ_{dv_i} for each t_j .
- $\sigma_{t_j}^2$: Variance of Measurement Differentials θ_{dv_i} for each t_j .
- σ_{t_j} : Experimental Standard Deviation of Measurement Differentials θ_{dv_i} for each t_j .
- $\bar{\mu}$: Mean of t_N samples.
- $\bar{\sigma}^2$: Mean Variance of t_N samples.
- $\bar{\sigma}$: Mean Standard Deviation of t_N samples, this value is associated to the Measurement Uncertainty estimation [SI].
- \bar{U} : Expanded uncertainty of Measurements.
- Z : Number of M_{dv_i} measurements in MZ ($Z = p$) or MS ($Z = q$) volume for each t_j .
- N : Sample Size defined by the number of Instants of Time (t_j).

3.2.2 Methodology to decouple systematic and random uncertainties of Type A samples

Within the thesis, a methodology to decouple the measurement uncertainties associated to the systematic and random errors for a Type A sample has been developed. The Measurement's Spatial Uncertainty $U_{M(SP)}$ includes the random causes of uncertainty, while the systematic errors are considered into the Measurement Sensor Uncertainty $U_{M(S)}$; these two uncertainties are independent of each other and are estimated as Expanded Uncertainties (\bar{U}). The Measurement Uncertainty (U_M) values include overall uncertainty sources, that is the $U_{M(S)}$ and $U_{M(SP)}$ values are included for any analysed volume (MZ or MS). Decoupling the U_M value, it is possible to estimate the $U_{M(SP)}$ value on the basis of the previous estimation of U_M and $U_{M(S)}$ through the statistical parameters set out above. The decoupling method is based on the sample's Mean Variance $\bar{\sigma}^2$ (Equation 3.15). Thus, through the analytical method of the mean-variance sum (Equation 3.22), it is possible to decouple the Measurement Uncertainties U_M (Equation 3.26), since the $U_{M(S)}$ value is independent of the rest of the causes of the Measurement Uncertainty, $U_{M(SP)}$, and both uncertainties make up the Measurement Uncertainty U_M value; then the Mean Variance $\bar{\sigma}^2$ associated to U_M is directly proportional to the sum of the mean variance associated to $U_{M(S)}$, $\bar{\sigma}_{(S)}^2$ and the mean variance associated to $U_{M(SP)}$, $\bar{\sigma}_{(SP)}^2$.

Equations 3.18, 3.19, 3.20, 3.21, 3.22, 3.23, 3.24, 3.25, 3.26 3.27, 3.28 and Equation 3.29 show the analytical development of the decoupling method of Measurement Uncertainty U_M (Equation 3.26), so it is possible to obtain $U_{M(SP)}$ with Equation 3.25.

$$U_M = 2\bar{\sigma}_M = 2\left(\sqrt{\bar{\sigma}_M^2}\right) = 2\left(\sqrt{\frac{1}{N} \sum_{t_N=1}^N \left[\sigma_{t_j(S)}^2 + \sigma_{t_j(SP)}^2\right]}\right) [SI] \quad (3.18)$$

$$\begin{aligned} \bar{\sigma}_M^2 &= \frac{1}{N} \sum_{t_N=1}^N \left[\sigma_{(S)}^2 + \sigma_{(SP)}^2\right] = \\ &= \frac{1}{N} \left(\sigma_{t_1(S)}^2 + \sigma_{t_1(SP)}^2 + \sigma_{t_2(S)}^2 + \sigma_{t_2(SP)}^2 + \dots + \sigma_{t_N(S)}^2 + \sigma_{t_N(SP)}^2\right) = \\ &= \frac{1}{N} \left(\sigma_{t_1(S)}^2 + \sigma_{t_2(S)}^2 + \dots + \sigma_{t_N(S)}^2 + \sigma_{t_1(SP)}^2 + \sigma_{t_2(SP)}^2 + \dots + \sigma_{t_N(SP)}^2\right) = \\ &= \frac{1}{N} \left(\sigma_{t_1(S)}^2 + \sigma_{t_2(S)}^2 + \dots + \sigma_{t_N(S)}^2\right) + \frac{1}{N} \left(\sigma_{t_1(SP)}^2 + \sigma_{t_2(SP)}^2 + \dots + \sigma_{t_N(SP)}^2\right) [SI] \quad (3.19) \end{aligned}$$

$$\bar{\sigma}_{t_N(S)}^2 = \frac{1}{N} \left(\sigma_{t_1(S)}^2 + \sigma_{t_2(S)}^2 + \dots + \sigma_{t_N(S)}^2\right) [SI] \quad (3.20)$$

$$\bar{\sigma}_{t_N(SP)}^2 = \frac{1}{N} \left(\sigma_{t_1(SP)}^2 + \sigma_{t_2(SP)}^2 + \dots + \sigma_{t_N(SP)}^2 \right) [SI] \quad (3.21)$$

$$\bar{\sigma}_M^2 = \sigma_{(S)}^2 + \sigma_{(SP)}^2 [SI] \quad (3.22)$$

$$\bar{\sigma}_{(SP)}^2 = \bar{\sigma}_M^2 - \bar{\sigma}_{(S)}^2 [SI] \quad (3.23)$$

$$\bar{\sigma}_{(SP)} = \sqrt[2]{\left(\bar{\sigma}_M^2 - \bar{\sigma}_{(S)}^2 \right)} [SI] \quad (3.24)$$

$$U_{M(SP)} = 2 \left(\bar{\sigma}_{(SP)} \right) [SI] \quad (3.25)$$

$$U_M = 2 \left(\sqrt[2]{\bar{\sigma}_{(S)}^2 + \bar{\sigma}_{(SP)}^2} \right) = 2 \left(\sqrt[2]{\bar{\sigma}_M^2} \right) = 2 \left(\bar{\sigma}_M \right) [SI] \quad (3.26)$$

$$\bar{\sigma}_{(S)}^2 = \bar{\sigma}_M^2 - \bar{\sigma}_{(SP)}^2 [SI] \quad (3.27)$$

$$\bar{\sigma}_{(S)} = \sqrt[2]{\left(\bar{\sigma}_M^2 - \bar{\sigma}_{(SP)}^2 \right)} [SI] \quad (3.28)$$

$$U_{M(S)} = 2 \left(\bar{\sigma}_{(S)} \right) = \sqrt[2]{\left(\bar{\sigma}_{(S)}^2 \right)} = \sqrt[2]{\left(\bar{\sigma}_M^2 - \bar{\sigma}_{(SP)}^2 \right)} [SI] \quad (3.29)$$

where,

- U_M : Measurement Uncertainty.

- $\bar{\sigma}_M^2$: Mean Variance of t_N samples associated to U_M .
- $\bar{\sigma}_M$: Mean Standard Deviation of t_N samples associated to U_M .
- $U_{M(SP)}$: Measurement's Spatial Uncertainty.
- $\bar{\sigma}_{(SP)}^2$: Mean Variance of t_N samples associated to $U_{M(SP)}$.
- $\bar{\sigma}_{(SP)}$: Mean Standard Deviation of t_N samples associated to $U_{M(SP)}$.
- $U_{M(S)}$: Measurement Sensor Uncertainty.
- $\bar{\sigma}_{(S)}^2$: Mean Variance of t_N samples associated to $U_{M(S)}$.
- $\bar{\sigma}_{(S)}$: Mean Standard Deviation of t_N samples associated to $U_{M(S)}$.
- $\sigma_{t_j}^2$: Variance of Z Measurement Differential (θ_{dv_i}) $((\theta_{dv_i})_{vw}$ (Equation 3.7) or $(\theta_{dv_i})_a$ (Equation 3.8)) for each t_j .
- $\sigma_{t_j(S)}^2$: Variance of Z Measurement Differential (θ_{dv_i}) $((\theta_{dv_i})_{vw}$ (Equation 3.7) or $(\theta_{dv_i})_a$ (Equation 3.8)) for each t_j due to Sensor Uncertainty $U_{M(S)}$.
- $\sigma_{t_j(SP)}^2$: Variance of Z Measurement Differential (θ_{dv_i}) $((\theta_{dv_i})_{vw}$ (Equation 3.7) or $(\theta_{dv_i})_a$ (Equation 3.8)) for each t_j due to Measurement Spatial Uncertainty $U_{M(SP)}$.

The decoupling method allows us to know the relation between the Sensor Mean Variance ($\bar{\sigma}_{(S)}^2$) and the Measurement Sensor Uncertainty ($U_{M(S)}$) with respect to the overall Mean Variance and the Measurement Uncertainty (U_M). This relation is called, in this manuscript, the Sensor Ratio (R_S) (Equation 3.30) and it represents the weight of the systematic causes over all uncertainties, where the $\bar{\sigma}_{(S)}^2$ value can also be defined through Equation 3.31.

$$R_{(S)} = \frac{\bar{\sigma}_{(S)}^2}{\bar{\sigma}_M^2} [SI] \quad (3.30)$$

$$\bar{\sigma}_{(S)}^2 = R_{(S)} (\bar{\sigma}_M^2) [SI] \quad (3.31)$$

where,

- $\bar{\sigma}_{(S)}^2$: Mean Variance of t_N samples associated to $U_{M(S)}$.
- $R_{(S)}$: Ratio of Mean Variance of t_N samples due to $U_{M(S)}$ with respect to Mean Variance of t_N Samples due to U_M .

On the other hand, it is possible to obtain the relation between the Mean Variance $\bar{\sigma}_{(SP)}$ associated to $U_{M(SP)}$ with respect to the Mean Variance $\bar{\sigma}^2$ associated to U_M through Equation 3.30, thus obtaining the Spatial Ratio R_{SP} through Equation 3.32, which represents the weight of the random causes over all uncertainties, where the $\bar{\sigma}_{(SP)}^2$ value can also be defined through Equation 3.33.

$$R_{(SP)} = \frac{\bar{\sigma}_{(SP)}^2}{\bar{\sigma}_M^2} [SI] \quad (3.32)$$

$$\bar{\sigma}_{(SP)}^2 = R_{(SP)} (\bar{\sigma}_M^2) [SI] \quad (3.33)$$

where,

- $\bar{\sigma}_{(SP)}^2$: Mean Variance of t_N samples associated to $U_{M(SP)}$.
- $R_{(SP)}$: Ratio of Mean Variance of t_N samples due to $U_{M(SP)}$ with respect to Mean Variance of t_N Samples due to U_M .

Knowing the $R_S, U_{M(S)}, \bar{\sigma}_{(S)}^2$ and $\bar{\sigma}_{(S)}$ values, for a Monitored Zone, it is possible to estimate the $\bar{\sigma}_{(SP)}^2, \bar{\sigma}_{(SP)}$ and $U_{M(SP)}$ values through Equations 3.34, 3.35 and 3.36, respectively, and also the $\bar{\sigma}^2, \bar{\sigma}$ and U_M values by applying Equations 3.37, 3.38 and 3.39, respectively.

$$\bar{\sigma}_{(SP)}^2 = \bar{\sigma}_M^2 - \bar{\sigma}_{(S)}^2 = \frac{\bar{\sigma}_{(S)}^2}{R_{(S)}} - \bar{\sigma}_{(S)}^2 = \bar{\sigma}_{(S)}^2 \left(\frac{1}{R_{(S)}} - 1 \right) = \bar{\sigma}_{(S)}^2 \left(\frac{1 - R_{(S)}}{R_{(S)}} \right) [SI] \quad (3.34)$$

$$\bar{\sigma}_{(SP)} = \sqrt{\bar{\sigma}_M^2 - \bar{\sigma}_{(S)}^2} = \sqrt{\frac{\bar{\sigma}_{(S)}^2}{R_{(S)}} - \bar{\sigma}_{(S)}^2} = \sqrt{\bar{\sigma}_{(S)}^2 \left(\frac{1}{R_{(S)}} - 1 \right)} = \sqrt{\bar{\sigma}_{(S)}^2 \left(\frac{1 - R_{(S)}}{R_{(S)}} \right)} [SI] \quad (3.35)$$

$$U_{M(SP)} = 2 (\bar{\sigma}_{(SP)}) = 2 \left(\sqrt{\bar{\sigma}_{(SP)}^2} \right) = 2 \left(\sqrt{\bar{\sigma}_M^2 - \bar{\sigma}_{(S)}^2} \right) = 2 \left(\sqrt{\frac{\bar{\sigma}_{(S)}^2}{R_{(S)}} - \bar{\sigma}_{(S)}^2} \right) = 2 \left(\sqrt{\bar{\sigma}_{(S)}^2 \left(\frac{1}{R_{(S)}} - 1 \right)} \right) = 2 \left(\sqrt{\bar{\sigma}_{(S)}^2 \left(\frac{1 - R_{(S)}}{R_{(S)}} \right)} \right) [SI] \quad (3.36)$$

$$\bar{\sigma}_M^2 = \frac{\bar{\sigma}_{(S)}^2}{R_{(S)}} = \frac{\bar{\sigma}_{(SP)}^2}{R_{(SP)}} [SI] \quad (3.37)$$

$$\bar{\sigma}_M = \sqrt[2]{\frac{\bar{\sigma}_{(S)}^2}{R_{(S)}}} = \sqrt[2]{\frac{\bar{\sigma}_{(SP)}^2}{R_{(SP)}}} [SI] \quad (3.38)$$

$$U_M = 2(\bar{\sigma}) = 2 \left(\sqrt[2]{\frac{\bar{\sigma}_{(S)}^2}{R_{(S)}}} \right) = 2 \left(\sqrt[2]{\frac{\bar{\sigma}_{(SP)}^2}{R_{(SP)}}} \right) [SI] \quad (3.39)$$

where,

- U_M : Measurement Uncertainty.
- $\bar{\sigma}_M^2$: Mean Variance of t_N samples associated to U_M .
- $\bar{\sigma}_M$: Mean Standard Deviation of t_N samples associated to U_M .
- $U_{M(SP)}$: Measurement's Spatial Uncertainty.
- $\bar{\sigma}_{(SP)}^2$: Mean Variance of t_N samples associated to $U_{M(SP)}$.
- $\bar{\sigma}_{(SP)}$: Mean Standard Deviation of t_N samples associated to $U_{M(SP)}$.
- $U_{M(S)}$: Measurement Sensor Uncertainty.
- $\bar{\sigma}_{(S)}^2$: Mean Variance of t_N samples associated to $U_{M(S)}$.
- $\bar{\sigma}_{(S)}$: Mean Standard Deviation of t_N samples associated to $U_{M(S)}$.
- $R_{(SP)}$: Ratio of Mean Variance of t_N samples due to $U_{M(SP)}$ with respect to Mean Variance of t_N Samples due to U_M .
- $R_{(S)}$: Ratio of Mean Variance of t_N samples due to $U_{M(S)}$ with respect to Mean Variance of t_N Samples due to U_M .

If the R_{SP} , $U_{M(SP)}$, $\bar{\sigma}_{(SP)}^2$ and $\bar{\sigma}_{(SP)}$ values are known, it is possible to estimate the $\bar{\sigma}_{(S)}^2$, $\bar{\sigma}_{(S)}$ and $U_{M(S)}$, values through Equations 3.40, 3.41 and 3.42, respectively.

$$\bar{\sigma}_{(S)}^2 = \bar{\sigma}_M^2 - \bar{\sigma}_{(SP)}^2 = \frac{\bar{\sigma}_{(SP)}^2}{R_{(SP)}} - \bar{\sigma}_{(SP)}^2 = \bar{\sigma}_{(SP)}^2 \left(\frac{1}{R_{(SP)}} - 1 \right) = \bar{\sigma}_{(SP)}^2 \left(\frac{1 - R_{(SP)}}{R_{(SP)}} \right) [SI] \quad (3.40)$$

$$\bar{\sigma}_{(S)} = \sqrt[2]{\bar{\sigma}_M^2 - \bar{\sigma}_{(SP)}^2} = \sqrt[2]{\frac{\bar{\sigma}_{(SP)}^2}{R_{(SP)}} - \bar{\sigma}_{(SP)}^2} = \sqrt[2]{\bar{\sigma}_{(SP)}^2 \left(\frac{1}{R_{(SP)}} - 1 \right)} = \sqrt[2]{\bar{\sigma}_{(SP)}^2 \left(\frac{1 - R_{(SP)}}{R_{(SP)}} \right)} [SI] \quad (3.41)$$

$$U_{M(S)} = 2 \left(\bar{\sigma}_{(S)} \right) = 2 \left(\sqrt[2]{\bar{\sigma}_{(S)}^2} \right) = 2 \left(\sqrt[2]{\bar{\sigma}_M^2 - \bar{\sigma}_{(SP)}^2} \right) = 2 \left(\sqrt[2]{\frac{\bar{\sigma}_{(SP)}^2}{R_{(SP)}} - \bar{\sigma}_{(SP)}^2} \right) = \\ 2 \left(\sqrt[2]{\bar{\sigma}_{(SP)}^2 \left(\frac{1}{R_{(SP)}} - 1 \right)} \right) = 2 \left(\sqrt[2]{\bar{\sigma}_{(SP)}^2 \left(\frac{1 - R_{(SP)}}{R_{(SP)}} \right)} \right) [SI] \quad (3.42)$$

where,

- $U_{M(S)}$: Measurement Sensor Uncertainty.
- $\bar{\sigma}_{(S)}^2$: Mean Variance of t_N samples associated to $U_{M(S)}$.
- $\bar{\sigma}_{(S)}$: Mean Standard Deviation of t_N samples associated to $U_{M(S)}$.
- $\bar{\sigma}_{(SP)}^2$: Mean Variance of t_N samples associated to $U_{M(SP)}$.
- $R_{(SP)}$: Ratio of Mean Variance of t_N samples due to $U_{M(SP)}$ with respect to Mean Variance of t_N Samples due to U_M .

Estimation of the range of the representative measurement through the uncertainty estimation

The Measurement Uncertainty (U_M) can be estimated for an MZ or MS independently, so it is possible to estimate the range where a representative measurement can be. In the case of estimating the measurement range for an MZ, it is necessary to identify whether the whole or a large part of the MZ is monitored, or if only one or some MS are monitored (the entire MZ volume is not usually monitored).

To estimate the ranges, it is first necessary to carried out a pre-monitoring to estimate the $(M_a)_{MS}$, $(M_a)_{MZ}$ and $(M_{vw})_{MZ}$ values. In this pre-monitoring, all or a large part of the whole MZ volume must be monitored, and their MSs must be monitored with more than one sensor.

Figures 3.2 and 3.3 show an scheme of the two estimation ranges of the representative measurements when the whole MZ is monitored and where one or several MSs are monitored. Henceforth, the measurements carried out after the pre-monitoring are called post-monitoring. Thus, the different cases are set out to below.

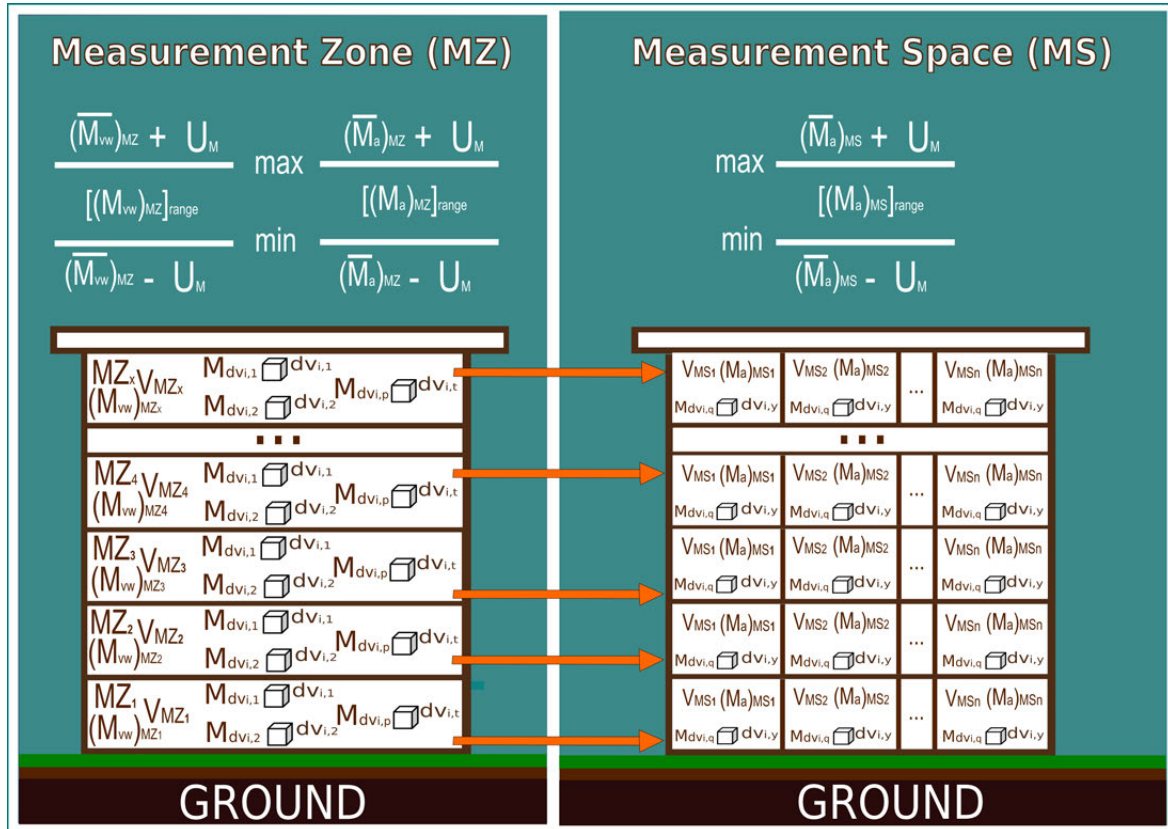


Figure 3.2: Scheme of $[(\bar{M}_{vw})_{MZ}]_{range}$ and $[(\bar{M}_a)_{MZ}]_{range}$ estimation based on the U_M estimation.

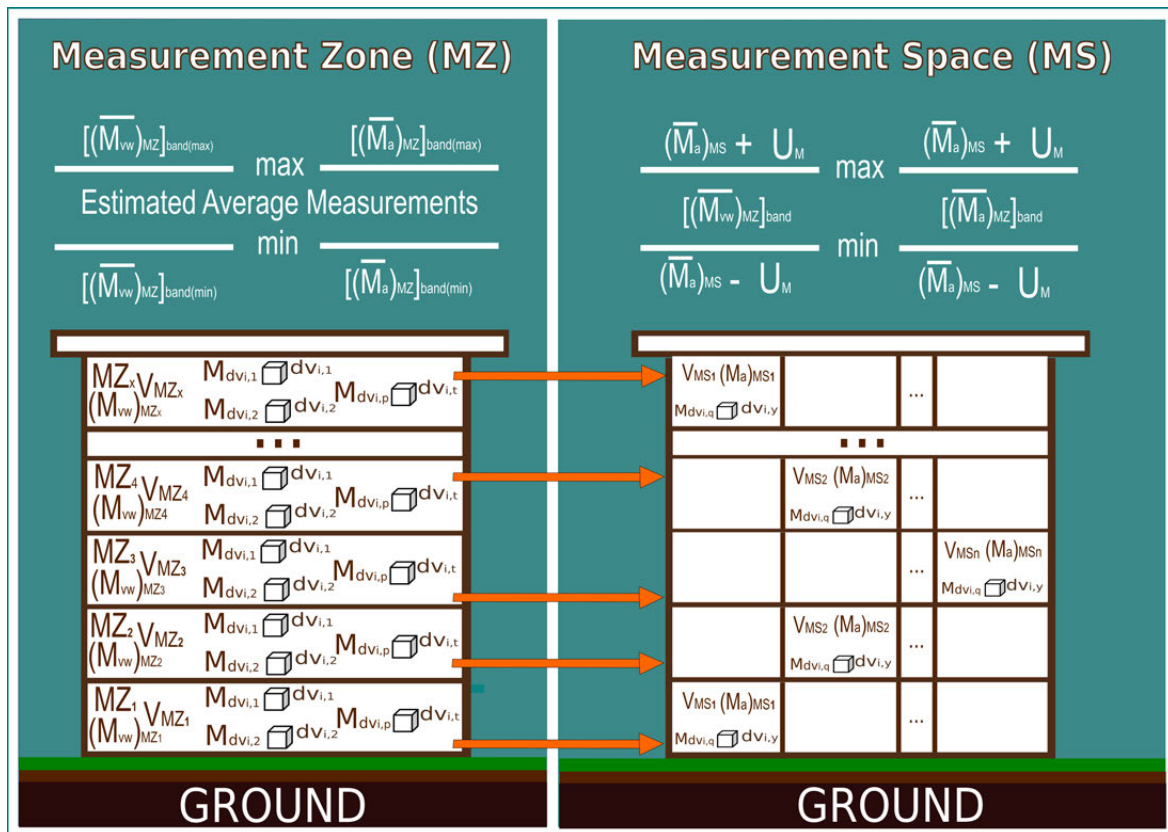


Figure 3.3: Scheme of $[(\bar{M}_{vw})_{MZ}]_{band}$ and $[(\bar{M}_a)_{MZ}]_{band}$ estimation when one or some MSs are monitored to measure a intensive variable in a MZ.

The overall MZ volume is monitored to obtain M_{dv_i} values

In this case, $(M_a)_{MZ}$ or $(M_{vw})_{MZ}$ values are calculated taking into account the M_{dv_i} of all the sensors installed in the whole MZ volume; while the U_M value is estimated for M_{dv_i} values centred on $(M_a)_{MZ}$ or $(M_{vw})_{MZ}$. To determine the range within which the representative measurement values of a monitored MZ lie, Equations 3.43 and 3.44, respectively, are used for the Volume Weighted Measurement of a t_N period ($(\overline{M}_{vw})_{MZ}$) or the Average Measurement of a t_N period ($(\overline{M}_a)_{MZ}$) values, obtained in a post-monitoring. Figure 3.2 shows a scheme of the range of measurement of the case described.

$$M_{vw} - 2 \left(\sqrt[2]{\frac{\overline{\sigma}_{(S)}^2}{R_{(S)}}} \right) = M_{vw} - U_M \leq [\overline{M}_{vw}]_{range} \leq M_{vw} + U_M = M_{vw} + 2 \left(\sqrt[2]{\frac{\overline{\sigma}_{(S)}^2}{R_{(S)}}} \right) [SI] \quad (3.43)$$

$$M_a - 2 \left(\sqrt[2]{\frac{\overline{\sigma}_{(S)}^2}{R_{(S)}}} \right) = M_a - U_M \leq [\overline{M}_a]_{range} \leq M_a + U_M = M_a + 2 \left(\sqrt[2]{\frac{\overline{\sigma}_{(S)}^2}{R_{(S)}}} \right) [SI] \quad (3.44)$$

where,

- M_{vw} : Volume Weighted Measurement of an MZ volume $(M_{vw})_{MZ}$ (Equation 3.6) for each t_j .
- M_a : Average Measurement of a volume $(M_a)_{MZ}$ (Equation 3.4) or $(M_a)_{MS}$ (Equation 3.5) for a t_N sample.
- $[\overline{M}_{vw}]_{range}$: Maximum and Minimum limits in which M_{vw} of t_N (\overline{M}_{vw}) fluctuates.
- $[\overline{M}_a]_{range}$: Maximum and Minimum limits in which M_a of t_N (\overline{M}_a) fluctuates.

One MS volume of an MZ volume is monitored to obtain M_{dv_i} values

This case is the most common as sensors are installed in one or some MSs to collect intensive measurement data for a studied MZ volume⁴, where the $(M_a)_{MZ}$ or $(M_{vw})_{MZ}$ values are unknown for a t_j or a period studied in a post-monitoring. However, through the procedure set out to below, it will be possible to estimate these values from the $(M_a)_{MS}$ value of a monitored MS.

In the pre-monitoring, the $(M_a)_{MZ}$ or $(M_{vw})_{MZ}$ values and $(M_a)_{MS}$ values should be calculated, together with the statistical parameters for the $(M_a)_{MS}$ centred on these $(M_a)_{MZ}$ or $(M_{vw})_{MZ}$ values to obtain the U_M estimation. This estimated U_M is based on the comparison between the average measurement of an MS ($(M_a)_{MS}$) and the average measurement of the MZ ($(M_a)_{MZ}$ or $(M_{vw})_{MZ}$).

⁴For example, sensors to measure temperature, relative humidity, CO₂, the thermostats, etc., are installed in one or some MSs (e.g. room or office) in an MZ (e.g., building or dwelling)

The information that gives this uncertainty is the amount of variation (accuracy) there is between the average measures of an MS with respect to the average measures of an MZ.

Once the U_M value has been estimated from the exposed average comparisons, it is possible to estimate a band within which $(\overline{M}_a)_{MZ}$ ($(M_a)_{MS}$ of the t_N sample) or the $(\overline{M}_{vw})_{MZ}$ ($(M_{vw})_{MS}$ of the t_N sample) values can be, if whole MZ volume was monitored, but having only one MS monitored. The estimation of the average measurement of an MZ is given by the Total Average Measurement Bandwidth [$(\overline{M}_{vw})_{MZ}]_{band}$ (Equation 3.45) or [$(\overline{M}_a)_{MZ}]_{band}$ (Equation 3.46)]. Figure 3.3 shows an scheme of the band in which the $(\overline{M}_a)_{MZ}$ of the MZ can be when there is only one monitored MS.

$$(M_a)_{MS} - U_M \leq [(\overline{M}_{vw})_{MZ}]_{band} \leq (M_a)_{MS} + U_M[SI] \quad (3.45)$$

$$(M_a)_{MS} - U_M \leq [(\overline{M}_a)_{MZ}]_{band} \leq (M_a)_{MS} + U_M[SI] \quad (3.46)$$

where,

- [$(\overline{M}_{vw})_{MZ}]_{band}$: Volume Weighted Measurement's Bandwidth. Maximum and Minimum limits in which M_{vw} of t_N ($(\overline{M}_{vw})_{MZ}$) of the MZ fluctuate, based on one measurement of an MS that forms part of it.
- [$(\overline{M}_a)_{MZ}]_{band}$: Average Measurement's Bandwidth of an MZ. Maximum and Minimum limit in which M_a of t_N ($(\overline{M}_a)_{MZ}$) of the MZ fluctuate, based on one measurement of an MS that forms part of it.

3.2.3 Vertical analysis of Measurement Uncertainty (U_M): vertical stratification's behaviour

The vertical analysis of the Measurement Uncertainty (U_M) is a particular study of the uncertainty analysis, where it is possible, through this study, to estimate the vertical stratification, as a cause of having changes at different heights in intensive variable measurements [137]. This analysis will be applied to measurements from the sensor group (the sensors located in the same vertical line make up a sensor group), where each sensor measures (M_{dv_i}) at different heights in an MZ or MS.

The M_{dv_i} values located in the same vertical line are centred on its M_a value (Equation 3.3). Then, for the new values obtained, $(\theta_{dv_i})_a$ for each t_j , several combinations of these sensors located at different heights (called sensor group) must be done. For these group of sensors with Z values of $(\theta_{dv_i})_a$ for each t_j , the statistical analysis has been carried out in order to estimate the Measurement Uncertainty (U_M) for vertical measurements. In this particular case, the estimated uncertainty is called the Vertical Measurement Uncertainty (U_{VM}), which includes systematic and random causes.

The Mean Variance and Mean Standard Deviation associated to U_{VM} are $\bar{\sigma}_{VM}^2$ and $\bar{\sigma}_{VM}$ respectively. For the $(\theta_{dv_i})_a$ values (Equation 3.8) obtained, Equations 3.15, 3.16 and 3.17 are used to estimate $\bar{\sigma}_{VM}$, $\bar{\sigma}_{VM}^2$ and U_{VM} , respectively. Likewise, it could be possible to decouple U_{VM} to obtain the U_S and U_{SP} associated to this uncertainty, applying the same procedure as for U_M (section 3.2.2).

3.2.4 Impact of spatial localisation over U_M

The aim of studying the impact of the spatial location of sensors over U_M is to find the best location to install the sensors so as to reduce the uncertainties associated to each measurement. The analysis should be done for sensors installed at the same height in order to eliminate the vertical stratification in the measures. To study the impact it is necessary to analyse a group of sensors installed in different horizontal locations in an MZ. The first step is to centre the M_{dv_i} values on M_a or M_{vw} of all the installed sensors to be studied, in order to obtain the new values, $(\theta_{dv_i})_a$ or $(\theta_{dv_i})_{vw}$ for each t_j . Then, a combination of sensors located in different spaces of the studied MZ are put together to create the group of sensors to be studied. Each group of sensors have their $(\theta_{dv_i})_a$ or $(\theta_{dv_i})_{vw}$, which have been obtained previously. The statistical analysis to obtain the U_M estimation for each group of sensors is carried out for their $(\theta_{dv_i})_a$ or $(\theta_{dv_i})_{vw}$.

3.2.5 Impact of number of sensors installed at the same height, but in different horizontal locations to decrease the Measurement Uncertainty (U_M) in an MZ

This study is implemented using a group of sensors installed at the same height and distributed in different horizontal locations. All M_{dv_i} values of each t_j are centred on M_a or M_{vw} to obtain $(\theta_{dv_i})_a$ or $(\theta_{dv_i})_{vw}$. Then, to each t_j (with Z $(\theta_{dv_i})_a$ or $(\theta_{dv_i})_{vw}$), the t-student method is applied to estimate the $\bar{\sigma}_M$ values for each t_j . Note that this mean standard deviation is over each instant of time t_j , not over the t_N sample). By plotting the $\bar{\sigma}_M$ of t_j , the evolution of $\bar{\sigma}_M$ for different numbers of sensors (Z θ_{dv_i} values) is obtained.

3.3 Design of Monitoring and Control Systems (MCS) for HLC estimation for buildings

As has been shown in the literature review of section 2.3.3, the Co-Heating Method [19] has been implemented in many projects since the 1970s, so this method can now be considered as a standard method to estimate the HLC in unoccupied buildings. The Average Method [24] to estimate the HLC in in-use buildings is currently it is being implemented in different research projects in order to be standardized.

To design and implement an MCS in a building in order to estimate the HLC through the Co-Heating Method and Average Method, it is necessary to identify the sensors and hardware to measure and collect data concerning the variables involved in the HLC estimation and its decoupling. For this, the MCS requirements for each method are set out below, together with other optional measurements to obtain the one dimensional Transmission Heat Transfer Coefficient (U-value), following the ISO 9869

method [20], and to estimate the heat loss through the Domestic Hot water (DHW) expelled from the dwelling or building.

HLC estimation through the Co-Heating Method: This method is used in unoccupied buildings and is based on Equation 2.22. The MCS requirements are:

- Electrical equipments:
 - Electrical radiators, heating system.
 - Fans to homogenize the indoor air temperature.
- Monitoring System sensors:
 - Indoor Air Temperature (T_{in}) sensors.
 - Outdoor Air Temperature (T_{out}) sensors.
 - Electrical energy meters.
 - Pyranometer (South vertical global solar radiation).
 - Superficial Temperature (T_{sup}) sensors (Optional): These measurements, together with the heat flux meter in the main typologies of the building walls, following the ISO 9869 method [20], could permit us to obtain the one dimensional transmission heat transfer coefficient (U-value) of the main wall typologies of the building envelope. Having these U-values could help us to understand the deviations between the design and actual HLC value of the analysed buildings.
 - Superficial heat flux sensors (Fluximeters) (Optional):
 - Blower door test or tracer gas test to estimate the infiltration heat loss coefficient (C_v) and permit the decoupling of the estimated HLC values into infiltration (C_v) and transmission (UA-value) heat loss coefficients [21] (see section 2.2.4).
- Controlling System
 - Hardware for data acquisition: Central Processing Unit (CPU).
 - Relay or controlling system for Indoor air temperature.
 - Supervisory Control And Data Acquisition (SCADA) [138].

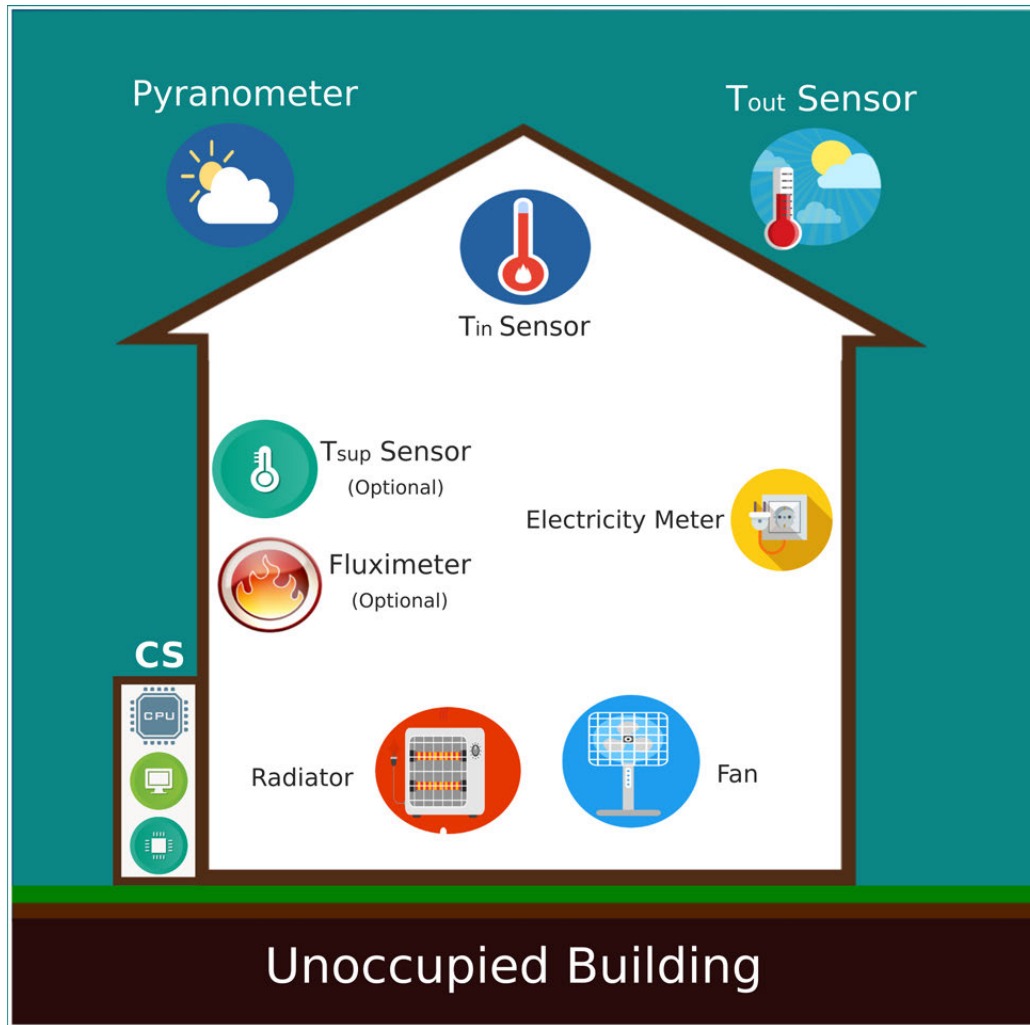


Figure 3.4: Scheme of MCS requirement of Co-Heating test to estimate the HLC.

HLC estimation through the Average Method: This method is applied to in-use buildings, the MCS requirements based on Equation 2.18 are:

- Monitoring System sensors:
 - Indoor Air Temperature (T_{in}) sensors.
 - Outdoor Air Temperature (T_{out}) sensors.
 - Electrical energy meters: These electrical meters should only measure the electricity consumption within the building envelope that will end up as a heat input to the indoor air. In other words, the electrical consumptions for heating domestic hot water, washing machine or dishwasher will mainly leave the building through the drain tubes and will not be used to heat up the indoor air. Then, this heat should not be considered in the energy balance presented in section 2.2.2, since this heat will not leave the building through the building envelope in the forms of transmission or infiltration/ventilation losses. Thus, to develop the Monitoring system for in-use buildings, it is crucial to understand which of the electrical consumptions within the building end up as heat in the indoor air and participate

in the energy balance that has permitted us to obtain the Equation 2.18.

- Calorimeters (for heating and DHW systems): When domestic hot water is produced together with the space heating, which part of the heat is used for Domestic Hot water (DHW) production and which part is used for space heating must be measured accurately. As for the electrical consumptions, the heat used to produce DHW mainly leaves the building through the hot water drain and is not transmitted to the indoor air, so it should not be considered in Equation 2.18.
- HVAC sensors: As presented in section 2.2.4, when we have ventilation systems, it is necessary to monitor them, adequately measuring the supply and exhaust mass flow rates together with the temperatures of the supply and exhaust air streams in order to be able to estimate the ventilation heat loss coefficient. If this is not measured, it will be impossible to decouple the estimated HLC values into the infiltration/ventilation (C_v) and transmission (UA) heat loss coefficients.
- Indoor and outdoor Carbon Dioxide (CO_2) sensor: Measuring the indoor and outdoor CO_2 concentration values could following the procedure presented in section 2.2.4 enable, the estimation of the overall infiltration plus ventilation rates. Then, combining these results with the HVAC system measurements, it could be possible to estimate the infiltration and ventilation heat loss coefficients (C_v) and finally decouple the estimated HLC value to obtain the transmission heat loss coefficient (UA -value) of the building envelope. Furthermore, the indoor CO_2 concentration, together with the infiltration/ventilation analysis, can permit us to estimate the metabolic heat generation within the occupied buildings with a certain accuracy.
- Gas meters (Optional): Measuring the gas consumption, together with the heat produced for space heating and Domestic Hot Water (DHW), will permit us (with just one more sensor) to correctly characterize the boiler's seasonal efficiencies and we will be able to compare them with the theoretical ones.
- Pyranometer (Horizontal global solar radiation) (Optional): In case there is not an available nearby meteorological station, this variable should be measured so as to be able to detect cloudy periods with just diffuse solar radiation and also allow as to make rough estimates of the solar gains.
- Superficial Temperature (T_{sup}) sensors (Optional): These measurements, together with the heat flux meter in the main typologies of the building walls, following the ISO 9869 method [20], could permit us to obtain the one-dimensional transmission heat transfer coefficient (U-value) of the main wall typologies of the building envelope. Having these U-values could help us to understand the deviations between the design and actual HLC values of the analysed buildings.

- Superficial heat flux sensors (Fluximeters) (Optional).
- Control System
 - Hardware for data acquisition: Central Processing Unit (CPU).
 - SCADA or BMS.

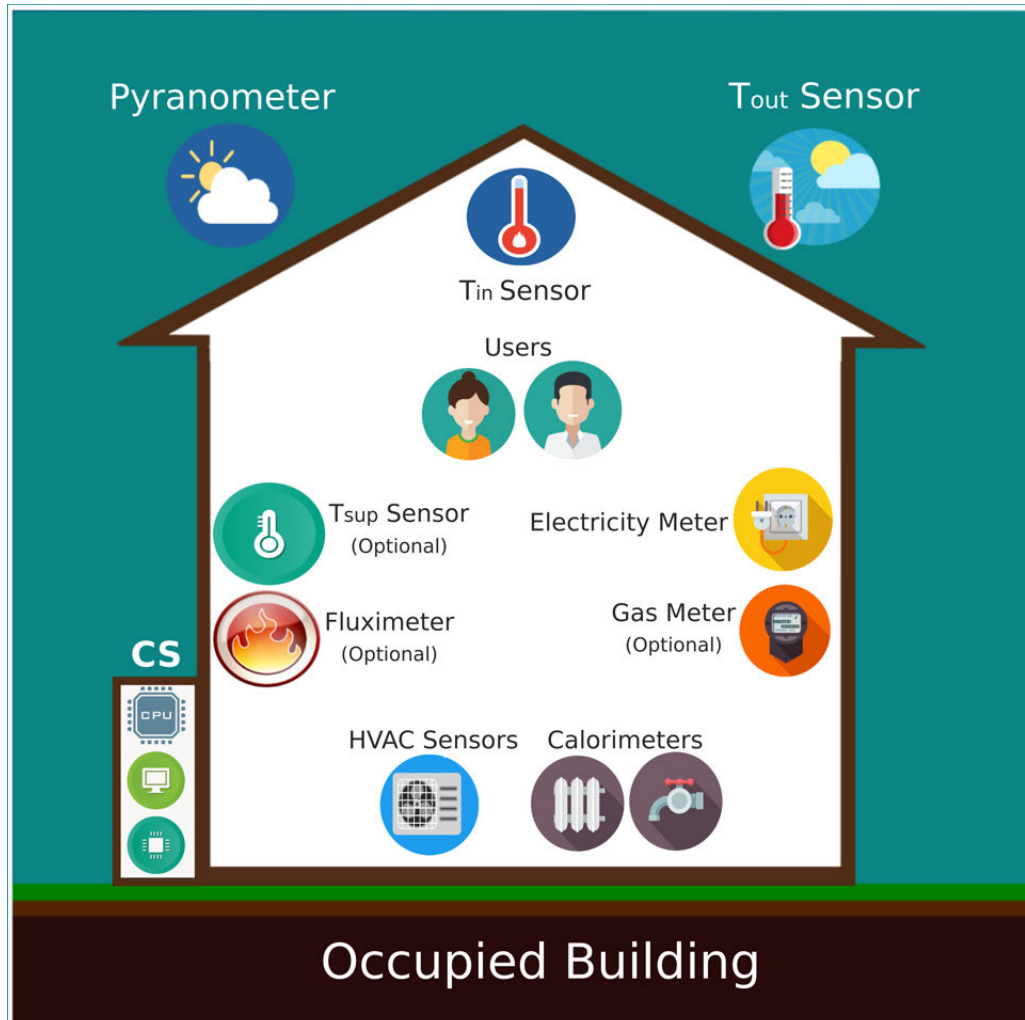


Figure 3.5: Scheme of MCS requirement of Average method to estimate the HLC.

3.4 Conclusions

The methodology developed allows the overall measurement uncertainty of such intensive variables as T_{in} and T_{out} to be estimated, with the aim of obtaining a more reliable estimation of the HLC of a building through the Co-Heating Method and the Average Method. It also allows us to know the weight of the random and systematic errors in the value of the total uncertainty of the measurement of these variables, through the decoupling method of overall uncertainty.

The identification of the equipment needed to measure the variables involved in the estimation of the HLC, and to collect these data, will allow the design and implementation of a comprehensive

Monitoring and Control System in a residential or tertiary building. This system will be oversized to measure all the possible variables that can affect the estimation and decoupling of the HLC. Then, through the analysis proposed in the next section, the minimum number of sensors needed to estimate and decouple the HLC through the Average Method will be proposed.

The study of measurement uncertainty, together with the identification of a minimum number of sensors required to estimate and decouple the HLC in in-use buildings, will make it possible to obtain a Monitoring Kit that minimises the measurement uncertainty of the variables involved in the estimation and the decoupling of the HLC using the Average Method.

Chapter 4

RESULTS AND DISCUSSION

Based on the study carried out in the literature review, two Monitoring and Control Systems (MCS) have been designed and installed, one in a tertiary building and the other one in a residential building.

The MCS of the tertiary building has been designed to deploy the uncertainty analysis of the indoor and outdoor air temperatures in the monitored tertiary building based on the developed methodology. The main aim of this study is to prove that the overall uncertainty of the indoor and outdoor air measurements is considerably higher than the manufacturer's uncertainty associated to the temperature sensors. Likewise, the experimental sensor accuracy of the sensor plus MCS (called Measurement Sensor Uncertainty due to systematic errors), is estimated so it can be compared with the manufacturer's accuracy. In addition, it will allow us to know the Measurement's Spatial Uncertainty (uncertainty due to random errors) through the decoupling method of Measurement Uncertainty. Furthermore, this study of the Measurement Uncertainty, which includes overall uncertainty sources due to systematic and random errors, will allow us to know the position in which to install the sensors within the monitored thermal zones with less uncertainty and more precision, as well as study the air temperature stratification.

Finally, based on the Average Method and Co-heating Method measurement requirements, a very detailed monitoring of a residential building is designed and deployed in order to be able to analyse in detail the minimum set of sensors that would be required to accurately estimate and decouple the HLC of a residential building. A cost analysis is also included so as to be able to decide which what the optimum monitoring kit would be, considering both the minimum uncertainty of the HLC, Cv and UA estimates with a reasonable cost.

4.1 Introduction

Taking into account the importance of sensor measurement uncertainty, two Monitoring and Control Systems (MCS) have been designed and implemented in two buildings, one tertiary building and one residential building. The technologies used are sensors and hardware with high accuracy, as those used in laboratory testing and industrial automation systems. Both MCS have been designed taking into account the conclusions of the Literature review chapter (2.3.3) and the Methodology chapter (section 3.4).

The literature review highlights the importance of the measurement uncertainty estimation of T_{in} and T_{out} to improve the estimation of HLC, as in the Co-Heating Method as Average Method. Based on this, an MCS has been designed in a tertiary building to estimate the uncertainties associated to these intensive variables, T_{in} and T_{out} . Likewise, the methodology of measurement uncertainty explained in section 3.2 has been applied to both these variables in order to estimate the uncertainties due to systematic and random errors, together with a study of the vertical and spatial stratification of air temperature. The influence of the effects of solar radiation, the heating system and electrical consumption on the T_{in} and T_{out} measurements, also has been studied based on the uncertainty analysis. The entire uncertainty analysis has been carried out in order to improve the MCS through the T_{in} and T_{out} measurements.

In addition, the MCS design of residential buildings has been conceived with the aim of characterizing the TEP and HLC in occupied and unoccupied buildings making different studies and analyses such as the uncertainty analysis, comparing sensor technologies, the optimisation of HVAC and heating system monitoring, among others; together with the HLC estimation using the Average Method (Equation 2.18), the Co-Heating Method (Equation 2.22) and its decoupling (Equation 2.10).

This chapter starts with the presentation of the experimental test carried out in a tertiary building followed by the uncertainty analysis of the T_{in} and T_{out} measurements, which have been obtained from the MCS of this tertiary building. Then, the experimental test carried out in a residential building is shown and the conclusions are given at the end.

4.2 Design of a Mobile Monitoring System (MMS) to analyse the overall uncertainties of T_{in} and T_{out} measurements in the administrative building of the UPV/EHU

A Mobile Monitoring System (MMS), integrated within the existing Building Automation System (BAS) of a tertiary building, has been designed taking into account the high sensor accuracy and the ability to be installed easily and quickly in different cardinal locations, distribution spaces, volumes and at different heights of a tertiary in-use building located in Leioa (Bilbao). Two types of MMS (interior MMS and exterior MMS) have been designed to be able to carry out studies to optimise the measurement intensive variables, such as the indoor and outdoor air temperature measurements of

the monitoring system to estimate the HLC through the Average Method for tertiary buildings. The experimental test shown in this chapter has been published in the Data in Brief called 'Dataset of an in-use tertiary building collected from a detailed 3D Mobile Monitoring System and Building Automation System for indoor and outdoor air temperature analysis' [139].

Eight tripods make up the interior MMS with twenty sensors at different heights, which have been installed in different offices in the building to collect indoor air temperature measurements at different heights and locations. In addition, eight sensors make up the exterior MMS to collect data from outdoor air temperature measurements around the building envelope. Both MMS have been integrated into the existing Building Automation System (BAS) of the tertiary building; some other data collected by the BAS have also been taken into account for the analysis of the measurement uncertainties.

The interior and exterior MMS datasets have been compiled based on a rigorous data collection process, with the potential to use the data to study the spatial measurement behaviour, taking into account the impact of solar radiation, the heating system and the electrical energy consumption. Furthermore, it enables the global uncertainty measurements on an in-use building to be estimated and to break it down into the different uncertainty sources, such as the sensor accuracy, vertical and horizontal temperature variability, solar radiation, occupancy and heating system effects. Finally, it enables the optimization of monitoring and control systems for BAS, heating and HVAC systems, as well as any monitoring system implemented in research tests.

The Monitoring and Control Systems

The designed Mobile Monitoring System (MMS) was implemented to collect data in spaces with different distributions, cardinal orientations, volumes and at different heights of a tertiary building located in Leioa (Bilbao) Figure 4.1. This building is the west block of the rectory building of the University of the Basque Country (UPV/EHU).

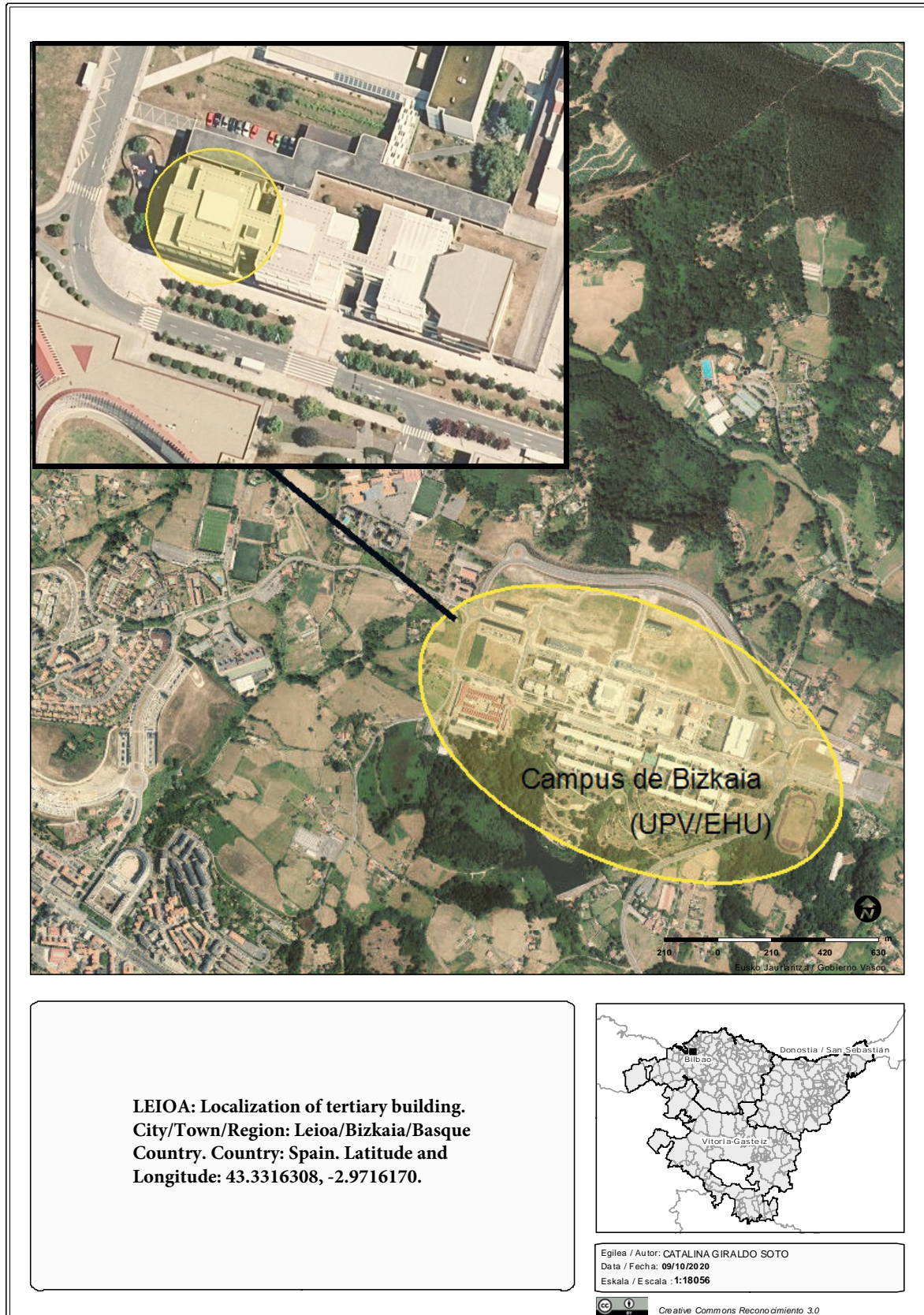


Figure 4.1: Location of tertiary building. City/Town/Region: Leioa/Bizkaia/Basque Country. Country: Spain. Latitude and longitude: 43.3316308, -2.9716170.

The in-use building had been retrofitted in 2018 as a demonstrator building of the project “Affordable and Adaptable Public Buildings through Energy Efficient Retrofitting (A2PBEER)” [76], and was equipped with a BAS system in 2013. The building after retrofitting is shown in Figure 4.2.



Figure 4.2: The UPV/EHU administrative building in Leioa post-retrofitting: a) northern façade, b) West Façade, c) southern façade, d) Roof.

There are three types of dataset; data collected from the existing Building Automation System (BAS) and from two Mobile Monitoring Systems (MMS), interior and exterior MMS. Each system is made up of different technologies.

For the interior experimental test, the Monitoring System (MS) has been conceived as a mobile system, so as to be able to quickly change the MS to different spaces and floors, adapting it to different distances, heights and geometrics in each space. Eight tripods, twenty sensors, two gateways, Modbus wire and aero-connectors make up the interior MMS. In the case of the MS for the exterior experimental test, eight sensors have been placed around the building at different heights and cardinal orientations. A gateway, Modbus wire and aero-connectors compose the exterior MMS.

The following is to describe the building’s characteristics and its existing BAS, along with the description of the interior and exterior MMS. Also, there is information on the technical specifications, experimental layout distribution and geometric information of each monitored area.

Technology and selected datasets from the Mobile Monitoring System (MMS) and existing Building Automation System (BAS)

There are three types of dataset; data collected from the existing Building Automation System (BAS) and from two Mobile Monitoring Systems (MMS), interior and exterior MMS. Each system is made up of different technologies.

For the interior experimental test, the Monitoring System (MS) has been conceived to be a mobile system, so as to be able to quickly change the MS to different spaces and floors, adapting it to different distances, heights and geometrics in each space. Eight tripods, twenty sensors, two gateways, Modbus wire and aero-connectors make up the interior MMS. In the case of the MS for the exterior experimental test, eight sensors have been placed around the building at different heights and cardinal orientations. A gateway, Modbus wire and aero-connectors compose the exterior MMS.

The technologies used for the interior and exterior MMS and the existing BAS of the tertiary building are:

1. Mobile Monitoring System (MMS) for interior measurement composed of:

(a) Tripods: Eight units.

(b) Sensors:

- i. Temperature, relative humidity and Carbon Dioxide (CO₂): EE800-M12J3 (E+E Elektronik) [140]. Protocol communication Modbus-RTUS485. Eighteen units.
- ii. Temperature and relative humidity: EE071-HTPC¹ with shielding (E+E Elektronik). Protocol communication Modbus-RTUS485. One unit.
- iii. Radiant temperature: WBGT-PT100 (4L) (Ahlborn) [143]. Analogical communication - resistive signal. One unit.

(c) Gateway:

- i. Modbus - KNX: KNXRTU1K (DEEI) [144]. Maximum number of points 1000. Supports Boolean data, 8 bits, 16 bits, 32 bits, 64 bits, float 16, float 32. 120-ohm resistor inside the gateway. One unit.

(d) Data collector:

- i. Analogical communication: Almemo 2590 (Ahlborn) [145]. One unit.

(e) Power supply:

- i. Output 24V - 4.2A: HDR-100-24N (Mean Well). One unit.

¹The name reference EE071-HTPC [141] of E+E plus manufacturer has been changed by the name reference EE071-HS1TT1F3 [142].

- ii. Output 5V - 3A: HDR-30-5 (Mean Well). One unit.

2. Mobile Monitoring System (MMS) for exterior measurement composed of:

(a) Sensors:

- i. Temperature and relative humidity: EE071-HTPC with shielding (E+E Elektronik). Protocol communication Modbus-RTUS485. Eight units.
- With radiation shielding, but without mechanical ventilation: seven units.
 - With radiation shielding and mechanical ventilation: one unit.

(b) Gateway:

- i. Modbus - KNX: IBOX-KNX-MBM (IntsisBox) [146]. One unit.

(c) Power supplies:

- i. Output 24V - 4.2A: HDR-100-24N (Mean Well). One unit.
- ii. Output 5V - 3A: HDR-30-5 (Mean Well). One unit.

3. The existing Building Automation System (BAS) of the Leioa building:

- (a) Composed of sensors with KNX protocol communication, gateways and power supplies installed by the A2PBEEER project of the European Union [76], which are:

i. Sensors (KNX):

- Electricity meters: EM/S3.16.1 and A43-211 (ABB).
- Calorimeters: Multical 602 (Kampstrup).
- Indoor comfort measurements: Temperature, relative humidity and carbon oxide: SK04-S8-CO₂-TF (ARCUS-EDS).
- Exterior variable measurements: Temperature and relative humidity: SK01-TFK-AFF and SK10-THC-CO₂-KF (ARCUS-EDS).
- Weather station: SK08-GLBS (ARCUS-EDS).
- Horizontal global solar radiation: SK08-GLBS (ARCUS-EDS).

- ii. Power supply: 2005 REG (JUNG). 320mA.

- iii. IP gateway: KNX IP Interface 730 (WEINZIERL).

- iv. Modules: ZS/S1.1 Meter interface (ABB).

(b) Web server [147]:

- i. Hardware: CBSE Evolution Server (IPAS). Intel N2930, 4x1.83 GHz, 4 GB RAM, 128 GB SSD, fanless, <18 Watt, 1x Ethernet, VGA and HDMI.
- ii. Software: IPAS visualisation software based on HTML technology (IPAS).

The existing Building Automation System (BAS) and selected measurements

The tertiary building studied is the west block of the administrative building of the University of the Basque Country (UPV/EHU) and consists of four floors. A nursery is located on the Ground Floor (F0) while the other three floors are made up of offices (Floor One (F1), Floor Two (F2) and Floor Three (F3)). There is currently an existing Building Automation System (BAS) which was implemented during the A2PBEER project, with KNX protocol communication [84]. The KNX sensors installed in the existing BAS are described in Table A.1. Figures A.1, A.2, A.3 and A.4 show the floor layouts for each building level, including the roof, and the selected BAS sensor references provided in this document.

The MMS experimental test was carried out on two of the four floors of this tertiary building, floors two (F2) and three (F3). These were selected because they can represent four different types of office layouts, each one representing a different office typology. F2 has the particularity that it is made up of three different, independent office spaces and F3 is a single office. Likewise, around the building eight sensors have been installed at different orientations and locations. Figures A.11 and A.17 show the installed sensors for the interior MMS and exterior MMS, respectively.

Office Typologies (OT)

The offices monitored in this experimental test have different cardinal orientations, distributions, geometry and volumes, each of them with different typologies. Each monitored office is identified as an Office Typology (OT), where each one has been classified according to the number of internal divisions called Workspaces (WS) and where each OT is located:

- Office Typology 1 (OT1): Located in F2.
- Office Typology 2 (OT2): Located in F2.
- Office Typology 3 (OT3): Located in F2.
- Office Typology 4 (OT4): Located in F3.

Table 4.1 shows the areas, heights and volumes of each OT and WS according to the architectural drawings shown in Figures A.6, A.7, A.8 and A.9.

Office	WS in drawings Reference	Area (m ²)	Height (m)	Volume(m ³)
OT1	2C1	126.03	3.39	427.24
	2C1.1	15.94	3.07	48.94
	2C1.2	16.25	3.10	50.38
	2C1.3	16.18	3.11	50.32
	2C1.4	16.25	3.12	50.62
	2C1.5	16.25	3.13	50.86
	2C1.6	18.06	3.16	56.98
OT2	2C2	62.45	3.15	196.72
	2C2.1	11.85	3.12	36.97
OT3	2C3	110.22	2.95	325.15
	2C3.2	15.97	3.13	49.99
	2C3.3	14.83	2.91	43.08
	2C3.4	30.70	2.98	91.49
	2C3.5	18.60	2.98	55.34
	2C3.6	18.60	3.13	50.86
	2C3.7	18.53	2.93	54.29
	2C3.8	18.60	2.93	54.41
	2C3.9	18.21	2.93	53.26
OT4	3C1*	400.40	3.55	1472.98
	3C1.1	16.10	3.36	54.02
	3C1.2	23.99	3.36	80.49
	3C1.3	23.99	3.36	80.49

*The 3C1 height shown is a mean value of this WS. Nevertheless, the volume shown takes into account the different heights within this WS. All southern façade windows have external shading elements, except in the WS reference 3C1.2. Windows in the north, east and west façades have no shading elements.

Table 4.1: Areas, heights and volumes of OT and WS based on the architectural drawings shown in Figure A.6, Figure A.7, Figure A.8 and Figure A.9.

Description of interior and exterior experimental tests using a 3D Mobile Monitoring System (MMS)

The criteria for choosing the technology for a monitoring and control system in a BAS or in experimental tests are important to determine the accuracy level of the sensors and their measurements. The technology currently used in domotic systems and BAS do not have the high precision and accuracy of laboratory technology; so it is necessary to introduce technology with greater accuracy and precision in order to increase the reliability of the building monitoring and control systems [148].

Based on this perspective, the technology selected for this experimental test has been chosen with high precision sensors in mind, such as the sensors used in laboratory tests. The selection criteria were:

1. Monitoring technology characterised by
 - (a) High accuracy.
 - (b) Monitoring systems used in industry.
2. Protocol communication:
 - (a) Digital protocol.
 - (b) Frequently used in industrial MCS and not in domotic systems.
 - (c) Protocol that can, in the future, be compared to Transmission Control Protocol/Internet Protocol (TCP/IP) protocol communication.
3. Hardware:
 - (a) Gateways with a capacity to integrate the new protocol communication and technology in the existing BAS of the tertiary building, which use KNX technology and protocol communication.
4. Viable costs.

The implemented interior and exterior MMS technology is described below, together with the MMS layout, where the sensors and hardware implemented in UPV/EHU administrator building are shown in Figure A.10, which is described in the following subsection:

Interior experimental test and its 3D MMS on the different OT

The Monitoring System (MS) implemented in the experimental test is a mobile system that uses eight tripods distributed in the different volumes of the monitored Office Typologies (OT). Twenty sensors have been installed on eight tripods at different heights (shown in Figure A.11), while the types of sensor and their accuracy are described in Table 4.2.

The protocol communication implemented in the MMS was Modbus RTU-RS485 [90]. For data collection, it was necessary to integrate the MMS into the admin building's BAS, which works with KNX protocol communication. It was necessary to use KNX Modbus RTU- RS485 gateways to integrate the MMS to the existing BAS [90]. The use of these gateways allowed the collected MMS data to be sent to the web server, and all the information to be exported to a single database. The gateway brand used is a DEEI KNX-Modbus RTU, whose reference is KNXRTU1K [144]. Table 4.2 shows a brief technical description of the installed gateway.

The eight tripods that make up the MMS were distributed spatially and temporally in different OTs

of F2 and F3. The tripods were interconnected using aero-connectors with different wire lengths, allowing for a quick installation of the MMS and adaption of the system to the different spatial geometries.

Table A.2 shows the position of each sensor on each tripod, as well as sensor and manufacturing references. Table A.3 shows the WS location in each OT with respect to the architectural drawings shown in Figures A.6, A.7, A.8 and A.9. The encoding of the dataset files is shown in Table A.5.

Two types of test have been carried out using the interior MMS:

Tripod Together (TT) test: The TT period test datasets are prefixed by TT.Tj with $j = 1$ to 8 (see Table A.5). All sensors were installed at the same height (at an average of 174 cm with a ± 12 cm strip) and the same location (see Figure A.5).

Office Typology (OT) test: The OT test period datasets are prefixed by OTp .Tj, with $p = 1$ to 4 and $j = 1$ to 8 (see Table A.5). Four office typologies were monitored, OT1, OT2, OT3 and OT4. The sensors were installed at different heights on each tripod:

- High (hg): Located 30 cm from the OT ceiling.
- Medium (md): Located midway between the ceiling and floor of each OT.
- Low (lw): Located 30 cm from the OT floor.

Exterior experimental test and its 3D MMS

Exterior MMS were located around the building's façade and roof. Eight sensors were located on the Exterior (E) of the building envelope at different heights:

- Façades (F): At F1 height and F2 height.
- Roof (R): At F3 height.

Furthermore, the sensors were located at different cardinal orientations: North (nt), South (st), East (et) and West (wt). Seven out of the eight installed EE071-HTP sensors were protected against solar radiation using shields without mechanical ventilation and one with mechanical ventilation. Table A.4 shows the sensor reA.14, A.15 and A.16 show, in the architectural drawings, the location of each sensor on the building envelope. Remember that these dataset file codifications are presented in Table A.6.

The exterior experimental test is composed of two tests:

Exterior Together (ET) test: The ET test period datasets are prefixed by ET.R3. All sensors are installed at the same location, five (sensor IDs 20 to 24) over the roof floor, while two (sensor IDs 25 to 26) are on the roof mast (see Figure A.12). The sensor ID 27 is also on a roof mast, but is not shown in Figure A.12.

Exterior (E) test: The E test period datasets are prefixed by E.Fn and E.R3, with n=1 or 2 (see Table A.6).

Datasets from the Mobile Monitoring System (MMS) and existing Building Automation System (BAS)

For the experimental test, some selected datasets measured by the existing Building Automation System (BAS) have been included along with the Mobile Monitoring System (MMS) datasets. The main variables affecting the behaviour of the MMS measurements, such as the heat power input of the heating system, the total electricity active power consumption within the analysed office, and the horizontal global solar radiation, have been included within the study. The dataset collected from the existing BAS of the in-use building consisted of data from some selected electricity meters (EM/S3.16.1), calorimeters (Multical 602) and the Horizontal Global Solar Radiation (SK08-GLBS (ARCUS-EDS)) sensors.

The collected data can be found in the Mendeley Data Repository called "Dataset of an in-use tertiary building collected from a detailed 3D Mobile Monitoring System and Building Automation System for indoor and outdoor air temperature analysis" [149].

The structure of the data files of the 3D MMS is divided into weeks and per unit of measurement. To identify the datasets for the experimental test, Tables A.5, A.6 and A.7 show the coding for the interior and exterior MMS sensors and the selected measurements of the existing BAS of the in-use building. Tables A.2, A.3 and A.4 show the sensor reference and location. To identify the MMS sensors in diagrams; Figures A.6, A.7, A.8, A.9, A.13, A.14, A.15 and A.16 show a schematic location of the sensors.

Investment analysis

The cost analysis carried out includes the direct costs of material and integration of the MMS to the BAS of the in-use administrative building of UPV/EHU. Table 4.3 shows the unit cost, total costs without taxes, while the budget and bills used for the cost calculation are shown in Appendix III. The total investment is equal to 15,709.56 €, where the 47.05% (7,391.70 €) has been invested in sensors of the monitoring kit, and 8.08% (1,269.50 €) corresponds to the controlling kit composed of hardware equipment. The integration and setup is 30.22% (4,747.00 €) of the total cost. The rest of the costs corresponding to the other installation costs being 14.65% (2,301.39 €) of the total cost.

The indirect costs of this project correspond to the electricity costs, but the hours spent by the doctoral candidate together with the support of the thesis directors and laboratory technician are not considered.

Typology	Product	Unit	Unit Cost	Total Cost	Cost Weigh
Sensor	EE800-M12J3	18	228.75 €	4,117.50 €	26.21%
Sensor	AMR - PT100 (4L)	1	510.00 €	510.00 €	3.25%
Sensor	EE071-HTPC	9	142.80 €	1,285.20 €	8.18%
Equipment	Shielding for EE071-HTPC	8	80.75 €	646.00 €	4.11%
Equipment	Mechanical Shielding for EE071-HTPC	1	833.00 €	833.00 €	5.30%
Monitoring Kit Total		28	1,795.30 €	7,391.70 €	47.05%
Hardware	KNXRTU1K Gateway	2	299.00 €	598.00 €	3.81%
Hardware	Configuration Kit EE800: HA011066	1	323.00 €	323.00 €	2.06%
Hardware	Configuration Kit EE870-EE871: HA011012	1	306.00 €	306.00 €	1.95%
Hardware	Wire 1.5m for kit EE870: HA010819	1	42.50 €	42.50 €	0.27%
Controlling Kit (Hardware) Total		5	970.50 €	1,269.50 €	8.08%
Setup	Exterior sensor Installation	1	1,856.00 €	1,856.00 €	11.81%
Setup	Data Base integration	1	840.00 €	840.00 €	5.35%
Setup	BAS integration	1	2,051.00 €	2,051.00 €	13.06%
Setup MCS Total		3	4,747.00 €	4,747.00 €	30.22%
Equipment	Female aero connectors	16	5.81 €	92.96 €	0.59%
Equipment	Male aero connectors	16	4.97 €	79.52 €	0.51%
Equipment	Adaptor with 3 ways	1	28.40 €	28.40 €	0.18%
Equipment	Power supply 12V	1	4.17 €	4.17 €	0.03%
Equipment	Power supply 24V	1	25.83 €	25.83 €	0.16%
Equipment	Wire 400m	1	1,578.24 €	1,578.24 €	10.05%
Equipment	Telescopic strut	8	37.00 €	296.00 €	1.88%
Equipment	Strut 1m	1	34.29 €	34.29 €	0.22%
Equipment	Concrete bass	1	45.95 €	45.95 €	0.29%
Rental Car	Van rental	1	116.03 €	116.03 €	0.74%
Installation Kit Total		47	1,880.69 €	2,301.39 €	14.65%
TOTAL COST			9,393.49€	15,709.59 €	100%

Table 4.3: Investment of MMS and its integration in the BAS of UPV/EHU building [139].

Detected challenges and improvements areas

The challenges detected during the design, installation and collection of the data have been:

- Design phase: Finding sensors with an accuracy similar to the sensors used in laboratory tests with a competitive price and according to the available budget.
- Setup: The gateway to convert protocol communication from Modbus RS485 to KNX has presented communication problems with the sensors. The gateway configuration delayed the installation in the OT and E tests.
- Collected data: Loss of registered data, the monitoring in each OT has taken longer than expected to ensure a minimum period of fifteen days of faultless data. The causes of lost data are associated with electrical switch-off or with external problems of the BAS data collector.

During the Exterior Together (ET) test, two tests were carried out for the data collection using the same hardware, software and wire longitude, but in different locations: in the first test, the sensors were put together, but due to the problems associated with the gateway configuration and their communications problems, the data were not stored correctly. The authorisation for installing the sensors around the building and the deadlines of the project planning made it impossible to repeat this test within the building. Therefore, the test was repeated by installing the sensors together on the roof of the building. In this test, two sensors were installed on the mast (E.R.st.25 and E.R.st.26 sensors) and six sensors were placed on the roof floor. In this second tests the data were correctly stored. However, once the data had been analysed, only the data from the sensors installed on the mast (E.R.st.25 and E.R.st.26) were taken into account for the study carried out in this research. This is because the data from the roof floor sensors were very dispersed, since the roof floor maintained the thermal inertia and this affected their measurements. A significant gap (bias) between their measurements with respect to the sensors installed on the mast (E.R.st.25 and E.R.st.26) was detected.

The improvement areas detected for future work are:

- Setup: Avoiding the use of gateways if the technology requirements allow. If the use of gateways is necessary, it is important to select very high quality ones, even if it means a higher hardware investment.
- Implement an FDD on the BAS and have a parallel system to register data in case of fault.

SENSORS			
Sensor Reference	Measure	Accuracy	Protocol Communication
EE+Plus:EE800-M12]3	Temperature	$\pm 0.3^{\circ}\text{C}$	Digital-Modbus RS485
	Relative Humidity	$\pm 3\% \text{ RH}(30..70\% \text{RH}). \pm 5\% \text{RH} (10-90\% \text{RH})$	
	Carbon Dioxide	$0 \dots 2000 \text{ppm} < \pm (50 \text{ppm} + 2\% \text{ of measured value})$	
EE+Plus EE071-HTPC	Temperature	$\pm 0.1^{\circ}\text{C}$ at 23°C	Digital-Modbus RS485
	Relative Humidity	$\pm 2\% \text{ RH} (0-90\% \text{RH}). \pm 3\% \text{ RH} (0-100\% \text{RH})$	
Ahlborn:WBG7 - PT100 (4L)	Radiant Temperature	PT 1000 Class B (-50°C to $+200^{\circ}\text{C}$)	Analogic-Resistive
GATEWAY			
Reference	Producer	Protocols	Description
KNXRTU1K [144]	DEEI	KNX to Modbus RTU-RS485	RS485 Half-Duplex interface for Modbus RTU. The 120-ohm RS485 termination resistor inside the gateway. Operating temperature -40 to $+85^{\circ}\text{C}$. Maximum number of points 1000. Supports Boolean data, 8 bits, 16 bits, 32 bits, 64 bits, float 16, float 32.

Table 4.2: Technical characteristics of sensors, gateway and protocol communications of interior MMS.

4.3 Measurement uncertainty analysis of indoor and outdoor air temperature in the administrative building of the UPV/EHU

For the MCS' optimization used to measure the variables involved in estimating and decoupling the HLC, an uncertainty analysis of the sensors' measurements must be carried out. Based on the theoretical frame of the Average Method (section 2.2.2), the Co-Heating Method (section 2.2.3) and the HLC decoupling method (section 2.2.4), the Measurement Uncertainty (U_M) of the Indoor Air Temperature (T_{in}) and the Outdoor Air Temperature (T_{out}) have been identified as crucial as a first step to optimising the MCS. As specified in the literature review (chapter 2.3.3), the overall uncertainty estimation of these two variables is necessary to estimate the HLC more accurately the HLC through the Co-Heating Method and Average Method. This study is based on the collected data from the MMS implemented on the in-use administrative building of UPV/EHU, which is shown and described in section 4.2.

The identification of all measurement uncertainties allows us to know with a certain level of confidence what the HLC estimation error is; one of these main measures being the intensive variables, T_{in} and T_{out} . These variables' measurement together with the heat gains from the heating system, and/or electricity gains, are required for the accurate estimation of the HLC in unoccupied buildings through the co-heating method. However, for the HLC estimation in in-use buildings through the average method, the accurate measurement (or estimation) of the heating system heat gains, electricity gains, occupancy gains, solar gains, outdoor air temperature and indoor air temperature of a building are required.

As proven in the literature review, the research works estimating the HLC of buildings only use the manufacturer's accuracy as the overall uncertainty for the indoor and outdoor temperature mismeasurements. In this section, it will be proven to what extent the manufacturer's accuracy differs from the overall uncertainty of the indoor air temperature of an in-use building thermal zone and from the outdoor air temperature.

Indoor Air Temperature (T_{in}) and Outdoor Air Temperature (T_{out}) in buildings are physical parameters that influences different aspects of scientific and technical works, studies and research. T_{in} and T_{out} values are collected from sensors as a unit of measurement, where the estimation of the Measurement Uncertainty (U_M) of T_{in} and T_{out} , called Temperature Uncertainty (U_T), should give the overall error (systematic and random errors) associated to the T_{in} and T_{out} measures and which are studied and estimated below. Based on the study of the literature review, the scientific experiments and publications do not usually specify the technical information from the manufacturer of the technology used for monitoring; likewise, measurement uncertainty values are not taken into account in experimental or simulation studies. In the cases where the uncertainties associated with the interior temperature are used, only the accuracy given by the manufacturer (uncertainty associated with systematic errors) is considered as a measurement uncertainty, without taking into account uncertainties associated with random effects. In other cases, there is no specification of the particular

methodology used to estimate the temperature uncertainty. The estimation of the overall Temperature Uncertainty (U_T) of indoor and outdoor air, has been based on the experimental test carried out in the tertiary in-use building with the monitoring system for the UPV/EHU administration building, where a Mobile Monitoring System (MMS) was installed to collect T_{in} and T_{out} data.

The study results are based on the global uncertainty analysis, which were described on the Methodology section of this document, developed within this research study. The scope of the obtained results is to estimate and decouple the overall U_T of indoor and outdoor air measurements of the studied tertiary in-use building and open a new methodology and analysis to be applied to other related studies. The results and discussion presented allow conclusions to be drawn on the analysis of the uncertainties.

Among others, the reliable measurement of the T_{in} and T_{out} play an important role in efficiently operating in-use buildings. Both are physical variables that are studied and analysed in multiple scientific fields of in-use buildings and other areas. These include tests related with air quality, thermal comfort, ventilation systems, pollution concentration and environmental conditions, meteorology studies, biotechnology, energy efficiency, engineer's designs, Energy Performance of Buildings (EPB), among others. Many publications deal with T_{in} and T_{out} , which play a key role in studies of in-use buildings. For example, it is currently possible to find around 71,647 and 67,084 T_{in} and T_{out} results, respectively, in buildings from Science Direct [150], around 784 and 388 T_{in} and T_{out} results, respectively, from the Institute of Electrical and Electronics Engineers (IEEE) [151] and around 13,470 and 14,638 T_{in} and T_{out} publications, respectively, in the Taylor & Francis Group [152].

The T_{in} and T_{out} measurements, as intensive variables, are used in the EPB analysis, the optimization of Building Automation Systems (BAS), buildings' ventilation system's controls and others building subsystems controls. In the same way, for the International Organization for Standardization (ISO) and the American Society of Heating, Refrigerating & Air-Conditioning Engineers (ASHRAE), in their standards and handbooks, the T_{in} and T_{out} of in-use buildings and their subsystems are an important physical parameter used to develop procedures, methodologies and calculations ([20, 44, 45, 153–162]). All this shows the importance of the T_{in} and T_{out} roles and the need to estimate both measures with precision and accuracy through proper measurements. To do so, it is necessary to estimate the overall Temperature Uncertainty (U_T) in order to have a better approximation of the true representative T_{in} and T_{out} values of different thermal zones of in-use buildings.

Thus, the uncertainty analysis for T_{in} and T_{out} measurements has been presented for the studied tertiary building, where the Measurement Zone (MZ) and Measurement Space (MS) specified in section 3.2.1 are identified as Thermal Zone (TZ) and Thermal Space (TS), respectively. In the analysis carried out, the measurements are exposed to several uncertainty sources, some of which are:

- The stratification of the air leads to different temperature measurement values at the different points where the sensors are installed in a thermal zone; the number of sensors installed in the monitoring systems (MS) to collect the temperature values of all points of this volume being

insufficient.

- Sensor uncertainty represented by manufacturer accuracy.
- Vertical and horizontal temperature stratification and/or variation.
- Solar radiation incidence.
- Thermal zones or volume geolocation.
- Heating incidence.
- Electricity heat gain incidence.
- User behaviour.
- Air currents.
- Thermal bridge.
- Volume insulation level with respect to exterior environment, etc.

4.3.1 Indoor air temperature global uncertainty results for the UPV/EHU administrative building

Taking into account the importance of properly estimating the overall Uncertainty value for T_{in} , the analysis and estimation of U_T has been developed for a multi-volume building (section 2.2.2) made up of four offices with different cardinal orientations, divisions, volumes and geometries. The monitored in-use building has been the UPV/EHU administrative building, whose experimental test is explained in section 4.2.

The results include the following analysis:

- Measurement Sensor Uncertainty $U_{M(S)}$ analysis of T_{in} , called, Temperature Sensor Uncertainty $U_{T(S)}$.
- Measurement Uncertainty U_M analysis of T_{in} , called, Temperature Uncertainty U_T .
- Measurement's Spatial Uncertainty $U_{M(SP)}$ analysis of T_{in} , called, Temperature's Spatial Uncertainty $U_{T(SP)}$.
- Estimation of the temperature range within which the representative value of T_{in} can lie, based on the uncertainty analysis.
- Measurement's Vertical Uncertainty analysis of T_{in} to study the vertical stratification.
- Effect of radiation, heating and electricity consumption on the Measurement Uncertainty U_M of T_{in} .
- Impact of the number of sensors and their location on the Measurement Uncertainty U_M of T_{in} .

Concepts and variables used in the methodology to estimate the uncertainty of T_{in}

Based on the methodology set out in section 3.2.1, the variables identified for the study case are specified for the in-use tertiary building of UPV/EHU. The experimental test carried out with an MMS integer in a BAS has been described in section 4.2 and in the Data in Brief [139]. The concept and variables used in the uncertainty analysis of T_{in} are set out below.

Thermal Zone (TZ) characterization

The Thermal Zone (TZ) and Thermal Space (TS) of the administrative building of UPV/EHU are identified as Office Typology (OT) and Workspace (WS), respectively. The OT are shown in Figure 4.3. An Office Typology (OT) is defined as a tertiary building volume composed of sub-volumes, which will be called Workspaces (WS). In the experimental test carried out, four-monitored OTs have been studied, composed of different WS distributions, for which two types of WS were identified in order to characterize the OT:

- **Open Workspace (OWS):** This is a large space where there are many workstations without dividing walls.
- **Compact Workspace (CWS):** This is a space with less volume than the OWS, where there is one or a maximum of two workstations.

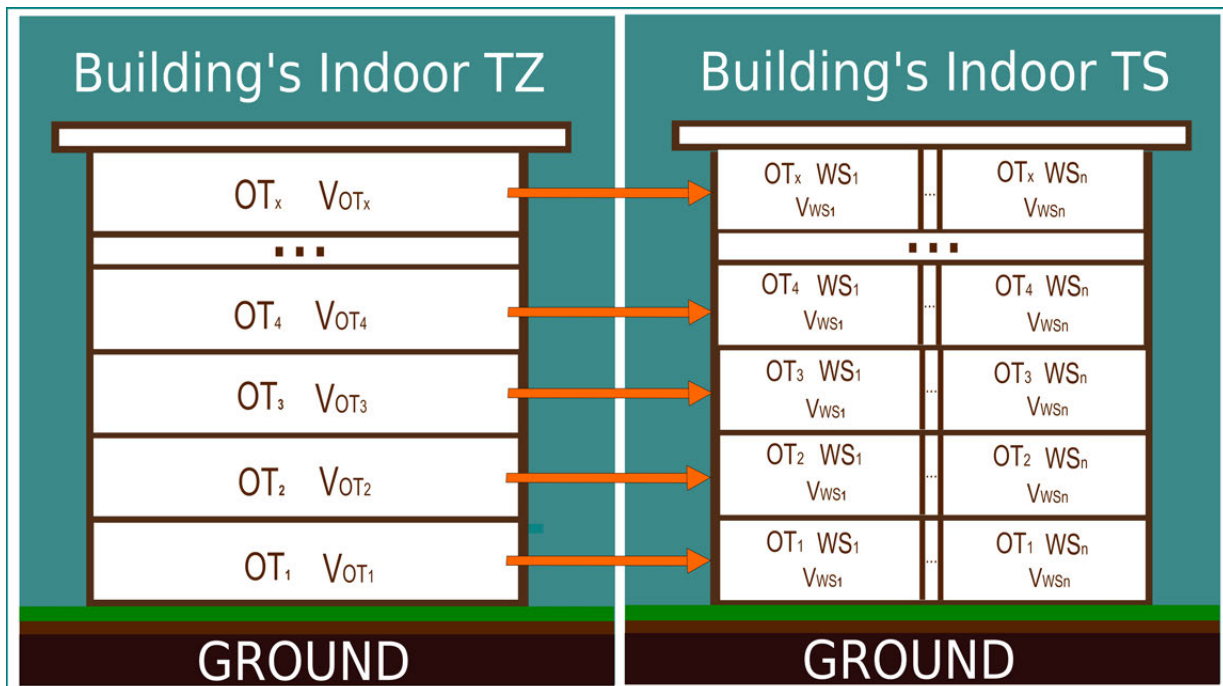


Figure 4.3: Scheme of the uncertainty of T_{in} measurement for different Thermal Zones (TZs) and Thermal Spaces (TSs) identified in the in-use tertiary building.

To characterize the OT, a relationship has been created based on the OWS volume and the number of CWS in each monitored space on each floor:

Open Workspace Ratio (OWSR): This is a percentage of the volume occupied by open workspaces

with respect to the OT volume; this ratio is calculated according to Equation 4.1.

$$OWSR_{OT} = \frac{V_{OWS}}{V_{OT}} 100[\%] \quad (4.1)$$

where,

- $OWSR_{OT}$: Open Workspace Ratio of Office Typology (OT).
- V_{OWS} : Open Workspace Volume within an Office Typology (OT) [m³].
- V_{OT} : Volume of Office Typology (OT) [m³].

Six typologies have been defined in Table 4.4 to characterize the volume occupied by the OWS and describe each typology.

OWS Typologies	OWSR	Description
A	$OWSR = 100\%$	Unique open workspace
B	$100 < OWSR < 75\%$	Big volume of OWS
C	$75\% \leq OWSR < 50\%$	Medium volume of OWS
D	$50\% \leq OWSR < 25\%$	Small volume of OWS
E	$25\% \leq OWSR < 0\%$	Very small volume of OWS
F	$OWSR = 0\%$	There is not OWS

Table 4.4: OWS typologies based on the OWSR.

Division Factor (DF): This ratio defines the number of CWSs in relation to the total number of WS in an OT, which is the sum of the number of OWSs and CWSs. This factor is calculated according to Equation 4.2.

$$DF_{OT} = \frac{N_{CWS}}{N_{CWS} + N_{OWS}} 100[\%] \quad (4.2)$$

where,

- DF_{OT} : Division Factor of a OT [%].
- N_{CWS} : Number of Compact Workspaces in Office Typology (OT).
- N_{OWS} : Number of Open Workspaces in Office Typology (OT).

In Table 4.5, six typologies have been defined relative to the number of CWS.

CWS Typologies	DF	Description
6	$DF = 100\%$	There is not OWS
5	$100\% < DF < 75\%$	Mainly CWS units
4	$75\% \leq DF < 50\%$	Many CWS units
3	$50\% \leq DF < 25\%$	Few CWS units
2	$25\% \leq DF < 0\%$	Very few CWS units
1	$DF = 0\%$	There is not CWS

Table 4.5: CWS Typologies based on DF.

Based on Equation 4.1, Table 4.4, Equation 4.2 and Table 4.5, the office zone's characterization results for the OWR and DF values have been obtained and are shown in Table 4.6: the OWS-CWS typology of office one is C5 (named OT1-C5); of office two, it is the B3 typology (named OT2-B3); of office three, it is D5 (named OT3-D5); and of office four, it is B4 (named OT4-B4). OT1-C5, facing north-west, has six CWSs, while OT3-D5, facing south-west, has eight CWSs; both OTs have similar OWR values and the same DF typology. Both these OTs have many CWSs and nearly 50% of the volume is occupied by an OWS. The OT2-B3, with a north orientation, has one CWS and 84.18% of the volume is occupied by an OWS. In addition, OT4-B4 (facing north, south and west), has three CWSs and the same proportion of OWS volume with respect to OT2-B3. This OT has the same OWS typology, but a total volume considerably greater than OT2-B3.

Office textbfReference	CWS Number	OWSR (Eq.4.1)	DF (Eq.4.2)	OWS-CWS Typology	Office Typology Name
OT1	6	58.10%	85.71%	C-5	OT1-C5
OT2	1	84.18%	50.00%	B-3	OT2-B3
OT3	8	41.59%	88.89%	D-5	OT3-D5
OT4	3	87.26%	75.00%	B-4	OT4-B4

Table 4.6: Results of the office characterization based on the studied thermal zones.

Identification of methodology's variables for the uncertainty analysis of Indoor Air Temperature (T_{in}) measurement

In order to relate the variable names of the methodology of sections 3.2.1 and 3.2.2 and the variable names of the results shown in this section, Table 4.6 shows the relation of variables for the uncertainty study and Figure 4.4 shows a scheme of the uncertainty of T_{in} measurement for different Thermal Zones (TZs) and Thermal Spaces (TSs) identified in an in-use tertiary building.

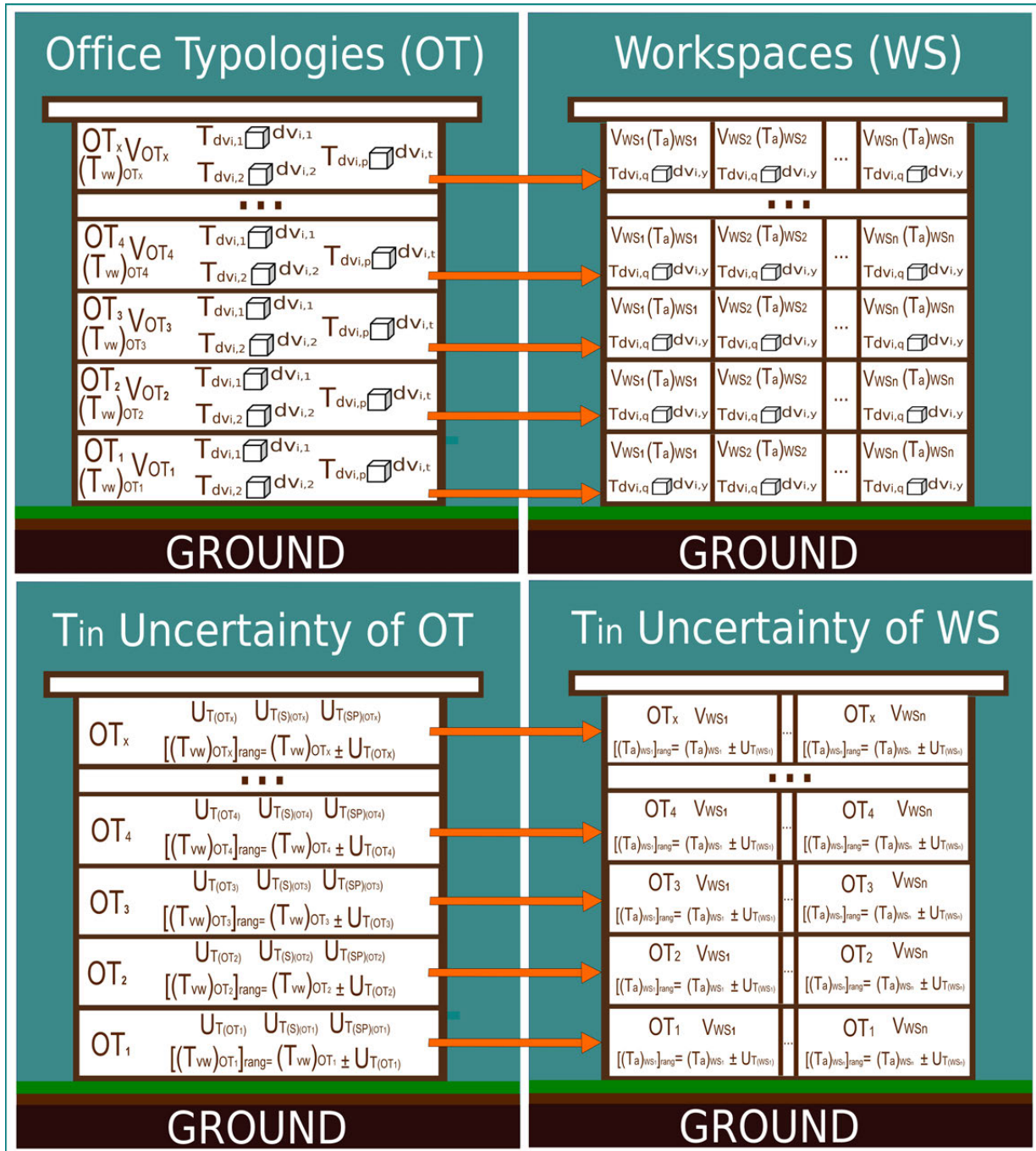


Figure 4.4: Scheme of the uncertainty of T_{in} measurement for different Thermal Zones (TZs) and Thermal Spaces (TSs) identified in an in-use tertiary building.

Temperature Sensor Uncertainty $U_{T(S)}$ analysis of the indoor air

The objective of this analysis is to obtain the experimental accuracy of the sensors plus the Mobile Monitoring System (MMS). To estimate this experimental value, for each time instant, t_j , nineteen temperature measurements, T_{dv_i} , have been obtained by installing nineteen sensors together at the same height in the same location of the same WS (section 4.2). The experimental accuracy of the sensors, or the Temperature Sensor Uncertainty $U_{T(S)}$, is given by the Expanded Uncertainty $2\bar{\sigma}_{(S)}$ value, as described in section 3.2.1, which is obtained from the differential temperature, $((\theta_{dv_i})_{WS})$

Variable names of section 3.4	Variable names of section 4.3.1	Description	Variable names of section 4.3.1		Description
			Variable names of section 3.4	Variable names of section 4.3.1	
t_N	t_N	Instants of Time.	U_T	U_T	Temperature Uncertainty.
N		Sample Size defined by the number of Instants of Time (t_N).	σ_M^2	σ_T^2	Mean Variance of t_N samples associated to U_M .
Z	Z	Number of T_{dvi} Temperature in OT ($Z = p$) or WS ($Z = q$) volume for each t_j .	σ_M^2	σ_T	Mean Standard Deviation of t_N samples associated to U_T
dvi	dvi	Differential Volume contained in and OT or a WS [m^3].	$U_{M(s)}$	$U_{T(s)}$	Temperature Sensor Uncertainty.
V_{MZ}	V_{OT}	OT Volume [m^3].	$\sigma_{(s)}^2$	$\sigma_{(s)}^2$	Mean Variance of t_N samples associated to $U_{M(s)}$.
V_{MS}	V_{WS}	WS Volume [m^3].	$\bar{\sigma}_{(s)}$	$\bar{\sigma}_{(s)}$	Mean Standard Deviation of t_N samples associated to $U_{M(s)}$.
g	g	Number of Differential Volume in an OT volume.	$U_{T(sP)}$	$U_{T(sP)}$	Temperature's Spatial Uncertainty.
y	y	Number of Differential Volume in a WS volume.	$\sigma_{(sP)}^2$	$\sigma_{(sP)}^2$	Mean Variance of t_N samples associated to $U_{M(sP)}$.
n	n	Number of WS volumes contained in a OT.	$\bar{\sigma}_{(sP)}$	$\bar{\sigma}_{(sP)}$	Mean Standard Deviation of t_N samples associated to $U_{M(sP)}$.
p	p	Number of T_{dvi} in a OT for each t_j .	$R_{(s)}$	$R_{(s)}$	Ratio of Mean Variance of t_N samples due to $U_{T(s)}$ with respect Mean Variance of t_N Samples due to U_T
q	q	Number of T_{dvi} in an WS for each t_j .	$R_{(sP)}$	$R_{(sP)}$	Ratio of Mean Variance of t_N samples due to $U_{T(sP)}$ with respect to Mean Variance of t_N Samples due to U_T
M_{dvi}	T_{dvi}	Temperature Measurement on an OT for each t_j .	$[\bar{M}_{vw}]_{range}$	$[(\bar{T}_{vw})_{OT}]_{range}$	Maximum and Minimum limit in which (T_{vw}) _{OT} of t_N sample ($(\bar{T}_{vw})_{OT}$) fluctuates
$(M_{dvi})_{MZ}$	$(T_{dvi})_{OT}$	Temperature (T_{dvi}) of a WS for each t_j .	$[\bar{M}_a]_{range}$	$[(\bar{T}_a)_{WS}]_{range}$	Maximum and Minimum limit in which (T_a) _{WS} of t_N sample ($(\bar{T}_a)_{OT}$) fluctuates
$(M_{dvi})_{MS}$	$(T_{dvi})_{WS}$	Temperature Measurement (T_{dvi}) on a WS for each t_j .	U_{VM}	U_{VT}	Vertical Measurement Uncertainty.
M_a	T_a	Average Temperature of OT or WS for each t_j .	σ_{VM}^2	σ_{VT}^2	Mean Variance of t_N samples associated to U_{VM} .
$(M_a)_{MZ}$	$(T_a)_{OT}$	Average Temperature of an OT Volume for each t_j .	σ_{VM}^2	σ_{VT}	Mean Standard Deviation of t_N samples associated to U_{VM} .
$(M_a)_{MS}$	$(T_a)_{WS}$	Average Temperature of a WS Volume for each t_j .			
$(M_{vw})_{MZ}$	$T_{vw}OT$	Volume-Weighted Temperature of and OT for each t_j .			
$(\theta_{dvi})_{vw}$	$(\theta_{dvi})_{vw}$	Temperature Differential with respect to the Volume-Weighted Temperature of a OT for each t_j .			
$(\theta_{dvi})_a$	$(\theta_{dvi})_a$	Temperature Differential of T_{dvi} centred on an Average Temperature for each t_j .			
$(\theta_{dvi})_{MZ}$	$(\theta_{dvi})_{OT}$	Temperature Differential of T_{dvi} centred on an Average Temperature of a OT for each t_j .			
$(\theta_{dvi})_{MS}$	$(\theta_{dvi})_{wsn}$	Temperature Differential of T_{dvi} centred on an Average Temperature of a WS for each t_j .			

Table 4.7: Names of particularized variables for the uncertainty study of the T_{in} measurement.

(Equation 3.10) values of each temperature T_{dv_i} value for each t_j . The $U_{T(S)}$ (Equation 3.17, Table 3.6) value represents the experimental accuracy of the sensor measurements plus MMS for a manufacturer’s specific technology within a specific monitoring system.

This study provides insights into the experimental measurement accuracy for the sensor technology installed in the MMS. In this experimental test, all the sensors were left together at the same height (at a medium level of 174 cm with a strip of ± 12 cm), measuring from 28th June 2019 at 11:55 am to 1st July 2019 at 12:10 am. Figure 4.5 shows the evolution of all T_{dv_i} during 24 hours of data collected from the TT test ([149]) on 30th June 2019 from 0:00 to 24:00.

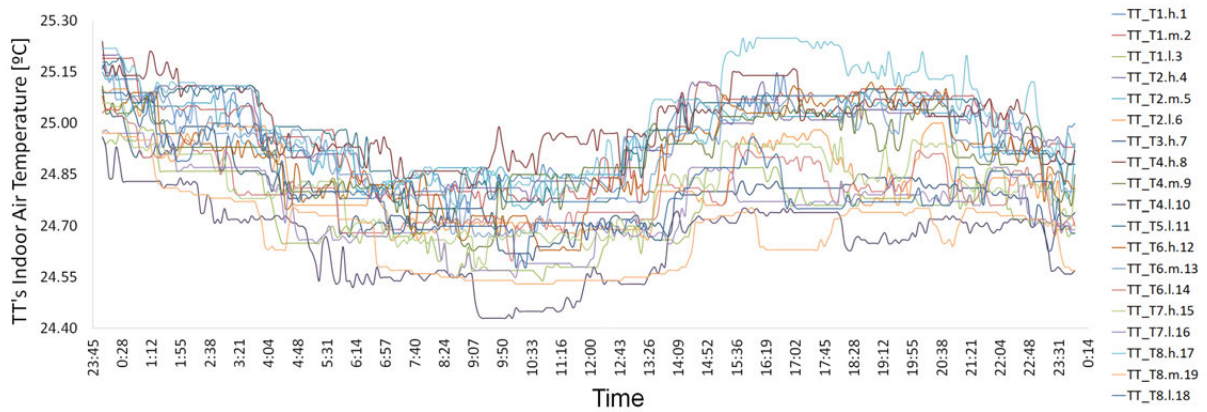


Figure 4.5: T_{dv_i} evolution in 24 hours of data collected from the TT test between 30th June 2019 at 0:00 to 24:00. (TT test ([149])).

Table 4.8 shows the statistical analysis results for a sample size of 868 t_N , each t_j with nineteen-temperature measurements collected at a measurement frequency of five minutes. Figures B.1 and B.2 show the temperature frequency diagram of the sample data analysed in this section for T_{dv_i} and $(\theta_{dv_i})_{wsm}$.

According to the methodology described in section 3.2.1, the normal distribution of the zero centred sample, $N(0,\sigma)$, has a $\bar{\sigma}$ value of $\pm 0.12^\circ\text{C}$, the $U_{T(S)}$ value being $\pm 0.24^\circ\text{C}$ for the MMS. The $U_{T(S)}$ value is less than the accuracy of the EE800-M1213 sensor based on the manufacturer’s values shown in Table 10, which is $\pm 0.3^\circ\text{C}$, with both values differing by 20% from the manufacturer’s accuracy.

The statistical parameters for the values with eighteen sensors, excluding the EE071-HTPC sensor, has a $U_{T(S)}$ value of $\pm 0.22^\circ\text{C}$, the MMS being more accurate using only EE800-M1213 sensors, and the $\bar{\sigma}$ value being $\pm 0.113^\circ\text{C}$, which is 0.006°C less than the $\bar{\sigma}$ value from the statistical analysis of the nineteen sensors. The $U_{T(S)}$ value for the MMS in the next estimates in this section will be $\pm 0.24^\circ\text{C}$, which consider the systematic errors of both the sensor technologies used (EE800-M1213 and EE071-HTPC) plus the MMS.

Statistical Analysis	Nineteen sensor	Eighteen sensors**	SI
Sample Size (N)	868	868	-
Samples' Mean ($\bar{\mu}$) (Eq.3.14)	0.00	0.00	[°C]
Mean Variance ($\bar{\sigma}^2 = \bar{\sigma}_{(S)}^2$) (Eq.3.15)	0.014	0.013	[K ²]
Mean Standard Deviation ($\bar{\sigma} = \bar{\sigma}_{(S)}$) (Eq.3.16)	0.119	0.113	[°C]
Expanded Uncertainty ($U_{T(S)}$) (Eq.3.17)	0.24	0.22	[°C]
Min	-0.44	-0.33	[°C]
Max	0.31	0.29	[°C]

**Excluding the EE071-HTPC sensor measurement.

Table 4.8: Statistical results of Temperature Sensor Uncertainty ($U_{T(S)}$) analysis for the Mobile Monitoring System (MMS).

Temperature Uncertainty (U_T) analysis of the MZ (OT) and MS (WS) of the tertiary building

The methodology used to estimate the Temperature Uncertainty is based on section 4.3.1 and the study has been carried out for OT and WS independently. Here, sensors are randomly distributed throughout the volume of each TZ for OT test, as detailed in section 4.2. For estimating the U_T value for an OT, the differential temperature, $((\theta_{dv_i})_{vw})$ (Equation 3.7), must first be calculated for each temperature value T_{dv_i} of each t_j and then the statistical analysis of these $(\theta_{dv_i})_{vw}$ values must be done. In addition, to estimate the U_T value for a WS, the $((\theta_{dv_i})_{wsm})$ (Equation 3.10) values must first be calculated for each temperature value T_{dv_i} of each t_j , after which the statistical analysis must be performed. The U_T value is calculated for both OT and WS using Equation 3.17, which includes $U_{T(S)}$ and all other uncertainty causes described in section 3.2.1.

The estimated U_T value includes all sources of uncertainty that have an impact on the indoor air temperature measurement of the considered volumes, the random errors (Temperature's Spatial Uncertainty $U_{T(SP)}$) and the systematic errors (Temperature Sensor Uncertainty $U_{T(S)}$). The OT figures of section 3.2.1 allow us to identify the interior and exterior CWSs facing north, south, west and with multiple cardinal orientations. In this section, Figure 4.6 shows the T_{dv_i} evolution during 24 hours of data collected from the OT test ([149]) for OT1, OT2, OT3 and OT4. Figures 4.7, B.4, B.6 and B.8 show the sample histogram for the T_{dv_i} collected by the sensors in OT1, OT2, OT3 and OT4, respectively. Likewise, the sample histogram for the $(\theta_{dv_i})_{vw}$ values for OT1, OT2, OT3 and OT4 are shown in Figures B.3, B.5, B.7 and B.9, respectively. The OT test was carried out in the following periods:

- OT1: From 6th June 2019 at 14:11:40 to 23rd June 2019 at 05:29:10, every 10 seconds.
- OT2: From 6th June 2019 at 14:20:50 to 23rd June 2019 at 05:07:30, every 10 seconds.
- OT3: From 19th May 2019 at 7:09:10 to 30rd May 2019 at 5:05:50, every 50 seconds.
- OT4: From 12th April 2019 at 14:43:20 to 29rd April 2019 at 00:06:40, every 40 seconds.

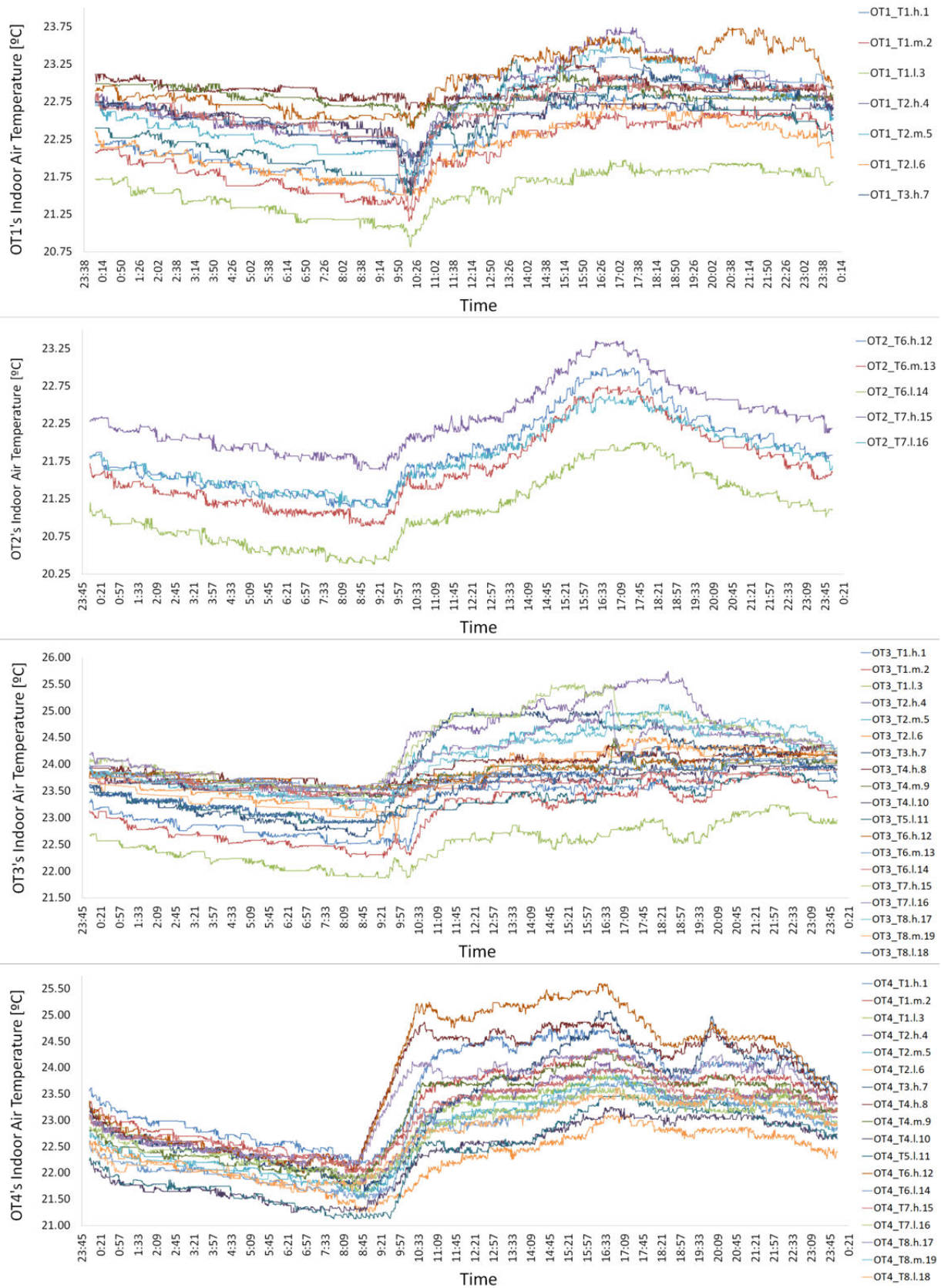


Figure 4.6: T_{dvi} evolution during 24 hours of data collected from the OT test ([149]): a. OT1 data 11th June 2019 from 0:00 to 24:00. b. OT2 data of 11th June 2019 from 0:00 to 24:00. c. OT3 data of 29th May 2019 from 0:00 to 24:00. d. OT4 data of 24th April 2019 from 0:00 to 24:00.

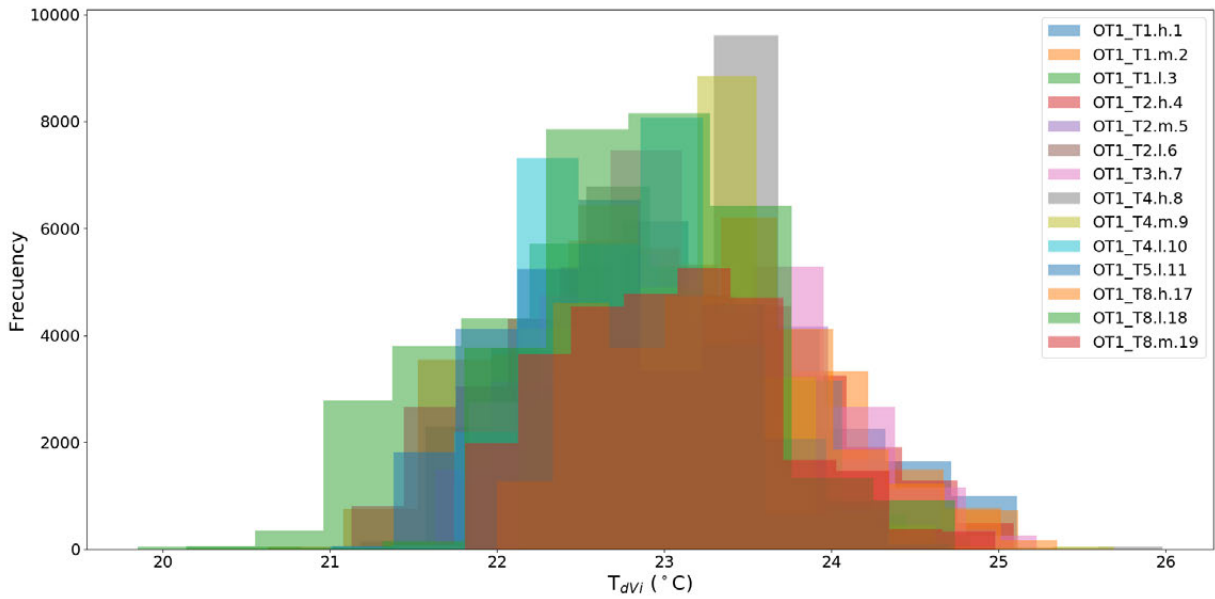


Figure 4.7: Temperature Histogram of T_{dvi} from MMS in OT1 for a sample size equal to 28,733 t_N with measurement frequency equal to ten seconds.

For each OT, Table 4.9 shows the statistical results of the $(\theta_{dvi})_{vw}$ values (Equation 3.7) for each sample t_j , where the T_{dvi} has been centred on $(Tvw)_{OT}$ (Equation 3.6). The OT1-C5, with fourteen temperature sensors, has its $\bar{\sigma}_T^2$, $\bar{\sigma}_T$ and U_T values equal to 0.127 K^2 , $\pm 0.356 \text{ }^\circ\text{C}$ and $\pm 0.71^\circ\text{C}$, respectively. OT2-B3, with five temperature sensors, has $\bar{\sigma}_T^2$, $\bar{\sigma}_T$ and U_T values equal to 0.135 K^2 , $\pm 0.368 \text{ }^\circ\text{C}$ and $\pm 0.74 \text{ }^\circ\text{C}$, respectively. OT3-D5, with nineteen temperature sensors, has $\bar{\sigma}_T^2$, $\bar{\sigma}_T$ and U_T values equal to 0.287 K^2 , $\pm 0.536 \text{ }^\circ\text{C}$ and $\pm 1.07 \text{ }^\circ\text{C}$, respectively. In addition, OT4-B4, with eighteen temperature sensors, has $\bar{\sigma}_T^2$, $\bar{\sigma}_T$ and U_T values equal to 0.172 K^2 , $\pm 0.414 \text{ }^\circ\text{C}$ and $\pm 0.83 \text{ }^\circ\text{C}$, respectively. The OT1-C5 and OT2-B3 OT have an almost equal uncertainty value and the lowest value of the four studied OT; both have the main façade oriented to the north, a very different OWS-CWS typology (Table 4.6), and a different number of sensors to measure the indoor air temperature. OT4-B4 has a similar U_T value with respect to OT1-C5 and OT2-B3; this OT has the same OWSR (Table 4.6) as OT2-B3, but different from OT1-C5. These three OTs have in common that they have one main façade oriented to the north. Finally, OT3-D5 has a greater U_T value than OT1-C5, OT2-B3 and OT4-B4; this OT has a different typology from the others and does not have any north-facing Façade, but it has its main façade to the south.

Data centred on $(Tvw)_{OT}$								
Office Typology	Sample Size	Measures (Z) by t_j	$\bar{\mu}[^\circ\text{C}]$ (Eq.3.14)	$\bar{\sigma}_T^2[\text{K}^2]$ (Eq.3.15)	$\bar{\sigma}_T[^\circ\text{C}]$ (Eq.3.16)	$U_T[^\circ\text{C}]$ (Eq.3.17)	Min	Max
OT1-C5	28,733	14	0.144	0.127	0.356	0.71	-2.336	1.882
OT2-B3	28,705	5	-0.174	0.135	0.368	0.74	-1.616	1.448
OT3-D5	18,861	19	-0.033	0.287	0.536	1.07	-4.145	2.732
OT4-B4	35,381	18	-0.031	0.172	0.414	0.83	-3.917	3.146

Table 4.9: Sample statistical results and Temperature Uncertainty (U_T) estimation of OT $(\theta_{dvi})_{vw}$ values (Equation 3.7), with temperature measurement (T_{dvi}) centred on $(Tvw)_{OT}$ (Equation 3.6).

Data centred on $(Ta)_{WS}$								
Office Typology	Sample Size	Measures (Z) by t_j	$\bar{\mu}$ [°C] (Eq.3.14)	$\bar{\sigma}_T^2$ [K ²] (Eq.3.15)	$\bar{\sigma}_T$ [°C] (Eq.3.16)	U_T [°C] (Eq.3.17)	Min	Max
OT1-2C1	28,733	3	0.000	0.044	0.209	0.42	-1.540	0.993
OT1-2C1.1	28,733	3	0.000	0.099	0.315	0.63	-1.117	0.937
OT1-2C1.3	28,733	1	n.a.	n.a.	n.a.	n.a.	n.a.	n.a.
OT1-2C1.4	28,733	1	n.a.	n.a.	n.a.	n.a.	n.a.	n.a.
OT1-2C1.5	28,733	3	0.000	0.081	0.285	0.57	-0.993	0.780
OT1-2C1.6	28,733	3	0.000	0.034	0.186	0.37	0.863	0.597
OT2-2C2	28,705	2	0.000	0.067	0.259	0.52	-1.280	1.280
OT2-2C2.1	28,705	3	0.000	0.094	0.306	0.61	0.833	0.637
OT3-2C3	18,861	3	0.000	0.097	0.311	0.62	-2.820	2.110
OT3-2C3.2	18,861	3	0.000	0.016	0.126	0.25	-0.963	0.620
OT3-2C3.3	18,861	3	0.000	0.016	0.128	0.26	-1.023	0.807
OT3-2C3.4	18,861	3	0.000	0.019	0.137	0.27	-0.540	0.540
OT3-2C3.5	18,861	3	0.000	0.074	0.271	0.54	-2.030	1.677
OT3-2C3.7	18,861	1	n.a.	n.a.	n.a.	n.a.	n.a.	n.a.
OT3-2C3.8	18,861	1	n.a.	n.a.	n.a.	n.a.	n.a.	n.a.
OT3-2C3.9	18,861	3	0.000	0.122	0.349	0.70	-0.920	0.747
OT4-3C1	35,381	16	0.000	0.110	0.332	0.66	-3.004	2.056
OT4-3C1.1	35,381	1	n.a.	n.a.	n.a.	n.a.	n.a.	n.a.
OT4-3C1.2	35,381	1	n.a.	n.a.	n.a.	n.a.	n.a.	n.a.

n.a. value means 'not applicable': the statistical analysis has not been applied to the WS with only one T_{dv_i} for each t_j (Z=1).

Table 4.10: Sample statistical results and Temperature Uncertainty (U_T) estimation of OT (θ_{dv_i})_{WSM} values (Equation 3.10), with temperature measurement (T_{dv_i}) centred on $(Ta)_{WS}$ (Equation 3.6).

For each WS, Table 4.10 shows the statistical results of $(\theta_{dv_i})_{WSM}$ (Equation 3.10) for each sample (t_N), where the T_{dv_i} has been centred on $(Ta)_{WS}$ (Equation 3.5). The methodology is not applicable to the WS with only one T_{dv_i} for each t_j (Z=1), these have been marked as n.a. (not applicable in the table). Unlike the $\bar{\mu}$ value of the OTs which were centred on $(Tvw)_{OT}$, the $\bar{\mu}$ values of all WS have been centred on $(Ta)_{WS}$ are thus are equal to zero.

The OWS of each analysed office typology, OT1-2C1, OT2-2C2, OT3-2C3 and OT4-3C1, have $\bar{\sigma}_T^2$ values between 0.044 K² and 0.110 K², $\bar{\sigma}_T$ values between ± 0.209 °C and ± 0.332 °C and U_T values between ± 0.42 °C and ± 0.66 °C. The OT1-2C1 has the lowest U_T values; this OWS has perimeter areas within OT1-C5 and one perimeter with west orientation, OT2-2C2 has a $\bar{\sigma}_T$ value ± 0.05 °C greater than OT3-2C3, this OWS has perimeter areas within OT3-D5 and one perimeter side facing north. OT3-2C3 and OT4-3C1 have worse U_T values with respect to OT1-2C1 and OT2-2C2, both OWSs have a perimeter side facing south and west; in addition, OT3-2C3 has a perimeter side facing north.

The interior CWS with three temperature measurements, OT1-2C1.6, OT3-2C3.2 and OT3-2C3.3 have $\bar{\sigma}_T^2$ values between 0.016 K² and 0.034 K², $\bar{\sigma}_T$ values between ± 0.126 °C and ± 0.186 °C and U_T values between ± 0.25 °C and ± 0.37 °C. These are the lowest U_T values of all the results. The $\bar{\sigma}_T^2$ value of OT1-2C1.6 is ± 0.06 °C higher because the door is open all the time with respect to OT3-2C3.2 and

OT3-2C3.3, which have the door closed most of the time. Analysing the exterior CWS, the OT3-2C3.4 has $\bar{\sigma}_T^2$, $\bar{\sigma}_T$ and U_T values equal to 0.019 K^2 , $\pm 0.137 \text{ }^\circ\text{C}$ and $\pm 0.27 \text{ }^\circ\text{C}$, respectively, which are the lowest values of all exterior CWSs. This CWS has two sensors to measure air temperature for each t_j ($Z=2$), the doors are closed most of the time and the windows are always closed, while all the other frequently occupied exterior CWSs behave similarly and have U_T values between $\pm 0.54 \text{ }^\circ\text{C}$ and $\pm 0.70 \text{ }^\circ\text{C}$, that is, they have greater uncertainties.

The U_T results of T_{in} shown in Table 4.9 plus the U_M values of the Q , K_e , K_o measurements of each Sub-Volume ($V_{i,j}$) or Thermal Zone (TZ) of the tertiary building, together with the U_M of the $S_a V_{sol}$ and T_{out} measurements, make it possible to obtain the U_{HLC} (Equation 2.29) of the HLC ($HLC_{F_{i,j}}$) (Equation 2.20) for each $F_{i,j}$, thus the estimation of the HLC can be obtained using Equation 2.32.

Decoupling Temperature Uncertainty (U_T) to estimate Temperature's Spatial Uncertainty ($U_{T(SP)}$) of the in-use tertiary building

Section 3.2.2 sets out the methodology for decoupling U_T to estimate the $U_{T(SP)}$ value from the already estimated $U_{T(S)}$ and U_T values. The $U_{T(S)}$ value is $\pm 0.24 \text{ }^\circ\text{C}$ that estimated in section 4.3.1 and the U_T values for the studied thermal zones (OT or WS) are estimated in section 4.3.1, whose values are shown in Tables 4.9 and 4.10.

Tables 4.11 and 4.10 show the results of the $U_{T(SP)}$ values decoupling U_T through the value of the associated Mean Variance of the sample $\bar{\sigma}_T^2$, this being equal to the sum of the sample's Mean Variance associated to $U_{T(S)}$ ($\bar{\sigma}_{(S)}^2$) and to $U_{T(SP)}$ ($\bar{\sigma}_{(SP)}^2$) (Equation 3.22) in order to estimate the $U_{T(SP)}$ value (Equations 3.23, 3.24 and 3.25).

The overall effect of $U_{T(S)}$ on U_T is based on the value of $R_{(S)}$. The effect of this on the analysis of the OT zone has values of between 4.91% and 11.14%, while the global effect of $U_{T(SP)}$, based on the value of the $R_{(SP)}$ value, has values of between 88.86% and 95.06% (Table 4.11). In general, there is the same trend in the global effects of $U_{T(S)}$ and $U_{T(SP)}$ with respect to U_T in the WS zone study shown in Table 4.12, where the $R_{(S)}$ values are between 11.62% and 32.26% and the $R_{(SP)}$ values are between 67.74% and 88.38%, for OT1-2C1, OT1-2C1.1, OT1-2C1.5, OT1-2C1.6, OT2-2C, OT2-2C2.1, OT3-2C3, OT3-2C3.5, OT3-2C3.9 and OT4-3C1. Here, the WSs have the doors open most of the time and there are occupants, solar radiation, heating effect and air currents, among other characteristics. This trend is different in three WSs , OT3-2C3.2, OT3-2C3.3 and OT3-2C3.4, where the values of $R_{(S)}$ are between 75.50% and 88.96% and the $R_{(SP)}$ values are between 11.31% and 24.50%, in which the global effect of $U_{T(S)}$ is greater with respect to the global effect of $U_{T(SP)}$. These WSs have the doors closed most of the time and there are neither occupants, air currents, solar radiation, or heating effects, among other types of uncertainty causes.

Values from $U_{T(S)}$ Analysis (Table 4.8): $\bar{\sigma}_{(S)}^2 = 0.014 \text{ K}^2$, $\bar{\sigma}_{(S)} = 0.119 \text{ }^\circ\text{C}$, $U_{T(S)} = 0.24 \text{ }^\circ\text{C}$

Office Typology	$\bar{\sigma}_T^* [^\circ\text{C}]$ (Eq.3.14)	$\bar{\sigma}_T^2 [K^2]$ (Eq.3.22)	$\bar{\sigma}_{(SP)}^2 [K^2]$ (Eq.3.23)	$\bar{\sigma}_{(SP)} [^\circ\text{C}]$ (Eq.3.24)	$U_{T(SP)} [^\circ\text{C}]$ (Eq.3.25)	$R_{(S)}$ (Eq.3.30)	$R_{(SP)}$ (Eq.3.32)
OT1-C5	0.356	0.127	0.113	0.335	0.67	11.14%	88.86%
OT2-B3	0.368	0.135	0.121	0.348	0.70	10.43%	89.57%
OT3-D5	0.536	0.287	0.273	0.523	1.05	4.91%	95.09%
OT4-B4	0.414	0.172	0.157	0.397	0.79	8.23%	91.77%

*Results obtained from Table 4.9.

Table 4.11: Decoupling of global standard deviation values of temperature measurement for four OT volumes.

Values from $U_{T(S)}$ Analysis (Table 4.8): $\bar{\sigma}_{(S)}^2 = 0.014 \text{ K}^2$, $\bar{\sigma}_{(S)} = 0.119 \text{ }^\circ\text{C}$, $U_{T(S)} = 0.24 \text{ }^\circ\text{C}$

Workspace	$\bar{\sigma}_T^* [^\circ\text{C}]$ (Eq.3.14)	$\bar{\sigma}_T^2 [K^2]$ (Eq.3.22)	$\bar{\sigma}_{(SP)}^2 [K^2]$ (Eq.3.23)	$\bar{\sigma}_{(SP)} [^\circ\text{C}]$ (Eq.3.24)	$U_{T(SP)} [^\circ\text{C}]$ (Eq.3.25)	$R_{(S)}$ (Eq.3.30)	$R_{(SP)}$ (Eq.3.32)
OT1-2C1	0.209	0.044	0.030	0.172	0.34	32.26%	67.74%
OT1-2C1.1	0.315	0.099	0.085	0.292	0.58	14.21%	85.79%
OT1-2C1.3	n.a.	n.a.	n.a.	n.a.	n.a.	n.a.	n.a.
OT1-2C1.4	n.a.	n.a.	n.a.	n.a.	n.a.	n.a.	n.a.
OT1-2C1.5	0.285	0.081	0.067	0.259	0.52	17.38%	82.62%
OT1-2C1.6	0.186	0.034	0.020	0.143	0.29	40.95%	59.05%
OT2-2C2	0.259	0.067	0.053	0.230	0.46	21.06%	78.94%
OT2-2C2.1	0.306	0.094	0.080	0.282	0.56	15.03%	84.97%
OT3-2C3	0.311	0.097	0.083	0.288	0.58	14.58%	85.42%
OT3-2C3.2	0.126	0.016	0.002	0.042	0.08	88.69%	11.31%
OT3-2C3.3	0.128	0.016	0.002	0.048	0.10	85.75%	14.25%
OT3-2C3.4	0.137	0.019	0.005	0.068	0.14	75.50%	24.50%
OT3-2C3.5	0.271	0.074	0.060	0.244	0.49	19.17%	80.83%
OT3-2C3.7	n.a.	n.a.	n.a.	n.a.	n.a.	n.a.	n.a.
OT3-2C3.8	n.a.	n.a.	n.a.	n.a.	n.a.	n.a.	n.a.
OT3-2C3.9	0.349	0.122	0.107	0.328	0.66	11.62%	88.38%
OT4-3C1	0.332	0.110	0.096	0.310	0.62	12.82%	87.18%
OT4-3C1.1	n.a.	n.a.	n.a.	n.a.	n.a.	n.a.	n.a.
OT4-3C1.2	n.a.	n.a.	n.a.	n.a.	n.a.	n.a.	n.a.

*Results obtained from Table 4.10.

n.a. value means “not applicable”: the statistical analysis cannot be applied to the WS with only one T_{dvi} for each t_j ($Z=1$).

Table 4.12: Decoupling of global standard deviation values of temperature measurement for each WS.

Estimation of the representative Indoor Air Temperature (T_{in}) of OT and WS of the studied in-use tertiary building

Estimating the U_T value, it is possible to know the Temperature Uncertainty (U_T) range in which the representative temperature could be for each OT and WS, based on Equations 3.43 and 3.44, respectively. Tables 4.14 and 4.13 show the results of the minimum and maximum limits of the indoor air temperature range for each OT and WS, regarding the whole averaged period for the temperature

of the OTs ($(\bar{T}_{vw})_{OT}$), so as to be able to apply the Temperature Uncertainty (U_T) for the experimental campaign carried out for this study.

Workspace	$(\bar{T}_a)_{WS}^*$ [°C]	U_T^{**} [°C]	$[(\bar{T}_a)_{WS}]_{range}$ (Equation 3.44)	
			Minimum Limit [°C]	Maximum Limit [°C]
OT1-2C1	23.10	±0.42	22.68	23.52
OT1-2C1.1	22.83	±0.63	22.20	23.46
OT1-2C1.3	n.a.	n.a.	n.a.	n.a.
OT1-2C1.4	n.a.	n.a.	n.a.	n.a.
OT1-2C1.5	22.98	±0.57	22.41	23.55
OT1-2C1.6	23.02	±0.37	22.65	23.39
OT2-2C2	22.63	±0.52	22.11	23.15
OT2-2C2.1	22.23	±0.61	21.62	22.84
OT3-2C3	23.29	±0.62	22.67	23.91
OT3-2C3.2	23.49	±0.25	23.24	23.74
OT3-2C3.3	23.45	±0.26	23.19	23.71
OT3-2C3.4	23.78	±0.27	23.51	24.05
OT3-2C3.5	23.50	±0.54	22.96	24.04
OT3-2C3.7	n.a.	n.a.	n.a.	n.a.
OT3-2C3.8	n.a.	n.a.	n.a.	n.a.
OT3-2C3.9	22.51	±0.70	21.81	23.21
OT4-3C1	22.96	±0.66	22.30	23.62
OT4-3C1.1	n.a.	n.a.	n.a.	n.a.
OT4-3C1.2	n.a.	n.a.	n.a.	n.a.

* $(\bar{T}_a)_{WS}$ is the Average Temperature of a WS for the whole monitored period.

** Values obtained from Table 4.10.

Table 4.13: Example of the range in which, the representative value of the Average Temperature of a WS for the whole monitored period ($(\bar{T}_a)_{WS}$) can be with a confidence interval of 95%.

Office Typology	$(\bar{T}_{vw})_{OT}^*$ [°C]	U_T^{**} [°C]	$[(\bar{T}_a)_{WS}]_{range}$ (Equation 3.44)	
			Minimum Limit [°C]	Maximum Limit [°C]
OT1-C5	22.83	±0.71	22.12	23.55
OT2-B3	22.57	±0.74	21.83	23.30
OT3-D5	23.33	±1.07	22.25	24.40
OT4-B4	22.99	±0.83	22.17	23.82

* $(\bar{T}_{vw})_{OT}$ is the Volume Weight Average Temperature of an OT for the whole monitored period.

** Values obtained from Table 4.9.

Table 4.14: Example of the range in which the representative value of the Volume Weight Average Temperature of a OT for the whole monitored period ($(\bar{T}_{vw})_{OT}$) can be with a confidence interval of 95%.

Vertical analysis of Temperature Uncertainty (U_T): vertical stratification's behaviour in TS of the in-use tertiary building

Vertical analysis of Temperature Uncertainty (U_T), called Vertical temperature Uncertainty (U_{VT}), was performed in OT3 as it is an office with more quantities of CWS, and with a greater number of monitored CWS with tripods during the OT test (the sensor layout is shown in Figure A.8 and is specified in Table A.3). The sensor groups are made up by combining the three sensors installed on a tripod (three sensors installed in the same vertical line), where the group of sensors to be studied can be made up of one, two or three sensors. Before the creation of the group of sensors to be studied, the $(\theta_{dv_i})_a$ values (Equation 3.8) are obtained, centring each T_{dv_i} of the studied tripod on its T_a^2 value (Equation 3.3). Then, the statistical analysis is carried out based on the studied group of sensors, where each t_j has $Z(\theta_{dv_i})_a$ values, and whose Z value depends on the number of sensors (or group of sensors) to analyse in the studied tripod or vertical line. The methodology applied in this analysis is described in section 3.2.3. In the studied OT, $(\theta_{dv_i})_a$ matches the $(\theta_{dv_i})_{wsm}$ value (Equation 3.10), the latter being the nomenclature used to carry out this analysis.

The objective of this study is to identify which is the optimal height to install a sensor or group of sensors in the same vertical line, reducing the measurement uncertainty associated with the vertical stratification of the T_{in} with respect to the T_a of the studied tripod, since the measurement of the temperature varies at different heights.

For the stratification analysis, the selected tripods of OT3 are those that have the three sensors with the same kind of reference, EE800-M12J3 (Table 4.2), the selected tripods being T1, T2, T4 and T6 (Table A.2) (T8 is not considered since it has the T8.m.19 sensor with reference: EE071-HTPC). Statistics analysis has developed independently for each studied tripod and for a sample size of 18,861 t_N . The study by tripod has been carried out for a combination of Z measurements by t_j . These Z values are made up by combining the tripod's sensors located at different heights. The studied period is from 19th May 2019 at 7:09:10 to 30th May 2019 at 5:05:50. Statistical parameters results are shown in Tables 4.15, 4.16 and 4.17.

Figures B.10, B.12, B.14 and B.16 show the histogram of T_{dv_i} for 18,8861 t_N of OT3.2C3.2, OT3.2C3.3, OT3.2C3.5 and OT3.2C3.9, respectively. Figures B.11, B.13, B.15 and B.17 show the histogram of $(\theta_{dv_i})_{wsm}$ for 18,8861 t_N of OT3.2C3.2, OT3.2C3.3, OT3.2C3.5 and OT3.2C3.9, respectively.

Statistical results from one sensor of each tripod located in a different CWS are shown in Table 4.15, where the results of each sensor measurement are with respect to the Average Temperature (T_a) of the tripod's sensors. Thus, in the studied case, this matches with the Average Temperature of the corresponding $((T_a)_{WS})$. The results show that all sensors located at medium level have lower U_{VT} , $\bar{\sigma}_{VT}$ and $\bar{\mu}$ values, their temperature measurement have better precision (lower $\bar{\sigma}_{VT}$ value) and better accuracy (lower $\bar{\mu}$ value) with respect to the T_a value of the studied tripod. This means that the sensors located at the medium level give a T_{dv_i} values closer to the T_a than the others sensors located on the

²The T_a of whole sensors installed on the same vertical, matches the T_a value of the sensors installed on a Tripod (T). Since each T is located in a WS, the average temperature of each T is the Average Temperature of a WS $((T_a)_{WS})$.

same tripod. The level with the greatest values of U_{VT} , $\bar{\sigma}_{VT}$ and $\bar{\mu}$ are the sensors located at the low height. Figures 4.8 and 4.9 show the $\bar{\sigma}_{VT}$ tendency by tripod and height level.

Analysing the statistical results by groups of three sensors (Table 4.17), where the temperature measurements of each tripod are included, it is possible to identify that the T1 and T2 values have higher values with respect to T4 and T6. For T2, the U_{VT} value is equal to ± 0.54 °C and the $\bar{\sigma}_{VT}$ value is equal to ± 0.271 °C; and for T1, the U_{VT} value is equal to ± 0.70 °C and the $\bar{\sigma}_{VT}$ value is equal to ± 0.349 °C. Likewise, for T4, the U_{VT} value is equal to ± 0.26 °C and the $\bar{\sigma}_{VT}$ value is equal to ± 0.128 °C; and for T6, the U_{VT} value is equal to ± 0.25 °C and the $\bar{\sigma}_{VT}$ value is equal to ± 0.126 °C. T1 and T2 are located in a CWS where doors are open most of the time, thus being influenced by a constant air current, occupations, solar radiations, and heating effects among other random incidences. In additions, T4 and T6 are located in a CWS where doors are closed most of the time, their statistical values being very similar, and the random incidences in both CWS have similar impacts on their temperature measurements.

The best combination two sensors with respect to the vertical location has been analysed in order to reduce the vertical stratification uncertainty. For this, Table 4.16 shows the results in two groups: tripods located in WS with closed doors most of the time (T4 and T6) and tripods located in WS with doors open most of the time (T1 and T2):

T4 and T6: In this case, the U_{VT} and $\bar{\sigma}_{VT}$ values are lowest for the sensor installed in the high and medium levels. This combination is the best from the point of view of precision, but with less accuracy (greater $\bar{\mu}$ values). For two sensors located in the high and low levels, the values have better accuracy (lowest $\bar{\mu}$ values) with less precision and greater values of U_{VT} and $\bar{\sigma}_{VT}$.

T1 and T2: In this case, the U_{VT} and $\bar{\sigma}_{VT}$ values are lowest for the sensors installed in the high and low levels. This combination is the best from the point of view of the precision, (lowest U_{VT} values) but with less accuracy (greater $\bar{\mu}$ values). For two sensors located in the high and medium levels, the values have better accuracy (lower $\bar{\mu}$ values) with less precision (greater U_{VT} and $\bar{\sigma}_{VT}$ values).

Figure 4.10 shows the $\bar{\sigma}_{VT}$ values by groups of two sensors at different heights, and their variation with respect to each tripod. In addition, Figure 4.11 shows the tendency of the $\bar{\sigma}_{VT}$ values by tripod for groups formed by two sensors at different heights.

The U_{VT} values in analysis by sensor are better than the analysis by groups of two sensors, accuracy the measure with one sensor at medium level having a better accuracy than the measure with a group of two sensors at the high and medium levels. Nevertheless, the T_{in} measurement with a group of two sensors, one located at the high level and other at the medium level, improves the accuracy of the temperature measure, obtaining lower $\bar{\mu}$ values and the U_{VT} values (measuring precision) if only the T_{in} is measured with a sensor installed at the medium level.

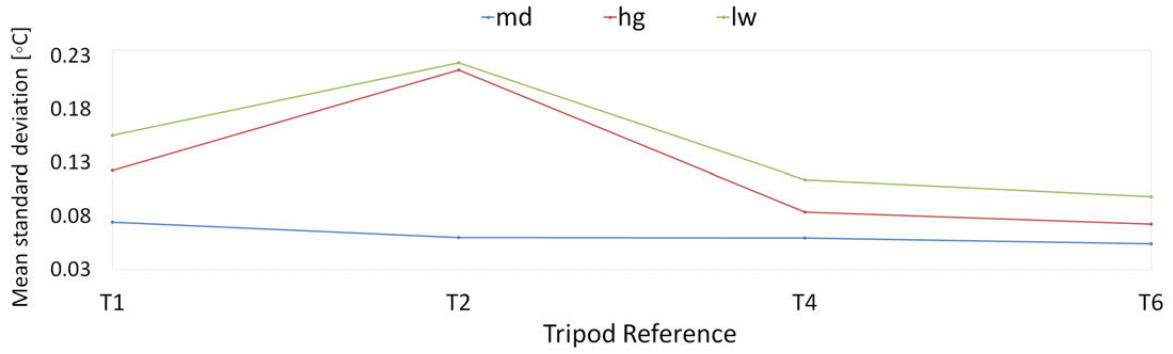


Figure 4.8: Standard deviation tendency by vertical height for each tripod with one sensor.

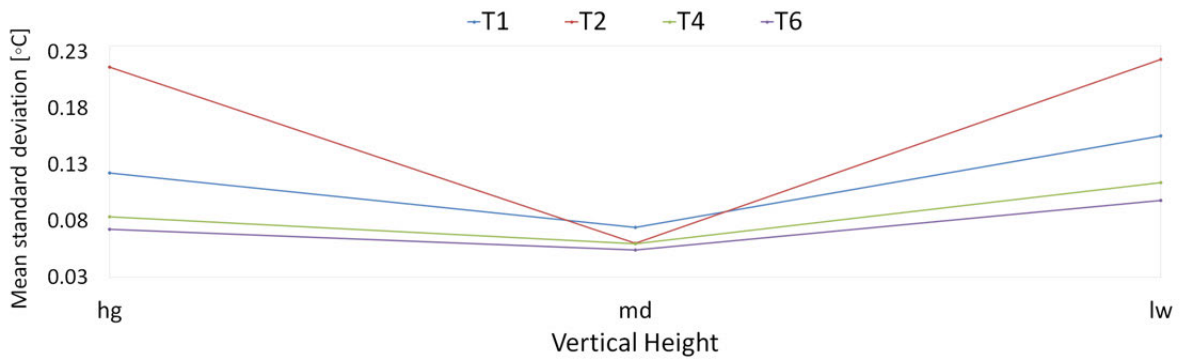


Figure 4.9: Standard deviation tendency by tripod with two sensors for each vertical height.

Data centred on T_a (Equation 3.3). Sample Size (N): 18,861				
OT3 Workspaces	Sensor ID	$\bar{\mu}$ [°C] (Eq.3.14)	$\bar{\sigma}_{VT}$ [°C] (Eq.3.16)	U_{VT} [°C] (Eq.3.17)
2C3.2	T6.h.12	0.078	0.068	0.14
	T6.m.13	0.068	0.049	0.10
	T6.l.14	-0.146	0.093	0.19
2C3.3	T4.h.8	0.124	0.079	0.16
	T4.m.9	-0.010	0.055	0.11
	T4.l.10	-0.114	0.109	0.22
2C3.5	T2.h.4	0.246	0.211	0.42
	T2.m.5	0.010	0.055	0.11
	T2.l.6	-0.255	0.218	0.44
2C3.9	T1.h.1	0.324	0.118	0.24
	T1.m.2	0.126	0.069	0.14
	T1.l.3	-0.450	0.151	0.30

Table 4.15: Statistical results of vertical uncertainty analysis by sensor in OT3.

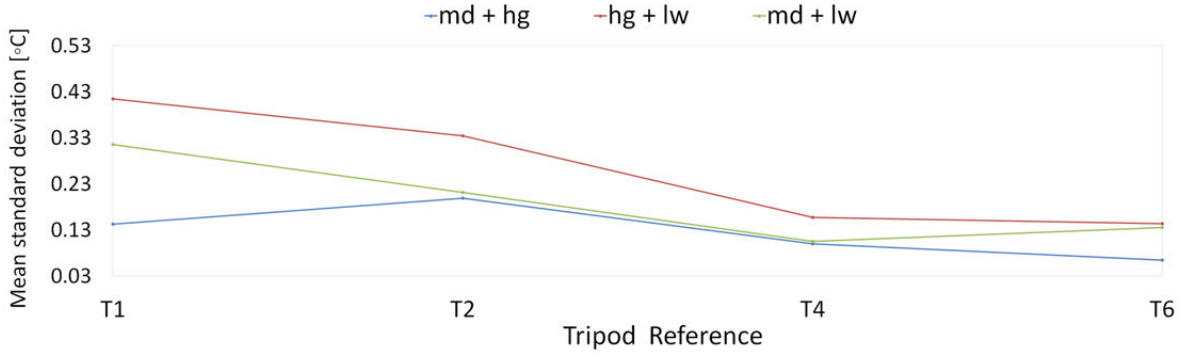


Figure 4.10: Standard deviation tendency by vertical height for each tripod with one sensors.

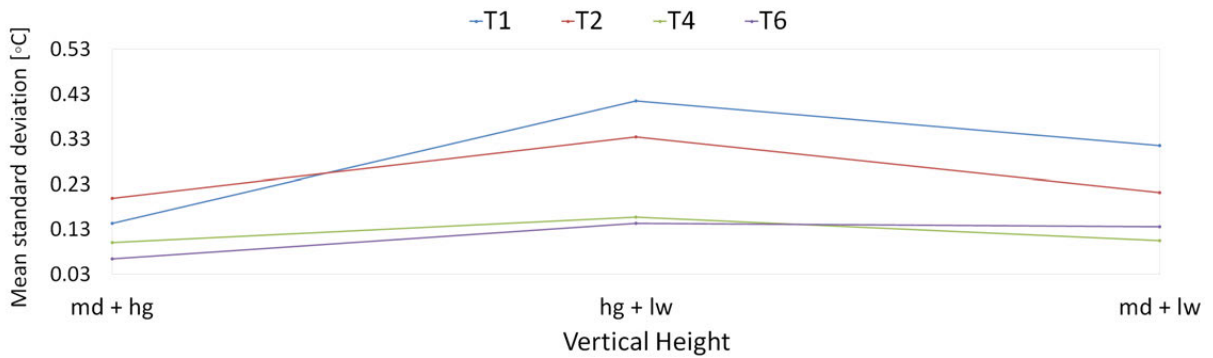


Figure 4.11: Standard deviation tendency by tripod with one sensor for each vertical height.

Data centred on T_a (Equation 3.3). Sample Size (N): 18,861				
OT3		$\bar{\mu}$ [°C]	$\bar{\sigma}_{VT}$ [°C]	U_{VT} [°C]
Workspaces	Sensor Group	(Eq.3.14)	(Eq.3.16)	(Eq.3.17)
2C3.2	T6.h.12 - T6.m.13	0.073	0.059	0.12
	T6.h.12 - T6.l.14	-0.034	0.138	0.28
	T6.m.13 - T6.l.14	-0.039	0.131	0.26
2C3.3	T4.h.8 - T4.m.9	0.057	0.095	0.19
	T4.h.8 - T4.l.10	0.005	0.152	0.30
	T4.m.9 - T4.l.10	-0.062	0.100	0.20
2C3.5	T2.h.4 - T2.m.5	0.128	0.194	0.39
	T2.h.4 - T2.l.6	-0.005	0.330	0.66
	T2.m.5 - T2.l.6	-0.123	0.207	0.41
2C3.9	T1.h.1 - T1.m.2	0.225	0.138	0.28
	T1.h.1 - T1.l.3	-0.063	0.410	0.82
	T1.m.2 - T1.l.3	-0.162	0.311	0.62

Table 4.16: Statistical results of vertical uncertainty analysis by group of two sensors in OT3.

Data centred on T_a (Equation 3.3). Sample Size (N): 18,861				
OT3		$\bar{\mu}$ [°C]	$\bar{\sigma}_{VT}$ [°C]	U_{VT} [°C]
Workspaces	Sensor Group	(Eq.3.14)	(Eq.3.16)	(Eq.3.17)
2C3.2	T6.h.12 – T6.l.13 – T6.m.14	0.000	0.126	0.25
2C3.3	T4.h.8 – T4.m.9 – T4.l.10	0.000	0.128	0.26
2C3.5	T2.h.4 – T2.m.5 – T2.l.6	0.000	0.271	0.54
2C3.9	T1.h.1 – T1.m.2 – T1.l.3	0.000	0.349	0.70

Table 4.17: Statistical results of vertical uncertainty analysis by group of three sensors in OT3.

Incidence of heating system, electricity consumption and solar radiation effects over Vertical Temperature Uncertainty (U_{VT})

This study is focused on the Vertical Temperature Uncertainty (U_{VT}) to analyse how it is affected by the On-Off cycles of the effects of the heating system, electricity consumption and solar radiation on the air temperature stratification. For this analysis, we selected groups of study with different sample sizes (t_N), called On-Off Sample Groups (OSGs), based on:

- Solar radiation effects: t_N group of periods With Solar Radiation (RAD ON) and Without solar radiation (RAD OFF) or only with solar diffuse radiation, in which, during the studied period, the t_N sample can have randomly On-Off cycles of the heating system and electricity consumption.
- Heating effect: t_N group of periods with Heating Power On (Ph ON) and another group with Heating Power Off (Ph OFF), in which, during the studied period, the t_N sample can have randomly On-Off cycles of solar radiation and electricity consumption.
- Electricity consumption effect: t_N group of periods with workers in OT or Active Power On (Pw ON) and without workers in OT or Active Power Off (Pw OFF), in which, during the studied period, the t_N sample can have randomly On-Off cycles of heating system and solar radiation.

The statistical analysis has been carried out on OT3 for tripods: T1, T2, T4 and T6, where each studied tripod has a sample size equal to 18,861 T_{dvi} . For these studied tripods, six OSGs with different T_{dvi} sample sizes have been selected. Each OSG, in turn, is made up of a group of sensors, as the groups of sensors were formed in the U_{VT} study of section 4.3.1, so as to be compared with respect to the U_{VT} results obtained in Tables 4.15, 4.16 and 4.17 of section 4.3.1. Table 4.18 shows the OSG to analyse the U_{VT} estimation for radiation, heating cycle and electricity consumption effects.

On-Off Study Groups (OSGs)		Incident effects		
OSG Name	Sample Size (N)	Solar Radiation	Heating Cycle	Electricity Consumption
Total Sample*	18,861	rad.on & rad.off	ph.on & ph.off	pw.on & pw.off
RAD ON Sample	7,000	rad.on rad.off	rad.on & rad.off	pw.on & pw.off
RAD OFF Sample	6,974	rad.off	rad.on & rad.off	pw.on & pw.off
Ph ON Sample	8,267	rad.on & rad.off	rad.on	pw.on & pw.off
Ph OFF Sample	7,411	rad.on & rad.off	rad.off	pw.on & pw.off
Pw ON Sample	5,905	rad.on & rad.off	rad.on & rad.off	pw.on
Pw OFF Sample	9,811	rad.on & rad.off	rad.on & rad.off	pw.off

* Section 4.3.1 shows and analyse the results of U_{VT} estimations.

Table 4.18: Relation of On-Off Sample Groups (OSGs) to analyse U_{VT} estimation based on radiation, heating cycle and electricity consumption effects.

For each sensor group of an OSG, which are installed in the same vertical or Tripod (T), the T_{dv_i} values have been centred on Ta^3 (Equation 3.3) to obtain the $(\theta_{dv_i})_a$ (Equation 3.8). In the experimental test carried out, the $(\theta_{dv_i})_a$ value matches with the $(\theta_{dv_i})_{wsm}$ value (Equation 3.10), the latter being the nomenclature used to carry out this analysis. The methodology to estimate the $\bar{\sigma}_{VT}$ (Equation 3.15), $\bar{\sigma}_{VT}^2$ (Equation 3.16) and U_{VT} (Equation 3.17) values are based on the methodology of section 3.2.1 for $(\theta_{dv_i})_{wsm}$ values.

Based on the results shown in Tables 4.19, 4.20 and 4.21, the inferior U_{VT} and $\bar{\mu}$ values are from the sensor installed at the medium level for all studied OSG. They are being also the sensor measurements with the better precision and accuracy with respect to the Ta of the studied tripod. Likewise, the sensors installed at the low level have greater U_{VT} and $\bar{\mu}$ values, the temperature measurements being those with the lowest accuracy and precision. Figures 4.12, 4.13 and 4.14 shows this result tendency through the evolution of the $\bar{\sigma}_{VT}$ values for the RAD ON and RAD OFF samples and Ph ON and Ph OFF samples, Pw ON and Pw OFF samples, respectively.

The effects of the Off cycles for all OSG have lower U_{VT} , $\bar{\sigma}_{VT}$ and $\bar{\mu}$ values than the effects of the On cycles.

³The T_a of whole sensors installed at the same vertical (located a Tripod (t)), matches the average temperature of each T with the Average Temperature of a WS $((T_a)_{WS})$.

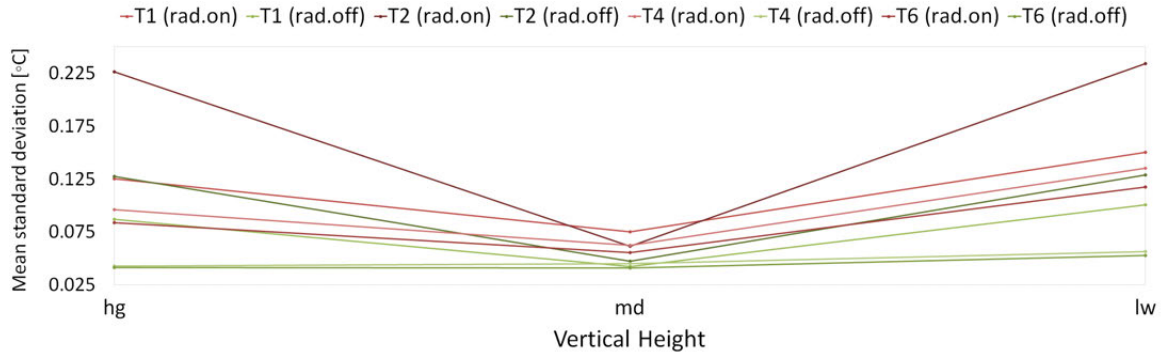


Figure 4.12: Mean standard deviation tendency by sensor based on vertical location for RAD ON and RAD OFF samples.

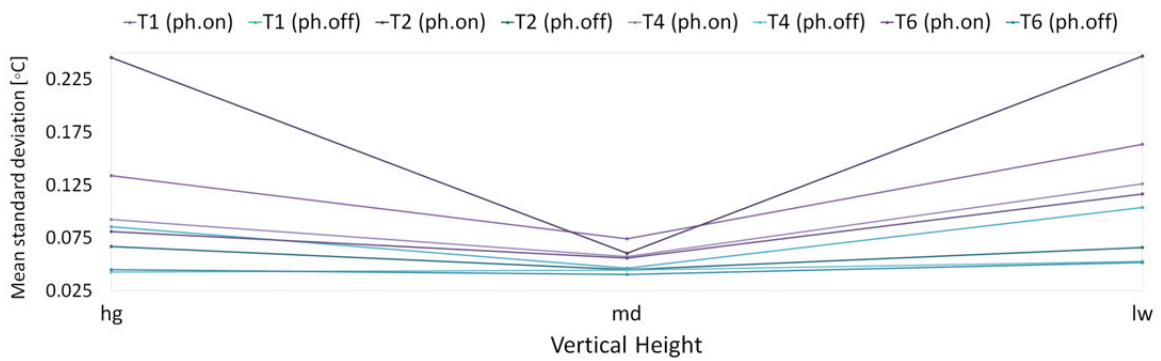


Figure 4.13: Mean standard deviation tendency by sensor based on vertical location for Ph ON and Ph OFF samples.

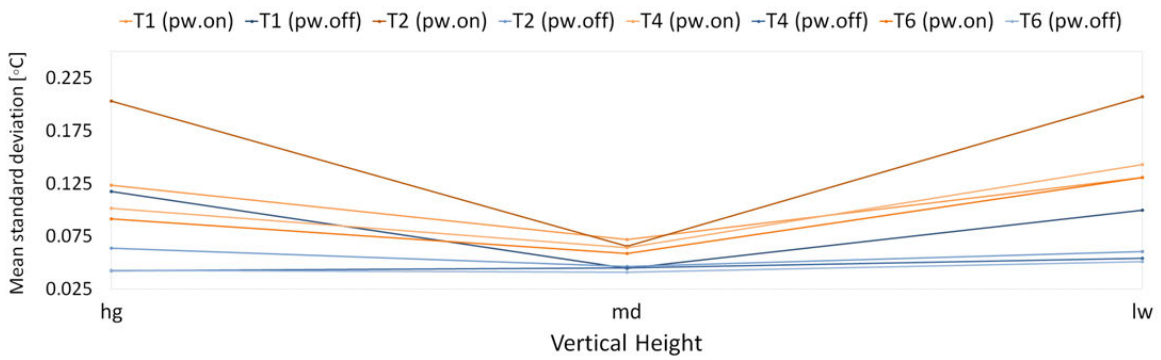


Figure 4.14: Mean standard deviation tendency by sensor based on vertical location for Pw ON and Pw OFF samples.

Data centred on		Total Sample			RAD ON sample			RAD OFF sample		
T_a		Sample Size (N): 18,861			Sample Size (N): 7,000			Sample Size (N): 6,974		
Tripod	Vertical Height	$\bar{\mu}$ [°C] (Eq.3.14)	$\bar{\sigma}_{VT}$ [°C] (Eq.3.16)	U_{VT} [°C] (Eq.3.17)	$\bar{\mu}$ [°C] (Eq.3.14)	$\bar{\sigma}_{VT}$ [°C] (Eq.3.16)	U_{VT} [°C] (Eq.3.17)	$\bar{\mu}$ [°C] (Eq.3.14)	$\bar{\sigma}_{VT}$ [°C] (Eq.3.16)	U_{VT} [°C] (Eq.3.17)
T1	h	0.324	0.118	0.24	0.369	0.125	0.25	0.277	0.087	0.17
	m	0.126	0.0769	0.14	0.158	0.075	0.15	0.093	0.042	0.08
	l	-0.450	0.151	0.30	-0.526	0.150	0.30	-0.370	0.101	0.20
T2	h	0.246	0.211	0.42	0.345	0.227	0.45	0.140	0.128	0.26
	m	0.010	0.055	0.11	0.014	0.062	0.12	0.005	0.047	0.09
	l	-0.255	0.218	0.44	-0.360	0.234	0.47	-0.145	0.129	0.26
T4	h	0.124	0.079	0.16	0.150	0.096	0.19	0.097	0.043	0.09
	m	-0.010	0.055	0.11	0.003	0.062	0.12	-0.018	0.045	0.09
	l	-0.114	0.109	0.22	-0.147	0.135	0.27	-0.079	0.056	0.11
T6	h	0.078	0.068	0.14	0.092	0.084	0.17	0.063	0.041	0.08
	m	0.068	0.049	0.10	0.075	0.056	0.11	0.061	0.041	0.08
	l	-0.146	0.093	0.19	-0.167	0.117	0.23	-0.124	0.053	0.11

Table 4.19: Statistical parameters by one sensor of the OSGs to study the solar radiation effect on the vertical uncertainty.

Data centred on		Total Sample			Ph ON sample			Ph OFF sample		
T_a		Sample Size (N): 18,861			Sample Size (N): 8,267			Sample Size (N): 7,411		
Tripod	Vertical Height	$\bar{\mu}$ [°C] (Eq.3.14)	$\bar{\sigma}_{VT}$ [°C] (Eq.3.16)	U_{VT} [°C] (Eq.3.17)	$\bar{\mu}$ [°C] (Eq.3.14)	$\bar{\sigma}_{VT}$ [°C] (Eq.3.16)	U_{VT} [°C] (Eq.3.17)	$\bar{\mu}$ [°C] (Eq.3.14)	$\bar{\sigma}_{VT}$ [°C] (Eq.3.16)	U_{VT} [°C] (Eq.3.17)
T1	h	0.324	0.118	0.24	0.352	0.134	0.27	0.293	0.086	0.17
	m	0.126	0.0769	0.14	0.154	0.074	0.15	0.095	0.046	0.09
	l	-0.450	0.151	0.30	-0.506	0.163	0.33	-0.388	0.104	0.21
T2	h	0.246	0.211	0.42	0.344	0.245	0.49	0.136	0.067	0.13
	m	0.010	0.055	0.11	0.021	0.061	0.12	0.002	0.045	0.09
	l	-0.255	0.218	0.44	-0.364	0.247	0.49	-0.133	0.066	0.13
T4	h	0.124	0.079	0.16	0.151	0.093	0.19	0.094	0.043	0.09
	m	-0.010	0.055	0.11	0.007	0.057	0.11	-0.029	0.045	0.09
	l	-0.114	0.109	0.22	-0.158	0.126	0.25	-0.064	0.053	0.11
T6	h	0.078	0.068	0.14	0.089	0.081	0.16	0.066	0.045	0.09
	m	0.068	0.049	0.10	0.073	0.056	0.11	0.063	0.040	0.08
	l	-0.146	0.093	0.19	-0.162	0.117	0.23	-0.129	0.052	0.10

Table 4.20: Statistical parameters by one sensor of the OSGs to study the heating system effect on the vertical uncertainty.

Data centred on		Total Sample			Pw ON sample			Pw OFF sample		
T_a		Sample Size (N): 18,861			Sample Size (N): 5,905			Sample Size (N): 9,811		
Tripod	Vertical Height	$\bar{\mu}$ [°C] (Eq.3.14)	$\bar{\sigma}_{VT}$ [°C] (Eq.3.16)	U_{VT} [°C] (Eq.3.17)	$\bar{\mu}$ [°C] (Eq.3.14)	$\bar{\sigma}_{VT}$ [°C] (Eq.3.16)	U_{VT} [°C] (Eq.3.17)	$\bar{\mu}$ [°C] (Eq.3.14)	$\bar{\sigma}_{VT}$ [°C] (Eq.3.16)	U_{VT} [°C] (Eq.3.17)
T1	h	0.324	0.118	0.24	0.401	0.12	0.25	0.324	0.118	0.24
	m	0.126	0.0769	0.14	0.178	0.07	0.14	0.095	0.044	0.09
	l	-0.450	0.151	0.30	-0.579	0.13	0.26	-0.372	0.100	0.20
T2	h	0.246	0.211	0.42	0.456	0.20	0.41	0.119	0.064	0.13
	m	0.010	0.055	0.11	0.019	0.07	0.13	0.004	0.047	0.09
	l	-0.255	0.218	0.44	-0.475	0.21	0.41	-0.123	0.061	0.12
T4	h	0.124	0.079	0.16	0.169	0.10	0.20	0.97	0.042	0.08
	m	-0.010	0.055	0.11	0.007	0.06	0.13	-0.021	0.045	0.09
	l	-0.114	0.109	0.22	-0.176	0.14	0.29	-0.076	0.054	0.11
T6	h	0.078	0.068	0.14	0.099	0.09	0.18	0.065	0.043	0.09
	m	0.068	0.049	0.10	0.079	0.06	0.12	0.061	0.041	0.08
	l	-0.146	0.093	0.19	-0.179	0.13	0.26	-0.126	0.051	0.10

Table 4.21: Statistical parameters by one sensor of the OSGsto study the electricity consumption effect on the vertical uncertainty.

The results shown in Tables 4.22, 4.23 and 4.24, can be seen that the sensor group with more precision is the combination of the medium and high levels, which has lower U_{VT} values. On the other hand, these groups have lower accuracy with respect with T_a , having greater $\bar{\mu}$ values than other groups. The group of sensors installed at the high and low levels has greater U_{VT} values and the lower $\bar{\mu}$ value; the combination of two sensors having greater accuracy and lower precision with respect to T_a . Figures 4.15, 4.16 and 4.17 shows this result tendency through the evolution of the $\bar{\sigma}_{VT}$ values for the RAD ON and RAD OFF samples, Ph ON and Ph OFF samples and Pw ON and Pw OFF samples, respectively.

The effects of the Off cycles for all OSG with groups of two sensors have lower $U_{VT}, \bar{\sigma}_{VT}$ and $\bar{\mu}$ values than the effects of the On cycles. The statistical results of the impact on the U_{VT} of the On-Off cycles of the studied OSGs: solar radiation, heating system and electricity consumption show the same tendency as the Total Sample results, which has been studied in section 4.3.1. These results are consistent from the point of view of the vertical stratification of T_{in} .

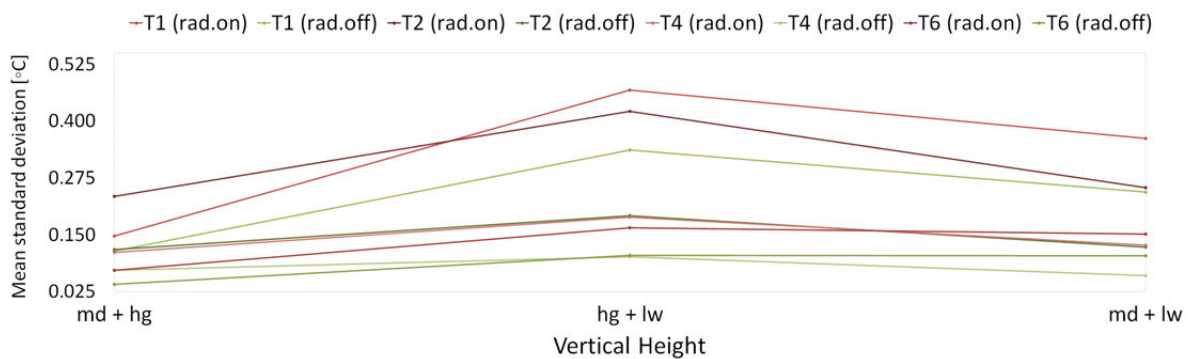


Figure 4.15: Mean standard deviation tendency by sensor based on vertical location for RAD ON and RAD OFF samples.

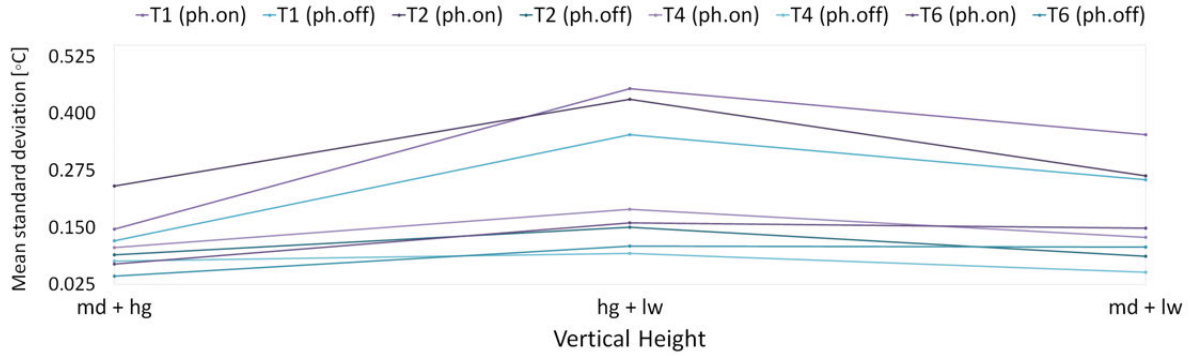


Figure 4.16: Mean standard deviation tendency by sensor based on vertical location for Ph ON and Ph OFF samples.

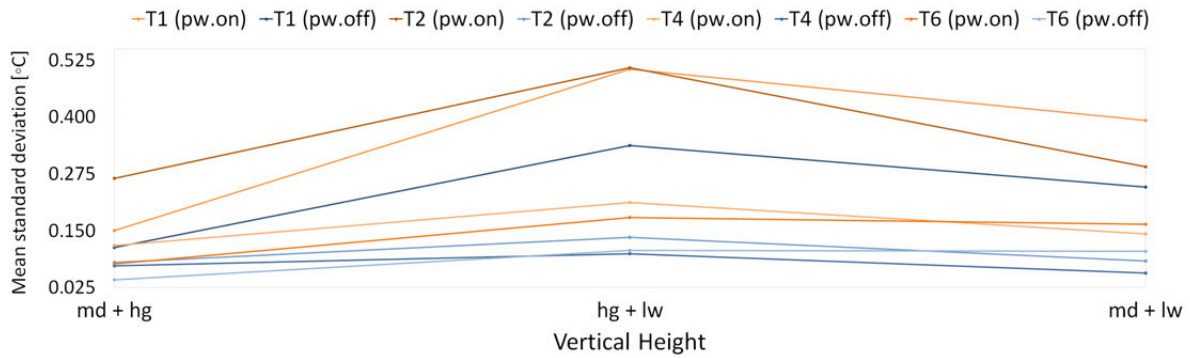


Figure 4.17: Mean standard deviation tendency by sensor based on vertical location for Pw ON and Pw OFF samples.

Data centred on		Total Sample			RAD ON sample			RAD OFF sample		
		Sample Size (N): 18,861			Sample Size (N): 7,000			Sample Size (N): 6,974		
T_a	Vertical Height	$\bar{\mu}$ [°C] (Eq.3.14)	$\bar{\sigma}_{VT}$ [°C] (Eq.3.16)	U_{VT} [°C] (Eq.3.17)	$\bar{\mu}$ [°C] (Eq.3.14)	$\bar{\sigma}_{VT}$ [°C] (Eq.3.16)	U_{VT} [°C] (Eq.3.17)	$\bar{\mu}$ [°C] (Eq.3.14)	$\bar{\sigma}_{VT}$ [°C] (Eq.3.16)	U_{VT} [°C] (Eq.3.17)
T1	m - h	0.225	0.138	0.28	0.263	0.148	0.30	0.185	0.114	0.23
	h - l	-0.063	0.410	0.82	-0.079	0.468	0.94	-0.047	0.337	0.67
	m - l	-0.162	0.311	0.62	-0.184	0.362	0.72	-0.138	0.244	0.49
T2	m - h	0.128	0.194	0.39	0.180	0.234	0.47	0.073	0.117	0.23
	h - l	0.005	0.330	0.66	-0.007	0.421	0.84	0.003	0.192	0.38
	m - l	-0.123	0.207	0.41	-0.173	0.253	0.51	-0.070	0.123	0.25
T4	m - h	0.057	0.095	0.19	0.073	0.111	0.22	0.040	0.072	0.14
	h - l	0.005	0.152	0.30	0.002	0.189	0.38	0.009	0.101	0.20
	m - l	-0.062	0.100	0.20	-0.075	0.127	0.25	-0.049	0.060	0.12
T6	m - h	0.073	0.059	0.12	0.084	0.072	0.14	0.062	0.041	0.08
	h - l	-0.034	0.138	0.28	-0.037	0.165	0.33	-0.031	0.105	0.21
	m - l	-0.039	0.131	0.26	-0.046	0.152	0.30	-0.032	0.104	0.21

Table 4.22: Statistical parameters by two sensors of the OSGs to study the solar radiation effect on the vertical uncertainty.

Data centred on		Total Sample			Ph ON sample			Ph OFF sample		
T_a		Sample Size (N): 18,861			Sample Size (N): 8,267			Sample Size (N): 7,411		
Tripod	Vertical Height	$\bar{\mu}[^\circ\text{C}]$ (Eq.3.14)	$\bar{\sigma}_{VT}[^\circ\text{C}]$ (Eq.3.16)	$U_{VT}[^\circ\text{C}]$ (Eq.3.17)	$\bar{\mu}[^\circ\text{C}]$ (Eq.3.14)	$\bar{\sigma}_{VT}[^\circ\text{C}]$ (Eq.3.16)	$U_{VT}[^\circ\text{C}]$ (Eq.3.17)	$\bar{\mu}[^\circ\text{C}]$ (Eq.3.14)	$\bar{\sigma}_{VT}[^\circ\text{C}]$ (Eq.3.16)	$U_{VT}[^\circ\text{C}]$ (Eq.3.17)
T1	m - h	0.225	0.138	0.28	0.253	0.147	0.29	0.194	0.120	0.24
	h - l	-0.063	0.410	0.82	-0.077	0.454	0.91	-0.048	0.353	0.71
	m - l	-0.162	0.311	0.62	-0.176	0.354	0.71	-0.146	0.254	0.51
T2	m - h	0.128	0.194	0.39	0.182	0.241	0.48	0.067	0.090	0.18
	h - l	0.005	0.330	0.66	-0.010	0.431	0.86	0.001	0.150	0.30
	m - l	-0.123	0.207	0.41	-0.172	0.263	0.53	-0.068	0.087	0.17
T4	m - h	0.057	0.095	0.19	0.079	0.105	0.21	0.032	0.076	0.15
	h - l	0.005	0.152	0.30	0.003	0.190	0.38	0.015	0.093	0.19
	m - l	-0.062	0.100	0.20	-0.075	0.128	0.26	-0.047	0.052	0.10
T6	m - h	0.073	0.059	0.12	0.081	0.070	0.14	0.064	0.043	0.09
	h - l	-0.034	0.138	0.28	-0.036	0.160	0.32	-0.032	0.109	0.22
	m - l	-0.039	0.131	0.26	-0.044	0.149	0.30	-0.033	0.107	0.21

Table 4.23: Statistical parameters by two sensors of the OSGs to study the heating system effect on the vertical uncertainty.

Data centred on		Total Sample			Pw ON sample			Pw OFF sample		
T_a		Sample Size (N): 18,861			Sample Size (N): 5,905			Sample Size (N): 9,811		
Tripod	Vertical Height	$\bar{\mu}[^\circ\text{C}]$ (Eq.3.14)	$\bar{\sigma}_{VT}[^\circ\text{C}]$ (Eq.3.16)	$U_{VT}[^\circ\text{C}]$ (Eq.3.17)	$\bar{\mu}[^\circ\text{C}]$ (Eq.3.14)	$\bar{\sigma}_{VT}[^\circ\text{C}]$ (Eq.3.16)	$U_{VT}[^\circ\text{C}]$ (Eq.3.17)	$\bar{\mu}[^\circ\text{C}]$ (Eq.3.14)	$\bar{\sigma}_{VT}[^\circ\text{C}]$ (Eq.3.16)	$U_{VT}[^\circ\text{C}]$ (Eq.3.17)
T1	m - h	0.225	0.138	0.28	0.289	0.150	0.30	0.186	0.114	0.23
	h - l	-0.063	0.410	0.82	-0.089	0.506	1.01	-0.047	0.338	0.68
	m - l	-0.162	0.311	0.62	-0.200	0.393	0.79	-0.139	0.246	0.49
T2	m - h	0.128	0.194	0.39	0.238	0.265	0.53	0.061	0.080	0.16
	h - l	0.005	0.330	0.66	-0.010	0.509	1.02	0.002	0.136	0.27
	m - l	-0.123	0.207	0.41	-0.228	0.291	0.58	-0.059	0.083	0.17
T4	m - h	0.057	0.095	0.19	0.088	0.117	0.23	0.038	0.073	0.15
	h - l	0.005	0.152	0.30	0.003	0.212	0.42	0.010	0.099	0.20
	m - l	-0.062	0.100	0.20	-0.084	0.143	0.29	-0.048	0.057	0.11
T6	m - h	0.073	0.059	0.12	0.089	0.077	0.15	0.063	0.042	0.08
	h - l	-0.034	0.138	0.28	-0.040	0.179	0.36	-0.031	0.107	0.12
	m - l	-0.039	0.131	0.26	-0.050	0.164	0.33	-0.033	0.105	0.21

Table 4.24: Statistical parameters by two sensors of the OSGs to study the electricity consumption effect on the vertical uncertainty.

Impact of spatial location on U_T

The statistical analysis has been carried out to collected data from seven sensors located at the high level of the tripods in OT4, with the objective of identifying the lowest U_T value obtained to determine the best location to reduce the random causes of uncertainty. OT4 has been chosen as this OT has the highest number of tripods and sensors installed in an OWS, so it is possible to analyse many groups of sensors in different orientations within an OT. On the other hand, the sensors located at the high level have been selected for this study, since there are more EE800-M12J3 sensors with respect to the medium level, where, based on section 4.3.1, measures from the medium level have lower U_{VT} values, followed by the high level.

To study the impact of spatial location on the U_T , the statistical analysis carried out is based on the $(\theta_{dvi})_{vw}$ values, which are calculated for each t_j , centring their T_{dvi} on the T_{vw} of OT4. Then, only with the sensors installed at the high level of OT4's Tripods (T) (Figure A.9), a different group of sensors has been formed. Making different combinations of sensor layout, it is possible to determine what is the best sensor location to decrease the U_T value, taking into account the number of sensors installed to monitor a volume. The statistical analysis described in section 3.2.1 is applied for each $(\theta_{dvi})_{vw}$ value of the group of sensors to be studied. In this way, the estimation of U_T and $\bar{\sigma}_T$ values has been carried out for each studied group of sensors, formed by sensors installed at the high level in OT4.

The data analysed for this study was collected between 12th April 2019 at 14:43:20 and 29th April 2019 at 00:06:40; with a collection frequency of 40 seconds. For OT4, Figures B.8 and B.9 show the histogram of T_{dvi} and $(\theta_{dvi})_a$, respectively, for a sample size equal to 35,381 t_N .

Table 4.25 shows the statistical results for one sensor. T3.h.7 has U_T greater than the U_T values of the rest of the sensors. Sensor T3.h.7, installed in 3C1.2 CWS (Figure A.9), does not have shadings to cover their windows, this WS more exposed to solar radiation. This is the reason why the T_{dvi} of this CWS is higher than the rest of the OT4 workspaces during the testing period, which is also why current analysis does not consider the T3.h.7 sensor measurement. Tables 4.26, 4.27, 4.28, 4.29 and 4.30 show the result excluding sensor T3.h.7 as this CWS has windows without shadings and its sensor measurements present values with great randomness with respect to the rest of the south facing sensors (tripods T1 and T2).

Sample Size (N): 35,381			
Sensor ID	$\bar{\mu}$ [°C] (Eq.3.14)	$\bar{\sigma}_T$ [°C] (Eq.3.16)	U_T [°C] (Eq.3.17)
T1.h.1	0.363	0.243	0.49
T2.h.4	0.046	0.102	0.20
T3.h.7	0.459	0.788	1.58
T4.h.8	0.212	0.314	0.63
T6.h.12	0.280	0.413	0.83
T7.h.15	0.133	0.168	0.34
T8.h.17	0.176	0.179	0.36

Table 4.25: Statistics results by sensor analysing values of $(\theta_{dvi})_{vw}$ for high-level sensors in OT4 in order to determine the best spatial location.

T4.h.8 and T6.h.12 sensors, with U_T values equal to ± 0.63 °C and ± 0.83 °C, respectively, have the lowest U_T value. Both are located at the northern façade, where sensor T4.h.8 has a pillar between the north window and is thus more protected from the exterior incidence through the window. Sensor T6.h.12 does not have any protection with respect to the window area and it is more exposed to northern exterior temperatures through the window, as well as radiation exchange (the northern

façade has no shadings for the windows). Sensors T1.h.1 and T2.h.4 are also near window influences, but this southern façade has shadings to protect it from the influence of solar radiation, so their U_T values are equal to ± 0.49 °C and ± 0.20 °C, respectively. These sensors are more protected by the window shielding than T1.h.1 due to its position with respect to the exterior shielding. On the other hand, the U_T values of T7.h.15 and T8.h.17 are equal to ± 0.34 °C and ± 0.36 °C. Both sensors are located in the interior zone of OT4, further away from the windows. The sensors with lower U_T values are T1.h.1, T7.h.15 and T8.h.17, which are less exposed to outside conditions impacting through the window. Further more, the accuracy of these T7.h.15 and T8.h.17 sensors is better than the rest, except sensor T2.h.4, with $\bar{\mu}$ values equal to 0.046 °C. In general, sensors closer to windows have a greater uncertainty than sensors located in the interior of the OWS.

Using two sensors, the best location and sensor combination are groups of two T2.h.4-T7.h.15 and T2.h.4-T8.h.17 with U_T values equal to ± 0.29 °C and ± 0.32 °C, $\bar{\sigma}_T$ values equal to ± 0.145 °C and ± 0.159 °C and $\bar{\mu}$ values equal to 0.090 °C and 0.111 °C, respectively (Table 4.26). Of these two-sensor groups, the combination with better accuracy and precision is the T2.h.4-T7.h.15 group, being the best location to install two sensors for monitoring OT4.

Sample Size (N): 35,381			
Sensor Group	$\bar{\mu}$ [°C] (Eq.3.14)	$\bar{\sigma}_T$ [°C] (Eq.3.16)	U_T [°C] (Eq.3.17)
T1.h.1-T2.h.4	0.204	0.245	0.49
T1.h.1-T4.h.8	0.287	0.291	0.58
T1.h.1-T6.h.12	0.321	0.341	0.68
T1.h.1-T7.h.15	0.248	0.238	0.48
T1.h.1-T8.h.17	0.269	0.233	0.47
T2.h.4-T4.h.8	0.129	0.248	0.50
T2.h.4-T6.h.12	0.163	0.323	0.65
T2.h.4-T7.h.15	0.090	0.145	0.29
T2.h.4-T8.h.17	0.111	0.159	0.32
T4.h.8-T6.h.12	0.246	0.369	0.74
T4.h.8-T7.h.15	0.172	0.255	0.51
T4.h.8-T8.h.17	0.194	0.256	0.51
T6.h.12-T7.h.15	0.207	0.323	0.65
T6.h.12-T8.h.17	0.228	0.322	0.64
T7.h.15-T8.h.17	0.154	0.175	0.35

Table 4.26: Statistics results by two-sensor group analysing values of $(\theta_{dv_i})_{vw}$ for high-level sensors in OT4 in order to determine the best spatial location.

Using three sensors (Table 4.27), the best combination of sensors is the T2.h.4-T7.h.15-T8.h.17 group. Which, whose U_T values equal ± 0.32 °C, $\bar{\sigma}_T$ values equal ± 0.162 °C and $\bar{\mu}$ values equal to 0.118°C. The

following best combination using three sensors are the groups T1.h.1-T2.h.4-T7.h.15, T1.h.1-T2.h.4-T8.h.17 and T2.h.4-T4.h.8-T7.h.15, with U_T values equal to ± 0.45 °C for these three groups and $\bar{\mu}$ values equal to 0.181 °C, 0.195 °C and 0.130 °C, respectively. The sensor group with the best accuracy the T2.h.4-T4.h.8-T7.h.15 combination. On the other hand, the combinations T4.h.8-T7.h.15-T8.h.17 and T6.h.12-T7.h.15-T8.h.17 have the U_T value equal to ± 0.46 °C and ± 0.57 °C, respectively. These sensor groups have values approximately equal to the T1.h.1-T2.h.4-T7.h.15, T1.h.1-T2.h.4-T8.h.17 and T2.h.4-T4.h.8-T7.h.15 U_T values, but they have some variation in their accuracy with $\bar{\mu}$ values equal to 0.174 °C and 0.196 °C, respectively.

Sample Size (N): 35,381			
Sensor Group	$\bar{\mu}$ [°C] (Eq.3.14)	$\bar{\sigma}_T$ [°C] (Eq.3.16)	U_T [°C] (Eq.3.17)
T1.h.1-T2.h.4-T4.h.8	0.207	0.270	0.54
T1.h.1-T2.h.4-T6.h.12	0.230	0.313	0.63
<i>T1.h.1-T2.h.4-T7.h.15</i>	<i>0.181</i>	<i>0.224</i>	<i>0.45</i>
<i>T1.h.1-T2.h.4-T8.h.17</i>	<i>0.195</i>	<i>0.225</i>	<i>0.45</i>
T1.h.1-T4.h.8-T6.h.12	0.285	0.337	0.67
T1.h.1-T4.h.8-T7.h.15	0.236	0.267	0.53
T1.h.1-T4.h.8-T8.h.17	0.250	0.264	0.53
T1.h.1-T6.h.12-T7.h.15	0.259	0.308	0.62
T1.h.1-T6.h.12-T8.h.17	0.273	0.305	0.61
T1.h.1-T7.h.15-T8.h.17	0.224	0.223	0.45
T2.h.4-T4.h.8-T6.h.12	0.179	0.321	0.64
<i>T2.h.4-T4.h.8-T7.h.15</i>	<i>0.130</i>	<i>0.224</i>	<i>0.45</i>
T2.h.4-T4.h.8-T8.h.17	0.144	0.228	0.46
T2.h.4-T6.h.12-T7.h.15	0.153	0.281	0.56
T2.h.4-T6.h.12-T8.h.17	0.167	0.283	0.57
T2.h.4-T7.h.15-T8.h.17	0.118	0.162	0.32
T4.h.8-T6.h.12-T7.h.15	0.208	0.321	0.64
T4.h.8-T6.h.12-T8.h.17	0.222	0.320	0.64
<i>T4.h.8-T7.h.15-T8.h.17</i>	<i>0.174</i>	<i>0.232</i>	<i>0.46</i>
<i>T6.h.12-T7.h.15-T8.h.17</i>	<i>0.196</i>	<i>0.284</i>	<i>0.57</i>

Table 4.27: Statistics results by three-sensor group analysing values of $(\theta_{dv_i})_{vw}$ for high-level sensors in OT4.

The measurement analysis of groups made up of four sensors (Table 4.28), T1.h.1-T2.h.4-T7.h.15-T8.h.17 and T2.h.4-T4.h.8-T7.h.15-T8.h.17, have the same U_T value equal to ± 0.43 °C and $\bar{\mu}$ value equal to 0.179°C and 0.142 °C, respectively. The T2.h.4-T4.h.8-T7.h.15-T8.h.17 group has more measurement accuracy with respect to the T1.h.1-T2.h.4-T7.h.15-T8.h.17 group. The sensor group T2.h.4-T6.h.12-T7.h.15-T8.h.17 has better measurement accuracy with respect to T1.h.1-T2.h.4-

T7.h.15-T8.h.17, with a $\bar{\mu}$ value equal to 0.159 °C, but lower precision with the $\bar{\sigma}_T$ and U_T values equal to ± 0.259 °C and ± 0.52 °C, respectively.

Sample Size (N): 35,381			
Sensor Group	$\bar{\mu}$ [°C] (Eq.3.14)	$\bar{\sigma}_T$ [°C] (Eq.3.16)	U_T [°C] (Eq.3.17)
T1.h.1-T2.h.4-T4.h.8-T6.h.12	0.225	0.313	0.63
T1.h.1-T2.h.4-T4.h.8-T7.h.15	0.188	0.250	0.50
T1.h.1-T2.h.4-T4.h.8-T8.h.17	0.199	0.251	0.50
T1.h.1-T2.h.4-T6.h.12-T7.h.15	0.206	0.287	0.57
T1.h.1-T2.h.4-T6.h.12-T8.h.17	0.216	0.286	0.57
T1.h.1-T2.h.4-T7.h.15-T8.h.17	0.179	0.214	0.43
T1.h.1-T4.h.8-T6.h.12-T7.h.15	0.247	0.310	0.62
T1.h.1-T4.h.8-T6.h.12-T8.h.17	0.258	0.309	0.62
T1.h.1-T4.h.8-T7.h.15-T8.h.17	0.221	0.249	0.50
T1.h.1-T6.h.12-T7.h.15-T8.h.17	0.238	0.284	0.57
T2.h.4-T4.h.8-T6.h.12-T7.h.15	0.168	0.291	0.58
T2.h.4-T4.h.8-T6.h.12-T8.h.17	0.178	0.292	0.58
T2.h.4-T4.h.8-T7.h.15-T8.h.17	0.142	0.215	0.43
T2.h.4-T6.h.12-T7.h.15-T8.h.17	0.159	0.259	0.52
T4.h.8-T6.h.12-T7.h.15-T8.h.17	0.200	0.292	0.58
T1.h.1-T2.h.4-T4.h.8-T6.h.12	0.225	0.313	0.63

Table 4.28: Statistics results by four-sensor group analysing values of $(\theta_{dv_i})_{vw}$ for high-level sensors in OT4 in order to determine the best spatial location.

Using five sensors for measurements (Table 4.29), the combination with more precision is T1.h.1-T2.h.4-T4.h.8-T7.h.15-T8.h.17, with the $\bar{\sigma}_T$ and U_T values equal to ± 0.238 °C and ± 0.48 °C, respectively, and the $\bar{\mu}$ value equal to 0.186 °C. The T2.h.4-T4.h.8-T6.h.12-T7.h.15-T8.h.17 group has more measurement accuracy with a $\bar{\mu}$ value equal to 0.169 °C, and the U_T value equal to ± 0.54 °C for a $\bar{\sigma}_T$ value equal to ± 0.272 °C.

Sample Size (N): 35,381			
Sensor Group	$\bar{\mu}$ [°C] (Eq.3.14)	$\bar{\sigma}_T$ [°C] (Eq.3.16)	U_T [°C] (Eq.3.17)
T1.h.1-T2.h.4-T4.h.8-T6.h.12-T7.h.15	0.207	0.293	0.59
T1.h.1-T2.h.4-T4.h.8-T6.h.12-T8.h.17	0.215	0.292	0.58
T1.h.1-T2.h.4-T4.h.8-T7.h.15-T8.h.17	0.186	0.238	0.48
T1.h.1-T2.h.4-T6.h.12-T7.h.15-T8.h.17	0.200	0.269	0.54
T1.h.1-T4.h.8-T6.h.12-T7.h.15-T8.h.17	0.233	0.290	0.58
T2.h.4-T4.h.8-T6.h.12-T7.h.15-T8.h.17	0.169	0.272	0.54

Table 4.29: Statistics results by five-sensor group analysing values of $(\theta_{dv_i})_{vw}$ for high-level sensors in OT4 in order to determine the best spatial location.

Analysing the five-sensors group, T1.h.1-T2.h.4-T4.h.8-T7.h.15-T8.h.17 combination, with U_T , $\bar{\sigma}_T$ and $\bar{\mu}$ values equal to ± 0.55 °C, ± 0.277 °C and 0.202 °C, respectively, the U_T value increases as this group includes the sensor with greater U_T values based on results by sensors of Table 4.25. Likewise, in the results of the two, three and four-sensor groups, it has been observed that the sensor combination with lower U_T values, are the groups where sensors with the lower U_T values from the results of the sensors from Table 4.25 are included.

The uncertainty are increases along with the number of sensors a the location in which some sensors are installed, can have greater uncertainty values due to random errors, thus increasing the value of the quadratic sum of the variance in the estimation of the $\bar{\sigma}_T^2$ and, therefore, the $\bar{\sigma}_T$ and its U_T value.

Sample Size (N): 35,381			
Sensor Group	$\bar{\mu}$ [°C] (Eq.3.14)	$\bar{\sigma}_T$ [°C] (Eq.3.16)	U_T [°C] (Eq.3.17)
T1.h.1-T2.h.4-T4.h.8-T6.h.12-T6.h.15-T6.h.17	0.202	0.277	0.55

Table 4.30: Statistics results for six-sensor group analysing values of $(\theta_{dv_i})_{vw}$ for high-level sensors in OT4 in order to determine the best spatial location.

Impact of number of sensors installed at the same height, but in different horizontal locations to decrease the Measurement Uncertainty (U_T) of T_{in} in a TZ

To analyse the impact of the number of sensors on U_T in the temperature measurement, the t-student method is applied to different sensor groups installed at high level in OT4. All T_{dv_i} are centred on T_{vw} to obtain the $(\theta_{dv_i})_{vw}$ for each t_j , and then, for these values, the $\bar{\sigma}_T$ of each t_j is estimated (see section 3.2.5). Each group is made up of a variable number of sensors, so each group has Z values of T_{dv_i} in each t_j (where Z matches the number of sensors in a studied group). Plotting the $\bar{\sigma}_T$ values of each t_j for each group, it is possible to obtain the $\bar{\sigma}_T$ evolution over time with a confidence interval of 95%

for each group of sensors.

Figure 4.18 shows the σ_T evolution, with a confidence interval of 95%, applying the t-student method to each t_j in each group characterized by the number of sensors or sensor measurement, Z T_{dv_i} , values. In addition, this figure shows an example of the uncertainty evolution due to the number of sensor measurements located at the high level in OT4. Graphically, it is possible to observe how the uncertainty decreases when the number of measurements (T_{dv_i}) increase for each t_j in the experimental test carried out.

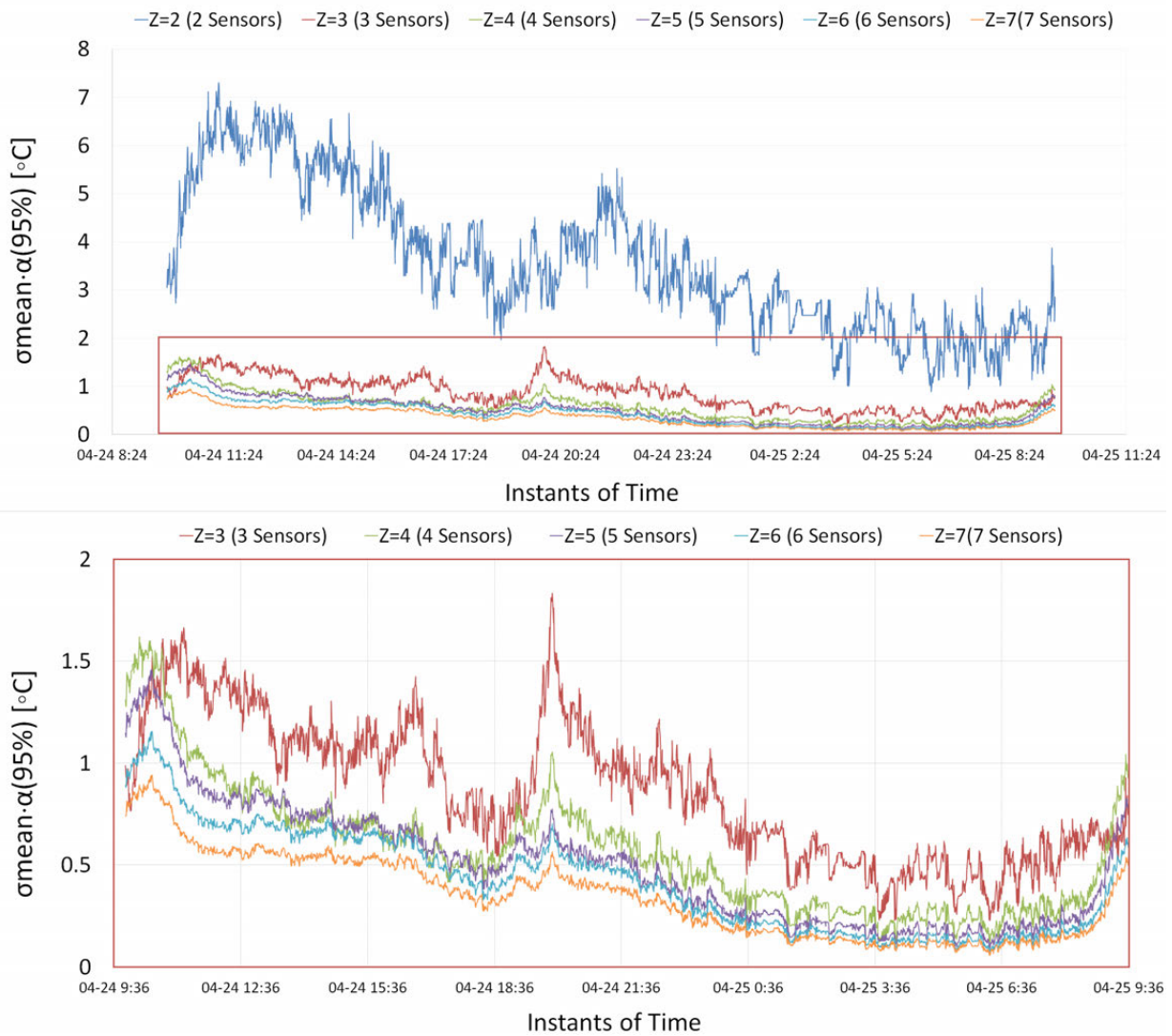


Figure 4.18: Uncertainty evolution for each $(\theta_{dv_i})_{vw}$ by Instant of Time (t_N), in function of the number of sensors (T_{dv_i} values) installed at high level in OT4.

4.3.2 Outdoor air temperature global uncertainty results for the UPV/EHU administrative building

Based on the importance of properly estimating the overall Uncertainty value for T_{out} , the analysis and estimation of U_T has been developed for an administrative in-use building monitored at UPV/EHU. This experimental test has been described in section 4.2.

The results show the following analysis:

- Measurement Sensor Uncertainty $U_{M(S)}$ analysis of T_{out} , called, Temperature Sensor Uncertainty $U_{T(S)}$.
- Measurement Uncertainty U_M analysis of T_{out} , called Temperature Uncertainty U_T .
- Measurement's Spatial Uncertainty $U_{M(SP)}$ analysis of T_{out} , called, Temperature's Spatial Uncertainty U_T .
- Estimation of the temperature range in which the representative value of T_{out} can lie, based on the uncertainty analysis.
- Temperature Uncertainty U_T analysis for outdoor air temperature measurements protected with solar radiation shield with and without mechanical ventilation.
- Estimation of the temperature bandwidth in which the Average Temperature of the air surrounding the building, called the Total Average Temperature ($(T_a)_{ta}$), can be, if measured only from one outdoor Measurement Space (MS) of the building.

Conception and variables used in the methodology to estimate the uncertainty of T_{out}

Based on the methodology set up in section 3.2.1, the variables identified for the study case are specified for the in-use tertiary building of UPV/EHU, where the experimental test carried out with an MMS integer in a BAS has been described in section 4.4. The conception and variables used in the uncertainty analysis of T_{out} are set out below.

Thermal Zone (TZ) characterization

The outdoor Thermal Zone (TZ) and Thermal Space (TS) of the administrative building of UPV/EHU are identified as Building Air Volume (BAV) and Building Envelope Area (BEA), respectively, where:

- **Building Air Volume (BAV):** This TZ refers to the air surrounding the studied building.
- **Building Envelope Area (BEA):** This TS refers to the envelope areas of the building, where, for the studied case, they are made up of the north façade (F_{nd}), south façade (F_{st}), east Façade (F_{wt}) and Roof (R).

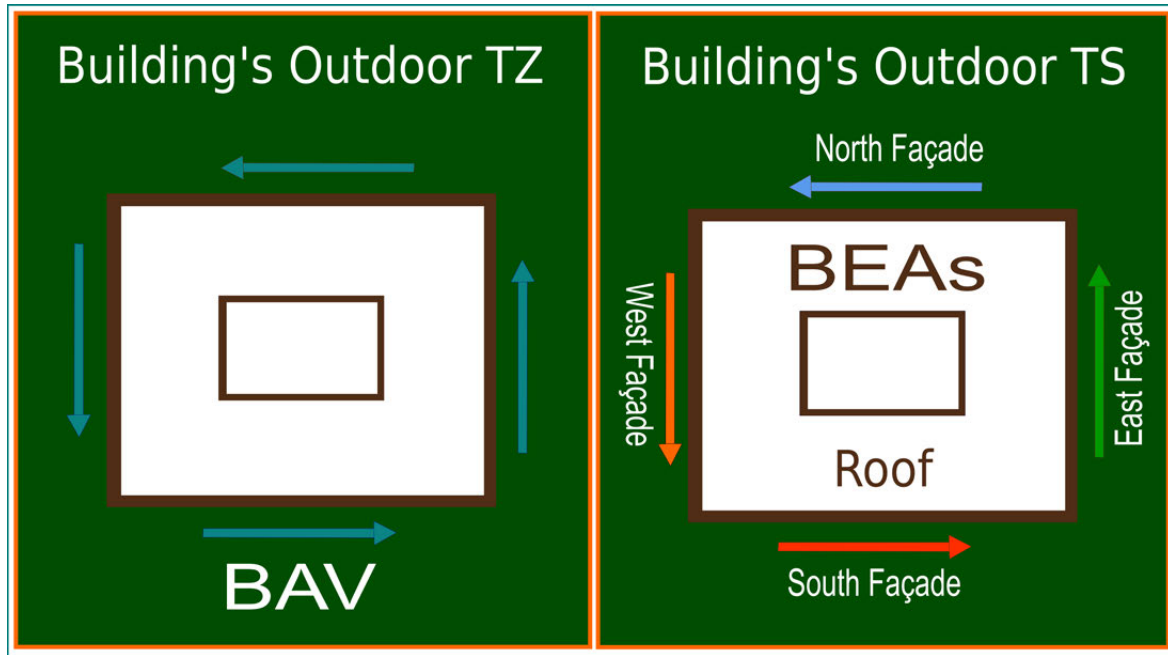


Figure 4.19: Scheme of the uncertainty of the T_{out} measurement for different Thermal Zones (TZs) and Thermal Spaces (TSs) identified in an in-use tertiary building.

Identification of methodology's variables for the uncertainty analysis of Outdoor Air Temperature (T_{out}) measurement

The variable names of the results shown in this section, are related to the variable names of the methodology of sections 3.2.1 and 3.2.2. Table 4.31 shows the relation of the variables for the uncertainty study, while Figure 4.20 shows a scheme of the uncertainty of the T_{out} measurement for different Thermal Zones (TZs) and Thermal Spaces (TSs) identified in an in-use tertiary building.

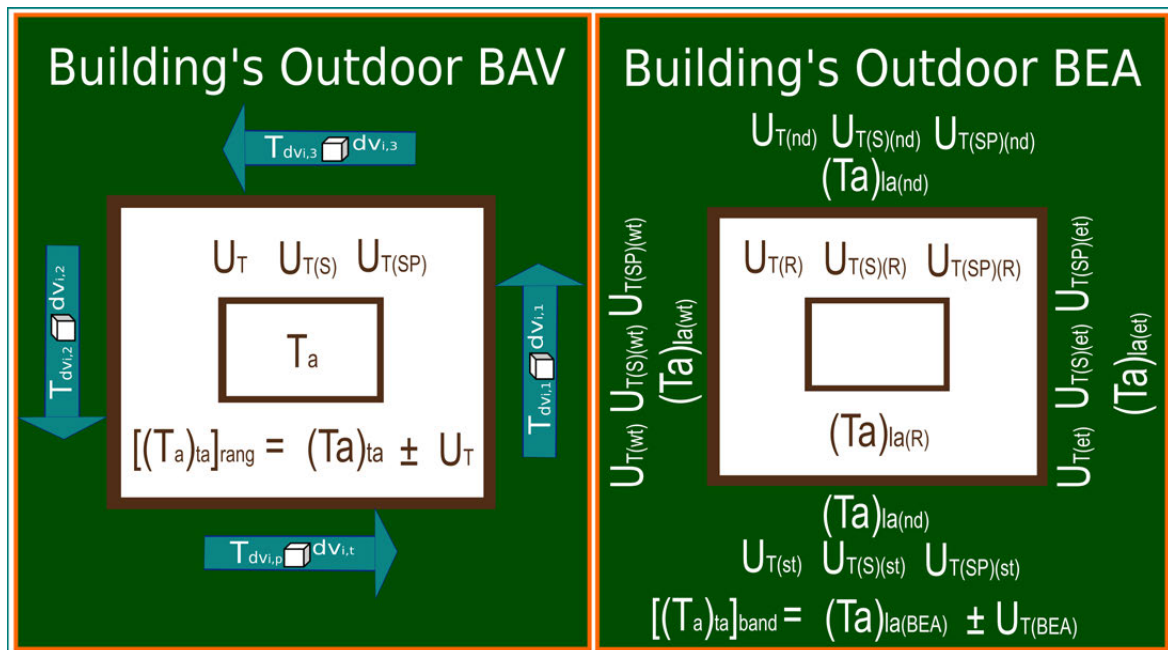


Figure 4.20: Scheme of the uncertainty of the T_{out} measurement for different Thermal Zones (TZs) and Thermal Spaces (TSs) identified in an in-use tertiary building.

Outdoor Air Temperature T_{out} data

The data analysis has been carried out using the data sets available in the data repository [149] specified and described in section 4.2.

In the analysed period, 407,664 data points have been collected in 50,958 Instants of Time (t_N) from 7th October 2019 at 12:42:20 to 6th January 2020 at 3:53:00, during the Exterior (E) Test (section 4.2). The results show three analysed cases for periods with different t_N sizes: periods only With Solar Radiation (RAD ON) incidence, Without Solar Radiation (RAD OFF) incidence and With and Without Solar Radiation (RAD ON-OFF) incidence, and whose sample sizes (N) are equal to 17,527; 29,065 and 50,958 Instants of Time (t_N), respectively.

In the RAD ON-OFF case, with a sample size equal to 50,958 t_N , not all the t_j have solar radiation data registered from the sensor E.T9.m.1413 (section 4.2), of which 8% of these t_j do not have registered data for solar radiation, while the other 92% (46,952 t_N) do have registered solar radiation data. The statistical analysis of the RAD ON-OFF case carried out in this section is based on a sample size equal to 50,958 t_N . The RAD ON-OFF case with a sample size equal to 46,952 t_N is shown only in subsection 2.2.2 in order to analyse the U_T value of the whole BAV with a smaller sample size.

Temperature Uncertainty (U_T) analysis for outdoor air temperature measurements protected with solar radiation shield, with and without mechanical ventilation

The purpose of this first analysis is to demonstrate that the solar radiation shielded outdoor air temperature sensors are only measuring the convection air temperature, excluding any solar radiation effect on these temperature measurements. Solar radiation shields without mechanical ventilation are usually used to protect the outdoor air temperature sensors against solar radiation effects on their measurements. In this research, one of the temperature sensors has been protected by a mechanically ventilated solar shield, while the rest have been protected by naturally ventilated solar radiation shields. Thus, it has been possible first of all to demonstrate that the not mechanically ventilated solar radiation protected air temperature measurements are not affected by the solar radiation. For this, two sensors, one with a mechanically ventilated solar shielding and the other with a not mechanically ventilated solar shielding, were installed in the same place measuring next to each other in a BA at the same height. Then, the Temperature Sensor Uncertainty ($U_{T(S)}$) for these two sensors has been estimated for a sample with N Instants of Time t_N , where the T_{dv_i} measurements have been centred with respect to $(T_a)_{la}$, in order to obtain the new data values, $(\theta_{dv_i})_{la}$. The statistical analysis has been applied to the $(\theta_{dv_i})_{la}$ values based on the methodology explained in section 3.2.1.

The analysed data have been collected by the E.R3.s.25 and E.R3.s.26 sensors, with and without mechanical ventilation within the solar radiation shield, respectively, from 7th October 2019 at 12:42:20 to 6th January 2020 3:53:00 during the Exterior E test (section 4.2). Figure 4.21 shows the temperature evolution of both air temperature sensors, together with the horizontal global solar radiation measurements on the 19th October, 2020 from 0:00 to 23:59. Likewise, Figure C.1 shows the histogram of all t_N with two T_{dv_i} measurements per sample ($Z=2$) (E.R3.s.25 and E.R3.s.26 sensors).

Variable names of section 3.4	Variable names section 4.3.1	Description	Variable names of section 3.4	Variable names section 4.3.1	Description
t_N	t_N	Instants of Time.	U_M	U_T	Temperature Uncertainty.
N	Z	Sample Size defined by the number of Instants of Time (t_N).	σ_M^2	σ_T^2	Mean Variance of t_N samples associated to U_M .
Z	Z	Number of $T_{d_{t_i}}$ Measurements in BAV ($Z = p$) or BEA ($Z = q$) volume for each t_j .	σ_M	σ_T	Mean Standard Deviation of t_N samples associated to U_T .
d_{t_i}	d_{t_i}	Differential Volume contained in BAV or a BEA [m^3].	$U_{M(S)}$	$U_{T(S)}$	Temperature Sensor Uncertainty.
M_{MZ}	V_{BAV}	BAV Volume [m^3].	$\sigma_{(S)}^2$	$\sigma_{(S)}^2$	Mean Variance of t_N samples associated to $U_{M(S)}$.
M_{MS}	V_{BEA}	BEA Volume [m^3].	$\bar{\sigma}_{(S)}$	$\bar{\sigma}_{(S)}$	Mean Standard Deviation of t_N samples associated to $U_{M(S)}$.
g	g	Number of Differential Volume in an BAV volume.	$U_{T(SP)}$	$U_{T(SP)}$	Temperature's Spatial Uncertainty.
y	y	Number of Differential Volume in a BEA volume.	$\sigma_{(SP)}^2$	$\sigma_{(SP)}^2$	Mean Variance of t_N samples associated to $U_{T(SP)}$.
n	n	Number of Building Envelope Areas (BEAs).	$\bar{\sigma}_{(SP)}$	$\bar{\sigma}_{(SP)}$	Mean Standard Deviation of t_N samples associated to $U_{T(SP)}$.
p	p	Number of $T_{d_{t_i}}$ in a BAV for each t_j .	$R(S)$	$R(S)$	Ratio of Mean Variance of t_N samples due to $U_{T(S)}$ with respect Mean Variance of t_N Samples due to U_T .
q	q	Number of $T_{d_{t_i}}$ in a BEA for each t_j .	$R(SP)$	$R(SP)$	Ratio of Mean Variance of t_N Samples due to $U_{T(SP)}$ with respect to Mean Variance of t_N Samples due to U_T .
$M_{d_{t_i}}$	$T_{d_{t_i}}$	Sensor Temperature for each t_j .	$[(\bar{M}_a)_{MZ}]_{range}$	$[(\bar{T}_a)_{t_{i_a}}]_{range}$	Maximum and Minimum limit in which $(T_a)_{t_{i_a}}$ of t_N Sample $(\bar{T}_a)_{t_{i_a}}$ fluctuates
$(M_{d_{t_i}})_{MZ}$	$(T_{d_{t_i}})_{BAV}$	Temperature Measurement ($T_{d_{t_i}}$) within a BAV for each t_j .	$[(\bar{M}_a)_{MZ}]_{range}$	$[(\bar{T}_a)_{t_{i_a}}]_{range}$	Maximum and Minimum limit in which $(T_a)_{t_{i_a}}$ of t_N Sample $(\bar{T}_a)_{t_{i_a}}$ fluctuates
$(M_{d_{t_i}})_{MS}$	$(T_{d_{t_i}})_{BEA}$	Temperature Measurement ($T_{d_{t_i}}$) within a BEA for each t_j .	$[(\bar{M}_a)_{MZ}]_{band}$	$[(\bar{T}_a)_{t_{i_a}}]_{band}$	Maximum and Minimum limit in which T_a of t_N Sample $(\bar{T}_a)_{t_{i_a}}$ of the MZ fluctuate, based on the one measurement of a MS that make it up.
M_a	T_a	Average Temperature of a Volume or Area (BAV or BEA).			
$(M_a)_{MZ}$	$(T_a)_{t_{i_a}}$	Total Average Temperature of $T_{d_{t_i}}$ collected around BAV for each t_j .			
$(M_a)_{MS}$	$(T_a)_{t_{i_a}}$	Local Average Temperature of $T_{d_{t_i}}$ collected on BEA for each t_j .			
$(\theta_{d_{t_i}})_{MZ}$	$(\theta_{d_{t_i}})_{t_{i_a}}$	Temperature Differential of $T_{d_{t_i}}$ centred on Total Average Temperature ($(T_a)_{t_{i_a}}$) for each t_j .			
$(\theta_{d_{t_i}})_{MS}$	$(\theta_{d_{t_i}})_{t_{i_a}}$	Temperature Differential of $T_{d_{t_i}}$ centred on Local Average Temperature ($(T_a)_{t_{i_a}}$) for each t_j .			

Table 4.3.1: Names of particularized variables for the uncertainty study of the T_{out} measurement.

In addition, Figures C.2, C.3 and C.4 show the histograms of t_N with the T_{dvi} data, centred with respect to $(T_a)_{la}$ for the RAD ON-OFF, RAD ON and RAD OFF periods, respectively.

The results of this statistical analysis are shown in Table 4.32 for t_N , considering the RAD ON-OFF, RAD ON and RAD OFF periods, respectively, where the U_T are equal to ± 0.091 °C, ± 0.112 °C and ± 0.077 °C for the RAD ON-OFF, RAD ON and RAD OFF periods, respectively. The case with the highest U_T value occurs in the periods with radiation incidence and the lowest U_T value is for the periods without radiation incidence. Analysing the U_T difference value regarding the solar radiation effect, it is possible to obtain two values in order to compare the RAD ON-OFF and RAD OFF periods with respect to the RAD ON periods. UD is obtained by subtracting the U_T value of periods with RAD ON-OFF and RAD OFF, from the U_T of periods with radiation (RAD ON):

- The difference RAD ON and RAD OFF is equal to 0.035 °C.
- The difference RAD ON and RAD ON-OFF is equal to 0.022 °C.

Both difference results are very low, which is a clear sign that the measured temperature is the air temperature excluding any solar radiation effect in any of the solar radiation shielding types, with and without mechanical ventilation.

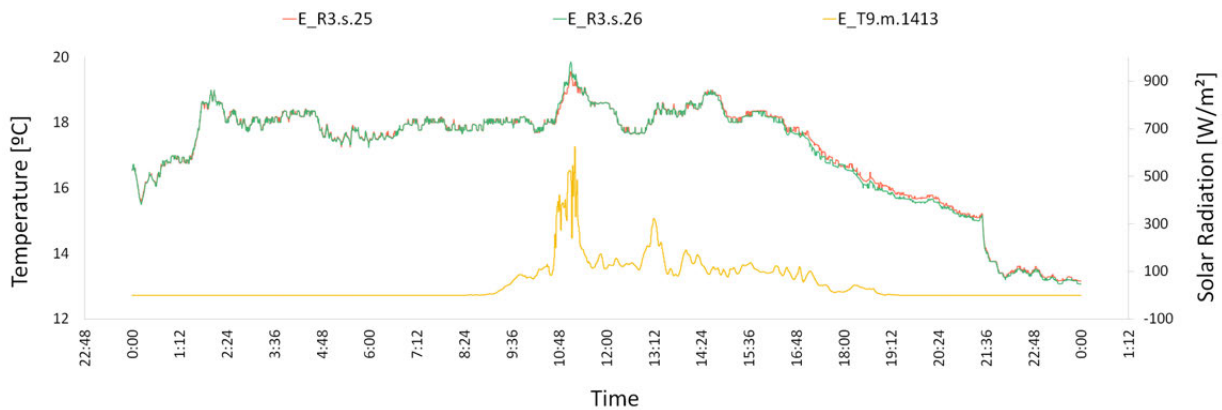


Figure 4.21: T_{dvi} evolution for October 19th, 2020 from 0:00 to 23:59 of data collected from the E.R3.s.25 and E.R3.s.26 sensors of the MMS.

Data centred on the local average temperature for E.R3.s.25 and E.R3.s.26 (Roof (R))			
Statistical Parameters	t_N with RAD ON-OFF N=50,958	t_N with RAD ON N=17,527	t_N with RAD OFF N=29,065
Z Measures by t_j	2	2	2
$(\bar{\mu})$ [°C] (Eq.3.14)	0.000	0.000	0.000
$(\bar{\sigma}_T^2)$ [K ²] (Eq.3.15)	0.002	0.003	0.001
$(\bar{\sigma}_T)$ [°C] (Eq.3.16)	0.045	0.056	0.039
(U_T) [°C] (Eq.3.17)	0.091	0.112	0.077
Min	-0.289	-0.230	-0.289
Max	0.290	0.230	0.290

Table 4.32: Temperature Uncertainty (U_T) estimation of $(\theta_{dvi})_{ia}$ with data centred on the Local Average Temperature $((T_a)_{ia})$ of the E.R3.s.25 and E.R3.s.26 sensors for each t_j with and without solar radiation, with solar radiation and without solar radiation cases.

Temperature Uncertainty (U_T) analysis of Outdoor Air surrounding the UPV/EHU Building or Building Air Volume (BAV)

This section shows the overall uncertainty of the T_{out} measurement surrounding the tertiary building or BAV, as well as the estimation of the T_{out} measurement surrounding the building when only one BEA of the building is monitored. The statistical results of this section have been obtained based on the methodology described in subsection 3.2.1, with data centred on $(T_a)_{ta}$ (Equation 3.4) to obtain $(\theta_a)_{ta}$ (Equation 3.9), which were calculated from the data of the eight-temperature sensors installed around the building envelope (E.F1.n.20, E.F1.n.21, E.F1.w.22, E.F1.s.23, E.F2.s.24, E.R3.s.25, E.R3.s.26 and E.R3.n.27 references).

The figures and tables shown in this section are:

- In Figure 4.22, the T_{dvi} evolution on October 19, 2020 from 0:00 to 23:59 of all data collected from E.F1.n.20, E.F1.n.21, E.F1.w.22, E.F1.s.23, E.F2.s.24, E.R3.s.25, E.R3.s.26 and E.R3.n.27 sensors of the MMS is shown. The locally measured horizontal global solar radiation is also shown in the right axis.
- For the data collected from the eight sensors installed around the building (E.F1.n.20, E.F1.n.21, E.F1.w.22, E.F1.s.23, E.F2.s.24, E.R3.s.25, E.R3.s.26 and E.R3.n.27 references):
 - Figure C.5 (RAD ON-OFF case), Figure C.6 (RAD ON case) and Figure C.7 (RAD OFF case) show the histogram of the eight T_{dvi} measurements ($Z=8$) for all the t_N samples considered in each case;
 - Figure C.8 (RAD ON-OFF case), Figure C.9 (RAD ON case) and Figure C.10 (RAD-OFF case) show the histogram of the eight T_{dvi} measurements ($Z=8$) centred with respect to $(T_a)_{ta}$ for all the t_N samples considered in each case.

- For the data analysis of the sensor measurements installed per BEAs regarding the Total Average Temperature ($(T_a)_{ta}$) calculated for the whole BAV, the histograms of the data centred on $(T_a)_{ta}$ are shown in:
 - Figure C.11 (RAD ON-OFF case), Figure C.12 (RAD ON case) and Figure C.13 (RAD-OFF case) for E.F1.n.20 and E.F1.n.21 sensors (Northern façade);
 - Figure C.14 (RAD ON-OFF case), Figure C.15 (RAD ON case) and Figure C.16 (RAD-OFF case) for E.F1.s.23 and E.F2.s.24 sensors (Southern façade);
 - Figure C.17 (RAD ON-OFF case), Figure C.18 (RAD ON case) and Figure C.19 (RAD-OFF case) for E.R3.s.25, E.R3.s.26 and E.R3.n.27 sensors (Roof).

Tables 4.33, 4.34 and 4.35 show the results of the statistical analysis for the three studied cases, RAD ON-OFF (N=50,958), RAD ON (N=17,527) and RAD OFF (N=29,065). Table 4.36 shows the results of RAD ON-OFF for a smaller sample size equal to 46,952 t_N of the eight sensors: E.F1.n.20, E.F1.n.21, E.F1.w.22, E.F1.s.23, E.F2.s.24, E.R3.s.25, E.R3.s.26 and E.R3.n.27, where there were both, temperature and global horizontal solar radiation measurements. Finally, Table 4.37 shows the Total Average Temperature Band ($[(\bar{T}_a)_{ta}]_{band}$) (Equation 3.45) in which the average temperature of BAV $(\bar{T}_a)_{ta}$ for the whole monitored period can lie if only one of the three BEA is monitored.

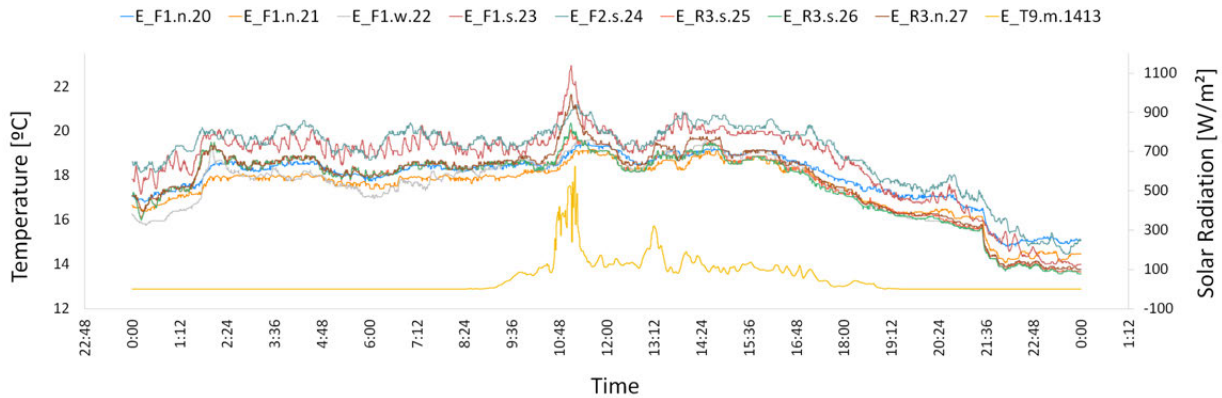


Figure 4.22: T_{dv_i} evolution on October 19th, 2020 from 0:00 to 23:59 of data collected from E.F1.n.20, E.F1.n.21, E.F1.w.22, E.F1.s.23, E.F2.s.24, E.R3.s.25, E.R3.s.26 and E.R3.n.27 sensors of the MMS.

Temperature Uncertainty (U_T) estimation of whole Building Air Volume (BAV)

The results of this subsection show the Temperature Uncertainty (U_T) of the T_{out} surrounding the tertiary building for the three study cases (RAD ON-OFF, RAD ON and RAD OFF). Table 4.33 (RAD ON-OFF periods), Table 4.34 (RAD ON periods) and Table 4.35 (RAD OFF periods) show the U_T results for the analysed t_N samples.

Data centred on $(T_a)_{ta}, t_N$ with RAD ON-OFF - N=50,958									
BEA	Sensor Reference	Measures (Z) by t_N	$(\bar{T}_{dvi})_{ta}/(\bar{T}_{dvi})_{la}$ [°C] Eq.3.4/Eq.3.5	$\bar{\mu}$ [°C] (Eq.3.14)	$\bar{\sigma}_T^2$ [K ²] (Eq.3.15)	$\bar{\sigma}_T$ [°C] (Eq.3.16)	U_T [°C] (Eq.3.17)	Min	Max
F _{nd}	E.F1.n.20 E.F1.n.21	2	17.414*	-0.396	0.899	0.948	1.90	-4.501	2.279
F _{st}	E.F1.s.23 E.F2.s.24	2	19.021*	1.211	1.527	1.236	2.47	-0.997	7.079
R	E.R3.s.25 E.R3.s.26 E.R3.n.27	3	17.489*	-0.321	0.240	0.490	0.98	-2.488	2.240
F _{nd} F _{st} F _{wt} R	E.F1.n.20 E.F1.n.21 E.F1.w.22 E.F1.s.23 E.F2.s.24 E.R3.s.25 E.R3.s.26 E.R3.n.27	8	17.810**	0.000	1.230	1.109	2.22	-4.501	7.079
*Local Average Temperature $((T_a)_{la})$ for the whole monitored period (Equation 3.5)									
**Total Average Temperature $((T_a)_{ta})$ for the whole monitored period (Equation 3.4)									

Table 4.33: Temperature Uncertainty (U_T) estimation of $((\theta_{dvi})_{ta})$ for each BEA with data centred on the Total Average Temperature $((T_a)_{ta})$ for each t_j with and without solar radiation. Including data with and without solar radiation measurement data.

Data centred on $(T_a)_{ta}$. t_N with RAD ON - N=17,527									
BEA	Sensor Reference	Measures (Z) by t_N	$(\bar{T}_{dvi})_{ta}/(\bar{T}_{dvi})_{la}$ [°C] Eq.3.4/Eq.3.5	$\bar{\mu}$ [°C] (Eq.3.14)	$\bar{\sigma}_T^2$ [K ²] (Eq.3.15)	$\bar{\sigma}_T$ [°C] (Eq.3.16)	U_T [°C] (Eq.3.17)	Min	Max
F_{nd}	E.F1.n.20 E.F1.n.21	2	19.286*	-1.149	1.116	1.056	2.11	-4.501	1.214
F_{st}	E.F1.s.23 E.F2.s.24	2	22.353*	1.918	2.852	1.689	3.38	-0.285	7.079
R	E.R3.s.25 E.R3.s.26 E.R3.n.27	3	20.096*	-0.339	0.453	0.673	1.35	-2.488	2.240
F_{nd}	E.F1.n.20	8	20.435**	0.000	2.541	1.594	3.19	-4.501	7.079
F_{st}	E.F1.n.21								
F_{wt}	E.F1.w.22								
R	E.F1.s.23								
	E.F2.s.24								
	E.R3.s.25								
	E.R3.s.26								
	E.R3.n.27								
*Local Average Temperature $((T_a)_{la})$ for the whole monitored period (Equation 3.5)									
**Total Average Temperature $((T_a)_{ta})$ for the whole monitored period (Equation 3.4)									

Table 4.34: Temperature Uncertainty (U_T) estimation of $((\theta_{dvi})_{ta})$ for each BEA with data centred on the Total Average Temperature $((T_a)_{ta})$ for each t_j with solar radiation.

In the case of the RAD ON and RAD OFF periods, the U_T values are equal to ± 3.19 °C (Table 4.34) and ± 1.38 °C (Table 4.35), respectively. The RAD ON period uncertainty values are considerably higher than those of the RAD OFF periods. The uncertainty of the outdoor air temperature surrounding the tertiary building in periods with and without radiation (RAD ON-OFF) is equal to ± 2.22 °C (Table 4.33). Thus, the minimum uncertainty for the overall outdoor air temperature measurements is obtained when it is measured during periods without solar radiation.

Finally, comparing the U_T value equal to ± 2.22 °C of the sample with 50,958 t_N to the U_T value of ± 2.24 °C (Table 4.36) of the sample size of 46,592 t_N , it is possible to affirm that the t_N equal to ± 2.22 °C is a consistent value of the temperature uncertainty of the air surrounding the building for the RAD ON-OFF case.

Data centred on $(T_a)_{ta} \cdot t_N$ with RAD OFF - N=29,065									
BEA	Sensor Reference	Measures (Z) by t_N	$(\bar{T}_{dvi})_{ta}/(\bar{T}_{dvi})_{la}$ [°C] Eq.3.4/Eq.3.5	$\bar{\mu}$ [°C] (Eq.3.14)	$\bar{\sigma}_T^2$ [K ²] (Eq.3.15)	$\bar{\sigma}_T$ [°C] (Eq.3.16)	U_T [°C] (Eq.3.17)	Min	Max
F_{nd}	E.F1.n.20 E.F1.n.21	2	16.677*	0.004	0.309	0.556	1.11	-1.854	2.279
F_{st}	E.F1.s.23 E.F2.s.24	2	17.471*	0.798	0.284	0.533	1.07	-0.997	5.396
R	E.R3.s.25 E.R3.s.26 E.R3.n.27	3	16.395*	-0.278	0.124	0.352	0.70	-1.492	1.449
F_{nd} F_{st} F_{wt} R	E.F1.n.20 E.F1.n.21 E.F1.w.22 E.F1.s.23 E.F2.s.24 E.R3.s.25 E.R3.s.26 E.R3.n.27	8	16.673**	0.000	0.478	0.691	1.38	-2.899	5.396

*Local Average Temperature $((T_a)_{la})$ for the whole monitored period (Equation 3.5)

**Total Average Temperature $((T_a)_{ta})$ for the whole monitored period (Equation 3.4)

Table 4.35: Temperature Uncertainty (U_T) estimation of $((\theta_{dvi})_{ta})$ for each BEA with data centred on the Total Average Temperature $((T_a)_{ta})$ for each t_j without solar radiation.

Data centred on $(T_a)_{ta} \cdot t_N$ with RAD ON - N=46,592									
BEA	Sensor Reference	Measures (Z) by t_N	$\bar{\mu}$ [°C] (Eq.3.14)	$\bar{\sigma}_T^2$ [K ²] (Eq.3.15)	$\bar{\sigma}_T$ [°C] (Eq.3.16)	U_T [°C] (Eq.3.17)	Min	Max	
F_{nd} F_{st} F_{wt} R	E.F1.n.20 E.F1.n.21 E.F1.w.22 E.F1.s.23 E.F2.s.24 E.R3.s.25 E.R3.s.26 E.R3.n.27	8	0.000	1.254	1.120	2.24	-4.501	7.079	

Table 4.36: Temperature Uncertainty (U_T) estimation of $((\theta_{dvi})_{ta})$ for the eight installed sensors with data centred on the Total Average Temperature $((T_a)_{ta})$ for each t_j with and without solar radiation.

Estimation of the Total Average Temperature $((T_a)_{ta})$ of whole Building Air's Volume (BAV) when only one Building Envelope Area (BEA) is monitored

The T_{out} is usually measured with sensors installed in one BEA, as for instance the northern façade and roof of buildings. However, the $(T_a)_{ta}$ obtained from the T_{dvi} of one BEA, is not the same $(T_a)_{ta}$ value of the BAV. Through the uncertainty analysis of T_{dvi} data of BEA centred with respect to the $(T_a)_{ta}$ value, which has been obtained from the eight sensors installed around the building, it is possible to estimate a band of values in which the $(T_a)_{ta}$ can lie when only is the T_{out} is measured from the sensors installed in one BEA.

The statistical study has been carried out to estimate the Total Average Temperature $((T_a)_{ta})$ of the air surrounding the building when only one BEA (roof, north and south façade) is monitored to collect data. The methodology used to obtain the statistical results is based on section 3.2.2, whose results are shown in Table 4.33 (RAD ON-OFF period), Table 4.34 (RAD ON period) and Table 4.35 (RAD OFF period) where: the $\bar{\mu}$ values of the sensor measurements installed on the northern façade, (E.F1.n.20 and E.F1.n.21 sensors) are equal to -0.396 °C, -1.149 °C and 0.004 °C for the RAD ON-OFF, RAD ON and RAD OFF periods, respectively. The results show that the northern temperature sensors with respect to the air temperature surrounding the building measure 0.396 °C and 1.149 °C less in periods with and without solar radiation and in periods with solar radiation, respectively; and 0.004 °C higher in periods without solar radiation. However, at night or in periods without solar radiation, the temperature measurements from these sensors give a representative measurement of the $(T_a)_{ta}$ surrounding the building. The $\bar{\mu}$ values of the sensors installed on the roof (E.R3.s.25, E.R3.s.26 and E.R3.n.27 sensors) are equal to -0.321 °C, -0.339 °C and -0.278 °C, respectively, for the RAD ON-OFF, RAD ON and RAD OFF periods. The mean values show that the sensors installed in the roof measure 0.321 °C, 0.339 °C and 0.278 °C less than the average air temperature that surrounds the building during periods with and without solar radiation, with solar radiation and without solar radiation incidence, respectively. The temperature measured by these sensors give the best value of the $(T_a)_{ta}$ value and are more homogenous than northern sensor in the three studied periods. The $\bar{\mu}$ values of sensor installed on the southern façade (E.F1.s.23 and E.F2.s.24 sensors) are equal to 1.211 °C, 1.918 °C and 0.798 °C, respectively, for the RAD ON-OFF, RAD ON and RAD OFF periods. These results show that the southern sensors measure 1.211 °C, 1.918v and 0.798 °C higher than the $(T_a)_{ta}$ surrounding the building during with and without solar radiation, with solar radiation and without solar radiation incidence, respectively. The temperatures measured by these sensors give the worst value of the $(T_a)_{ta}$ estimation.

Analysing the measurements per BEAs, it is clear that the roof is the most appropriate place for measuring the outdoors air temperature for this building for the three cases, RAD ON-OFF, RAD ON and RAD OFF. In fact, since we have centred the T_{dvi} of each t_j on the $(T_a)_{ta}$ calculated with the eight temperature measurements of each t_j , the column $\bar{\mu}$ is only zero for the case that studies the entire BAV measurements. Then, for the individual BEAs analyses, the column $\bar{\mu}$ is giving the difference between the average of all the T_{dvi} of all t_N in each BEA and the average of all the T_{dvi} of all t_N in the

entire BAV. Then, the tables for the RAD ON-OFF and RAD ON cases give reasonable results, since the southern façade $\bar{\mu}$ must obviously be higher than the northern or roof $\bar{\mu}$ values. However, even for the RAD OFF analysis, the southern façade $\bar{\mu}$ is higher than the northern or roof $\bar{\mu}$ values.

Furthermore, from Tables 4.33, 4.34 and 4.35, it can also be stated that the measurements on the roof are the ones with the lowest local uncertainty, since its U_T value is always the minimum among the BEAs. Thus, the roof provides the closest value to the total average value of the air surrounding the whole building and, furthermore, it gives this value with the least local spread on the measurements. Note, that having the least local spread has nothing to do with the overall uncertainty for the outdoor air temperature measurement. The overall outdoor air temperature measurement is given by the U_T provided by the statistical analysis of the eight outdoor air temperature measurements. Obviously, considering the eight air temperature measurements on all the BEAs, the total spread of the measurements is considerably higher than the local spread of the measurements carried out solely on the roof. Nevertheless, since the overall uncertainty for the air temperature representing the whole building envelope is usually the objective, the statistical analysis of the total spread of all the measurements is the one that gives the uncertainty level for the whole BAV air temperature.

Thus, having the Local Average Temperature $(\bar{T}_a)_{la}$ of one BEA: the roof, northern façade or southern façade, and the uncertainty values obtained from data centre on $(T_a)_{ta}$; it is possible to obtain a temperature range in which the Total Average Temperature $(\bar{T}_a)_{ta}$ of the BAV can be valid for the whole monitored period. This range of temperatures is called, the Total Average Temperature Band $[(\bar{T}_a)_{ta}]_{band}$ (Equation 3.45). This air temperature band can be estimated subtracting and adding the estimated U_T to the $(\bar{T}_a)_{la}$ (Equation 3.5) of the monitored BEA, whose values are shown in Tables 4.33, 4.34 and 4.35. The $[(\bar{T}_a)_{ta}]_{band}$ of the BAV estimated from the U_T results is shown below:

For measurements from the northern sensor:

- $[(\bar{T}_a)_{ta}]_{band} = (\bar{T}_a)_{la} \pm 1.90$ °C in periods with/without solar radiation.
- $[(\bar{T}_a)_{ta}]_{band} = (\bar{T}_a)_{la} \pm 2.11$ °C in periods with solar radiation.
- $[(\bar{T}_a)_{ta}]_{band} = (\bar{T}_a)_{la} \pm 1.11$ °C in periods without solar radiation.

For measurements from the roof sensors:

- $[(\bar{T}_a)_{ta}]_{band} = (\bar{T}_a)_{la} \pm 0.98$ °C in periods with/without solar radiation.
- $[(\bar{T}_a)_{ta}]_{band} = (\bar{T}_a)_{la} \pm 1.35$ °C in periods with solar radiation.
- $[(\bar{T}_a)_{ta}]_{band} = (\bar{T}_a)_{la} \pm 0.70$ °C in periods without solar radiation.

For measurements from the southern sensors:

- $[(\bar{T}_a)_{ta}]_{band} = (\bar{T}_a)_{la} \pm 2.47$ °C in periods with/without solar radiation.
- $[(\bar{T}_a)_{ta}]_{band} = (\bar{T}_a)_{la} \pm 3.38$ °C in periods with solar radiation.

- $[(\bar{T}_a)_{ta}]_{band} = (\bar{T}_a)_{la} \pm 1.07 \text{ }^\circ\text{C}$ in periods without solar radiation.

Based on these U_T estimations, the $[(\bar{T}_a)_{ta}]_{band}$ limits (Equation 3.45) have been estimated for each BEA of the studied building and these results are shown in Table 4.37. The roof with the $[(\bar{T}_a)_{ta}]_{band}$ value equal to $1.243 \text{ }^\circ\text{C}$ in RAD ON period, has the lowest bandwidth for the RAD ON-OFF and RAD OFF periods being equal to $0.845 \text{ }^\circ\text{C}$ and $0.510 \text{ }^\circ\text{C}$, respectively. After the roof, the monitored BEA with low $[(\bar{T}_a)_{ta}]_{band}$ value is the northern façade, where the $[(\bar{T}_a)_{ta}]_{band}$ value is equal to $1.058 \text{ }^\circ\text{C}$, $0.828 \text{ }^\circ\text{C}$ and $1.129 \text{ }^\circ\text{C}$, respectively, for the RAD ON-OFF, RAD ON and RAD OFF periods. The northern façade has the lowest $[(\bar{T}_a)_{ta}]_{band}$ value in the RAD ON periods. The widest band for the RAD ON-OFF, RAD ON and RAD OFF cases is obtained in the monitored southern façade, being equal to $2.165 \text{ }^\circ\text{C}$, $2.939 \text{ }^\circ\text{C}$ and $1.521 \text{ }^\circ\text{C}$, respectively.

BEA	Sensor Reference	Studied Cases	$(\bar{T}_a)_{la}^* \text{ [}^\circ\text{C]}$ (Eq.3.5)	$U_T^{**} \text{ [}^\circ\text{C]}$ (Eq.3.17)	$[(\bar{T}_a)_{la}]_{band} \text{ [}^\circ\text{C}]$ (Equation 3.45)	
					Minimum Limit $[\text{ }^\circ\text{C}]$	Maximum Limit $[\text{ }^\circ\text{C}]$
F_{nd}	E.F1.n.20	RAD ON-OFF	17.414	1.90	15.517	19.310
	E.F1.n.21	RAD ON	19.286	2.11	17.174	21.399
		RAD OFF	16.677	1.11	15.565	17.789
F_{st}	E.F1.s.23	RAD ON-OFF	19.021	2.47	16.549	21.492
	E.F2.s.24	RAD ON	22.353	3.38	18.975	25.731
		RAD OFF	17.471	1.07	16.404	18.537
R	E.R3.s.25	RAD ON-OFF	17.489	0.98	16.509	18.469
	E.R3.s.26	RAD ON	20.096	1.35	18.750	21.442
	E.R3.n.27	RAD OFF	16.395	0.70	15.691	17.099

** $(\bar{T}_a)_{la}$ is the average temperature of air surrounding a BEA for the whole monitored periods.

** Obtained from Tables 4.33, 4.34 and 4.35

Table 4.37: Example of the Total Average Temperature Band $[(\bar{T}_a)_{ta}]_{band}$ analysis, in which the average temperature of air surrounding the tertiary building or BAV for the whole monitored period $(\bar{T}_a)_{ta}$ can lie, if only one Building Envelope Area (BEA) is monitored.

Temperature Uncertainty (U_T) analysis of the air surrounding the Building Envelope Areas (BEAs): roof, northern and southern façades

This section shows the U_T value of the air surrounding the three BEAs: the roof, northern and southern façades. The data have been analysed independently by monitored area; for this, each BEA dataset has been centred on its Local Temperature Average $(T_a)_{la}$ (Equation 3.5) to estimate the statistical parameters based on Subsection 3.2.1.

The figures and tables shown in this section are:

The evolution of the temperatures during 24 hours are shown on Figure 4.23, in October 19, 2020 from 0:00 to 23:59 for the group of sensors E.F1.n.20 - E.F1.n.21, E.F1.s.23 - E.F2.s.24 and E.R3.s.25 -

E.R3.s.26 - E.R3.n.27. The T_{dvi} Histogram of the t_N samples for the three cases (RAD ON-OFF, RAD ON, RAD OFF) are shown, respectively, in Figures C.20, C.21 and C.22 for E.F1.n.20 and E.F1.n.21 sensors, Figures C.23, C.24 and C.25 for E.F1.s.23 and E.F2.s.24 sensors, Figures C.26, C.27 and C.28 for E.R3.s.25, E.R3.s.26 and E.R3.n.27.

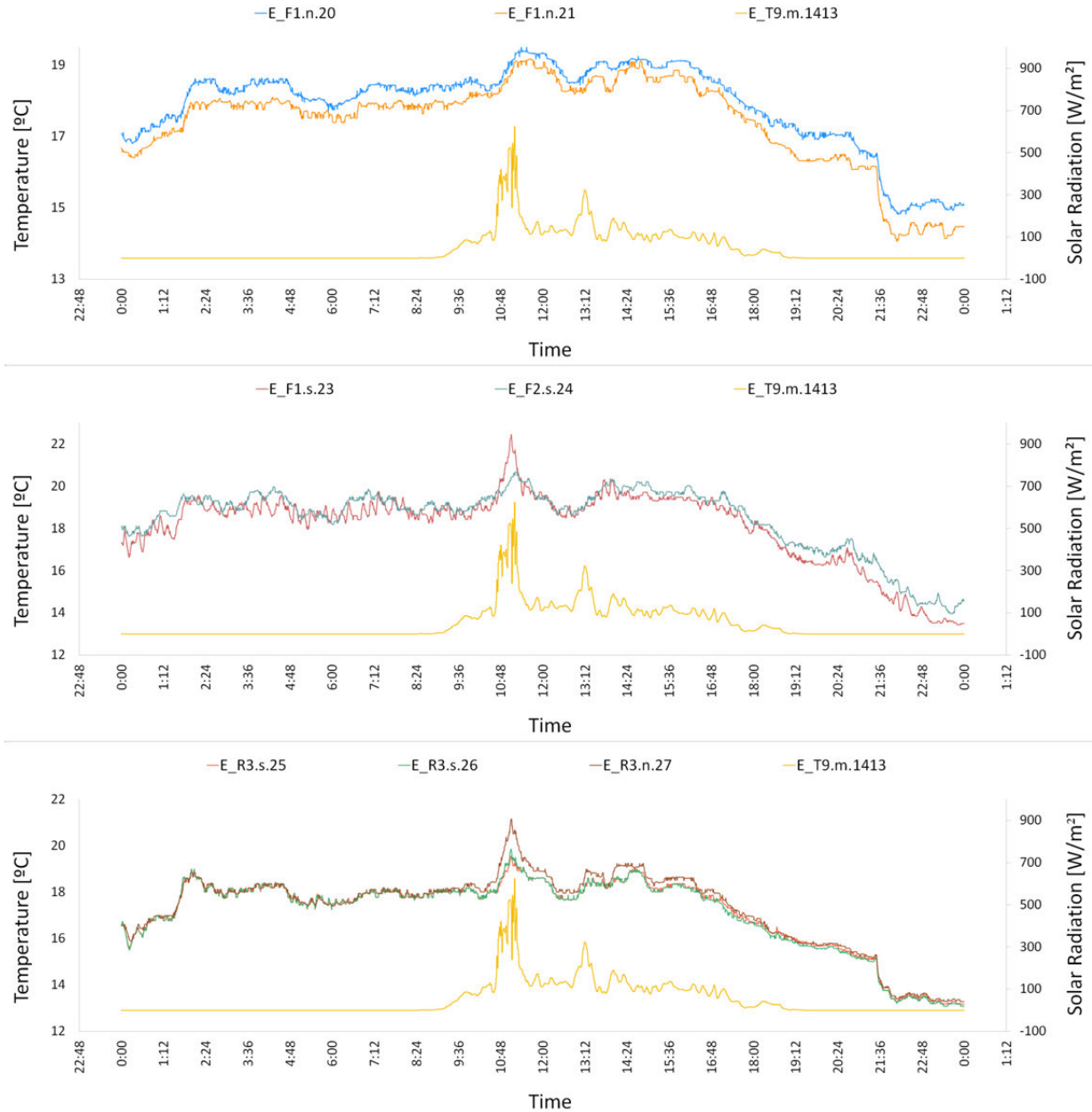


Figure 4.23: T_{dvi} and solar radiation evolution on October 19th, 2020 from 0:00 to 23:59 of data collected from MMS' BEAs (north Façade, southern façade and roof).

The histogram of the T_{dvi} measurements centred on the $(T_a)_{la}$ for the three cases (RAD ON-OFF, RAD ON, RAD OFF) are shown, respectively, in Figures C.29, C.30 and C.31 for E.F1.n.20 and E.F1.n.21 sensors, Figures C.32, C.33 and C.34 for E.F1.s.23 and E.F2.s.24 sensors, Figures C.35, C.36 and C.37 for E.R3.s.25, E.R3.s.26 and E.R3.n.27.

Tables 4.38, 4.39 and 4.40 show the U_T for the air surrounding each BEA where:

- Sensors installed on the northern façade (E.F1.n.20 and E.F2.n.21) have Temperature Uncertainty (U_T) values of the air surrounding the northern façade of the building equal to $\pm 0.53^\circ\text{C}$, $\pm 0.41^\circ\text{C}$ and $\pm 0.56^\circ\text{C}$, respectively, for the RAD ON-OFF, RAD ON and RAD OFF cases.
- The sensor, installed on the southern façade, (E.F1.s.23 and E.F2.s.24) have U_T values of the air surrounding the southern façade of the building equal to $\pm 1.08^\circ\text{C}$, $\pm 1.47^\circ\text{C}$ and $\pm 0.76^\circ\text{C}$, respectively, for the RAD ON-OFF, RAD ON and RAD OFF cases.
- Sensors installed on the roof (E.R3.s.25, E.R3.s.26 and E.R3.n.27) have U_T values of the air surrounding the building roof equal to $\pm 0.42^\circ\text{C}$, $\pm 0.62^\circ\text{C}$ and $\pm 0.25^\circ\text{C}$, respectively, for the RAD ON-OFF, RAD ON and RAD OFF.

Data centred on $(T_a)_{ta}^* \cdot t_N$ with RAD ON-OFF - N=50,958									
BEA	Sensor Reference	Measures (Z) by t_N	$(\bar{T}_a)_{la}^{***} [^\circ\text{C}]$ (Eq.3.5)	$\bar{\mu} [^\circ\text{C}]$ (Eq.3.14)	$\bar{\sigma}_T^2 [\text{K}^2]$ (Eq.3.15)	$\bar{\sigma}_T [^\circ\text{C}]$ (Eq.3.16)	$U_T [^\circ\text{C}]$ (Eq.3.17)	Min	Max
F_{nd}	E.F1.n.20 E.F1.n.21	2	17.414	0.000	0.070	0.264	0.53	-0.885	0.885
F_{st}	E.F1.s.23 E.F2.s.24	2	19.021	0.000	0.293	0.541	1.08	-2.865	2.865
R	E.R3.s.25 E.R3.s.26 E.R3.n.27	3	17.489	0.000	0.045	0.211	0.42	-0.957	1.303

* $(T_a)_{ta}$ is the average temperature of air surrounding the building or BAV in each t_j .
** $(\bar{T}_a)_{la}$ is the average temperature of air surrounding a BEA for the whole monitored periods.

Table 4.38: Temperature Uncertainty (U_T) estimation of $(\theta_{dvi})_{la}$ for each BEA with data centred on the Local Average Temperature $((T_a)_{la})$ for each t_j with and without solar radiation.

Data centred on $(T_a)_{ta}^* \cdot t_N$ with RAD ON - N=17,527									
BEA	Sensor Reference	Measures (Z) by t_N	$(\bar{T}_a)_{la}^{**} [^\circ\text{C}]$ (Eq.3.5)	$\bar{\mu} [^\circ\text{C}]$ (Eq.3.14)	$\bar{\sigma}_T^2 [\text{K}^2]$ (Eq.3.15)	$\bar{\sigma}_T [^\circ\text{C}]$ (Eq.3.16)	$U_T [^\circ\text{C}]$ (Eq.3.17)	Min	Max
F_{nd}	E.F1.n.20 E.F1.n.21	2	19.286	0.000	0.043	0.207	0.41	-0.640	0.640
F_{st}	E.F1.s.23 E.F2.s.24	2	22.353	0.000	0.540	0.735	1.47	-2.865	2.865
R	E.R3.s.25 E.R3.s.26 E.R3.n.27	3	20.096	0.000	0.097	0.311	0.62	-0.957	1.303

* $(T_a)_{ta}$ is the average temperature of air surrounding the building or BAV in each t_j .
** $(\bar{T}_a)_{la}$ is the average temperature of air surrounding a BEA for the whole monitored periods.

Table 4.39: Temperature Uncertainty (U_T) estimation of $(\theta_{dvi})_{la}$ for each BEA with data centred on the Local Average Temperature $((T_a)_{la})$ for each t_j with solar radiation.

Data centred on $(T_a)_{ta}^* \cdot t_N$ with RAD OFF - N=29,065									
BEA	Sensor Reference	Measures (Z) by t_N	$(\bar{T}_a)_{la}^{**}$ [°C] (Eq.3.5)	$\bar{\mu}$ [°C] (Eq.3.14)	$\bar{\sigma}_T^2$ [K ²] (Eq.3.15)	$\bar{\sigma}_T$ [°C] (Eq.3.16)	U_T [°C] (Eq.3.17)	Min	Max
F_{nd}	E.F1.n.20 E.F1.n.21	2	16.677	0.000	0.080	0.282	0.56	-0.885	0.885
F_{st}	E.F1.s.23 E.F2.s.24	2	17.471	0.000	0.145	0.380	0.76	-1.880	1.880
R	E.R3.s.25 E.R3.s.26 E.R3.n.27	3	16.395	0.000	0.016	0.127	0.25	-0.630	1.160

* $(T_a)_{ta}$ is the average temperature of air surrounding the building or BAV in each t_j .

** $(\bar{T}_a)_{la}$ is the average temperature of air surrounding a BEA for the whole monitored periods.

Table 4.40: Temperature Uncertainty (U_T) estimation of $(\theta_{dvi})_{la}$ for each BEA with data centred on the Local Average Temperature $((T_a)_{la})$ for each t_j without solar radiation.

The group of sensors installed in the southern façade (E.F1.s.23 and E.F2.s.24) are those with highest uncertainty values in the RAD ON-OFF, RAD-ON and RAD OFF cases. These highest values are due to the higher exposition of this façade to the solar radiation, which can have a greater impact on the air temperature measurement variation between the two sensors. In addition, the group of sensors with the lowest measurement uncertainty in the RAD ON-OFF, RAD ON and RAD OFF cases, are the sensors installed on the roof (E.R3.s.25, E.R3.s.26 and E.R3.n.27), having even lower values than the sensors installed on the northern Façade, where the T_{out} sensors are usually installed. The sensors on the roofs of buildings are also exposed to solar radiation, but in this area, the airflow comes from all directions, which can reduce the air temperature variation with respect to the façade that is more exposed to the solar radiation, the southern façade.

Temperature Sensor Uncertainty ($U_{T(S)}$) analysis

The objective of this analysis is to estimate the uncertainty sources due to systematic errors of the installed sensors plus monitoring and control system (Temperature Sensor Uncertainty ($U_{T(S)}$)). To carry out this study, the sensors must measure together (Exterior Together (ET) Test (section 4.2)) in the same place in a BEA. Then, using the collected T_{out} data, the $U_{T(S)}$ has been estimated for Z T_{dvi} values, which were centred with respect to $(T_a)_{la}$ to obtain the $(\theta_a)_{la}$. The statistical analysis has been applied to these $(\theta_a)_{la}$ values based on the methodology set out in section 3.2.1.

The $U_{T(S)}$ value considers the uncertainty due to the systematic errors. This value is given by the sensor manufacturer through the sensor accuracy and can also be obtained experimentally.

Data from the sensors E.R3.s.25 and E.R3.s.26 of the ET test have been used to estimate the outdoor air's Temperature Sensor Uncertainty ($U_{T(S)}$), these sensors were installed together on a mast (Figure A.12). The period analysed has been from 4th May 2019 at 0:15:00 to 5th May 2019 at 10:05:00 Without Solar Radiation (RAD OFF) during the test. Figures C.38 and C.39 show the histogram of the

analysed period. Likewise, Figure 4.24 shows the 10 hours evolution of the E.R3.s.25 and E.R3.s.26 sensors, in which values with and without solar radiation are included.

The experimental accuracy of the sensor reference EE071-HTPC is equal to $\pm 0.06^\circ\text{C}$ (Table 4.42); this value is less than the manufacturer's accuracy, which is equal to $\pm 0.1^\circ\text{C}$ (Table A.1). Table 4.41 shows the mean variance and mean standard deviation calculated from the manufacturer's accuracy data. This manufacturer $U_{T(S)}$ value is estimated with a confidence value equal to 95%, so the k value is equal to 2 [103]. The methodology applied to make this estimation is based on Equations 3.15, 3.16 and 3.17.

The value of U_T includes both the uncertainties due to systematic errors ($U_{T(S)}$) and random errors ($U_{T(SP)}$) (Equation 3.18 and 3.26). Thus, the U_T value should be higher than $U_{T(S)}$ and $U_{T(SP)}$. Based on the U_T values shown in Table 4.32 of section 4.3.2 for the E.R3.s.25 and E.R3.s.26 sensors during the E test, the $U_{T(S)}$ must be less than U_T equal to $\pm 0.091^\circ\text{C}$, $\pm 0.112^\circ\text{C}$ and $\pm 0.077^\circ\text{C}$ for the cases the RAD ON-OFF, RAD ON and RAD OFF, respectively. If, comparing these U_T values with the manufacturer's accuracy with a $U_{T(S)}$ equal to $\pm 0.10^\circ\text{C}$, it is possible to identify that this value is higher than the U_T value of Table 4.32. This demonstrates that the estimated value of $U_{T(S)}$ should be lower than the accuracy given by the sensor manufacturer. Thus, for the decoupling analysis, the experimental $U_{T(S)}$ value equal to $\pm 0.06^\circ\text{C}$ will be used. Note that using the manufacturer's accuracy for the decoupling ($U_{T(S)}$ equal to $\pm 0.10^\circ\text{C}$) of the overall uncertainty will provide very similar results.

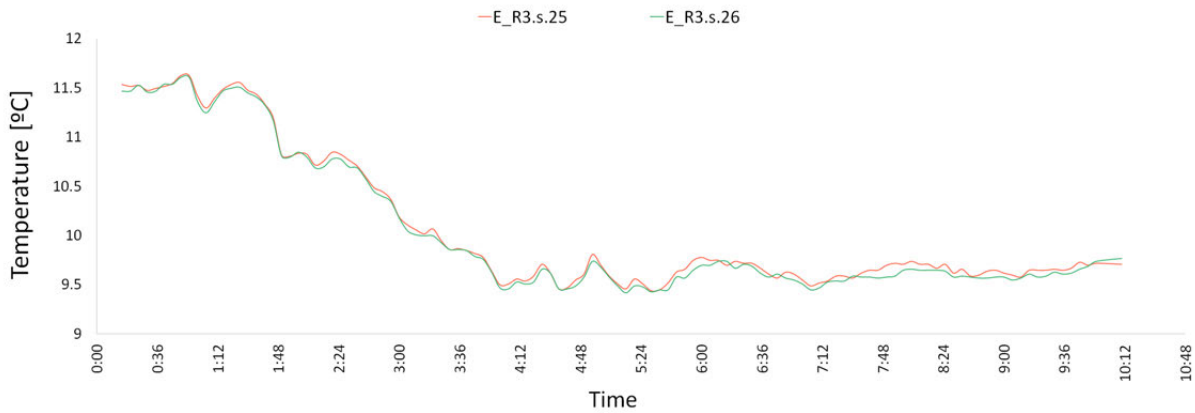


Figure 4.24: (T_{dv_i}) evolution during 10 hours from 4th May 2019 at 0:15:00 to 10:10:00 of data collected from the E.R3.s.25 and E.R3.s.26 sensors, there is no solar radiation.

Statistical Analysis of Manufacturer's Accuracy	Sensor Reference	
Statistical Analysis with a confidence level of 95% using k=2	EE071-HTPC	Units
Mean Variance ($\bar{\sigma}^2 = \bar{\sigma}_{(S)}^2$) (Equation 3.15)	0.0025	[K ²]
Mean Standard Deviation ($\bar{\sigma} = \bar{\sigma}_{(S)}$) (Equation 3.16)	0.0500	[°C]
Expanded Uncertainty ($U_{T(S)}$) (Equation 3.17)	0.10	[°C]

Table 4.41: Statistical results from manufacturer's accuracy of the EE071-HTPC sensor.

Statistical Analysis of Experimental Accuracy	Sensor Reference	
	E.R3.s.25 - E.R3.s.26	Units
Sample Size (N)	233	-
Samples' Mean ($\bar{\mu}$) (Equation 3.14)	0.000	[°C]
Mean Variance ($\bar{\sigma}^2 = \bar{\sigma}_{(S)}^2$) (Equation 3.15)	0.001	[K²]
Mean Standard Deviation ($\bar{\sigma} = \bar{\sigma}_{(S)}$) (Equation 3.16)	0.029	[°C]
Expanded Uncertainty ($U_{T(S)}$) (Equation 3.17)	0.06	[°C]
Min	-0.1050	[°C]
Max	0.1050	[°C]

Table 4.42: Statistical results from experimental accuracy of the EE071-HTPC sensor.

Decoupling Temperature Uncertainty (U_T) by means of the Temperature Sensor Uncertainty ($U_{T(S)}$) to estimate the Temperature's Spatial Uncertainty ($U_{T(SP)}$)

In this section, the decoupling method has been carried out to estimate the Temperature's Spatial Uncertainty ($U_{T(SP)}$) in order to know the influence of the random uncertainties in the Temperature Uncertainty (U_T), together with the systematic errors through the Temperature Sensor Uncertainty $U_{T(S)}$. Likewise, the range in which the representative temperature value of the BAV lies has been estimated with a 95% of confidence.

The results of decoupling the Temperature Uncertainty (U_T) from the Temperature Sensor Uncertainty ($U_{T(S)}$) to estimate the Temperature's Spatial Uncertainty ($U_{T(SP)}$) are shown below for the whole BAV and each BEA.

Decoupling of Temperature Uncertainty (U_T) of whole the Building's Air Volume (BAV)

This section shows the decoupling method results of the uncertainties estimated for the T_{out} of BAV with a 95% confidence. For this, the data analysed is based on the temperature measurements from the eight sensors installed around the building envelope for the RAD ON-OFF, RAD ON and RAD OFF cases. Decoupling the U_T value has allowed us to obtain the uncertainty due to the random errors of the T_{out} , called in this document Temperature's Spatial Uncertainty ($U_{T(SP)}$). This value has been calculated using the $U_{T(S)}$ value equal to $\pm 0.06^\circ\text{C}$ (Table 4.42).

The results of decoupling the Temperature Uncertainty (U_T) from the Temperature Sensor Uncertainty ($U_{T(S)}$) to estimate the Temperature Spatial Uncertainty ($U_{T(SP)}$) are shown below for the whole BAV. The outdoor air overall Temperature Uncertainty (U_T) value equal to $\pm 2.22^\circ\text{C}$, $\pm 3.19^\circ\text{C}$ and 1.38°C , together with its associated values of mean variance and mean standard deviation (Tables 4.33, 4.34 and 4.35) have been taken into account to obtain the results of the decoupling method, for the RAD ON-OFF, RAD ON and RAD OFF cases. Decoupling the (U_T) value has allowed us to obtain the uncertainty due to the random errors affecting the T_{out} measurement, called in this document Temperature Spatial Uncertainty ($U_{T(SP)}$). This value has been calculated using the $U_{T(S)}$ value equal to

$\pm 0.06^\circ\text{C}$ (from Table 4.42).

Based on the methodology of section 3.2.2, the $U_{T(SP)}$ (Equations 3.35 and 3.36), R_S (Equation 3.30) and R_{SP} (Equation 3.32) values have been estimated. For the RAD ON-OFF case, the $U_{T(SP)}$ value is equal to $\pm 2.22^\circ\text{C}$, while the R_S and R_{SP} values are equal to 0.07% and 99.93%, respectively (Table 4.43). The $U_{T(SP)}$ value of the RAD ON case is equal to $\pm 3.19^\circ\text{C}$, the R_S and R_{SP} values are equal to 0.03% and 99.97%, respectively (Table 4.43). For the RAD OFF case, the $U_{T(SP)}$ value is equal to $\pm 1.38^\circ\text{C}$, the R_S and R_{SP} values are equal to 0.018% and 99.83%, respectively (Table 4.43). The R_{SP} values for all cases are three orders of magnitude higher than the R_S values. Thus the temperature measurement uncertainties associated to the random errors are those with the main incidence on the T_{out} measurement. The systematic errors can be considered negligible in this case.

Finally, Table 4.44 shows an example of the limits within which the representative average temperature of the BAV $((\bar{T}_a)_{ta})$ for the monitored period can lie with a 95% confidence:

- $15.591^\circ\text{C} \leq [(\bar{T}_a)_{ta}]_{range} \leq 20.028^\circ\text{C}$ for RAD ON-OFF periods.
- $17.247^\circ\text{C} \leq [(\bar{T}_a)_{ta}]_{range} \leq 23.624^\circ\text{C}$ for RAD ON periods.
- $15.291^\circ\text{C} \leq [(\bar{T}_a)_{ta}]_{range} \leq 18.056^\circ\text{C}$ for RAD OFF periods.

E.F1.n.20 - E.F1.w.21 (F_{nd}), E.F1.w.22 (F_{wt}), E.F1.s.23 - E.F2.s.24 (F_{st}), E.R3.s.25 - E.R3.s.26 - E.R3.n.27 (R)									
Values from $U_{T(S)}$ Analysis (Table 4.42): $\bar{\sigma}_{(S)}^2 = 0.001 \text{ K}^2$, $\bar{\sigma}_{(S)} = 0.029^\circ\text{C}$, $U_{T(S)} = 0.06^\circ\text{C}$									
Study Case	Sample Size (N)	$\bar{\sigma}_T^2 [\text{K}^2]^*$ (Eq.3.22)	$\bar{\sigma}_T [^\circ\text{C}]^*$ (Eq.3.14)	$U_T [^\circ\text{C}]^*$ (Eq.3.17)	$\bar{\sigma}_{(SP)}^2 [\text{K}^2]$ (Eq.3.23)	$\bar{\sigma}_{(SP)} [^\circ\text{C}]$ (Eq.3.24)	$U_{T(SP)} [^\circ\text{C}]$ (Eq.3.25)	$R_{(S)}$ (Eq.3.30)	$R_{(SP)}$ (Eq.3.32)
RAD ON-OFF	50,958	1.23028	1.10918	2.22	1.22944	1.10805	2.22	0.07%	99.93%
RAD ON	17,527	2.54138	1.59417	3.19	2.54054	1.59339	3.19	0.03%	99.97%
RAD OFF	29,065	0.47779	0.69122	1.38	0.47696	0.68941	1.38	0.18%	99.83%

*Values from Table 4.33 (RAD ON-OFF), Table 4.34 (RAD ON) and Table 4.35 (RAD OFF).
In order to appreciate the differences between the different values, the results are shown with five decimals.

Table 4.43: Decoupling of T_{out} measurement with data centred on the Total Average Temperature $((T_a)_{ta})$ for the eight installed sensors around the building for the RAD ON-OFF, RAD ON and RAD OFF cases.

E.F1.n.20 - E.F1.w.21 (F_{nd}), E.F1.s.23 - E.F2.s.24 (F_{st}), E.F1.w.22 (F_{wt}), E.R3.s.25 - E.R3.s.26 - E.R3.n.27 (R)				
[[$(\bar{T}_a)_{ta}$]] _{range} (Eq.3.44)				
Study Case	[[$(\bar{T}_a)_{ta}$]]* [°C] (Eq.3.5)	U_T [°C] (Eq.3.17)	Minimum Limit [°C]	Maximum Limit [°C]
RAD ON-OFF	17.810	± 2.22	15.591	20.028
RAD ON	20.435	± 3.19	17.247	23.624
RAD OFF	16.673	± 1.38	15.291	18.056

* $(\bar{T}_a)_{ta}$ is the average temperature of air surrounding the building or BAV for the whole monitored periods.

Table 4.44: Example of estimation the Average Temperature Range $[[(\bar{T}_a)_{ta}]_{range}]$, within which the representative temperature of the air surrounding the building or BAV for the whole monitored period $(\bar{T}_a)_{ta}$, can lie with a 95% confidence for the studied tertiary building.

Decoupling of Temperature Uncertainty (U_T) of air surrounding the Building Envelope Area (BEA)

The following results show the $U_{T(SP)}$ values of the (T_{out}) surrounding the three BEAs: the northern façade, southern façade and roof; whose uncertainty results have been set out in Tables 4.38, 4.39 and 4.40 of section 4.3.2. The decoupling method of Temperature Uncertainty (U_T) has been applied to data from sensors installed on the northern façade (E.F1.n.20 and E.F1.n.21), southern façade (E.F1.s.23 and E.F2.s.24) and roof (E.R3.s.25, E.R3.s.26 and E.R3.n.27).

Table 4.45 (RAD ON-OFF case), 4.46 (RAD ON-OFF case) and 4.46 (RAD OFF case) show the following results:

- The $U_{T(SP)}$ value of air temperature surrounding the northern façade is equal to ±0.53, the R_S and R_{SP} values are equal to 1.20% and 98.80%, respectively, for the RAD ON-OFF period. Likewise, the $U_{T(SP)}$ value is equal to ±0.41°C, the R_S and R_{SP} are equal to 1.95% and 98.05%, respectively, for the RAD ON period. In addition, for the RAD OFF period, the $U_{T(SP)}$ value is equal to ±0.56°C, and the R_S and R_{SP} are equal to 1.05% and 98.95%, respectively.
- The $U_{T(SP)}$ value of air temperature surrounding the southern façade is equal to ±1.08°C, the R_S and R_{SP} values are equal to 0.29% and 99.71%, respectively, for the RAD ON-OFF period. Likewise, the $U_{T(SP)}$ value is equal to ±1.47°C, the R_S and R_{SP} values are equal to 0.15% and 99.85%, respectively, for the RAD ON period. In addition, for the RAD OFF period the $U_{T(SP)}$ value is equal to ±0.76°C, and the R_S and R_{SP} values are equal to 0.58% and 99.42%, respectively.
- The $U_{T(SP)}$ value of air temperature surrounding the roof of building is equal to ±0.42°C, the R_S and R_{SP} values are equal to 1.88% and 98.12%, respectively, for the RAD ON-OFF period. Likewise, the $U_{T(SP)}$ value is equal to ±0.62°C, and the R_S and R_{SP} values are equal to 0.87% and 99.82%, respectively, for RAD ON period. In addition, for the RAD OFF period, the $U_{T(SP)}$ value is equal to ±0.25°C, and the R_S and R_{SP} are equal to 5.16% and 94.84%, respectively.

t_N with RAD ON-OFF - N=50,958Values from $U_{T(S)}$ Analysis (Table 4.42): $\bar{\sigma}_{(S)}^2 = 0.001 \text{ K}^2$, $\bar{\sigma}_{(S)} = 0.029 \text{ }^\circ\text{C}$, $U_{T(S)} = 0.06 \text{ }^\circ\text{C}$

BEA	Sensor Reference	$\bar{\sigma}_T^2$ [K ²] (Eq.3.22)	$\bar{\sigma}_T$ [°C] (Eq.3.14)	U_T [°C] (Eq.3.17)	$\bar{\sigma}_{(SP)}^2$ [K ²] (Eq.3.23)	$\bar{\sigma}_{(SP)}$ [°C] (Eq.3.24)	$U_{T(SP)}$ [°C] (Eq.3.25)	$R_{(S)}$ (Eq.3.30)	$R_{(SP)}$ (Eq.3.32)
F _{nd}	E.F1.n.20 E.F1.n.21	0.070	0.264	0.53	0.069	0.263	0.53	1.20%	98.80%
F _{st}	E.F1.s.23 E.F2.s.24	0.293	0.541	1.08	0.292	0.540	1.08	0.29%	99.71%
R	E.R3.s.25 E.R3.s.26 E.R3.n.27	0.045	0.211	0.42	0.044	0.209	0.42	1.88%	98.12%

*Results obtained from Table 4.38

Table 4.45: Decoupling of the T_{out} measurement from the BEA with data centred on the Local Average Temperature ($(T_a)_{la}$) for each t_j with and without solar radiation. t_N with RAD ON - N=17,527Values from $U_{T(S)}$ Analysis (Table 4.42): $\bar{\sigma}_{(S)}^2 = 0.001 \text{ K}^2$, $\bar{\sigma}_{(S)} = 0.029 \text{ }^\circ\text{C}$, $U_{T(S)} = 0.06 \text{ }^\circ\text{C}$

BEA	Sensor Reference	$\bar{\sigma}_T^2$ [K ²] (Eq.3.22)	$\bar{\sigma}_T$ [°C] (Eq.3.14)	U_T [°C] (Eq.3.17)	$\bar{\sigma}_{(SP)}^2$ [K ²] (Eq.3.23)	$\bar{\sigma}_{(SP)}$ [°C] (Eq.3.24)	$U_{T(SP)}$ [°C] (Eq.3.25)	$R_{(S)}$ (Eq.3.30)	$R_{(SP)}$ (Eq.3.32)
F _{nd}	E.F1.n.20 E.F1.n.21	0.043	0.207	0.41	0.042	0.205	0.41	1.95%	98.05%
F _{st}	E.F1.s.23 E.F2.s.24	0.540	0.735	1.47	0.539	0.734	1.47	0.15%	99.85%
R	E.R3.s.25 E.R3.s.26 E.R3.n.27	0.097	0.311	0.62	0.096	0.309	0.62	0.87%	99.13%

*Results obtained from Table 4.38

Table 4.46: Decoupling of the T_{out} measurement from the BEA with data centred on the Local Average Temperature ($(T_a)_{la}$) for each t_j with solar radiation.

t_N with RAD OFF - N=29,065									
Values from $U_{T(S)}$ Analysis (Table 4.42): $\bar{\sigma}_{(S)}^2 = 0.001 \text{ K}^2$, $\bar{\sigma}_{(S)} = 0.029 \text{ }^\circ\text{C}$, $U_{T(S)} = 0.06 \text{ }^\circ\text{C}$									
BEA	Sensor Reference	$\bar{\sigma}_T^2$ [K ²] (Eq.3.22)	$\bar{\sigma}_T$ [°C] (Eq.3.14)	U_T [°C] (Eq.3.17)	$\bar{\sigma}_{(SP)}^2$ [K ²] (Eq.3.23)	$\bar{\sigma}_{(SP)}$ [°C] (Eq.3.24)	$U_{T(SP)}$ [°C] (Eq.3.25)	$R_{(S)}$ (Eq.3.30)	$R_{(SP)}$ (Eq.3.32)
F _{nd}	E.F1.n.20 E.F1.n.21	0.080	0.282	0.56	0.079	0.281	0.56	1.05%	98.95%
F _{st}	E.F1.s.23 E.F2.s.24	0.145	0.380	0.76	0.144	0.379	0.76	0.58%	99.42%
R	E.R3.s.25 E.R3.s.26 E.R3.n.27	0.016	0.127	0.25	0.015	0.124	0.25	5.16%	94.84%

*Results obtained from Table 4.38

Table 4.47: Decoupling of the T_{out} measurement from the BEA with data centred on the Local Average Temperature $((T_a)_{la})$ for each t_j without solar radiation.

Regarding all these results, it is possible to observe that in the northern façade, southern façade and roof the $U_{T(SP)}$ values of the three studied cases are similar, where the R_{SP} values, which represents the random error's weight, are much higher than the R_S values; this is due to the uncertainties associated to the random errors being predominant as compared to the systematic errors. The $U_{T(SP)}$ estimation associated to random errors is lower on the roof than the northern and southern façades. Here the T_{out} measurement, for the three studied cases (RAD ON-OFF, RAD ON and RAD OFF periods), in the southern façade has higher uncertainty values, since the effect of the random errors is greater with respect to the roof and northern façade. The $U_{T(SP)}$ values are greater in the RAD ON period than the RAD ON-OFF and RAD OFF periods; where the latter has lower $U_{T(SP)}$ values (less randomness associated with temperature measurement).

The roof is the best location with the lowest measurement uncertainty due to random errors, so its R_S value, which represents the weight of the systematic error, is greater than the northern and southern façades in the three cases. Even so, in all studied locations and studied cases the uncertainty due to systematic errors is almost negligible. Likewise, in the RAD OFF period, the uncertainty due to the random errors decreases a little because the incidence of solar radiation on the Spatial Uncertainty ($U_{T(SP)}$) disappears without reducing the weight of the Temperature Sensor Uncertainty ($U_{T(S)}$) value. Likewise, the range limits within which the representative temperature of the air surrounding a BEA can lie for the studied building, has been estimated in Table 4.48 as an application example, where the minimum and maximum limits are equal:

For the northern façade:

- $16.885 \text{ }^\circ\text{C} \leq [(\bar{T}_a)_{la}]_{range} \leq 17.943 \text{ }^\circ\text{C}$ for RAD ON-OFF periods.
- $18.872 \text{ }^\circ\text{C} \leq [(\bar{T}_a)_{la}]_{range} \leq 19.700 \text{ }^\circ\text{C}$ for RAD ON periods.
- $16.113 \text{ }^\circ\text{C} \leq [(\bar{T}_a)_{la}]_{range} \leq 17.242 \text{ }^\circ\text{C}$ for RAD OFF periods.

For the southern façade:

- $17.938\text{ °C} \leq [(\bar{T}_a)_{la}]_{range} \leq 20.103\text{ °C}$ for RAD ON-OFF periods.
- $20.884\text{ °C} \leq [(\bar{T}_a)_{la}]_{range} \leq 23.822\text{ °C}$ for RAD ON periods.
- $16.710\text{ °C} \leq [(\bar{T}_a)_{la}]_{range} \leq 18.231\text{ °C}$ for RAD OFF periods.

For the roof:

- $17.067\text{ °C} \leq [(\bar{T}_a)_{la}]_{range} \leq 17.911\text{ °C}$ for RAD ON-OFF periods.
- $19.475\text{ °C} \leq [(\bar{T}_a)_{la}]_{range} \leq 20.717\text{ °C}$ for RAD ON periods.
- $16.141\text{ °C} \leq [(\bar{T}_a)_{la}]_{range} \leq 16.650\text{ °C}$ for RAD OFF periods.

BEA	Sensor Reference	Studied Cases	$[(\bar{T}_a)_{la}]^*$ [°C] (Eq.3.5)	U_T [°C] (Eq.3.17)	$[(\bar{T}_a)_{la}]_{range}$ (Eq.3.44)	
					Minimum Limit [°C]	Maximum Limit [°C]
F_{nd}	E.F1.n.20	RAD ON-OFF	17.414	0.53	16.885	17.943
	E.F1.n.21	RAD ON	19.286	0.41	18.872	19.700
		RAD OFF	16.677	0.56	16.113	17.242
F_{st}	E.F1.s.23	RAD ON-OFF	19.021	1.08	17.938	20.103
	E.F2.s.24	RAD ON	22.353	1.47	20.884	23.822
		RAD OFF	17.471	0.76	16.710	18.231
R	E.R3.s.25	RAD ON-OFF	17.489	0.42	17.067	17.911
	E.R3.s.26	RAD ON	20.096	0.62	19.475	20.717
	E.R3.n.27	RAD OFF	16.395	0.25	16.141	16.650

* $(\bar{T}_a)_{la}$ is the average temperature of air surrounding a BEA for the whole monitored periods.

Table 4.48: Example of the estimation of the limits of the range within which the average temperature of the air surrounding the Building Envelope Area (BEA) $(\bar{T}_a)_{la}$ can lie for the whole monitored period. $[(\bar{T}_a)_{la}]_{range}$ (Equation 3.44)

4.4 Design and deployment of an Experimental Monitoring and Control System (MCS) for an in-use residential building of Vitoria-Gasteiz to analyse the sensor requirements so as to be able to estimate and decouple the HLC

Taking into account the conclusions of the state of the art, the methodology monitoring criteria section and the results regarding the indoor and outdoor uncertainty measurements, an MCS has been designed and installed in a residential building of Vitoria-Gasteiz. This MCS has been extremely oversized to be able to monitor in detail all the possible variables that could affect the energy balance presented in the literature review. The ventilation system and the heat pumps have been monitored in detail to understand their effect on the HLC estimation and decoupling. The MCS selection criteria have been briefly presented in the methodology section. The MCS has been integrated in all the phases of the building retrofitting project.

The residential building is a demonstrator building in Vitoria-Gasteiz (Figure 4.26) [163] within the ENERPAT - SUDOE project⁴, [164–166] which has been planned in two monitoring phases: the first before and the second after the eco-renovation actions (Figure 4.25). Although the objectives of both monitoring sessions are essentially identical, the scope, conditioning factors, number of sensors and approach differ significantly. Here, only the post-retrofitting detailed monitoring is presented.

Due to the Covid-19 lock-down, even if the monitoring system have been installed and is already storing data since January 2020, the final tuning of the MCS was not finished in March due to the lock-down. Thus, the data analysis part of this monitoring system has not been included in this Thesis, since not enough quality data has been available with sufficient time.

⁴Co-creation of Energetically efficient territorial solutions of Patrimonial Residential habitat Ecorenovation in SUDOE historical centres. Where, the Interreg SUDOE is the Southwest European Space Territorial Cooperation programme

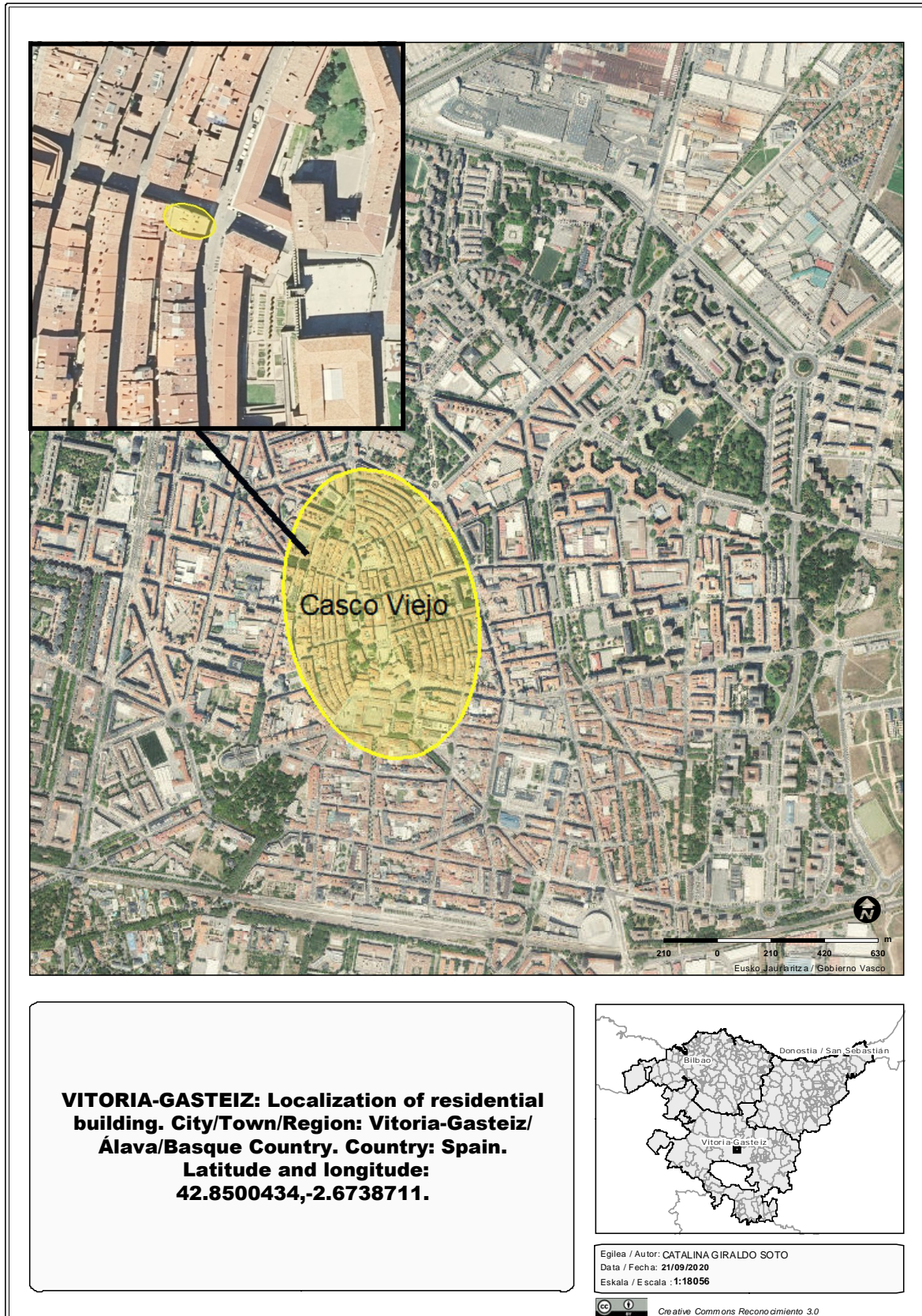


Figure 4.25: Location of residential building. City/Town/Region: Vitoria-Gasteiz/Álava/Basque Country. Country: Spain. Latitude and longitude: 42.8500434, -2.6738711.



Figure 4.26: The residential building in Vitoria-Gasteiz: a) Pre-retrofitting, b) Post-retrofitting.

The pre-retrofitting monitoring has been based on a standard configuration, with the aim of finding a balance between the greatest possible knowledge of the building's behaviour and the least possible effect on the users of the homes, since half of the homes were inhabited in this demonstrator. This research work has been focused on the post-retrofitting monitoring, whose scope is much more ambitious, since the aim is to integrate the MCS within the retrofitting. This allows for much more intensive monitoring, while at the same time enabling the sensors to be optimised (type, number, communication protocols, control, etc.). In this sense, the monitoring proposed for the post-rehabilitation phase has been highly innovative, with important scientific work, which will facilitate the design and definition of the future monitoring requirements that would permit a reliable HLC estimation and its decoupling.

The global aims of the post-rehabilitation monitoring have been to design an energy MCS in order to optimise the monitoring system using technology with a high accuracy that are also used in inmotric systems and laboratory tests. The first design goals have been:

- To design an MCS to characterize the TEP and Energy EPB using different methods, and also to

quantify the gap between the design and post-construction phase.

- To integrate the energy MCS in the design and construction phase as an active part within the building construction project.
- To use different technologies, analogical and digital, to compare them, and to optimise and standardise the MCS.
- Use a control system in order to guarantee that the technologies are accurate, reliable, profitable, and safe from cyber-attacks, also making it possible to quickly and easily identify the fault in the MCS with the possibility that an FDD can be integrated.
- To include the measurements of the energy systems that will permit the characterization of the TEP under in-use conditions.

Scope of monitoring systems for residential buildings

The Vitoria-Gasteiz demonstrator incorporates an MCS to evaluate the impact of the innovative rehabilitation, which has been designed for a building that belongs to the built heritage of the historical centre of the city, within the medieval quarter of the city. It will provide information on the energy improvement of the building's eco-rehabilitation and the efficiency of its thermal envelope, making it possible to check the level of energy efficiency of the building in post-rehabilitation use; while at the same time providing a better understanding of how the energy systems of the building work (ventilation system, heating system), by knowing the energy consumption of each home, the thermal comfort and air quality for the users. At the same time, it will allow the user's behaviour to be understood, as can be done within a Building Management System (BMS) [167], but using scientific and technical analysis techniques that different groups of researchers are currently working on.

Similarly, the scientific study with the MCS will allow progress to be made towards integrating energy monitoring into existing Building Automation Systems (BAS) and home automation systems, with reliable technologies, greater precision in sensors and communication protocols that guarantee cyber security [168], with the aim of initiating technology transfer with an investment and economic feasibility study. This will allow the end user to know the profitability in economic and comfort terms, in order to increase its marginal utility to motivate such investment, and thus ensure the integration of the new BAS with energy monitoring systems in the market.

From the point of view of cultural heritage, the MCS to be implemented in the building provides a value enhancement in the environment of the medieval quarter of Vitoria-Gasteiz, being a reference in the integral rehabilitation of the buildings and dwellings of the historical centre from the point of view of eco-rehabilitation, energy improvement and automation of buildings catalogued as historical heritage.

To know the energy behaviour of the building before refurbishment, a set of tests was carried out and included [169]: infrared thermography to detect the presence of thermal bridges and/or insulation

faults, blower door test according to the standard EN 13829 [170] to assess the airtightness of the building, and in-situ measurement of thermal resistance and thermal transmittance of the Façade walls of the ground and first floors, according to the standard ISO 9869 [20]. In order to cover the scope of the energy MCS and thus to know the energy behaviour after refurbishment, there are a total of 199 sensors, 70 hardware elements in the control system, 2 software 7, radiators and 7 fans, with which different types of data will be obtained, processed and analysed. In addition, the following tests and studies will be carried out with the designed MCS:

- Tracer gas test [171].
- Co-Heating test [19].
- Study of the building's energy behaviour by estimating the Heat Loss Coefficient (HLC) [24] of the building under in-use conditions, including all the building's subsystems and the users' behaviour. The estimation of this coefficient with the building in use will make it possible to know the thermal behaviour of the building, taking into account the behaviour of the users together with the building subsystems.
- Study of the thermal behaviour of the building envelope by estimating the thermal resistance (R-value) and thermal transmittance (U-value) of some building envelope elements according to the ISO 9869-1 - 2014 standard [20, 45].
- Study of the energy improvement with respect to the electrical and thermal consumption of the building.
- Study of the thermal comfort and air quality with respect to the CO₂ level, ventilation and air renewal ratio.
- Study of the stratification of air temperature, relative humidity and CO₂.
- Study of different high precision technologies used in energy monitoring in the building.
- Study and compare different sensor technologies.
- Study the optimisation of energy MCSs.
- Technical and economic feasibility of the technology to implement the energy MCSs in Building Automation Systems (BAS), with the objective of enabling the estimation, in real time, of the HLC of an in-use building and also to evaluate the EPB.
- Study of the discrepancy in the energy behaviour of the building envelope between the design phase, post-construction and the building in use.

Design of the residential building's MCS

The MCS has been designed and is made up of 199 sensors, 70 hardware and 2 software elements. The design integrates two MCS, one Fixed MCS and another mobile MCS, this last has been designed

in order to carry out the Co-Heating test:

Fixed MCS: This has a total of 154 sensors, of which 85 are digital with ModBus Protocol Communication (PC), 2 sensors have Wi-Fi and 67 sensors are analogical, of which, 41 are resistive and 26 thermocouples. In turn, this system has 44 hardware elements and one software as part of the Control System (CS). Within the Fixed MCS, a 3D monitoring has been implemented in two zones of the first floor, in Zones 2 (Z2) and 4 (Z4) (see Figure D.2). The objective of this 3D monitoring is to study the stratification and overall uncertainty of measurement, while at the same time making a comparison of sensor technologies. The layout of 3D monitoring is shown in Figure D.9.

Mobile MCS or Mobile Co-Heating System: This has been designed for the Co-Heating test and has a total of 45 sensors, of which 8 are digital with ModBus PC and 38 are analogical, of which, 27 are resistive and 10 thermocouples. This system has 26 hardware elements and one software elements as part of the control system. The control system of each MCS has been implemented with Beckhoff [172] hardware and software, which is made up of a Central Processing Unit (CPU), analogue and digital terminals, Bus coupler and TwinCat software. This MMS is also composed of 7 fans and 7 electric radiators, which are controlled on the basis of the set-points assigned to the control system on the basis of the indoor air temperature of the studied dwelling.

The number of sensors installed in each dwelling, and the total number of sensors installed in the building (199 sensors), has been determined by: The distribution of the dwellings; the characteristics of the building envelope, which has several construction phases and different construction materials; the requirements set out in section 3.3, which specifies the necessary and optional measurements to estimate and decouple the HLC through the Average Method and Co-heating Method; and finally by the design criteria of the MCS, which are:

- High measurement precision of the sensors, similar or superior to those used in laboratory tests.
- Sensors with digital communication protocol used in industrial automation.
- Analogical sensors used in laboratory tests as an alternative to sensors with digital communication protocol, in case it is not economically viable or the technology does not exist.
- Economic viability.
- Control system without the use of gateways.
- Control system with remote access that allows interaction with various communication protocols without the use of gateways, but with the capacity to capture and store data with the recommended frequency in each of the planned tests and studies.
- Control hardware and software used in industrial automation, with high reliability and precision of the equipment.
- Equipment with the possibility of being acquired through various suppliers at a national and

international level.

- The sensors to be chosen must be of different measurement typologies:
 - Indoor and outdoor air temperature: Used to know the thermal comfort, estimation of HLC (Equation 2.18 and Equation 2.22), to study indoor air temperature uncertainty.
 - Indoor and outdoor relative humidity: Used to know the user comfort, to study the indoor relative humidity uncertainty.
 - Indoor radiant temperature: Used to know the user comfort level.
 - Indoor and outdoor CO₂: Used to know the user comfort, air quality, to decouple the HLC (Equation 2.10) and to study indoor CO₂ uncertainty.
 - Air temperature in ducts and inside houses: Used to the control of the HVAC system, to decouple the HLC (Equation 2.10).
 - Relative humidity of the air in ducts and inside houses: Used to the control of the HVAC system.
 - Air speed in ducts: Used to control the HVAC system and estimate the ventilation mass flow rates for HLC decoupling.
 - Surface temperature in walls and floors: Used to estimate the R-value and U-value, estimation of heat transfer through the walls, floors and roofs.
 - Heat flux in surfaces: Used to estimate the R-value and U-value, estimation of heat transfer through the walls.
 - Air, water and water-glycolic flows in ducts: Used to estimate the heat gains due to the heating system.
 - Temperature of liquids in ducts: Used to estimate the heat gains due to the heating system.
 - Wind speed: Used to estimate the air infiltration to the dwelling.
 - Wind direction outside: Used to estimate the air infiltration to the dwelling.
 - Direct solar radiation: Used to estimate the solar gains for the estimation of HLC (Equations 2.18 and 2.22).
 - Electrical consumption: Used to estimate the electricity gains for the estimation of HLC (Equations 2.18 and 2.22). Note that individual pieces of equipment are considered in order to know their weight in the electricity consumption. Part of the electricity consumed by devices that heat up water might not be considered within the HLC estimation equations.

- Gas consumption: Used to estimate the seasonal energy efficiencies of systems for producing space heating and DHW.
- The distribution and number of measurement units has been determined by:
 - Number of volumes or rooms in the house.
 - Stratification studies in the study areas with different orientations.
 - Co-Heating test requirements.

Architecture of the residential building's MCS

The Vitoria-Gasteiz demonstrator consists of three floors and a Basement (B0), where the Ground Floor (F0), First Floor (F1) and Second Floor (F2) include a ventilation system with heat recovery. In turn F0 and F1 include aerothermal energy for the heating system and Domestic Hot Water (DHW) production. On the other hand, F2 uses natural gas for the heating system and DHW.

In the Basement (B0), only surface temperature and heat flow measurements are taken in its ceiling slab for the Co-Heating test. It is a space for commercial use, is uninhabited and its current use is for storage. The F0 has a dwelling and a Facility Room (FR). The F0 dwelling had an integral rehabilitation and is inhabited, it has a total of 41 fixed sensors, the FR has the aerothermal and electrical system of building, which is only monitored for the Co-Heating test. The F1, with a partial refurbishment that includes a ventilation system and aerothermal energy, will have two study phases. The first phase of monitoring will be carried out with the uninhabited dwelling, while in the second phase of monitoring it will be occupied. The total number of fixed sensors in the uninhabited house is 77 and in the inhabited house 67. The F2, with 28 sensors, has two levels and a fireplace on the first level. To measure the Exterior (E) conditions, 5 fixed sensors are installed, four of them on the roof of the building.

There are four fixed CS connected in series, one per dwelling floor and one in the Facilities Room (FR). The E sensors are controlled by the F2 control system. The aerothermal system of F1 and F2, together with the natural gas consumption of F2, are controlled by the FR's CS. The mobile MCS has an independent CS.

One of the objectives of estimating the HLC through the Average Method and the Co-Heating Method is to have a reference HLC value obtained through the co-heating test that will permit us to compare the results of the HLC values obtained with the average method when the building is occupied. Thus, the average method in-use HLC values discrepancies will be understood thanks to the detailed monitoring of all the variables that are considered in the energy balance developed in the literature review section.

The installed sensors reference and the manufacturer's accuracy of the Monitoring System (MS) is shown in Table 4.53 and 4.54. Likewise, Table D.1 plus Figure D.1 show the layout of F0 plus FR sensors; Table D.2 plus Figure D.2 show the layout of F1 sensors; finally, Table D.3 plus Figures D.3

and D.4 show the layout of F2 plus E sensors. On the other hand, Table D.3 plus Figures D.5, D.6 and D.7 show the sensors layout of the Co-Heating test for F1, F0 and f2, respectively.

Some pictures of installed sensors and CS of fixed MCS are shown in Figures D.10, D.11, D.12 and D.13 of F0, F1, F2, and roof, respectively. In addition some pictures of the mobile MCS for doing the Co-Heating test are shown in Figure D.14. The sensors and hardware implemented in the residential building are shown in Figure D.8, which is described in the following subsection:

MONITORING SYSTEMS (MSs) OF THE RESIDENTIAL BUILDING					
MCS	Digital Sensors		Analogue Sensors		Total by
	Type	ModBus	Wi-fi	Resistive	
Fixed MCS	85	2	48	19	154
Mobile MCS	8	0	27	10	45
Total	93	2	75	29	199

Table 4.49: Number of sensors installed in the Fixed MCS and Mobile MCS of the residential building.

FIXED MONITORING SYSTEM (MS) OF THE RESIDENTIAL BUILDING					
MS	Digital Sensors		Analogue Sensors		Total by
	Location	ModBus	Wi-fi	Resistive	
F0	23	0	14	7	424
F1	31	2	34	10	77
F2	27	0	0	1	28
E	4	0	0	1	5
Total	85	2	41	26	154

Table 4.50: Number of sensors installed in the Fixed MCS of the residential building.

CONTROL SYSTEMS (CSs) OF THE RESIDENTIAL BUILDING												
MCS	Hardware										Software	Total by
	Type	CX2020-0121	EK1100	EL6021	EL3202	EL3602	EL3064	EL1502	EL2622	KL9100		
Fixed MCS	1	3	4	21	9	2	1	0	3	1	45	
Mobile MCS	1	0	1	14	5	0	0	4	1	1	27	
Total	2	3	5	35	14	2	1	4	4	2	72	

Table 4.51: Number of hardware and software elements used in the Fixed MCS and Mobile MCS of the residential building.

FIXED CONTROL SYSTEM (CS) OF THE RESIDENTIAL BUILDING											
CS	Hardware									Software	Total by
Location	CX2020-0121	EK1100	EL6021	EL3202	EL3602	EL3064	EL1502	EL2622	KL9100	TwinCat	MCS
FR	1	0	1	0	0	0	1	0	0	1	4
F0	0	1	1	7	4	0	0	0	1	0	14
F1	0	1	1	14	5	2	0	0	2	0	25
F2+E	0	1	1	0	0	0	0	0	0	0	2
Total	1	3	4	21	9	2	1	0	3	1	45

Table 4.52: Number of hardware and software elements used in the Fixed MCS of the residential building.

Investment analysis

The investment analysis carried out includes the direct investment of material, the installation and setup of the residential building's MCS in Vitoria-Gasteiz, the investment estimation including bills and budget of stock sensors and hardware with the price of the purchase year. These prices are taken into account for the analysis, since there is the documentation to justify the investment made at the time of purchase. Tables 4.55, 4.56, 4.57, 4.58, 4.59 and 4.60 show the unit cost and total costs without taxes, where the budget and bills used for the investment are shown in Appendix IV, in which the price of the stock and new sensor equipment and hardware.

The installation has been carried out in parallel with the retrofitting. The total investment shown in Table 4.60, is equal to 99,556.11 €, where 55.50% (55,249.76 €) has been invested in the sensors for the monitoring kit, a 12.05% (111,995.19 €) corresponds to the control kit composed of hardware and software equipment. The programming and setup take up 13.94%% (13,877.10 €) of the total cost. The rest of the costs correspond to the calibration of the sensors from stock, while the equipment and rentals of the installation account for 14.82% (14,775.76 €) of the total cost.

Within the monitoring kit (Table 4.55), all the digital sensors, the AMR-PT100 (4L), 23 units of Phymeas-Type7 and 13 units of 515-720 are new acquisitions corresponding to 34.69% (34,536.30 €). The rest of the sensors are stock provided by the UPV/EHU [173] and the ENERPAT project cofunder, Tecnalía [174]. Within the Hardware equipment (Table 4.56), the stock represents 5.44% (5,415.74 €), with 2 units of CX2020-0121, 17 units of EL3202, 6 units of EL3602, 2 units of EL3064, and 1 unit of EL1502. This equipment has been supplied by Tecnalía. The rest of the hardware equipment is of new acquisition, accounting for 6.61% (6,579.45 €). The total investment, excluding the stock, is equal to 46,409,41€, the stock investment being equal to 53,146.70 €.

The indirect cost of this project corresponding to the electricity costs and the hours spent by the doctoral candidate during the design phase, installing and setup phases, together with the support of the thesis directors during the design and setup phases, are not considered.

INSTALLED DIGITAL SENSOR			
PC	Sensor Reference	Measure	Accuracy
ModBus RS485:	EE800-M12J3	Temperature	±0.3 °C
		Relative Humidity	±3% RH(30...70%RH). ±5% RH(10...90%RH)
		Carbon Dioxid	At 25 °C and 1013mbar: 0...2000ppm < ±(50ppm +2% of measuring value)
	EE071-HTPC	Temperature	±0.1°C at 23°C
		Relative Humidity	Hysteresis: ±2% RH (0...90% RH). Non-linearity: ±3% RH (0...100% RH)
	MM880-DMF	Electricity consumption	Volt and Amp: 0,5% of reading ±2 digits. Frequency:0.1HZ ±1 digit. Active, Reactive and Apparent power: 1% of reading ± 2 digits. Power factor: 1% range. Energy: IEC 1036 class 1
	MultiCal-403	Integrator Pair of probes	Ec= ±(0.15 + 2/Δθ)% ET= ±(0.4 + 4/Δθ)%
	EE650-T2J3L100P1	Air velocity	0.2...10m/s ±(0.2m/s + 3% of m.v.). 0.2...15m/s ±(0.2m/s + 3% of m.v.). 0.2...20m/s ±(0.2m/s + 3% of m.v)
	EE160-HTX3XPBB	Temperature Relative Humidity	±0.03°C. Pt1000 class B 2.5% RH
	EE850-M12J3P1	Temperature Relative Humidity Carbon Dioxid	±0.3°C ±3% RH (20...80%RH) 0...2000ppm < ±(50ppm +2% of measuring value)
SMP6	Radiation	Spectral range (20% point): 280 to 3000 nm and (50% points): 285 to 2800 nm. Response time (63%): < 1.5 s and (95%): < 12 s. Zero offset A < 10 W/m ² and B < 4 W/m ² . Directional response: (up to 80° with 1000 W/m ² beam): < 15 W/m ² . Temperature dependence of sensitivity: (-40 °C to +70 °C) < 3%.	
4.920.00.000	Wind Speed Wind Direction Virtual Temperature	±0.3 m/s rms (< 5m/s). ±3 % rms (5m/s...60m/s) ±2° W-S > 2m/s ±0.5 K	
Wi-fi:	HD35ED1NB	Temperature	±0.2°C(0...+60 °C). ±(0.2-0.05*T)°C at (0...+40°C). ±(0.2+0.032*(T-60))°C at (0...-60°C). Stability: 0.05°C/year
	(HD 35APW)	Relative Humidity Carbon Dioxide	±2.5% RH (0...85% RH). ±3.5% RH (0...100% RH). (T=23°C). Stability: -1%/year ±(50ppm + 3% of measurement at 25°C and 1013 hPa. Stability: 51% of measurement/5years.
TOTAL SENSORS			95

Table 4.53: Accuracy and references of digital sensors installed in Fixed MCS and Mobile MCS of the residential building.

INSTALLED ANALOGUE SENSOR				
PC	Sensor Reference	Measure	Accuracy	Total
Electric	AMR-PT100(4L)	Radiant Temperature	PT 1000 Class B (-50 °C to +200 °C)	1
Resistance:	515-720	Air Temperature	±0.03°C sensor. ±0.06°C probes	16
	KPC1-5	Relative Humidity	0...1 V (-27...80 °C)...±0.2 K. 0..10 V(-29...80 °C)...±0.2 K. 4..20mA (-0.3...-0.6 K)	7
	2113-1-073	Superficial Temperature	5% at 25°C	44
	578-062	Superficial Temperature	±1/10 (0.3 + 0.005 t)°C. (0 to 100 °C) (Class 1/10DIN)	7
Voltage:	GMP-220	Carbon Dioxide	0...2000ppm (±1.5% of range +2% of reading)	1
	Phymeas-Type7	Heat Flux	5% at 25 °C	27
	5561515-Itron	Gas Consumption	±1.5°C (Class 1 DIN 584 N,K,J). ±0.5°C (Class 1 DIN584T)	1
TOTAL SENSORS				104

Table 4.54: Accuracy and references of analogue sensors installed in Fixed MCS and Mobile MCS of the residential building.

Typology	Product	Units	Unit Cost	Total Cost	Cost Weigh
Sensor	EE800-M12J3	39	305.00 €	11,895.00 €	11.84%
Sensor	HD 35ED 1NB (HD 35APW)	2	465.00 €	930.00 €	0.93%
Sensor	Wifi data concentrator	1	365.00 €	365.00 €	0.36%
Sensor	EE071-HTPC	1	140.25 €	140.25 €	0.14%
Sensor	Shielding EE071-HTPC	1	80.75 €	80.75 €	0.08%
Sensor	MultiCal-403	6	267.00 €	1,602.00 €	1.60%
Sensor	EE650-T2J3L100-P1	6	229.50 €	1,377.00 €	1.37%
Sensor	EE160-HTX3XPBB	6	174.25 €	1,045.50 €	1.04%
Sensor	EE850-M12-J3-P1	6	340.00 €	2,040.00 €	2.03%
Sensor	MM880-DMF	26	127.50 €	3,315.00 €	3.30%
Sensor	SMP6	2	667.50 €	1,335.00 €	1.33%
Sensor	4.920.00.000	1	2,200.00 €	2,200.00 €	2.19%
Sensor	GMP-220	1	280.00 €	280.00 €	0.28%
Sensor	5561515-Itron	1	22 €	22 €	0.02%
Sensor	AMR - PT100 (4L)	1	510.00 €	510.00 €	0.51%
Sensor	515-720	16	66.60 €	1,065.60 €	1.06%
Sensor	KPC1-5	7	162.18 €	1,135.26 €	1.13%
Sensor	2113-1-073	44	410.00 €	18,040.00 €	17.96%
Sensor	578-062	7	25.20 €	176.40 €	0.18%
Sensor	Phymeas-Type7	27	285.00 €	7,695.00 €	7.68%
Monitoring Kit Total		201	7,122.73 €	55,249.76 €	55.02%

Table 4.55: Monitoring kit's investment of Vitoria-Gasteiz' MCS.

Typology	Product	Units	Unit Cost	Total Cost	Cost Weigh
Hardware	PLC -CX2020-0121	2	187.01 €	374.02 €	0.38%
Hardware	Heat-EK1100	3	44.65 €	133.95 €	0.13%
Hardware	EL6021	5	176.59 €	882.95 €	0.89%
Hardware	EL3202	35	191.63 €	6,707.05 €	6.74%
Hardware	EL3602	14	233.89 €	3,274.46 €	3.29%
Hardware	EL3064	2	117.93 €	235.86 €	0.24%
Hardware	EL1502	1	144.81 €	144.81 €	0.15%
Hardware	EL2622	4	35.67 €	142.68 €	0.14%
Hardware	KL9100	4	12.58 €	50.32 €	0.05%
Software	TwinCat	1	49.09 €	49.09 €	0.05%
Controlling Kit Total		71	1,139.85 €	11,995.19 €	12.05%

Table 4.56: Control kit's investment of Vitoria-Gasteiz' MCS.

Typology	Product	Unit Cost	Total Cost	Cost Weigh	
Equipment	Wire, fans, radiators, boxes, connectors...	1	2,703.30 €	2,703.30 €	2.72%
Equipment	Weather tower mast	1	480.00 €	480.00 €	0.48%
Equipment	Wire exterior sensor	3	165.00 €	495.00 €	0.50%
Equipment Total		5	3,348.30 €	3,678.30 €	3.69%

Table 4.57: Equipment investment of Vitoria-Gasteiz' MCS.

Typology	Product	Unit Cost	Total Cost	Cost Weigh	
Installing	Installing of MCS	1	12,671.24 €	12,671.24 €	12.73%
Calibration	Fluximeter calibration	1	576.00 €	576.00 €	0.58%
Calibration	GMP-220 Calibration	1	1,440.00 €	1,440.00 €	1.45%
Rent Car	Vant rent	1	68.52 €	68,52 €	1.17%
Installing Total		3	13,877.10 €	13,877.10 €	14.82%

Table 4.58: Installing investment of Vitoria-Gasteiz' MCS.

Typology	Product	Unit Cost	Total Cost	Cost Weigh	
Setup	Programming Fixed MCS	1	12,337.00 €	12,337.00 €	12.39%
Setup	Programming Modification	1	371.00 €	371.00 €	0.37%
Setup	Programming Mobile MCS	1	1,169.10 €	1,169.10 €	1.17%
Setup Total		3	13,877.10 €	13,877.10 €	13.94%

Table 4.59: Setup investment of Vitoria-Gasteiz' MCS.

Product	Total Cost	Cost Weigh
Monitoring Kit Total	55,227.76 €	55.50%
Equipment Total	3,678.30 €	3.69%
Controlling Kit Total	12,720.68 €	12.05%
Installing Total	14,755.76 €	14.82%
Setup Total	13,877.10 €	13.94%
Total MCS of Residential Building	99,556.11 €	100%

Table 4.60: Total investment of Vitoria-Gasteiz' MCS.

Detected challenges and improvements areas

The challenges detected during the design, installation and collection of the data have been:

- Design phase: Finding sensors with an accuracy similar of those used in laboratory tests with a competitive price and according to the available budget.
- Installation: Coordination and integration within construction phases.
- Setup: Problems with extranet connections with the programming company to make the tests. The internet connection was implemented by a router with a data card, the facilities room does not have ADSL or optical fibre connection.
- Collected data: The update of the firewall has led to cuts in data recording.

The improvement areas detected for the future:

- Design: Update and optimise the economic investment with updated prices of sensors, hardware, software, installation and labour force, taking into account the estimated investment presented in the 4.4 section.
- Setup: Improve the extranet connection using optical fibre for example.
- Implement a parallel system to register data in case of fault.

During the lock-down, in March, April, May and June of 2020, because of the COVID-19 pandemic, failures in the communication with the MCS and the data storage were detected, making it impossible to act on the system to correct them in time. The COVID-19 crisis is currently a challenge for the future research work based on the MCS of the Vitoria-Gasteiz building, and the research project is being adapted to ensure the data collection to achieve the objectives set out in this research.

4.5 Conclusions

Measurement of indoor air temperature:

In this paper, high quality indoor air temperature measurements of different thermal zones of an in-use office building have been statistically analysed to evaluate different components of indoor Temperature Uncertainty. The main conclusion is that the temperature sensor uncertainty of the monitored thermal zones is 2 to 10.7 times bigger than the manufacturer's accuracy for sensors. Thus, using the manufacturer's accuracy as the overall temperature uncertainty value of the indoor air temperature measurement of a thermal zone could underestimate the uncertainty of the thermal zone temperature.

This research has developed a method that permits monitored indoor air temperature measurements to be analysed in order to estimate both the overall temperature uncertainty of a thermal zone and the uncertainty associated to the systematic error of the temperature sensors, including the uncertainty associated to the monitoring system where the sensor has been installed. Furthermore, through the decoupling method developed in this study, it is possible to analytically estimate the uncertainty associated to the random errors of temperature sensor measurements of a thermal zone.

The results show that there is even a discrepancy between the sensor accuracy given by the manufacturer and the experimental accuracy of the sensor plus the monitoring equipment. In the studied case, the manufacturer's accuracy for the sensors used was 0.3 °C and 0.1 °C; while the uncertainty associated to the used temperature sensor technology plus the uncertainty associated to the monitoring system has been estimated to be of 0.24 °C.

In addition, a classification of office typologies has been developed to better understand and analyse the uncertainty analysis results. Based on this Office Typology classification, four thermal zones with different geometric and spatial characteristics have been selected for monitoring in an in-use office building. The following overall uncertainty values have been obtained after applying the developed statistical method: $\pm 0.71^\circ\text{C}$, $\pm 0.74^\circ\text{C}$, $\pm 1.07^\circ\text{C}$ and $\pm 0.83^\circ\text{C}$. These values allow an estimate of the upper and lower limits of the real representative indoor air temperature value. The offices with a larger south-facing Façade area have greater Temperature Uncertainties than the offices with a larger north-facing Façade area. The offices with large south and north facing façade areas have uncertainty values close to the offices with only one large north-facing Façade area. During this study, two different types of sensors have been used, some with a 0.3 °C manufacturer accuracy and other with a 0.1°C manufacturer accuracy. Then, it can be seen that the overall uncertainties calculated, with a 95% confidence interval, are 2.4 to 3.6 higher than the $\pm 0.3^\circ\text{C}$ manufacturer's sensor accuracy, or they are 7 to 10.7 higher than the $\pm 0.1^\circ\text{C}$ manufacturer's sensor accuracy.

Finally, based on a proposed decoupling method, the estimated overall temperature uncertainties have been decoupled using the already estimated sensor plus monitoring system uncertainty to obtain the Temperature's Spatial Uncertainty. In this Temperature's Spatial Uncertainty, all the other sources of uncertainty, excluding the sensor plus monitoring system, are considered. To estimate the weight of the different sources of uncertainty, the Ratio of Mean Variance due to Sensor Uncertainty over the Mean Variance due to the overall Temperature Uncertainty has been defined as $R_{(S)}$. This ratio has allowed us to know the percentage weight of the sensor plus monitoring system uncertainty over the overall temperature uncertainty for the four studied Office Typologies and studied Workspaces. In the case of the Office Typologies, the weight has values between 4.91% and 11.14%. In addition, the Ratio of Mean Variance due to Spatial Temperature Uncertainty ($R_{(SP)}$) has been defined in an analogous way and the obtained values range between 88.86% and 95.09%. Both ratio values, $R_{(S)}$ and $R_{(SP)}$, allow us to know the degree of importance of all Spatial Uncertainties $U_{T(SP)}$, excluding $U_{T(S)}$, over thermal zones where the temperature measurements have been performed.

Analysing individual work spaces or volumes that make up the four analysed thermal zones, in the individual volumes most exposed to the random effects of the air temperature measurement, such as the air flow, occupants, solar radiation, or heating effect, among others, the Spatial Uncertainty has more weight with respect to the overall Temperature Uncertainty than the volumes less exposed to these random effects. The studied cases show the $R_{(S)}$ values are between 11.62% and 32.26%, and the $R_{(SP)}$ values are between 67.74% and 88.38% in volumes exposed to many random effects; while the $R_{(S)}$ values are between 75.50% and 88.96%, and the $R_{(SP)}$ values are between 11.31%

and 24.50% in volumes with a low exposition to random effects.

As for temperature stratification or Vertical Uncertainty (U_{VT}), the best location for sensors in order to have a temperature measurement with more precision and accuracy, is to install one sensor at the medium level; the high level location being the next best position to locate the sensor. If two sensors are installed to monitor a volume, with a temperature measurement with better precision, one sensor should be located at the medium level and another at high level.

The results show as increasing the number of sensors can decrease the Temperature Uncertainty (U_T) value. Furthermore, the best spatial location to install sensors in a Workspace (WS) is away from windows and centred on the volume, as uncertainty causes derived from the exterior environment have a greater impact over the temperature measurements. If only one sensor is installed, based on the results, this should be at the middle level and located in the centre of the volume. If two sensors are installed, the best location is to locate them in the centre of volume.

As for the temperature stratification or Vertical Uncertainty (U_{VT}), the best location of sensors, in order to have a temperature measurement of monitored volume with more precision and accuracy, is the medium height if only one sensor is installed, followed by the high level. Measuring with two sensors, it is possible to have a better precision if one sensor is installed at the high height and the other at medium height. If on the contrary it interests more, have temperature measurement with better precision, the best two positions to install two sensors are one high and the other low. Based on the study of the effects of solar radiation, heating and electricity consumption, the above locations remain the same as those already mentioned.

Measurement of outdoor air temperature:

In the outdoor air temperature measurements for a four-floor building, the uncertainties associated to the random effects are predominant compared to the systematic errors; the overall Temperature Uncertainty value and the Temperature Spatial Uncertainty values being practically the same.

The outdoor air temperature sensors with and without mechanical ventilation shielding measure the convection temperature, not the radiant temperature of the air. This is evidenced by the low uncertainty values of sensors with and without mechanical ventilation installed in the solar radiation shield, which are equal to ± 0.091 °C for the analysed periods with and without radiation, ± 0.112 °C for periods with solar radiation, and ± 0.077 °C for periods without solar radiation.

Before installing the sensors in a monitoring system, it is important to experimentally estimate the accuracy of the sensors plus the monitoring and control system, because this estimated value is different from the manufacturer's accuracy of the sensors. The measurement uncertainty study due to systematic errors of the outdoor air temperature shows that the sensor uncertainty given by the sensor's manufacturer (equal to ± 0.10 °C) is superior to the experimental accuracy or Temperature Sensor Uncertainty estimated experimentally, which is equal to ± 0.06 °C, being a 98% higher than the accuracy given by the manufacturer.

The overall Temperature Uncertainty (in which all the measurement uncertainty sources are included) of the air surrounding the building is equal to ± 2.22 °C in periods with and without solar radiation incidence, ± 3.19 °C in periods with solar radiation incidence, and ± 1.38 °C in periods without solar radiation incidence. For estimations or studies where only cloudy periods are considered, the Temperature Uncertainty is considerably lower; in the analysed building, this was equal to ± 1.38 °C.

The Temperature Spatial Uncertainties (which include the random errors) of the air surrounding the building have the same values as the estimated Temperature Uncertainties, being equal to ± 2.22 °C in periods with and without solar radiation incidence, ± 3.19 °C in periods with solar radiation incidence, and ± 1.38 °C in periods without solar radiation incidence. Likewise, they represent, 99.93%, 99.97% and 99.83%, respectively, of the total uncertainty of temperature. Thus, only considering the manufacturer's uncertainty as the overall uncertainty of the outdoor air measurement, leads to strongly underestimating the uncertainty value of the outdoor air measurements.

If outdoor air temperature sensors are measuring only in one exterior area of the building, through the uncertainty analysis, it is possible to estimate the range in which the average temperature of air surrounding the building can lie. Likewise, it is possible to identify the best location area to install the outdoor air temperature sensors in order to obtain a measurement with the lowest uncertainty value with respect to the air temperature surrounding the building in the event of sensors being installed around it. To estimate this band in the studied case of tertiary buildings if the temperature sensors are only measuring on the northern façade, it is necessary to add the ± 1.90 °C, ± 2.11 °C and ± 1.11 °C for periods with/without solar radiation incidence and with solar radiation incidence, respectively, to the average temperature. Likewise, if the temperature sensors are measuring on the roof, it is necessary to add ± 0.98 °C, ± 1.35 °C and ± 0.70 °C for periods with/without solar radiation incidence and with solar radiation incidence, respectively, to the average temperature. In addition, if the temperature sensors are measuring on the southern façade, it is necessary to add ± 2.47 °C, ± 3.38 °C and ± 1.07 °C for periods with/without solar radiation incidence and with solar radiation incidence, respectively, to the average temperature.

To know with a 95% of confidence the temperature ranges of the representative temperature of the air surrounding one area of the building envelope (one façade or roof), the measurement must be collected from sensors installed in the corresponding studied area to estimate the measurement uncertainty value in order to add this value to the average temperature of the area to be studied. For the studied tertiary building, to obtain the representative temperature of the southern façade, it is necessary to add ± 3.14 °C, ± 4.41 °C and ± 1.57 °C for periods with/without solar radiation, with solar radiation and without solar radiation incidence, respectively. For the roof, it is necessary to add ± 0.42 °C, ± 0.62 °C and ± 0.25 °C, respectively. Moreover, for the northern façade, it is necessary to add ± 0.53 °C, ± 0.41 °C and ± 0.56 °C, respectively.

The Temperature Spatial Uncertainties (which include the random errors) of the air surrounding the areas of building have the same values of estimated Temperature Uncertainties. For the roof of building, this uncertainty is equal to ± 0.42 °C, ± 0.62 °C and ± 0.25 °C for periods with and without

solar radiation, with solar radiation and without solar radiation incidence, respectively. Moreover, these random effects represent 98.12%, 99.13% and 94.84% of the total uncertainty of temperature in the same respective periods. In the case of the air surrounding the northern façade, this uncertainty is equal to ± 0.53 °C, ± 0.41 °C and ± 0.56 °C for periods with and without solar radiation, with solar radiation and without solar radiation incidence, respectively. Where these random effects represent the 98.80%, 98.05% and 98.95% of the total uncertainty of temperature in the same respective periods. In addition, for the southern façade, this uncertainty is equal to ± 1.08 °C, ± 1.47 °C and ± 0.76 °C for periods with and without solar radiation, with solar radiation and without solar radiation incidence, respectively. Its random effects represent the 99.93%, 99.97% and 99.83% of the total uncertainty of temperature in periods with and without solar radiation incidence and with solar radiation incidence, respectively.

Chapter 5

Final Conclusions, contributions and New Research Lines

This chapter presents a recapitulation of the conclusions obtained in this doctoral thesis. In addition, the main research contributions of this doctoral thesis and the contributions related to the thesis are also listed. Likewise, the new research lines opened by this thesis are also presented with the objective to continue the research works to improve the Energy Performance of Buildings and in consequence help to meet the global target to reduce buildings' CO₂ emissions and its impact on global climate change.

5.1 Final conclusions

It has been proven in the literature review that in Building Automation Systems, there is currently no evidence of the integration of in-use building energy monitoring systems to characterize the Thermal Envelope Performance. However, it would be useful to know how efficient the envelope is after the construction or retrofit in order to determine the discrepancy between the building's design and the building in-use, and to identify future retrofit requirements of the building envelope.

The equipment necessary to carry out the Thermal Envelope Performance characterization includes sensors, controllers, software, hardware, communication protocols, and other devices and components of Monitoring and Control Systems. At the end of the 1970s and the beginning of the 1980s, studies were undertaken regarding the different monitoring technologies and cost/precision criteria for equipment selection used in the energy monitoring of buildings to characterize their Thermal Envelope Performance through the estimation of the Heat Loss Coefficient. Currently, there is no evidence for which monitoring systems should be used to characterize the Thermal Envelope Performance in Building Automation Systems or domotic systems.

The reviewed publications do not specify the selection criteria of the monitoring systems used in research projects, which shows that there is no standardization in the type of Monitoring and Controlling System that should be used to perform experimental tests in these estimations. It is also evident that experimental tests tend to focus more on developing methods to estimate the Heat Loss Coefficient and other parameters estimations to characterize the Thermal Envelope Performance, rather than carrying out an analysis to determine the criteria to choose the Monitoring and Control Systems. This trend is apparent even though the sensors used to measure physical variables are critical for the reliability of the data collected to perform the Thermal Envelope Performance characterization. It has also been observed that the Monitoring and Control Systems used to estimate Heat Loss Coefficient allow the analysis and estimation of other parameters used to characterize buildings' Thermal Envelope Performance.

The standardisation of the Monitoring and Control Systems used for the Thermal Envelope Performance characterization in experimental tests needs further research in order to ensure the physical data are accurate enough to rigorously apply the Heat Loss Coefficient estimation and decoupling methods. Remember that the Heat Loss Coefficient (HLC) is the sum of the building envelope transmission heat loss coefficient (UA) plus the infiltration and/or ventilation heat loss coefficient (C_v). In this way, if for example the HLC and the C_v are estimated, the HLC could be decoupled using the following simple subtraction: $UA = HLC - C_v$.

When the measurement uncertainty or measurement error is taken into account in the literature reviewed, only the manufacturer's accuracy (systematic errors) of sensors is taken into account, without considering the measurement uncertainties associated to random errors or other uncertainty sources.

The Co-Heating Method for HLC estimation has the advantage of being a method in which the random

errors are minimised. The random errors due to solar radiation disappear since they are estimated through the regression method together with the HLC value. The rest of the variables (indoor air temperature, electricity consumption and heating) have associated only systematic errors, so the outdoor air temperature is the only variable that has associated systematic and random errors. In this method, thanks to the air fans that are used to continuously mix the indoor air, the indoor air temperature measurement does not have associated random errors. On the other hand, this method to estimate the HLC does not consider user behaviour, since the dwelling or building must be unoccupied during the considerable period of time that takes to carry out this test. The latter makes it difficult to carry out this type of tests on dwellings or buildings that are already inhabited.

The Average Method has the advantage that it is possible to estimate the impact of the user behaviour in the estimated Heat Loss Coefficient, since it is not necessary to have the dwelling or building unoccupied. Furthermore, the effect of the random errors in the estimated HLCs are considerably increased with respect to the co-heating method, since the variables such as solar radiation gains are measured from sensors and not estimated by the method. The estimation of users' metabolic gains must also be taken into account and the indoor air temperature is a measure that is not homogeneous within the thermal zones that make up the building. These uncertainty variables, together with the outdoor air temperature uncertainty, give the average method HLC value a higher uncertainty, where systematic and random errors are associated to more variables with respect to the HLC estimation of the co-heating method.

The methodology developed in this thesis allows the overall measurement uncertainty of the intensive variables, such as indoor air temperature and outdoor air temperature to be estimated, with the aim of obtaining a more reliable estimation of the HLC of a building through the co-heating method and the average method. It has also allowed us to know the weight of the random and systematic errors in the the total uncertainty of the measurement of these intensive variables, through the decoupling method of the overall uncertainty.

Based on the developed methodology for overall uncertainty estimation, high quality three dimensional indoor air temperature measurements of different thermal zones of an in-use office building have been statistically analysed to evaluate the different components of the indoor Temperature Uncertainty. The main conclusion is that the overall temperature uncertainty of the monitored thermal zones is 2.4 to 10.7 times bigger than the manufacturer's accuracy for sensors. Thus, using the manufacturer's accuracy as the overall temperature uncertainty value of the indoor air temperature measurement of a thermal zone could underestimate the uncertainty of the thermal zone temperature.

This thesis has developed a method that permits monitored indoor air temperature measurements to be analysed in order to estimate both, the overall temperature uncertainty of a thermal zone and the uncertainty associated to the systematic error of the temperature sensors, including the uncertainty associated to the monitoring system where the sensor has been installed. Furthermore, through the decoupling method developed in this study, it has been possible to analytically estimate the uncertainty associated to the random errors of temperature sensor measurements of a thermal

zone.

The results show that there is even a discrepancy between the sensor accuracy given by the manufacturer and the experimental accuracy of the sensor plus the monitoring equipment. In the studied case, the manufacturer's accuracy for the sensors used was 0.3 °C and 0.1 °C; while the uncertainty associated to the used temperature sensor technology plus the uncertainty associated to the monitoring system has been estimated to be of 0.24 °C.

In addition, a classification of office typologies has been developed to better understand and analyse the uncertainty analysis results. Based on this Office Typology classification, four thermal zones with different geometric and spatial characteristics have been selected for monitoring in an in-use office building. There, these overall uncertainty values have been obtained after applying the developed statistical method: ± 0.71 °C, ± 0.74 °C, ± 1.07 °C and ± 0.83 °C. The offices with a larger south-facing façade area have greater Temperature Uncertainties than the offices with a larger north-facing façade area. The offices with large south and north facing façade areas have uncertainty values close to the offices with only one large north-facing façade area. During this study, two different types of sensors have been used, some of them with a 0.3 °C manufacturer's accuracy and others with a 0.1 °C manufacturer's accuracy. So, it can be seen that the overall uncertainties calculated, with a 95% confidence, are 2.4 to 3.6 higher than the ± 0.3 °C manufacturer's sensor accuracy, or 7 to 10.7 higher than the ± 0.1 °C manufacturer's sensor accuracy.

Finally, based on a proposed decoupling method, the estimated overall temperature uncertainties have been decoupled using the already estimated sensor plus monitoring system uncertainty to obtain the Temperature's Spatial Uncertainty, where all the other sources of uncertainty, excluding the sensor plus monitoring system, are considered. To estimate the weight of the different sources of uncertainty, the Ratio of Mean Variance due to Sensor Uncertainty over the Mean Variance due to the overall Temperature Uncertainty has been defined as $R_{(S)}$. This ratio has allowed us to know the percentage weight of the sensor plus monitoring system uncertainty over the overall temperature uncertainty for the four studied Office Typologies and studied Workspaces. In the case of the Office Typologies, the weight has values between 4.91% and 11.14%. In addition, the Ratio of Mean Variance due to Spatial Temperature Uncertainty ($R_{(SP)}$) has been defined in an analogous way and the obtained values range between 88.86% and 95.09%. Both ratio values, $R_{(S)}$ and $R_{(SP)}$, allow us to know the degree of importance of all Spatial Uncertainties $U_{T(SP)}$, excluding the uncertainty associated to the sensors plus monitoring system, over thermal zones where the temperature measurements have been performed.

In the outdoor air temperature measurements for the analysed four-floor building, to a greater extent than for the indoor air temperature, the uncertainties associated to the random effects are predominant compared to the systematic errors; the overall Temperature Uncertainty value and the Temperature Spatial Uncertainty value being practically the same.

Before performing the overall uncertainty analysis, it has been proven that the outdoor air temper-

ature sensors, with and without mechanical ventilation within the solar shielding, measure the convection temperature, not affected by the possible radiation effects on the temperature sensor. This is evidenced by the low uncertainty values of sensors with and without mechanical ventilation installed in the solar radiation shield, which are equal to ± 0.091 °C for the analysed periods with and without radiation, ± 0.112 °C for periods with solar radiation, ± 0.077 °C for periods without solar radiation.

To perform the decoupling analysis to the overall uncertainty, it has been important to experimentally estimate the accuracy of the sensors plus monitoring and control system, because this estimated value is again different from the manufacturer's accuracy of the sensors. The measurement uncertainty study due to systematic errors of outdoor air temperature shows that the sensor uncertainty given by the sensor's manufacturer (equal to ± 0.10 °C) is superior to the experimental accuracy or Temperature Sensor Uncertainty estimated experimentally, which is equal to ± 0.06 °C.

The overall Temperature Uncertainty (which includes all the measurement uncertainty sources) of the air surrounding the building was equal to ± 2.22 °C in periods with and without solar radiation incidence, ± 3.19 °C in periods with solar radiation incidence and ± 1.38 °C in periods without solar radiation incidence. For estimations or studies where only cloudy periods are considered (such as in the average method), the Temperature Uncertainty is considerably lower; in the analysed building, this was equal to ± 1.38 °C.

The Temperature Spatial Uncertainties (which include only the random errors) of the air surrounding the building have the same values as the estimated overall Temperature Uncertainties, being equal to ± 2.22 °C in periods with and without solar radiation incidence, ± 3.19 °C in periods with solar radiation incidence and ± 1.38 °C in periods without solar radiation incidence. Likewise, they represent 99.93%, 99.97% and 99.83% of the total uncertainty of temperature in periods with and without solar radiation incidence, with solar radiation incidence and without solar radiation incidence, respectively. Thus, only considering the manufacturer's accuracy as the overall uncertainty of the outdoor air measurement, leads to strongly underestimating the uncertainty value of the outdoor air measurements.

The second objective of this thesis deals with the minimum monitoring requirements that could provide reliable Energy Performance Certificates of buildings based on real monitored data. For this, based on the Co-heating Method requirements for the HLC estimation of unoccupied buildings, a mobile monitoring and control system has been designed and deployed to carry out the co-heating test in a three floor residential building in Vitoria-Gasteiz. Furthermore, based on the average method requirements for the HLC estimation and decoupling for occupied buildings, an extremely detailed monitoring and control system has also been designed and deployed in the three floors of this residential building. It has have been possible to design and implement these two monitoring systems thanks to the detailed analysis of both methods and following the criteria developed in the methodology section for selecting the required sensors. Due to Covid-19, even though the MCS had been installed by January 2020, it has not been possible to obtain enough reliable data to perform the detailed analysis that could lead to a specification of the minimum monitoring kit requirements so as

to reliably estimate and decouple the HLC of this in-use building.

Furthermore, proving the reliability of the average method, could open a door to the reliable estimation of Key Performance Indicators (KPI) related to building users. By using the building envelope in-use performance KPIs (in-use HLC, UA and C_v values) and the currently existing building systems' in-use KPIs, it would be possible to estimate the in-use building energy consumption in an hypothetical case where the in-use building systems are used in an optimal manner to produce optimal comfort and air quality conditions within the building. This optimal energy consumption value would be based on real building envelopes and real building systems and would then be compared to the real energy consumption monitored data. The difference in consumption could be assigned to the building user misuse and a KPI could be defined to make this effect easily understandable this effect to the wider public. Once different KPIs regarding the three main energy consumption discrepancy sources for the in-use building energy consumption are available, the most user-friendly KPIs for the general public could be selected for a new building certification scheme based on in-use data. In addition, if the HLC is decoupled, it will be possible to analyse the real origin of the heat losses of the buildings and, in such a case, the disagreement with the design parameters will be easier to understand. If the reason for the losses comes from the transmission part (UA), an envelope insulation improvement should be performed. On the other hand, if the cause were the Infiltration/Ventilation losses (C_v), it would be necessary to check the ventilation system and the building's airtightness.

5.2 Contributions

The scientific publications carried out during the development of this thesis, have been framed within the following areas of study: Mathematical development of the Average Method for the estimation of HLC and its decoupling; study of the state of the art of the Monitoring and Control Systems used in different methods to characterize the thermal envelope of the building; analysis of the Measurement Uncertainty of the indoor and outdoor temperature; implementation of the Monitoring and Control System in the studied in-use tertiary building; presentation of the energy retrofiting of the two buildings studied in this research: the administrative building of the University of the Basque Country (UPV/EHU) and the residential building of Vitoria-Gasteiz.

Part of the results of this research have been disseminated through the following scientific publications and have also been presented at the following congresses:

5.2.1 Research papers of this thesis

1. C. Giraldo-Soto, A. Erkoreka, L. Mora, I. Uriarte and L. A. Del Portillo. **Monitoring system analysis for evaluating a building's envelope energy performance through estimation of its heat loss coefficient.** *Sensors*, vol. 18, no. 7, p. 2360, Jul. 2018. DOI: 10.3390/s18072360. (Published).

2. C. Giraldo-Soto, A. Ekoreka, A. Barragan and L. Mora, **Dataset of an in-use tertiary building collected from a detailed 3d mobile monitoring system and building automation system for indoor and outdoor air temperature analysis**. *Data in Brief*, p. 105 907, 23rd Jun. 2020. DOI: 10.1016/j.dib.2020.105907. (Published).
3. C. Giraldo-Soto, L. Mora, A. Erkoreka, I. Uriarte and P. Eguia. **Overall uncertainty analysis of zonal indoor air temperature measurement in an in-use office building**. *Energy and Buildings*. (Under review).
4. C. Giraldo-Soto, A. Erkoreka, L. Mora, A. Uriarte and E. Granada. **Measurement uncertainty analysis of the outdoor air temperature surrounding a building**. *Building and Environment*. (To be sent shortly).

5.2.2 Research papers related to this thesis work

1. I. Uriarte, A. Erkoreka, C. Giraldo-Soto, K. Martin, A. Uriarte and P. Eguia. **Mathematical development of an average method for estimating the reduction of the heat loss coefficient of an energetically retrofitted occupied office building**. *Energy and Buildings*, vol. 192, pp. 101–122, 1st Jun. 2019. DOI:10.1016/j.enbuild.2019.03.006. (Published).
2. A. Egusquiza, S. Ginestet, J. C. Espada, I. Flores-Abascal, C. Garcia-Gafaro, C. Giraldo-Soto, S. Claude and G. Escadeillas. **Co-creation of local eco-rehabilitation strategies for energy improvement of historic urban area**. *Renewable and Sustainable Energy Reviews*, vol. 135, p. 110 332, 1st Jan. 2021. DOI:10.1016/j.rser.2020.110332. (Published).
3. I. Uriarte, A. Erkoreka, A. Legorburu, K. Martin-Escudero, C. Giraldo-Soto, M. Odriozola-Maritorea. **Decoupling the Heat Loss Coefficient of an in-use office building into its Transmission and Infiltration heat loss coefficients**. *Building and Environment*. (Under review).

5.2.3 Data repositories related to this thesis work

1. C. Giraldo-Soto, A. Erkoreka, A. Barragan and L. Mora. **Dataset of an in-use tertiary building collected from a detailed 3d mobile monitoring system and building automation system for indoor and outdoor air temperature analysis**. Mendeley Data, vol. 3, 5th Jun. 2020. DOI: 10.17632/fc2r9rdxbt.3. (Published).

5.2.4 International conferences

1. C. Giraldo-Soto, I. Uriarte, L. Mora, E. Granada and A. Erkoreka. **Monitoring systems analysis for building's envelope energy performance evaluation**. *11th European Conference on Energy Efficiency and Sustainability in Architecture and Planning*, Donostia-San Sebastian, Spain: Universidad del País Vasco/Euskal Herriko Unibersitatea, 1st Dec. 2020.

2. X. Aparicio, A. Erkoreka, L. A. Del Portillo, C. Giraldo-Soto, A. Uriarte, P. Eguia, A. Sánchez-Ostiz **Vacuum Insulation Panels in Building Sector: Case study in Spain of Vacuum insulation panels in construction for energy efficient retrofitting of buildings.** *35th PLEA 2020 - Planning Post Carbon Cities*, A Coruña, Spain. 1st-3rd September 2020.
3. F. Troncoso¹, A. Ogando, P. Eguía, E. Granada, C. Giraldo-Soto. **Artificial Lighting Data Acquisition in Buildings for BIM Integration Based on Computer Vision.** *11 CNIT-XX-2018: XI National and II International Engineering Thermodynamics Congress*, Albacete, Spain. 12th - 13th June 2018.
4. I. Uriarte¹, C. Giraldo, K. Martin, L. A. Del Portillo, A. Erkoreka **Estimating the Heat Loss Coefficient of an in-use office building, floor by floor and as a whole, through basic monitoring and modelling.** *10CNIT-XX-2017: X National and I International Engineering Thermodynamics Congress*, Lleida, Spain. 28th - 30th June 2017.
5. C Giraldo-Soto, I. Uriarte, A. Erkoreka, J. Sala and P. Eguia. **Applying the decay method to the CO₂ produced by occupants for decoupling the heat loss coefficient of an in-use office building.** *8th European Conference on Energy Efficiency and Sustainability in Architecture and Planning*, Donostia-San Sebastian, Spain: Universidad del País Vasco/Euskal Herriko Unibersitatea, 5th Jul. 2017, pp. 95–104. ISBN: 978-84-9082-668-3.

5.3 New research lines:

In the coming months, the Co-heating test will be applied on a floor by floor basis to the Vitoria-Gasteiz residential building. The test, will also include the measurements of the heat exchanges between adjacent floors and dwellings. These Co-heating tests will provide reliable HLC results for this residential building based on the only well-established methodology that allows us to obtain the HLC of unoccupied buildings. It is also planned to perform a tracer gas test for the unoccupied building floors in order to be able to measure their infiltration heat loss coefficients. The latter will provide us with the possibility of decoupling this Co-heating HLC into its transmission heat loss coefficient (UA-Value) and the infiltration heat loss coefficient ($C_{v_{infiltration}}$). Remember that the $HLC = UA + C_v$.

Furthermore, the Vitoria-Gasteiz building will be inhabited while being monitored by the extremely detailed monitoring system presented in chapter 3.4. This extremely detailed MCS will permit us to accurately measure all the energy flows occurring within the building while it is occupied and it will also provide detailed weather and indoor conditions data so as to be able to estimate and decouple the HLC using the Average Method. These in-use HLC values, alongside the issues dealt with in the chapter 3.4, will have a reference HLC value for comparison from the Co-heating test. As commented before, we also expect to have their respective decoupled UA and C_v values. Then, having both the extremely detailed data sets of all the energy flows, detailed indoor conditions and weather data, together with the reference HLC, UA and C_v values from the Co-heating test, it will be possible to know what the key measurements are that provide reliable HLC, UA and C_v values with a minimum number of sensors

by means of the Average Method in this occupied building case.

In a dwelling of the Vitoria-Gasteiz building, an analytical study of the estimated HLC values through the Co-Heating Method (with the dwelling unoccupied) and the Average Method (with the dwelling occupied) will be carried out, in order to know what is the impact of the user behaviour on the estimated HLC value in the dwelling when is occupied. Also, it will allow us to know the experimental value of the heat gain variable due to occupation, together with the study of methods to estimate the uncertainty associated to this variable. Likewise, it will open a new way to analyse and develop a new methodology to estimate the number of occupants from the estimation of the experimental heat gains due to occupancy, and then compare the developed methodology with the estimation of the number of occupants through the CO₂ measurement and another estimation techniques, currently used.

The latter analysis will permit us to define a monitoring kit for occupied residential buildings, as well as the guides of where and how the sensors should be installed, together with the required accuracy for each of the sensor types. For the main intensive variable measurements: indoor and outdoor air temperature (required for the HLC estimation) and indoor and outdoor CO₂ concentrations (required for the HLC decoupling), the uncertainty method developed in this thesis will be crucial, since it will allows us to reliably estimate the overall uncertainty of these variables. Only then, these monitoring kits should permit the reliable HLC estimation and decoupling. Therefore, with a few extra sensors providing the fuel or electricity consumption of the systems that produce the space heating and domestic hot water, it will also permit us to reliably obtain the seasonal efficiencies of such systems.

Thanks to the detailed economic analysis presented in the thesis, this experimental test will also open the way to performing the economic optimisation of in-motic technologies to be integrated into in-use dwellings in order to know, in real time, their energy behaviour, including the yearly re-estimation and decoupling of the Heat Loss Coefficient.

To finish, we must remember that the design and implementation of reliable monitoring and control systems for estimating and decoupling the HLC of in-use buildings will, in the near future, allow us to generate reliable Energy Performance Certificates based on in-use data. These certificates will be able to better explain the reasons for the energy performance gap between the design and operation phases of buildings and evaluate the user behaviour and the building subsystems.

This study will also open the way to starting the uncertainty propagation and sensitivity analysis on the Heat Loss Coefficients (HLC) estimations of in-use buildings with monitoring in real-time, in order to improve our knowledge of energy performance concerning the buildings and their energy efficiency. Estimating the overall Measurement Uncertainty of other intensive variables (such as CO₂ concentrations or relative humidity), through the statistical method developed in this research, will also help to improve the estimation of thermal comfort, air quality, heating and HVAC controls, among others. Finally, trying to develop a new methodology to more accurately estimate the heat gains due to the occupants' metabolic heat generation, by means of measuring the CO₂ concentrations of the indoor thermal zones and estimating its associated measurement uncertainty, is another open line of

research, where the number of occupants can be estimated with more precision and accuracy through the machine learning techniques.

With the estimated overall Temperature Uncertainty values, it will be possible to study the propagation of the indoor air temperature overall uncertainty in different fields, where the thermal zones' indoor air temperature is used for calculation purposes, such as for the case of the estimation of the Heat Loss Coefficient (HLC) of in-use buildings.

In further research, studying the interior temperature in residential buildings will enable us to know the behaviour of the Temperature Uncertainty (U_T) in order to compare the results and conclusions of this experimental test on tertiary buildings, and also be able to make the interior temperature uncertainty propagation for Heat Loss Coefficient (HLC) estimation to this type of buildings.

Bibliography

- [1] 'nZEB definitions across europe BPIE - buildings performance institute europe,' [Online]. Available: <https://www.bpie.eu/publication/nzeb-definitions-across-europe-2015/> (visited on 15/10/2020).
- [2] 'Ministerio para la transición ecológica y el reto demográfico - rite - reglamento instalaciones térmicas en los edificios,' [Online]. Available: <https://energia.gob.es/desarrollo/EficienciaEnergetica/RITE/Paginas/InstalacionesTermicas.aspx> (visited on 13/11/2020).
- [3] 'Passivhaus institut,' [Online]. Available: <https://passivehouse.com/> (visited on 13/11/2020).
- [4] P. de Wilde, 'The gap between predicted and measured energy performance of buildings: A framework for investigation,' *Automation in Construction*, vol. 41, pp. 40–49, 1st May 2014, ISSN: 0926-5805. DOI: 10.1016/j.autcon.2014.02.009.
- [5] L. De Boeck, S. Verbeke, A. Audenaert and L. De Mesmaeker, 'Improving the energy performance of residential buildings: A literature review,' *Renewable and Sustainable Energy Reviews*, vol. 52, pp. 960–975, 1st Dec. 2015, ISSN: 1364-0321. DOI: 10.1016/j.rser.2015.07.037.
- [6] R. Lowe, J. Wingfield, M. Bell and J. Bell, 'Evidence for heat losses via party wall cavities in masonry construction,' *Building Services Engineering Research and Technology*, vol. 28, no. 2, pp. 161–181, 1st May 2007, ISSN: 0143-6244. DOI: 10.1177/0143624407077196.
- [7] M. Bell and R. Lowe, 'Energy efficient modernisation of housing: A UK case study,' *Energy and Buildings*, vol. 32, no. 3, pp. 267–280, 1st Sep. 2000, ISSN: 0378-7788. DOI: 10.1016/S0378-7788(00)00053-0.
- [8] D. Johnston, D. Farmer, M. Brooke-Peat and D. Miles-Shenton, 'Bridging the domestic building fabric performance gap,' *Building Research & Information*, vol. 44, no. 2, pp. 147–159, 17th Feb. 2016, ISSN: 0961-3218. DOI: 10.1080/09613218.2014.979093.
- [9] S. Baldi, T. L. Quang, O. Holub and P. Endel, 'Real-time monitoring energy efficiency and performance degradation of condensing boilers,' *Energy Conversion and Management*, vol. 136, pp. 329–339, 15th Mar. 2017, ISSN: 0196-8904. DOI: 10.1016/j.enconman.2017.01.016.
- [10] A. Stafford and D. Lilley, 'Predicting in situ heat pump performance: An investigation into a single ground-source heat pump system in the context of 10 similar systems,' *Energy and Buildings*, vol. 49, pp. 536–541, 1st Jun. 2012, ISSN: 0378-7788. DOI: 10.1016/j.enbuild.2012.03.001.

- [11] D. Bourgeois, C. Reinhart and I. Macdonald, 'Adding advanced behavioural models in whole building energy simulation: A study on the total energy impact of manual and automated lighting control,' *Energy and Buildings*, Special Issue on Daylighting Buildings, vol. 38, no. 7, pp. 814–823, 1st Jul. 2006, ISSN: 0378-7788. DOI: 10.1016/j.enbuild.2006.03.002.
- [12] C. Aghemo, J. Virgone, G. V. Fracastoro, A. Pellegrino, L. Blaso, J. Savoyat and K. Johannes, 'Management and monitoring of public buildings through ICT based systems: Control rules for energy saving with lighting and HVAC services,' *Frontiers of Architectural Research*, vol. 2, no. 2, pp. 147–161, 1st Jun. 2013, ISSN: 2095-2635. DOI: 10.1016/j.foar.2012.11.001.
- [13] R. Gupta and S. Chandiwala, 'Understanding occupants: Feedback techniques for large-scale low-carbon domestic refurbishments,' *Building Research & Information*, vol. 38, no. 5, pp. 530–548, 1st Oct. 2010, ISSN: 0961-3218. DOI: 10.1080/09613218.2010.495216.
- [14] F. Stevenson and H. B. Rijal, 'Developing occupancy feedback from a prototype to improve housing production,' *Building Research & Information*, vol. 38, no. 5, pp. 549–563, 1st Oct. 2010, ISSN: 0961-3218. DOI: 10.1080/09613218.2010.496182.
- [15] 'Energy statistics - an overview - statistics explained,' [Online]. Available: https://ec.europa.eu/eurostat/statistics-explained/index.php?title=Energy_statistics_-_an_overview#Final_energy_consumption; (visited on 13/11/2020).
- [16] 'Final report. annex 58: Reliable building energy performance characterisation based on full scale dynamic measurement,' 2015.
- [17] *Directive 2010/31/EU of the european parliament and fo the council of 19 may 2010 on the energy performance of buildings*, 19th May 2010.
- [18] J. Chapman, R. Lowe and R. Everett, 'The pennyland project,' Energy Technology Support Unit (ETSU) prepared for The U.S. Department of Energy under Contract No. E5A/CON/1046/174/040, Milton Keynes, UK, ERG 053. ETSU-S-1046, Jul. 1985.
- [19] D. Butler and A. Dengel, 'Review of co-heating test methodologies,' NHBC Foundation, Knowhill, UK, 2013.
- [20] 'ISO.thermal insulation - building elements - in-situ measurement of thermal resistance and thermal transmittance - part 1: Heat flow meter method; ISO standard 9869-1,' AENOR, Genoa, 2014.
- [21] C Giraldo-Soto, I Uriarte, A Erkoreka, J. Sala and P Eguia, 'Applying the decay method to the CO₂ produced by occupants for decoupling the heat loss coefficient of an in-use office building,' in *Estrategia para la construcción inteligente y sostenible. 8th European Conference on Energy Efficiency and Sustainability in Architecture and Planning*, Donostia-San Sebastian, Spain: Universidad del País Vasco/Euskal Herriko Unibersitatea, 5th Jul. 2017, pp. 95–104, ISBN: 978-84-9082-668-3.
- [22] O. Mejri, E. Palomo Del Barrio and N. Ghrab-Morcos, 'Energy performance assessment of occupied buildings using model identification techniques,' *Energy and Buildings*, vol. 43, no. 2, pp. 285–299, 1st Feb. 2011, ISSN: 0378-7788. DOI: 10.1016/j.enbuild.2010.09.010.
- [23] I. Uriarte, A. Erkoreka, C. Giraldo-Soto, K. Martin, A. Uriarte and P. Eguia, 'Mathematical development of an average method for estimating the reduction of the heat loss coefficient of

- an energetically retrofitted occupied office building,' *Energy and Buildings*, vol. 192, pp. 101–122, 1st Jun. 2019, ISSN: 0378-7788. DOI: 10.1016/j.enbuild.2019.03.006.
- [24] A. Erkoreka, E. Garcia, K. Martin, J. Teres-Zubiaga and L. Del Portillo, 'In-use office building energy characterization through basic monitoring and modelling,' *Energy and Buildings*, vol. 119, pp. 256–266, 1st May 2016, ISSN: 0378-7788. DOI: 10.1016/j.enbuild.2016.03.030.
- [25] *Remote monitoring and control*, in *Wikipedia*, 18th Jul. 2019.
- [26] P. H. Shaikh, N. B. M. Nor, P. Nallagownden, I. Elamvazuthi and T. Ibrahim, 'A review on optimized control systems for building energy and comfort management of smart sustainable buildings,' *Renewable and Sustainable Energy Reviews*, vol. 34, pp. 409–429, 1st Jun. 2014, ISSN: 1364-0321. DOI: 10.1016/j.rser.2014.03.027.
- [27] 'Implementing the energy performance of buildings directive (EPBD) – featuring country reports.'
- [28] 'Smart home - europe | statista market forecast,' [Online]. Available: <https://www.statista.com/outlook/279/102/smart-home/europe#> (visited on 16/05/2018).
- [29] 'Digitalization and energy,' Digitalization and Energy Working Group - International Energy Agency (IEA), Paris, France, 2017.
- [30] 'Buildings - energy - european commission,' Energy, [Online]. Available: <https://ec.europa.eu/energy/en/topics/energy-efficiency/buildings> (visited on 29/05/2018).
- [31] 'Report on an action plan for energy efficiency realising the potential (2007/2106 (INI)),' European Parliament, Brussels, A6-0003/2008, 8th Jan. 2008.
- [32] *Proposal for a directive of the european parliament and of the council amending directive 2010/31/EU on the energy performance of buildings*, 30th Nov. 2016.
- [33] 'Energy performance of buildings: Impact assessment (SWD (2016) 414, SWD (2016) 415 (summary)) of a commission proposal for a directive of the european parliament and of the council amending directive 2010/31/EU on the energy performance of buildings (COM (2016) 765),' European Parliament, Brussels, Feb. 2017.
- [34] *Directive 2012/27/EU of the european parliament and fo the council of 25 october 2012 on energy efficiency, amending directives 2009/125/EC and 2010/30/EU and repealing directives 2004/8/EC and 2006/32/EC*, 25th Oct. 2012.
- [35] 'Commission proposes new rules for consumer centred clean energy transition - european commission,' [Online]. Available: <https://ec.europa.eu/energy/en/news/commission-proposes-new-rules-consumer-centred-clean-energy-transition> (visited on 16/05/2018).
- [36] *Action plan for energy efficiency: Realising the potential. COM (2006) 545 final. european commission*. 19th Oct. 2006.
- [37] *Green paper on energy efficiency or doing more with less. COM(2005) 265 final*, 22nd Jun. 2005.
- [38] 'Energy technology RD&d budgets overview,' The IEA energy efficiency indicators statistical report, Paris, France, The IEA energy RD&D data collection and the analysis, 2017.
- [39] *Regulation (EU) no 182/2011 of the european parliament and of the council of 16 february 2011, laying down the rules and general principles concerning mechanisms for control by member states of the commission's exercise of implementing powers*, 16th Feb. 2011.

- [40] *Proposal for of the european parliament and of the council amending directive 2010.31.EU on the energy performance of buildings. general approach*, 19th Jun. 2017.
- [41] O. Brajterman, M. Jamieson, Y. Verstraeten and J. Arbon, 'EPBD compliance study - final report. energy performance of buildings directive (EPBD) compliance study specific contract no. MOVE/ENER/SRD.1/2012-409-lot3/ENER/c3/2014-542/s12.701648,' European Union, Luxembourg, 088586.0.004.00, 8th Dec. 2018. DOI: 10.2833/281509.
- [42] D. Johnston, D. Miles-Shenton, J. Wingfield, D. Farmer and M. Bell, 'Whole house heat loss test method (coheating),' International Energy Agency Annex 58: Reliable Building Energy Performance Characterisation Based on Full Scale Dynamic Measurements, Bilbao, Spain, 2nd Apr. 2012.
- [43] 'ISO - international organization for standardization,' ISO, [Online]. Available: <https://www.iso.org/home.html> (visited on 02/10/2020).
- [44] 'ISO. energy performance of buildings - energy needs for heating and cooling, internal temperatures sensible and latent heat loads; ISO standard 52016-1,' AENOR, Genoa, 2017.
- [45] 'ISO. thermal performance of buildings - calculation of energy use for space heating; ISO standard 13790,' AENOR, Genoa, 2008.
- [46] G. B. Murphy, M. Kummert, B. R. Anderson and J. Counsell, 'A comparison of the UK standard assessment procedure (SAP) and detailed simulation of building-integrated renewable energy systems,' in *Building Simulation 2009, 11th International Building Performance Simulation Association Conference*, Glasgow, Scotland, 27th Jul. 2009.
- [47] R. Sutton, A. Stafford and C. Gorse, 'The co-heating test: The value of a number,' International Energy Agency Annex 58: Reliable Building Energy Performance Characterisation Based on Full Scale Dynamic Measurements, Bilbao, Spain, NF54, 2nd Apr. 2012.
- [48] M. R. Brambley, P. Haves, S. C. McDonald, P. Torcellini, D. Hansen, D. R. Holmberg and K. W. Roth, 'Advanced sensors and controls for building applications: Market assessment and potential r&d pathways,' Pacific Northwest National Laboratory, prepared for the U.S. Department of Energy under Contract DE-AC05-76RL01830, Washington, DC, USA, PNNL-15149, Apr. 2005, p. 163. DOI: 10.2172/1217909.
- [49] R. H. Socolow and P. U. C. f. E. Studies, *Saving energy in the home : Princeton's experiments at Twin Rivers*. Cambridge, Massachusetts, USA: Ballinger Publishing Company, Apr. 1978, 180 pp., ISBN: 0-88410-080-4.
- [50] M. Kapsalaki. (24th Apr. 2017). 'IEA-EBC annex 71,' Build Up, [Online]. Available: <http://www.buildup.eu/en/explore/links/iea-ebc-annex-71-0> (visited on 04/06/2019).
- [51] A. J. Summerfield, T. Oreszczyn, I. G. Hamilton, D. Shipworth, G. M. Huebner, R. J. Lowe and P. Ruyssevelt, 'Empirical variation in 24-h profiles of delivered power for a sample of UK dwellings: Implications for evaluating energy savings,' *Energy and Buildings*, vol. 88, pp. 193–202, 1st Feb. 2015, ISSN: 0378-7788. DOI: 10.1016/j.enbuild.2014.11.075.
- [52] X. Lü, T. Lu, C. J. Kibert and M. Viljanen, 'Modeling and forecasting energy consumption for heterogeneous buildings using a physical–statistical approach,' *Applied Energy*, vol. 144, pp. 261–275, 15th Apr. 2015, ISSN: 0306-2619. DOI: 10.1016/j.apenergy.2014.12.019.

- [53] S. Roels, P. Bacher, G. Bauwens, H. Madsen and M. J. Jiménez, 'Characterising the actual thermal performance of buildings: Current results of common exercises performed in the framework of the IEA EBC annex 58-project,' *Energy Procedia*, 6th International Building Physics Conference, IBPC 2015, vol. 78, pp. 3282–3287, 1st Nov. 2015, ISSN: 1876-6102. DOI: 10.1016/j.egypro.2015.11.726.
- [54] M. J. Jiménez and M. R. Heras, 'Application of multi-output ARX models for estimation of the u and g values of building components in outdoor testing,' *Solar Energy*, vol. 79, no. 3, pp. 302–310, 1st Sep. 2005, ISSN: 0038-092X. DOI: 10.1016/j.solener.2004.10.008.
- [55] M. J. Jiménez, B. Porcar and M. R. Heras, 'Estimation of building component UA and gA from outdoor tests in warm and moderate weather conditions,' *Solar Energy*, vol. 82, no. 7, pp. 573–587, 1st Jul. 2008, ISSN: 0038-092X. DOI: 10.1016/j.solener.2008.02.013.
- [56] K. K. Andersen, H. Madsen and L. H. Hansen, 'Modelling the heat dynamics of a building using stochastic differential equations,' *Energy and Buildings*, vol. 31, no. 1, pp. 13–24, 2000, Publisher: Elsevier, ISSN: 0378-7788. DOI: 10.1016/S0378-7788(98)00069-3.
- [57] P. Bacher and H. Madsen, 'Identifying suitable models for the heat dynamics of buildings,' *Energy and Buildings*, vol. 43, no. 7, pp. 1511–1522, 1st Jul. 2011, ISSN: 0378-7788. DOI: 10.1016/j.enbuild.2011.02.005.
- [58] N. R. Kristensen, H. Madsen and S. B. Jørgensen, 'Parameter estimation in stochastic grey-box models,' *Automatica*, vol. 40, no. 2, pp. 225–237, 1st Feb. 2004, ISSN: 0005-1098. DOI: 10.1016/j.automatica.2003.10.001.
- [59] A. C. Menezes, A. Cripps, D. Bouchlaghem and R. Buswell, 'Predicted vs. actual energy performance of non-domestic buildings: Using post-occupancy evaluation data to reduce the performance gap,' *Applied Energy*, Energy Solutions for a Sustainable World - Proceedings of the Third International Conference on Applied Energy, May 16-18, 2011 - Perugia, Italy, vol. 97, pp. 355–364, 1st Sep. 2012, ISSN: 0306-2619. DOI: 10.1016/j.apenergy.2011.11.075.
- [60] P. Eguía Oller, J. M. Alonso Rodríguez, n. Saavedra González, E. Arce Fariña and E. Granada Álvarez, 'Improving transient thermal simulations of single dwellings using interpolated weather data,' *Energy and Buildings*, vol. 135, pp. 212–224, 15th Jan. 2017, ISSN: 0378-7788. DOI: 10.1016/j.enbuild.2016.11.030.
- [61] *Implementing of the Energy Performance of Buildings directive (EPBD) - 2016*. Lisbon (Portugal): Co-funded under the Intelligent Energy-Europe Programme of the European Union., Sep. 2015, 110 pp., ISBN: 978-972-8646-32-5.
- [62] martizr. (7th May 2015). 'Intelligent energy europe,' EASME - European Commission, [Online]. Available: <https://ec.europa.eu/easme/en/section/energy/intelligent-energy-europe> (visited on 31/08/2020).
- [63] G. Bauwens and S. Roels, 'Co-heating test: A state-of-the-art,' *Energy and Buildings*, vol. 82, pp. 163–172, 1st Oct. 2014, ISSN: 0378-7788. DOI: 10.1016/j.enbuild.2014.04.039.
- [64] M. Marzouk and N. Seleem, 'Assessment of existing buildings performance using system dynamics technique,' *Applied Energy*, vol. 211, pp. 1308–1323, 1st Feb. 2018, ISSN: 0306-2619. DOI: 10.1016/j.apenergy.2017.10.111.

- [65] X. Liang, T. Hong and G. Q. Shen, 'Improving the accuracy of energy baseline models for commercial buildings with occupancy data,' *Applied Energy*, vol. 179, pp. 247–260, 1st Oct. 2016, ISSN: 0306-2619. DOI: 10.1016/j.apenergy.2016.06.141.
- [66] M. J. Moran, H. N. Shapiro, D. D. Boettner and M. B. Bailey, *Fundamentals of Engineering Thermodynamics*, 8th. John Wiley & Sons, 2014, 1056 pp., ISBN: 9781118412930.
- [67] J. A. Duffie and W. A. Beckman, *Solar Engineering of Thermal Processes*, 4th. John Wiley & Sons, 2013, 944 pp., ISBN: 9780471698678.
- [68] D. Arasteh, J. Carmody, L. Heschong and S. Selkowitz, *Residential Windows: A Guide to New Technologies and Energy Performance*, 3th. 2007, 264 pp., ISBN: 9780393732252.
- [69] M. Fletcher, C. Gorse, A. Stafford and R. Sutton, 'Full scale dynamic building testing: Roadmap document 1:1 outline of test methods and equipment,' International Energy Agency Annex 58: Reliable Building Energy Performance Characterisation Based on Full Scale Dynamic Measurements, Bilbao, Spain, 2nd Apr. 2012.
- [70] 'Selected papers from the first international conference a companion to: 'sustainable ecological engineering design - selected proceedings,' presented at the International Conference of Sustainable Ecological Engineering Design for Society (SEEDS), Leeds, UK: LSIPublishing, 17th Sep. 2015, ISBN: 978-0-9955690-0-3.
- [71] S. Van Buggenhout, T. Zerihun Desta, A. Van Brecht, E. Vranken, S. Quanten, W. Van Malcot and D. Berckmans, 'Data-based mechanistic modelling approach to determine the age of air in a ventilated space,' *Building and Environment*, vol. 41, no. 5, pp. 557–567, 1st May 2006, ISSN: 0360-1323. DOI: 10.1016/j.buildenv.2005.02.029.
- [72] *ASTM d6245 - 12: Standard guide for using indoor carbon dioxide concentrations to evaluate indoor air quality and ventilation*, 2012.
- [73] *ASTM e741 - 11: Standard test method for determining air change in a single zone by means of a tracer gas dilution*, 2011.
- [74] J. R. Taylor, *Introduction to Error Analysis, 2nd Ed. (cloth)*. California, Florida, USA: University Science Books, 1997, 448 pp., ISBN: 0-935702-42-3.
- [75] 'What is FP7? - FP7 in brief - research - EUROPA,' [Online]. Available: https://ec.europa.eu/research/fp7/understanding/fp7inbrief/what-is_en.html (visited on 29/05/2018).
- [76] 'Affordable and adaptable public buildings through energy efficient retrofitting (a2pbeer),' [Online]. Available: <http://www.a2pbeer.eu/> (visited on 16/05/2018).
- [77] 'Affordable and adaptable public buildings through energy efficient retrofitting | projects | FP7-NMP| european commission,' CORDIS | European Commission, [Online]. Available: https://cordis.europa.eu/project/rcn/108894_es.html (visited on 16/05/2018).
- [78] P. Domingues, P. Carreira, R. Vieira and W. Kastner, 'Building automation systems: Concepts and technology review,' *Computer Standards & Interfaces*, vol. 45, pp. 1–12, 1st Mar. 2016, ISSN: 0920-5489. DOI: 10.1016/j.csi.2015.11.005.
- [79] O. Gassmann and H. Meixner, *Sensors in intelligent buildings*. Weinheim: Wiley-VCH Verlag GmbH, 2001, vol. 2, 585 pp., ISBN: 3-527-29557-7.

- [80] S. Millán-Anglés, A. García-Santos, F. J. Jiménez-Leube and O. Higuera-Rincón, 'Estudio de la influencia de la automatización en el proyecto arquitectónico,' *Informes de la Construcción*, vol. 66, no. 534, e020, 1st Jun. 2014, ISSN: 0020-0883, 1988-3234. DOI: 10.3989/ic.12.081.
- [81] G. Lilis, G. Conus, N. Asadi and M. Kayal, 'Towards the next generation of intelligent building: An assessment study of current automation and future IoT based systems with a proposal for transitional design,' *Sustainable Cities and Society*, vol. 28, pp. 473–481, 1st Jan. 2017, ISSN: 2210-6707. DOI: 10.1016/j.scs.2016.08.019.
- [82] N. Aste, M. Manfren and G. Marenzi, 'Building automation and control systems and performance optimization: A framework for analysis,' *Renewable and Sustainable Energy Reviews*, vol. 75, pp. 313–330, 1st Aug. 2017, ISSN: 1364-0321. DOI: 10.1016/j.rser.2016.10.072.
- [83] W. Granzer, C. Reinisch and W. Kastner, 'Future challenges for building automation: Wireless and security,' in *2010 IEEE International Symposium on Industrial Electronics*, Bari, Italy, 4th Jul. 2010, pp. 4415–4467. DOI: 10.1109/ISIE.2010.5637840.
- [84] 'KNX association - KNX association [official website],' [Online]. Available: <https://www.knx.org/knx-en/index.php> (visited on 16/05/2018).
- [85] 'LonMark - news & events - LON achieves ISO/IEC standardization,' [Online]. Available: http://www.lonmark.org/news_events/press/2008/1208_iso_standard (visited on 16/05/2018).
- [86] 'BACnet website,' [Online]. Available: <http://www.bacnet.org/> (visited on 16/05/2018).
- [87] 'Energy harvesting wireless sensor solutions and networks from EnOcean,' [Online]. Available: <https://www.enocean.com/en/> (visited on 29/05/2018).
- [88] 'Zigbee alliance,' [Online]. Available: <http://www.zigbee.org/> (visited on 16/05/2018).
- [89] 'Technology — insteon,' [Online]. Available: <https://www.insteon.com/technology/> (visited on 29/05/2018).
- [90] 'The modbus organization,' [Online]. Available: <http://www.modbus.org/> (visited on 20/05/2018).
- [91] 'Z-wave for OEMs & developers,' Z-Wave Alliance, [Online]. Available: <https://z-wavealliance.org/z-wave-oems-developers/> (visited on 29/05/2018).
- [92] 'OCF - UPnP standards & architecture,' Open Connectivity Foundation (OCF), [Online]. Available: <https://openconnectivity.org/developer/specifications/upnp-resources/upnp> (visited on 29/05/2018).
- [93] 'OSGi™ alliance – the dynamic module system for java,' [Online]. Available: <https://www.osgi.org/> (visited on 29/05/2018).
- [94] W. Granzer, W. Kastner and C. Reinisch, 'Gateway-free integration of BACnet and KNX using multi-protocol devices,' in *2008 6th IEEE International Conference on Industrial Informatics*, Daejeon, South Korea, 13th Jul. 2008, pp. 973–978. DOI: 10.1109/INDIN.2008.4618243.
- [95] S. Wendzel, B. Kahler and T. Rist, 'Covert channels and their prevention in building automation protocols: A prototype exemplified using BACnet,' in *2012 IEEE International Conference on Green Computing and Communications*, Besancon, France, 20th Nov. 2012, pp. 731–736. DOI: 10.1109/GreenCom.2012.120.

- [96] J. Singh, N. Hassanzadeh, S. Rea and D. Pesch, 'Semantics-empowered middleware implementation for home ecosystem gateway,' in *2014 IEEE International Conference on Pervasive Computing and Communication Workshops (PERCOM WORKSHOPS)*, Budapest, Hungary, 24th Mar. 2014, pp. 449–454. DOI: 10.1109/PerComW.2014.6815248.
- [97] Z. Pan, J. Pacheco and S. Hariri, 'Anomaly behavior analysis for building automation systems,' in *2016 IEEE/ACS 13th International Conference of Computer Systems and Applications (AICCSA)*, Agadir, Morocco, 29th Dec. 2016, pp. 1–8. DOI: 10.1109/AICCSA.2016.7945692.
- [98] M. Jung, C. Reinisch and W. Kastner, 'Integrating building automation systems and IPv6 in the internet of things,' in *2012 Sixth International Conference on Innovative Mobile and Internet Services in Ubiquitous Computing*, Palermo, Italy, 4th Jul. 2012, pp. 683–688. DOI: 10.1109/IMIS.2012.134.
- [99] M. Armbrust, A. Fox, R. Griffith, A. Joseph, R. Katz, A. Konwinski, G. Lee, D. Patterson, A. Rabkin, I. Stoica and M. Zaharia, 'A view of cloud computing,' *Commun. ACM*, vol. 53, no. 4, pp. 50–58, Apr. 2010, ISSN: 0001-0782. DOI: 10.1145/1721654.1721672.
- [100] I. Stojmenovic and S. Wen, 'The fog computing paradigm: Scenarios and security issues,' in *2014 Federated Conference on Computer Science and Information Systems*, Warsaw, Poland, 7th Sep. 2014, pp. 1–8. DOI: 10.15439/2014F503.
- [101] Y. Agarwal, B. Balaji, R. Gupta, J. Lyles, M. Wei and T. Weng, 'Occupancy-driven energy management for smart building automation,' in *Proceedings of the 2Nd ACM Workshop on Embedded Sensing Systems for Energy-Efficiency in Building*, ser. BuildSys'10, Zurich, Switzerland: ACM, 3rd Nov. 2010, pp. 1–6, ISBN: 978-1-4503-0458-0. DOI: 10.1145/1878431.1878433.
- [102] A. Ting-pat So and W. Chan, *Intelligent Building Systems*. New York, USA: Springer Science & Business Media, 1999, 175 pp., ISBN: 978-1-4613-7280-6.
- [103] 'Evaluation of measurement data. bipm - guide to the expression of uncertainty in measurement,' Working Group 1 of the Joint Committee for Guides in Metrology (JCGM/WG 1), France, JCGM 100:2008, GUM 1995, Sep. 2008, p. 134.
- [104] S. Stamp, H. Altamirano-Medina and R. Lowe, 'Measuring and accounting for solar gains in steady state whole building heat loss measurements,' *Energy and Buildings*, vol. 153, pp. 168–178, 15th Oct. 2017, ISSN: 0378-7788. DOI: 10.1016/j.enbuild.2017.06.063.
- [105] S. Yoon and Y. Yu, 'Hidden factors and handling strategies on virtual in-situ sensor calibration in building energy systems: Prior information and cancellation effect,' *Applied Energy*, vol. 212, pp. 1069–1082, 15th Feb. 2018, ISSN: 0306-2619. DOI: 10.1016/j.apenergy.2017.12.077.
- [106] K. O. Roper and R. P. Payant, *The Facility Management Handbook*, 4th ed. New York: American Management Association, 2014, ISBN: 978-0-8144-3215-0.
- [107] M. Basarkar, X. Pang, L. Wang, P. Haves and T. Hong, 'Modeling and simulation of HVAC faults in energyplus,' presented at the Building Simulation 2011 | IBPSA: 12th Conference of International Building Performance Simulation Association, Sydney, Australia, 14th Nov. 2011, pp. 2897–2903.

- [108] R. Zhang and T. Hong, 'Modeling of HVAC operational faults in building performance simulation,' *Applied Energy*, vol. 202, pp. 178–188, 15th Sep. 2017, ISSN: 0306-2619. DOI: 10.1016/j.apenergy.2017.05.153.
- [109] J. Verhelst, G. V. Ham, D. Saelens and L. Helsen, 'Economic impact of persistent sensor and actuator faults in concrete core activated office buildings,' *Energy and Buildings*, vol. 142, pp. 111–127, 2017, ISSN: 0378-7788. DOI: <https://doi.org/10.1016/j.enbuild.2017.02.052>.
- [110] K. Roth, D. Westphalen, P. Llana and M. Feng, 'The energy impact of faults in u.s. commercial buildings,' in *International Refrigeration and Air Conditioning Conference*, Lafayette, USA, 12th Jul. 2014.
- [111] J. Y. Kao and E. T. Pierce, 'Sensor errors: Their effects on building energy consumption,' *ASHRAE J.; (United States)*, vol. 25:12, 1st Dec. 1983.
- [112] W. Kim, 'Fault detection and diagnosis for air conditioners and heat pumps based on virtual sensors,' Ph.D. dissertation, Purdue University, Ann Arbor, United States, 2013, 307 pp.
- [113] W. Kim and S. Katipamula, 'A review of fault detection and diagnostics methods for building systems,' *Science and Technology for the Built Environment*, vol. 24, no. 1, pp. 3–21, 2nd Jan. 2018, ISSN: 2374-4731. DOI: 10.1080/23744731.2017.1318008.
- [114] S. Katipamula and M. R. Brambley, 'Review article: Methods for fault detection, diagnostics, and prognostics for building systems-a review, part i,' *HVAC&R Research*, vol. 11, no. 1, pp. 3–25, 1st Jan. 2005, ISSN: 1078-9669. DOI: 10.1080/10789669.2005.10391123.
- [115] ———, 'Review article: Methods for fault detection, diagnostics, and prognostics for building systems-a review, part II,' *HVAC&R Research*, vol. 11, no. 2, pp. 169–187, 1st Apr. 2005, ISSN: 1078-9669. DOI: 10.1080/10789669.2005.10391133.
- [116] 'OSTI.GOV | OSTI, US dept of energy office of scientific and technical information,' [Online]. Available: <https://www.osti.gov/> (visited on 16/05/2018).
- [117] R. Jack, D. Loveday, D. Allinson and K. Lomas, 'First evidence for the reliability of building co-heating tests,' *Building Research & Information*, vol. 46, no. 4, pp. 383–401, 19th May 2018, ISSN: 0961-3218. DOI: 10.1080/09613218.2017.1299523.
- [118] M. P. Modera, 'Electric co-heating: A method for evaluating seasonal heating efficiencies and heat loss rates in dwellings,' Lawrence Berkeley Laboratory of University of California/Berkeley prepared for US Department of Energy under Contract No. W-7405-ENG-48, California, Florida, USA, Mar. 2018.
- [119] L. S. Palmiter, L. B. Hamilton and M. J. Holtz, 'Low cost performance evaluation of passive solar buildings,' Solar Energy Research Institute prepared for The U.S. Department of Energy under Contract No. EG-77-C-01-4042, Golden, CO, USA, SERI/RR-63-223, Oct. 1979. DOI: 10.2172/5857852.
- [120] R. C. Sonderegger, P. E. Condon and M. P. Modera, 'In-situ measurements of residential energy performance using electric co-heating,' California Univ., Berkeley (USA). Lawrence Berkeley Lab., LBL-10117; CONF-800206-4, Jan. 1980.

- [121] R. Everett, A. Horton, J. Doggart and J. Willoughby, 'Linford low energy houses, technical report,' Energy Technology Support Unit (ETSU) prepared for The U.S. Department of Energy under Contract No. E/SA/CON/1025/174/020, ERG 50. ETSU-S-1025, Jan. 1985.
- [122] H. Madsen and J. Holst, 'Estimation of continuous-time models for the heat dynamics of a building,' *Energy and Buildings*, vol. 22, no. 1, pp. 67–79, 1st Mar. 1995, ISSN: 0378-7788. DOI: 10.1016/0378-7788(94)00904-X.
- [123] V. Richalet, F. P. Neirac, F. Tellez, J. Marco and J. J. Bloem, 'HELP (house energy labeling procedure): Methodology and present results,' *Energy and Buildings*, vol. 33, no. 3, pp. 229–233, 1st Feb. 2001, ISSN: 0378-7788. DOI: 10.1016/S0378-7788(00)00086-4.
- [124] V. D. Meulenaer, J. V. d. Veken, G. Verbeeck and H. Hens, 'Comparison of measurements and simulations of passive house,' in *9th International IBPSA Building Simulation Conference*, Montréal, Canada, 15th Aug. 2005, pp. 769–775. DOI: 10.4028/www.scientific.net/AMR.1041.158.
- [125] O. Guerra-Santin, C. Tweed, H. Jenkins and S. Jiang, 'Monitoring the performance of low energy dwellings: Two UK case studies,' *Energy and Buildings*, vol. 64, pp. 32–40, 1st Sep. 2013, ISSN: 0378-7788. DOI: 10.1016/j.enbuild.2013.04.002.
- [126] G. Lethé, 'A new experiment and modelling work to jointly identify the building envelope's thermal parameters and a physical solar aperture,' in *Sustainable Ecological Engineering Design*, Springer, Cham, 2015, pp. 163–180, ISBN: 978-3-319-32645-0 978-3-319-32646-7.
- [127] D. Rodriguez-Gracia, J. A. Piedra-Fernández and L. Iribarne, 'Adaptive domotic system in green buildings,' in *2015 IIAI 4th International Congress on Advanced Applied Informatics*, Okayama, Japan, 12th Jul. 2015, pp. 593–598. DOI: 10.1109/IIAI-AAI.2015.281.
- [128] R. Jack, D. Loveday, D. Allinson and K. Lomas, 'Quantifying the effect of window opening on the measured heat loss of a test house,' in *Sustainable Ecological Engineering Design*, Springer, Cham, 2015, pp. 183–196, ISBN: 978-3-319-32645-0 978-3-319-32646-7. DOI: 10.1007/978-3-319-32646-7_13.
- [129] M.-B. Carutasiu, V. Tanasiev, C. Ionescu, A. Danu, H. Necula and A. Badea, 'Reducing energy consumption in low energy buildings through implementation of a policy system used in automated heating systems,' *Energy and Buildings*, vol. 94, pp. 227–239, 1st May 2015, ISSN: 0378-7788. DOI: 10.1016/j.enbuild.2015.03.008.
- [130] E. Latif, M. Lawrence, A. Shea and P. Walker, 'In situ assessment of the fabric and energy performance of five conventional and non-conventional wall systems using comparative coheating tests,' *Building and Environment*, vol. 109, pp. 68–81, 15th Nov. 2016, ISSN: 0360-1323. DOI: 10.1016/j.buildenv.2016.09.017.
- [131] D. Farmer, D. Johnston and D. Miles-Shenton, 'Obtaining the heat loss coefficient of a dwelling using its heating system (integrated coheating),' *Energy and Buildings*, vol. 117, pp. 1–10, 1st Apr. 2016, ISSN: 0378-7788. DOI: 10.1016/j.enbuild.2016.02.013.
- [132] A. Marshall, R. Fitton, W. Swan, D. Farmer, D. Johnston, M. Benjaber and Y. Ji, 'Domestic building fabric performance- closing the gap between the in situ measured and modelled performance,'

- Energy and Buildings*, vol. 150, pp. 307–317, 1st Sep. 2017, ISSN: 0378-7788. DOI: 10.1016/j.enbuild.2017.06.028.
- [133] D. Farmer, C. Gorse, W. Swan, R. Fitton, M. Brooke-Peat, D. Miles-Shenton and D. Johnston, 'Measuring thermal performance in steady-state conditions at each stage of a full fabric retrofit to a solid wall dwelling,' *Energy and Buildings*, vol. 156, pp. 404–414, 1st Dec. 2017, ISSN: 0378-7788. DOI: 10.1016/j.enbuild.2017.09.086.
- [134] S. Roels, P. Bacher, G. Bauwens, S. Castaño, M. J. Jiménez and H. Madsen, 'On site characterisation of the overall heat loss coefficient: Comparison of different assessment methods by a blind validation exercise on a round robin test box,' *Energy and Buildings*, vol. 153, pp. 179–189, 15th Oct. 2017, ISSN: 0378-7788. DOI: 10.1016/j.enbuild.2017.08.006.
- [135] F. Alzetto, D. Farmer, R. Fitton, T. Hughes and W. Swan, 'Comparison of whole house heat loss test methods under controlled conditions in six distinct retrofit scenarios,' *Energy and Buildings*, vol. 168, pp. 35–41, 1st Jun. 2018, ISSN: 0378-7788. DOI: 10.1016/j.enbuild.2018.03.024.
- [136] P. Fornasini, *The Uncertainty in Physical Measurements: An Introduction to Data Analysis in the Physics Laboratory*. New York, NY, USA: Springer Science+Business Media, LLC, 2008, 288 pp., ISBN: 978-0-387-78649-0.
- [137] Q. Kong and B. Yu, 'Numerical study on temperature stratification in a room with underfloor air distribution system,' *Energy and Buildings*, vol. 40, no. 4, pp. 495–502, 1st Jan. 2008, ISSN: 0378-7788. DOI: 10.1016/j.enbuild.2007.04.008.
- [138] (23rd Sep. 2020). 'SCADA,' Wikipedia, la enciclopedia libre, [Online]. Available: <https://en.wikipedia.org/wiki/SCADA> (visited on 27/09/2020).
- [139] C. Giraldo-Soto, A. Erkoreka, A. Barragan and L. Mora, 'Dataset of an in-use tertiary building collected from a detailed 3d mobile monitoring system and building automation system for indoor and outdoor air temperature analysis,' *Data in Brief*, vol. 31, p. 105 907, 1st Aug. 2020, ISSN: 2352-3409. DOI: 10.1016/j.dib.2020.105907.
- [140] 'CO₂, RH and t room transmitter for indoor applications,' [Online]. Available: <https://www.epluse.com/en/products/co2-measurement/co2-carbon-dioxide-transmitters/ee800/> (visited on 05/01/2020).
- [141] 'Digital humidity and temperature probe with modbus RTU,' [Online]. Available: <https://www.epluse.com/en/products/humidity-instruments/humidity-measuring-modules/ee071/> (visited on 05/01/2020).
- [142] 'Modbus RTU humidity and temperature probe,' [Online]. Available: <https://www.epluse.com/en/products/humidity-instruments/humidity-measuring-modules/ee072/> (visited on 22/07/2020).
- [143] 'Room air conditions - ahlborn meß- und regelungstechnik GmbH,' [Online]. Available: https://www.ahlborn.com/en_UK/products/room-air-conditions (visited on 11/02/2020).
- [144] 'Pasarelas - DEEI,' [Online]. Available: https://deei.es/?product_cat=pasarelas (visited on 10/02/2020).

- [145] 'Professional measuring instrument and data logger ALMEMO® 2590a - ahlborn meß- und regelungstechnik GmbH,' [Online]. Available: https://www.ahlborn.com/en_UK/products/professional-measuring-instrument-and-data-logger-almemo-2590a (visited on 11/02/2020).
- [146] 'Modbus TCP & RTU master to KNX TP gateway,' [Online]. Available: <https://www.intesis.com/products/protocol-translator/modbus-gateways/modbus-rtu-tcp-knx-ibox-knx-mbm?ordercode=INKNXMBM1000000> (visited on 11/02/2020).
- [147] 'IPAS - smart building concepts - ComBridge studio evolution | ipas-products,' [Online]. Available: <https://ipas-products.de/en/products/combridge-visualization/combridge-studio-evolution/> (visited on 11/02/2020).
- [148] C. Giraldo-Soto, A. Erkoreka, L. Mora, I. Uriarte and L. A. Del Portillo, 'Monitoring system analysis for evaluating a building's envelope energy performance through estimation of its heat loss coefficient,' *Sensors*, vol. 18, no. 7, p. 2360, Jul. 2018. DOI: 10.3390/s18072360.
- [149] C. Giraldo-Soto, A. Erkoreka, A. Barragan and L. Mora, 'Data repository. dataset of an in-use tertiary building collected from a detailed 3d mobile monitoring system and building automation system for indoor and outdoor air temperature analysis,' vol. 3, 5th Jun. 2020. DOI: 10.17632/fc2r9rdxht.3.
- [150] 'ScienceDirect.com | science, health and medical journals, full text articles and books,' [Online]. Available: <https://www.sciencedirect.com/> (visited on 09/02/2020).
- [151] 'IEEE xplore digital library,' [Online]. Available: <https://ieeexplore.ieee.org/Xplore/home.jsp> (visited on 09/02/2020).
- [152] 'Taylor & francis group,' [Online]. Available: <https://www.tandfonline.com/> (visited on 10/09/2020).
- [153] *Handbook: Fundamentals*, 2017.
- [154] *Handbook: HVAC applications*, 2018.
- [155] *Handbook: HVAC refrigeration*, 2019.
- [156] *Handbook: HVAC systems and equipment*, 2016.
- [157] 'ISO. building environment design - indoor air quality - methods of expressing the quality of indoor air for human occupancy; ISO standard 16814,' AENOR, Genoa, 2008.
- [158] 'ISO. energy performance of buildings - overall energy performance assessment procedures - part 2: Guideline for using indoor environmental input parameters for the design and assessment of energy performance of buildings; ISO standard 17772-2,' AENOR, Genoa, 2018.
- [159] 'ISO. energy performance of buildings - overarching EPB assessment - part 1: General framework and procedures; ISO standard 52000-1,' AENOR, Genoa, 2017.
- [160] 'ISO. heating and cooling systems in buildings -method for calculation of the system performance and system design for heat pump systems - part 1: Design and dimensioning; ISO standard 13612-1,' AENOR, Genoa, 2014.
- [161] 'ISO. heating and cooling systems in buildings - method for calculation of the system performance and system design for heat pump systems - part 2: Energy calculation; ISO standard 13612-2,' AENOR, Genoa, 2014.

- [162] 'ISO. heating systems in buildings - method and design for calculation of the system energy performance - combustion systems (boilers); ISO standard 13675,' AENOR, Genoa, 2013.
- [163] 'Obras correspondientes a la rehabilitación energética del edificio situado en la calle correría, 119 de vitoria-gasteiz,' [Online]. Available: <https://www.contratacion.euskadi.eus/w32-1084/es/v79aWar/comunJSP/v79aSubmitMostrarHistoricoExpediente.do?a=Anuncio&b=83115&R01HNoPortal=true> (visited on 04/09/2020).
- [164] 'V sudoe interreg - interreg program sudoe - home,' [Online]. Available: <https://interreg-sudoe.eu/gbr/home> (visited on 04/06/2019).
- [165] 'V sudoe interreg - interreg program sudoe - co-creation of energetically efficient territorial solutions of patrimonial residential habitat ecorenovation in SUDOE historical centres,' [Online]. Available: <https://www.interreg-sudoe.eu/gbr/projects/the-approved-projects/170-co-creation-of-energetically-efficient-territorial-solutions-of-patrimonial-residential-habitat-ecorenovation-in-sudoe-historical-centres> (visited on 04/09/2020).
- [166] 'Accueil - Présentation du projet d'expérimentation Ener'pat Sudoe,' Ener'pat Sudoe, [Online]. Available: <https://www.enerpatsudoe.fr/> (visited on 04/09/2020).
- [167] E. Sirombo, M. Filippi, A. Catalano and A. Sica, 'Building monitoring system in a large social housing intervention in northern italy,' *Energy Procedia*, Beyond NZEB Buildings (AiCARR 50th International Congress, Matera (I), 10-11 May 2017), vol. 140, pp. 386–397, 1st Dec. 2017, ISSN: 1876-6102. DOI: 10.1016/j.egypro.2017.11.151.
- [168] 'ENEDI (UPV-EHU) research group's introduction,' ENEDI (UPV-EHU) Research Group, [Online]. Available: <https://www.ehu.eus/en/web/enedi/presentation> (visited on 04/06/2019).
- [169] A. Egusquiza, S. Ginestet, J. C. Espada, I. Flores-Abascal, C. Garcia-Gafaro, C. Giraldo-Soto, S. Claude and G. Escadeillas, 'Co-creation of local eco-rehabilitation strategies for energy improvement of historic urban areas,' *Renewable and Sustainable Energy Reviews*, vol. 135, p. 110 332, 1st Jan. 2021, ISSN: 1364-0321. DOI: 10.1016/j.rser.2020.110332.
- [170] 'UNE-EN 13829:2002 aislamiento térmico. determinación de la est...,' [Online]. Available: <https://www.une.org/encuentra-tu-norma/busca-tu-norma/norma?c=N0026148> (visited on 30/10/2020).
- [171] *AENOR norma e741-11(2017). standard test method for determining air change in a single zone by means of a tracer gas dilution.*
- [172] 'BECKHOFF new automation technology,' [Online]. Available: <https://www.beckhoff.com> (visited on 23/09/2020).
- [173] 'Inicio - UPV/EHU,' [Online]. Available: <https://www.ehu.eus/es/> (visited on 12/10/2020).
- [174] 'Tecnalia. inspiring business,' [Online]. Available: <https://www.tecnalia.com/en/> (visited on 12/10/2020).

Appendix A

MMS' sensor installed in the in-use tertiary building

Tripod Number	Sensor Reference	Height	Sensor ID	Sensor Manufacture Reference
T1	T1.hg.1	hg	1	EE800-M12J3
	T1.md.2	md	2	EE800-M12J3
	T1.lw.3	lw	3	EE800-M12J3
T2	T2.hg.4	hg	4	EE800-M12J3
	T2.md.5	md	5	EE800-M12J3
	T2.lw.6	lw	6	EE800-M12J3
T3	T3.hg.7	hg	7	EE800-M12J3
T4	T4.hg.8	hg	8	EE800-M12J3
	T4.md.9	md	9	EE800-M12J3
	T4.lw.10	lw	10	EE800-M12J3
T5	T5.lw.11	lw	11	EE800-M12J3
T6	T6.hg.12	hg	12	EE800-M12J3
	T6.md.13	md	13	EE800-M12J3
	T6.lw.14	lw	14	EE800-M12J3
T7	T7.hg.15	hg	15	EE800-M12J3
	T7.md.30	md	30	WBGT - PT100
	T7.lw.16	lw	16	EE800-M12J3
T8	T8.hg.17	lw	17	EE800-M12J3
	T8.md.19	hg	19	EE071-HTPC*
	T8.lw.18	md	18	EE800-M12J3

* EE071-HTP with radiation shielding without mechanical ventilation [139].

Office Typology	Number of WS	WS Reference	Sensor Reference
OT1	6	2C1	T8.hg.17 - T8.md.19 - T8.lw.18
		2C1.1	T1.hg.1 - T1.md.2 - T1.lw.3
		2C1.2	No tripod
		2C1.3	T5.lw.11
		2C1.4	T3.hg.7
		2C1.5	T2.hg.4 - T2.md.5 - T2.lw.6
		2C1.6	T4.hg.8 - T4.md.9 - T4.lw.10
OT2	1	2C2	T7.hg.15 - T7.md.30 - T7.lw.16
		2C2.1	T6.hg.12 - T6.md.13 - T6.lw.14
OT3	8	2C3	T8.hg.17 - T8.md.19 - T8.lw.18
		2C3.2	T6.hg.12 - T6.md.13 - T6.lw.14
		2C3.3	T4.hg.8 - T4.md.9 - T4.lw.10
		2C3.4	T7.hg.15 - T7.md.30 - T7.lw.16
		2C3.5	T2.hg.4 - T2.md.5 - T2.lw.6
		2C3.6	No tripod
		2C3.7	T5.lw.11
		2C3.8	T3.hg.7
		2C3.9	T1.hg.1 - T1.md.2 - T1.lw.3
OT4	3	3C1	T1.hg.1 - T1.md.2 - T1.lw.3 - T2.hg.4 - T2.md.5 - T2.lw.6 - T4.hg.8 - T4.md.9 - T4.lw.10 - T6.hg.12 - T6.lw.14 - T7.hg.15 - T7.md.30 - T7.lw.16 - T8.hg.17 - T8.md.19 - T8.lw.18
		3C1.1	T5.lw.11
		3C1.2	T3.hg.7
		3C1.3	No tripod

Table A.3: Sensor layout by OT in each OT volume [139].



Figure A.5: Interior 3D MMS tripods and sensors all together during the TT test [139].

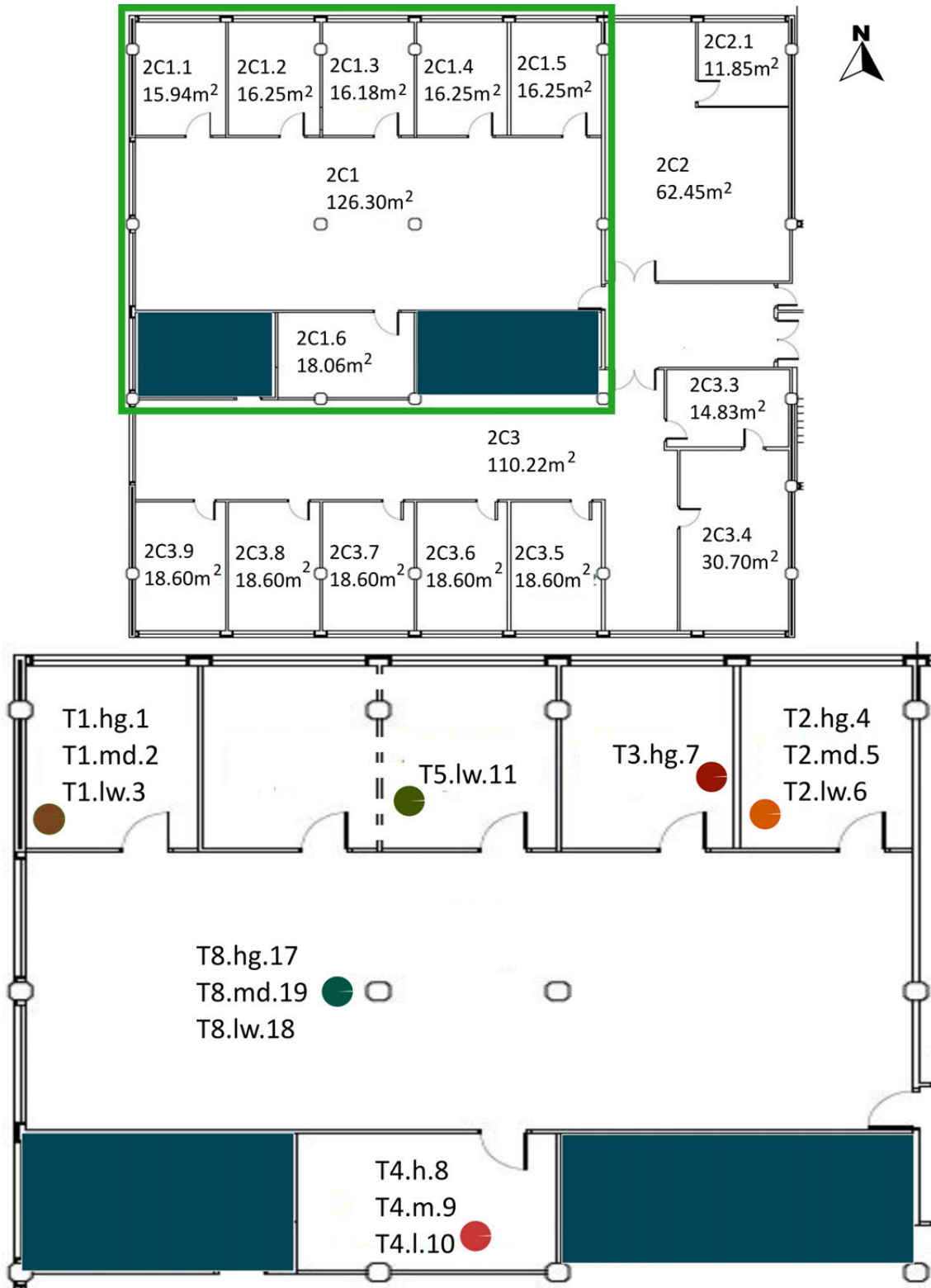


Figure A.6: OT1 sensor layout, located in F2. Based on A2PBEER project's architecture plans [76] [139].

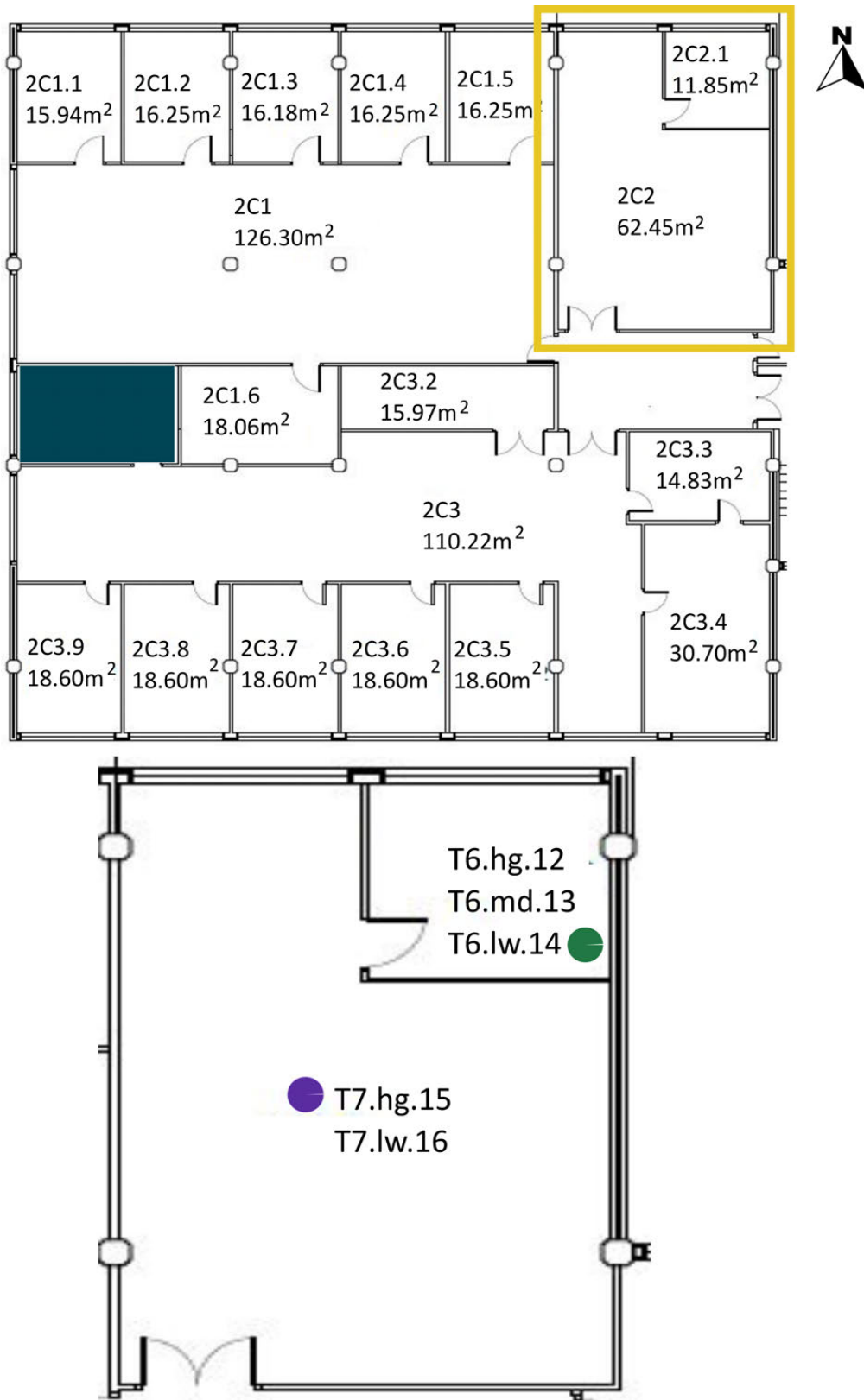


Figure A.7: OT2 sensor layout, located in F2. Based on A2PBEER project's architecture plans [76] [139].

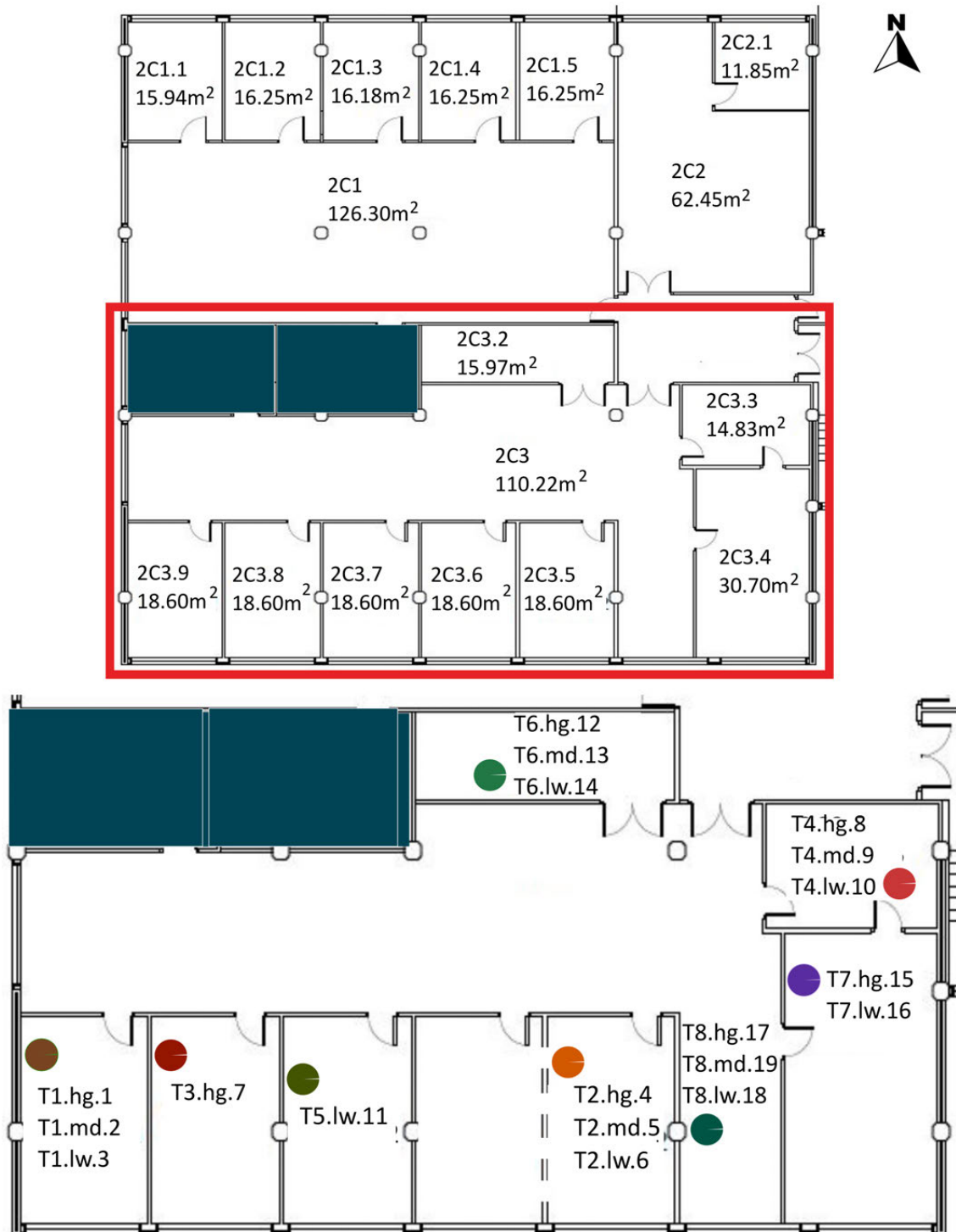


Figure A.8: OT3 sensor layout, located in F2. Based on A2PBEEER project's architecture plans [76] [139].

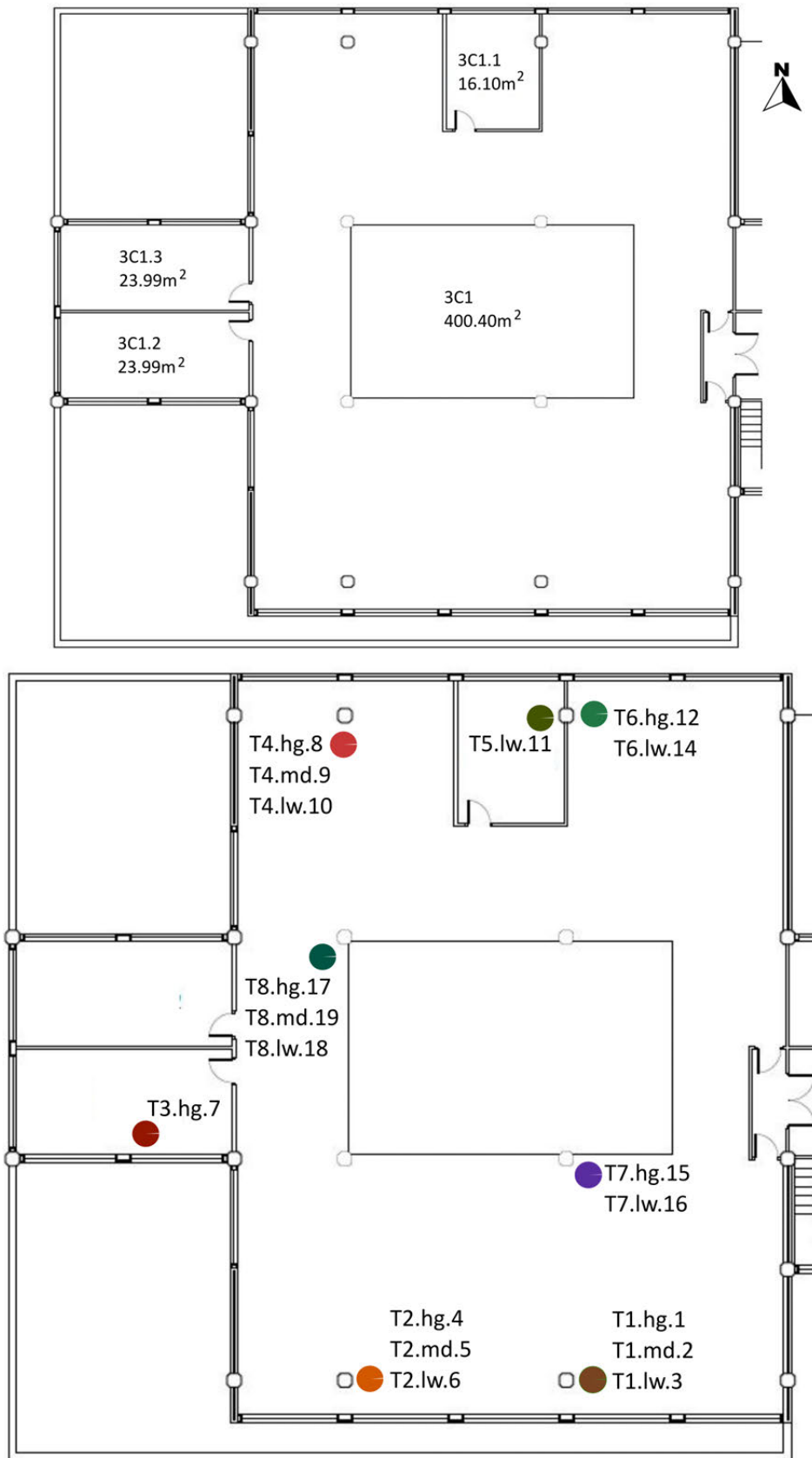


Figure A.9: OT4 sensor layout, located in F3. Based on A2PBEER project's architecture plans [139].

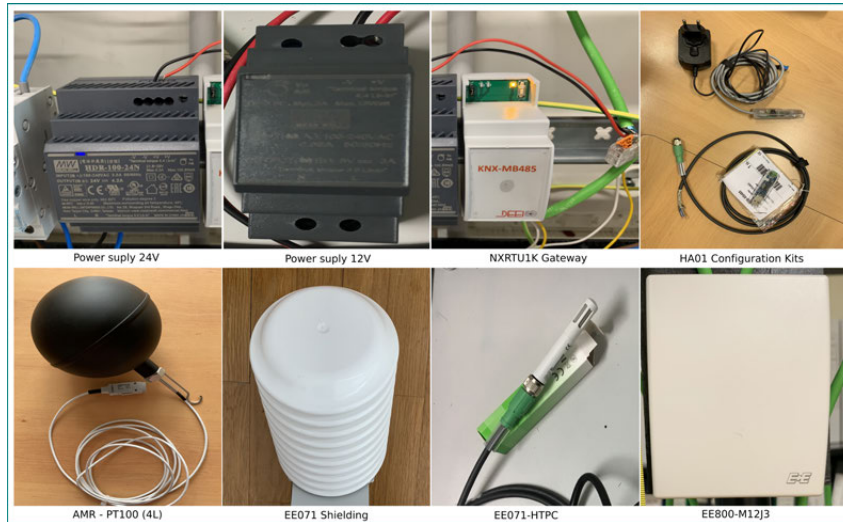


Figure A.10: Sensors and Hardware installed in UPV/EHU administrator building [139].



Figure A.11: Installed interior MMS' pictures [139].

Sensor Reference	Façade (F)/ Roof (R)	Cardinal Floor Orientation	Sensor ID	Sensor Manufacture Reference	
E.F1.nt.20	F	1	nt	20	EE071-HTP*
E.F1.nt.21	F	1	nt	21	EE071-HTP*
E.F1.wt.22	F	1	wt	22	EE071-HTP*
E.F1.st.23	F	1	st	23	EE071-HTP*
E.F2.st.24	F	2	st	24	EE071-HTP*
E.R3.st.25	R	3	st	25	EE071-HTP**
E.R3.st.26	R	3	st	26	EE071-HTP*
E.R3.nt.27	R	3	nt	27	EE071-HTP*

*EE071-HTP protected with solar radiation shielding without mechanical ventilation.

**EE071-HTP protected with solar radiation shielding with mechanical ventilation.

Table A.4: Exterior (E) Layout of EE071-HTPC sensors installed around the building envelope [139].



Figure A.12: Exterior Together (ET) test pictures [139].

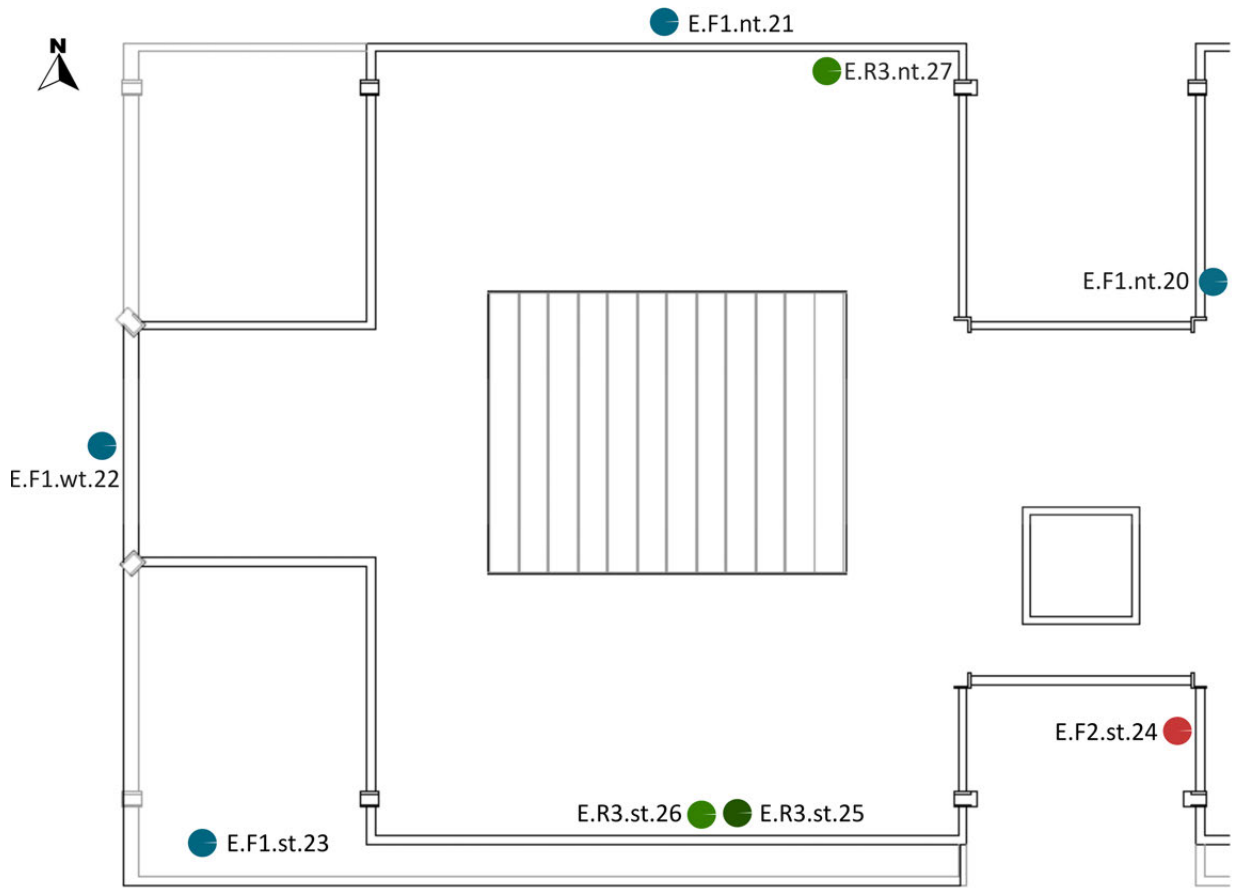


Figure A.13: Exterior MMS' layout [139].

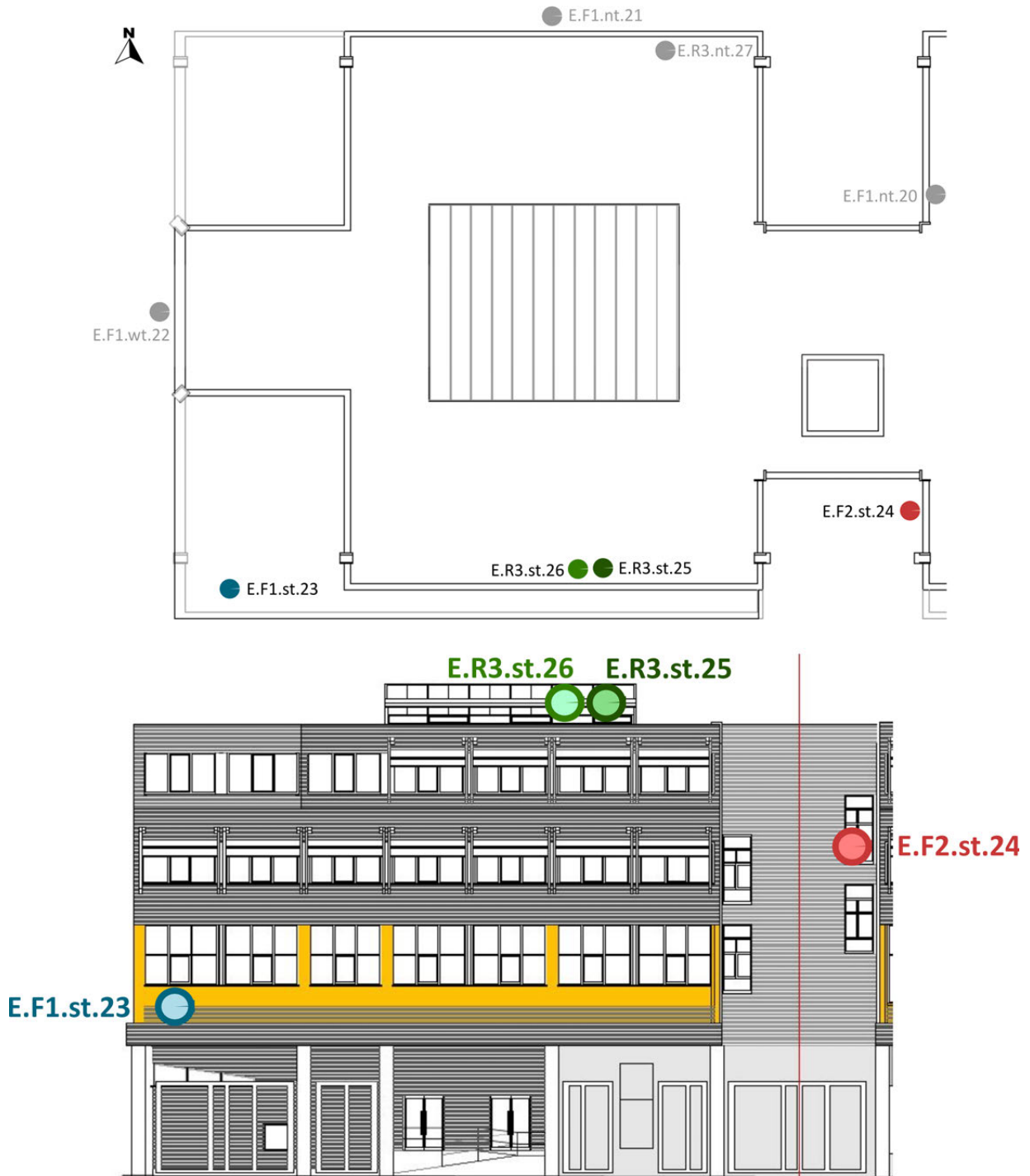


Figure A.14: Southern sensors layout of Exterior MMS [139].

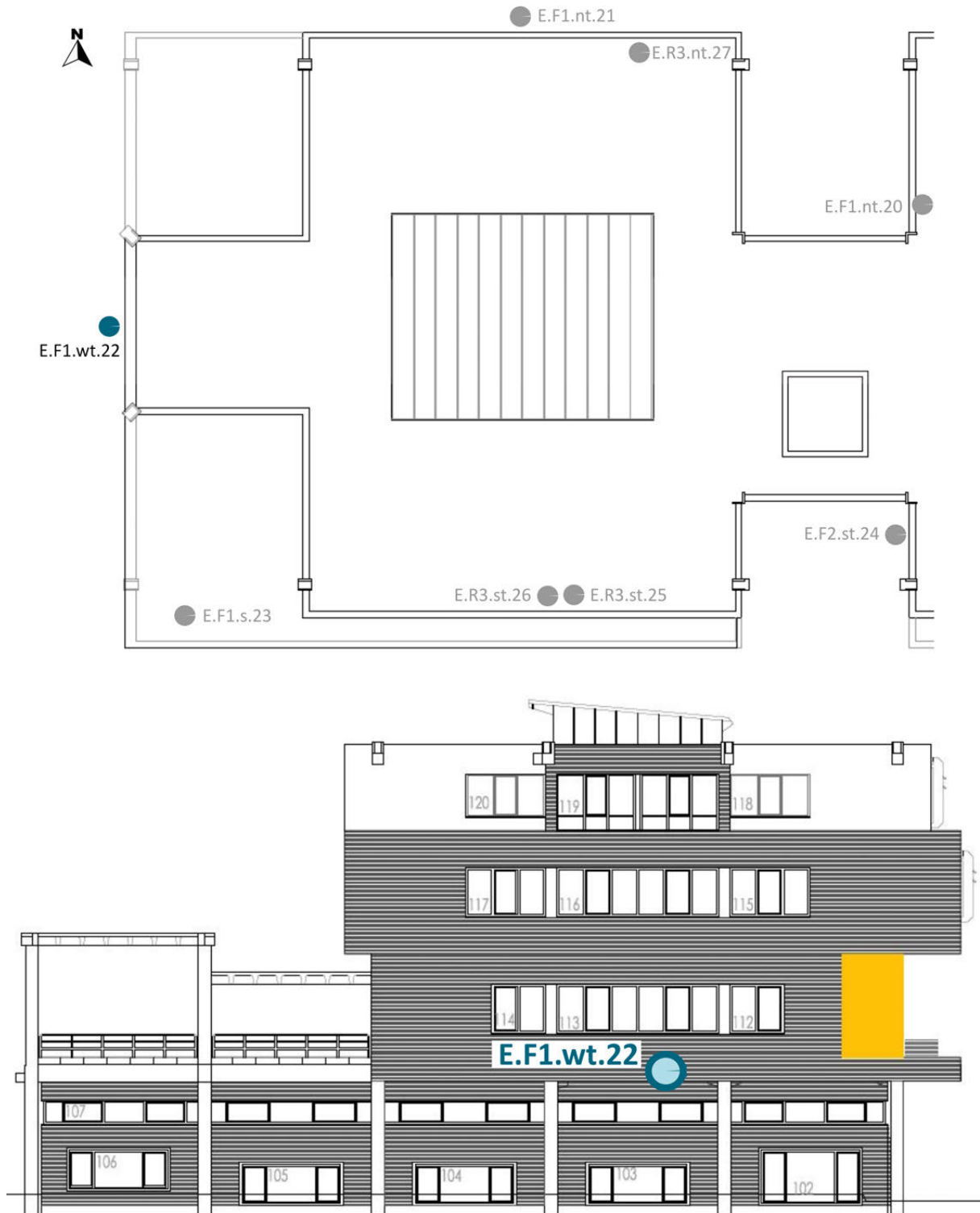


Figure A.15: Western sensor layout of Exterior MMS [139].

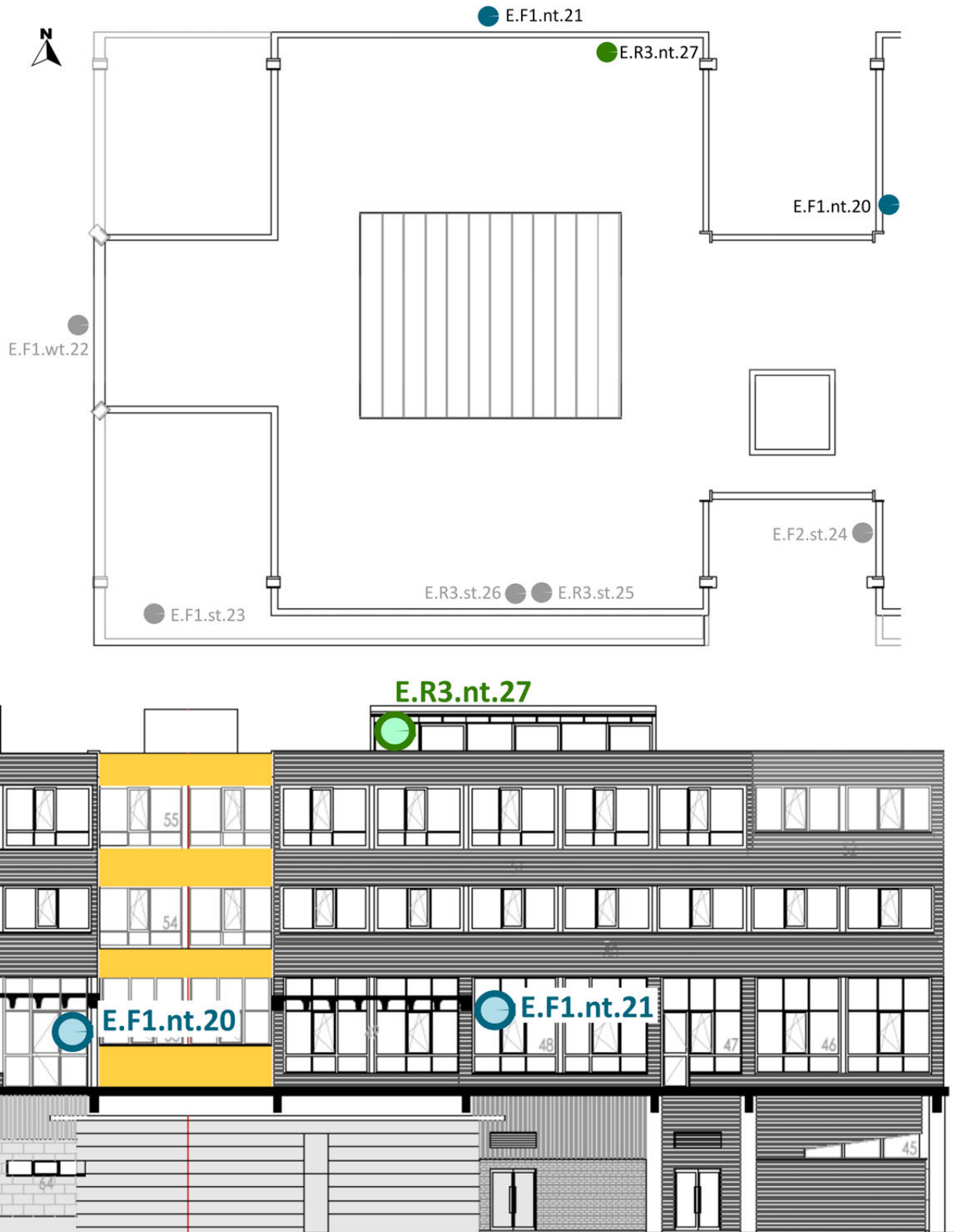


Figure A.16: Northern sensors layout of Exterior MMS [139].



Figure A.17: Installed exterior MMS sensors' pictures [139].

Sensor Reference	Measure	Accuracy	Protocol Communication
KAMSTRUP: Multical 602	Heat Energy and/or power	ET $\pm(0.4 + 4/\Delta T)\%$	Digital - KNX
ABB:a. A43-211, b.EM/S 3.16.1	a. Lighting power/consumption, b. Rest of electricity power/consumption except a, Total power/consumption: a+b	a. $\pm 2\%$, b. $\pm 1\%$, Total consumption $\pm 3\%$	Digital - KNX
	Illuminance (lux)	—	
Energy Consumption	Air Quality (ppm CO ₂)	$\pm 1\%$ Measurement Error	Digital - KNX
	Temperature (°C)	± 0.5 °C	
	Relative Humidity (%)	$\pm 3\%$ RH	
	Illuminance (lux)	$\pm 35\%$ at 0...150,000 lux	
ELSNER:3595 Sun tracer	Temperature (°C)	± 0.5 °C	Digital - KNX
	Wind Speed (m/s)	$\pm 25\%$ at 0...15 m/s	
	Rain (yes/no)	—	
ARCUS: SK01-TFK-AFF	Temperature (°C)	± 0.5 °C	Digital - KNX
	Relative Humidity (%)	Relative Humidity (%)	
	Temperature (°C)	± 0.4 °C (5 to 60°C), else ± 0.8 °C	
ARCUS:SK10-THC-CO ₂ -KF	Relative Humidity (%)	$\pm 3\%$ RH	Digital - KNX
	Air Quality (ppm CO ₂)	$\pm(50\text{ppm} + 3\% \text{ Measurement})$	
ARCUS:SK08-GLBS	Horizontal Global Solar Radiation (W/m^2)	$\pm 5\%$	Digital - KNX

Table A.1: BAS sensors installed at the UPV/EHU administrative building in Leioa: Reference, measurements, accuracies and protocol communication.

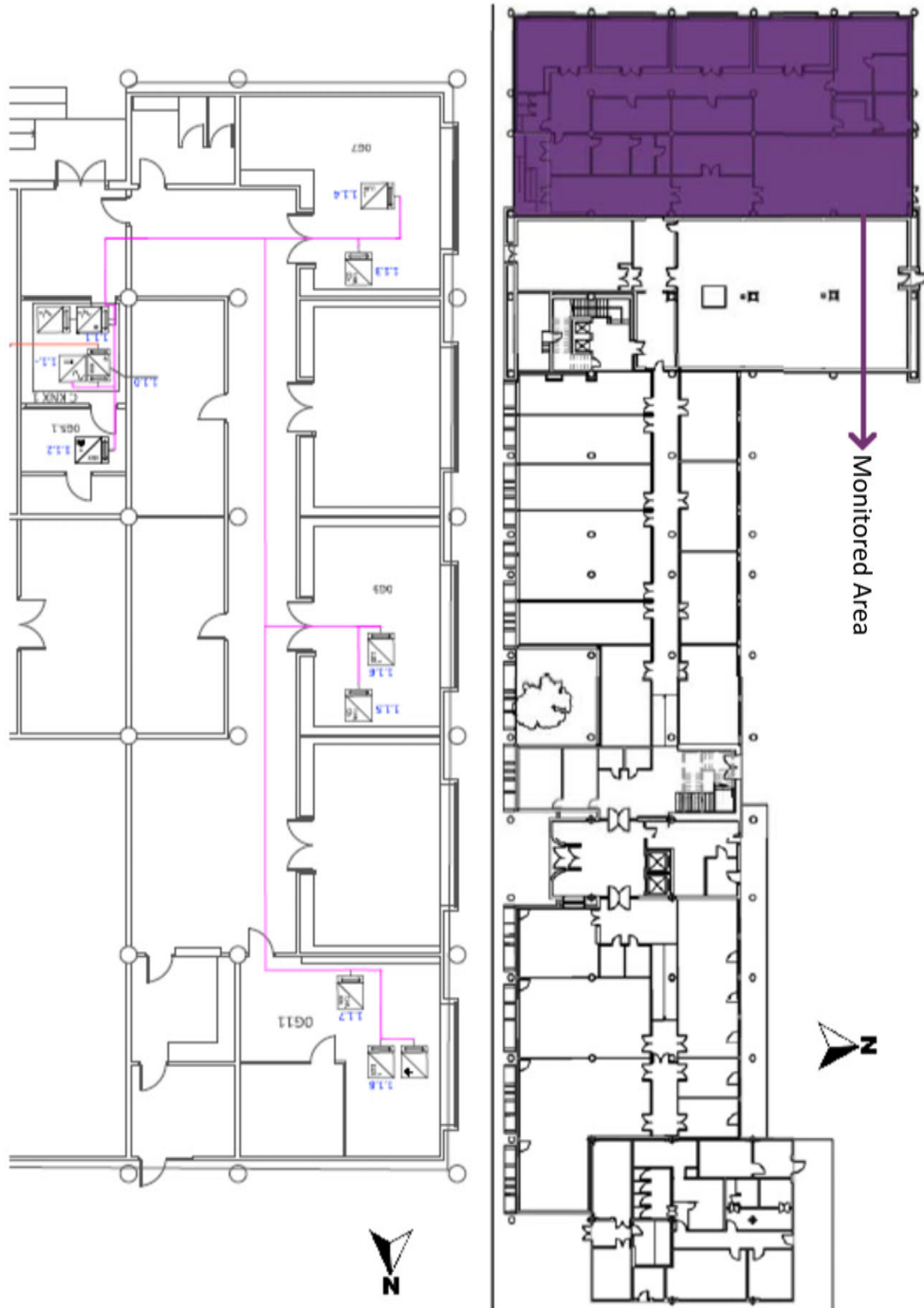


Figure A.1: F0 of the UPV/EHU admin building in Leioa. Based on A2PBBER project's architecture plans [76].

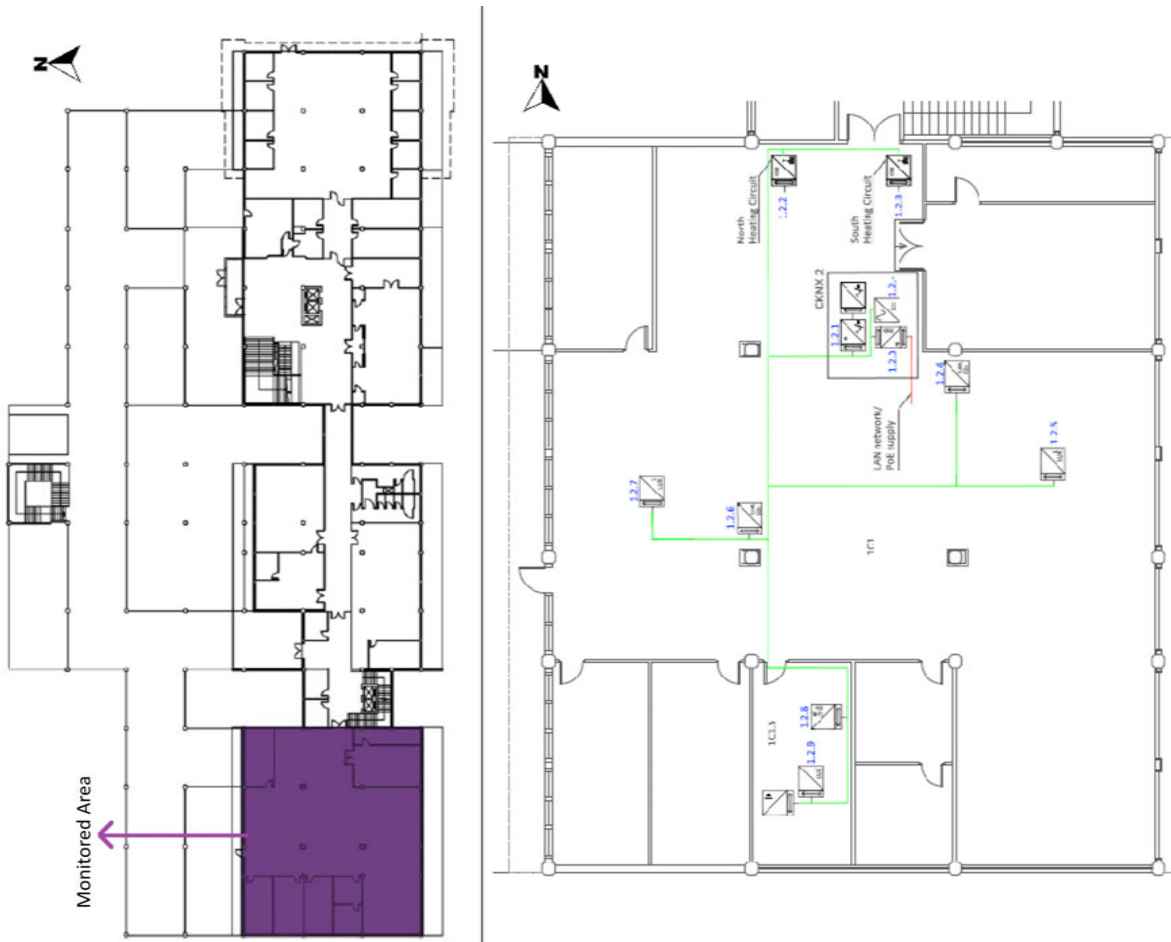


Figure A.2: F1 of the UPV/EHU admin building in Leioa. Based on A2PBEER project's architecture plans [76].

Figure A.3: F2 of the UPV/EHU admin building in Leioa. Includes the position of the three selected measurement points of the existing BAS referred to in Table A.6. Based on A2PBEEER project's architecture plans [76].





Figure A.4: F3 of the UPV/EHU admin building in Leioa, including the position of the three selected measurement points of the existing BAS referred to in Table A.6. Note that T9.md.142143 is the signal created by adding the measurements T9.md.142 and T9.md.143. Based on A2PBEER project's architecture plans [76].

File Name Codes of Interior Mobile Monitoring System (MMS)						
OT#: Tp#.H.ID#_XY(SI)_w# // TT#.Tp#.H.ID#_XY(SI)_w#						
File Column Codes of Interior Mobile Monitoring System (MMS)						
OT#: Tp#.H.ID#_XY(SI) // TT#.Tp#.H.ID#_XY(SI)						
Codes of Interior MMS Sensor (Sensor Reference)						
T#.H.ID#						
Office Typology (OT) and Tripod Together (TT) Test** (OT#)/(TT)	Tripod Reference (T#)	Height Location (H)	ID Sensor (ID#)	Sensor Measurement (XY)* and its International System Unit (SI)** (XY(SI))	Week of Year w#	
OT1	T1	md	2	T(C)	w#	
	T1	lw	3	T(C)	w#	
	T2	hg	4	T(C)	w#	
	T2	md	5	T(C)	w#	
	T2	lw	6	T(C)	w#	
	T3	hg	7	T(C)	w#	
	T4	hg	8	T(C)	w#	
	T4	md	9	T(C)	w#	
	T4	lw	10	T(C)	w#	
	T5	lw	11	T(C)	w#	
	T6	hg	12	T(C)	w#	
	T6	md	13	T(C)	w#	
OT4	T6	lw	14	T(C)	w#	
	T7	hg	15	T(C)	w#	
	T7	md	30	Trad(C)	w#	
TT	T7	lw	16	T(C)	w#	
	T8	hg	17	T(C)	w#	
	T8	mg	19	T(C)	w#	
	T8	lw	18	T(C)	w#	

*Sensor measurement: Air Temperature (T) and Radiant Temperature (Trad).

**SI: Symbol (C) represents Degrees Celsius [°C].

***The OT test is the information collected from the interior MMS installed in four offices, where each tripod has been distributed in different locations within the monitored office.

The TT test is the information collected from interior MMS where the tripods have been situated in the same place so that the twenty sensors have been measuring together at the same height.

Table A.5: Interior MMS codes: file name codes, file column code and sensor reference [139].

File Name Codes of Exterior Mobile Monitoring System (MMS)									
E.F#.CO.ID#_XY(SI)_w# // E.R#.CO.ID#_XY(SI)_w# // ETR3.CO.ID#_XY(SI)_w#									
File Column Codes of Exterior Mobile Monitoring System (MMS)									
E.F#.CO.ID#_XY(SI) // E.R#.CO.ID#_XY(SI) // ETR3.CO.ID#_XY(SI)									
Codes of Interior MMS Sensor (Sensor Reference)									
F#.CO.ID# // R#.CO.ID#									
Exterior (E) and Exterior Together (ET) Test* **	Façade(F)/Roof (R)/ Location (F/R)	Floor (#) Roof(#)	Cardinal Orientation (CO)	Sensor ID (ID#)	Sensor Measurement (XY)* and its International System Unit (SI)** (XY(SI))	Week of Year (w#) Week of Year (w#)			
F	1	1	nt	20	T(C)	w#			
F	1	1	nt	21	T(C)	w#			
E	F	1	wt	22	T(C)	w#			
F	1	1	st	23	T(C)	w#			
ET	F	2	st	24	T(C)	w#			
R	3	3	st	25	T(C)	w#			
R	3	3	st	26	T(C)	w#			

*Sensor measurement: Air Temperature (T).
 **SI: (C) represent Degrees Celsius [°C].
 ***The E test is the information collected from the exterior MMS installed around the building envelope; the ET test is the information collected from exterior MMS where the eight sensors have been measuring together at the same place on the roof of the building.

Table A.6: Exterior MMS codes: file name codes, file column code and sensor reference [139].

Codes of existing Building Automation System (BAS)						
OT#.T9.md.ID#_XY(SI)_w# // E:T9.md.ID#_XY(SI)_w#						
File Column Codes of existing Building Automation System (BAS)						
OT#.T9.md.ID#_XY(SI) // E:T9.md.ID#_XY(SI)						
Codes of BAS Sensor (Sensor Reference)						
T9.md.ID#						
Office Typology (OT#) Test/ Exterior (E) Test	Virtual Tripod Reference (T#)	Virtual Height location (H)	ID sensor (ID#)***	Sensor Measurement (XY) * and its International System Unit (SI) ** (XY(SI))	Week of Year (w#)	
	T9	md	132	ph(W)	w#	
	T9	md	133	ph(W)	w#	
OT1	T9	md	142	ph(W)	w#	
OT2	T9	md	143	ph(W)	w#	
OT3	T9	md	142143	ph(W)	w#	
OT4	T9	md	131	pw(W)	w#	
E	T9	md	141	pw(W)	w#	
	T9	md	1413	rad(W/m ²) or rad(W-m2)	w#	

*Sensor measurement: Heating Power (ph) from calorimeter; Active Power (pw) from electricity meters; Solar Radiation (rad).
 **SI: W represents Watts [W] and m² represents Square Meter [m2]. W-m2 and W/m² represent Watt per square meter [W/m²].
 ***ID sensors: 131 is the total electric power on F2 (F2 is composed of OT1, OT2 and OT3). 141 is the total electric power on F3 (OT4). 132 is the power supplied by the heating system to the north oriented offices at F2 (OT1 and OT2). 133 is the power supplied by the heating system to the south oriented offices at F2 (OT3). 142 is the power supplied by the heating system to the north oriented areas at F3 (OT4). 143 is the power supplied by the heating system to the south oriented areas at F3 (OT4). 142143 is the total heating power supplied by the heating system to the F3 (sum of 142 and 143). 1413 is the horizontal global solar radiation. 1413 is the horizontal global solar radiation. The measurement of 1413 is the only data that have been taken into account in both the OT test and the E test; the rest of the sensor measurements are taken into account only in the OT test, depending on the floor where the test is done.
 All data are supplied by the existing BAS.

Table A.7: Existing BAS codes: file name codes, file column code and sensor reference [139].

Appendix B

Histograms of T_{in} uncertainty for tertiary building

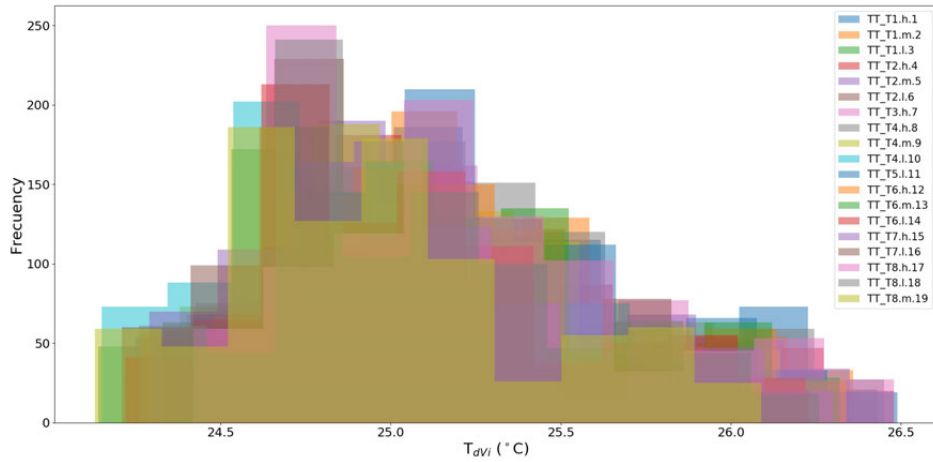


Figure B.1: Temperature Histogram of T_{dvi} from nineteen sensors measuring together (eighteen EE800-M1213 sensors and one EE071-HTPC sensor), for a sample size equal to $868 t_N$ with measurement frequency equal to five minutes.

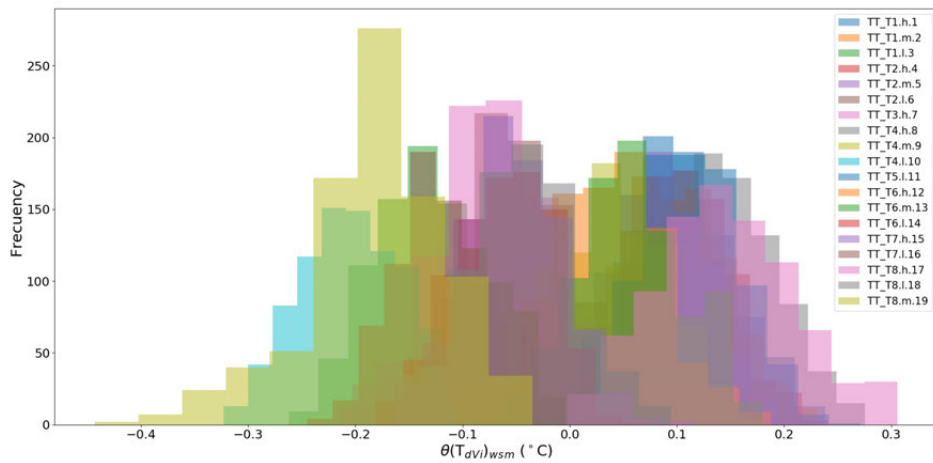


Figure B.2: Temperature Histogram of $(\theta_{dvi})_{wsm}$ from nineteen sensors measuring together (eighteen EE800-M1213 sensors and one EE071-HTPC sensor), for a sample size equal to $868 t_N$ with measurement frequency equal to five minutes.

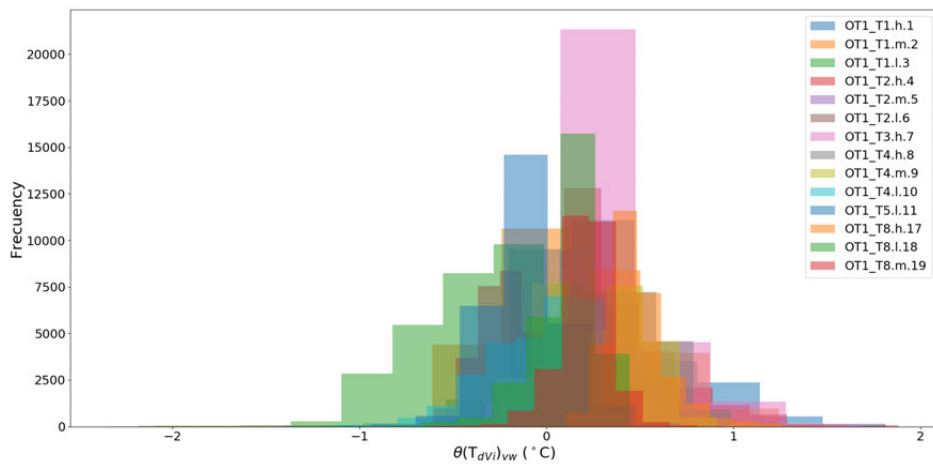


Figure B.3: Temperature Histogram of $(\theta_{dvi})_{vw}$ from MMS in OT1 for a sample size equal to $28,733 t_N$ with measurement frequency equal to ten seconds.

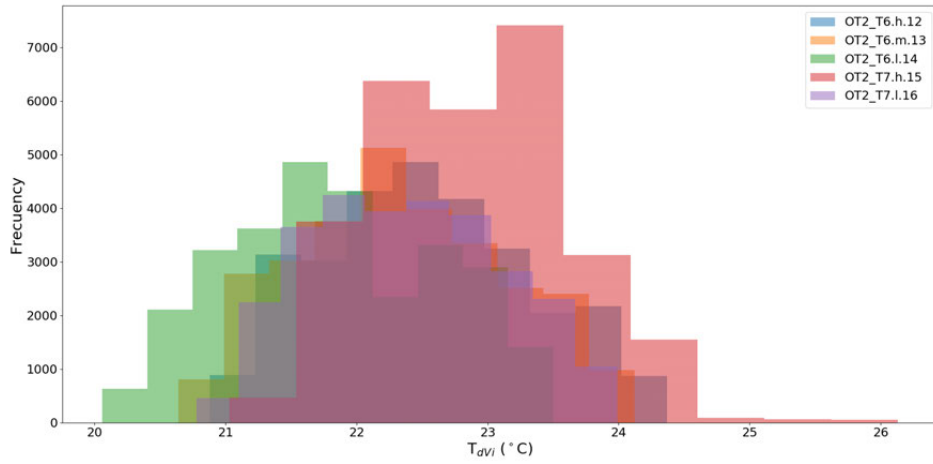


Figure B.4: Temperature Histogram of T_{dv_i} from MMS in OT2 for a sample size equal to $28,705 t_N$ with measurement frequency equal to ten seconds.

Figure C.9.

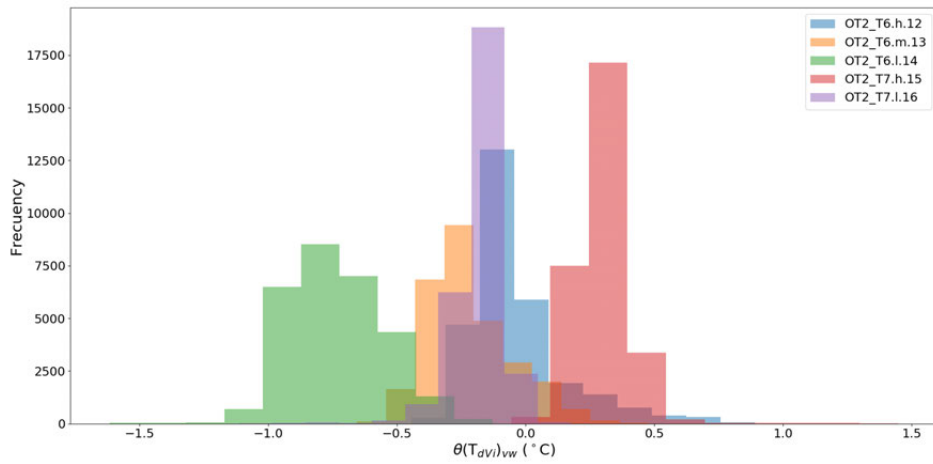


Figure B.5: Temperature Histogram of $(\theta_{dv_i})_{vw}$ from MMS in OT2 for a sample size equal to $28,705 t_N$ with measurement frequency equal to ten seconds.

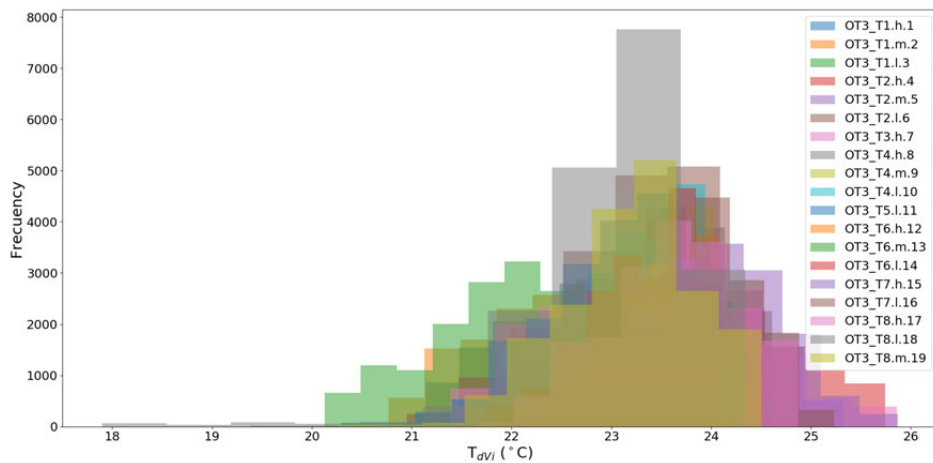


Figure B.6: Temperature Histogram of T_{dv_i} from MMS in OT3 for a sample size equal to $18,861 t_N$ with measurement frequency equal to fifty seconds.

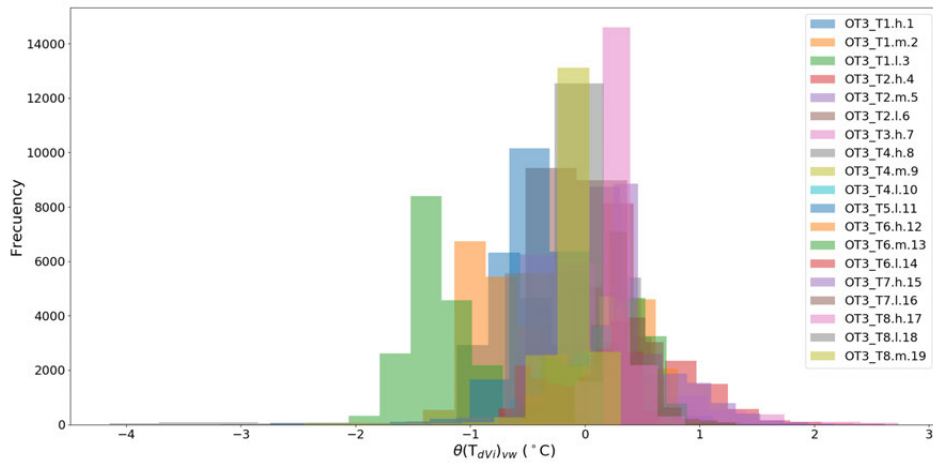


Figure B.7: Temperature Histogram of $(\theta_{dv_i})_{vw}$ from MMS in OT3 for a sample size equal to 18,861 t_N with measurement frequency equal to fifty seconds.

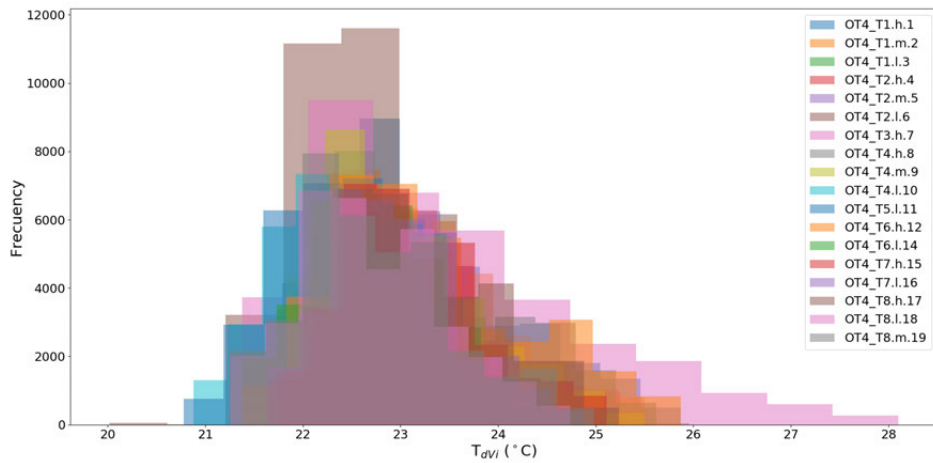


Figure B.8: Temperature Histogram of T_{dv_i} from MMS in OT4 for a sample size equal to 35,381 t_N with measurement frequency equal to forty seconds.

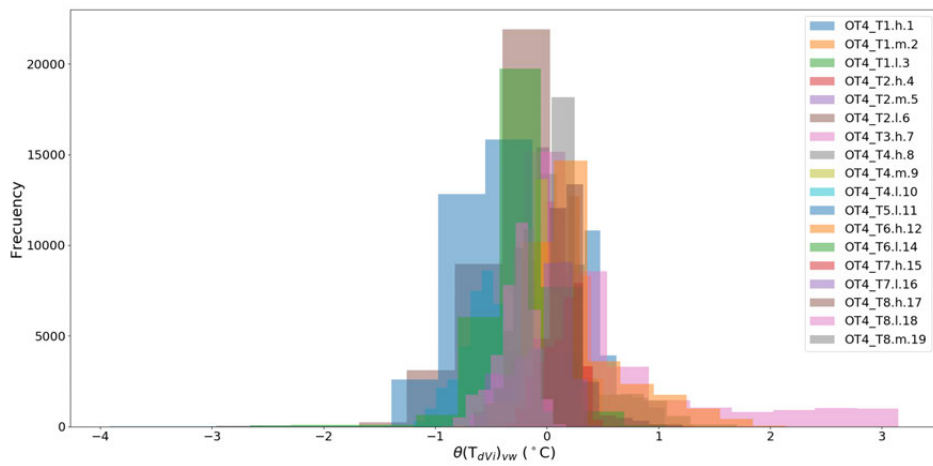


Figure B.9: Temperature Histogram of $(\theta_{dv_i})_{vw}$ from MMS in OT4 for a sample size equal to 35,381 t_N with measurement frequency equal to forty seconds.

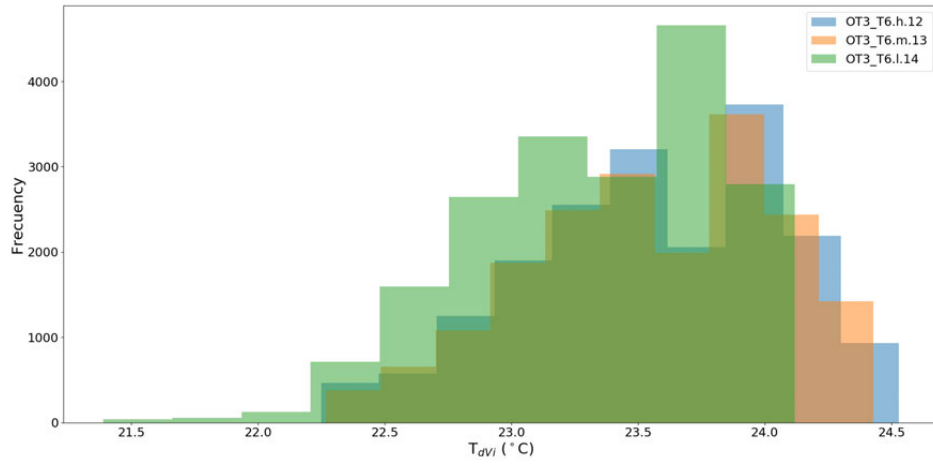


Figure B.10: Temperature Histogram of T_{dv_i} from MMS in OT3.2C3.2 for a sample size equal to 18,861 t_N with measurement frequency equal to fifty seconds.

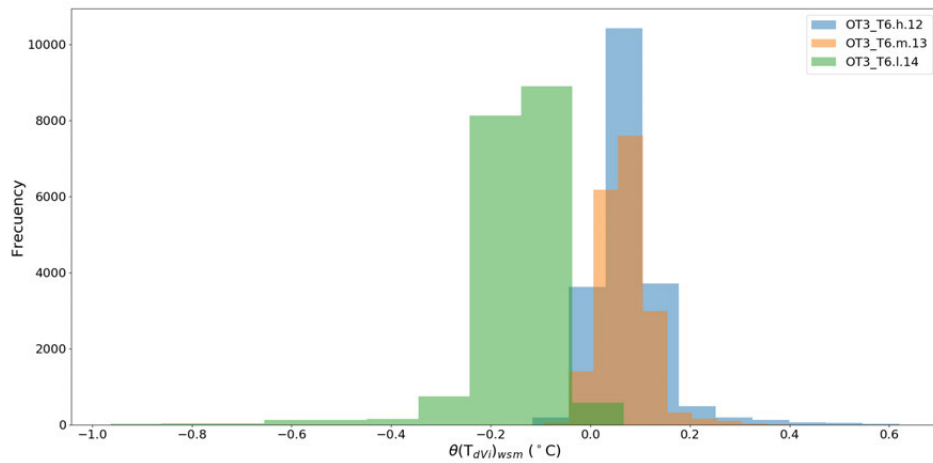


Figure B.11: Temperature Histogram of $(\theta_{dv_i})_{wsm}$ from MMS in OT3.2C3.2 for a sample size equal to 18861 t_N with measurement frequency equal to fifty seconds.

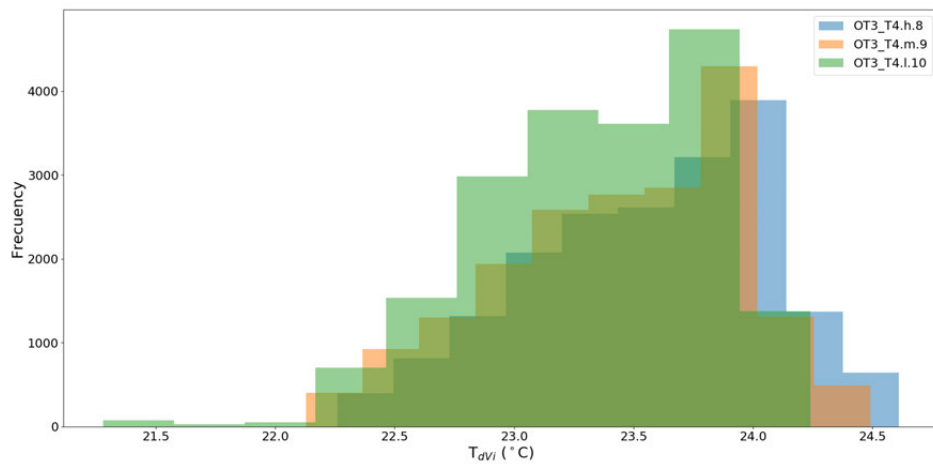


Figure B.12: Temperature Histogram of T_{dv_i} from MMS in OT3.2C3.3 for a sample size equal to 18,861 t_N with measurement frequency equal to fifty seconds.

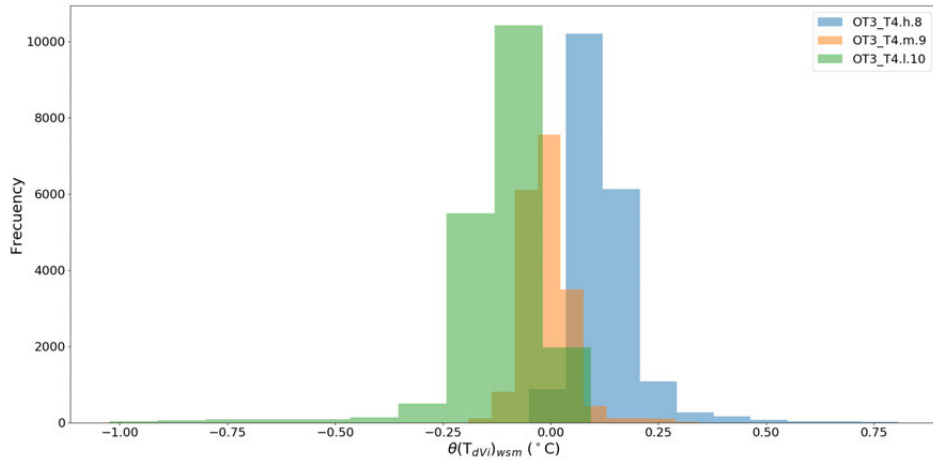


Figure B.13: Temperature Histogram of $(\theta_{dv_i})_{wsm}$ from MMS in OT3.2C3.3 for a sample size equal to 18,861 t_N with measurement frequency equal to fifty seconds.

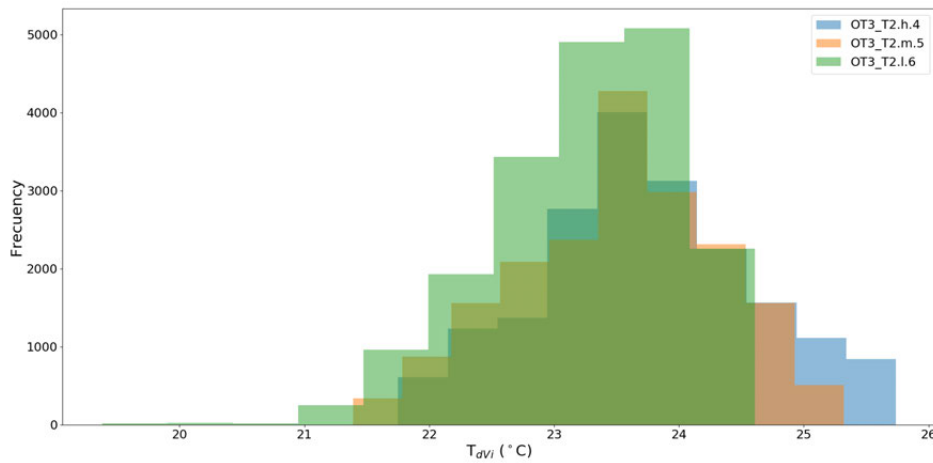


Figure B.14: Temperature Histogram of T_{dv_i} from MMS in OT3.2C3.5 for a sample size equal to 18,861 t_N with measurement frequency equal to fifty seconds.

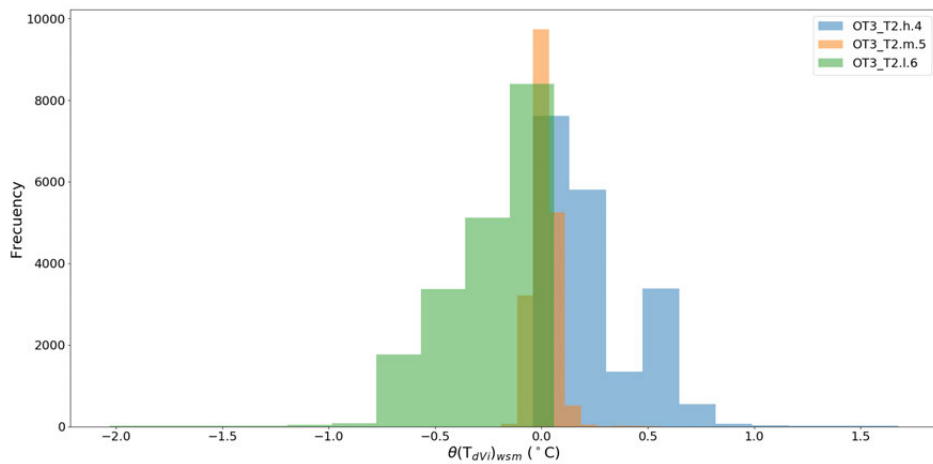


Figure B.15: Temperature Histogram of $(\theta_{dv_i})_{wsm}$ from MMS in OT3.2C3.5 for a sample size equal to 18,861 t_N with measurement frequency equal to fifty seconds.

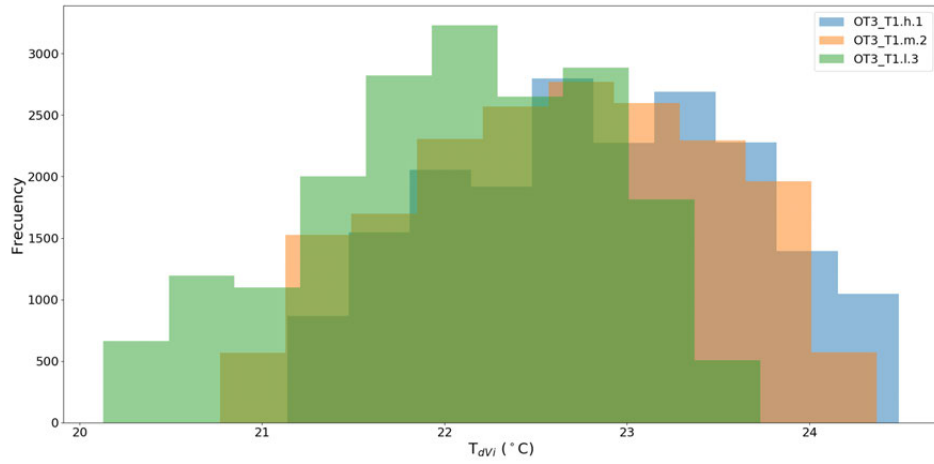


Figure B.16: Temperature Histogram of T_{dv_i} from MMS in OT3.2C3.9 for a sample size equal to 18,861 t_N with measurement frequency equal to fifty seconds.

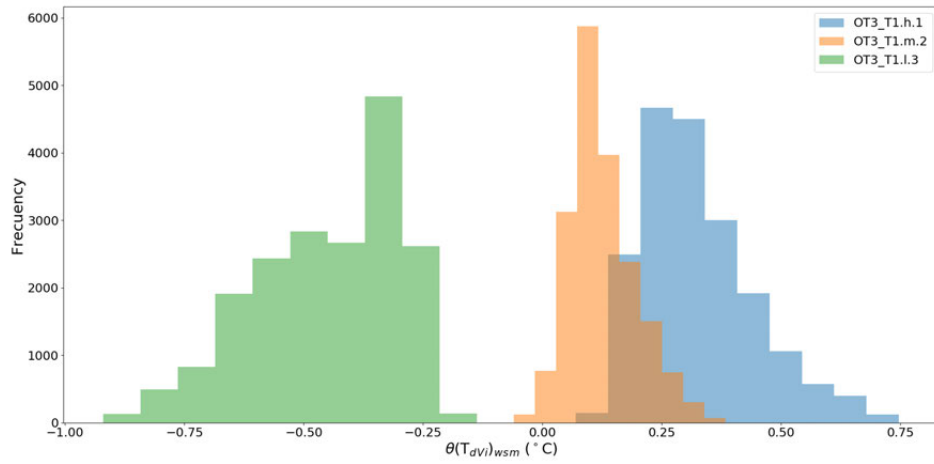


Figure B.17: Temperature Histogram of $(\theta_{dv_i})_{wsm}$ from MMS in OT3.2C3.9 for a sample size equal to 18,861 t_N with measurement frequency equal to fifty seconds.

Appendix C

Histograms of T_{out} uncertainty for tertiary building

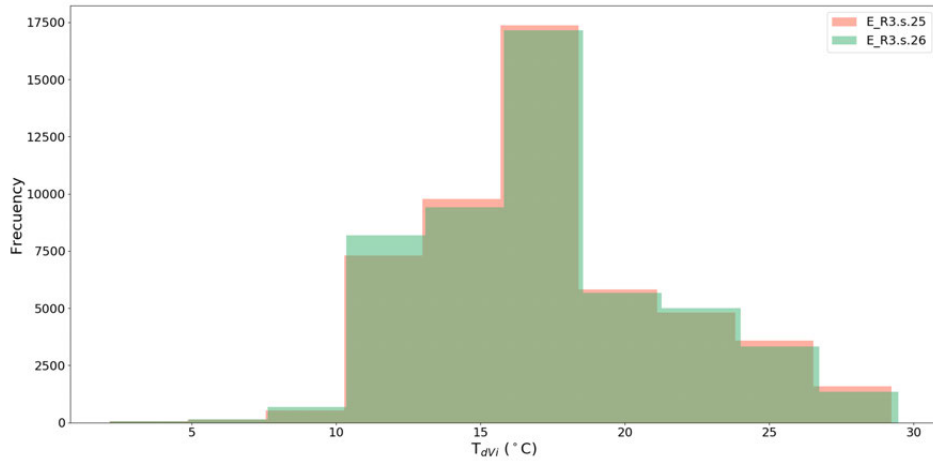


Figure C.1: Temperature Histogram of T_{dv_i} from E.R3.s.25 and E.R3.s.26 sensors of the MMS for a sample size equal to 50,958 t_N with and without solar radiation.

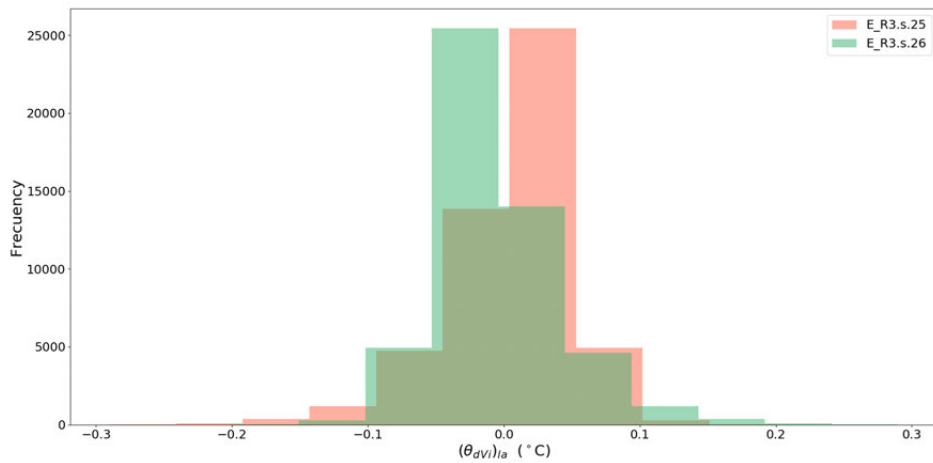


Figure C.2: Temperature Histogram of $(\theta_{dv_i})_{la}$ with data centred on the Local Average Temperature $(T_a)_{la}$ for E.R3.s.25 and E.R3.s.26 sensors of the MMS for a sample size equal to 50,958 t_N with and without solar radiation.

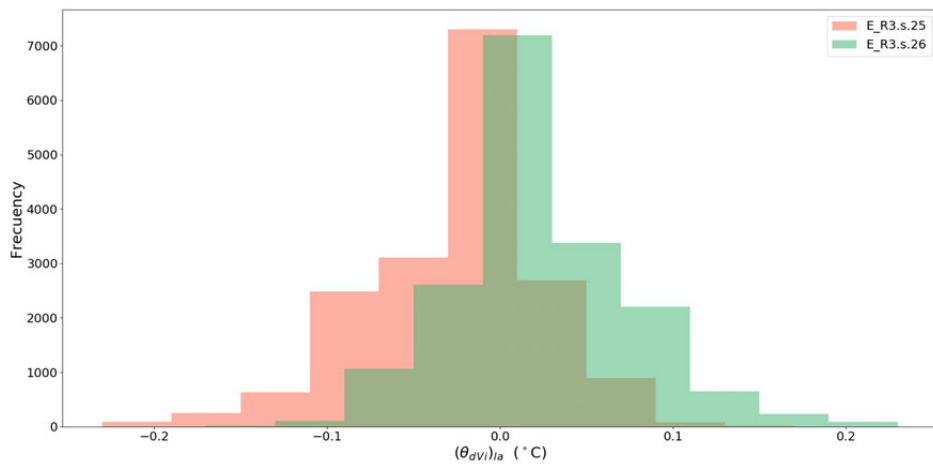


Figure C.3: Temperature Histogram of $(\theta_{dv_i})_{la}$ with data centred on the Local Average Temperature $(T_a)_{la}$ for E.R3.s.25 and E.R3.s.26 sensors of the MMS for a sample size equal to 17,527 t_N with solar radiation.

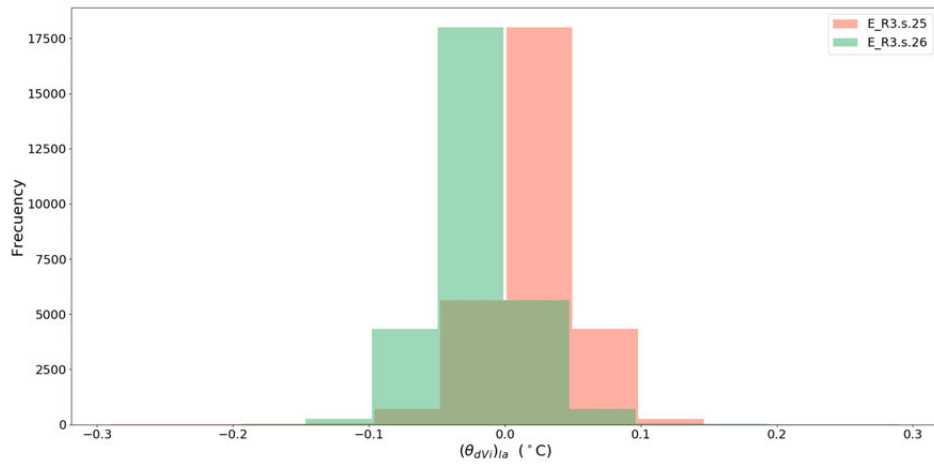


Figure C.4: Temperature Histogram of $(\theta_{dvi})_{la}$ with data centred on the Local Average Temperature $(T_a)_{la}$ for E.R3.s.25 and E.R3.s.26 sensors of the MMS for a sample size equal to $29,05 t_N$ without solar radiation.

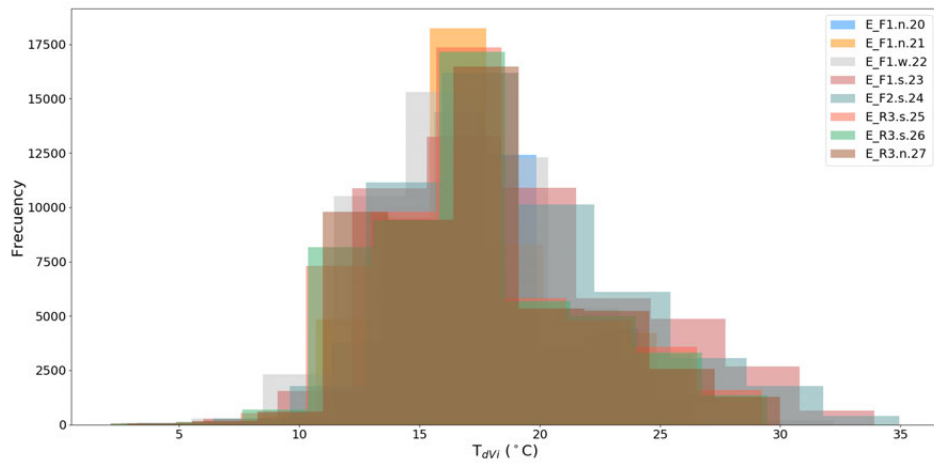


Figure C.5: Temperature Histogram of (T_{dvi}) from E.F1.n.20, E.F1.n.21, E.F1.w.22, E.F1.s.23, E.F2.s.24, E.R3.s.25, E.R3.s.26 and E.R3.n.27 sensors of MMS for a sample size equal to $50,958 t_N$ with and without solar radiation.

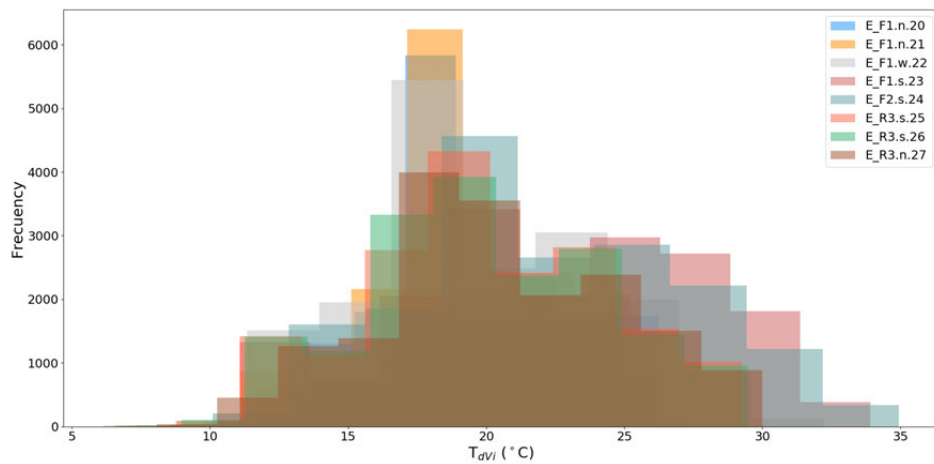


Figure C.6: Temperature Histogram of (T_{dvi}) from E.F1.n.20, E.F1.n.21, E.F1.w.22, E.F1.s.23, E.F2.s.24, E.R3.s.25, E.R3.s.26 and E.R3.n.27 sensors of the MMS for a sample size equal to $17,527 t_N$ with solar radiation.

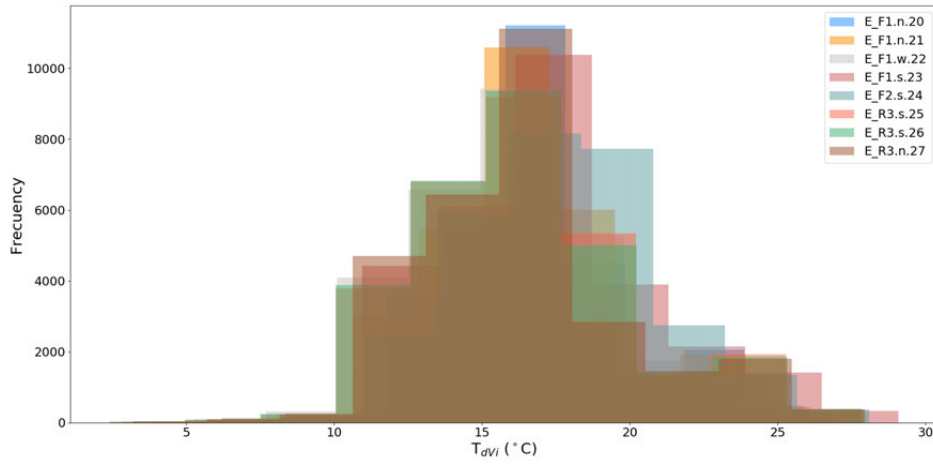


Figure C.7: Temperature Histogram of (T_{dvi}) from E.F1.n.20, E.F1.n.21, E.F1.w.22, E.F1.s.23, E.F2.s.24, E.R3.s.25, E.R3.s.26 and E.R3.n.27 sensors of the MMS for a sample size equal to 29,05 t_N without solar radiation.

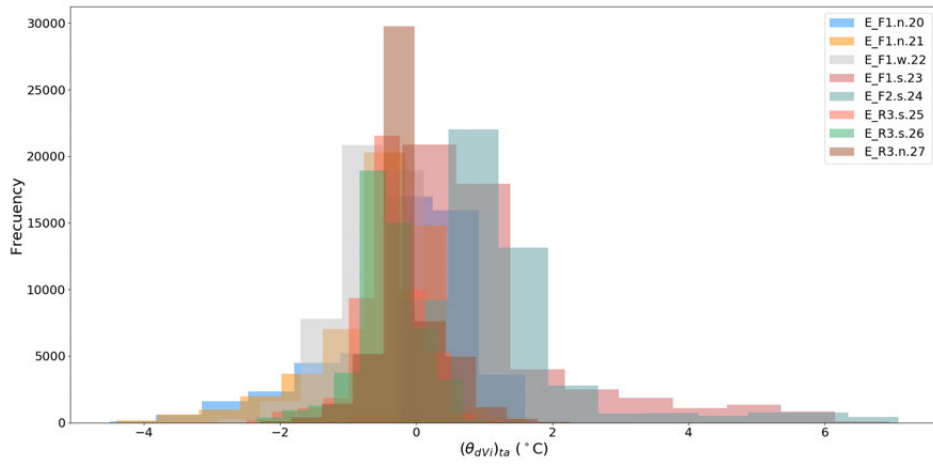


Figure C.8: Temperature Histogram of $(\theta_{dvi})_{ta}$ with data centred on the Total Average Temperature $((T_a)_{ta})$ for E.F1.n.20, E.F1.n.21, E.F1.w.22, E.F1.s.23, E.F2.s.24, E.R3.s.25, E.R3.s.26 and E.R3.n.27 sensors of MMS for a sample size equal to 50,958 t_N with and without solar radiation.

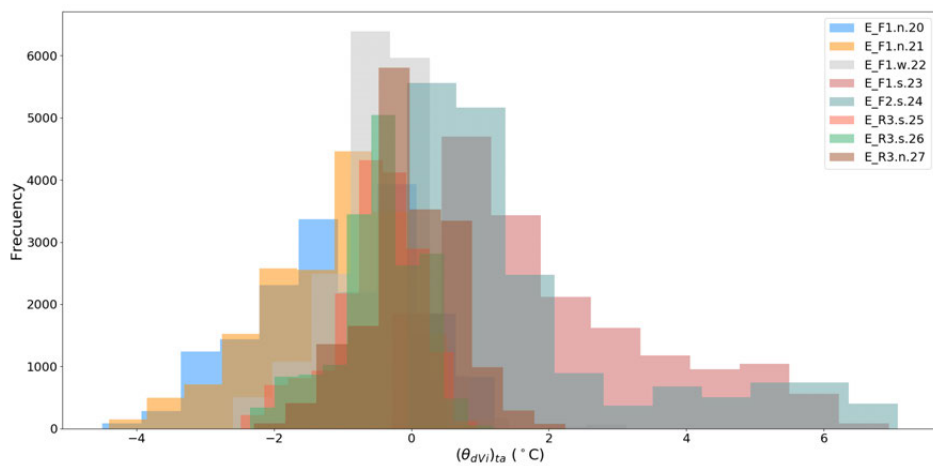


Figure C.9: Temperature Histogram of $(\theta_{dvi})_{ta}$ with data centred on the Total Average Temperature $((T_a)_{ta})$ for E.F1.n.20, E.F1.n.21, E.F1.w.22, E.F1.s.23, E.F2.s.24, E.R3.s.25, E.R3.s.26 and E.R3.n.27 sensors of MMS for a sample size equal to 17,527 t_N with solar radiation.

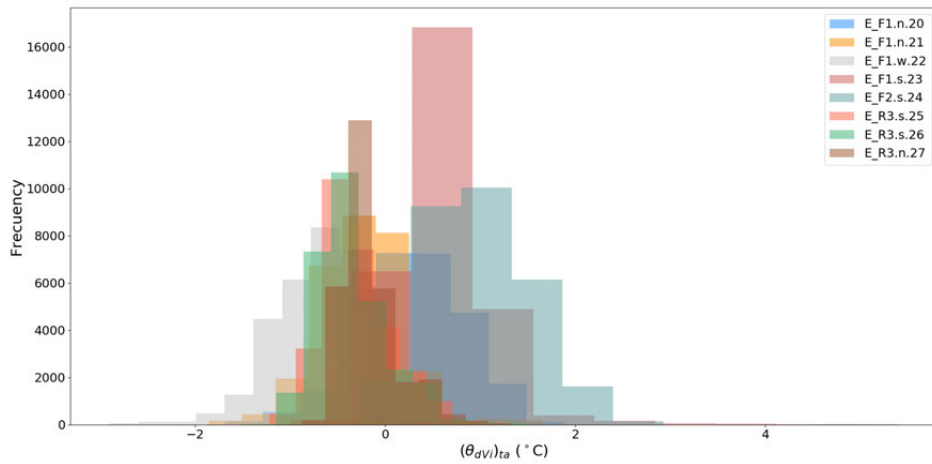


Figure C.10: Temperature Histogram of $((\theta_{dvi})_{ta})$ with data centred on the Total Average Temperature $((T_a)_{ta})$ for E.F1.n.20, E.F1.n.21, E.F1.w.22, E.F1.s.23, E.F2.s.24, E.R3.s.25, E.R3.s.26 and E.R3.n.27 sensors of MMS for a sample size equal to 29,05 t_N without solar radiation.

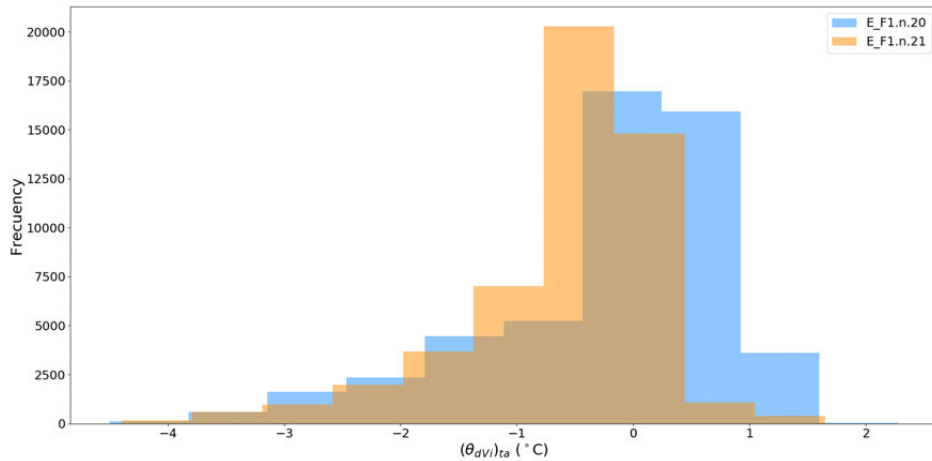


Figure C.11: Temperature Histogram of $(\theta_{dvi})_{ta}$ with data centred on the Total Average Temperature $((T_a)_{ta})$ for E.F1.n.20 and E.F1.n.21 sensors of MMS for a sample size equal to 50,958 t_N with and without solar radiation.

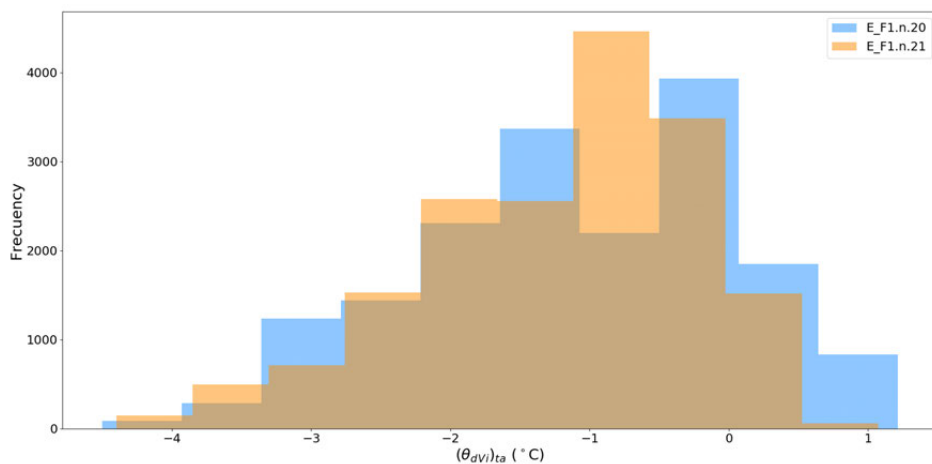


Figure C.12: Temperature Histogram of $(\theta_{dvi})_{ta}$ with data centred on the Total Average Temperature $((T_a)_{ta})$ for E.F1.n.20 and E.F1.n.21 sensors of MMS for a sample size equal to 17,527 t_N with solar radiation.

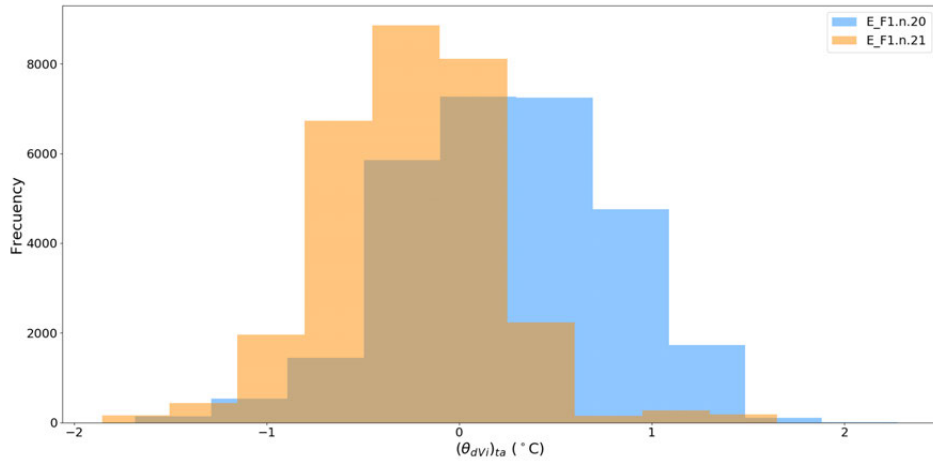


Figure C.13: Temperature Histogram of $((\theta_{dvi})_{ta})$ with data centred on the Total Average Temperature $((T_a)_{ta})$ for E.F1.n.20 and E.F1.n.21 sensors of MMS for a sample size equal to $29,05 t_N$ without solar radiation.

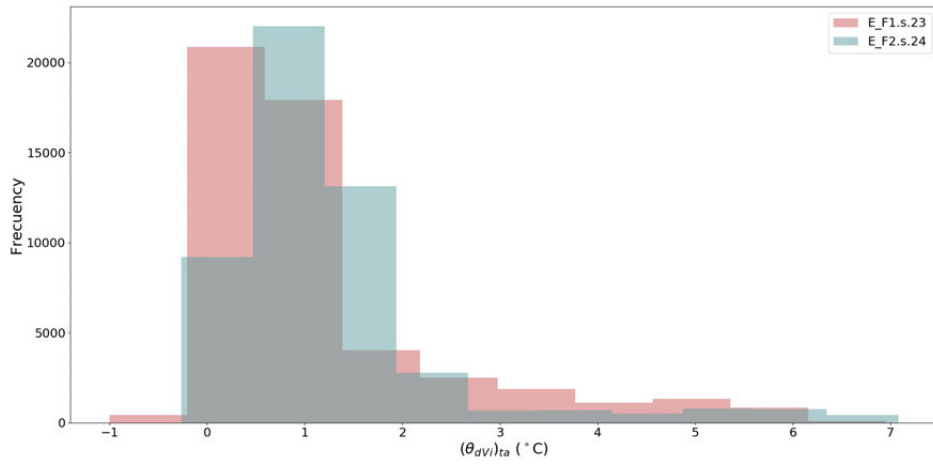


Figure C.14: Temperature Histogram of $((\theta_{dvi})_{ta})$ with data centred on the Total Average Temperature $((T_a)_{ta})$ for E.F1.s.23 and E.F2.s.24 sensors of MMS for a sample size equal to $50,958 t_N$ with and without solar radiation.

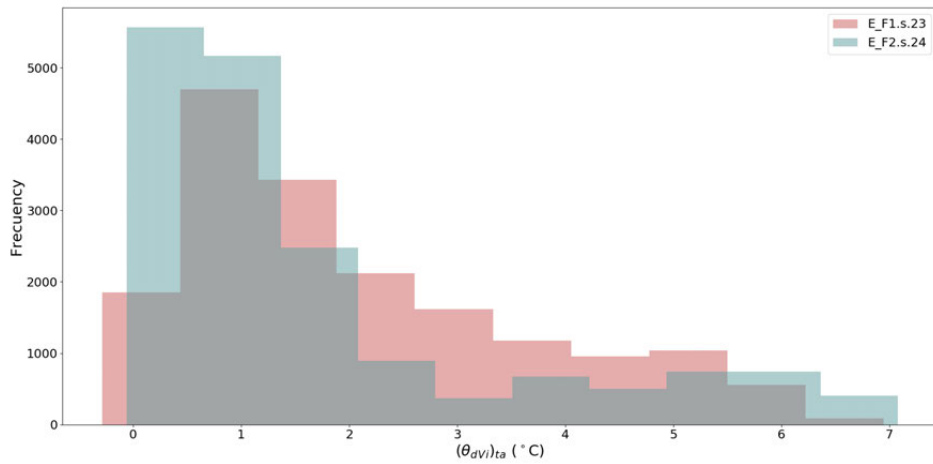


Figure C.15: Temperature Histogram of $((\theta_{dvi})_{ta})$ with data centred on the Total Average Temperature $((T_a)_{ta})$ for E.F1.s.23 and E.F2.s.24 sensors of MMS for a sample size equal to $17,527 t_N$ with solar radiation.

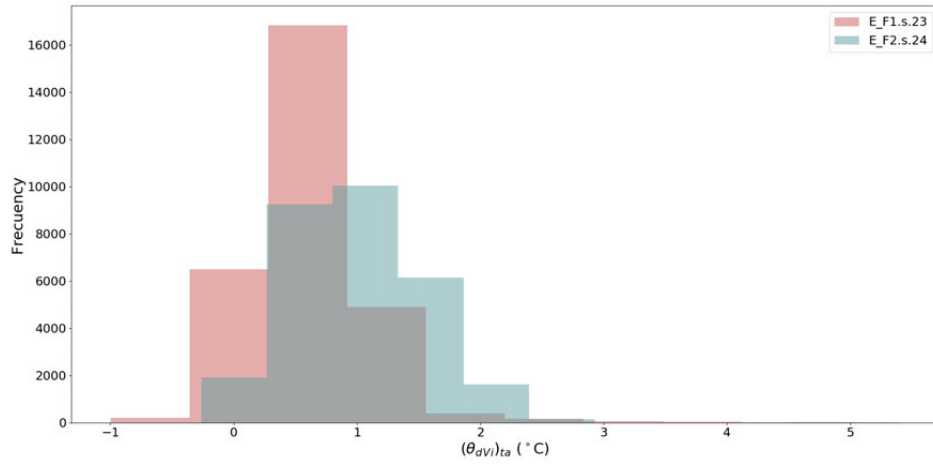


Figure C.16: Temperature Histogram of $((\theta_{dv_i})_{t_a})$ with data centred on the Total Average Temperature $((T_a)_{t_a})$ for E.F1.s.23 and E.F2.s.24 sensors of MMS for a sample size equal to $29,05 t_N$ without solar radiation.

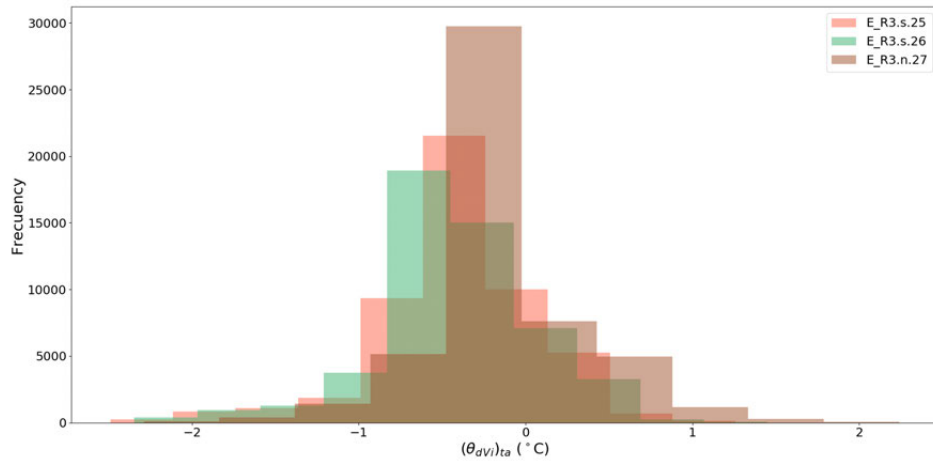


Figure C.17: Temperature Histogram of $(\theta_{dv_i})_{t_a}$ with data centred on the Total Average Temperature $((T_a)_{t_a})$ for E.R3.s.25, E.R3.s.26 and E.R3.n.27 sensors of MMS for a sample size equal to $50,958 t_N$ with and without solar radiation.

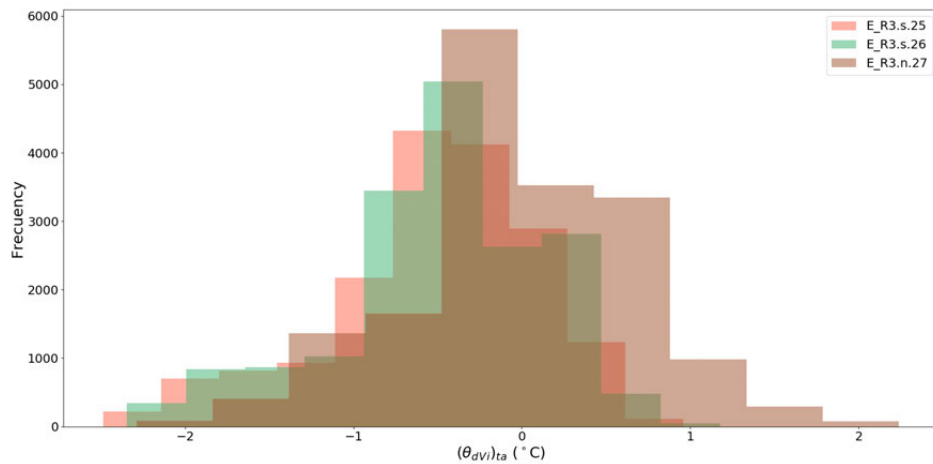


Figure C.18: Temperature Histogram of $(\theta_{dv_i})_{t_a}$ with data centred on the Total Average Temperature $((T_a)_{t_a})$ for E.R3.s.25, E.R3.s.26 and E.R3.n.27 sensors of MMS for a sample size equal to $17,527 t_N$ with solar radiation.

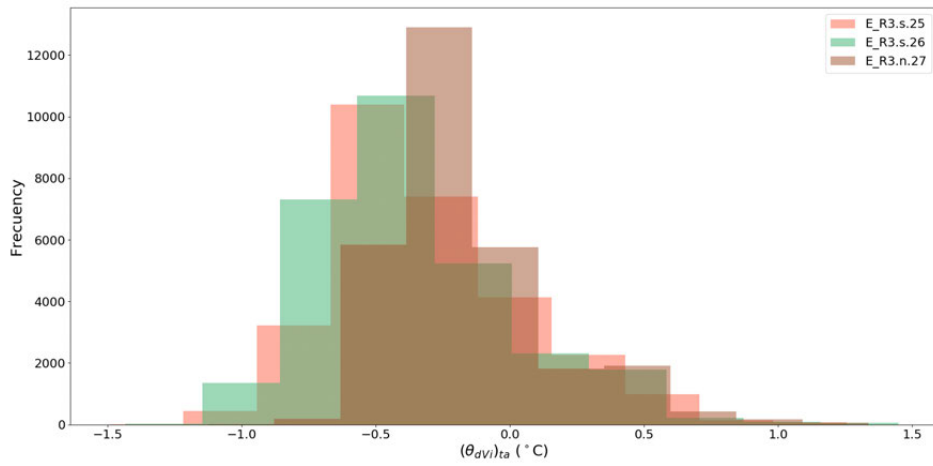


Figure C.19: Temperature Histogram of $(\theta_{dvi})_{ta}$ with data centred on the Total Average Temperature $((T_a)_{ta})$ for E.R3.s.25, E.R3.s.26 and E.R3.n.27 sensors of MMS for a sample size equal to 29,05 t_N without solar radiation.

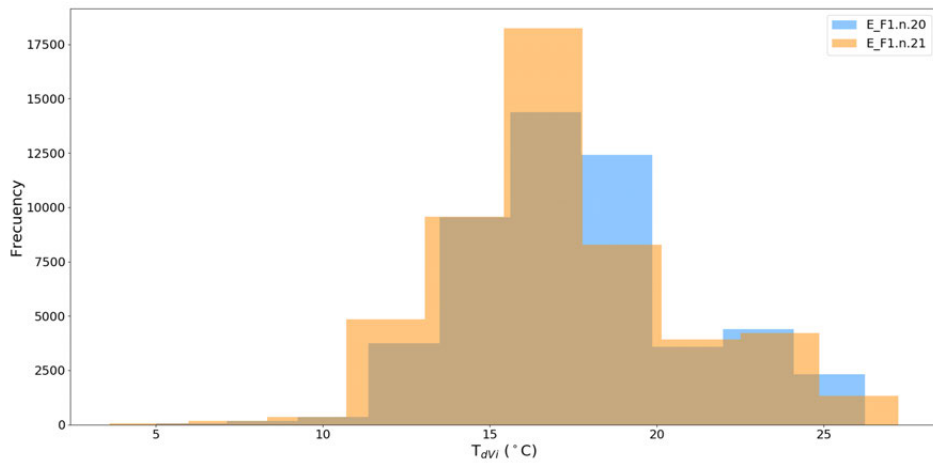


Figure C.20: Temperature Histogram of T_{dvi} from E.F1.n.20 and E.F1.n.21 sensors of the MMS for a sample size equal to 50,958 t_N with and without solar radiation.

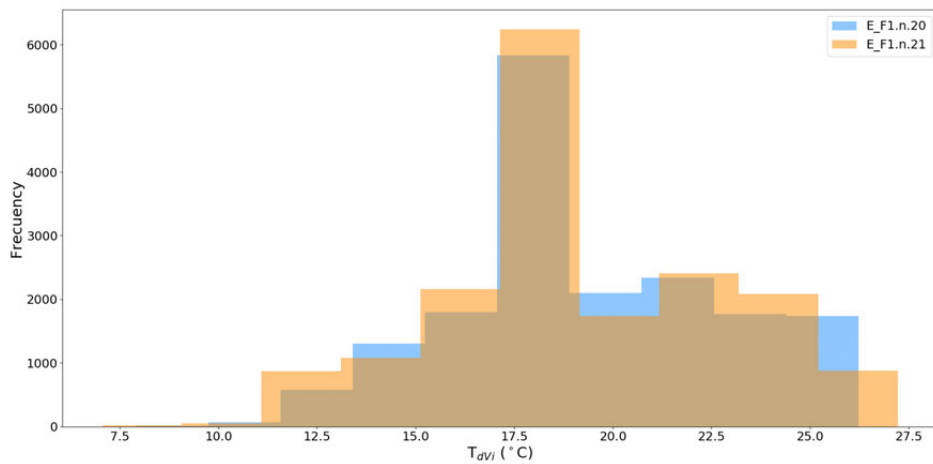


Figure C.21: Temperature Histogram of T_{dvi} from E.F1.n.20 and E.F1.n.21 sensors of the MMS for a sample size equal to 17,527 t_N with solar radiation.

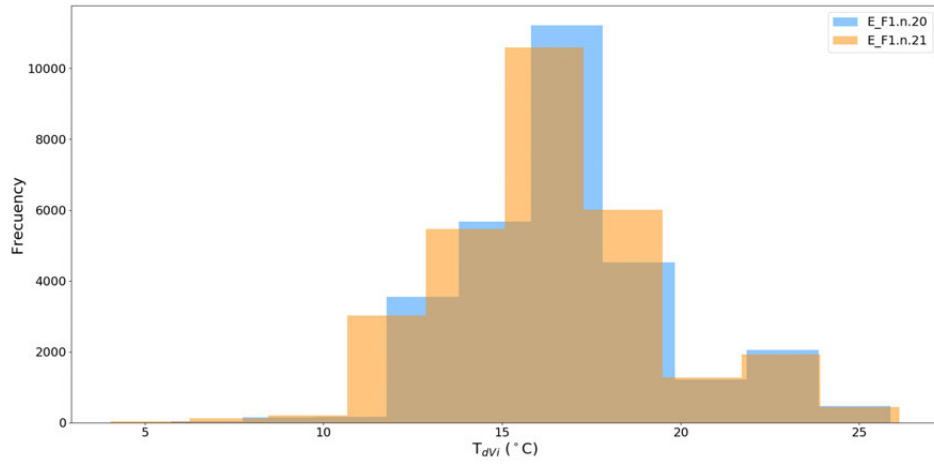


Figure C.22: Temperature Histogram of T_{dv_i} from E.F1.n.20 and E.F1.n.21 sensors of MMS for a sample size equal to 29,05 t_N without solar radiation.

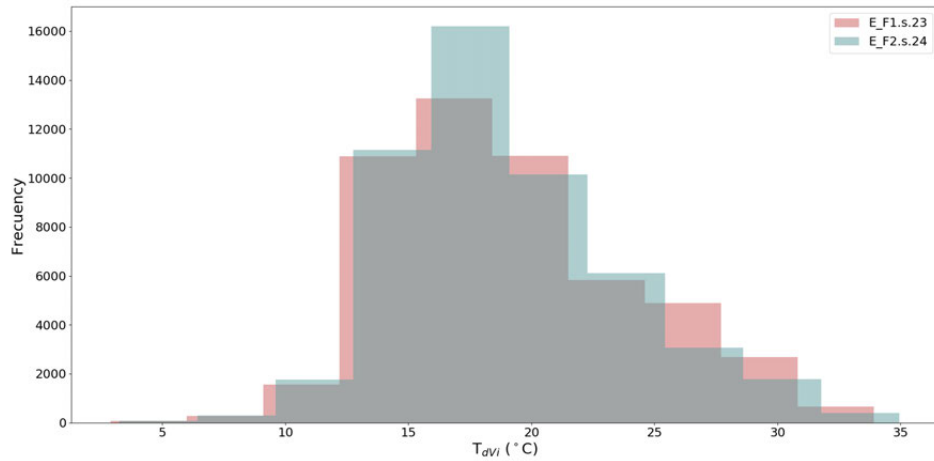


Figure C.23: Temperature Histogram of T_{dv_i} from E.F1.s.23 and E.F2.s.24 sensors of the MMS for a sample size equal to 50,958 t_N with and without solar radiation.

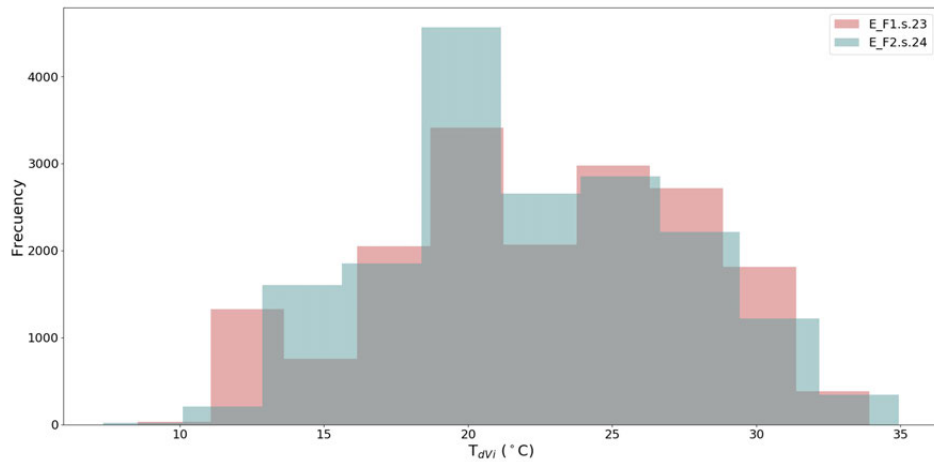


Figure C.24: Temperature Histogram of T_{dv_i} from E.F1.s.23 and E.F2.s.24 sensors of the MMS for a sample size equal to 17,527 t_N with solar radiation.

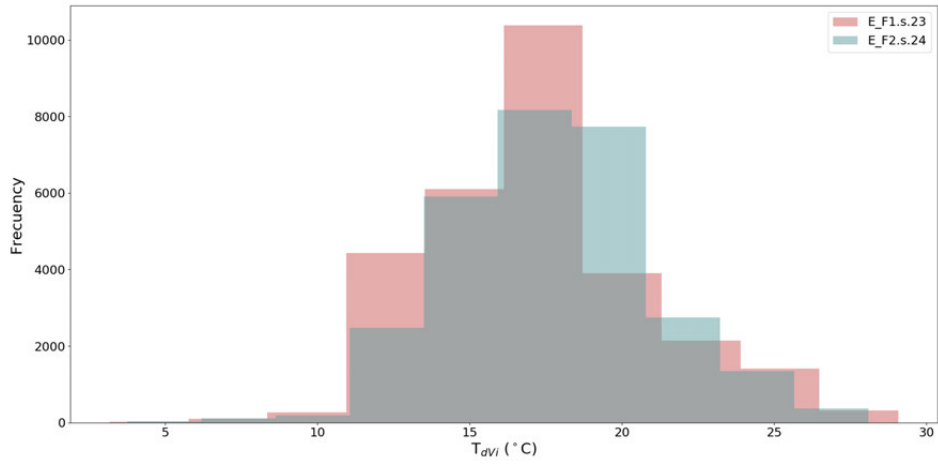


Figure C.25: Temperature Histogram of T_{dvi} from E.F1.s.23 and E.F2.s.24 sensors of the MMS for a sample size equal to 29,05 t_N without solar radiation.

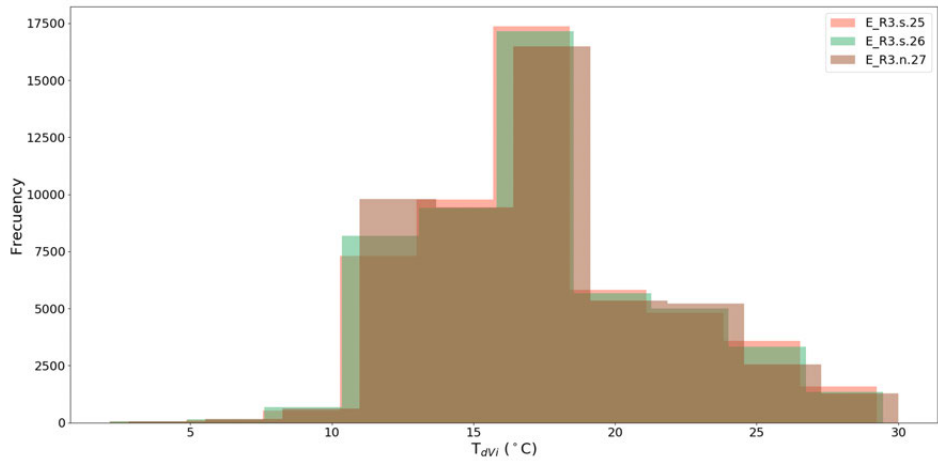


Figure C.26: Temperature Histogram of T_{dvi} from E.R3.s.25, E.R3.s.26 and E.R3.n.27 sensors of the MMS for a sample size equal to 50,958 t_N with and without solar radiation.

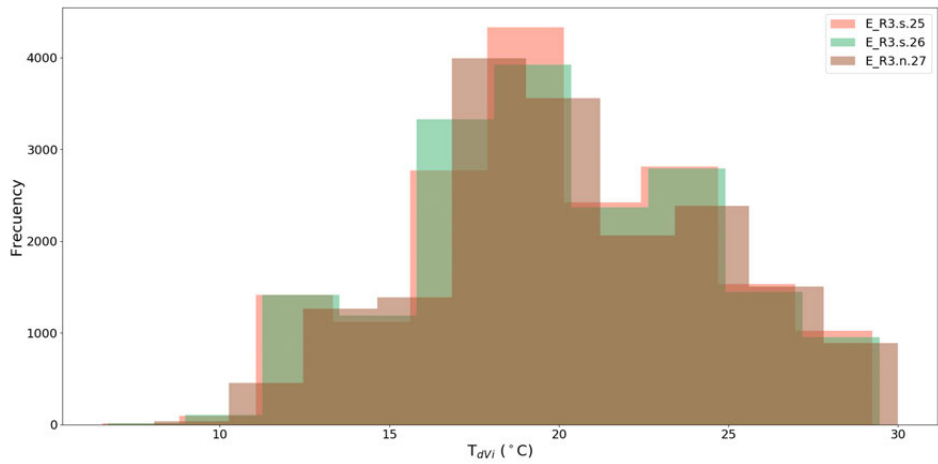


Figure C.27: Temperature Histogram of T_{dvi} from E.R3.s.25, E.R3.s.26 and E.R3.n.27 sensors of the MMS for a sample size equal to 17,527 t_N with solar radiation.

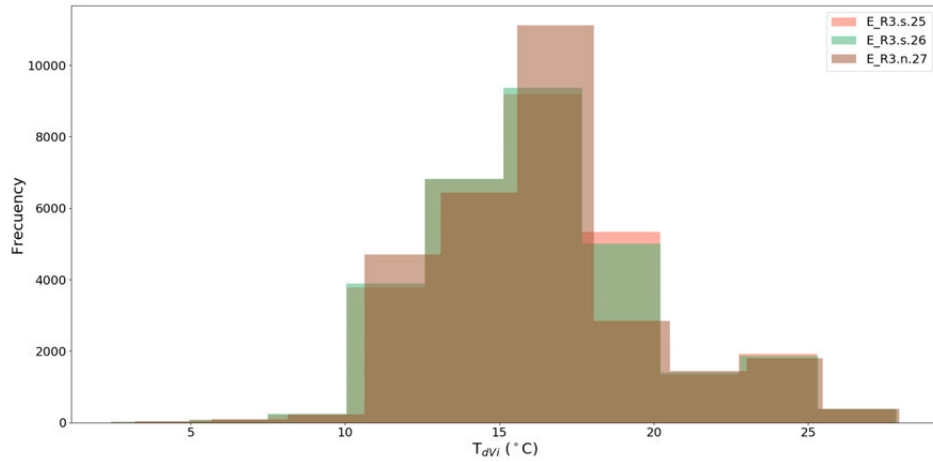


Figure C.28: Temperature Histogram of T_{dv_i} from E.R3.s.25, E.R3.s.26 and E.R3.n.27 sensors of MMS for a sample size equal to $29,05 t_N$ without solar radiation.

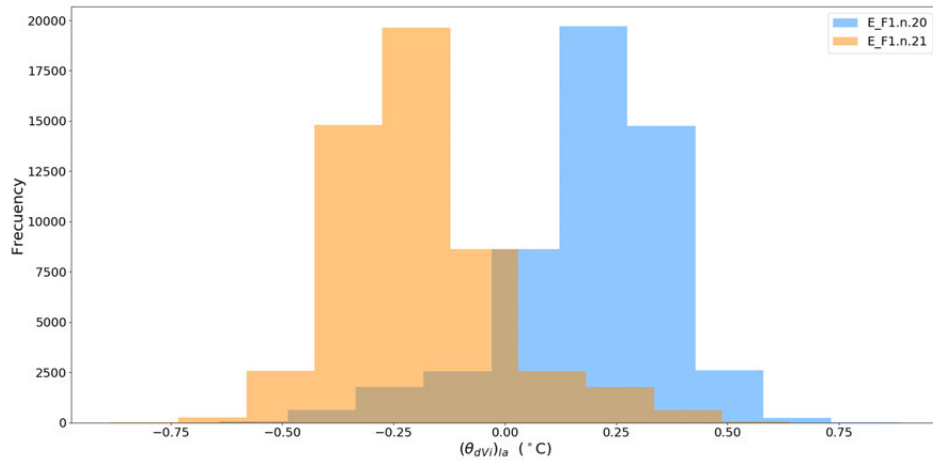


Figure C.29: Temperature Histogram of $(\theta_{dv_i})_{la}$ with data centred on the Local Average Temperature $((T_a)_{la})$ for E.F1.n.20 and E.F1.n.21 sensors of MMS for a sample size equal to $50,958 t_N$ with and without solar radiation.

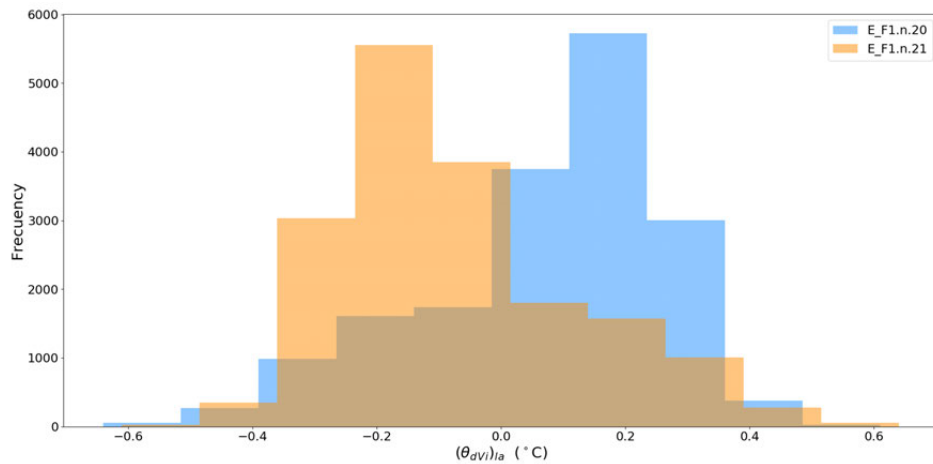


Figure C.30: Temperature Histogram of $(\theta_{dv_i})_{la}$ with data centred on Local Average Temperature $((T_a)_{la})$ for E.F1.n.20 and E.F1.n.21 sensors of MMS for a sample size equal to $17,527 t_N$ with solar radiation.

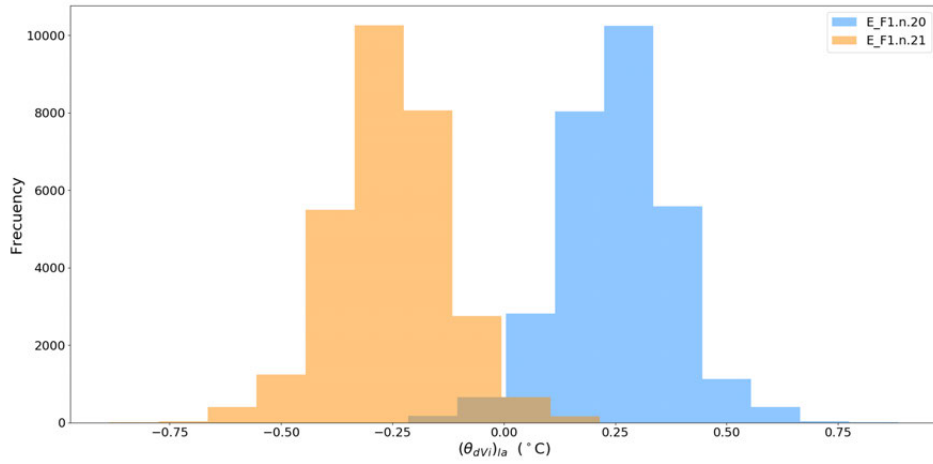


Figure C.31: Temperature Histogram of $(\theta_{dvi})_{la}$ with data centred on Local Average Temperature $((T_a)_{la})$ for E.F1.n.20 and E.F1.n.21 sensors of the MMS for a sample size equal to 29,05 t_N without solar radiation.

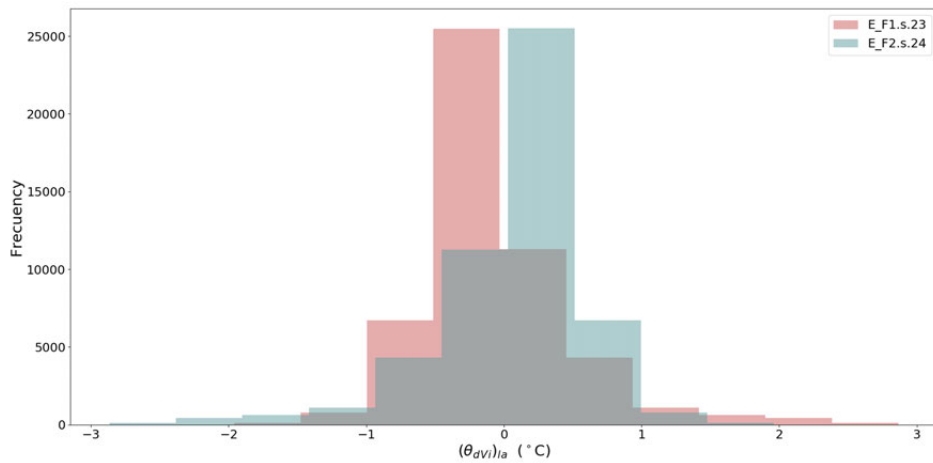


Figure C.32: Temperature Histogram of $(\theta_{dvi})_{la}$ with data centred on Local Average Temperature $((T_a)_{la})$ for E.F1.s.23 and E.F2.s.24 sensors of the MMS for a sample size equal to 50,958 t_N with and without solar radiation.

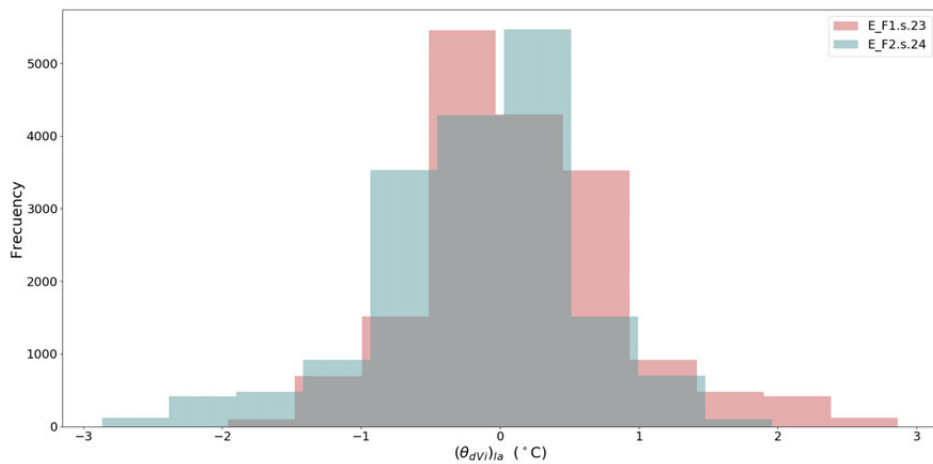


Figure C.33: Temperature Histogram of $(\theta_{dvi})_{la}$ with data centred on Local Average Temperature $((T_a)_{la})$ for E.F1.s.23 and E.F2.s.24 sensors of MMS for a sample size equal to 17,527 t_N with solar radiation.

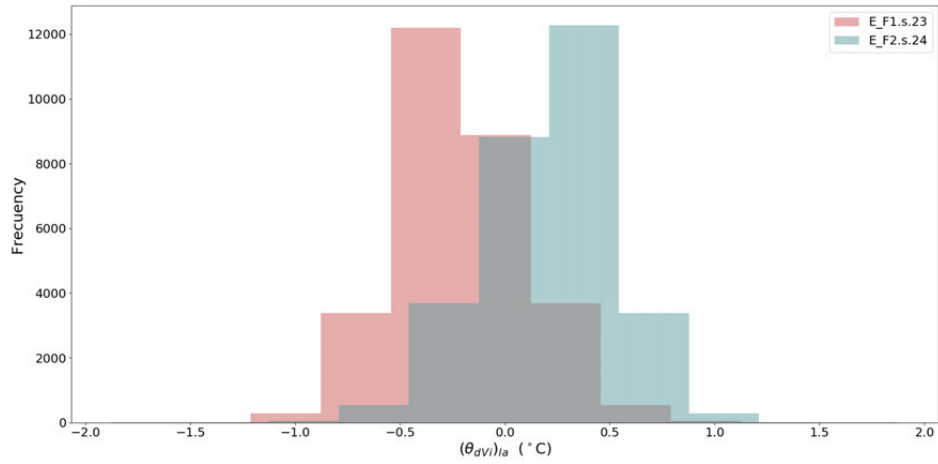


Figure C.34: Temperature Histogram of $(\theta_{dvi})_{la}$ with data centred on Local Average Temperature $((T_a)_{la})$ for E.F1.s.23 and E.F2.s.24 sensors of the MMS for a sample size equal to $29,05 t_N$ without and without solar radiation.

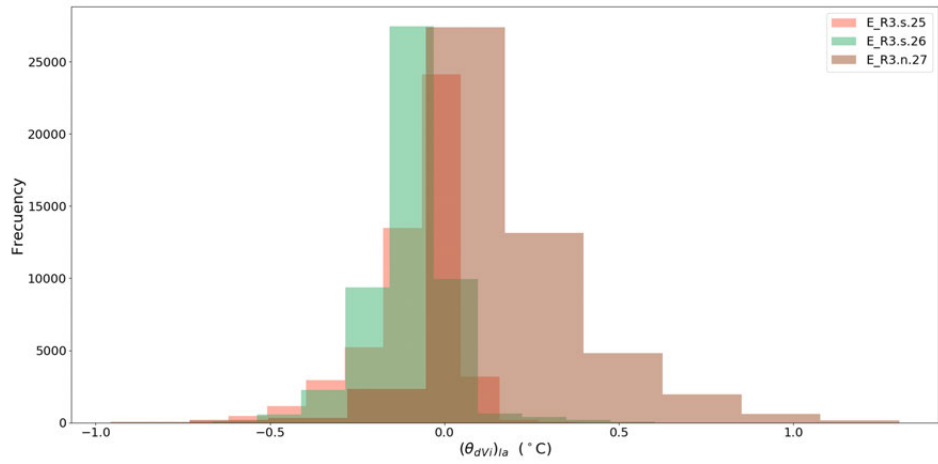


Figure C.35: Temperature Histogram of $(\theta_{dvi})_{la}$ with data centred on Local Average Temperature $((T_a)_{la})$ for E.R3.s.25, E.R3.s.26 and E.R3.n.27 sensors of MMS for a sample size equal to $50,958 t_N$ with and without solar radiation.

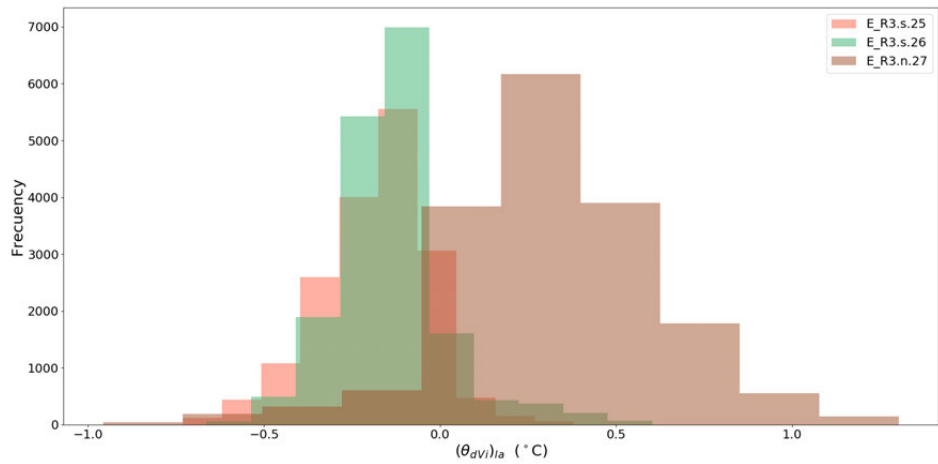


Figure C.36: Temperature Histogram of $(\theta_{dvi})_{la}$ with data centred on Local Average Temperature $((T_a)_{la})$ for E.R3.s.25, E.R3.s.26 and E.R3.n.27 sensors of the MMS for a sample size equal to $17,527 t_N$ with solar radiation.

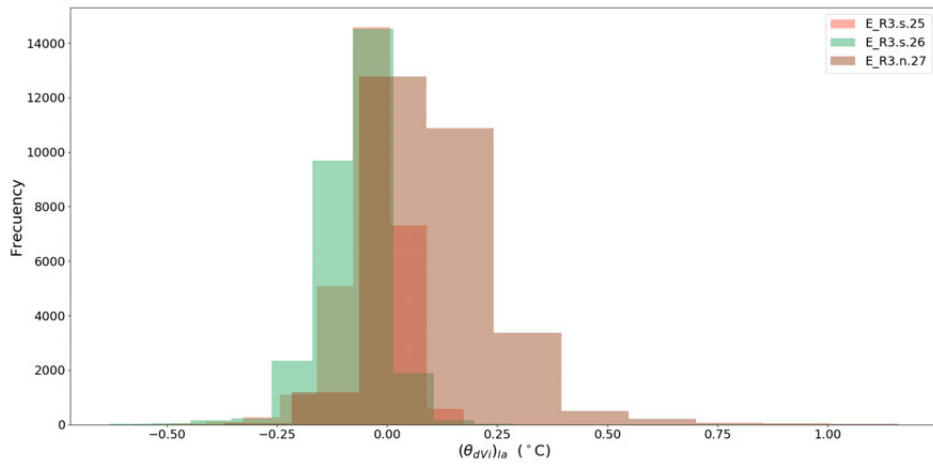


Figure C.37: Temperature Histogram of $(\theta_{dv_i})_{la}$ with data centred on Local Average Temperature $((T_a)_{la})$ for E.R3.s.25, E.R3.s.26 and E.R3.n.27 sensors of the MMS for a sample size equal to 29,05 t_N without solar radiation.

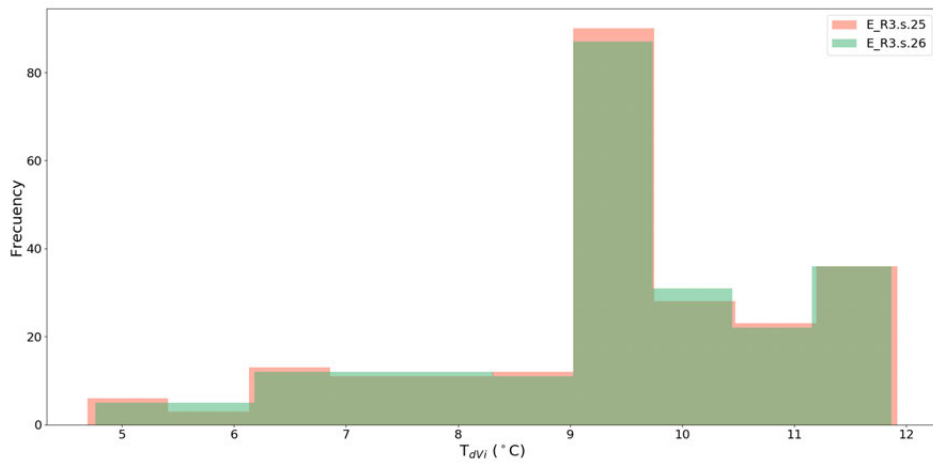


Figure C.38: Temperature Histogram of T_{dv_i} from E.R3.s.25 and E.R3.s.26 sensors of MMS for a sample size equal to 233 t_N with measurement frequency equal to five minutes and without solar radiation.

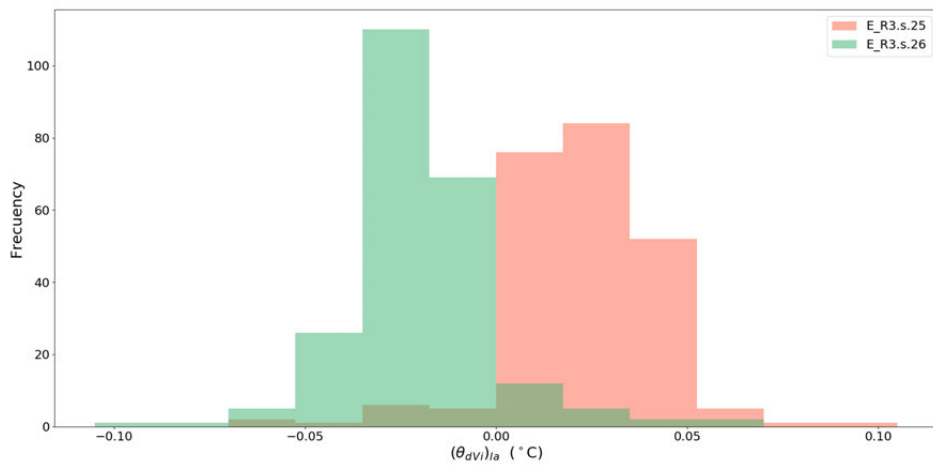


Figure C.39: Temperature Histogram of $(\theta_{dv_i})_{la}$ with data centred on Local Average Temperature $((T_a)_{la})$ for E.R3.s.25 and E.R3.s.26 sensors of MMS for a sample size equal to 233 t_N with measurement frequency equal to five minutes and without solar radiation.

Appendix D

MCS' sensor installed in the residential building

Spatial Localization of Fixed MMS' Sensor based on Figure D.1

Digital Sensors				Analogue Sensors			
Sensor ID	Floor	Zone	Reference	Sensor ID	Floor	Zone	Reference
01	F0	Z3	EE800-M12J3	18	F0	Z1	2113-1-073
02	F0	Z2	EE800-M12J3	19	F0	Z6	2113-1-073
03	F0	Z4	EE800-M12J3	20	F0	Z1	2113-1-073
04	F0	Z1	EE800-M12J3	21	F0	ZE	578-062
05	F0	Z6	EE800-M12J3	22	F0	Z1	2113-1-073
06	F0	Z7	EE800-M12J3	23	F0	ZE	578-062
07	F0	Z1	MM880-DMF	24	F0	Z1	2113-1-073
08	F0	Z1	MM880-DMF	25	F0	ZN	578-062
09	F0	Z1	MM880-DMF	26	F0	Z1	2113-1-073
10	F0	Z1	MM880-DMF	27	F0	ZN	578-062
11	F0	Z1	MM880-DMF	28	F0	Z1	2113-1-073
39	F0	Z1	MM880-DMF	29	F0	ZW	578-062
12	F0	Z1	EE650-T2J3L100-P1	30	F0	Z3	2113-1-073
13	F0	Z1	EE650-T2J3L100-P1	31	F0	Z5	2113-1-073
14	F0	Z1	EE160-HTX3XPBB	32	F0	Z3	Phymeas-Type7
15	F0	Z1	EE160-HTX3XPBB	33	F0	Z2	Phymeas-Type7
16	F0	Z1	EE850-M12-J3-P1	34	F0	Z1	Phymeas-Type7
17	F0	Z1	EE850-M12-J3-P1	35	F0	Z1	Phymeas-Type7
				36	F0	Z1	Phymeas-Type7
				37	F0	Z1	Phymeas-Type7
				38	F0	Z1	Phymeas-Type7
				41	F0	Z5	MM880-DMF
294	APPENDIX D. MCS' SENSOR INSTALLED IN THE RESIDENTIAL BUILDING			42	F0	Z5	MultiCal-403
				43	F0	Z5	MultiCal-403
				44	F0	Z5	MultiCal-403

Spatial Localization of Fixed MMS' Sensor based on Figure D.2

Digital Sensors				Analogue Sensors			
Sensor ID	Floor	Zone	Reference	Sensor ID	Floor	Zone	Reference
47	F1	Z1	EE800-M12J3	82	F1	Z8	2113-1-073
48	F1	Z2	EE800-M12J3	83	F1	Z2	2113-1-073
49	F1	Z2	EE800-M12J3	84	F1	Z1	2113-1-073
50	F1	Z2	EE800-M12J3	85	F1	Z2	2113-1-073
51	F1	Z2	EE800-M12J3	86	F1	ZE	2113-1-073
52	F1	Z2	EE800-M12J3	87	F1	ZN	2113-1-073
53	F1	Z2	EE800-M12J3	88	F1	Z2	2113-1-073
54	F1	Z2	EE800-M12J3	89	F1	Z2	578-062
55	F1	Z3	EE800-M12J3	90	F1	ZN	2113-1-073
56	F1	Z4	EE800-M12J3	91	F1	Z2	2113-1-073
57	F1	Z4	EE800-M12J3	92	F1	ZW	2113-1-073
58	F1	Z4	EE800-M12J3	93	F1	Z4	2113-1-073
59	F1	Z4	EE800-M12J3	94	F1	Z6	2113-1-073
60	F1	Z4	EE800-M12J3	95	F1	Z6	2113-1-073
61	F1	Z4	EE800-M12J3	96	F1	Z8	2113-1-073
62	F1	Z4	EE800-M12J3	97	F2	Z6	2113-1-073
63	F1	Z5	EE800-M12J3	98	F1	Z1	515-720
64	F1	Z6	EE800-M12J3	99	F1	Z2	515-720
65	F1	Z7	EE800-M12J3	100	F1	Z2	515-720
68	F1	Z2	HD 35ED 1NB (HD 35APW)	101	F1	Z2	515-720
69	F1	Z3	HD 35ED 1NB (HD 35APW0)	102	F1	Z2	515-720
70	F1	ZN	EE071-HTPC	103	F1	Z2	515-720
71	F1	Z7	MM880-DMF	104	F1	Z2	515-720
72	F1	Z7	MM880-DMF	105	F1	Z2	515-720
73	F1	Z7	MM880-DMF	106	F1	Z4	515-720
74	F1	Z7	MM880-DMF	107	F1	Z2	AMR-PT100(4L)
75	F1	Z7	MM880-DMF	201	F1	Z2	578-062
40	F1	Z7	MM880-DMF	108	F1	Z2	Phymeas-Type7
76	F1	Z7	EE650-T2J3L100-P1	109	F1	Z1	Phymeas-Type7
77	F1	Z7	EE650-T2J3L100-P1	110	F1	Z2	Phymeas-Type7
78	F1	Z7	EE160-HTX3XPBB	111	F1	Z2	Phymeas-Type7
79	F1	Z7	EE160-HTX3XPBB	112	F1	Z2	Phymeas-Type7
80	F1	Z7	EE850-M12-J3-P1	113	F1	Z2	Phymeas-Type7
81	F1	Z7	EE850-M12-J3-P1	114	F1	Z4	Phymeas-Type7
				115	F1	Z6	Phymeas-Type7
				116	F1	Z6	Phymeas-Type7
				117	F2	Z6	Phymeas-Type7
				118	F1	Z2	KPC1-5
				119	F1	Z2	KPC1-5
				120	F1	Z2	KPC1-5
				121	F1	Z2	KPC1-5
				122	F1	Z2	KPC1-5
				123	F1	Z2	KPC1-5
				124	F1	Z2	KPC1-5

Table D.2: Spatial Location in F1 of Fixed MMS' Sensor based on Figure D.2.

Spatial Localization of Fixed MMS' Sensor based on Figures D.3 and D.4

Digital Sensors				Analogue Sensors			
Sensor ID	Floor	Zone	Reference	Sensor ID	Floor	Zone	Reference
126	F2	Z6	EE800-M12J3	125	F2	Z13	GMP-220
127	F2	Z6	EE800-M12J3	46	F0	Z6	5561515-Itron
128	F2	Z1	EE800-M12J3				
129	F2	Z2	EE800-M12J3				
130	F2	Z3	EE800-M12J3				
131	F2	Z4	EE800-M12J3				
132	F2	Z4	EE800-M12J3				
133	F2	Z5	EE800-M12J3				
134	F2	Z7	EE800-M12J3				
135	F2	Z7	EE800-M12J3				
136	F2	Z8	EE800-M12J3				
137	F2	Z9	EE800-M12J3				
138	F2	Z10	EE800-M12J3				
139	F2	Z11	EE800-M12J3				
140	F2	Z13	4.920.00.000				
141	F2	Z13	SMP6				
142	F2	Z13	SMP6				
143	F2	Z5	MM880-DMF				
144	F2	Z5	MM880-DMF				
145	F2	Z5	MM880-DMF				
146	F2	Z5	MM880-DMF				
147	F2	Z5	MM880-DMF				
148	F2	Z12	MultiCal-403				
149	F2	Z12	MultiCal-403				
195	F2	Z12	EE650-T2J3L100-P1				
196	F2	Z12	EE650-T2J3L100-P1				
197	F2	Z12	EE160-HTX3XPBB				
198	F2	Z12	EE160-HTX3XPBB				
199	F2	Z12	EE850-M12-J3-P1				
200	F2	Z12	EE850-M12-J3-P1				

Table D.3: Spatial Location in F2 of Fixed MMS' Sensor based on Figures D.3 and D.4.

Spatial Localization of Mobile MMS' Sensor for Co-Heating Test based on Figure D.5

Digital Sensors				Analogue Sensors			
Sensor ID	Floor	Zone	Reference	Sensor ID	Floor	Zone	Reference
150	n.a.	n.a.	MM880-DMF	158	F0	Z6	2113-1-073
151	n.a.	n.a.	MM880-DMF	159	F0	Z1	2113-1-073
152	n.a.	n.a.	MM880-DMF	160	F0	Z1	2113-1-073
153	n.a.	n.a.	MM880-DMF	161	F0	Z1	2113-1-073
154	n.a.	n.a.	MM880-DMF	162	F0	Z2	2113-1-073
155	n.a.	n.a.	MM880-DMF	163	F0	Z2	2113-1-073
156	n.a.	n.a.	MM880-DMF	164	F0	Z2	2113-1-073
157	n.a.	n.a.	MM880-DMF	165	F0	Z5	2113-1-073
				166	F1	Z1	2113-1-073
				167	F1	Z1	2113-1-073
				168	F1	Z2	2113-1-073
				169	F1	Z2	2113-1-073
				170	F1	Z4	2113-1-073
				171	F1	Z4	2113-1-073
				172	F1	Z6	2113-1-073
				173	F1	Z6	2113-1-073
				174	F2	Z1	2113-1-073
				175	F2	Z2	2113-1-073
				176	F2	Z4	2113-1-073
				177	F2	Z5	2113-1-073
				178	n.a.	n.a.	515-720
				179	n.a.	n.a.	515-720
				180	n.a.	n.a.	515-720
				181	n.a.	n.a.	515-720
				182	n.a.	n.a.	515-720
				183	n.a.	n.a.	515-720
				184	n.a.	n.a.	515-720
				185	F0	Z6	Phymeas-Type7
				186	F0	Z1	Phymeas-Type7
				187	F0	Z1	Phymeas-Type7
				188	F1	Z2	Phymeas-Type7
				189	F0	Z2	Phymeas-Type7
				190	F0	Z5	Phymeas-Type7
				191	F1	Z1	Phymeas-Type7
				192	F1	Z2	Phymeas-Type7
				193	F1	Z4	Phymeas-Type7
				194	F2	Z6	Phymeas-Type7

Table D.4: Spatial Location of Mobile MMS' Sensor of Co-Heating test based on Figure D.5, Figure D.6 and Figure D.7.

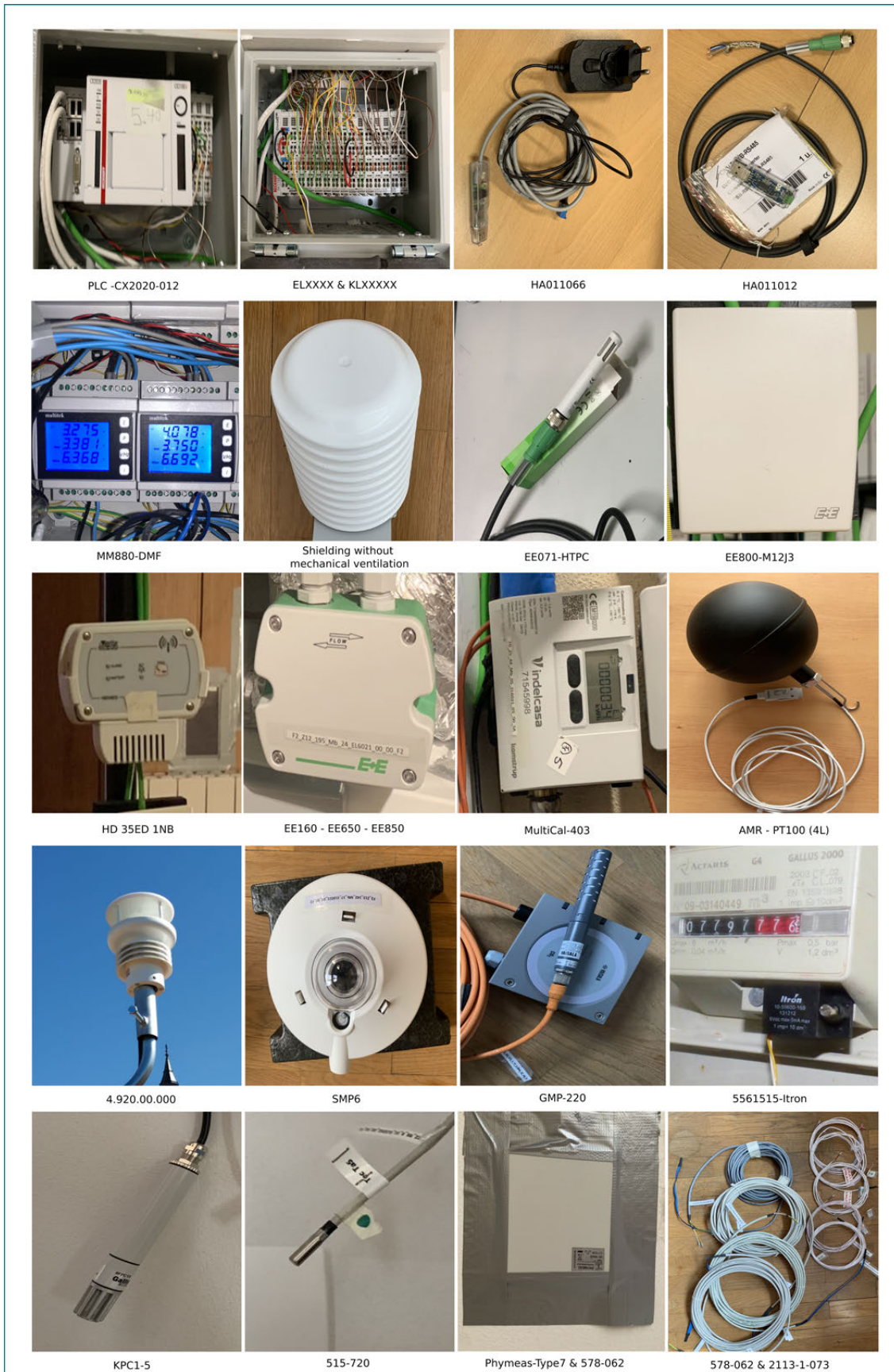


Figure D.8: Sensors and Hardware installed in residential building at Vitoria-Gasteiz.

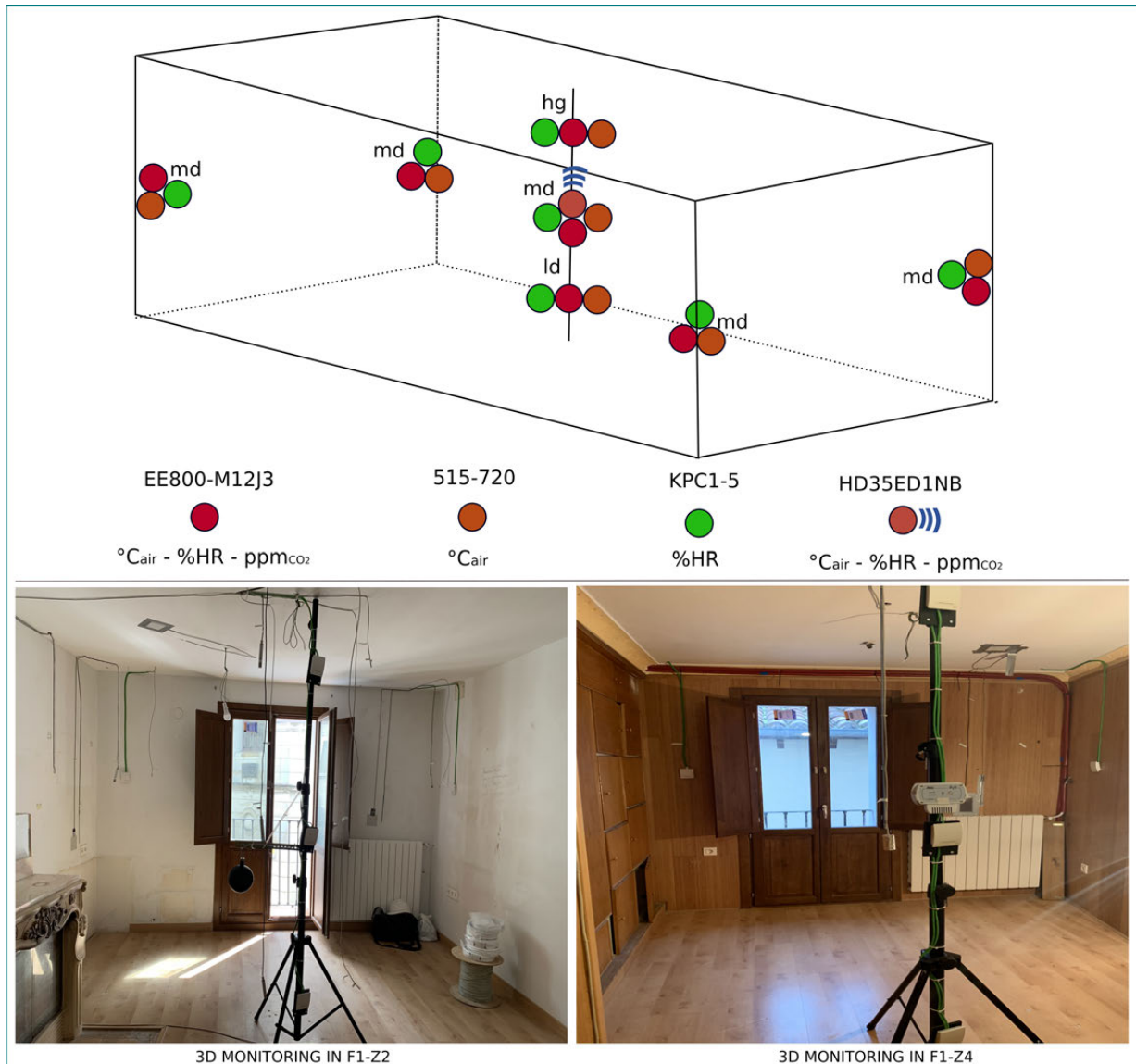


Figure D.9: Layout of 3D monitoring in Z2 and Z4 of F1.

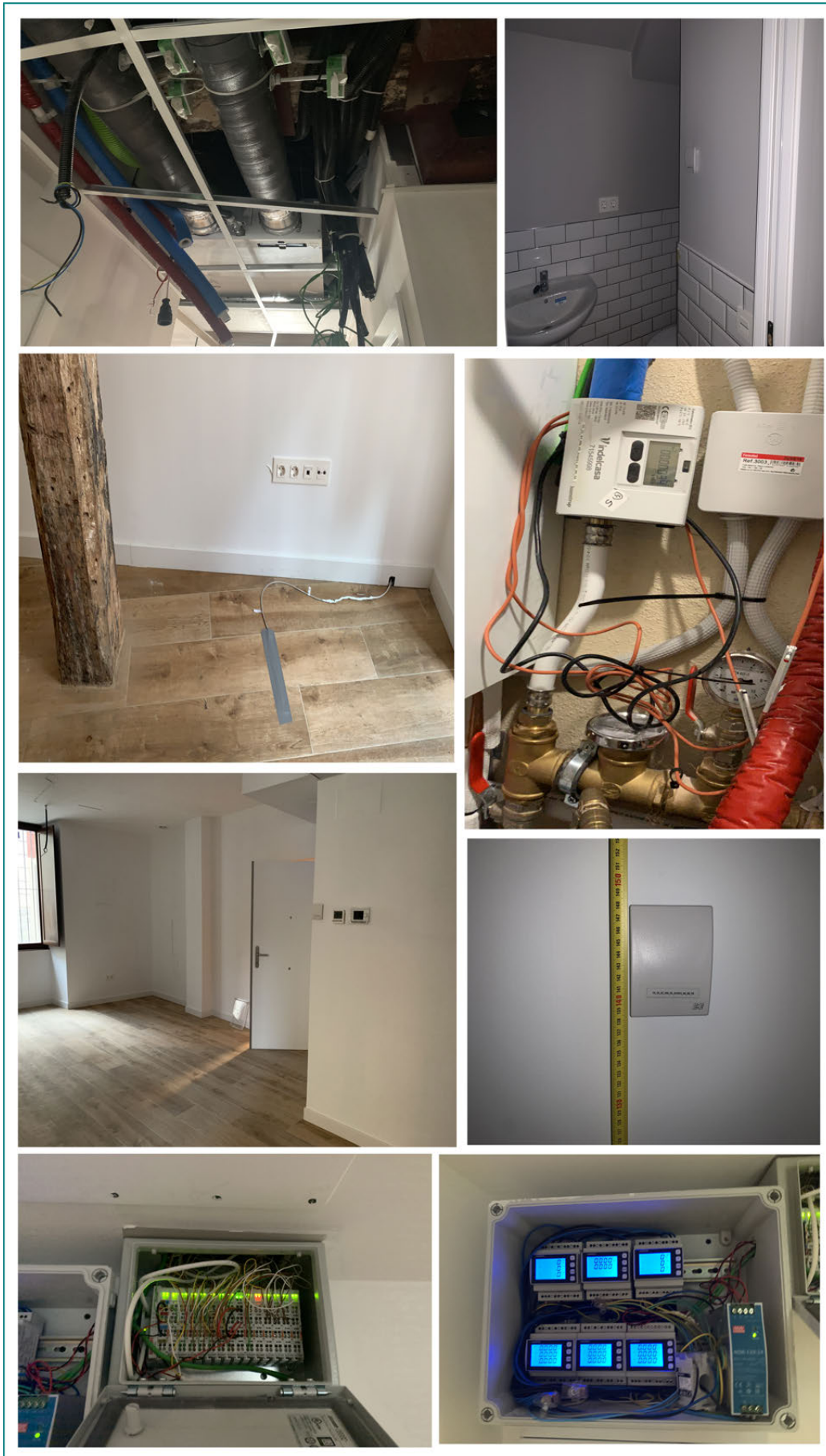


Figure D.10: Installed indoor sensors of Fixed MCS pictures in F0.



Figure D.11: Installed indoor sensors of Fixed MCS pictures in F1.

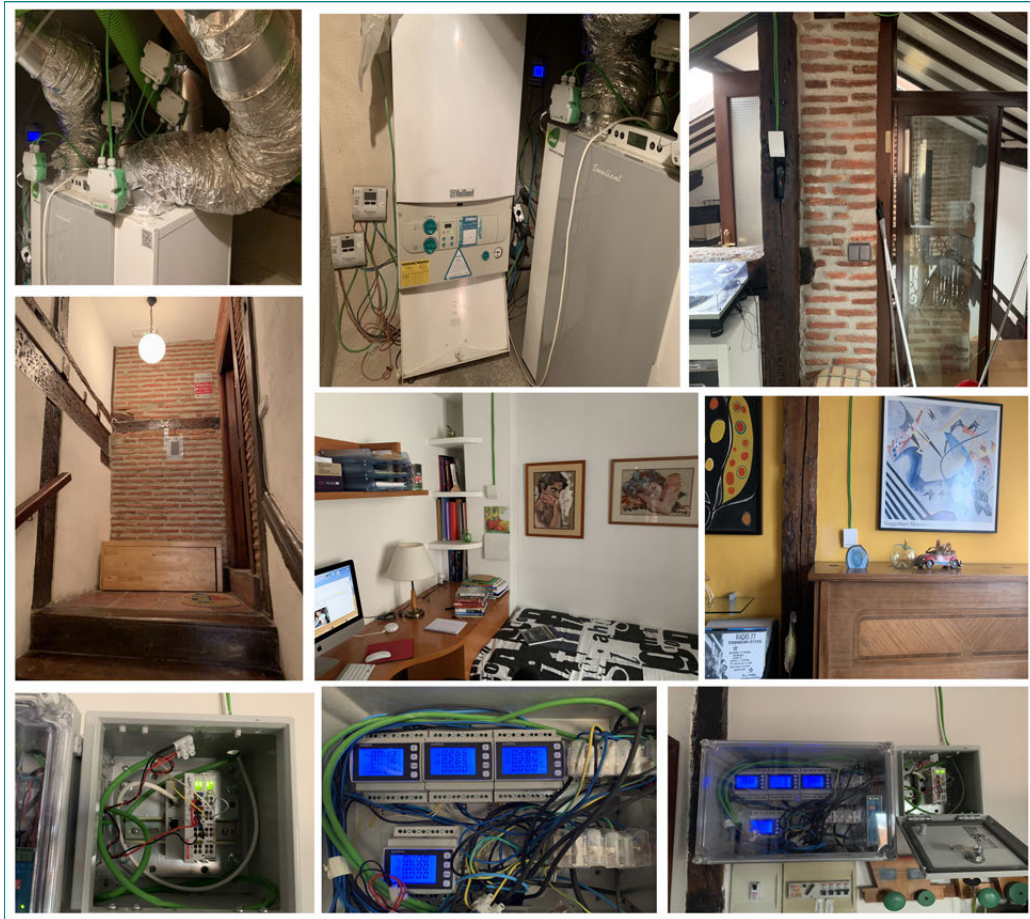


Figure D.12: Installed indoor sensors of Fixed MCS pictures in F2.



Figure D.13: Installed outdoor sensors of Fixed MCS pictures in roof.



Figure D.14: Hardware and electricity meters of Mobile MCS (Co-Heating Co-Heating).



Figure D.15: Hardware and electricity meters of Mobile MCS (mobile Co-Heating).

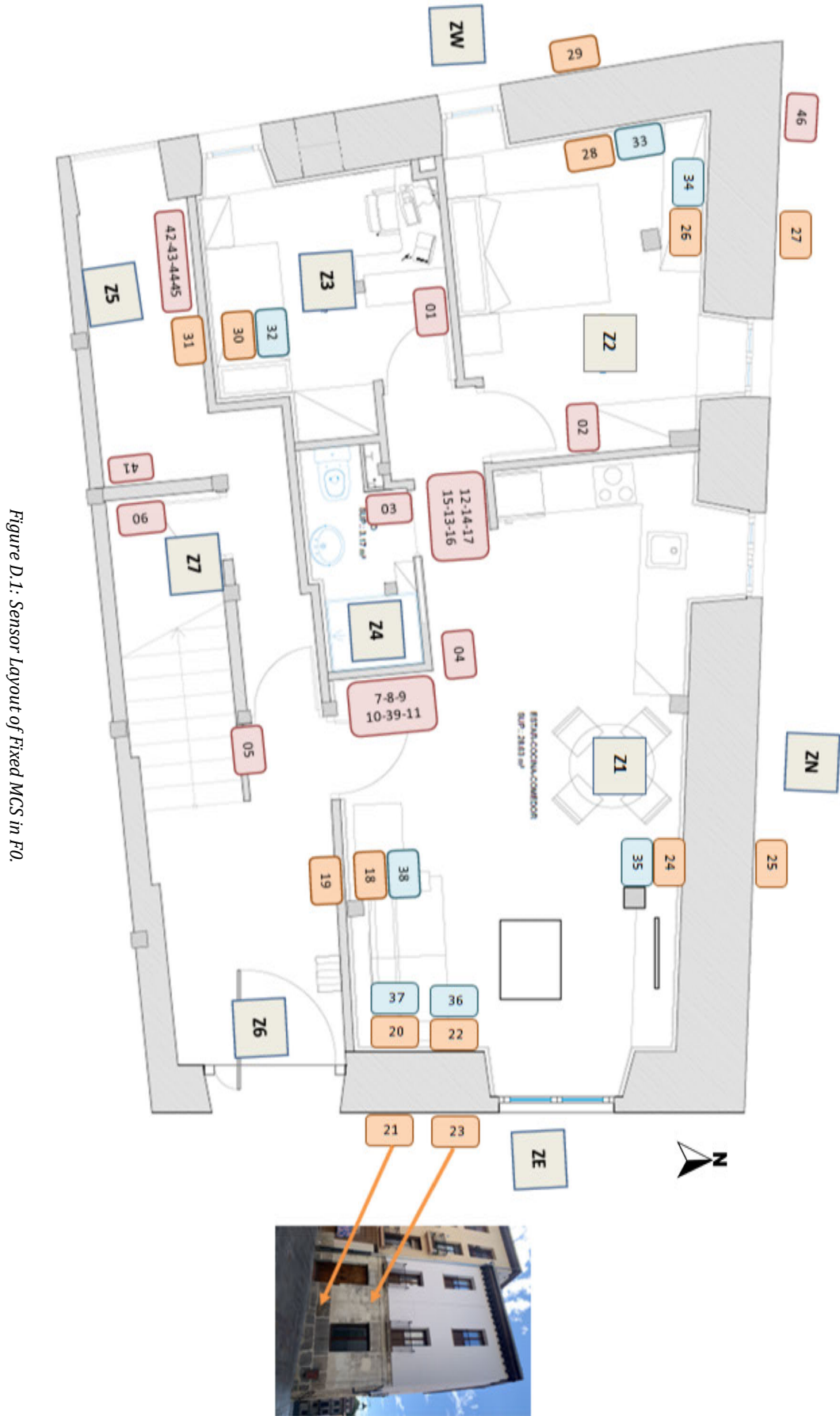


Figure D.1: Sensor Layout of Fixed MCS in F0.



Figure D.2: Sensor Layout of Fixed MCS in F1.

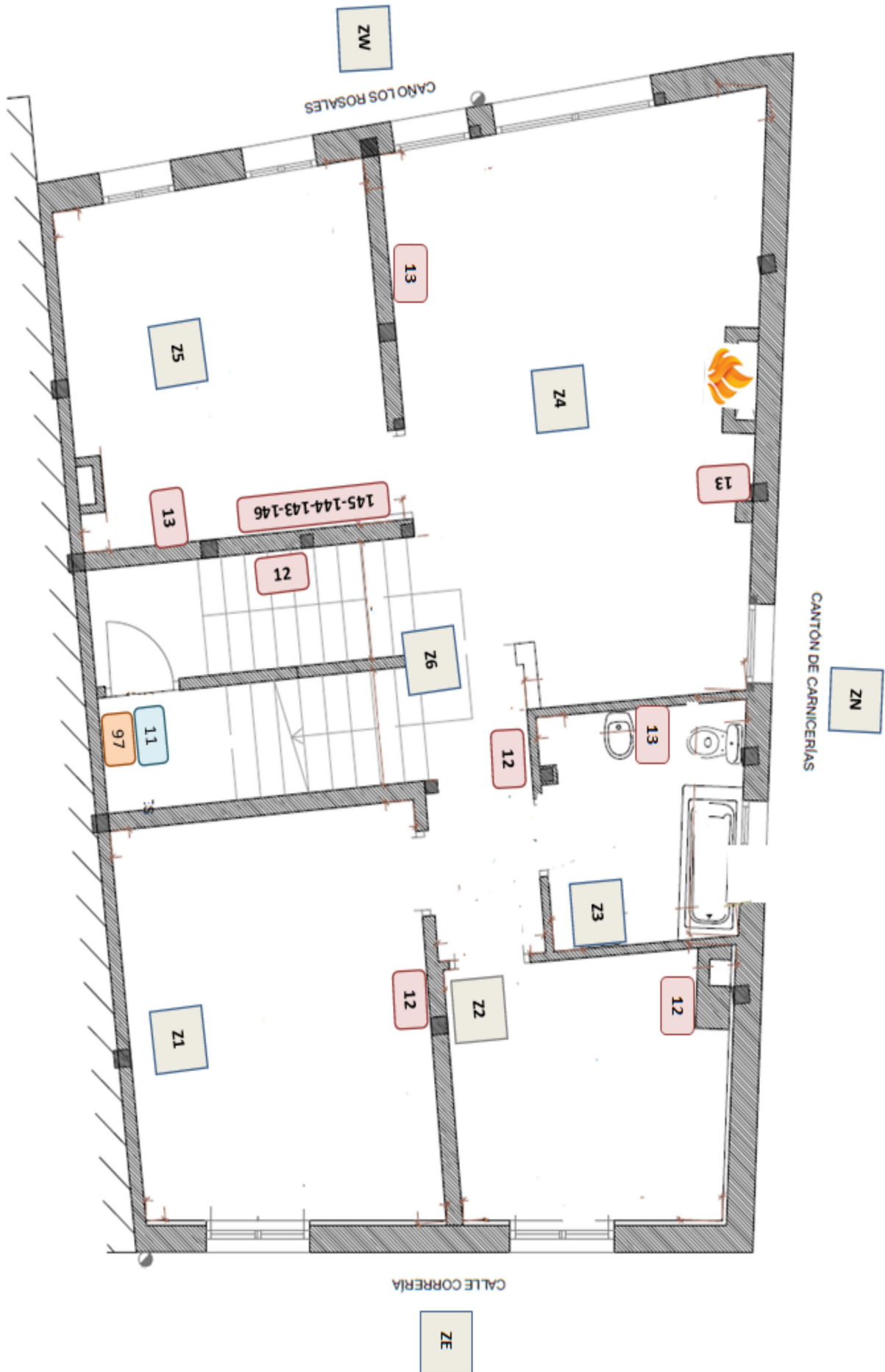


Figure D.3: Sensor Layout of Fixed MCS in first level of F2.

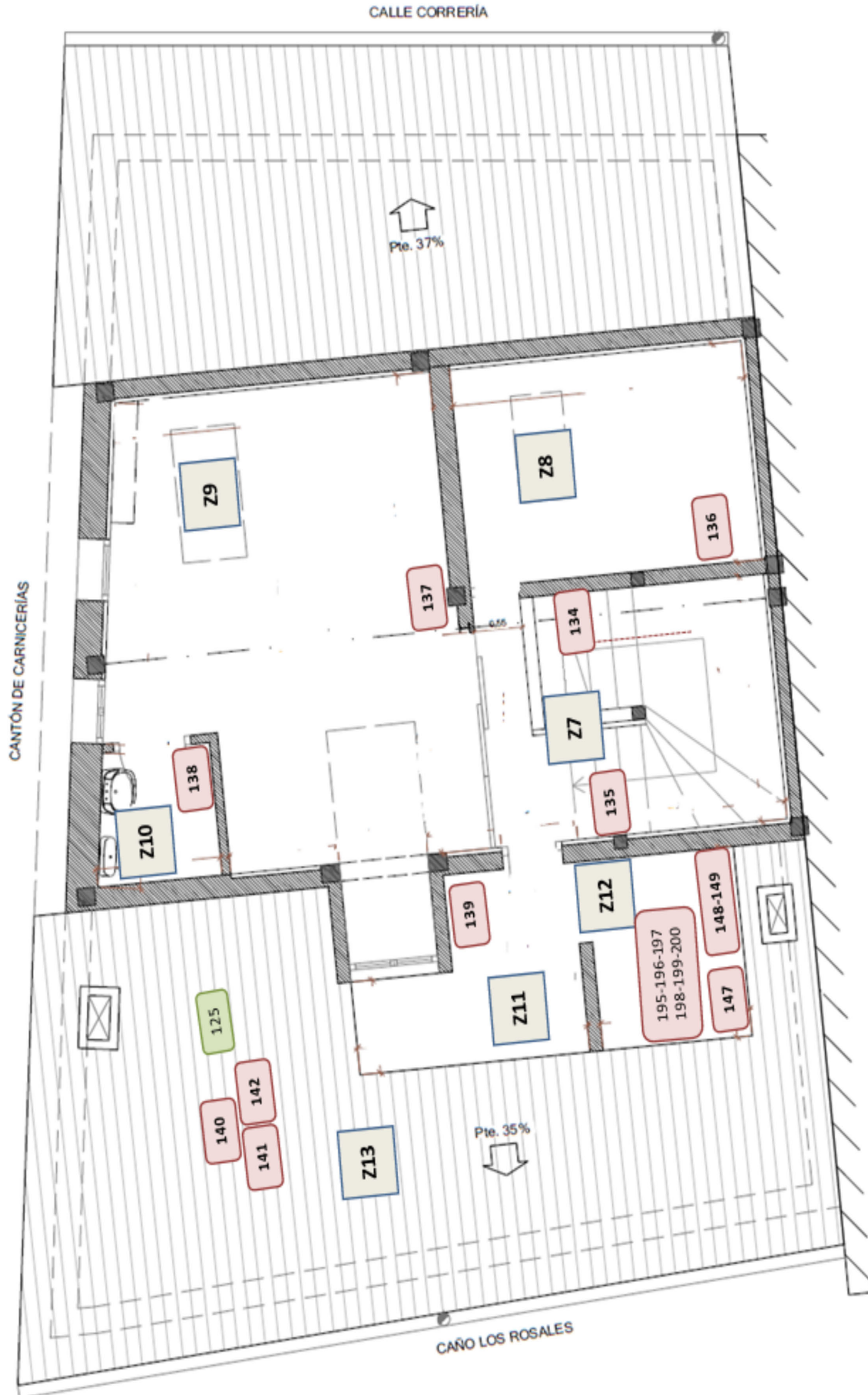


Figure D.4: Sensor Layout of Fixed MCS in second level of F2.



Figure D.5: Sensor Layout of Mobile MCS in F0 for Co-Heating test.



Figure D.6: Sensor Layout of Mobile MCS in F1 for Co-Heating test.



Figure D.7: Sensor Layout of Mobile MCS in F2 for Co-Heating test.

Appendix E

Budgets and invoices for the investment of tertiary building's MMS

SENSOVANT, S.L.
NIF B30706634

Av. Benjamin Franklin, 28-B. (Valencia Parc Tecnologic)
46980 PATERNA (VALENCIA) ESPAÑA
Teléf. 96 8162005, 672402132
admon@sensovant.com - www.sensovant.com

S.U.M. ENSANCHE 21 ZABALGUEÑA, S.A.
NIF A-01302462

Paseo Fray Francisco, 21 - C
01007 - VITORIA - GASTEIZ
ÁLAVA - ESPAÑA

Cliente: 2.265

Divisa: EUR

Transportista: C-EXPRESS

Referencia	Descripción	Cantidad	Precio	% Dto.	Importe
EE800-M12J3P1	SENSOR CO2-TEMPERATURA Y HUMEDAD SUPERFICIE CAJA EMBELLECIDA, MODBUS RS485 Part. Arancelaria: 90271010	21	305,00	25%	4.803,75



M12-J3-PY0-BT2 ModBus RTU



DATOS BANCARIOS CAJAMAR: ES79 3058 0311 7027 2030 1396

Suma Importes	% Dcto. PP	Portes	Gastos	Cuota de I.V.A.	Cuota R.E.	Retención	TOTAL
4.803,75				1.008,79			5.812,54

Desglose del I.V.A.			Recargo de Equivalencia		Retención		Forma de Pago
Base	% IVA	Cuota IVA	% R.E.	Cuota R.E.	Base	% Ret.	
4.803,75	21%	1.008,79					CONTADO PREVIO ENVIO MATERIAL. FACTURA PROFORMA

CONTROL LLEVANT INSTRUMENTACION Y CONTROL, SL
NIF B30706634

Av. Benjamin Franklin, 28-B. Valencia Parc Tecnologic
46980 PATERNA (VALENCIA) ESPAÑA
Teléf. 96 8162005, 672402132
admon@sensovant.com - www.sensovant.com


UNIVERSIDAD DEL PAIS VASCO/EHU
NIF Q4818001B

ATT. AITOR ECORECA GONZALEZ
DPTO. DE MAQUINAS Y MOTORES TERMICOS, Alameda
Urquijo, s/n
48013 - BILBAO
BIZKAIA - ESPAÑA

Cliente: 1.110

Divisa: EUR

Transportista: C-EXPRESS

Referencia	Descripción	Cantidad	Precio	% Dto.	Importe
EE071-HTPC	EE071-HTPC Part. Arancelaria: 90258040	9	165,00	15%	1.262,25
	 <p>SONDA HUMEDAD-TEMPERATURA E+E SALIDA MODBUS, CONECTOR M12 MACHO. FILTRO MALLA</p> <p>EE071-HTPC-CAN2</p>				



DATOS BANCARIOS CAJAMAR: ES79 3058 0311 7027 2030 1396

Suma Importes	% Dcto. PP	Portes	Gastos	Cuota de I.V.A.	Cuota R.E.	Retención	TOTAL
1.262,25		10,00		267,17			1.539,42

Desglose del I.V.A.			Recargo de Equivalencia		Retención		Forma de Pago	
Base	% IVA	Cuota IVA	% R.E.	Cuota R.E.	Base	% Ret.	ORGANISMOS Y ENTIDADES PUBLICOS CAJAMAR	
1.272,25	21%	267,17						

IBAN ES** **** **** 1396



SAFER INSTRUMENTACIÓN S.L

Elizalde, 4 lonja dcha.
Teléfono: 94-4129981
48006 BILBAO.
CIF : B95039210
safer@saferinstrument.com

MOTORIZACION Y AUTOMATIZACION
INSTRUMENTOS DE MEDIDA
ANALISIS Y CONTROL

S.U.M. ENSANCHE 21 ZABALGUNEA, S.A.
Paseo Fray Francisco, 21 C
01.007- VITORIA-GASTEIZ.
(ARABA)

FACTURA Nº 2019/ 366

Nº PEDIDO : PEDIDO 31.05.19

FECHA 18-06-19

C.I.F./D.N.I. A-01302462

Albarán nº	ARTICULO	Cant.	Precio Euros	Dto.	IMPORTE Euros
375	Sensor de Medida de Temperatura Globométrica (PT100 4 L) AMR, modelo FPA805GTS, salida hilos. - Rango de Temperatura: -50 a +200º C. - Precisión: PT100 Clase B. Su Pedido del 31.05.19. N/Oferta Nº. 19/479-FG-FGC. Lugar de Entrega: S.U.M. ENSANCHE 21 ZABALGUNEA, S.A. Paseo Fray Francisco , 21 C 01.007-VITORIA-GASTEIZ (ÁLAVA). AT. SRA. CRISTINA GÓMEZ. AT. SRA. ISABEL PINEDA. TELF: 945-16.26.00.	1	510,00		510,00
IMPORTE MERCANCIA Euros		% I.V.A.	IMPORTE I.V.A. Euros		IMPORTE FACTURA Euros
510,00		21	107,10		617,10

Forma de Pago : 30 DIAS TRANSFERENCIA.

25-07-19 617,10

BCO. LABORAL KUTXA BILBAO.

C/C. 3035017431 1740024460

SAFER INSTRUMENTACION,S.L. Inscrita en el R.M. de Bizkaia, Tomo 3.802, Folio 117, Hoja B1025459.

Nº PRODUCTOR REI-RAEE 6271

CONTROL LLEVANT INSTRUMENTACION Y CONTROL, SL
NIF B30706634

Av. Benjamin Franklin, 28-B. Valencia Parc Tecnologic
46980 PATERNA (VALENCIA) ESPAÑA
Teléf. 96 8162005, 672402132
admon@sensovant.com - www.sensovant.com

UNIVERSIDAD DEL PAIS VASCO/EHU
NIF Q4818001B

Alameda Urquijo, s/n
48013 - BILBAO
VIZCAYA - ESPAÑA

Cliente: 1.110

Divisa: EUR

Referencia	Descripción	Cantidad	Precio	% Dto.	Importe
	Albarán A/181147 de 12/12/2018.				
	Pedido A/181129 de 12/12/2018.				
	Proforma A/180285 de 11/12/2018.				
EE871-HR2000-F5-1AN2	SENSOR CO2 E+E 2000 PPM SALIDA MODBUS RS485, FILTRO TEFLON	2	420,00	15%	714,00
RSHIELD-PM20	PROTECTOR SOLAR INTEMPERIE SONDAS HUMEDAD/TEMPERATURA DIAMETRO 6-12MM Part. Arancelaria: 90158020	8	95,00	15%	646,00
RSHIELD-CO2	PROTECTOR SOLAR INTEMPERIE SONDAS CO2 EE870/871 CON CAJA CONEXIONES IP65	2	180,00	15%	306,00
HA010508	PROTECTOR SOLAR INTEMPERIE VETILACION MECANICA FORZADA	1	980,00	15%	833,00
HA011066	KIT CONFIGURACION USB SONDAS E+E	1	380,00	15%	323,00
HA010819	CONECTOR M12 + CABLE 1.5 METROS	1	50,00	15%	42,50
HA011012	CONVERTIDOR RS485-USB	1	360,00	15%	306,00



DATOS BANCARIOS CAJAMAR: ES79 3058 0311 7027 2030 1396

Suma Importes	% Dcto. PP	Portes	Gastos	Cuota de I.V.A.	Cuota R.E.	Retención	TOTAL
---------------	------------	--------	--------	-----------------	------------	-----------	--------------

Desglose del I.V.A.			Recargo de Equivalencia		Retención		Fechas de Pago		Forma de Pago
Base	% IVA	Cuota IVA	% R.E.	Cuota R.E.	Base	% Ret.	Fecha	Importe	
							12/12/2018	3.848,41	

FACTURA

ARQUEDOMO ESTUDIO, S.L.
San Antonio, 10-1º
41100 Coria del Rio (Sevilla)
Tel. 900 52 51 08
CIF. B-91960823
arquedomo@arquedomo.com



Numero Factura: 1808	Fecha factura: 11/12/2018
--------------------------------	-------------------------------------

Aitor Ercoreca Gonzalez
UPV / EHU
Departamento de Máquinas y Motores Térmicos
Alameda Urquijo s/n
48013 BILBAO
CIF: Q-48/18001-B

Descripción

Concepto	Precio	Cantidad	Total
Suministro de 2 pasarelas de comunicaciones Modbus – KNX según oferta N°1913	299,00 €	2	598,00 €

Base Impon. 598,00 €	IVA 21%	Importe IVA 125,58 €	Total Factura 723,58 €
--------------------------------	-------------------	--------------------------------	----------------------------------

Forma de pago

Tranferencia a N° de cuenta: ES79 2100 2518 16 0210119583

Contacto: José Manuel Alonso



Amidata S.A.U.
 Avda. Europa 19 Edif.3
 28224 Pozuelo de Alarcón
 Madrid

COPIA DE FACTURA

Fecha de Factura 14.03.2019
 Pagador nº 11589965
 Dirección de envío de factura nº 14513297
 CIF ESQ4818001B
 Factura Nº 61609197
 Página 1 de 1

DIRECCIÓN DE PAGO
 UNIVERSIDAD DEL PAIS VASCO
 E.T.S.DE INGENIERIA
 Plaza Torres Quevedo 1
 48013 Bilbao-VIZCAYA

DIRECCION ENVIO FACTURA
 UNIVERSIDAD DEL PAIS VASCO
 U02000279
 U02000001
 U02000137
 48013 Bilbao

Referencia pedido cliente	Pedido RS	Cliente	Código cliente
149010526	149010526	Catalina Giraldo Soto 94-6017322	76786381

Código destino	DIRECCION ENTREGA PEDIDO
11589965	UNIVERSIDAD DEL PAIS VASCO E.T.S.DE INGENIERIA Catalia Giraldo Soto - Dpto. Máquinas y Motores TérmicosC. Plaza Torres Quevedo 1 48013 Bilbao-VIZCAYA

Albarán 1154512964 Fecha de envío 14.03.2019

Artículo	Código RS	Descripción	Cantidad	Unidad de venta	Precio Unitario	Importe línea	IVA
10	7080448	Operación exenta art. 25 Ley 37/1992 del IVA Power Supply Step, 12V 1A 1AC HS code 85044082 *** SERVICIO ESTANDAR ***	1	C/U	41,17	41,17	21,00%
						Base Imponible	41,17
						IVA	8,65
						Total - EUR	49,82

Valor neto Total	Base Imponible	%IVA	IVA (EUR)
41,17	41,17	21,00%	8,65

Términos de pago
 60 días desde fecha factura
 Hasta el 13.05.2019 sin deducción 13.05.2019 49,82

NOTA IMPORTANTE : Les informamos que nuestro sistema informático no tiene la flexibilidad de retrasar las fechas de pago por motivo vacacional.Les rogamos que efectúen los pagos sin demoras, a fin de evitar la suspensión de envío de material.

Su pedido queda aceptado bajo las condiciones de ventas publicadas en nuestro catálogo. En caso de de que tenga que realizar una reclamación sobre el contenido de esta factura, por favor contacte con nosotros dentro de los 10 días siguientes a la fecha de emisión de este documento

Pago. Los cheques deben ser enviados a la dirección que aparece reflejada en el principio de este documento, y nominativo a AMIDATA S.A.U. En el caso de que deseen pagar por transferencia, le remitimos nuestros datos bancarios: BNP Paribas, Ribera del Loira, nº28, 28042, Madrid IBAN= ES1301490101110060198001 - SWIFT CODE= BNPAESMSXXX. Les rogamos que indiquen como referencia el número de factura/as que abonen.

Inscrito en el Registro Mercantil de Madrid, tomo 73, libro 67, sección 3ª, folio 24, Hoja 61026-1, inscripción 1ª, con CIF A78913993 No. R.I. AEE Productor 3457



Amidata S.A.U.
 Avda. Europa 19 Edif.3
 28224 Pozuelo de Alarcón
 Madrid

COPIA: ABONO POR DEVOLUCIÓN

Fecha nota de abono 19.03.2019
 Pagador nº 11589965
 Dirección de envío de factura nº 14513297
 CIF ESQ4818001B
 Nota de abono numero 10286365
 Numero Factura original 61599826
 Fecha Factura original 05.03.2019
 Página 1 de 1

DIRECCIÓN DE PAGO
 UNIVERSIDAD DEL PAIS VASCO
 E.T.S.DE INGENIERIA
 Plaza Torres Quevedo 1
 48013 Bilbao-VIZCAYA

DIRECCION ENVIO FACTURA
 UNIVERSIDAD DEL PAIS VASCO
 U02000279
 U02000001
 U02000137
 48013 Bilbao

Referencia pedido cliente	Pedido RS	Cliente	Código cliente
148822649	239709871	Catalina Giraldo Soto 94-6017322	76786381

Código destino 11589965
 DIRECCION ENTREGA PEDIDO
 UNIVERSIDAD DEL PAIS VASCO
 E.T.S.DE INGENIERIA
 MAQUINAS Y MOTORES TERMICOS
 Catalina Giraldo Soto
 Plaza Torres Quevedo 1
 48013 Bilbao-VIZCAYA

Artículo	Código RS	Descripción	Cantida d de venta	Unidad de venta	Suministrado en múltiplos de	Precio unitario	Importe línea	IVA
20	6925438	Operación exenta art. 25 Ley 37/1992 del IVA 4 way shielded plastic DIN cable socket	5	C/U	5	3,182	15,91	21,00%
40	1368315	HS code 85366990 Din Rail Power Supply, 70W, 24V Output	1	C/U		25,83	25,83	21,00%
60	7211406	HS code 85044084 SAC-5P-Y/2XFS VP SCO	1	C/U		21,70	21,70	21,00%
80	6925472	HS code 85366990 4 way shielded plastic DIN cable plug	5	C/U	5	4,124	20,62	21,00%
		HS code 85366990						

Base Imponible 84,06
IVA 17,65
Total - EUR 101,71

Valor neto Total	Base Imponible	%IVA	IVA (EUR)
84,06	84,06	21,00%	17,65

NOTA IMPORTANTE : Les informamos que nuestro sistema informático no tiene la flexibilidad de retrasar las fechas de pago por motivo vacacional.Les rogamos que efectúen los pagos sin demoras, a fin de evitar la suspensión de envío de material.

Su pedido queda aceptado bajo las condiciones de ventas publicadas en nuestro catálogo. En caso de de que tenga que realizar una reclamación sobre el contenido de esta factura, por favor contacte con nosotros dentro de los 10 días siguientes a la fecha de emisión de este documento

Pago. Los cheques deben ser enviados a la dirección que aparece reflejada en el principio de este documento, y nominativo a AMIDATA S.A.U. En el caso de que deseen pagar por transferencia, le remitimos nuestros datos bancarios: BNP Paribas, Ribera del Loira, nº28, 28042, Madrid IBAN= ES1301490101110060198001 - SWIFT CODE= BNPAESMSXXX. Les rogamos que indiquen como referencia el número de factura/as que abonen.

Inscrito en el Registro Mercantil de Madrid, tomo 73, libro 67, sección 3ª, folio 24, Hoja 61026-1, inscripción 1ª, con CIF A78913993 No. R.I. AEE Productor 3457

Factura

Farnell Components, S.L. (sociedad unipersonal)

Parque Empresarial Cityparc
Edificio Londres, 2ª Planta
Ctra. de Hospitalet, 147-149
08940 Cornellá (Barcelona)

Tel: 93 475 88 05
Fax: 93 474 52 88



es.farnell.com

element14

www.element14.com

Nº Factura	2940046
Fecha Factura	7 MAR 2019
Fecha Pedido	7 MAR 2019
Nº Cuenta Cliente	890210
Nº Albarán	
Página	1

Universidad Pais Vasco UPV/EHU
Plaza Ingeniero Torres Quevedo
1
BILBAO
48013 BIZKAIA
SPAIN

UNIVERSIDAD DEL PAÍS VASCO UPV/EHU.
PL. INGENIERO TORRES QUEVEDO 1
ESCUELA INGENIEROS DE BILBAO
48013 BILBAO
BIZKAIA Spain

Dirección de Envío

C.I.F.: Q4818001B

Nº Pedido	-	Nuestra Ref:	6670-0220/01
-----------	---	--------------	--------------

N Linea	Cod Farnell / Descripción	U.E.	Cantidad Enviada	Precio Unitario	Precio Neto	IVA	Importe
1	2918314 120068-8009 EMPALME DE SENSOR, ESTILO T, TPU, NEGRO Despatch Note No GB1-004877348 Tariff Code: 85366990	UD	10	28.4000	28.4000	21.00	284.00
2	2080256 ES: ACCOUNT WELCOME OBSEQUIO DE BIENVENIDA Despatch Note No LG1-008296839 Tariff Code: 49111010 OFICINA CONTABLE U02000279 ORGANO GESTOR U02000001 UNIDAD TRAMITADORA U02000137 PEDIDO REALIZADO POR CATALINA GIRALDO SOLTO RII AEE : nÂ° 2340 REI RPA : nÂ° 980	UD	1	0.0000	0.0000	21.00	0.00

Conforme a lo establecido en la Ley Orgánica 15/1999, de Protección de Datos de Carácter Personal y su normativa de desarrollo, le informamos que los datos personales proporcionados son confidenciales y forman parte de los ficheros titularidad de FARNELL COMPONENTS, S.L. con la finalidad de gestionar la relación comercial y contractual, para la que son necesarios, así como proporcionarle información referente a nuestros productos y servicios, vinculados directamente con la relación comercial y/o contractual que nos une, ya sea por correo electrónico, postal o fax.
En cualquier caso podrá ejercer los derechos de acceso, rectificación, cancelación y oposición previstos en la ley mediante escrito dirigido a FARNELL COMPONENTS, S.L. Parque Empresarial Cityparc, Edificio Londres 2º, Crta. Hospitales, 147-149 08940 Cornellá Barcelona o mediante correo electrónico a la dirección spmarketing@farnell.com junto con su identificación a través del DNI.

Aviso Importante La no entrega o cualquier discrepancia en la misma debe notificarse, por escrito a Farnell Components, S.L. (sociedad unipersonal) en un plazo máximo de 3 días desde la recepción del material, en otro caso ninguna reclamación será aceptada. El propietario de la mercancía es Farnell Components, S.L. (sociedad unipersonal) hasta la recepción del pago total de la misma. Condiciones de venta indicadas en el catálogo actual.	IVA %	Base Imponible	IVA		
	21.00	284.00	59.64	Subtotal	284.00
				IVA	59.64
				Total Factura	EUR 343.64

Fecha de vencimiento: 6 ABR 2019	Forma de pago: 30 días, fecha factura
-------------------------------------	--

Reg. Merc. Madrid:
Tomo 13.951, Libro 0, Folio 143, Sección 8, hoja M.-228575,
Insc. 1ª - C.I.F.: B82229907

Bank of America N.A. Sucursal en España
IBAN: ES09 1485 0001 0100 3567 4015
BIC: BOFAES2X

NUESTRA CUENTA BANCARIA			
BANCO	OFICINA	D.C.	CUENTA
1485	0001	01	0035674015

ELEKTRA S.A. (VITORIA)

Capelamendi, 10

1013 Vitoria

Tel: 945253300

Fax: 945283900



Oferta Número

138702 / 1

Fecha Oferta

22/02/2019

Fecha Validez

22/03/2019

Nuestra Referencia

Catalina

Asunto

Hoja

1

Vendedor

JONATHAN

071577

UPV/EHU UNIVERSIDAD DEL PAIS VASCO

COMANDANTE IZARDUY, 2

01006 VITORIA

De acuerdo con su petición , nos es grato presentarle la siguiente oferta económica

Artículo	Concepto	Cantidad	Precio	Dto	Importe
90213	LAPP 2170204 UNITONIC BUS LD 2X2X0,22 Plazo: 1 semana	400,00	83,33/C		333,32
622938	LAPP 0030922 UNITRONIC-FD-CP(TP)PLUS 5x2x0,25 Plazo: Inmediato	400,00	311,23/C		1.244,92

Precios en blanco=Unidad, D=Decena, C=Centena, M=Millar

Suma Oferta	% Portes y embalajes	% Dto. pronto pago	% Gastos financieros	% Gastos gestión	
1.578,24					
Base Imponible		% I.V.A.	% Rec. equivalencia		
1.578,24		21,00	331,43		
					TOTAL
					1.909,67 €



Invoice Nr.: 40178730

Thomann GmbH, Hans-Thomann-Str. 1, D-96138 Burgebrach

Universidad del País Vasco (UPV/EHU)
Nif Q4818001b Dept. Maquinas y Motores Termicos
Alameda Urquijo S/n,

E-48013 Bilbao

Delivery address:

Universidad del País Vasco (UPV/EHU)
Aitor Ercoreca González Pl. Ingeniero Torres Quevedo 1. Esc Inge
de Bilabao.Dpto.Máq. y Motores Térmicos

E-48013 Bilbao

Invoice Nr.: 40178730

Date: 05.02.2019

Your customer no.: 10686704

Order No.: 201906.396880 / 2195

Sales Person: Christian Carrión Pérez

Telephone: 0049 9546 / 9223 644

Method of Shipment: UPS

Your Reference:

N.I.F. Nr.: ES N2760245G

**Please include your customer no.: 10686704 with
payment by bank transfer!**

Pos.	Article	Amount	Unit	Unit Price	Total Price
001.00	287838	8	piece	37,00 EUR	296,00 EUR
Stairville BLS-315 Pro lighting and speaker stand with 35mm Adapter, black. Professional and stable light stand, Magnesium compound. Single reinforced legs for a high Stability. Technical specifications: Material: Steel and magnesium, Height: 150 cm - 310 cm (Transport Length: 124 cm) footprint diameter: Ø 120 cm, tube diameter: Ø 28 mm + 35,5 mm (fits not on all speakers!), adapter, max. Load 30 kg, weight: 5.60 kg, color: black, Made in Europe, Optional accessories (not included): crossbar 100 cm: #293501, crossbar 120 cm: #293504, adapter for single light: #293511, matching bag: #293512					

Value of goods: **296,00 EUR**

Net amount: 244,63 EUR

21,00% Vat.: 51,37 EUR

Total amount: 296,00 EUR

Method of payment:

Visa Card 296,00 EUR

Thank you for your purchase!

Please see overleaf for our standard terms and conditions.
Unless otherwise specified the invoice date accounts for the date of payment /delivery.

Thomann GmbH
Hans-Thomann-Str.1
D-96138 Burgebrach

info@thomann.de
Tel +49 (0)9546 9223-66
Fax +49 (0)9546 9223-24

Geschäftsführer: Hans Thomann
Amtsgericht Bamberg: HRB 5862
Sitz der Gesellschaft: Burgebrach

USt.-IdNr.: DE 257375233
Steuernummer: 207/132/90050
WEEE-Reg.-Nr.: DE 18280160

Bank Sparkasse Bamberg
IBAN DE97 7705 0000 0000 1030 85
BIC BYLADEM1SKB

Raiffeisenbank Burgebrach
DE58 7706 2014 0000 0056 30
GENODEF1BGB

Postbank Nürnberg
DE41 7601 0085 0283 5648 54
PBNKDEFF

Deutsche Bank 24
DE19 7607 0024 0811 5008 00
DEUTDEB3760

Es gelten unsere umseitig abgedruckten Allgemeinen Geschäftsbedingungen.



Alutec Metallbau GmbH, Blumenstraße 24, 72285

Universidad del País Vasco UPV/EHU
NIF Q4818001B
Dpto Máquinas y Motores Térmicos
C/ Alameda de Urquijo s/n. CP
48013 Bilbao
Spanien

Alutec Metallbau GmbH
Dominik Gonser
Blumenstraße 24
72285 Pfalzgrafenweiler
Tel: +49 7445 85210
Fax: +49 7445 852120
Web: www.alutec-racingparts.de
E-Mail: racing@alutec-metallbau.de
Bearbeiter: Administrator

Rechnung

Seite: 1

04.02.2019

Rechnungsnr. RE2019-21344 bzgl. Auftragsnummer: AU2019-24296

Kundennummer: KN22523

Pos.	Menge	ArtNr	Bezeichnung	Ust.	E-Preis	G-Preis
1	1 Stück	ESR501000	50mm Edelstahlrohr 1m	19%	13,36	13,36
2	1		GLS	19%	20,92	20,92

Gesamt Netto (19,00%) 34,29 €

zzgl. 19,00% MwSt. 6,51 €

Gesamtbetrag 40,80 €

Zahlung (Amazon Payment) vom 04.02.2019 40,80 €

Offener Betrag 0,00 €

Amazon Order 404-4919501-8814704

GLS

Das Rechnungsdatum entspricht dem Lieferdatum.

Vielen Dank für Ihren Auftrag.


[Ayuda compra on-line](#)


Gracias por tu compra

Catalina Giraldo Soto , muchas gracias por hacer tu compra en Leroy Merlin.

Producto	Cantidad	Precio
 Pie de parasol HORMIGON BLANCO ref. 17853724 Más info	1	45,95€
Subtotal		45,95€
Gastos de envío		0,00€
Importe total (1 producto)		45,95€
Plazo de entrega estimado en 5 días excepto sábados, domingos y festivos		

Datos para el envío

Catalina Giraldo Soto
 Zaramaga
 Álava,01013
 Spain
 675975866

Para retirar tus productos es imprescindible mostrar el DNI del propietario del pedido o de la persona autorizada



Tienda Vitoria
 Centro Comercial Centro Comercial
 Boulevard.
 Zaramaga
 01013 Vitoria - Álava.
 Tel. 945129900

Horarios
 De Lunes a Sábado de 09:00 a 22:00

[Ver en Google Maps](#)

Número de pedido:

2713884

GRUPE *adeo*

[Aviso legal](#) @ Leroy Merlin España S.L.U. 2015

De: UPV_EHU_BCDTRAVEL
A: [Catalina Giraldo Soto](mailto:Catalina.Giraldo.Soto)
Asunto: Fwd: GIRALDO/CATALINA 01JUL2019 BILBAO
Fecha: viernes, 28 de junio de 2019 15:05:50

----- Forwarded message -----

De: <UPV-EHU@bcdtravel.es>
Date: vie., 28 jun. 2019 a las 15:03
Subject: GIRALDO/CATALINA 01JUL2019 BILBAO
To: <CINEA.VIAJES@bcdtravel.es>

BCD TRAVEL
AVDA MAZARREDO 16-18
48009 BILBAO
VIZCAYA
SPAIN

TELEFONO: +34946050000
FAX: TBA
E-MAIL: BILBAO.EMP@BCDTRAVEL.ES

CODIGO DE RES.: U35FBB
FECHA: 28 JUNIO 2019
GIRALDO/CATALINA

COCHE
2019

LUN 01 JULIO

RECOGIDA: BILBAO 01
JUL
DEVOLUCION: 02
JUL

REFERENCIA DE LA RESERVA 1106531501

INFORMACION DE VEHICULO: EQUIPAMIENTO COMPLETO FURGONETA (6 O
MAS PASAJEROS) MANUAL AIRE
ACONDICIONADO

CIA-EUROPCAR
ARR-0800
RT-0800
DO-BIO
TARIFA-EUR46.03
VV-EUR46.03
TXT-
CONFIRMADO

CONFIRMADO

INFORMACION GENERAL

***COMPRUEBE SU DOCUMENTAC. ANTES DEL VIAJE

POR SU INTERES, LE ROGAMOS COMPRUEBE SU DOCUMENTACION ANTES DE
LA SALIDA. LE INFORMAMOS QUE BCD TRAVEL, DISPONE DE UN SERVICIO
EXCLUSIVO DE ATENCION PARA EMERGENCIAS FUERA DEL HORARIO DE
OFICINA PUEDE CONTACTAR A TRAVES DEL TELEFONO 902995365
(LLAMADAS NACIONALES) O +34971070551 (LLAMADAS DESDE EL
EXTRANJERO). ESTE SERVICIO PUEDE TENER COSTE ADICIONAL.
BCD TRAVEL LE DESEA UN FELIZ VIAJE.

VERIFIQUE SU VIAJE ONLINE
[CLICK HERE GIRALDO CATALINA](#)

AVISO DE PROTECCIÓN DE DATOS: SUS DATOS PERSONALES SE PROCESARÁN DE
ACUERDO



MONTAJES IRURA, S.L.

JOSE MANUEL NUÑEZ ESPAÑOL

C/Padurea 19
Polígono Ind. Gojain
01170 LEGUTIANO
TFNO. 945 465 550
FAX. 945 465 481
irura@m-irura.com
CIF. B01057082

UNIVERSIDAD DEL PAIS VASCO
ESCUELA DE INGENIERIA DE BILBAO
PL. INGENIERO TORRES QUEVEDO 1
48013 BILBAO
VIZCAYA

Nº FACTURA	FECHA	COD.CLIENTE	CIF/DNI	S/PROVEEDOR	PAG.
2680	24-05-2019	43000420	Q4818001B		1

CODIGO	DESCRIPCIÓN	IMPORTE
	OBRA: REPARACIONES UPV - DEPARTAMENTO DE MAQUINAS Y MOTORES TÉRMICOS. Cableado e instalación de sensores exteriores en el edificio del rectorado de la Universidad del Pais Vasco UPV/EHU.	1.856,00

BASE IMPONIBLE	ANTICIPO	RETENCION	I.V.A.	TOTAL FACTURA
1.856,00			21 % 389,76	2.245,76

Nº Cuenta Banco	/ / /	Forma de pago Vencimientos Retención	PAGARE 24-06-2019 2.245,76
--------------------	-------	--	----------------------------------

FACTURA

ARQUEDOMO ESTUDIO, S.L.
San Antonio, 10-1º
41100 Coria del Rio (Sevilla)
Tel. 900 52 51 08
CIF. B-91960823
arquedomo@arquedomo.com



Numero Factura: 1819	Fecha factura: 05/11/2019
--------------------------------	-------------------------------------

Aitor Ercoreca Gonzalez
UPV / EHU
Departamento de Máquinas y Motores Térmicos
Alameda Urquijo s/n
48013 BILBAO
CIF: Q-48/18001-B

Descripción
Se corresponde con el presupuesto N° 1956. Nuevas tablas SQL

Concepto	Precio	Cantidad	Total
Creación de nuevas tablas de exportación de todos los datos recibidos por los sensores.	840,00 €	1	840,00 €

Base Impon. 840,00 €	IVA 21%	Importe IVA 176,40 €	Total Factura 1.016,40 €
--------------------------------	-------------------	--------------------------------	------------------------------------

Forma de pago
Tranferencia a N° de cuenta: ES79 2100 2518 16 0210119583
Contacto: José Manuel Alonso

FACTURA

ARQUEDOMO ESTUDIO, S.L.
San Antonio, 10-1º
41100 Coria del Rio (Sevilla)
Tel. 900 52 51 08
CIF. B-91960823
arquedomo@arquedomo.com



Numero Factura: 1817	Fecha factura: 05/03/2019
--------------------------------	-------------------------------------

Aitor Ercoreca Gonzalez
UPV / EHU
Departamento de Máquinas y Motores Térmicos
Alameda Urquijo s/n
48013 BILBAO
CIF: Q-48/18001-B

Descripción

Concepto	Precio	Cantidad	Total
Integración de nueva instalación de sensores en el edificio del Rectorado, según oferta N°1904.1 (Se corresponde con el 70% restante del total)	1.421,00 €	1	1.421,00 €

Base Impon. 1.421,00 €	IVA 21%	Importe IVA 298,41 €	Total Factura 1.719,41 €
----------------------------------	-------------------	--------------------------------	------------------------------------

Forma de pago
Tranferencia a N° de cuenta: ES79 2100 2518 16 0210119583
Contacto: José Manuel Alonso

FACTURA

ARQUEDOMO ESTUDIO, S.L.
San Antonio, 10-1º
41100 Coria del Rio (Sevilla)
Tel. 900 52 51 08
CIF. B-91960823
arquedomo@arquedomo.com



Numero Factura: 1816	Fecha factura: 05/09/2019
--------------------------------	-------------------------------------

Aitor Ercoreca Gonzalez
UPV / EHU
Departamento de Máquinas y Motores Térmicos
Alameda Urquijo s/n
48013 BILBAO
CIF: Q-48/18001-B

Descripción

Concepto	Precio	Cantidad	Total
Sobrecostes en la Integración de nueva instalación de sensores en el edificio del Rectorado, (oferta N°1904.1). Se han contemplado 2 jornadas de trabajo adicionales.	630,00 €	1	630,00 €

Base Impon. 630,00 €	IVA 21%	Importe IVA 132,30 €	Total Factura 762,30 €
--------------------------------	-------------------	--------------------------------	----------------------------------

Forma de pago
Tranferencia a N° de cuenta: ES79 2100 2518 16 0210119583
Contacto: José Manuel Alonso

Appendix F

Budgets and invoices for the investment of residential building's MCS

SENSOVANT, S.L.
NIF B30706634

Av. Benjamin Franklin, 28-B. (Valencia Parc Tecnologic)
46980 PATERNA (VALENCIA) ESPAÑA
Teléf. 96 8162005, 672402132
admon@sensovant.com - www.sensovant.com

S.U.M. ENSANCHE 21 ZABALGUEA, S.A.
NIF A-01302462

Paseo Fray Francisco, 21 - C
01007 - VITORIA - GASTEIZ
ÁLAVA - ESPAÑA

Cliente: 2.265
Divisa: EUR
Transportista: C-EXPRESS

Referencia	Descripción	Cantidad	Precio	% Dto.	Importe
EE800-M12J3P1	SENSOR CO2-TEMPERATURA Y HUMEDAD SUPERFICIE CAJA EMBELLECIDA, MODBUS RS485 Part. Arancelaria: 90271010	21	305,00	25%	4.803,75



DATOS BANCARIOS CAJAMAR: ES79 3058 0311 7027 2030 1396

Suma Importes	% Dcto. PP	Portes	Gastos	Cuota de I.V.A.	Cuota R.E.	Retención
---------------	------------	--------	--------	-----------------	------------	-----------

4.803,75

1.008,79

TOTAL

5.812,54

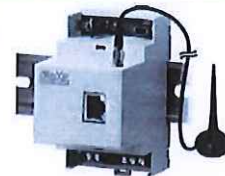
Desglose del I.V.A.			Recargo de Equivalencia		Retención		Forma de Pago
Base	% IVA	Cuota IVA	% R.E.	Cuota R.E.	Base	% Ret.	
4.803,75	21%	1.008,79					CONTADO PREVIO ENVIO MATERIAL. FACTURA PROFORMA

V.B

(Handwritten signature/initials)

S.U.M. ENSANCHE 21 ZABALGUEÑA S.A.
Pº FRAY FRANCISCO Nº 21 C
EDIF. GURE TXOKOA
01007 VITORIA-GASTEIZ
N.I.F. A01302462

ITEM	CONCEPTO	CANT	PRECIO UNIT.	TOTAL
1	EQUIPO INTEGRADO DELTA OHM HD 35ED 1NB Equipo de interior alimentado con pilas y con comunicación radio 868MHz. Este equipo mide temperatura, humedad, CO2. Alcance de 100m en interiores con posibilidad de montar repetidores para ampliar distancias. Sin pantalla Rangos de temperatura:-40...+85°C, humedad relativa : 0...100% RH y CO2: 0...5000 ppm Vida útil con las pilas incluidas de 1,5 años ESTE EQUIPO PERMITE MONTAR HASTA 255 EQUIPOS DISTRIBUIDOS Y SE PUEDE MONTAR EN DIVERSOS PUNTOS DEL EDIFICIO SIN NECESIDAD DE CABLES	2	465,00 €	930,00 €
2	Concentrador de datos HD 35APW Concentrador de datos, que recibe los datos con radio a 868MHz, y los pone a disposición del software HD35S (que permite configurar la red y el modbus), un puerto RS485 con Modbus RTU y un puerto Ethernet que permite también Modbus TCP	1	365,00 €	365,00 €



TOTAL	1.295,00 €
IVA	271,95 €
TOTAL + IVA	1.566,95 €

CONDICIONES PARTICULARES DE LA OFERTA

Plazo de entrega: 8 semanas, sujeto a la entrega por parte del suministrador y/o incidencias del transporte, a partir de la recepción del pedido oficial y aprobación por parte del departamento de Administración.

Validez de la oferta: La oferta tiene una validez de 1 mes a partir de la fecha de emisión indicada.

Garantía: 24 meses contra cualquier defecto de fabricación.

Forma de pago: A convenir

Pedidos: La formalización del pedido requiere la aceptación electrónica (alava@grupoalava.com) por parte del cliente, haciendo referencia expresa al nº de oferta, así como de los ítems objeto de interés.

Ver condiciones de la oferta completas en : www.alavaingenieros.com

V.B.

CONTROL LLEVANT INSTRUMENTACION Y CONTROL, SL
NIF B30706634

Av. Benjamin Franklin, 28-B. Valencia Parc Tecnologic
46980 PATERNA (VALENCIA) ESPAÑA
Teléf. 96 8162005, 672402132
admon@sensovant.com - www.sensovant.com

FUNDACION TECNALIA RESEARCH AND INNOVATION
TECNALIA RESEARCH & INNOVATION
NIF G-48975767

Paseo Mikeletegi, 2
20009 - DONOSTIA
GIPUZKOA - ESPAÑA

Cliente: 1.510
Divisa: EUR
Transportista: C-EXPRESS
Su Pedido: PC18-10264-100
12/12/18

Referencia	Descripción	Cantidad	Precio	% Dto.	Importe
	Proforma A/180287 de 13/12/2018. S/Proforma /MAIL AMAIA URIARTE de 12/12/2018.				
EE071-HTPC	EE071-HTPC Part. Arancelaria: 90258040 SONDA HUMEDAD-TEMPERATURA E+E SALIDA MODBUS, CONECTOR M12 MACHO, FILTRO MALLA	1	165,00	15%	140,25
RSHIELD	PROTECTOR SOLAR INTEMPERIE PARA Sonda HUMEDAD/TEMPERATURA EE210HTXXPBX Part. Arancelaria: 90158020	1	95,00	15%	80,75
MM880-DMF	ANALIZADOR REDES ELECTRICAS CARRIL DIN, MULTITEK, SALIDA RS485 MODBUS	22	150,00	15%	2.805,00
EE650-T2J3L100-P1	SENSOR VELOCIDAD AIRE CONDUCTO, 100MM, 20 M/S, SALIDA RS485 MODBUS Part. Arancelaria: 90268020	4	270,00	15%	918,00
EE850-M12-J3-P1	TRANSMISOR CO2 + HUMEDAD + TEMPERATURA E+E, CONDUCTO CAÑA 200MM, SALIDA RS485 MODBUS, 2000 PPM Part. Arancelaria: 90271010	4	400,00	15%	1.360,00
EE160-HTX3XPBB-XXXXX	SONDA HUMEDAD/TEMPERATURA HVAC, MONTAJE CONDUCTO, CAÑA 200MM FILTRO MEMBRANA, SALIDAS MODBUS RS485 Part. Arancelaria: 90258040 CONFIGURACION: EE160-HTX3-A-PB-B-TX-003-M/1-A-N-2-M	4	205,00	15%	697,00

Suma Importes	% Dcto. PP	Portes	Gastos	Cuota de I.V.A.	Cuota R.E.	Retención	TOTAL
---------------	------------	--------	--------	-----------------	------------	-----------	--------------

Desglose del I.V.A.			Recargo de Equivalencia		Retención		Forma de Pago	
Base	% IVA	Cuota IVA	% R.E.	Cuota R.E.	Base	% Ret.		

CONTROL LLEVANT INSTRUMENTACION Y CONTROL, SL
NIF B30706634

Av. Benjamin Franklin, 28-B. Valencia Parc Tecnologic
46980 PATERNA (VALENCIA) ESPAÑA
Teléf. 96 8162005, 672402132
admon@sensovant.com - www.sensovant.com

UNIVERSIDAD DEL PAIS VASCO/EHU
NIF Q4818001B

Alameda Urquijo, s/n
48013 - BILBAO
VIZCAYA - ESPAÑA

Cliente: 1.110

Divisa: EUR

Referencia	Descripción	Cantidad	Precio	% Dto.	Importe
	Albarán A/181147 de 12/12/2018.				
	Pedido A/181129 de 12/12/2018.				
	Proforma A/180285 de 11/12/2018.				
EE871-HR2000-F5-1AN2	SENSOR CO2 E+E 2000 PPM SALIDA MODBUS RS485, FILTRO TEFLON	2	420,00	15%	714,00
RSHIELD-PM20	PROTECTOR SOLAR INTEMPERIE SONDAS HUMEDAD/TEMPERATURA DIAMETRO 6-12MM Part. Arancelaria: 90158020	8	95,00	15%	646,00
RSHIELD-CO2	PROTECTOR SOLAR INTEMPERIE SONDAS CO2 EE870/871 CON CAJA CONEXIONES IP65	2	180,00	15%	306,00
HA010508	PROTECTOR SOLAR INTEMPERIE VETILACION MECANICA FORZADA	1	980,00	15%	833,00
HA011066	KIT CONFIGURACION USB SONDAS E+E	1	380,00	15%	323,00
HA010819	CONECTOR M12 + CABLE 1.5 METROS	1	50,00	15%	42,50
HA011012	CONVERTIDOR RS485-USB	1	360,00	15%	306,00



DATOS BANCARIOS CAJAMAR: ES79 3058 0311 7027 2030 1396

Suma Importes	% Dcto. PP	Portes	Gastos	Cuota de I.V.A.	Cuota R.E.	Retención	TOTAL
---------------	------------	--------	--------	-----------------	------------	-----------	--------------

Desglose del I.V.A.			Recargo de Equivalencia		Retención		Fechas de Pago		Forma de Pago
Base	% IVA	Cuota IVA	% R.E.	Cuota R.E.	Base	% Ret.	Fecha	Importe	
							12/12/2018	3.848,41	

Facturar a

 FUNDACION TECNALIA RESEARCH & INNOVATION
 FUNDACION TECNALIA RESEARCH & INNOVATION
 CL GELDO, EDIFICIO 700
 PARQUE CIENTÍFICO Y TECNOLÓG. DE BIZKAIA
 48160 - DERIO
 BIZKAIA

Dirección de envío

 PARQUE CIENTÍFICO Y TECNOLÓGICO DE BIZKAIA
 CL ASTONDO, EDIFICIO 700

 DERIO BIZKAIA
 AMAIA URIARTE ARRIEN
 902.760000 / 607.168992

S/Pedido	
S/Referencia	PC19-01269-100-

Hoja	N/Referencia	Código Cliente	DNI/NIF	Fecha Confirm. Pedido	Confirmación Pedido
1/1	352019099	48327	G48975767	13/02/2019	000/27.609

Cód. Artículo	Descripción	Cantidad	P.V.P.		Neto	F. salida
KC403W4021511767	MULTICAL 403 CALOR 1,5 M3/H 110x3/4" MULTICAL 403 Tarjeta ModBus RTU con 2 entradas de pulsos Caudalimetro Calor 110xG3/4" PN16 Sondas directas cable 1,5 m Alimentación 230 VAC Adaptador para sonda 1/2" Soporte plano de pared Caudal 1,5 m3/h Programación 6731100 Velocidad 9600 Paridad None (1 stop bit) Paquetes datos Default Datagram	6,00	267,00		1.602,00	05/03/2019

Forma de pago : PAGO ANTICIPADO TRANSFERENCIA

Portes :
Observaciones:
Total Neto..... 1.602,00

Portes.....

Dto P.P...... %.....

I.V.A...... 21.%..... 336,42

Carqo financiero.... %.....

TOTAL PEDIDO
1.938,42€

C/ Caléndula 93 - Edificio G - Miniparc III
28109 Alcobendas - Madrid
T 913450006
F 913450186
www.dilus.es - dilus@dilus.es



DILUS
INSTRUMENTACIÓN Y SISTEMAS

OFERTA: OVDIL18.317

TECNALIA

Geldo sn, Edificio 700

48160, Derio (vizcaya)

Att.. Inés Apraiz Egaña

Fecha	Nº Cliente	S/Referencia	Elaborada
24/07/2018	C00074	e-mail 19/07/2018	Alberto Pérez

ASUNTO: Suministro Estacion Meterologica

Muy Sres. nuestros:

De acuerdo con su atenta solicitud de oferta, por la presente tenemos el gusto de remitirles nuestra mejor oferta, como sigue:

Item	Ref.	Descripción	Unids.	Dto.	Precio Unit.	Precio Tot.
1	DT4DT80	Datalogger Mod. Data TAKER DT80 Serie 4 , con 5-15 entradas analógicas, 12 canales digitales	1		2.906,00€	2.906,00€
El suministro del datalogger incluye el software para volcado y visualización de datos en PC remoto Mod. dEX.						
2	SSA-LOGGER-ARMAF	Sistema de Adquisición de Datos Dilus en armario de intemperie, que incluye:	1		755,00€	755,00€
<ul style="list-style-type: none">- Armario de intemperie IP66- Fuente de alimentación- Elementos de protección eléctrica (magnetotérmica, diferencial y toma de corriente tipo schuko)- Prensaestopas- Batería recargable autonomía 24 horas- Regulador de carga para batería- Montado y probado						
3	0374920-202	PIRANOMETRO INTELIGENTE SMP6-A, 4-20mA, 10 m cable	2		1.335,00€	2.670,00€
4	0362703	SOPORTE DE MONTAJE CMF4 PARA SENSORES CON/SIN VENTILACIÓN	1		330,00€	330,00€
5	0369701	ABRAZADERA CMB1 PARA MONTAR SOPORTES A MÁSTIL O PARED	1		205,00€	205,00€
6	4.9200.00.001	Estacion Meteorológica compacta CLIMA SENSOR US, para medida de VV,DV,Tª, HR, PB; salida MODBUS RTU	1		2.200,00€	2.200,00€
7	509311	CABLE DE CONEXIÓN DE 10 METROS	1		165,00€	165,00€
8	TORRE 3M. 360	TORRE DE 3 METROS DE 360 TELEVÉS	1		480,00€	480,00€

Safer Instrumentación S.L.
 CIF: B95039210
 Elizalde 4 - 48006 Bilbao
 Telf.: 944129981 Fax: 944730585

safer@saferinstrument.com
 www.saferinstrument.com
 www.safer-instrumentacion.blogspot.com

Oferta

OFERTA Nº: 19/479-FG-FGC
 FECHA: 24/05/2019

S.U.M. ENSANCHE 21 ZABALGUEÑA, S.A.
 CIF: A01302462
 Paseo Fray Francisco , 21 C
01.007-VITORIA-GASTEIZ (ÁLAVA).

Muy Sres. Nuestros:

De acuerdo con su atenta consulta, les detallamos oferta del material por el que Vds. se han interesado, que esperamos sea de su interés.

POS.	CANT.	DESCRIPCIÓN.	EUROS UNIDAD.	DTO.
1	1	Sensor de Medida de Temperatura Globométrica (PT100 4 L) AMR, modelo FPA805GTS, salida hilos. - Rango de Temperatura: -50 a +200º C. - Precisión: PT100 Clase B.	510,-	Neto.

PLAZO DE ENTREGA: 3/4 Semanas.

IVA + 21 %

PORTES PAGADOS.

VALIDEZ DE LA OFERTA: 1 mes



LOPD: Le informamos que sus datos forman parte de nuestros ficheros con la finalidad de hacer efectiva nuestra relación comercial. Si lo desea podrá ejercer sus derechos A.R.C.O en Safer Instrumentación S.L. C/ Elizalde nº4 ,Lonja – Bilbao - Bizkaia (48006).

DPT. MAQUINAS Y MOTORES TERMICOS - (UPV/EHU)
Escuela de Ingeniería de Bilbao, Pl. Ingeniero Torres Quevedo 1 - 48013 BILBAO
ATT: CATALINA GIRALDO
Tel. +34946017322

ITEM	CONCEPTO	CANT.	PRECIO UNIT.	TOTAL
1	<p>Standard Humidity Calibration GMT222 + GMP222 S/N H3330053</p> <p>ISO 9001 carbon dioxide calibration at the pre-defined points over the measurement range within 1000...10000ppm. The calibration points are to cover the whole measurement range (min and max).</p> <p>The service includes:</p> <ul style="list-style-type: none">• Functional testing• Wearing parts• Calibration certificate with as-found and as-left results• Instrument adjustment to meet its specification• Service report• Service code: CO2CAL• Portes de envío incluidos desde la recepción del equipo en nuestro almacén.	1.00	280,00 €	280,00 €

NOTA: La oferta no incluye reparaciones. Si se detectar alguna anomalía en la calibración se enviará nueva oferta de reparación.

TOTAL	280,00 €
--------------	-----------------

En Stock Sondas Pt100

Sonda Pt100 con Conector Lemo de Tamaño 1

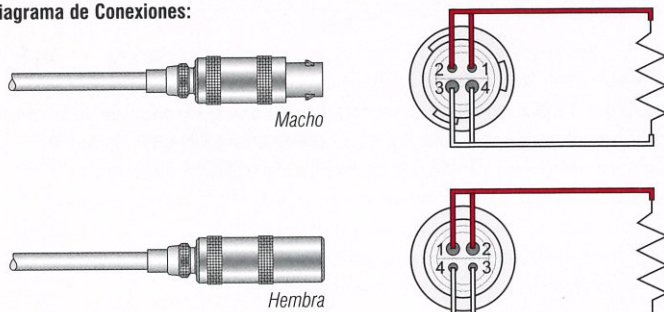


¿Necesita un racor? Ver página 88

Estos sensores rígidos tienen una vaina de acero inoxidable cerrada por un extremo. El elemento sensor Pt100 tiene una longitud de 10mm y está situada en el extremo de la vaina. Se recomienda una profundidad de inmersión de 50mm. La temperatura máxima es de 250°C. Como terminación se utiliza un conector Lemo macho de tamaño 1, sensor recomendado para una rápida y sencilla conexión. En este catálogo puede encontrar conectores hembra o macho, una amplia gama de cables de extensión y racores ajustables para completar este producto.

- Configuración a 4 hilos
- El elemento Pt100 cumple con la norma IEC 60751 clase B : 2008
- Vaina: acero inoxidable AISI 316, diámetro 3mm
- Disponibilidad en distintas longitudes (no incluye la longitud del conector)
- Rango de funcionamiento: -75°C a +250°C
- Terminado en conector macho o hembra Lemo de tamaño 1

Diagrama de Conexiones:



Contacte con nosotros para otras diferentes configuraciones de conexionado.

Sonda Pt100 con Conectores Lemo

Código Macho	Código Hembra	Descripción	Precio unitario		
			1-9	10-24	25-49
514-950	514-951	Ø 3mm x 150mm de longitud	€57,90	€54,90	€48,30
514-955	514-956	Ø 3mm x 300mm de longitud	€58,70	€55,80	€49,00
514-960	514-961	Ø 3mm x 500mm de longitud	€59,40	€56,50	€49,70
514-965	514-966	Ø 6mm x 150mm de longitud	€57,90	€54,90	€48,30
514-970	514-971	Ø 6mm x 300mm de longitud	€58,70	€55,80	€49,00
514-975	514-976	Ø 6mm x 500mm de longitud	€59,40	€56,50	€49,70

Conectores Lemo

Código	Descripción	Precio unitario		
		1-9	10-24	25-49
514-995	Conector hembra LEMO	€16,80	€15,50	€13,60
514-996	Conector macho LEMO	€16,80	€15,50	€13,60

Pt100 de Precision



Esta sonda Pt100 permite efectuar medidas de temperatura muy precisas. Sonda de referencia cuya precisión es suficiente para la mayoría de las operaciones de control o calibración de otros sensores de temperatura. Se puede suministrar acompañado de un certificado de calibración UKAS.

- El elemento Pt100 cumple con la norma IEC 60751 clase 1/10 : 2008
- Precisión: $\pm 0.03^\circ\text{C}$ (elemento sensor), $\pm 0.06^\circ\text{C}$ (sonda completa) a 0°C
- Configuración a 4 hilos, posibilidad a 3 hilos (no conectar uno de los conductores blancos)
- Se recomienda una profundidad mínima de inmersión de 150mm
- Longitud del elemento sensor: los primeros 20mm
- Rango de funcionamiento: -50°C a 250°C
- Vaina en acero inoxidable AISI 316, diámetro 3 ó 6mm con 250mm de longitud.
- Cable: 2 metros aislado con PFA.
- Disponible, como opción, de certificado de calibración UKAS en 3 puntos: 0°C , 100°C y 200°C o seleccionados por el cliente (plazo de entrega 4/5 días)

Pt100 de Precisión

Código	Descripción	Precio unitario		
		1-9	10-24	25-49
515-720	Pt100 de precisión Ø 3mm x 250mm long	€77,20	€66,80	€58,80
515-725	Pt100 de precisión Ø 6mm x 250mm long	€77,20	€66,80	€58,80
515-730	515-720 + certificado en 0, 100 y 200°C	€212,20	€194,20	€170,90
515-735	515-720 + certificado en 3 pto. (a elegir)	€222,00	€202,30	€178,10
515-740	515-725 + certificado en 0, 100 y 200°C	€225,30	€205,80	€181,20
515-745	515-725 + certificado en 3 pto. (a elegir)	€235,10	€215,50	€189,60

Sonda Pt100 con Conector Hirschmann



Sensor con vaina rígida de acero inoxidable cerrada por un extremo. El elemento Pt100 situado en la punta de la vaina tiene una longitud de unos 10mm, para realizar una correcta medida la profundidad de inmersión deber ser al menos de 20mm. Terminado en conector Hirschmann con protección IP65 que proporciona un fácil y rápido montaje, instalación y mantenimiento.

- Configuración a 3 hilos
- El elemento Pt100 cumple con la norma IEC 60751 clase B : 2008
- Vaina de acero inoxidable 316 de 3mm ó 6mm de diámetro
- Varias longitudes disponibles
- Rango de funcionamiento: -50°C a 200°C
- Protección IP65

Sonda Pt100 con Conector Hirschmann

Código	Descripción	Precio unitario		
		1-9	10-24	25-49
514-933	Ø 3mm x 150mm de longitud	€57,80	€54,90	€48,30
514-936	Ø 3mm x 300mm de longitud	€58,70	€55,70	€49,00
514-939	Ø 3mm x 500mm de longitud	€59,40	€56,40	€49,70
514-942	Ø 6mm x 150mm de longitud	€57,80	€54,90	€48,30
514-945	Ø 6mm x 300mm de longitud	€58,70	€55,70	€49,00
514-948	Ø 6mm x 500mm de longitud	€59,40	€56,40	€49,70



91 840 6695



Safer Instrumentación S.L.
 CIF: B95039210
 Elizalde 4 - 48006 Bilbao
 Telf.: 944129981 Fax: 944730585

safer@saferinstrument.com
 www.saferinstrument.com
 www.safer-instrumentacion.blogspot.com

Oferta

OFERTA Nº: 18/418-FG-RL-FGC
 FECHA: 08/05/2017

TECNALIA RESEARCH & INNOVATION.
 Parque Tecnológico de Bizkaia
 C/ Geldo, Edificio 700
48.160-DERIO (BIZKAIA).
AT. SRA. AMAIA URIARTE.

Muy Sres. Nuestros:

De acuerdo con su atenta consulta, les detallamos oferta del material por el que Vds. se han interesado, que esperamos sea de su interés.

POS.	CANT.	DESCRIPCIÓN.	EUROS UNIDAD.	DTO.
1	11	Placa de flujo Térmico 120 x 120 x 1.5 mm Serie 118 de resina epoxy AMR, modelo FQA018C, con cable de 2 metros de longitud.	410,- X11 <u>4.510,-</u>	Neto.

PLAZO DE ENTREGA: 3/4 Semanas.

IVA + 21 %

PORTES PAGADOS.

VALIDEZ DE LA OFERTA: 1 mes



Phymeas GbR - Ahornring 21 – D-03055 Cottbus

Inés Apraiz Egaña
TECNALIA
C/Geldo – Parque Tecnológico de Bizkaia
Edificio 700

48160 DERIO Bizkaia
SPAIN

Cottbus, May 8, 2018

Offer

Your enquiry: from May 8, 2018
Offer: 28 019 0801

Pos.	Quantity	Commodity	Unit-price [€]	price [€]
01	11	Heat flux sensor type 7 120mm*120mm*1,5mm with Calibration certificate at ca. 25°C bulk temperature	285,00	3.135,00
		Quantity rebate -5%		156,75
		Postal rate		20,00
All round price				2.998,25

Delivery time: ca. 2 weeks after ordering date
Conditions of payment: strictly net in the space of 21 days
Our general terms and conditions apply

Invoice without VAT due to intra-community delivery
Your VAT-Number: ESG48975767

Bankverbindung

Phymeas GbR
Cronbank Dreieich
IBAN: DE11 5053 0000 0000 2577 02
BIC: GENODE51CRO

VAT-Number

DE138781480

En Stock Calibración y Elementos Pt100

Servicio de Calibración para Sensores

El grupo TC ofrece un servicio de calibración para sondas Pt100 y termopares en su propio laboratorio el cual dispone de acreditación UKAS. Existe un reconocimiento mutuo entre los laboratorios de calibración acreditados UKAS y los laboratorios de calibración acreditados ENAC.



Nuestro laboratorio se acredita para las calibraciones de -100°C a 1590°C . Las calibraciones que proponemos se realizan en un plazo corto y a un precio muy interesante. Si lo desea, se puede poner en contacto con nosotros para conocer la incertidumbre de calibración y la longitud mínima de los sensores a calibrar. Estamos también en condiciones de fabricar los sensores idóneos para su aplicación y adaptados a la calibración pedida.

- **Calibración UKAS en laboratorio propio**
- **Rango de Calibración desde -100°C a 1590°C (también en -196°C como punto fijo - por favor contacte con nosotros para más detalles)**
- **Longitud mínima de los sensores a calibrar: 490mm (esta longitud puede ser menor para algunas aplicaciones de baja temperatura). Póngase en contacto con nosotros para más información**
- **Plazo de entrega: 4/5 días (se puede reducir en caso necesario)**
- **Certificado de calibración completo disponible en un plazo muy corto**
- **Calibración disponible tanto para nuestros equipos como para los de cualquier otro fabricante**

Calibración

Código	Descripción	Precio por calibración
998-002	1 sensor en 1 punto	€133,00
998-008	1 sensor en 2 puntos	€154,00
998-014	1 sensor en 3 puntos	€168,00
998-020	1 sensor en 4 puntos	€182,00
998-026	2 sensores en 1 punto	€147,00
998-032	2 sensores en 2 puntos	€168,00
998-038	2 sensores en 3 puntos	€210,00
998-044	3 sensores en 1 punto	€154,00
998-050	3 sensores en 2 puntos	€210,00
998-056	3 sensores en 3 puntos	€252,00
998-998	Cualquier otra combinación	Solicitar precio

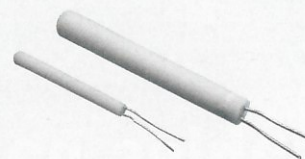
Pago

Se le puede abrir una cuenta de cliente de forma inmediata. Si ya tiene cuenta con el Grupo TC no es necesario que recuerde su número de cliente al ponerse en contacto con nosotros ya que le encontraremos con facilidad. ¡Nosotros haremos el trabajo! También puede pagar con Visa o Mastercard.



Elemento Cilíndrico Cerámico Pt100

Estos elementos Pt100 son recomendados para aquellas aplicaciones que requieran buena resistencia al choque térmico, buena estabilidad de medida y temperaturas altas. Disponibles en diferentes tolerancias. El valor nominal de resistencia es de 100 Ohms a 0°C , el hilo de medida se encuentra bobinado alrededor de un soporte y está encapsulado bajo un cilindro cerámico. Se aconseja que como mínimo se realice una conexión a 3 hilos.



- **Resistencia nominal: 100ohms a 0°C (138.5ohms a 100°C)**
- **Clase de tolerancia: B y A según la norma IEC 60751 : 2008 de clase 1/3, 1/5 y 1/10**
- **Rango: -200°C a 600°C**
- **Dimensiones: 3 x 25mm ó 1.6 x 15mm (diámetro x longitud)**
- **Hilos: 10mm de longitud (el valor nominal es medido a 5mm del extremo)**

Elemento Cilíndrico Cerámica 3mm x 25mm

Código	Descripción	Precio unitario		
		1-9	10-24	25-49
578-050	Clase B	€10,90	€10,00	€9,20
578-053	Clase A	€12,30	€11,20	€10,30
578-056	Clase 1/3	€14,70	€13,40	€12,30
578-059	Clase 1/5	€16,90	€15,40	€14,20
578-062	Clase 1/10	€25,20	€23,10	€21,30

Elemento Cilíndrico Cerámica 1.6mm x 15mm

Código	Descripción	Precio unitario		
		1-9	10-24	25-49
578-072	Clase B	€10,90	€10,00	€9,20
578-075	Clase A	€12,30	€11,20	€10,30
578-078	Clase 1/3	€14,70	€13,40	€12,30
578-081	Clase 1/5	€16,90	€15,40	€14,20
578-084	Clase 1/10	€25,20	€23,10	€21,30

Elemento Plano Pt100

Elementos Pt100 de película fina para medidas de temperatura precisas y económica. Construidos por deposición al vacío de platino sobre un sustrato cerámico y ajustado por láser para formar un elemento resistivo altamente estable. El valor nominal de resistencia es de 100 Ohms a 0°C . Se aconseja que como mínimo se realice una conexión a 3 hilos.



- **Resistencia nominal: 100 Ohms a 0°C (138.5 Ohms a 100°C)**
- **Clase de tolerancia: B y A según la norma IEC 60751 : 2008**
- **Rango: -100°C a 500°C**
- **Dimensiones: 2 x 2 x 0.4mm (largo x ancho x espesor, sin incluir el sellante azul)**
- **Hilos: 10mm de longitud (el valor nominal es medido a 5mm del extremo)**

Elemento Plano Pt100

Código	Descripción	Precio unitario		
		1-9	10-24	25-49
578-090	Clase B	€7,60	€6,90	€6,30
578-093	Clase A	€8,60	€7,80	€7,20

Fax: 91 850 8302

E-mail: info@tcdirect.es Web: www.tcdirect.es





Fundacion Tecnalia Res.&Innov.
Parque Cientifico de Bizkaia
C/Geldo, Edificio 700

ES-48160 Derio (Bizkaia)
Spain

tel 0034-94-6073300
fax 0034-94-6073349

inquiry dated 24.05.2018
E-mail sent by Amaia Uriarte

OFFER

offer no. T0486
date 28.05.2018

customer no.16687

operator Klaus Schwanke
extension +49/7457-9453-25 Fax -3758
e-mail k.schwanke@galltec.de

We thank you very much for your inquiry and are pleased to quote according to our general terms of trade and delivery:

pos.	description	quantity	list price	net/unit	amount EUR
001	art. nr. 57013400PC5	2.00	180.20		
	basic discount 10%		-18.02	162.18	324.36
	FPC1/5 Humidity Sensor, compact design gauze filter ZE17 measuring range humidity: 0 ... 100 % rh output humidity: 0 ... 1 V DC supply voltage: 6 ... 30 V DC				
	Further data according to data sheet Subject to technical modifications				

	goods value	EUR	324,36
	transport insurance	EUR	1,12
	net amount	EUR	325,48
excluding tax	% VAT	EUR	
	invoice amount	EUR	325,48

valid until 28.08.2018
date of delivery 3-4 weeks after order receipt
terms of payment 8 days 2% discount or 30 days net
terms of delivery ex works Bondorf / Germany
mode of shipment DPD- parcel service

Ajouter au panier

Le produit a été ajouté au panier

Le stock est insuffisant. unités ont été rajoutées au panier

Total:

Stock épuisé:

sous 72h sur commande

Quantité minimum d'achat

La quantité minimum d'achat n'est pas atteinte

- [Accueil](#)
- [Emetteurs d'Impulsion Gaz](#)
- [Emetteur d'impulsion ITRON pour compteur G4 Gallus](#)

Compteur-energie.com vous propose un éventail de produits pour maîtriser votre consommation d'énergie ou répartir les charges énergétiques des bâtiments. Accéder aux données énergétiques de vos compteurs grâce aux produits de Compteur-energie.com.

Retrouvez une sélection de compteurs d'énergie d'eau, de gaz, d'électricité, de fioul, d'énergie thermique ainsi que des émetteurs d'impulsions et système radio pour réaliser simplement vos projets d'efficacité énergétique et de télérelève.

ABB, Adeunis, Antarc Automation, Aqua Metro, B-Meters, Carlo Gavazzi, Chauvin-Arnaux, Circutor, Connit, Diehl, Dresser, Elster, Fludia, Georin, Imeys, Itron, Maddalena, Micronics, OTMetric, Pietro Fiorentini, Relay, Sensus, SigFox, Socomec, Webdyn, Zenner

En poursuivant votre navigation sur ce site, vous acceptez l'utilisation de Cookies à des fins statistiques et commerciales.

Emetteur d'impulsion ITRON pour compteur G4 Gallus

Itron - Ref : 10-59600-169

Itron



zoom



voir aussi :

photos non contractuelles

Neuf 22.00 € H.T.

Remise quantitative

- De 5 à 9 unités : -5%
- De 10 à 29 unités : -10%
- De 30 à 99 unités : -15%
- De 100 et plus : -20%

Quantité

Alerte réapprovisionnement

Recevez une alerte par email dès que votre choix sera de retour en stock

Votre e-mail*:

[Envoyer cette page à un\(e\) ami\(e\)](#)

Détails Produit

Emetteur d'impulsion ITRON pour compteur G4 Gallus

Itron - Ref : 10-59600-169

Disponibilité : **En Stock**



Nº OFERTA: 181107-O-16/1	Cliete:	Fundación Tecnalia Research & Innovation.
	Contacto:	Amaia Uriarte
FECHA: 30 – Enero – 2018	Dirección:	Parque Tecnológico de Bizkaia C/ Geldo Edif. 700 48160 Derio (Bizkaia)
	Tlfno:	902 760 000
	E-mail:	amaia.uriarte@tecnalia.com

1. ENSAYO:

Calibración de 24 medidores de flujo de calor mediante ensayos en equipo de medida de la conductividad térmica por el método de flujo de calor, HFM 436/3/0 Lambda de la marca NETZSCH.

2. NORMAS DE REFERENCIA:

El equipo de medida de la conductividad térmica HFM 436/3/0 Lambda de la marca NETZSCH esta homologado para la ejecución de ensayos según UNE-EN 12667:2002

3. MUESTRA:

24 medidores de flujo de calor, con señal de medida en mV.

4. CONDICIONES:

Se determinará el factor de calibración de cada medidor de flujo de calor en $mV/(W/m^2)$. Dicho factor resultará de la ejecución de un ensayo en el equipo de medida NETZSCH de una muestra formada por uno o dos (según sean sus dimensiones) medidores de flujo de calor a calibrar en medio de capas de manta de espuma aislante térmica, asociando el flujo de calor estabilizado del ensayo con la señal en mV obtenida de cada medidor.

La lectura y registro de la señal en mV de los medidores de flujo se hará con el adquirente que corresponda, o en su defecto se dispone de un equipo adquirente por multiplexión Agilent 34980A.

Los factores de calibración de los 24 medidores de flujo de calor serán determinados a una temperatura media de 20°C y un salto térmico de 10 °C.

El plazo de ejecución de las 24 calibraciones será de una semana, dependiendo de la disponibilidad del equipo de medida.

Los resultados del presente servicio serán consignados en un único informe, identificando cada medidor de flujo de calor según la codificación indicada por el cliente.

5. OFERTA ECONÓMICA:

Determinación del factor de calibración de 24 medidores de flujo de calor mediante ensayos en conductivímetro HFM 436/3/0 Lambda de la marca NETZSCH y emisión de un único informe (60€/unidad).....1440,00 €

TOTAL OFERTA1440,00 €

En ese precio no está incluido el IVA.

El plazo de validez de la oferta es de 60 días.

Ivan Flores

Laboratorio de Control de Calidad de la Edificación

Aceptado

El cliente

Phymeas GbR - Ahornring 21 – D-03055 Cottbus

Inés Apraiz Egaña
TECNALIA
C/Geldo – Parque Tecnológico de Bizkaia
Edificio 700

48160 DERIO Bizkaia
SPAIN

Cottbus, May 8, 2018

Offer

Your enquiry: from May 8, 2018
Offer: 28 020 0801

Pos.	Quantity	Commodity	Unit-price [€]	price [€]
01	8	Calibration of Heat flux sensor type 7 Calibration certificate at ca. 25°C bulk temperature	72,00	576,00
		Postal rate		20,00
All round price				596,00

Delivery time: ca. 2 weeks after ordering date
Conditions of payment: strictly net in the space of 21 days
Our general terms and conditions apply

Invoice without VAT due to intra-community delivery
Your VAT-Number: ESG48975767

OFERTA VENTA Nº 9102820

Fecha Oferta: 24/07/2019

Validez de la oferta:

Referencia: ENSANCHE 21

De: ANA

Para:

Cod.Cli. 00505 - Cod. Pro.

S.U.M. ENSANCHE 21 ZABALGUNEA, S.A.

PºFRAY FRANCISCO, 21 C

01007 VITORIA-GASTEIZ Alava

Telf:

Fax:

Página 1 de 1

Ref. Fab.	Descripción	Cantidad	Precio	Descuento	Importe
76DAT0220R25	CABLE BUS 2x2x0,8 (ROLLO 100m)	1.248,00	408,0000 (1000)	NETO	509,18
26MFP0112R25	CABLE TFCCO.C/PANT.4x0,2mm2 LH (RO.100m)	2.055,00	176,0000 (1000)	NETO	361,68
26MFP0100R25	CABLE TFCCO.C/PANT.2x0,2mm2 LH (RO.100m)	975,00	113,0000 (1000)	NETO	110,18
2123	CABLE UTP CAT6 LSFH	54,00	0,3430	NETO	18,52
NDR-75-24	FUENTE ALIM.CARRIL90-246VAC-24V DC 3.2A 75W	2,00	23,5000	NETO	47,00
NDR-120-24	FUENTE ALIM.CARRIL90-246VAC-24V DC 5A 120W	2,00	27,6000	NETO	55,20
NDR-240-24	FUENTE ALIM.CARRIL90-246VAC-24V DC 6.5A 240W	1,00	50,7000	NETO	50,70
MDR-10-5	FUENTE ALIM.CARRIL 5V 5MA	1,00	11,4000	NETO	11,40
MDR-10-24	FUENTE ALIM.24VCA 0,25A	5,00	11,1000	NETO	55,50
0779912	EMPALME PUNTA/PUNTA KPC 1,5 ROJO	700,00	6,1500 (100)	NETO	43,05
209902	CONECTOR DATO RJ45 UTP CAT-6 M	20,00	0,3400	NETO	6,80
SE72300	PLACA DF-23 P/CAJA CC-23	4,00	8,0000	40,00	19,20
AC73017	CAJA MODULAR CC-25T 570x285x185mm	1,00	66,5000	40,00	39,90
SE72500	PLACA DF-25 P/CAJA CC-25 Y CC-25A	1,00	10,5000	40,00	6,30
AC73016	CAJA MODULAR CC-23T 380x285x185mm	4,00	55,1250	40,00	132,30
MAS0302521R5	ARM.C/PLACA MAS-300x250x210 RAL7035	2,00	89,6500	42,00	103,99
MAS0252015R5	ARM.C/PLACA MAS-250x200x155 RAL7035	1,00	73,7200	42,00	42,76
MAS0403021R5	ARM.C/PLACA MAS-400x300x210 RAL7035	1,00	108,3100	42,00	62,82
MAS0503021R5	ARM.C/PLACA MAS-500x300x210 RAL7035	1,00	118,0000	42,00	68,44
ALL508	CIERRE C/LLAVE RONIS No.C21323 para armarios	5,00	21,8300	30,00	76,41
F-224A	PERFIL OMEGA PERFORADO BARRAS 2 MTS	10,00	2,5400	45,00	13,97
PB25	TRANSFORMADOR MONO S.P 12/24V 25VA	5,00	24,3600	20,00	97,44
CE	CALEFACTOR ELECTRICO 3000W	7,00	56,8900	NETO	398,23
VP	VENTILADOR PIE	7,00	53,1900	NETO	372,33

BRUTO	R.A.E.E	Base imp.	% IVA	Importe IVA	TOTAL OFERTA VENTA
2.703,30	0,00	2.703,30	21,00	567,69	3.270,99 eur

OBSERVACIONES:

UGA: 314818 BUD
 GASTO DE

RESUMEN DEL L

NÚMERO ESB0701210719F1628S00001590	VERSIÓN 3.2	MODALIDAD INDIVIDUAL
EMISOR DE LA FACTURA TERCERO	NUM. FACTURAS 1	MONEDA DE FACTURACIÓN EUR

FACTURA NÚMERO 19F1628S00001590

[VOLVER A LA FACTURA](#)

IMPORTE

IMPORTE TOTAL FACTURAS	46,03
IMPORTE TOTAL A PAGAR	46,03
IMPORTE TOTAL A EJECUTAR	46,03

DATOS EMISOR

[Ocultar](#)

RAZÓN SOCIAL: AVORIS RETAIL DIVISION S.L. **NIF/CIF:** ESB07012107
TIPO PERSONA: **TIPO RESIDENCIA:**
DIRECCIÓN: CL/ JOSE ROVER MOTTA, 27 **NOMBRE COMERCIAL:** AVORIS RETAIL DIVISION S.L.
 N: 07006PALMA DE MALLORCA
 BALEARES
 ESP

DATOS DE CONTACTO:

Teléfono: 944257055 **Fax:** **Web:** **Email:** upv-ehu@bcdtravel.es
Personas contacto: **CnoCnae:** **Código INE:** **Otros:** PAIS VASCO

CENTROS

Número	Tipo rol	Nombre	Dirección	Datos de contacto	GLN Físico	Pto op. lógico	Descripción
E00/16 28		BCD M. OUT 302	AL/ ALAMEDA MAZARREDO, 1655 48009BILBAO BIZKAIA ESP	Teléfono: 9442570 Fax: Web: Contacto: Cód. INE:			BCD M. OUT 302
				Email: upv-ehu@bcdtravel.es CnoCnae: Otros: PAIS VASCO			

DATOS RECEPTOR

[Ocultar](#)

RAZÓN SOCIAL: UNIVERSIDAD DEL PAIS VASCO - EHU **NIF/CIF:** ESQ4818001B
TIPO PERSONA: **TIPO RESIDENCIA:**
IDENTIFICACIÓN: 173516
DIRECCIÓN: CL/ BARRIO SARRIENA, S/N **NOMBRE COMERCIAL:** UNIVERSIDAD DEL PAIS VASCO - EHU
 N: 48940LEIOA BIZKAIA
 ESP

CENTROS

Número	Tipo rol	Nombre	Dirección	Datos de contacto	GLN Físico	Pto op. lógico	Descripción
U020002 79	Fiscal	OFICINA CONTABLE	CL/ BARRIO SARRIENA, S/N 48940LEIOA BIZKAIA ESP				SERVICIO DE CONTABILIDAD
U020000 01	Receptor	ORGANO GESTOR	CL/ BARRIO SARRIENA, S/N 48940LEIOA BIZKAIA ESP				UPV/EHU
U020001 37	Pagador	UNIDAD TRAMITADORA	CL/ BARRIO SARRIENA, S/N 48940LEIOA BIZKAIA ESP				3148 DEPARTAMENTO MAQUINAS Y MOTORES TERMICOS
3148	Comprador	ORGANO PROPONENTE	CL/ BARRIO SARRIENA, S/N 48940LEIOA BIZKAIA ESP				3148

DATOS TERCERO

[Ocultar](#)

RAZÓN SOCIAL: Bansabadell Factura, SL Unipersonal **NIF/CIF:** ESB63448526
TIPO PERSONA:
DIRECCIÓN: C/Sena, 12 Nucli B, 4 planta - Pol. Ind. Can Sant Joan
 N: 08190Sant Cugat del Vallès
 BARCELONA
 ESP

imp. gasta 44696
 an. ento - 139182

Razón fiscal:

UNIVERSIDAD DEL PAIS VASCO

PL INGENIERO TORRES QUEVEDO, 1
48013 BILBAO
Vizcaya

UNIVERSIDAD DEL PAIS VASCO

PL INGENIERO TORRES QUEVEDO, 1
48013 BILBAO
VIZCAYA

FACTURA	OBRA	FECHA	C.I.F.	COD. CLIENTE	
8192277	9191039	20/12/19	Q4818001B	02856	Página 1 de 6
Concepto		Cantidad	Precio Unitario	Importe	
-INSTALACION Y CONEXIONADO DE ELEMENTOS PARA HACER MEDICIONES EN EDIFICIO DE C/CORRERIA EN VITORIA					
Parte 900192637 - 29/07/19 REF.: 8068					
-CABLEAR SENSORES DE FACHADA Y CONECTAR					
HORAS DE OFICIAL ELECTRICISTA		7,50	29,740	223,05	
HORAS DE OFICIAL ELECTRICISTA		7,50	29,740	223,05	
Parte 900192638 - 30/07/19 REF.: 8069					
-CABLEAR SENSORES Y CONEXIONAR					
HORAS DE OFICIAL ELECTRICISTA		8,50	29,740	252,79	
HORAS DE OFICIAL ELECTRICISTA		8,50	29,740	252,79	
Parte 900192639 - 31/07/19 REF.: 8070					
-CABLEAR Y MARCAR CABLEADO					
HORAS DE OFICIAL ELECTRICISTA		5,00	29,740	148,70	
Parte 900192640 - 08/08/19 REF.: 8071					
-INSTALACION DE CABLEADO PARA SENSORES EN FACHADA TRASERA Y EMPALMAR					
HORAS DE OFICIAL ELECTRICISTA		6,50	29,740	193,31	
HORAS DE OFICIAL ELECTRICISTA		6,50	29,740	193,31	
Parte 900192641 - 02/09/19 REF.: 8075					

SUMA Y SIGUE:

Calle Correría 119			
Planta segunda-Atico	cant	unitario	total
Contadores de energía			
Intercalar sensores en tubería existente	2,00	42,29 €	84,58 €
Colocación contadores de energía	2,00	75,63 €	151,26 €
Modificación de tubería para colocación contadores de energía	1,00	498,58 €	498,58 €
TOTAL PRESUPUESTO			734,42 €

De: Tomás Martínez
Departamento: Comercial
Tlfno: 943-729006
Fax: 943-729147
Móvil: 617480661

E-mail: tmartinez@garapen.es

Empresa	TECNALIA
Att. De:	Amaia Uriarte Arrien
Dirección:	C/ Geldo, Edificio 700
C.Post./Pob.	48160 Derio
Provincia:	Bizkaia
Telef./ Fax:	667 119 810
E-mail:	amaia.uriarte@tecnalia.com

PROGRAMACIÓN PARA LA ADQUISICIÓN DE DATOS EN EDIFICIO DE VITORIA.

Tomás Martínez Noguera
tmartinez@garapen.es
Móvil: 617480661



GARAPEN, S.L.
Fecha: 15 de mayo de 2019
Saludos cordiales,

Presupuesto N°: 4.161

Fecha: 15/07/2019 0:

S/Ref.

FUND.TECNALIA RESEARCH & INNOVATION

Parque Científico y Tecn. de Bizkaia

48160 - Derio (Bizkaia)

CIF: G48975767

Tfno.

Fax.

- ()

Amaia Uriarte Arrien

Condiciones Particulares

F. de Pago: Transferencia a 60 días

Portes: Pagados

Envio: Pagados

Cant.	Ref./Descripción	Precio	Dto.	Importe	F. Entrega
1,00	PORTES DE VENTA LANGARRI	7,00 €	0,00	7,00 €	15/07/2019
7,00	SAT_ING_SOF_GAR Ampliación de proyecto "PROGRAMACIÓN PARA LA ADQUISICIÓN DE DATOS EN EDIFICIO DE VITORIA". Inclusión de seis nuevos equipos Modbus en planta F2. Programación de comunicaciones en PLC, inclusión de estos nuevos equipos en el programa de testeo de la instalación y pruebas. Esta oferta contempla la inclusión de equipos iguales a los que ya han sido utilizados en el desarrollo inicial.	65,00 €	20,00	364,00 €	15/07/2019

TOTAL PRESUPUESTO SIN IVA

371,00 €

Factura Nº: 6.923

Fecha: 24/06/2019

S/Ref.:

UNIVERSIDAD DEL PAIS VASCO

Barrio Sarriena s/n
48940 - Leioa (BIZKAIA)

CIF: Q4818001B

Tfno. Fax.

UNIVERSIDAD DEL PAIS VASCO
Barrio Sarriena s/n

48940 - Leioa (BIZKAIA)

Condiciones Particulares

F. de Pago: Transferencia

F. VTO. 24/06/2019

Cant.	Ref./Descripción	Precio	Dto.	Importe	F. Entrega
1,00	<p>VALB 8203 SAT_ING_SOF_GAR Desarrollo de software para:</p> <p>" PROGRAMACIÓN PARA LA ADQUISICIÓN DE DATOS EN EDIFICIO DE VITORIA, APARTADO COHEATING. REV_2 "</p> <p>Según oferta que obra en su poder. 30% a la realización del pedido.</p> <p>Relación de Cuentas Corrientes CAJA LABORAL POPULAR - ES77 3035 0132 54 1320030001</p>	1.169,10 €	0	1.169,10 €	24/06/2019

B .Imponible	% IVA	IVA	Total
1.169.10 €	21	245.51€	1.414.61€

BECKHOFF

Para:

Fund. Tecnalia Research&Innovation
 Mikeletegi Pasealekua, 2
 20009 Donostia - San Sebastián
 Guipuzkoa
 G48975767

Oferta

24/05/2018

OFV005624

Estimado Sr./Sra.: Amaia Uriarte Arrien
 De acuerdo con su solicitud detallamos oferta económica.

Código	Cantidad	Descripción	Precio Un.	Importe
BK1250	4	EtherCAT "Compact" Coupler between EtherCAT Terminals (E-bus) and Bus Terminals (K-bus), adapter terminal	107,76	431,03
KL6781	4	M-Bus master terminal	171,59	686,34
EL6021	4	Serial interface RS422/RS485	176,89	707,56
EL3202-0010	12	2-channel input terminal PT100 (RTD) for 4-wire connection, high-precision	191,63	2.299,58
EL3602-0010	7	2-channel analog input terminal -75...+75 mV, differential input, 24 bit	233,89	1.637,24
EL3064	3	4-channel analog input terminal 0...10 V, single-ended, 12 bit, 4 x 2-wire system	117,93	353,79
EL2024	9	4-channel digital output terminal 24 V DC, 2 A, 2-wire system	41,77	375,92
EL9100	4	Passive potential feed terminal, 24 V DC	12,58	50,32
TS6255-0001	2	TwinCAT PLC Modbus RTU	49,09	98,18
				6.639,96

Condiciones comerciales:

Precios: Netos
 IVA 21%: No incluido

Plazo de entrega estimado: 4 Semanas

Validez de la Oferta: 30 Días

Portes: CARGO

Forma de Pago: Transferencia

Plazo máximo 60 días según la Ley 15/2010 referente a las medidas adoptadas contra la morosidad en operaciones comerciales.

Todas las operaciones de Beckhoff están aseguradas en Crédito y Caución.

Esperando sea de su interés, aprovechamos la ocasión para saludarles.

Mikel Marin
 Ingeniero de Ventas
 48170 Zamudio
 Bizkaia

BECKHOFF AUTOMATION, S.A. Edificio Testa Sant Cugat Avda. Alcalde Barnils, 64-68 Módulo A, Planta 3, Local 1 y 2 08174 Sant Cugat del Vallès Barcelona	Nº teléfono +34 93 584 49 97 Fax: +34 93 584 40 84 Página Web http://www.beckhoff.es Correo electrónico info@beckhoff.es CIF/NIF A64161722	CaixaBank, S.A. CCC 21000104820201132450 IBAN ES62 2100 0104 8202 0113 2450 SWIFT CAIXESBXXXX
---	---	--

